



# **Design and development of novel organocatalytic artificial enzymes**

A thesis submitted in accordance with the conditions governing candidates for the degree of

**Philosophiae Doctor at Cardiff University**

**Nicolò Santi**

Under the supervision of **Dr Louis Luk**

July 2020

Cardiff School of Chemistry

Cardiff University

## Acknowledgement

Firstly, I would like to thank my supervisor, Dr Louis Luk, for giving me the opportunity for this PhD. I am incredibly grateful for the constant guidance and the excellent support he provided during these years and for all the precious lessons I have learnt from him. My gratitude goes to Cardiff University for this opportunity and for all the support I have received throughout the years.

My most excellent thanks go to all the people I have met during the last three years, all of them equally contributed to making this experience invaluable. A million thanks to my friend and colleague Dr Alexander Nödling for his incredible brilliance, for all the lessons and tricks he taught me, for being such a supportive friend and for all his help during these years. An enormous thank you also goes to Tom, Davide, Martin, and Victor to create a fantastic atmosphere in the labs and be great friends and amazing people outside the workplace. I would like to thank all the past and present Luk/Tsai/Jin's groups for the long chats in the office/labs, all the fantastic moments together and the lovely time we spend together. I am deeply thankful to all the big group of people who shared remarkable experiences in Cardiff, including Mauro, Mike, Alberto and Kim. They have contributed to making this journey unforgettable and have always been there for me. A big thanks also go to my friends in Italy, which have always been present for me and will always be. The biggest thanks go to my fantastic mom and the rest of my beloved family, for everything they have done for me, for being patient and for all the advises and immense love and support. You are special. Finally, I would like to thank Gilda, my beloved girlfriend, who has shared part of this journey with me and has shown to be a fantastic, beautiful and unique person. I hope this will be only a small part of the path we will walk together, hand by hand.

## Abstract

The creation of organocatalysts which function efficiently in aqueous or biocompatible environments can be useful for different applications, including soft robotics, self-healing materials, controlled drug delivery or on-demand drug synthesis in tumour cells. Thus, enabling organocatalysis under biologically benign conditions is still an essential challenge in chemical biology. This work aims to create a family of streptavidin-based artificial enzymes able to mediate organocatalysis in a biocompatible environment. Inspired by previous work in our group, the streptavidin-biotin technology was used to design organocatalytic artificial enzymes for iminium and enamine catalysis. In particular, two different proteins, tetrameric streptavidin (Sav) and its monomeric variant (M-Sav) were tested as hosts using the biotinylated organocatalyst **73** and **74** as ligands. In the first part of this work, two novel artificial enzymes, M-Sav:**73** and M-Sav:**74**, were created and tested for iminium catalysis. In the second part, Sav:**73** was employed for iminium catalysed transfer hydrogenations, whereas in the last chapter enamine catalysis was performed using Sav:**73** complex. Furthermore, optimisation of the protein scaffolds was carried out to design artificial enzymes with improved activity and selectivity. Moreover, an insight into the mechanism of action of these artificial complexes was provided.

## Abbreviations and Acronyms

4-OT: 4-Oxalocrotonate tautomerase

6xHis: hexahistidine protein tag

ALBP: Adipocyte lipid binding protein

Boc: *Tert*-butyloxycarbonyl protecting group

Bn: Benzyl

BNAH: *N*-benzyl-1,4-dihydronicotinamide

CAN: Ceric ammonium nitrate

CDCl<sub>3</sub>: Deuterated chloroform

C-FLAG: DYKDDDDK protein tag

D<sub>2</sub>O: Deuterium oxide

DCC: *N,N'*-Dicyclohexylcarbodiimide

DCM: Dichloromethane

DMAP: 4-Dimethylamino pyridine

DME: Dimethoxyethane

DMF: *N,N*-Dimethylformamide

DMSO: Dimethyl sulfoxide

dNTPs: Generic deoxynucleotide phosphate

E: Generic electrophile

$E_a$ : Energy of activation

EDTA: Ethylenediaminetetraacetic acid

Et<sub>2</sub>O: Diethyl ether

EtOH: Ethanol

GdnHCl: Guanidium hydrochloride

$k_{cat}$ : Catalytic rate constant

$K_M$ : Michaelis constant

KP<sub>i</sub>: Potassium phosphate buffer

h: Hour(s)

HABA: 2-(4-hydroxyphenylazo)benzoic acid

HCl: Hydrochloric acid

HClO<sub>4</sub>: Perchloric acid

HCO<sub>2</sub>H: Formic acid

HEPES: 2-[4-(2-hydroxyethyl)piperazin-1-yl]ethanesulfonic acid

HOMO: Highest occupied molecular orbital

HRMS: High resolution mass spectrometry

*i*-Pr: Isopropyl

LA: Lewis acid

LUMO: Lowest unoccupied molecular orbital

Me: Methyl

MeCN: Acetonitrile

MeNO<sub>2</sub>: Nitromethane

MES: 2-(*N*-morpholino)ethanesulfonic acid

min: Minute(s)

MOPS: 3-(*N*-morpholino)propanesulfonic acid

M-Sav: Monomeric streptavidin

NaCl: Sodium chloride

Na<sub>2</sub>CO<sub>3</sub>: Sodium carbonate

NADH: Nicotinamide adenine dinucleotide

NaHCO<sub>3</sub>: Sodium bicarbonate

NaOH: Sodium hydroxide

Naph: Naphthyl

NaP<sub>i</sub>: Sodium phosphate buffer

Nu: Generic nucleophile

PBS: Phosphate-buffered saline

PCR: Polymerase chain reaction

Ph: Phenyl

ppm: parts per million

*p*-TsOH: *p*-Toluenesulfonic acid

RA: Retro-aldolase

s: Second(s)

Sav: Tetrameric streptavidin

SEC: Size exclusion column

SDS-PAGE: Sodium dodecyl sulphate – polyacrylamide gel electrophoresis

SOMO: Single occupied molecular orbital

TBS: *t*-Butyldimethylsilyl

TDS: Tetryldimethylsilyl

TfO: Triflate or trifluoromethanesulfonate

TFA: Trifluoroacetic acid

T<sub>m</sub>: Melting temperature

TMS: Trimethylsilyl

TRIP: (*R*)-3,3'-Bis(2,4,6-triisopropylphenyl)-1,1'-binaphthyl-2,2'-diyl hydrogen phosphate

Tris: Tris(hydroxymethyl)aminomethane

## Table of Contents

	<u>Contents</u>
Chapter 1: Introduction	1
1.1 Organocatalysis	1
1.1.1 History and development	1
1.1.2 Generic activation modes in aminocatalysis	8
1.1.2.1 HOMO-raising catalysis	9
1.1.2.2 LUMO-lowering catalysis	10
1.1.3 Properties and applications of chiral aminocatalysts	12
1.2 Protein as host for biocompatible organocatalysis	16
1.2.1 Introduction	16
1.2.2 Site-selective chemical modification of proteins	17
1.2.3 <i>De novo</i> enzymes	20
1.2.4 N-terminal proline	23
1.2.5 Genetic code expansion	26
1.2.6 Protein as supramolecular host	29
1.2.6.1 Introduction	29
1.2.6.2 Anion- $\pi$ -catalysts	31
1.2.6.3 Tetrameric streptavidin as host	32
1.2.6.4 Monomeric streptavidin as host	35
1.3 Aim of the project	37
Chapter 2: Monomeric streptavidin as host for iminium catalysis	38
2.1 Introduction	38
2.2 Synthesis of organocatalysts 73 and 74	39
2.3 Expression and purification of M-Sav	40
2.4 M-Sav:73 and M-Sav:74 stability	45

---

2.5 Screening reactions	48
2.6 Analysis of M-Sav:74 crystal structure	53
2.7 Site-directed mutagenesis on Y111 residue	54
2.8 Conclusions	58
Chapter 3: Tetrameric Streptavidin as Host for Iminium Catalysis	60
3.1 Introduction	60
3.2 Screening reactions	61
3.3 Substrate scope for aromatic $\alpha,\beta$ -unsaturated aldehydes	63
3.4 Synthesis of aromatic $\beta$ -branched $\alpha,\beta$ -unsaturated aldehydes	66
3.5 Substrate scope for aromatic $\beta$ -methylated $\alpha,\beta$ -unsaturated aldehydes	67
3.6 Synthesis of deuterated analogues for mechanistic studies	70
3.7 KIE studies for Sav-based transfer hydrogenation	71
3.8 Kinetic measurement	73
3.9 Conclusions	74
Chapter 4: Tetrameric Streptavidin as Host for Enamine Catalysis	76
4.1 Introduction	76
4.2 Screening for optimised conditions	78
4.3 Site-directed mutagenesis of the protein host	79
4.4 Substrate scope	81
4.5 Conclusions	83
Chapter 5: Conclusion and future perspectives	84
5.1 Conclusion	84
5.1.1 Monomeric streptavidin-hosted 1,4-Michael addition	84
5.1.2 Tetrameric streptavidin-hosted transfer hydrogenation	85
5.1.3 Tetrameric streptavidin-hosted aldol addition	86
5.2 Future perspectives	86
5.2.1 Monomeric streptavidin-hosted 1,4-Michael addition	87



---

5.2.2 Tetrameric streptavidin-hosted transfer hydrogenations and aldol additions	87
Chapter 6: Experimental part	89
6.1 General information	89
6.1.1 Chemistry	89
6.1.2 Circular dichroism experiments	90
6.2 Monomeric streptavidin as host for iminium catalysis	91
6.2.1 Synthesis of catalyst 73 and 74	91
6.2.1.1 Synthesis of (+)-Biotin NHS ester 81	91
6.2.1.2 Synthesis of catalyst 73	92
6.2.1.3 Synthesis of catalyst 74	92
6.2.2 Experimental details for the preparation and purification of M-Sav and mutants	93
6.2.2.1 Expression and Purification	93
6.2.2.2 Site-directed mutagenesis	94
6.2.2.3 HRMS of M-Sav	95
6.2.3 Experimental details for the 1,4-Michael addition activity screening	96
6.2.3.1 General procedure for the $^1\text{H-NMR}$ based screening for yield determination	96
6.2.3.2 $^1\text{H-NMR}$ based determination of the reaction conversion	96
6.2.4 $^1\text{H-NMR}$ determination for substrates and compounds	97
6.2.4.1 Isolation and characterisation of product 75	97
6.2.4.2 Isolation and characterisation of the side-product 83	98
6.2.5 $^1\text{H-NMR}$ details for the activity screening of Table 2	98
6.2.5.1 Buffer screening for 1,4-Michael addition in Tris pH 7.0	98
6.2.5.2 Buffer screening for 1,4-Michael addition in Tris pH 7.5	99
6.2.5.3 Buffer screening for 1,4-Michael addition in Tris pH 8.0	100
6.2.5.4 Buffer screening for 1,4-Michael addition in HEPES pH 7.0	101

---

6.2.5.5 Buffer screening for 1,4-Michael addition in HEPES pH 7.5	102
6.2.5.6 Buffer screening for 1,4-Michael addition in HEPES pH 8.0	103
6.2.5.7 Buffer screening for 1,4-Michael addition in KP <sub>i</sub> pH 7.0	104
6.2.5.8 Buffer screening for 1,4-Michael addition in KP <sub>i</sub> pH 7.5	105
6.2.5.9 Buffer screening for 1,4-Michael addition in KP <sub>i</sub> pH 8.0	106
6.2.5.10 Buffer screening for 1,4-Michael addition in NaP <sub>i</sub> pH 7.0	107
6.2.5.11 Buffer screening for 1,4-Michael addition in NaP <sub>i</sub> pH 7.5	108
6.2.5.12 Buffer screening for 1,4-Michael addition in NaP <sub>i</sub> pH 8.0	109
6.2.5.13 Buffer screening for 1,4-Michael addition in PBS pH 7.0	110
6.2.5.14 Buffer screening for 1,4-Michael addition in PBS pH 7.5	111
6.2.5.15 Buffer screening for 1,4-Michael addition in PBS pH 8.0	112
6.2.5.16 Buffer screening for 1,4-Michael addition in H <sub>2</sub> O	113
6.2.6 <sup>1</sup> H-NMR details for the activity screening of Table 3	114
6.2.6.1 Buffer screening for 1,4-Michael addition in KP <sub>i</sub> pH 7.0 25 mM	114
6.2.6.2 Buffer screening for 1,4-Michael addition in KP <sub>i</sub> pH 7.0 50 mM	115
6.2.6.3 Co-solvent screening for 1,4-Michael addition in 50% KP <sub>i</sub> pH 7.0 10 mM and 50% EtOAc	116
6.2.6.4 Co-solvent screening for 1,4-Michael addition in 50% KP <sub>i</sub> pH 7.0 10 mM and 50% CDCl <sub>3</sub>	117
6.2.6.5 Co-solvent screening for 1,4-Michael addition in 50% KP <sub>i</sub> pH 7.0 10 mM and 50% MeOH	118
6.2.6.6 Co-solvent screening for 1,4-Michael addition in 50% KP <sub>i</sub> pH 7.0 10 mM and 50% MeCN	119
6.2.7 <sup>1</sup> H-NMR details for the activity screening of Table 4	120
6.2.7.1 Buffer screening for 1,4-Michael addition in KP <sub>i</sub> pH 7.0 (10% MeOH) using M-Sav:73	120
6.2.7.2 Buffer screening for 1,4-Michael addition in KP <sub>i</sub> pH 7.0 (20% MeOH) using M-Sav:73	121

---

6.2.7.3 Buffer screening for 1,4-Michael addition in $KP_i$ pH 7.0 (30% MeOH) using M-Sav:73	122
6.2.7.4 Buffer screening for 1,4-Michael addition in $KP_i$ pH 7.0 (40% MeOH) using M-Sav:73	123
6.2.7.5 Buffer screening for 1,4-Michael addition in $KP_i$ pH 7.0 (0% MeOH) using catalyst 73	124
6.2.7.6 Buffer screening for 1,4-Michael addition in $KP_i$ pH 7.0 (10% MeOH) using catalyst 73	125
6.2.7.7 Buffer screening for 1,4-Michael addition in $KP_i$ pH 7.0 (20% MeOH) using catalyst 73	126
6.2.7.8 Buffer screening for 1,4-Michael addition in $KP_i$ pH 7.0 (30% MeOH) using catalyst 73	127
6.2.7.9 Buffer screening for 1,4-Michael addition in $KP_i$ pH 7.0 (40% MeOH) using catalyst 73	128
6.2.7.10 Buffer screening for 1,4-Michael addition in $KP_i$ pH 7.0 (50% MeOH) using catalyst 73	129
6.2.7.11 Buffer screening for 1,4-Michael addition in $KP_i$ pH 7.0 (0% MeOH) using M-Sav:74	130
6.2.7.12 Buffer screening for 1,4-Michael addition in $KP_i$ pH 7.0 (10% MeOH) using M-Sav:74	131
6.2.7.13 Buffer screening for 1,4-Michael addition in $KP_i$ pH 7.0 (20% MeOH) using M-Sav:74	132
6.2.7.14 Buffer screening for 1,4-Michael addition in $KP_i$ pH 7.0 (30% MeOH) using M-Sav:74	133
6.2.7.15 Buffer screening for 1,4-Michael addition in $KP_i$ pH 7.0 (40% MeOH) using M-Sav:74	134
6.2.7.16 Buffer screening for 1,4-Michael addition in $KP_i$ pH 7.0 (50% MeOH) using M-Sav:74	135
6.2.7.17 Buffer screening for 1,4-Michael addition in $KP_i$ pH 7.0 (0% MeOH) using catalyst 74	136

---

6.2.7.18 Buffer screening for 1,4-Michael addition in KP <sub>i</sub> pH 7.0 (10% MeOH) using catalyst 74	137
6.2.7.19 Buffer screening for 1,4-Michael addition in KP <sub>i</sub> pH 7.0 (20% MeOH) using catalyst 74	138
6.2.7.20 Buffer screening for 1,4-Michael addition in KP <sub>i</sub> pH 7.0 (30% MeOH) using catalyst 74	139
6.2.7.21 Buffer screening for 1,4-Michael addition in KP <sub>i</sub> pH 7.0 (40% MeOH) using catalyst 74	140
6.2.7.22 Buffer screening for 1,4-Michael addition in KP <sub>i</sub> pH 7.0 (50% MeOH) using catalyst 74	141
6.2.8 <sup>1</sup> H-NMR details for the activity screening of Table 5	142
6.2.8.1 Buffer screening for 1,4-Michael addition in KP <sub>i</sub> pH 7.0 (20% MeOH) using Y111S:74	142
6.2.8.2 Buffer screening for 1,4-Michael addition in KP <sub>i</sub> pH 7.0 (20% MeOH) using Y111T:74	143
6.2.8.3 Buffer screening for 1,4-Michael addition in KP <sub>i</sub> pH 7.0 (20% MeOH) using Y111V:74	144
6.2.8.4 Buffer screening for 1,4-Michael addition in KP <sub>i</sub> pH 7.0 (20% MeOH) using Y111K:74	145
6.2.8.5 Buffer screening for 1,4-Michael addition in KP <sub>i</sub> pH 7.0 (20% MeOH) using Y111A:74	146
6.3 Tetrameric streptavidin as host for iminium catalysis	147
6.3.1 Synthesis of BNAH	147
6.3.1.1 Synthesis of <i>N</i> -benzyl-3-carbamoylpyridinium bromide (148, BNA <sup>+</sup> )	147
6.3.1.2 Synthesis of <i>N</i> -benzyl-1,4-dihydronicotinamide (87, BNAH)	147
6.3.2 Synthesis of <i>d</i> <sub>2</sub> -BNAH	148
6.3.2.1 Synthesis of 1-benzyl-1,4-dihydropyridine-4,4- <i>d</i> <sub>2</sub> -3-carboxamide (146, <i>d</i> <sub>2</sub> -BNAH)	148
6.3.2.2 <sup>1</sup> H-NMR spectrum of <i>d</i> <sub>2</sub> -BNAH	150

---

6.3.2.3 HRMS of <i>d</i> <sup>2</sup> -BNAH	151
6.3.3 Synthesis of the $\alpha,\beta$ -unsaturated aldehydes 89-90 and 92-95	151
6.3.3.1 <sup>1</sup> H-NMR assignment for ( <i>E</i> )-3-( <i>o</i> -fluoro) acrylaldehyde (89)	152
6.3.3.2 <sup>1</sup> H-NMR assignment for ( <i>E</i> )-3-( <i>o</i> -bromo) acrylaldehyde (90)	152
6.3.3.3 <sup>1</sup> H-NMR assignment for ( <i>E</i> )-3-( <i>o</i> -tolyl) acrylaldehyde (92)	152
6.3.3.4 <sup>1</sup> H-NMR assignment for ( <i>E</i> )-3-( <i>m</i> -fluoro) acrylaldehyde (93)	152
6.3.3.5 <sup>1</sup> H-NMR assignment for ( <i>E</i> )-3-( <i>m</i> -bromo) acrylaldehyde (94)	152
6.3.3.6 <sup>1</sup> H-NMR assignment for ( <i>E</i> )-3-( <i>m</i> -tolyl) acrylaldehyde (95)	153
6.3.4 Synthesis of the $\beta$ -branched $\alpha,\beta$ -unsaturated aldehydes 115-120	153
6.3.4.1 Synthesis of compounds 127-132	153
6.3.4.2 <sup>1</sup> H-NMR assignment for ethyl ( <i>E</i> )-3-phenylbut-2-enoate (127)	154
6.3.4.3 <sup>1</sup> H-NMR assignment for ethyl ( <i>E</i> )-3-( <i>p</i> -chlorophenyl) but-2-enoate (128)	154
6.3.4.4 <sup>1</sup> H-NMR assignment for ethyl ( <i>E</i> )-3-( <i>p</i> -fluorophenyl) but-2-enoate (129)	154
6.3.4.5 <sup>1</sup> H-NMR assignment for ethyl ( <i>E</i> )-3-( <i>o</i> -tolyl) but-2-enoate (130)	154
6.3.4.6 <sup>1</sup> H-NMR assignment for ethyl ( <i>E</i> )-3-( <i>m</i> -tolyl) but-2-enoate (131)	154
6.3.4.7 <sup>1</sup> H-NMR assignment for ethyl ( <i>E</i> )-3-( <i>p</i> -tolyl) but-2-enoate (132)	154
6.3.4.8 Synthesis of compounds 133-138	155
6.3.4.9 Synthesis of compounds 115-120	155
6.3.4.10 <sup>1</sup> H-NMR assignment for ( <i>E</i> )-3-phenylbut-2-enal (115)	155
6.3.4.11 <sup>1</sup> H-NMR assignment for ( <i>E</i> )-3-( <i>p</i> -chlorophenyl) but-2-enal (116)	155
6.3.4.12 <sup>1</sup> H-NMR assignment for ( <i>E</i> )-3-( <i>p</i> -fluorophenyl) but-2-enal (117)	156
6.3.4.13 <sup>1</sup> H-NMR assignment for ( <i>E</i> )-3-( <i>o</i> -tolyl) but-2-enal (118)	156
6.3.4.14 <sup>1</sup> H-NMR assignment for ( <i>E</i> )-3-( <i>m</i> -tolyl) but-2-enal (119)	156
6.3.4.15 <sup>1</sup> H-NMR assignment for ( <i>E</i> )-3-( <i>p</i> -tolyl) but-2-enal (120)	156
6.3.5 Experimental details for the transfer hydrogenation activity screening	156

---

6.3.5.1	General procedure for the $^1\text{H-NMR}$ based screening for yield determination	156
6.3.5.2	$^1\text{H-NMR}$ based determination of the reaction conversion	157
6.3.6	$^1\text{H-NMR}$ details for the activity screening of Table 6	159
6.3.6.1	Catalyst screening for transfer hydrogenation using no catalyst	159
6.3.6.2	Catalyst screening for transfer hydrogenation using catalyst 73	160
6.3.6.3	Catalyst screening for transfer hydrogenation using catalyst 74	161
6.3.6.4	Catalyst screening for transfer hydrogenation using Sav	162
6.3.6.5	Catalyst screening for transfer hydrogenation using M-Sav	163
6.3.6.6	Catalyst screening for transfer hydrogenation using Sav:73	164
6.3.6.7	Catalyst screening for transfer hydrogenation using Sav:73 (2 mol%)	165
6.3.6.8	Catalyst screening for transfer hydrogenation using Sav:73 (5 equivalents BNAH, 25% MeOH)	166
6.3.6.9	Catalyst screening for transfer hydrogenation using Sav:73, no shaking (0 rpm)	167
6.3.6.10	Catalyst screening for transfer hydrogenation using Sav:74	168
6.3.6.11	Catalyst screening for transfer hydrogenation using M-Sav:73	169
6.3.6.12	Catalyst screening for transfer hydrogenation using M-Sav:74	170
6.3.6.13	Catalyst screening for transfer hydrogenation using Sav:73 and NADH (86)	171
6.3.6.14	Catalyst screening for transfer hydrogenation using Sav:73 and Hantzsch ester (84)	172
6.3.7	$^1\text{H-NMR}$ details for the activity screening of Table 7	173
6.3.7.1	Transfer hydrogenation to ( <i>E</i> )-3-( <i>o</i> -fluorophenyl) acrylaldehyde	173
6.3.7.2	Transfer hydrogenation to ( <i>E</i> )-3-( <i>o</i> -bromophenyl) acrylaldehyde	174
6.3.7.3	Transfer hydrogenation to ( <i>E</i> )-3-( <i>o</i> -nitrophenyl) acrylaldehyde	175
6.3.7.4	Transfer hydrogenation to ( <i>E</i> )-3-( <i>o</i> -tolyl) acrylaldehyde	176

---

6.3.7.5	Transfer hydrogenation to ( <i>E</i> )-3-( <i>m</i> -fluorophenyl) acrylaldehyde	177
6.3.7.6	Transfer hydrogenation to ( <i>E</i> )-3-( <i>m</i> -bromophenyl) acrylaldehyde	178
6.3.7.7	Transfer hydrogenation to ( <i>E</i> )-3-( <i>m</i> -tolyl) acrylaldehyde	179
6.3.7.8	Transfer hydrogenation to ( <i>E</i> )-3-( <i>p</i> -chlorophenyl) acrylaldehyde	180
6.3.7.9	Transfer hydrogenation to ( <i>E</i> )-3-( <i>p</i> -fluorophenyl) acrylaldehyde	181
6.3.7.10	Transfer hydrogenation to ( <i>E</i> )-3-( <i>p</i> -bromophenyl) acrylaldehyde	182
6.3.7.11	Transfer hydrogenation to ( <i>E</i> )-3-( <i>p</i> -methoxyphenyl) acrylaldehyde	183
6.3.7.12	Transfer hydrogenation to ( <i>E</i> )-3-( <i>p</i> -nitrophenyl) acrylaldehyde	184
6.3.7.13	Transfer hydrogenation to ( <i>E</i> )-3-( <i>p</i> -tolyl) acrylaldehyde	185
6.3.8	<sup>1</sup> H-NMR details for the activity screening of Table 8	186
6.3.8.1	Transfer hydrogenation to ( <i>E</i> )-3-phenylbut-2-enal	186
6.3.8.2	Transfer hydrogenation to ( <i>E</i> )-3-( <i>p</i> -chlorophenyl) but-2-enal	187
6.3.8.3	Transfer hydrogenation to ( <i>E</i> )-3-( <i>p</i> -fluororophenyl) but-2-enal	188
6.3.8.4	Transfer hydrogenation to ( <i>E</i> )-3-( <i>o</i> -tolyl) but-2-enal	189
6.3.8.5	Transfer hydrogenation to ( <i>E</i> )-3-( <i>m</i> -tolyl) but-2-enal	190
6.3.8.6	Transfer hydrogenation to ( <i>E</i> )-3-( <i>p</i> -tolyl) but-2-enal	191
6.3.9	<sup>1</sup> H-NMR details for the activity screening of Table 9	192
6.3.9.1	Transfer hydrogenation to ( <i>E</i> )-3-( <i>o</i> -tolyl) but-2-enal in presence of BNAH	192
6.3.10	<sup>1</sup> H-NMR details for the activity screening of Table 10	193
6.3.10.1	Transfer hydrogenation to cinnamaldehyde in presence of <i>d</i> <sub>2</sub> -BNAH	193
6.3.11	Michaelis-Menten kinetics for the reaction between 14 and 87	194
6.3.11.1	Procedure for the kinetic assessment	194
6.4	Tetrameric streptavidin as host for enamine catalysis	195
6.4.1	General procedure for the <sup>1</sup> H-NMR based screening for yield determination	195
6.4.2	<sup>1</sup> H-NMR based determination of the reaction conversion	195

---

6.4.3 <sup>1</sup> H-NMR details for the activity screening of Table 11	196
6.4.3.1 Catalyst screening for aldol additions using no catalyst	197
6.4.3.2 Catalyst screening for aldol additions using catalyst 73	198
6.4.3.3 Catalyst screening for aldol additions using Sav (0.1 mol%)	199
6.4.3.4 Catalyst screening for aldol additions using Sav (0.5 mol%)	200
6.4.3.5 Catalyst screening for aldol additions using Sav (1 mol%)	201
6.4.3.6 Catalyst screening for aldol additions using Sav:73 (0.1 mol%)	202
6.4.3.7 Catalyst screening for aldol additions using Sav:73 (0.5 mol%)	203
6.4.3.8 Catalyst screening for aldol additions using Sav:73 (1 mol%)	204
6.4.3.9 Catalyst screening for aldol additions using Sav:73 (1 mol%) and 1 mol% of TFA	205
6.4.3.10 Catalyst screening for aldol additions using Sav:73 (1 mol%) at 10 °C	206
6.4.3.11 Catalyst screening for aldol additions using Sav:73 (5 equivalents of acetone and 25% methanol)	207
6.4.3.12 Catalyst screening for aldol additions using Sav:73 (5 equivalents of acetone and 25% acetonitrile)	208
6.4.3.13 Catalyst screening for aldol additions using Sav:73 (5 equivalents of acetone and 25% iso-propanol)	209
6.4.3.14 Catalyst screening for aldol additions using Sav:73 (10 equivalents of acetone and 25% iso-propanol)	210
6.4.3.15 Catalyst screening for aldol additions using Sav:73 (20 equivalents of acetone and 25% iso-propanol)	211
6.4.3.16 Catalyst screening for aldol additions using Sav:73 (50 equivalents of acetone and 25% iso-propanol)	212
6.4.4 <sup>1</sup> H-NMR details for the activity screening of Table 12	213
6.4.4.1 Catalyst screening for aldol additions using T-rSav:73 as catalyst	213
6.4.4.2 Catalyst screening for aldol additions using S112E:73 as catalyst	214
6.4.4.3 Catalyst screening for aldol additions using K121A:73 as catalyst	215



---

6.4.5 <sup>1</sup> H-NMR details for the activity screening of Table 13	216
6.4.5.1 Catalyst screening for aldol additions using <i>o</i> -nitrobenzaldehyde as substrate	216
6.4.5.2 Catalyst screening for aldol additions using <i>m</i> -nitrobenzaldehyde as substrate	217
6.4.5.3 Catalyst screening for aldol additions using <i>o</i> -chlorobenzaldehyde as substrate	218
6.4.5.4 Catalyst screening for aldol additions using <i>m</i> -chlorobenzaldehyde as substrate	219
6.4.5.5 Catalyst screening for aldol additions using <i>m</i> -bromobenzaldehyde as substrate	220
6.4.5.6 Catalyst screening for aldol additions using <i>p</i> -bromobenzaldehyde as substrate	221
6.4.5.7 Catalyst screening for aldol additions using <i>m</i> -iodobenzaldehyde as substrate	222
6.4.5.8 Catalyst screening for aldol additions using <i>o</i> -methoxybenzaldehyde as substrate	223
6.4.5.9 Catalyst screening for aldol additions using <i>p</i> -methoxybenzaldehyde as substrate	224
6.4.5.10 Catalyst screening for aldol additions using pentafluorobenzaldehyde as substrate	225
6.4.5 Chiral HPLC data of activity and selectivity screening	226
6.4.5.1 Chiral HPLC data for Table 11	226
6.4.5.1.1 Racemate of 13	227
6.4.5.1.2 L-proline	228
6.4.5.1.3 Catalyst 73 (1 mol%)	229
6.4.5.1.5 Sav:1 (0.1 mol%)	231
6.4.5.1.6 Sav:1 (0.5 mol%)	232
6.4.5.1.7 Sav:1 (1 mol%)	233

---

6.4.5.1.8 Sav:1 (1 mol%) and TFA (1 mol%)	234
6.4.5.1.9 Sav:1 (1 mol%) at 10 °C	235
6.4.5.1.10 Sav:1 (5 equivalents of acetone and 25% methanol)	236
6.4.5.1.11 Sav:1 (5 equivalents of acetone and 25% acetonitrile)	237
6.4.5.1.12 Sav:1 (5 equivalents of acetone and 25% iso-propanol)	238
6.4.5.1.13 Sav:1 (50 equivalents of acetone and 25% iso-propanol)	239
6.4.5.2 Chiral HPLC data for Table 12	240
6.4.5.2.1 T-rSav:73	240
6.4.5.2.2 S112E:73	241
6.4.5.2.3 K121A:73	242
6.4.5.3 Chiral HPLC data for Table 13	243
6.4.5.3.1 ( <i>S/R</i> )-4-hydroxy-4-( <i>m</i> -nitrophenyl) butan-2-one	243
6.4.5.3.2 ( <i>S/R</i> )-4-hydroxy-4-( <i>m</i> -chlorophenyl) butan-2-one	244
6.4.5.3.3 ( <i>S/R</i> )-4-hydroxy-4-( <i>m</i> -bromophenyl) butan-2-one	245
6.4.5.3.4 ( <i>S/R</i> )-4-hydroxy-4-( <i>p</i> -bromophenyl) butan-2-one	246
6.4.5.3.5 ( <i>S/R</i> )-4-hydroxy-4-( <i>m</i> -iodophenyl) butan-2-one	247
6.4.5.3.6 ( <i>S/R</i> )-4-hydroxy-4-(perfluorophenyl) butan-2-one	248
6.5 References	249

## List of Figures

- Figure 1. a)** Example of a catalytic cycle. **b)** Diagram of catalysed (green) and uncatalysed (black) reactions. 1
- Figure 2.** Classification of enantioselective catalysis into three main branches: organocatalysis (red box), biocatalysis (black box) and metal catalysis (blue box). 2
- Figure 3.** Timeline of some of the most significant generic activation modes for organocatalysis. Within each area are presented the corresponding organocatalysts employed in the first example reported for each activation protocol. 8
- Figure 4.** HOMO-raising catalysis. The formation of the enamine intermediate raises the HOMO and decrease the energy gap between LUMO and HOMO. 9
- Figure 5.** Enamine-catalysed nucleophilic attack of carbonyl to a generic electrophile E. 10
- Figure 6.** LUMO-lowering catalysis. The formation of the iminium intermediate lowers the LUMO and decrease the energy gap between the frontier orbitals. 11
- Figure 7.** Iminium-catalysed nucleophilic attack to carbonyl with a generic nucleophile. 11
- Figure 8.** Some representative organocatalysts employed in aminocatalysis. On the top part, secondary aminocatalysts, meanwhile on the bottom are located the primary amine-based organocatalysts. 12
- Figure 9.** The five approaches to design organocatalytic artificial enzymes. 17
- Figure 10.** Creation of organocatalytic artificial enzymes through site-selective modification. On the right, thiazolopapain generated from papain (PDB: 9PAP) after insertion of a catalyst. The replacement of cysteine with selenocysteine to form selenosubtilisin from subtilisin (PDB: 1YU6) is on the left. 18
- Figure 11.** Iminium-catalysed cleavage of **42** by de novo designed retro-aldolases and intermediates. In the middle an overview of the crystal structure of RA95.0 (magenta, PDB: 4A29), in which Lys210 (orange) is responsible for forming the Schiff base intermediate with a 1,3-diketone inhibitor (yellow). 22
- Figure 12.** The cycle of incorporation of unnatural amino acids by genetic code expansion in *E. coli*. **a)** Double transformation of two plasmids bearing exogenous amino acid tRNA synthetase (RS) and the gene of interest (GOI). **b)** Expression of the tRNA synthetase and addition of the unnatural amino acid (UAA). **c)** Ribosomal translation of the GOI with the unnatural amino acid incorporated site-specifically into the protein. 27
- Figure 13.** Linking a catalytically competent moiety to a ligand and insertion into a protein host to create a protein-catalyst assembly. 30
- Figure 14.** Series of biotinylated catalysts **67-74** created by Luk's group. 33
- Figure 15.** Overview of the biotin binding site of Sav:**73** in the crystal structure (green) and as aminol adduct with cinnamaldehyde obtained from QM/MM simulations (light blue). 34
- Figure 16.** Creation of organocatalytic enzymes using a supramolecular approach. 37
- Figure 17.** Biotinylated organocatalysts **73** and **74**. 39
- Figure 18.** pRSET-mSA plasmid. 41
- Figure 19.** 15% w/v SDS-PAGE after expression showing M-Sav band around 18 kDa. MW= Molecular weight; PM= Protein Marker; BI= Before Induction; AI= After Induction. 43

- Figure 20.** M-Sav before and after Ni-column. MW= Molecular weight; PM= Protein Marker; P= Pellet; SN= Supernatant; W1 Wash 1; W2 Wash 2; EI= Elution. 44
- Figure 21.** M-Sav:ligand complex after size exclusion chromatography. MW= Molecular weight; PM= Protein Marker. 45
- Figure 22.** CD spectra of M-Sav (top left), M-Sav:**79** (top right), M-Sav:**73** (bottom left) and M-Sav:**74** (bottom right). 46
- Figure 23.**  $T_m$  of M-Sav, M-Sav: **79**, M-Sav:**74** and M-Sav:**73**. 47
- Figure 24.** CD spectrum of M-Sav using different concentration of methanol: 10% (solid red line), 20% (dashed dotted green line), 30% (dashed blue line), 40% (short dashed red line), 50% (dotted black line). 48
- Figure 25.** Cartoon overview of the crystal structure of M-Sav:**74** (PDB: TBA, 1.68 Å). Catalyst **74** is coloured in beige. In dark blue are identified critical residues for site-directed mutagenesis after visual inspection. 53
- Figure 26.** Cartoon overview of the crystal structure of Sav:**73** (PDB: 6GH7), Sav:**74** (PDB: TBA) and M-Sav:**74** (PDB: TBA). In green are highlighted residue from Sav:**73/74** (subunit A or B), whereas in ochre M-Sav:**74** residues. Catalyst **74** is coloured in red and beige, while catalyst **73** is coloured in green. 54
- Figure 27.** Agarose gel for M-Sav mutants Y111S, Y111T, Y111V, Y111K and Y111A. The bands around 4000 bp confirm the M-Sav genes formation. S= serine; T= threonine; V= valine; K= lysine; A= alanine; bp= base pairs. 56
- Figure 28.** SDS-PAGE of the expression for the Y111V, Y111S, Y111K, Y111T and Y111A M-Sav mutants. MW= Molecular weight; PM= Protein Marker; BI= Before Induction; AI= After Induction. 57
- Figure 29.** Synthetic and natural hydrogen sources employed for hydrogenations. 61
- Figure 30. a)** Energy barriers involving C-H (light atom) and C-D (heavy atom) bonds. **b)** Employing KIE to define the rate-limiting step for Sav-based transfer hydrogenations. 70
- Figure 31.** Kinetic evaluation of Sav:**73** complex for transfer hydrogenation from BNAH to cinnamaldehyde. 74
- Figure 32.** Generation of the organocatalytic artificial enzyme Sav:**73** (step 1), followed by the formation of the enamine intermediate (step 2), the attack to a benzaldehyde derivative (step 3) and release of the aldol addition product (step 4). 77
- Figure 33.** Summary of the organocatalytic artificial enzymes presented in this work and their applications. 84
- Figure 34.**  $^1\text{H-NMR}$  spectrum of M-Sav catalysed 1,4-Michael addition. Each compound (**14**, **47**, **75** and **83**) and relative peaks are reported in the black box. The proton used for integration are drawn in red. 97
- Figure 35.**  $^1\text{H-NMR}$  spectrum of Sav catalysed transfer hydrogenation. In each row are reported the spectrum of the pure compounds **87**, **148**, **88** and **14**. In the middle is reported an exemplary of crude of reaction 158

**Figure 36.** <sup>1</sup>H-NMR spectrum of Sav catalysed aldol addition. For the addition of acetone to p-nitrobenzaldehyde, each compound (**11**, **13** and **13a**) and relative peaks are reported in the black box. The proton used for integration are drawn in red. 196

## List of Schemes

<b>Scheme 1.</b> The first organocatalytic reaction reported.	3
<b>Scheme 2.</b> L-Proline catalysed Hajos-Parrish reaction to yield: <b>a)</b> tetrahydroindandione and <b>b)</b> octahydronaphtalenedione.	4
<b>Scheme 3.</b> Eder-Sauer-Wiechert reaction to obtain <b>a)</b> compound <b>7</b> and <b>b)</b> compound <b>10</b> .	5
<b>Scheme 4.</b> L-Proline-catalysed intermolecular aldol reaction reported by Barbas, List and Lerner.	6
<b>Scheme 5.</b> Highly enantioselective organocatalytic Diels-Alder reaction using catalyst <b>16</b> .	7
<b>Scheme 6.</b> Selenosubtilisin catalyses the reduction of <b>a)</b> tert-butyl hydroperoxide and <b>b)</b> secondary alkyl hydroperoxide.	19
<b>Scheme 7.</b> Artificial enzymes created by covalent modification of cofactors: <b>a)</b> artificial flavopapain used for the oxidation of BNAH; <b>b)</b> artificial thiazolopapains for C-C bond formation; and <b>c)</b> artificial ALBP-pyridoxamine (PDB: 1ALB) for enantioselective reductive amination.	20
<b>Scheme 8.</b> Promiscuity of RA95.5-8 and variants for both iminium and enamine catalysis. Examples of iminium catalysis: <b>a)</b> conjugate addition of carbon nucleophiles; <b>b)</b> conjugate addition of nitromethane; <b>c)</b> Knoevenagel condensations of carbon nucleophiles with $\alpha,\beta$ -unsaturated aromatic aldehydes and <b>d)</b> Henry addition of nitromethane to aromatic aldehydes. Example of enamine catalysis: <b>e)</b> conjugate addition of acetone to nitrostyrene.	23
<b>Scheme 9.</b> Iminium- and enamine-catalysed reaction performed by 4-OT (PDB: 1OTF): <b>a)</b> Intermolecular aldol; <b>b)</b> Intramolecular aldol; <b>c)</b> Nitro-Michael addition; <b>d)</b> Enamine catalysed conjugate addition; <b>e)</b> Aldol condensation for aromatic aldehydes.	25
<b>Scheme 10.</b> <b>a)</b> Hydrazone and oxime ligation performed by p-amino phenylalanine incorporated onto LmrR (PDB: 3F8B). <b>b)</b> Michael addition using a novel dual catalyst within LmrR.	28
<b>Scheme 11.</b> Ester hydrolysis performed by BH32 (PDB: 6Q7N) with the unnatural amino acid Me-His produces fluorescein ( <b>60</b> ).	29
<b>Scheme 12.</b> Decarboxylative Michael addition reaction catalysed by <b>63</b> within S112Y (Sav cartoon from PDB: 6GH7) mutant streptavidin.	31
<b>Scheme 13.</b> Domino-Michael-Aldol-reaction catalysed by Sav: <b>63</b> assembly.	32
<b>Scheme 14.</b> 1,4-Michael addition reactions catalysed by <b>67-74</b> within a recombinant Sav (PDB: 6GH7).	34
<b>Scheme 15.</b> Tandem C-H activation and [4+2] annulation reaction catalysed by wt M-Sav: Cp*biotinRhCl.	36
<b>Scheme 16.</b> Synthesis of biotinylated organocatalysts <b>73-74</b> .	40
<b>Scheme 17.</b> Buffer screening for 1,4-Michael addition of <b>47</b> to <b>14</b> .	49
<b>Scheme 18.</b> Catalyst and concentration of methanol screening for 1,4-Michael addition of <b>47</b> to <b>14</b> .	51
<b>Scheme 19.</b> Reaction conditions screening for transfer hydrogenation from <b>87</b> to <b>14</b> .	62

<b>Scheme 20.</b> Sav: <b>73</b> tested for the transfer hydrogenation from <b>87</b> to aromatic $\alpha,\beta$ -unsaturated aldehydes ( <b>89-101</b> ).	64
<b>Scheme 21.</b> Three-step procedures to afford $\beta$ -methylated $\alpha,\beta$ -unsaturated aldehydes ( <b>115-120</b> ) starting from acetophenone derivatives ( <b>121-126</b> ).	66
<b>Scheme 22.</b> Sav: <b>73</b> promiscuity towards $\beta$ -methylated aromatic $\alpha,\beta$ -unsaturated aldehydes for transfer hydrogenation from <b>87</b> .	68
<b>Scheme 23.</b> Formation of the ( <i>Z</i> )-isomer ( <b>145</b> ) of the substrate <b>118</b> using Sav: <b>73</b> .	69
<b>Scheme 24.</b> The synthetic pathway from oxidised BNA <sup>+</sup> ( <b>148</b> ) to <i>d</i> 2-BNAH ( <b>146</b> ) involving 5 cycles of deuteration.	71
<b>Scheme 25.</b> Proposed transfer hydrogenation mechanism of action using Sav: <b>73</b> complex.	73
<b>Scheme 26.</b> Reaction conditions screening for aldol addition of <b>11</b> to <b>12</b> .	78
<b>Scheme 27.</b> Aldol addition of <b>11</b> to <b>12</b> using different protein hosts.	80
<b>Scheme 28.</b> Aldol additions of benzaldehyde derivatives ( <b>151-160</b> ) to <b>11</b> using Sav: <b>73</b> .	81

## List of Tables

<b>Table 1.</b> List of reactions for the main aminocatalysts.	14
<b>Table 2.</b> Buffer screening for 1,4-Michael addition of <b>47</b> to <b>14</b> . <sup>a</sup>	49
<b>Table 3.</b> Buffer strength and co-solvent screening for 1,4-Michael addition of <b>47</b> to <b>14</b> . <sup>a</sup>	50
<b>Table 4.</b> Catalyst and methanol screening for 1,4-Michael addition of <b>47</b> to <b>14</b> . <sup>a</sup>	52
<b>Table 5.</b> M-Sav mutants screening for 1,4-Michael addition of <b>47</b> to <b>14</b> . <sup>a</sup>	57
<b>Table 6.</b> Screening reaction for transfer hydrogenation from <b>87</b> to <b>14</b> . <sup>a</sup>	63
<b>Table 7.</b> Substrate scope for transfer hydrogenations from <b>87</b> to different $\alpha,\beta$ -unsaturated aldehydes. <sup>a</sup>	65
<b>Table 8.</b> Substrate scope for transfer hydrogenations from <b>87</b> to $\beta$ -methylated $\alpha,\beta$ -unsaturated aldehydes. <sup>a</sup>	68
<b>Table 9.</b> Screening to determine the isomerisation conditions for substrate <b>118</b> . <sup>a</sup>	69
<b>Table 10.</b> KIE determination for Sav: <b>73</b> catalysed transfer hydrogenation. <sup>a</sup>	72
<b>Table 11.</b> Screening for assessing the best conditions to perform enamine-catalysed aldol addition. <sup>a</sup>	79
<b>Table 12.</b> Screening for assessing the best conditions to perform enamine-catalysed aldol reactions. <sup>a</sup>	80
<b>Table 13.</b> Benzaldehyde derivatives scope for aldol addition catalysed by Sav: <b>73</b> complex. <sup>a</sup>	82
<b>Table 14.</b> List of primers used for the introduction of mutations in M-Sav at positions Y111.	94

## List of Equations

<b>Equation 1.</b> Arrhenius equation: $k$ is the rate constant, $T$ is the absolute temperature, $A$ is the frequency factor (a constant for each chemical reaction), $E_a$ is the energy of activation for the reaction and $R$ is the universal gas constant.	2
--	---

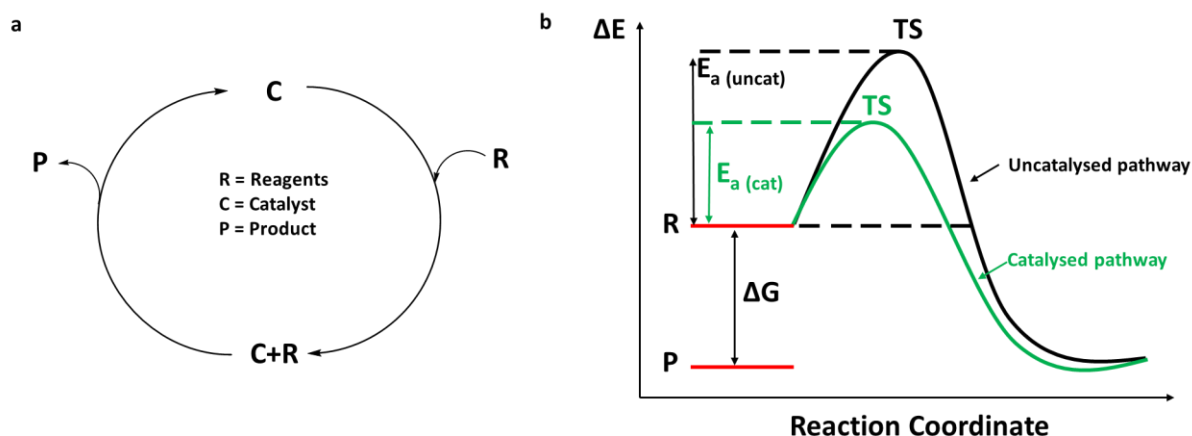
**Equation 2.** Mean residue molar ellipticity calculation. The unit of measure is deg·cm<sup>2</sup>/dmol.  $\theta$  is the ellipticity (mdeg); MRW is the mean residue weight (g/mol) calculated from the protein MW (g/mol) divided by the number of amino acid minus 1;  $l$  is the path length of the cell (cm);  $C$  is the protein concentration in g/L.

# Chapter 1: Introduction

## 1.1 Organocatalysis

### 1.1.1 History and development

The term catalysis, coined in 1835, describes “the property of exerting on other bodies an action which is very different from chemical affinity. By means of this action, they produce decomposition in bodies and form new compounds into the composition of which they do not enter”.<sup>1</sup> Before this moment, catalysis was not recognised as a phenomenon. Still, it was used in different processes, such as the production of alcohol by fermentation. In modern times, catalysts are defined as substances capable of enabling a chemical reaction to advance at a faster rate or under different conditions than otherwise possible.<sup>2</sup> A catalytic cycle describes the role of a catalyst in a chemical transformation (**Fig. 1a**). It illustrates the creation of a catalyst-reagent complex, followed by the acceleration of the rate of formation of one or more product(s). A catalysed process requires lower energy of activation ( $E_a$ ) to form the rate-limiting transition state compared to an uncatalysed one (**Fig. 1b**).



**Figure 1.** a) Example of a catalytic cycle. b) Diagram of catalysed (green) and uncatalysed (black) reactions.

The Arrhenius equation (**Equation 1**) explains the inverse proportionality between the rate constant of a reaction ( $k$ ) and the  $E_a$  to form a transition state.<sup>3</sup> Consequently, a

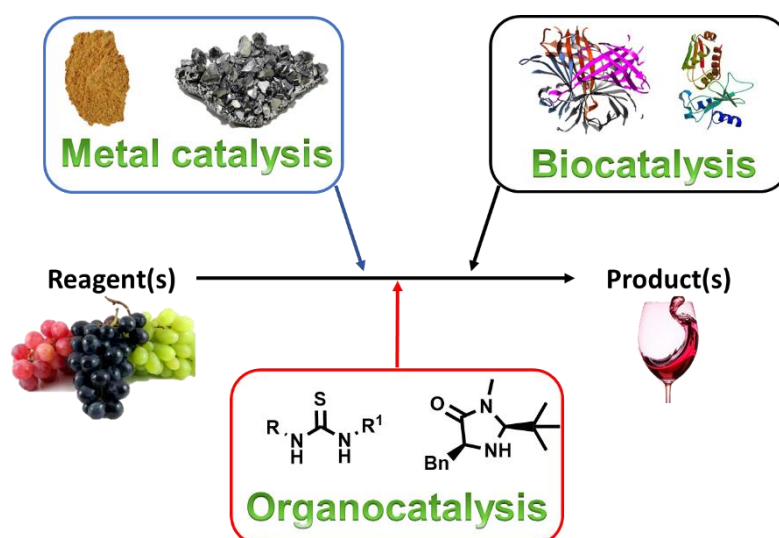


catalysed pathway with a lower  $E_a$  than an uncatalysed one will have a faster reaction rate.

$$k = A e^{-E_a/R.T}$$

**Equation 1.** Arrhenius equation:  $k$  is the rate constant,  $T$  is the absolute temperature,  $A$  is the frequency factor (a constant for each chemical reaction),  $E_a$  is the energy of activation for the reaction and  $R$  is the universal gas constant.

In modern organic chemistry, the concept of catalysis is often associated with stereoselectivity. A stereoselective reaction happens when a reactant forms predominantly one stereoisomer. The creation of catalysts able to transfer chiral information throughout a chemical process is defined as asymmetric or enantioselective catalysis. It is one of the critical aspects for the successful application of artificial molecules in synthetic and medicinal chemistry.<sup>4</sup> In this regard, asymmetric catalysis can be performed using three main catalysts: transition-metal based catalysts, biocatalysts and organocatalysts (**Fig. 2**).

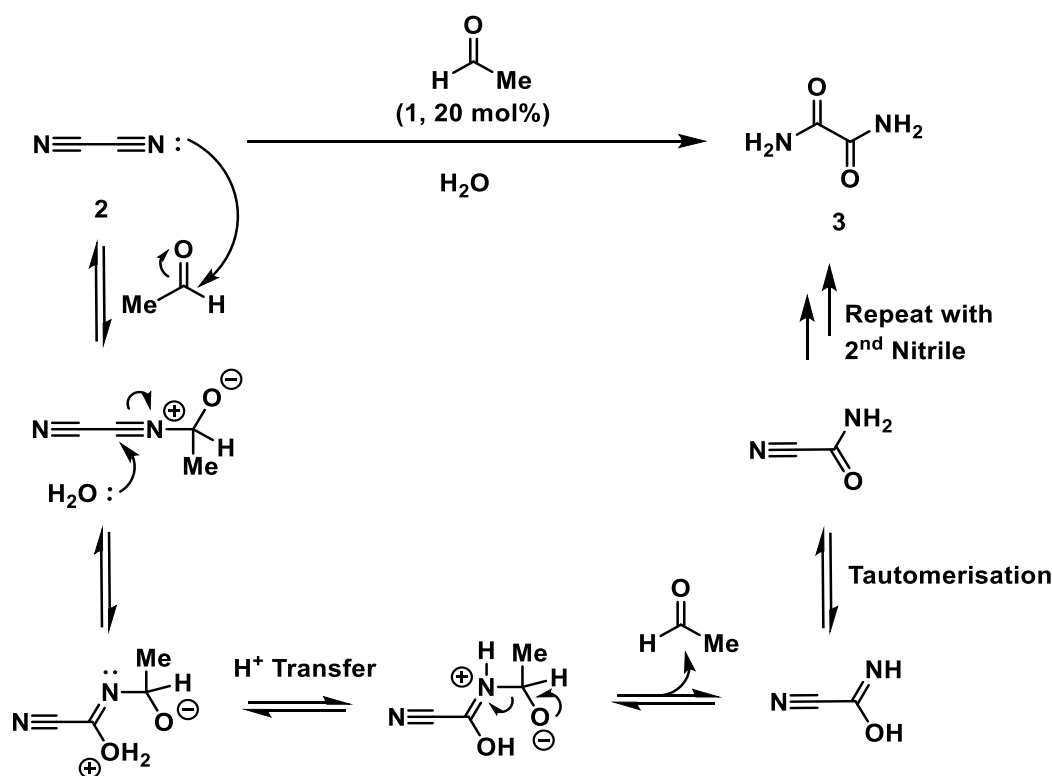


**Figure 2.** Classification of enantioselective catalysis into three main branches: organocatalysis (red box), biocatalysis (black box) and metal catalysis (blue box).

On the one hand, the use of transition-metal catalysts and enzymes for asymmetric catalysis is a powerful strategy to generate chiral molecules. On the other hand,

organocatalysis has become an appealing approach to create enantiomerically pure compounds.<sup>5-9</sup> Owing to this dissertation focus, the specific use of organocatalysis will be described in detail.

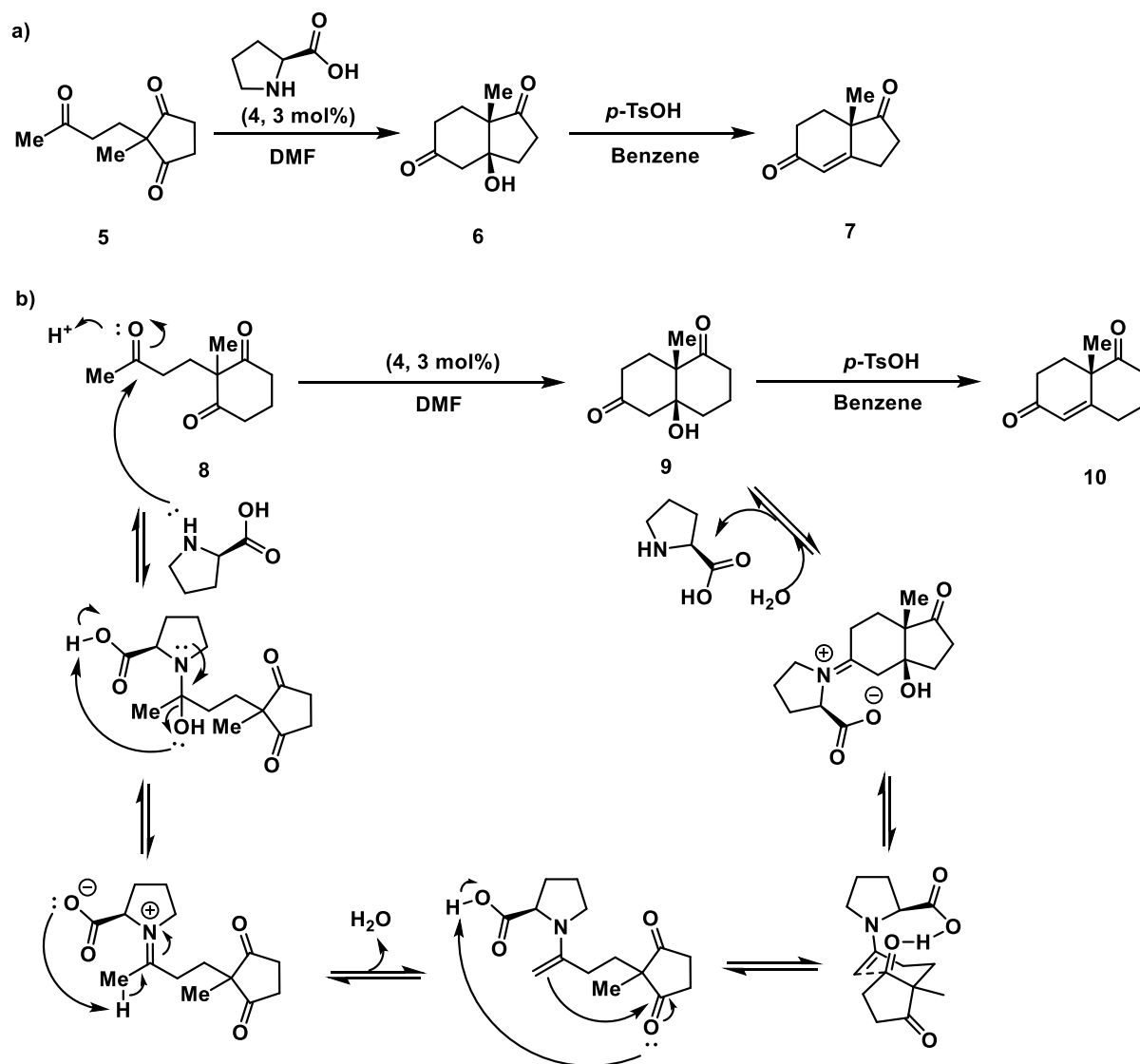
Organocatalysis refers to the use of a substoichiometric amount of any small organic molecule capable of accelerating the rate of a reaction.<sup>10</sup> While the term organocatalysis was coined only two decades ago,<sup>11</sup> the first report of an organocatalysed reaction was in 1860 when acetaldehyde (**1**, 20 mol%) was used to catalyse the conversion of the toxic gas cyanogen (**2**) to oxamide (**3**) in aqueous conditions (**Scheme 1**).<sup>12</sup> This transformation did not occur without **1**, and no metals were employed, thereby **1** can be described as the first example of an organocatalyst.



**Scheme 1.** The first organocatalytic reaction reported.

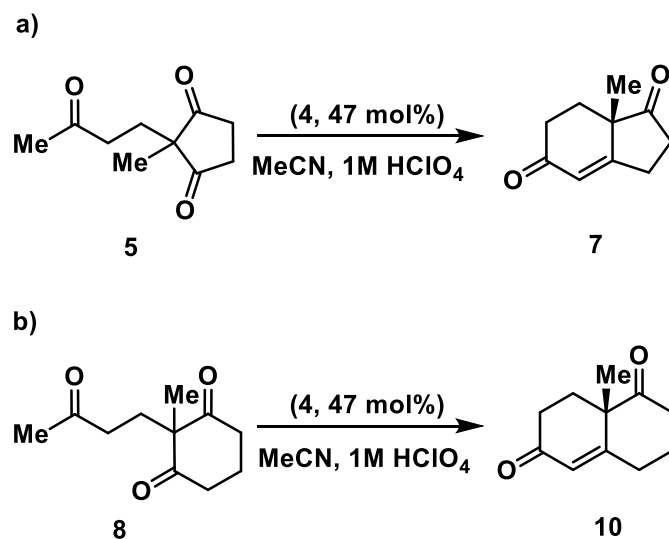
In the early '70s, two different industrial groups successfully reported a cyclisation reaction, now considered one of the milestones in the field of asymmetric organocatalysis. In 1974, Hajos and Parrish described L-proline (**4**) as an organocatalyst for the intramolecular asymmetric aldol reactions of two triketones. In

this work, the starting material **5**, a cyclopentanedione derivative, was fully converted to the bicyclic ketol **6** (93% ee) using only 3 mol% of **4** in 20 h at room temperature (**Scheme 2a**).<sup>13</sup> Similarly, using the same conditions, the triketone **8** was converted to the bicyclic ketol **9** in 72 h at room temperature with good yield and selectivity (**Scheme 2b**).<sup>14</sup> Acid-catalysed dehydration of ketols **6** and **9** provided diketones **7** and **10** (also called Wieland-Miescher ketone), which are elements of pivotal importance in the asymmetric total synthesis of steroids.<sup>15</sup>



**Scheme 2.** L-Proline catalysed Hajos-Parrish reaction to yield: **a)** tetrahydroindandione and **b)** octahydronaphthalenedione.

Previous studies conducted by Eder, Sauer and Wiechert achieved products **7** and **10** in a single step using high catalyst loading of **4** and an acid co-catalyst.<sup>16</sup> In this report, catalyst **4** converted both triketones **5** and **8** into products **7** and **10** with excellent yield and stereoselectivity (**Scheme 3a** and **3b**).

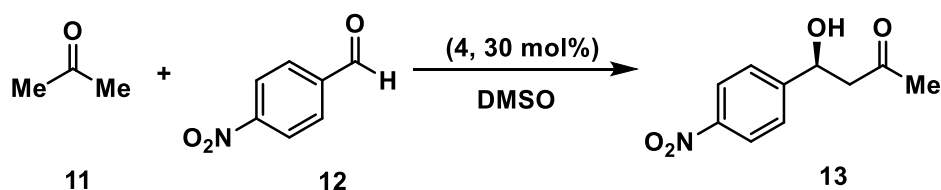


**Scheme 3.** Eder-Sauer-Wiechert reaction to obtain **a)** compound **7** and **b)** compound **10**.

Although the proline-catalysed aldol condensation, now known as Hajos-Parrish-Eder-Sauer-Wiechert reaction, constitutes a landmark for the renaissance of organocatalysis, the scientific community overlooked organocatalytic reactions until the late '90s. At that time, scientists lacked interest for organocatalysis mainly for three motivations.<sup>11</sup> As previously reported, one of the main reasons was that organocatalysis was not conceptualised as a field until the late '90s.<sup>11</sup> Second, scientists did not accredit importance to the advantages of organocatalytic transformations. Third, no predictions about the rapid growth of the field due to the advent of generic modes of catalyst activation, induction and reactivity were made.<sup>11</sup>

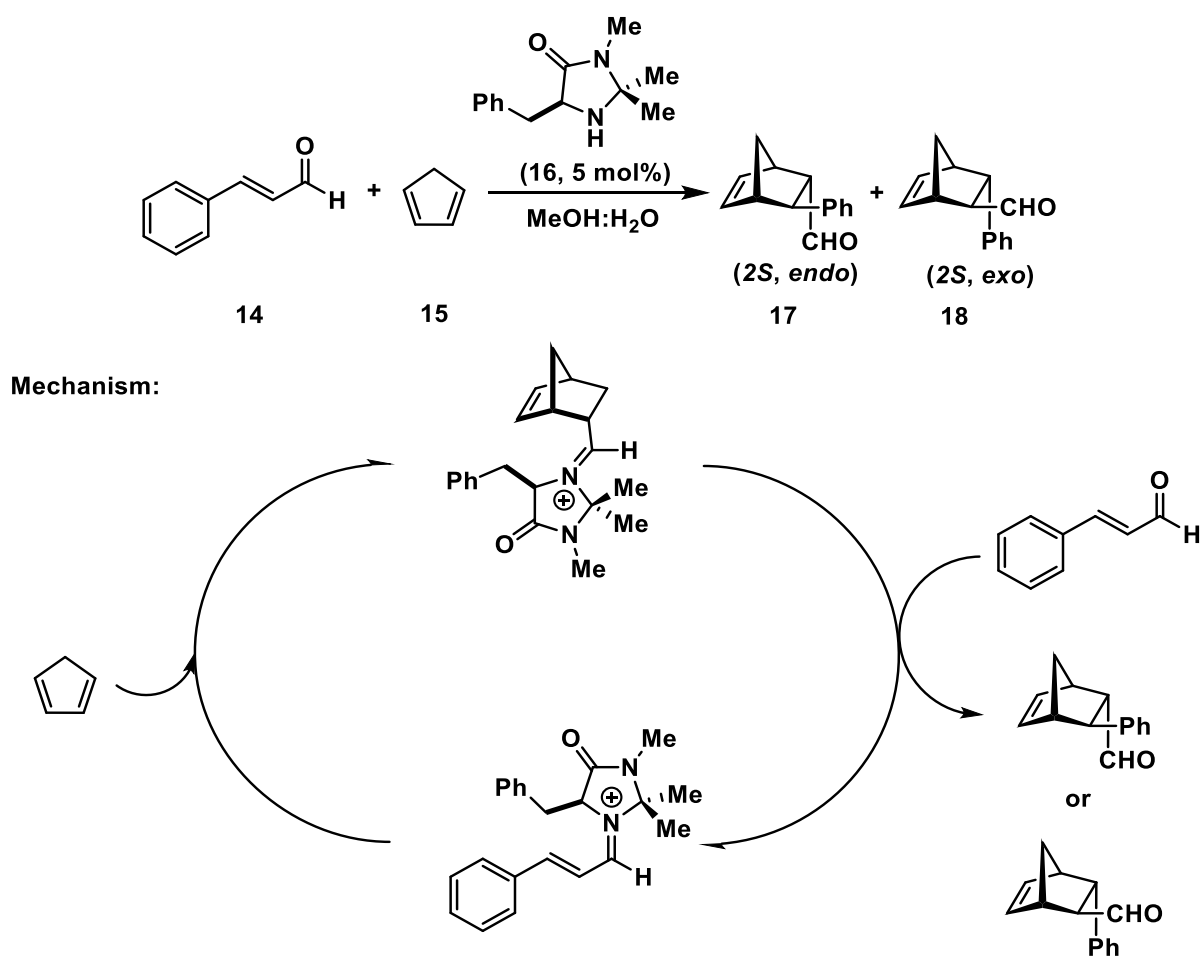
From the '70s to the '90s, some successful organocatalysed reactions were reported, including the first hydrogen-bonding catalysed reaction.<sup>17-27</sup> However, only at the beginning of the new century, the concept of organocatalysis was almost simultaneously described. The Barbas, Lerner, and List groups presented enamine catalysis as a generic activation mode.<sup>28</sup> In contrast, MacMillan's group introduced the concept of iminium organocatalysed organic transformations.<sup>29</sup> Barbas, List and

Lerner extended the seminal work made in the Hajos-Parrish-Eder-Sauer-Wiechert reaction to intermolecular aldol reactions (**Scheme 4**).<sup>28</sup> Although the reaction conditions were not fully optimised (30 mol% of **4**, 20 vol% of acetone (**11**) and in DMSO), this report described the first attempt to introduce enamine catalysis as a generic activation mode. In this case, catalyst **4** achieved moderate to good yield and selectivity when several aromatic and aliphatic aldehydes (*i.e.* *p*-nitrobenzaldehyde, **12**) and **11** were employed.



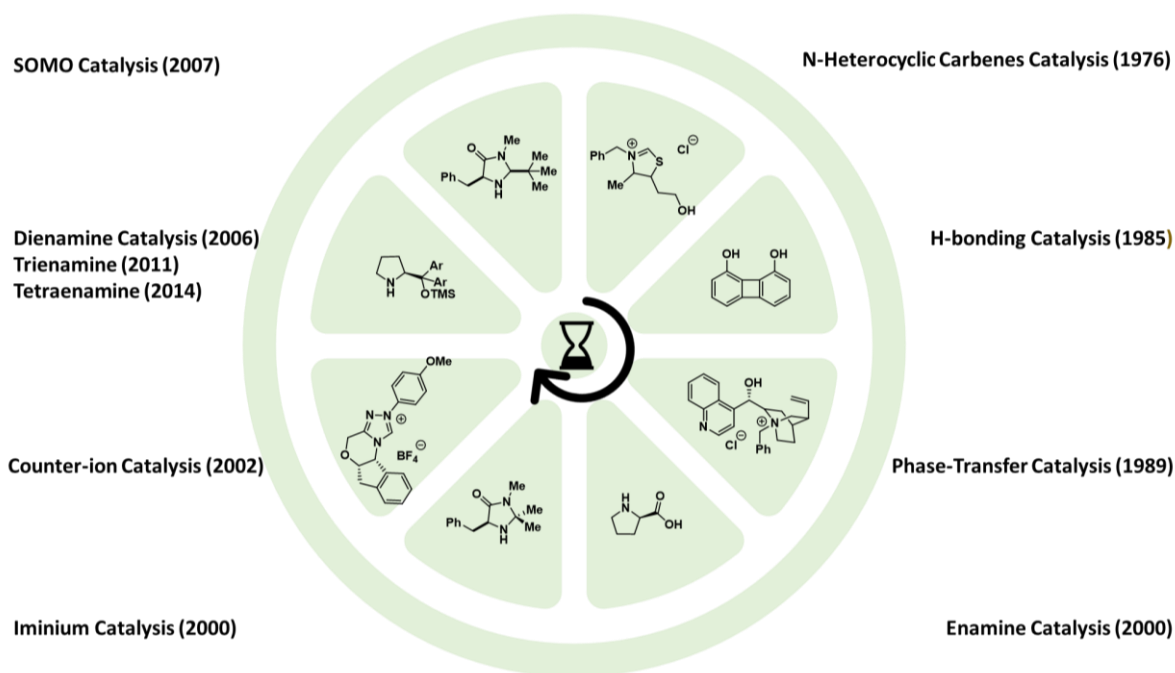
**Scheme 4.** L-Proline-catalysed intermolecular aldol reaction reported by Barbas, List and Lerner.

Simultaneously, the first enantioselective organocatalytic Diels-Alder reaction was reported (**Scheme 5**). In this paper, the formation of an iminium ion between  $\alpha,\beta$ -unsaturated aldehydes (*i.e.* cinnamaldehyde, **14**) and an imidazolidinone-based organocatalyst (1<sup>st</sup> generation MacMillan catalyst, **16**) was idealised as general activation mode.<sup>29</sup> Similarly to Lewis-acid catalysis, iminium catalysis was conceptualised as a pool of reactions where the newly formed iminium ion lowers the lowest unoccupied molecular orbital (LUMO) of the  $\alpha,\beta$ -unsaturated carbonyl yielding an increase of electrophilicity of the substrate. Indeed, in this specific case, **14** and cyclopentadiene (**15**) could react in a Diels-Alder reaction in the presence of only 5 mol% of catalyst **16**. Although both regioisomers *endo* and *exo* were generally obtained in a ratio 1:1, cinnamaldehyde was converted to *endo/exo* products **17-18** with good yield and enantioselectivity.



**Scheme 5.** Highly enantioselective organocatalytic Diels-Alder reaction using catalyst **16**.

Remarkably, this paper also defined “generic activation mode” as a way to describe “a reactive species that can participate in many reaction types with consistently high enantioselectivity (as opposed to one or two unique transformations)”.<sup>29</sup> Since then, organocatalysis has witnessed the discovery of novel activation protocols, which were crucial for the rapid growth of the field (**Fig. 3**).<sup>10, 30-33</sup> These different activation concepts are extended from covalent linkage to hydrogen-bonding interactions between catalyst and substrate.<sup>34, 35</sup> Although the listed activation modes have equally contributed to open new possibilities for novel stereoselective transformations in organocatalysis, the next part of the discussion will focus on the history and development of asymmetric aminocatalysis. Notably, the following paragraphs' emphasis will be given to aminocatalysis subfield, relying on amines' covalent activation of carbonyls.



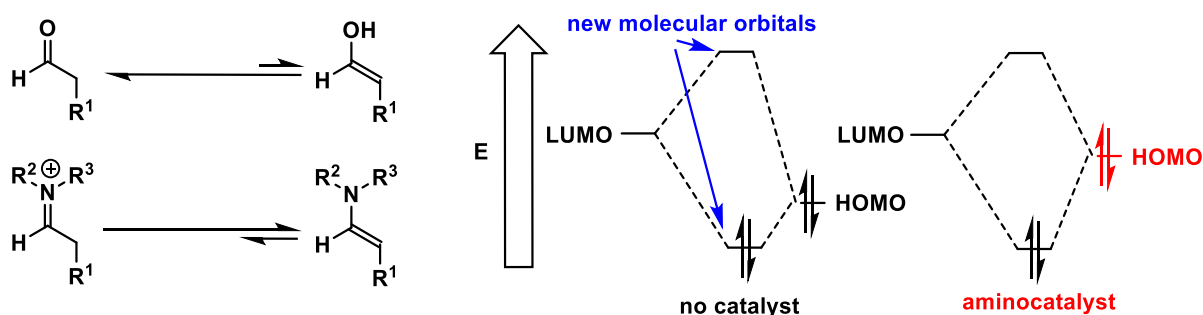
**Figure 3.** Timeline of some of the most significant generic activation modes for organocatalysis. Within each area are presented the corresponding organocatalysts employed in the first example reported for each activation protocol.

### 1.1.2 Generic activation modes in aminocatalysis

Aminocatalysis has evolved tremendously throughout the years, becoming a primary choice for asymmetric functionalisation of carbonyl compounds. Currently, the published literature on primary/secondary amine-based catalysts covers a broad range of stereoselective organic transformations, including  $\alpha$ -,  $\beta$ -,  $\gamma$ -,  $\epsilon$ -functionalisations of enals and  $\alpha,\beta$ -unsaturated aldehydes, in addition to domino, cascade and tandem processes of the carbonyl mentioned above.<sup>7, 33, 36</sup> Portion of the literature focuses on the role of aminocatalysts in total synthesis.<sup>30</sup> Moreover, a substantial number of reports focuses on organocatalysed reactions either in ionic liquids or using catalysts supported on polymeric resin, but will not be further discussed in this thesis.<sup>37</sup> Aminocatalytic pathways for functionalisation of carbonyls are based on either HOMO-raising (via enamine,<sup>28</sup> dienamine,<sup>38</sup> trienamine<sup>39</sup> and tetraenamine<sup>40</sup> intermediates), LUMO-lowering (via iminium-ion<sup>29</sup> and vinylogous iminium-ion intermediates<sup>41</sup>) or SOMO activation protocols.<sup>42</sup> In the interest of this dissertation, enamine and iminium catalysis will be further discussed.

### 1.1.2.1 HOMO-raising catalysis

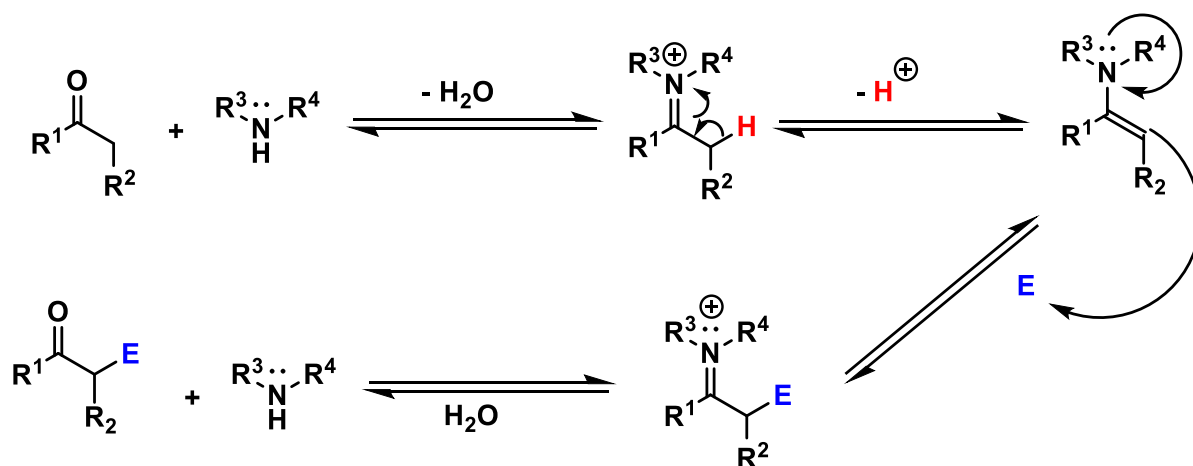
The concept of aminocatalysis is based on the variation of the energy gap between the frontier orbitals HOMO (Highest Occupied Molecular Orbital) and LUMO (Lowest Unoccupied Molecular Orbital).<sup>10</sup> In HOMO-raising catalysis the condensation of a carbonyl with a primary/secondary amine shifts the equilibrium towards the formation of the enamine intermediate, meanwhile in classic keto/enol tautomerisation the equilibrium is towards the keto form.<sup>43</sup> Moreover, the lone-pair on the nitrogen atom possesses higher energy than the oxygen atom, causing a raise in energy of the HOMO. Consequently, the energy gap between the enamine and the electrophilic substrate frontier orbitals decreases, causing an increase in the compound reactivity (**Fig. 4**).



**Figure 4.** HOMO-raising catalysis. The formation of the enamine intermediate raises the HOMO and decrease the energy gap between LUMO and HOMO.

Enamine catalysis pathway starts with the condensation of a carbonyl compound possessing an enolisable  $\alpha$ -hydrogen with an amino organocatalyst (**Fig. 5**). The catalytic cycle is continued after the newly formed iminium intermediate is deprotonated in position  $\alpha$  and generates an enamine. The equilibrium is shifted towards the formation of the enamine intermediate, which subsequently can attack a generic electrophile (E). Finally, the  $\alpha$ -functionalised product is formed, and the catalyst can be regenerated after water addition to the carbonyl group.<sup>10</sup>



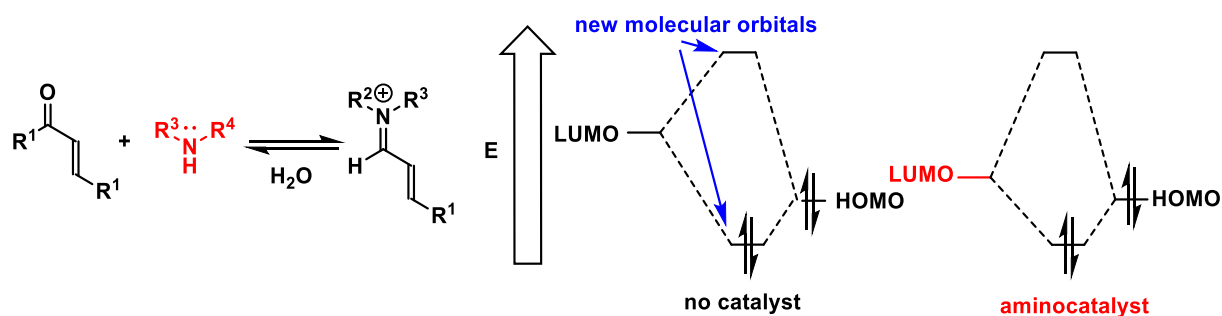


**Figure 5.** Enamine-catalysed nucleophilic attack of carbonyl to a generic electrophile E.

The emergence of enamine catalysis has paved the way for its application in asymmetric organocatalysis, including in the synthesis of precursors of pharmaceutical products,<sup>30</sup> reactions in ionic liquids or biocompatible environments,<sup>5, 6</sup> or solvent-free transformations.<sup>44</sup> A substantial amount of literature focusing on enamine catalysis has been collected in comprehensive reviews.<sup>4, 43, 45, 46</sup>

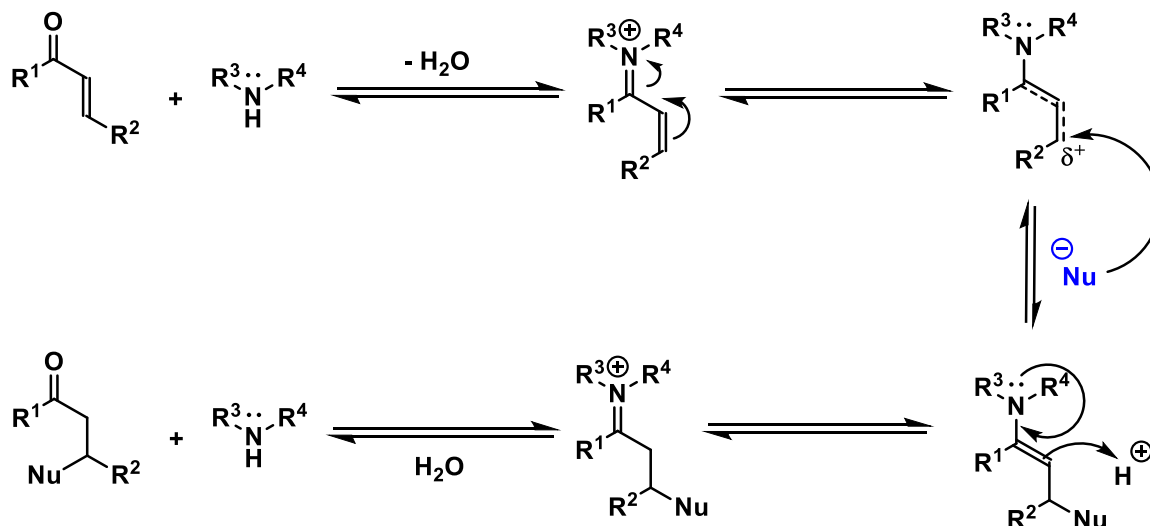
### 1.1.2.2 LUMO-lowering catalysis

LUMO-lowering catalysis involves the formation of an iminium ion after the condensation of an  $\alpha,\beta$ -unsaturated carbonyl with a primary/secondary amine (**Fig. 6**). The iminium ion formed possesses a lower LUMO in respect to the original carbonyl compound and facilitates the attack of nucleophiles to the  $\beta$  position of the  $\alpha,\beta$ -unsaturated carbonyl. This characteristic can also be found in Lewis Acid (LA) catalysis and has allowed a substantial amount of asymmetric  $\beta$ -functionalisations to generate C-H, C-C, and C-heteroatom bonds.



**Figure 6.** LUMO-lowering catalysis. The formation of the iminium intermediate lowers the LUMO and decrease the energy gap between the frontier orbitals.

Mechanistically, iminium catalysis activation starts with the condensation of an  $\alpha,\beta$ -unsaturated carbonyl with the amino organocatalysts and proceeds with the formation of an iminium ion (**Fig. 7**).



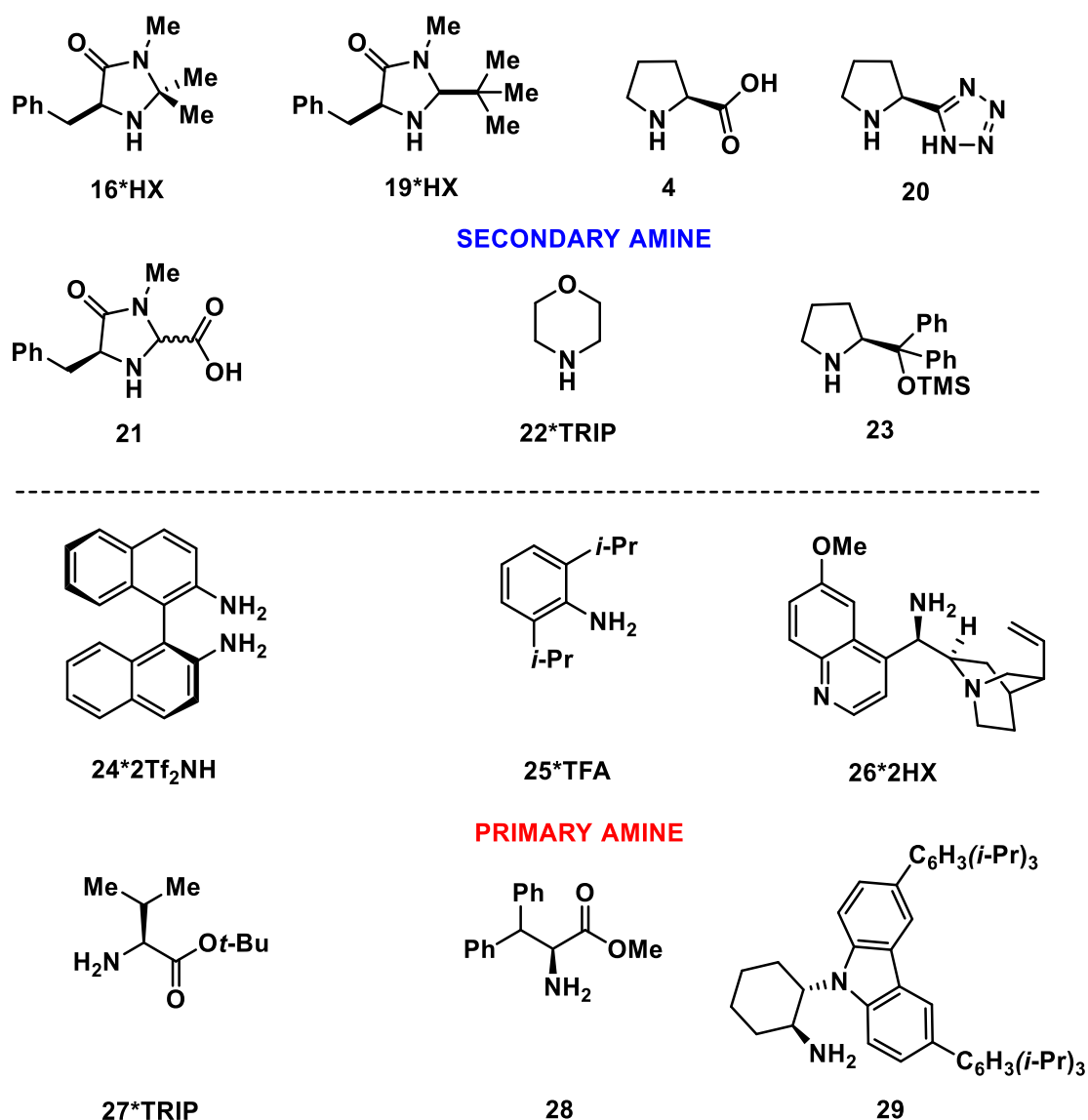
**Figure 7.** Iminium-catalysed nucleophilic attack to carbonyl with a generic nucleophile.

An electron shuffling towards the electronegative nitrogen causes a rearrangement where a partial positive charge is observed in position  $\beta$ . Thus, this intermediate can be sensitive either to nucleophilic attack or to cycloaddition reactions. After the nucleophilic attack, the newly formed  $\beta$ -substituted enamine adduct is then protonated in the  $C_\alpha$ . The subsequent addition of water regenerates the organocatalyst and the  $\beta$ -functionalised carbonyl compound.<sup>4, 37, 45, 46</sup> Summaries focusing on the origin, the

development and the massive impact of iminium catalysis in the field of asymmetric catalysis can be found in the appropriate reviews.<sup>4, 45, 47</sup>

### 1.1.3 Properties and applications of chiral aminocatalysts

The advent of generic activation protocols in organocatalysis has been accompanied by the creation of efficient aminocatalysts capable of being adapted to different reactions and conditions. Aminocatalysts for organocatalysis can be divided into primary and secondary amine-based catalysts (**Fig. 8**).



**Figure 8.** Some representative organocatalysts employed in aminocatalysis. On the top part, secondary aminocatalysts, meanwhile on the bottom are located the primary amine-based organocatalysts.

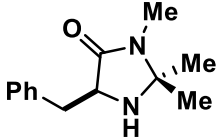
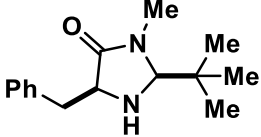
However, so far, chiral secondary amines-based organocatalysts dominated the field. The reasons behind this are threefold. First, primary amines often need to be activated by an external acid co-catalyst, whereas for secondary amines, the use of acid co-catalyst is recommended, but not mandatory.<sup>37</sup> Second, chiral secondary amines possess an inner conformational restraint in the amine structure, facilitating the transmission of the chiral information to create stereoselective adduct. Third, disubstituted nitrogens are slightly better nucleophiles than monosubstituted nitrogens, providing a higher rate of formation of the iminium ion between the catalyst and substrate.<sup>45-47</sup>

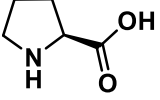
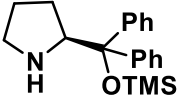
Among the secondary amine-based catalysts reported in **Fig. 8**, the family of imidazolidinone catalysts (**16** 1<sup>st</sup> generation, **19** 2<sup>nd</sup> generation), developed by the MacMillan group, has heavily contributed toward the evolution of the field.<sup>36</sup> In particular, aminocatalyst **16** has been employed for a plethora of enantioselective transformations (**Table 1, Entry 1**). Furthermore, the application of organocatalysis in the total synthesis of natural products has attracted great interest.<sup>48, 49</sup> Further efforts by the MacMillan group merged into creating the 2<sup>nd</sup> generation catalyst (**19**, see **Fig. 8**). This bulky and versatile chiral imidazolidinone-based catalyst was synthesised after structural refinement based on molecular modelling-aided studies, which provided a better insight into the properties of MacMillan's family of catalysts. Aminocatalyst **19** was extensively employed to discover numerous enantioselective organocatalytic reactions (**Table 1, Entry 2**). MacMillan catalysts of 1<sup>st</sup> and 2<sup>nd</sup> generation are versatile chiral compounds capable of producing stereoselective transformations for a broad range of substrate and reactions. However, these compounds have been reported to possess a limited functionality in aqueous media,<sup>50</sup> thus not allowing access to one-pot organocatalysis-biocatalysis reactions and impeding their application in a biological context. The reason for that can be found in the low solubility of most aminocatalysts (including catalyst **23**) and organic compounds in H<sub>2</sub>O, in addition to the poor hydrolytic stability of chemical compounds and catalytic intermediates.<sup>50</sup> Moreover, as a matter of more importance, to achieve high selectivity and yield, these chiral amines sometimes require high catalyst loading, extreme temperature (-78 °C) and acid co-catalysts.

Another class of catalysts, L-proline (**4**) and its derivatives are among the most simplistic version of amino organocatalysts. They have been very popular and applied to various iminium-catalysed reactions, especially ring-forming and domino reactions (**Table 1, Entry 3**).<sup>37</sup> Although its role in the history of organocatalysis has been of primary importance, L-proline suffers some drawbacks compared to the synthetic chiral secondary amine-based organocatalysts. Indeed, its simple structure does not help to gain orientation advantages in stereospecific transformation, where a bulky substituent can play a crucial role in forming a stereoselective product rather than another. Therefore, these restrictions associated with some common problems, such as high catalyst loading, and inconvenient working temperatures limited the use of this organocatalyst.

Eventually, another class of aminocatalysts based on secondary amine is the family of the diarylprolinol silyl ether derivatives introduced almost simultaneously by Jørgensen and Hayashi groups.<sup>51, 52</sup> These catalysts, such as catalyst **23**, enabled access to new activation protocols, including dienamine, trienamine and more recently tetraenamine catalysis (**Table 1, Entry 4**).<sup>45, 53, 54</sup> The majority of drawbacks reported for catalysts **16** and **19** are also associated to the Jørgensen-Hayashi family.

**Table 1.** List of reactions for the main aminocatalysts.

Entry	Catalyst	Reactions
1	“MacMillan 1 <sup>st</sup> generation” <b>16</b> 	Friedel-Crafts alkylation of pyrroles, <sup>55</sup> conjugate addition of pyrrole to cyclic enals, <sup>56</sup> vinylogous Michael Addition of dicyanoolefins, <sup>57</sup> and intramolecular Michael Addition <sup>58</sup>
2	“MacMillan 1 <sup>st</sup> generation” <b>19</b> 	Alkylation of indoles, <sup>59</sup> asymmetric conjugate additions of electron-rich benzenes to enals, <sup>60</sup> asymmetric intramolecular Diels-Alder reactions, <sup>61, 62</sup> enantioselective Mukaiyama-Michael reactions of silyloxyfurans, <sup>63</sup> enals and

		silyl enol ethers, <sup>64</sup> and asymmetric transfer hydrogenation of enals <sup>65</sup>
3	<p>L-Proline <b>4</b></p> 	Addition of nitroalkanes to cyclic enones, <sup>66</sup> intermolecular Baylis-Hillman, <sup>67</sup> formal [3+3]-dimerization of aliphatic and aromatic $\alpha,\beta$ -unsaturated aldehydes, <sup>68</sup> and domino Knoevenagel-formal Diels-Alder reaction. <sup>69</sup>
4	<p>Jørgensen-Hayashi <b>23</b></p> 	Epoxidation of $\alpha,\beta$ -unsaturated aldehydes, <sup>70</sup> formations of chiral aziridines and cyclopropanes, <sup>71</sup> synthesis of several different five- and six-membered hetero- and carbocycles. <sup>71-73</sup>

Generally, organocatalysis has become one of the most powerful tools to perform asymmetric catalysis and bioorthogonal transformations.<sup>11</sup> Notably, the development of catalysts tailored to the different activation protocols has implemented the versatility and the strength of organocatalysis to achieve several stereoselective C-X functionalisations. Often these reactions are catalysed in rates comparable to the metal counterpart. Both semi-synthetic and artificial organocatalysts are mostly non-toxic and highly stable in air and moisture. Also, recent seminal reports have indicated a terrific progression in the disclosure of metal-free catalysts capable of achieving excellent performances in both aqueous and solvent-free environment.<sup>44, 50, 74, 75</sup> However, only a few examples of organocatalysed reactions in a biological context are reported.<sup>5</sup> These include protein aldol ligation,<sup>76</sup> affinity protein-labelling and hydrazone/oxime bioconjugation.<sup>77</sup> Other organocatalytic reactions that can be potentially used *in vivo* were reported in a detailed review.<sup>50</sup> The limited application of organocatalytic reactions in biologically friendly environments can be associated with significant drawbacks, such as low solubility in buffer/H<sub>2</sub>O of substrates/catalysts, high catalyst loading, extreme temperature (-78 °C), cellular toxicity and the requirement of acid co-catalysts and co-solvents. In the next section, the potential solutions for enabling organocatalysis in a biocompatible context will be discussed.

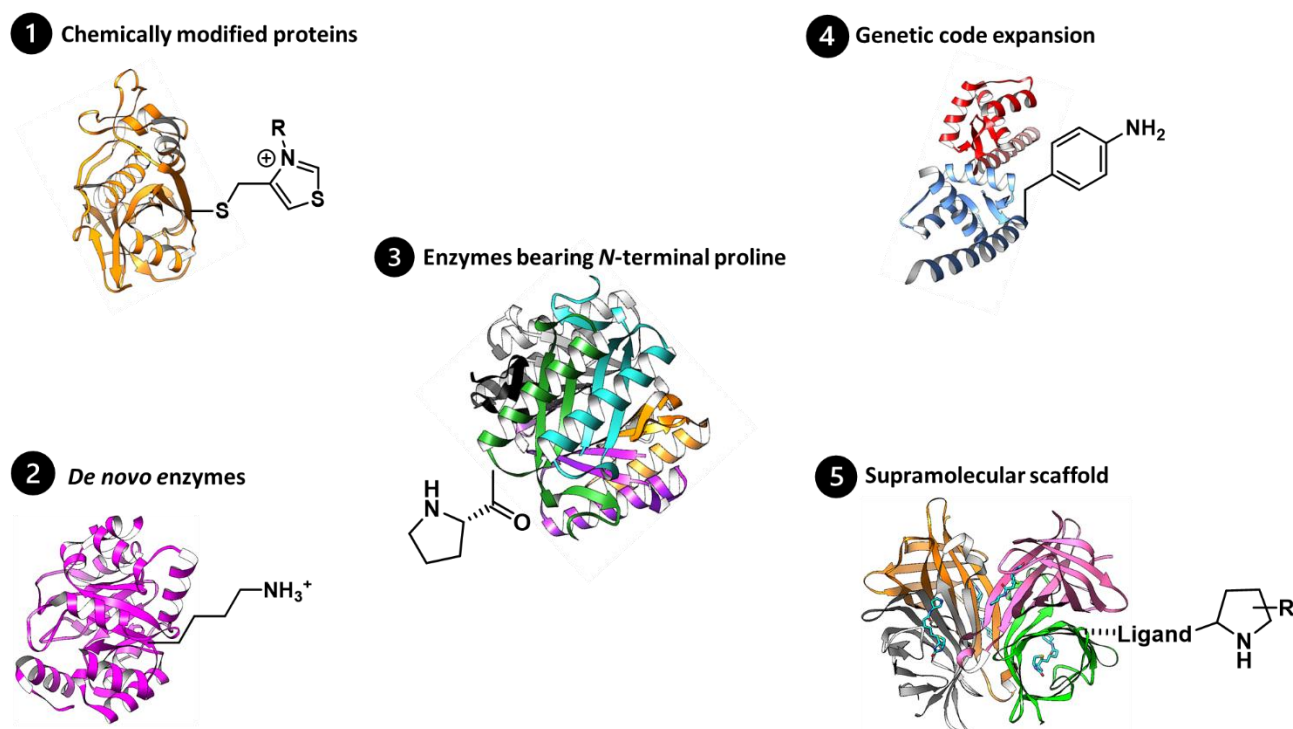
## 1.2 Protein as host for biocompatible organocatalysis

### 1.2.1 Introduction

The discovery and renaissance of enantioselective organocatalysis were discussed in the previous chapter.<sup>44, 78, 79</sup> At present times, scientists are gradually turning their interest in the role of biocompatible organocatalytic systems and their potential applications in chemical and synthetic biology.<sup>80-83</sup> Enabling organocatalysis under biologically benign conditions is still an essential challenge in chemical biology.<sup>81</sup> Different classes of organocatalysts, including MacMillan derivatives (*i.e.* **16** and **19**),<sup>84-86</sup> L-proline derivatives (**4**),<sup>87</sup> thiourea-based catalysts,<sup>88</sup> and anion- $\pi$ <sup>89</sup> derivatives were tested for biorthogonal reactions. For instance, aminocatalysts were used to mediate the bioconjugation of protein through aldol ligation,<sup>76, 90</sup> or, in combination with enzymes, they were employed for one-pot synthesis of chiral synthons.<sup>8, 91-93</sup> The majority of organocatalysts are barely functional in a biocompatible environment (*i.e.* physiological pH, room temperature and mostly aqueous environment),<sup>94</sup> limiting their applications to work described in only a few reports.<sup>9, 50, 81, 88, 95-104</sup> The creation of organocatalysts that function efficiently in aqueous or biocompatible environments can be useful for diverse applications, such as soft robotics and self-healing materials, controlled drug delivery or on-demand drug synthesis in tumour cells.<sup>50</sup> Several examples have been reported for organocatalytic reaction hosted within different biomolecules, such as DNA, RNA, oligopeptides and proteins.<sup>5, 105-115</sup> Given this thesis goal, the next paragraph will focus on the strategical advantages of using protein as a host for enabling biocompatible organocatalysis.

Proteins have been fruitfully and extensively used as the host for chemical catalysis.<sup>105, 116</sup> Remarkably, compared to other macromolecules, proteins bear some advantages. First, they can be easily expressed and engineered. Notably, laboratory evolution can alter protein functions,<sup>117</sup> using techniques such as molecular cloning, and in combination with appropriate screenings allows access to novel and improved reactivity.<sup>118</sup> Second, proteins are stable under biocompatible conditions. Third, proteins possess a relatively low dielectric constant, similar to most organic solvents.<sup>119</sup> Bearing in mind these features, protein have been shown to support the stabilisation of transition states during chemical transformation through a specific network of interactions.<sup>105, 120-122</sup> Moreover, the core that hosts the catalytic motif can

be altered genetically to improve the catalytic efficiency (selectivity and reactivity). Contrarily, limitations are still associated with exporting this “evolvability” in classic catalyst design.<sup>105, 107, 117, 120, 123-126</sup> To this extent, several protein scaffolds were used to develop biocompatible stereoselective artificial enzymes.<sup>107, 127</sup> In this chapter, the description of artificial enzymes, intended as protein-based systems modified to create enzymes with novel reactivities, will be provided.<sup>126</sup> For the story of this thesis, artificial organocatalytic enzymes reported in the literature will be introduced, paying close attention to artificial enzymes designed through the supramolecular approach. Synthetic polypeptides applied in organocatalysis will not be mentioned. However, a detailed description of them can be found in a recent summary.<sup>128</sup> Artificial organocatalytic enzymes will be categorised based on the strategy adopted for their design (**Fig. 9**).



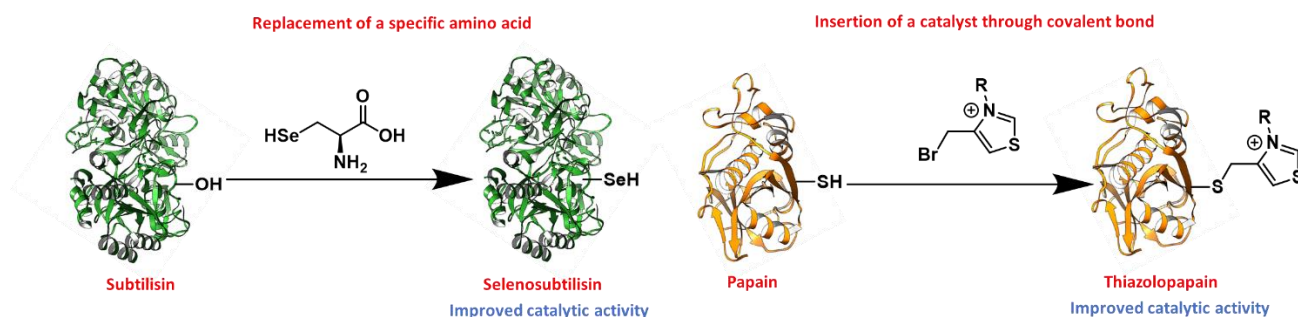
**Figure 9.** The five approaches to design organocatalytic artificial enzymes.

### 1.2.2 Site-selective chemical modification of proteins

Site-selective chemical modifications of proteins were used to design early examples of organocatalytic artificial enzymes.<sup>129-131</sup> This goal was achieved by modifying critical residues in the protein active site to alter the overall enzyme reactivity. These chemical modifications

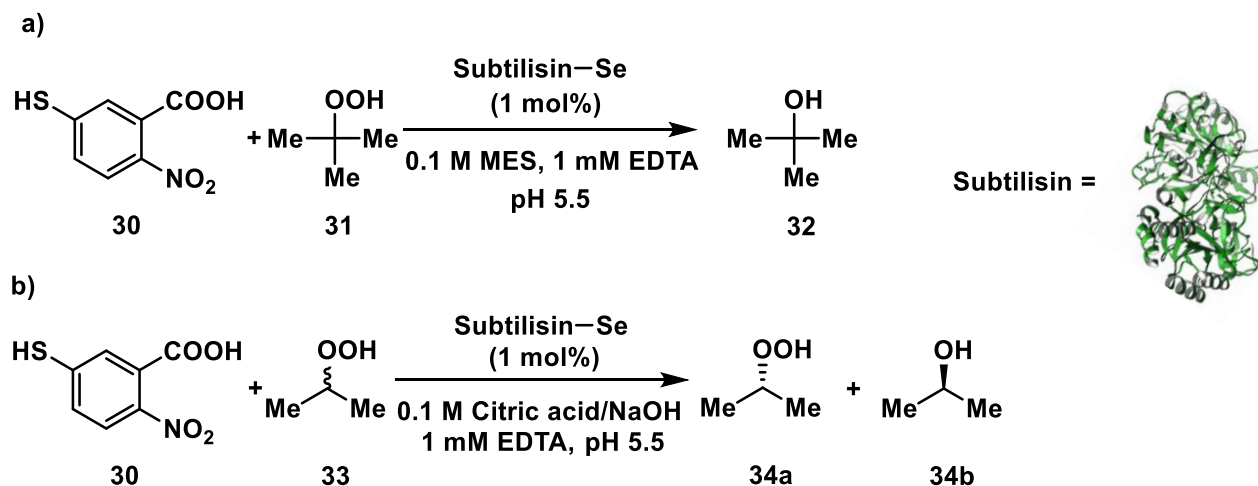


could be obtained through replacement of crucial amino acid, or in other cases via insertion of a chemical catalyst through covalent bonds (**Fig. 10**).



**Figure 10.** Creation of organocatalytic artificial enzymes through site-selective modification. On the right, thiazolopapain generated from papain (PDB: 9PAP) after insertion of a catalyst. The replacement of cysteine with selenocysteine to form selenosubtilisin from subtilisin (PDB: 1YU6) is on the left.

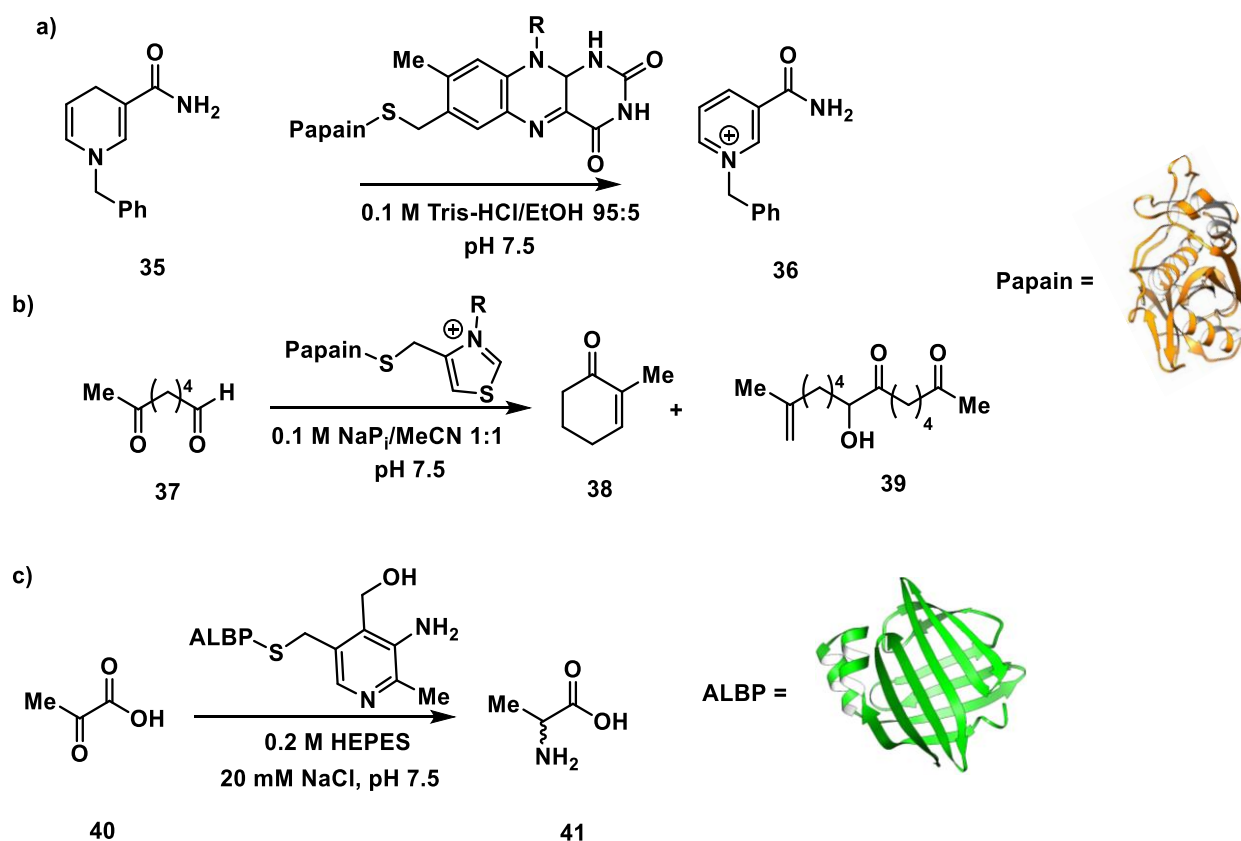
In the first case, organocatalytic artificial enzymes created by the replacement of specific amino acid were described for the protease subtilisin. When the serine located at the active site of subtilisin was replaced by cysteine or selenocysteine motifs, the resulting thiolsubtilisin and selenosubtilisin were tested for chemical catalysis.<sup>132, 133</sup> The resulting artificial enzymes showed a new activity as hydrolase for thiolsubtilisin and as reductase for selenosubtilisin. Interestingly, selenosubtilisin was employed to reduce hydroperoxides,<sup>132, 134, 135</sup> including *tert*-butyl hydroperoxide (**31**) to its alcohol equivalent **32** using thiophenol **30** as an oxidising agent (**Scheme 6a**).<sup>134</sup> A single mol% of selenosubtilisin led to a dramatic increase in the reaction rate, measured to be  $7 \cdot 10^5$  times faster than when the model selenium compound was used. Moreover, this artificial enzyme was also able to mediate the kinetic resolution of the racemic peroxide **33** (**Scheme 6b**), showing reaction rates comparable to those of subtilisin, although exhibiting an inverted enantioselectivity.<sup>132</sup>



**Scheme 6.** Selenosubtilisin catalyses the reduction of **a)** tert-butyl hydroperoxide and **b)** secondary alkyl hydroperoxide.

Alternatively, the insertion of a catalytically active motif on a selected residue of the protein was used to design organocatalytic artificial enzymes. For example, papain, an enzyme with native function as protease, was linked by covalent binding of its cysteine residues to chemical catalysts. Therefore, a semi-synthetic oxidoreductase could be generated by replacing the cysteine residue with semi-synthetic flavins. The resulting flavopapain was shown to be capable of oxidising NADH and other derivatives, including *N*-benzyl-1,4-dihydro nicotinamide (**35**, BNAH) to BNA<sup>+</sup> (**36**), with a detected rate of reaction 50-fold higher than the flavin itself (**Scheme 7a**).<sup>136</sup> Similarly, thiazolopapain was created by the reaction of the natural cofactor thiamine with the papain cysteine.<sup>137</sup> Thiazolopapain was also described as one of the first C-C bond formation examples by an organocatalytic artificial enzyme. Indeed, the slow cyclisation of 6-oxo heptanal (**37**) to achieve product **38** was observed in the presence of this artificial enzyme. However, the dimerisation by-product **39** was also observed (**Scheme 7b**). Eventually, the adipocyte lipid binding protein (ALBP) was covalently linked to the natural cofactor pyridoxamine (Py) to obtain ALBP-Py complex.<sup>138</sup> The resulting organocatalytic artificial enzyme could be successfully applied to synthesise a wide range of amino acids (including compound **40**) with modest to excellent enantioselectivity (up to 94%, **Scheme 7c**). Our group recently reported an approach to link penicillin derivatives to  $\beta$ -lactamase from *Mycobacterium tuberculosis*. In this case, the secondary amine moiety of the penicillin derivatives was able to mediate 1,4-Michael addition of nitromethane to cinnamaldehyde. However, poor yields and low enantioselectivities were observed (20-27%,

10% ee).<sup>139</sup> These reports were used as exemplary for the development of protein-hosted organocatalysis.<sup>134, 136, 140</sup> Considering the huge improvement achieved in the chemical methodologies for protein labelling in recent years, including signs of progress in fine-tuned reactivity, biocompatibility and labelling within live cells,<sup>141-148</sup> speculation regarding the possibility for creating efficient organocatalytic artificial enzymes by adapting these novel technologies can be made.

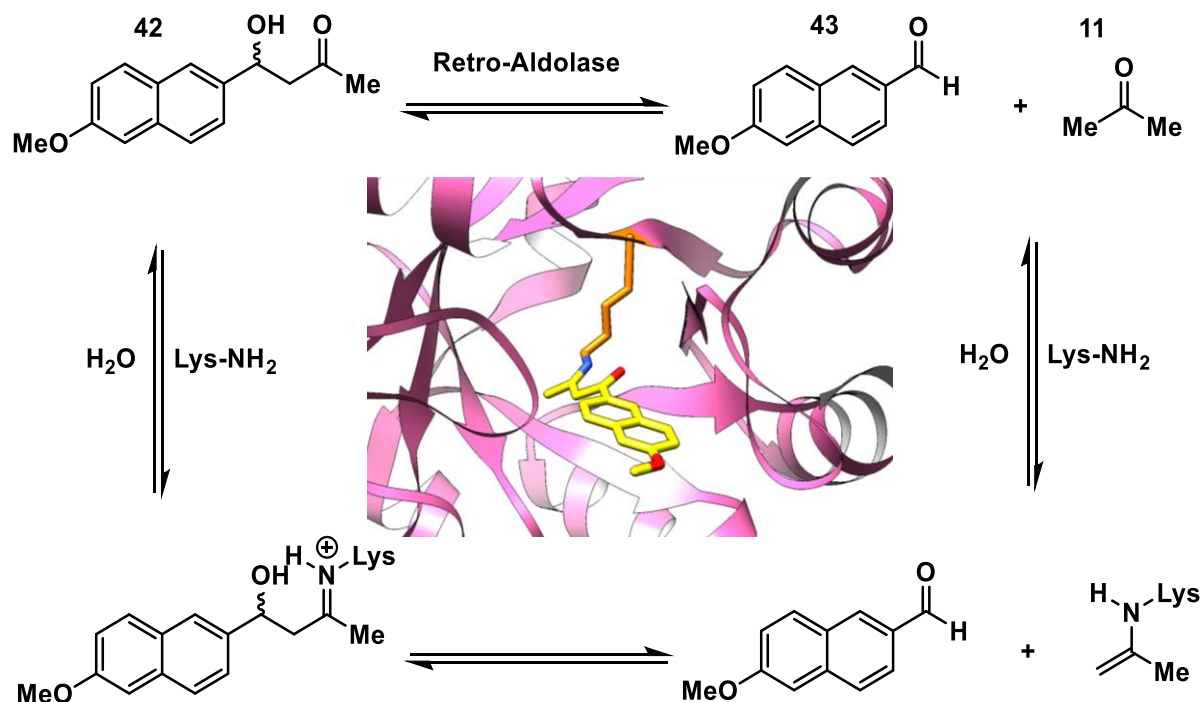


**Scheme 7.** Artificial enzymes created by covalent modification of cofactors: **a)** artificial flavopapain used for the oxidation of BNAH; **b)** artificial thiazolopapains for C-C bond formation; and **c)** artificial ALBP-pyridoxamine (PDB: 1ALB) for enantioselective reductive amination.

### 1.2.3 *De novo* enzymes

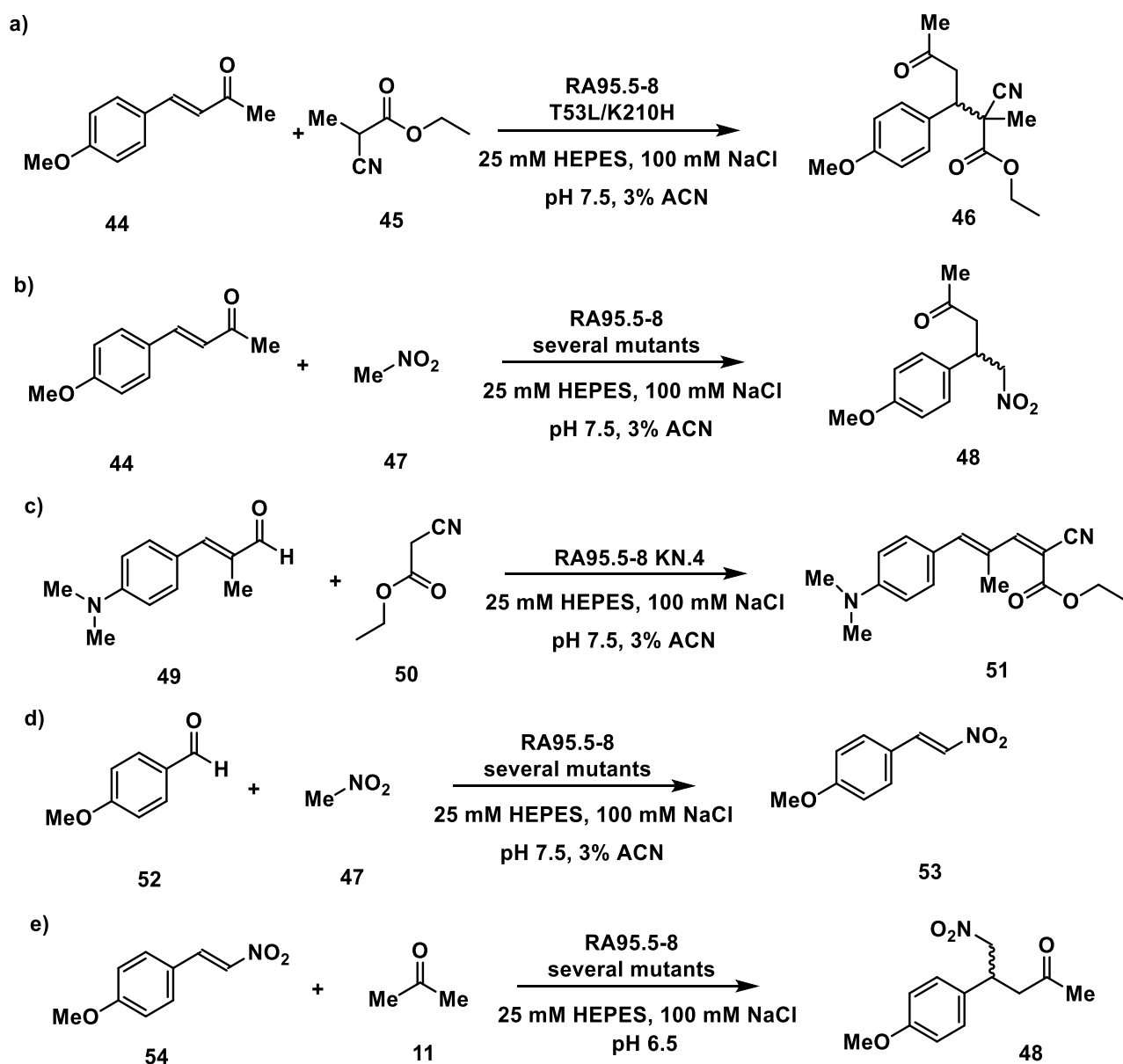
A second strategy adopted to design organocatalytic artificial enzymes is based on *de novo* enzymes originated from computational software, such as Rosetta and ORBIT.<sup>149-151</sup> The process of genesis of a *de novo* enzyme is the outcome of a substantial work articulated in different stages. The first phase involves creating a “theozyme”, which is a computational arrangement of several side-chain residues, water and ions that theoretically can stabilise

the rate-limiting transition state(s) of a determined model reaction.<sup>152</sup> The second stage consists of converting the “theozyme” into a protein structure potentially feasible for experimental work. This process can be achieved using a pool of computational software able to screen different tertiary structures of proteins. Successively, an extensive database of structural information and several variations of the transition state is evaluated.<sup>117, 149</sup> The initial design of these artificial enzymes is completed after evaluating different parameters, including geometry, energy and finally through visual inspection. At this stage, the best hits are assessed and produced recombinantly. The first models of *de novo* enzymes have typically poor catalytic efficiency and substrate promiscuity, and rounds of directed evolution are needed to enhance their model reaction performance. This protocol paved the way for the creation of several highly competent and promiscuous *de novo* enzymes, including Kemp eliminase,<sup>153, 154</sup> retro-aldolases (RA)<sup>111, 114, 115, 155-159</sup> and Diels-Alderases.<sup>124, 160</sup> Interestingly, retro-aldolases bearing a catalytically active lysine were reported to be able to mediate iminium and enamine catalysis. This family of *de novo* enzymes was initially described for the retro-aldol cleavage of the fluorogenic compound methodol (**42**) via formation of iminium intermediate with the catalytically active lysine of the enzyme (**Fig. 11**).<sup>158</sup> This reaction was easily screened through increased fluorescence of the C-C bond cleavage product naphthaldehyde (**43**).



**Figure 11.** Iminium-catalysed cleavage of **42** by de novo designed retro-aldolases and intermediates. In the middle an overview of the crystal structure of RA95.0 (magenta, PDB: 4A29), in which Lys210 (orange) is responsible for forming the Schiff base intermediate with a 1,3-diketone inhibitor (yellow).

Furthermore, retro-aldolases were generated by combining computer-aided design, analysis of the crystal structures and genetic manipulation techniques, such as directed evolution or cassette mutagenesis.<sup>5, 117</sup> Retro-aldolases were able to mediate both iminium catalysed reactions, such as conjugate additions of compound **45** or nitromethane (**47**) to the  $\alpha,\beta$ -unsaturated ketone **43** (Scheme 8a and b),<sup>111, 113, 115</sup> Knoevenagel (Scheme 8c)<sup>114</sup> and Henry condensations (Scheme 8d),<sup>112</sup> and enamine catalysed reactions, including the nitro-Michael addition of **11** to nitrostyrene derivative **54** (Scheme 8e).<sup>113</sup> In summary, the design and evolution of *de novo* enzymes, such as the promiscuous retro-aldolases is a powerful approach to create organocatalytic artificial enzymes.

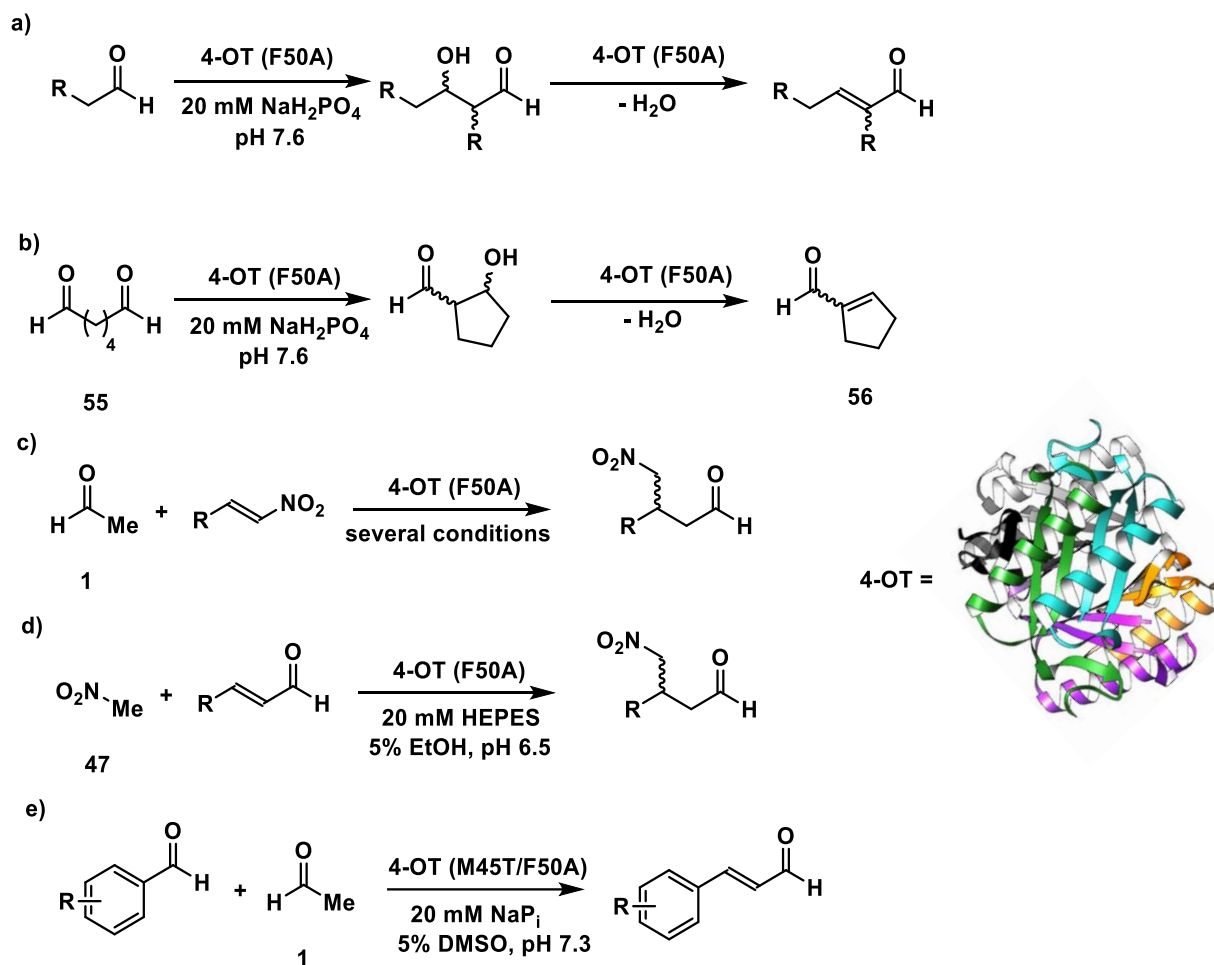


**Scheme 8.** Promiscuity of RA95.5-8 and variants for both iminium and enamine catalysis. Examples of iminium catalysis: **a)** conjugate addition of carbon nucleophiles; **b)** conjugate addition of nitromethane; **c)** Knoevenagel condensations of carbon nucleophiles with  $\alpha,\beta$ -unsaturated aromatic aldehydes and **d)** Henry addition of nitromethane to aromatic aldehydes. Example of enamine catalysis: **e)** conjugate addition of acetone to nitrostyrene.

### 1.2.4 N-terminal proline

In contrast to site-selective modification and *de novo* approaches, native enzymes bearing a catalytically active N-terminal proline can be employed as organocatalytic artificial enzymes. For example, 4-oxalocrotonate tautomerase (4-OT), a hexamer composed of six

homologous monomers bearing an N-terminal proline, was shown to mediate both iminium- and enamine-based organocatalysis.<sup>161</sup> In its natural form the N-terminal proline residue of 4-OT acts as a general base for the tautomerisation of a dienol into an unsaturated ketone.<sup>109, 162, 163</sup> As previously confirmed by mass spectrometry analysis,<sup>164</sup> when a carbonyl substrate interacts with this proline residue, an iminium intermediate is formed, thereby allowing 4-OT to become a promiscuous enzyme for organocatalytic transformations. 4-OT has been employed for enamine-based aldol reactions (**Scheme 9a and b**)<sup>108, 165</sup> and conjugate additions (**Scheme 9c**).<sup>166</sup> Moreover, this organocatalytic artificial enzyme could perform iminium catalysed reactions, such as the conjugate addition of nitromethane (**Scheme 9d**).<sup>167</sup> In a similar way to *de novo* enzymes, computational and experimental strategies were combined to improve 4-OT performances.<sup>168</sup> Eventually, 4-OT variant M45T/F50A was employed as carbonylase for the condensation of aromatic aldehydes with acetaldehyde with high enantioselectivity and in good yield (**Scheme 9e**).<sup>169</sup> Additionally, in the same report, an efficient one-pot two-step chemoenzymatic route for the formation of chiral aromatic 1,3-diols was described.



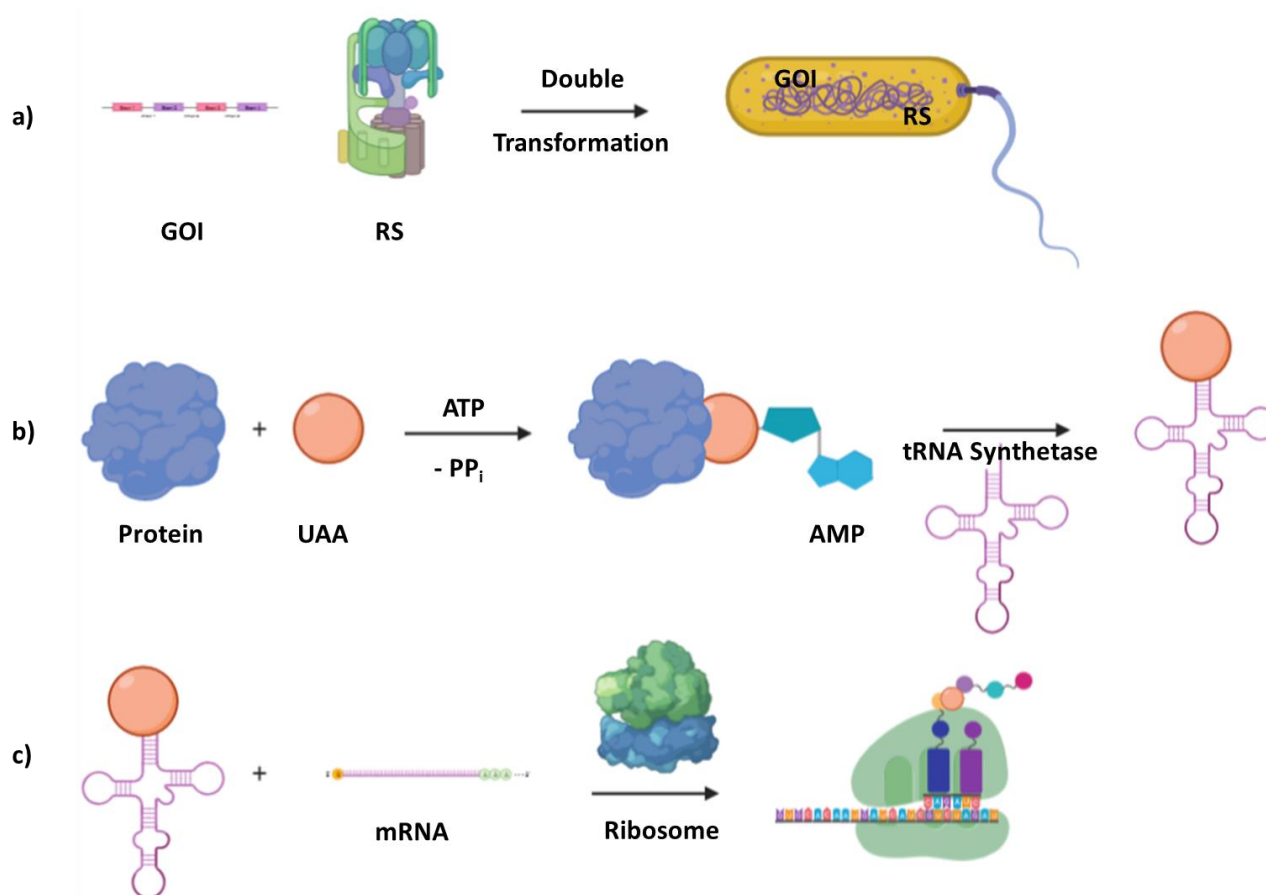
**Scheme 9.** Iminium- and enamine-catalysed reaction performed by 4-OT (PDB: 1OTF): **a)** Intermolecular aldol; **b)** Intramolecular aldol; **c)** Nitro-Michael addition; **d)** Enamine catalysed conjugate addition; **e)** Aldol condensation for aromatic aldehydes.

4-OT and its variants have been used for various applications, including enzymatic<sup>167</sup> and chemoenzymatic cascades,<sup>169, 170</sup> alongside whole cell catalytic systems.<sup>171-173</sup> Pregabalin, an anti-anxiety drug, and three of its derivatives were synthesised by coupling the 4-OT and aldehyde dehydrogenase. Among all different strategies to design organocatalytic artificial enzymes, the N-terminal proline approach is the easiest method to perform a biocompatible organocatalytic reaction. However, the scope of this organocatalytic artificial enzyme is limited to secondary aminocatalysis. Other useful organocatalytic transformations (e.g. thiourea and counterion based catalysis) are unavailable, and thus, other approaches must be employed.



### 1.2.5 Genetic code expansion

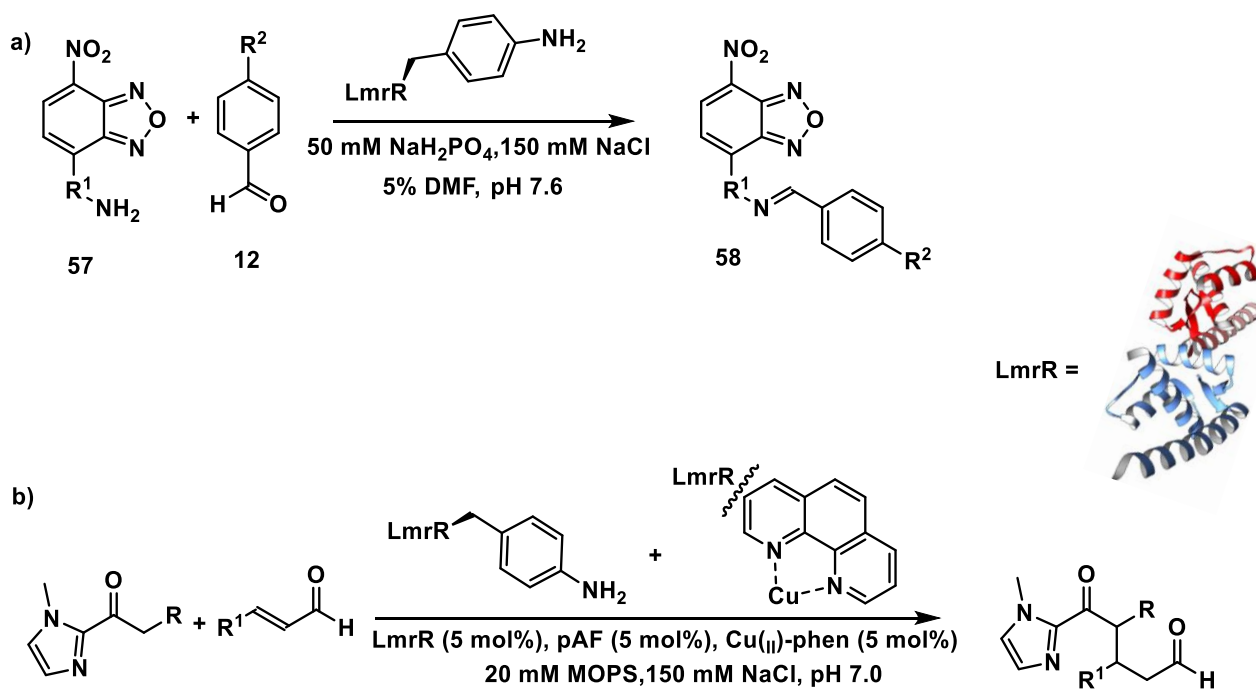
Biocompatible organocatalysis can also be enabled through the employment of genetic code expansion techniques. This methodology allows site-specific incorporation of unnatural amino acids, which can be used as catalysts to mediate organocatalytic reactions. Specifically, orthogonal tRNA synthetase and cognate tRNA employment can aid the incorporation of over 200 unnatural amino acids.<sup>146</sup> Among different choices, wild type and mutant variants of pyrrolysine and tyrosine tRNA synthetases are mostly selected due to their versatility and efficiency.<sup>174</sup> The TAG codon is used by pyrrolysine tRNA synthetase for recognition, whereas the tyrosyl tRNA synthetase necessitates a mutant tRNA able to recognise the TAG stop codon.<sup>175</sup> The incorporation of the unnatural amino acid is achieved by introducing a TAG mutation in a specific gene selected at the position of choice. Thus, the plasmids containing respectively the gene of interest (GOI) and the synthetase (RS) are subject to a double transformation in *E. coli* (**Fig. 12a**). The addition of the unnatural amino acid in the medium allows the synthetase to charge the respective mutant tRNA with it (**Fig. 12b**), thus enabling the full-length translation of the protein with the unnatural amino acid incorporated in the selected position (**Fig. 12c**).



**Figure 12.** The cycle of incorporation of unnatural amino acids by genetic code expansion in *E. coli*. **a)** Double transformation of two plasmids bearing exogenous amino acid tRNA synthetase (RS) and the gene of interest (GOI). **b)** Expression of the tRNA synthetase and addition of the unnatural amino acid (UAA). **c)** Ribosomal translation of the GOI with the unnatural amino acid incorporated site-specifically into the protein.

Genetic code expansion techniques were applied successfully to design both organocatalytic artificial enzymes and metalloenzymes.<sup>118, 122, 176</sup> The multidrug regulator protein LmrR, a dimeric protein isolated from *Lactococcus lactis* was tested for organocatalytic reactions after incorporation of *p*-aminophenylalanine (pAF). This protein contains a hydrophobic pore in the centre, which is favourable for recruiting organic molecules (**Scheme 10a**). The unnatural amino acid pAF was reduced to a catalytically active aniline, as direct incorporation was complicated.<sup>77</sup> The resulting organocatalytic artificial enzyme was tested for hydrazone and oxime formation, including the synthesis of product **58**. Interestingly, when the incorporation was placed at Val15 position, the most promising result was observed due to the appropriate positioning of the pAF inside the hydrophobic pore.<sup>77</sup> A library containing several variants was obtained by directed evolution and screened using a UV-based assay,<sup>118</sup> leading to an evolved variant with additional mutations.

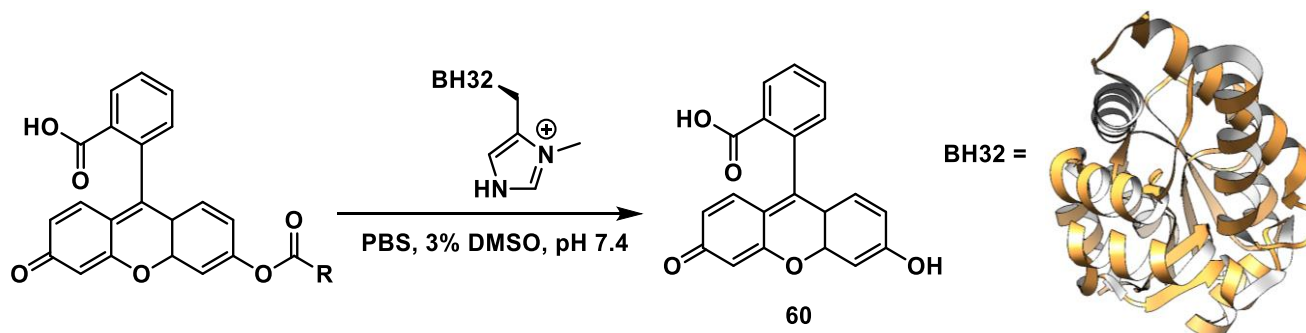
Previously, LmrR scaffold was also employed to create artificial metalloenzymes where an abiotic copper cofactor could act as Lewis acid for enantioselective Friedel–Crafts reactions.<sup>177</sup> Based on this work, LmrR was used to create an artificial enzyme with a second catalytic moiety. This innovative design consisted of the dual synergistic action of a pAF residue (genetically incorporated) and a supramolecular bound Lewis acidic Cu(II) complex.<sup>178</sup> This novel artificial enzyme was tested for Michael additions of imidazole-based ketones to  $\alpha,\beta$ -unsaturated aldehydes (**Scheme 10b**). Both catalysts were located within the hydrophobic cavity of the dimer interface of LmrR, where the pAF residue was responsible for the activation of the enal and Cu(II)-phen complex for the generating the enolate nucleophile. Among the several variants tested, LmrR\_V15pAF\_M8L+ Cu(II)-phen showed the best result with activity from good to excellent and optical purity (up to 99% ee).<sup>178</sup>



**Scheme 10.** a) Hydrazone and oxime ligation performed by p-amino phenylalanine incorporated onto LmrR (PDB: 3F8B). b) Michael addition using a novel dual catalyst within LmrR.

Genetic code incorporation was also applied to *de novo* designed enzyme BH32. Initially created to enable Morita-Baylis-Hillman reaction,<sup>160</sup> this organocatalytic artificial enzyme was recently reconverted into a hydrolase through the combined use of genetic code expansion and laboratory evolution.<sup>179</sup> In particular, replacement of the catalytic His23 with the unnatural amino acid methyl-histidine (Me-His) was achieved by an evolved variant of the pyrrolysine

tRNA synthetase and its cognate tRNA (**Scheme 11**). A 96-well plate fluorescence-based assay was employed to assess variants activity for ester hydrolysis to yield fluorescein (**11**).



**Scheme 11.** Ester hydrolysis performed by BH32 (PDB: 6Q7N) with the unnatural amino acid Me-His produces fluorescein (**60**).

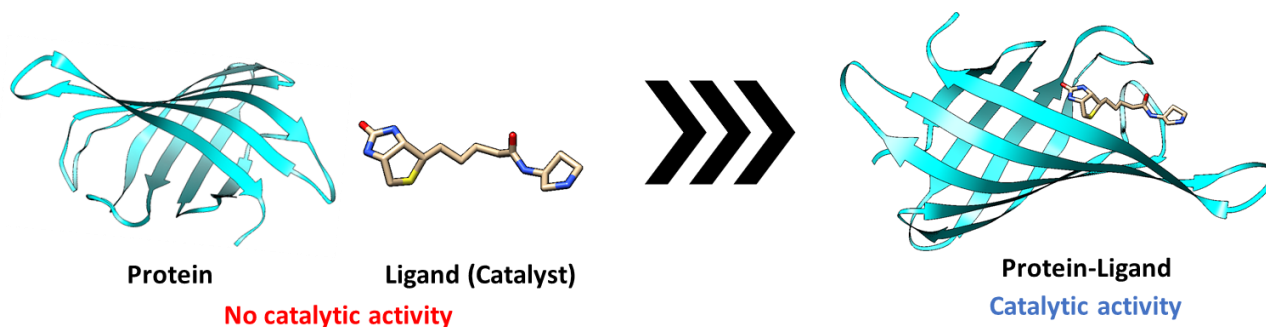
Techniques of genetic code expansion are a promising strategy to enable biocompatible organocatalysis. Incorporating a wide variety of unnatural amino acids *in vivo* can allow laboratory evolution similar to the one observed in natural enzymes. Consequently, an organocatalytic artificial enzyme created by genetic code expansion could be potentially employed for whole cell catalysis or synthetic biological pathways. However, incorporation efficiency is still limited to the type of amino acid used. Exogenous tRNA synthetases can be subject to evolution to increase their efficiency in incorporating new unnatural amino acids.<sup>180</sup> The selection process of an appropriate protein that embraces the unnatural amino acid also needs to be considered accurately. Both the examples presented herein, LmrR and BH32, were used for artificial enzyme design (LmrR for artificial metallo-enzymes and BH32 computationally designed for carbon-carbon bond forming transformations),<sup>122</sup> showing great potential for enabling biocompatible organocatalysis. At the time of writing, genetic code expansion holds great promises to become very popular for enzyme design in future.

## 1.2.6 Protein as supramolecular host

### 1.2.6.1 Introduction

Eventually, protein can be used as a supramolecular host to design organocatalytic artificial enzymes. This approach lays its basis on the non-covalent, but strong protein-ligand interactions. The design of these systems is based on the linkage between a catalytic moiety covalently attached to a portion of a ligand which is only weakly involved in protein binding

and introduced to the protein partner. The resulting protein-ligand complex is converted into a potential catalytic assembly (**Fig. 13**).



**Figure 13.** Linking a catalytically competent moiety to a ligand and insertion into a protein host to create a protein-catalyst assembly.

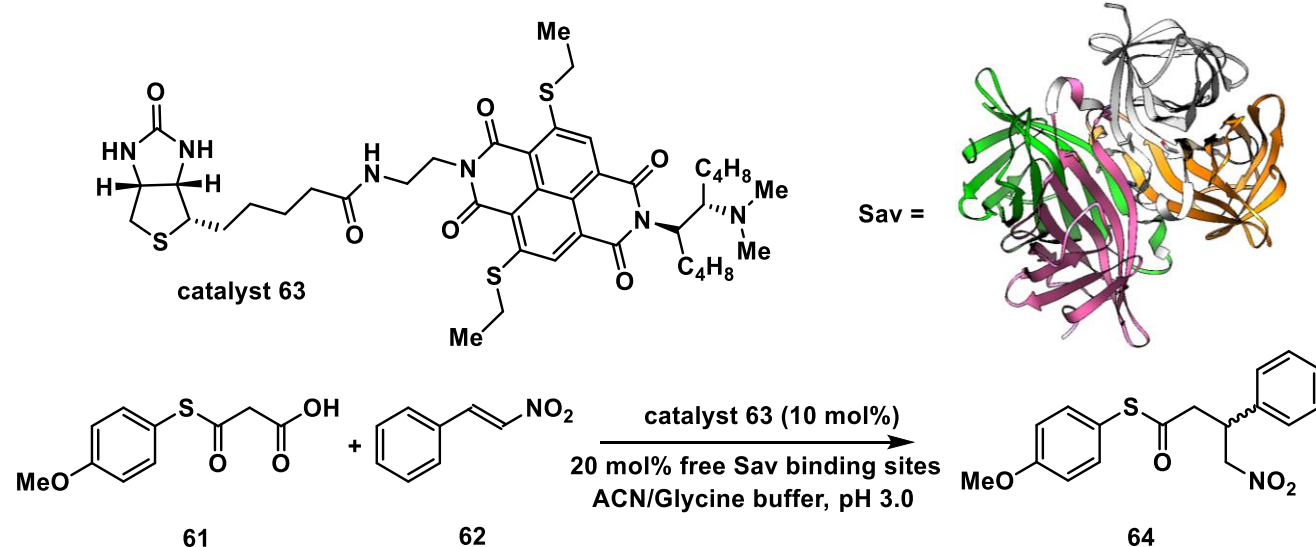
Generally, the modified ligands containing the catalytically active motif are prepared using one- or two-step procedures involving simple synthetic protocols, for example, amide bond coupling and click chemistry.<sup>106, 110, 181-184</sup> This approach allows screening a wide variety of catalysts for a broad range of chemical reactions within a limited amount of time. Moreover, modification of the protein hosts can be achieved through rational design or laboratory evolution.<sup>120, 121, 185-187</sup> To this extent, the supramolecular approach bears many advantages and can be seen as an essential technique to create artificial enzymes. The design of supramolecular complex for chemical catalysis relies on strong protein-ligand interactions with dissociation constants ( $K_d$ ) ranging from low  $\mu\text{M}$  to pM.<sup>181-183, 188</sup> Importantly, ligands tend to be functionalised only in the portion of molecule with few interactions with the protein host and this process should cause minimal effects on the protein-ligand binding. A well-known supramolecular assembly for chemical catalysis is the (strept)avidin (Sav) and biotin binding system. This complex possesses one of the most robust non-covalent interactions with an estimated  $K_d$  value of  $10^{-14}$  M.<sup>188</sup> Early reports focusing on the design of streptavidin-based artificial metalloenzymes were described in the late 1970s, where the valeric motif of biotin was functionalised with a rhodium catalyst and tested for asymmetric hydrogenations.<sup>189</sup> Later, several streptavidin-based artificial metallo-enzymes using iridium, rhodium, ruthenium and palladium catalysts were reported.<sup>106, 120, 181, 184, 185, 190, 191</sup> Similarly, different protein hosts and ligand-catalyst conjugates were described,<sup>182, 183, 192-199</sup> including siderophore binding protein-iron assemblies ( $K_d \approx 10^{-9}$  M)<sup>182</sup> and LmrR variants possessing strong affinity towards  $\pi$ -system ligands ( $K_d \approx 10^{-6}$  M).<sup>192</sup> Based on the artificial metallo-enzyme design,<sup>200, 201</sup> two

organocatalytic artificial enzymes operating using different mechanisms were designed via the supramolecular approach.

### 1.2.6.2 Anion- $\pi$ -catalysts

Anion- $\pi$ -catalysis is one of the most innovative and exciting strategies to perform organocatalysis within a protein host.<sup>89, 202-207</sup> Specifically, Matile and co-workers demonstrated that molecules possessing a positive quadrupole moment, such as naphthalenediimides, could stabilise anion intermediates formed during conjugate additions by  $\pi$ -acidic interactions. This stabilisation was proved to be useful for decarboxylative conjugate additions of **61** to **62** (**Scheme 12**). Although natural aromatic amino acids are  $\pi$ -basic and can interact with cations, the streptavidin-biotin technology was demonstrated to be useful for the creation of organocatalytic artificial enzymes driven by anion- $\pi$  catalysis.<sup>107,</sup>

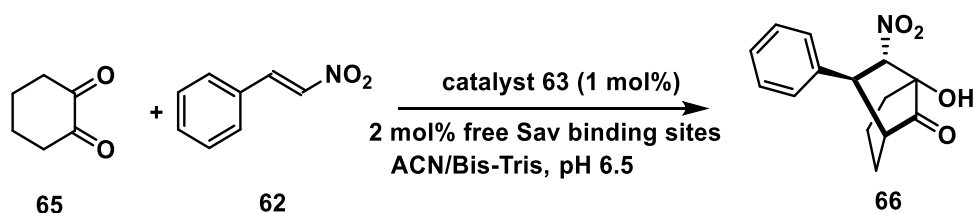
208



**Scheme 12.** Decarboxylative Michael addition reaction catalysed by **63** within S112Y (Sav cartoon from PDB: 6GH7) mutant streptavidin.

Interestingly, a combination of chemical and genetic screening aided the development of anion- $\pi$  catalysis. After screening a library of five bifunctional catalytic moieties attached to biotin, their ability to catalyse a decarboxylative alkylation between compound **61** and **62** was investigated.<sup>107</sup> All the catalysts tested contain both an NDI moiety, necessary for providing the  $\pi$ -acidic surface to stabilise the enolate intermediate, and tertiary amine, which acts as a

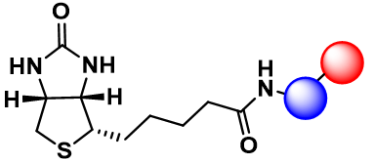
base and localises the enolate intermediate over the NDI moiety due to a short dimethylene bridge.<sup>209</sup> Among all the biotinylated catalysts tested, compound **63** was the most reactive and screened using a library of 20 streptavidin variants. Streptavidin variant S112Y, in combination with **63**, was found to lead to a selective formation of product **64**. Streptavidin-based systems for anion- $\pi$  catalysis were also tested for a biorthogonal domino-Michael-aldol reaction between diketone **65** and **62** (**Scheme 18**).<sup>208</sup> Using a range of catalyst loadings varying from 1 to 5 mol% and screening four different streptavidin variants, the bicyclic product **106** was obtained in moderate yields and enantioselectivities with significant diastereoselectivity. Interestingly, the protein-ligand complex showed inversion of stereoselectivity when compared to the biotin-catalyst conjugate.

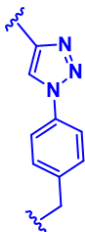
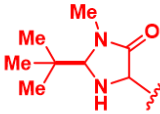

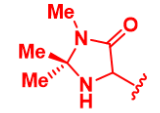
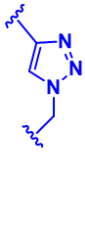
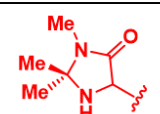
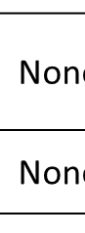
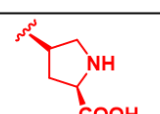
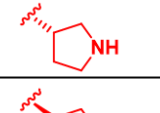
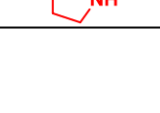
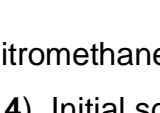
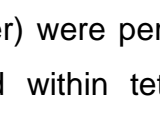


**Scheme 13.** Domino-Michael-Aldol-reaction catalysed by Sav:**63** assembly.

### 1.2.6.3 Tetrameric streptavidin as host

Our research group recently created one of the first secondary amine-based organocatalytic artificial enzyme using the streptavidin-biotin technology. A series of seven biotinylated secondary amines (ligands **67-74**) were prepared using either copper-catalysed azide-alkyne cycloaddition or amide bond coupling reactions.<sup>110</sup> These catalysts were inspired by three different categories of organocatalysts: MacMillan-like imidazolidinones, prolines and pyrrolidines (**Fig. 14**).

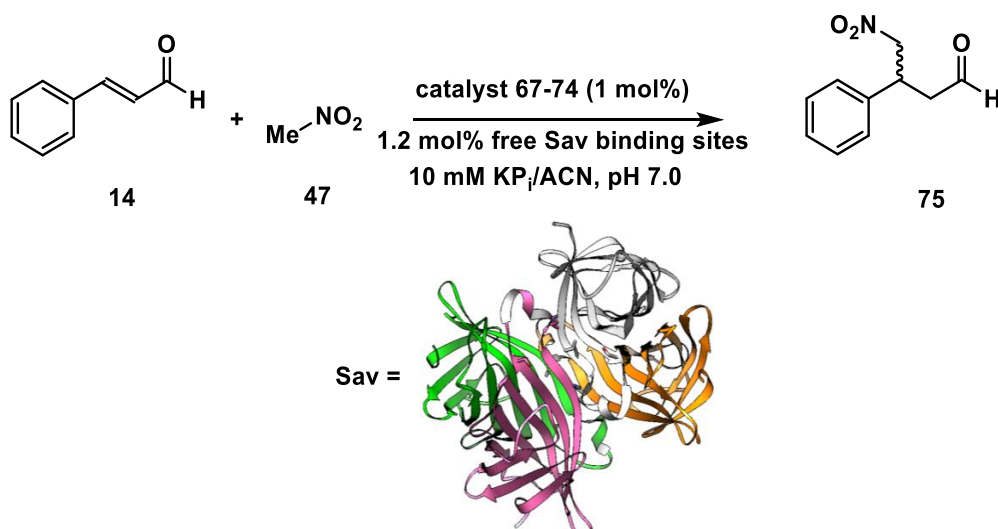


Compound	Spacer	Catalyst
67		
68		
69		
70		
71		
72	None	
73	None	
74	None	

**Figure 14.** Series of biotinylated catalysts **67-74** created by Luk's group.

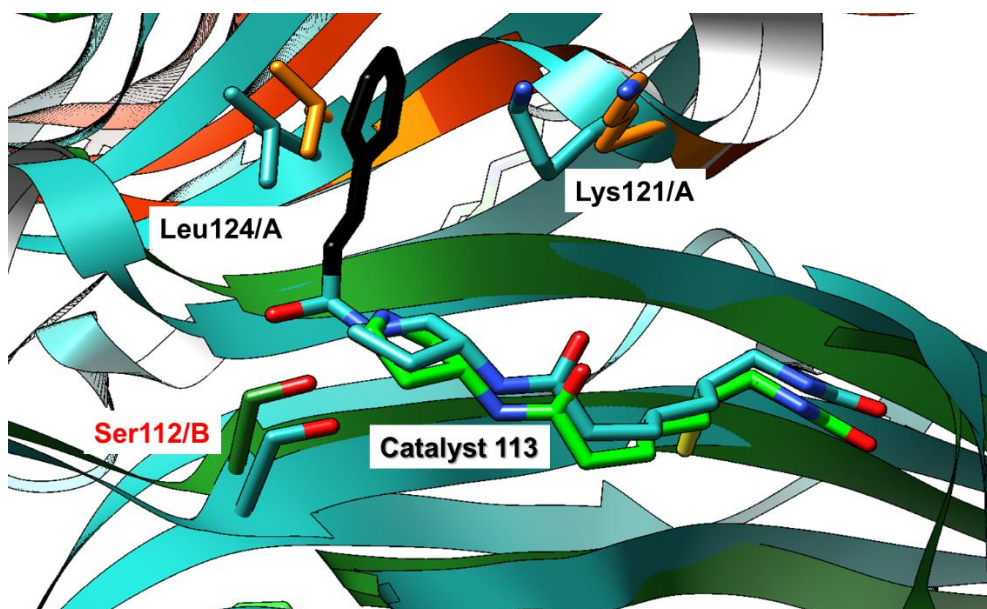
These biotinylated derivatives were screened for 1,4-Michael addition of nitromethane (**47**) to aromatic  $\alpha,\beta$ -unsaturated aldehydes, including compound **14** (**Scheme 14**). Initial screening reactions using both catalysts **73** (*R* enantiomer) and **74** (*S* enantiomer) were performed, showing no enantioselectivity. Once these ligands were introduced within tetrameric streptavidin, they were found capable of catalysing the model reaction with high conversion and stereoselectivity.<sup>110</sup> Interestingly, moderate to good yields (37-80%) were observed using only 1 mol% of protein catalyst and a mixture of 1:1 MeOH/KP<sub>i</sub> buffer as a reaction medium. In this case, Sav-based organocatalysts showed tolerance up to 50% to organic solvents, including ethyl acetate and acetonitrile. The two Sav-organocatalyst complexes, from here described as Sav:**73** and Sav:**74**, differed by only one chiral centre, but their stereoselectivity was opposite, with the former favouring for the *S* enantiomer and latter for the *R* enantiomer.





**Scheme 14.** 1,4-Michael addition reactions catalysed by **67-74** within a recombinant Sav (PDB: 6GH7).

Combined crystallographic and computational structural studies were employed to identify the secondary amine moiety within the Sav scaffold, which was located to be in proximity to Ser112<sub>B</sub>. Both lysine and leucine residues located at the dimer interface (Lys121<sub>A/B</sub> and Leu124<sub>A/B</sub>) were recognised to dictate the face for which the intermediate was exposed for nucleophilic addition, thereby dictating both regio- (1,2 vs 1,4-addition) and enantioselectivity (*R* and *S*) of the reaction (**Fig. 15**).<sup>110</sup>

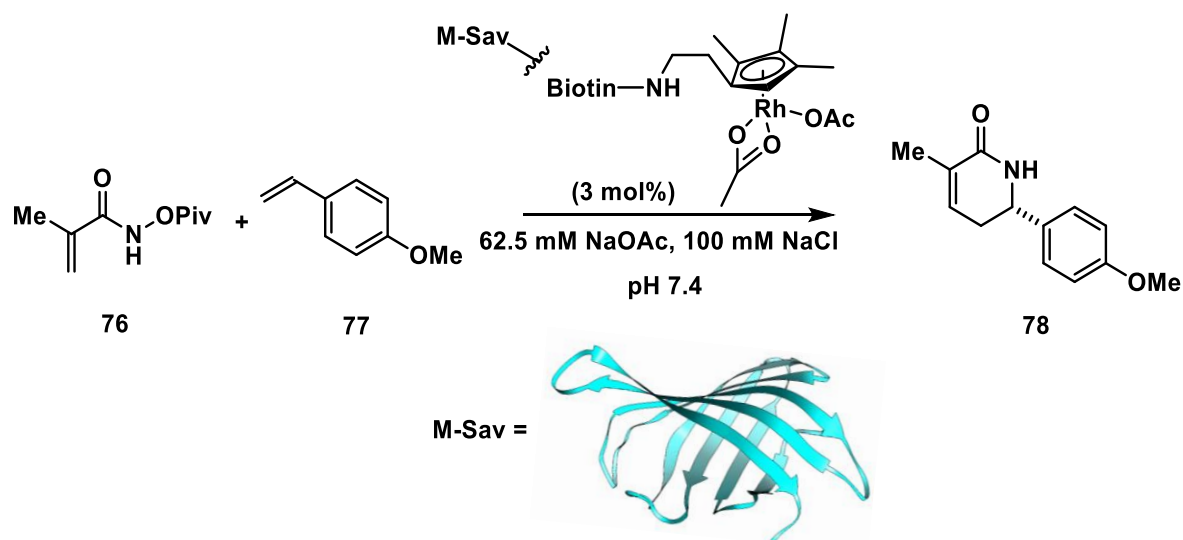


**Figure 15.** Overview of the biotin binding site of Sav:73 in the crystal structure (green) and as aminol adduct with cinnamaldehyde obtained from QM/MM simulations (light blue).

The supramolecular approach applied for anion- $\pi$ , and secondary amine-based artificial enzymes exhibited some notable advantages. However, the conditions of reactions need to be optimised to achieve full biocompatibility, as acidic conditions (pH 3.0) or a large volume of organic co-solvents are required (though the latter was mostly due to the use of a substrate with low solubility in aqueous environments).<sup>9</sup> Moreover, these non-covalent assemblies' activity is still subject to improvement, and laboratory evolution techniques were shown to be effective.<sup>120, 121, 185, 186</sup> Though being a reliable and robust system, issues related to the symmetry of the intersubunit interface of Sav was only recently addressed by the creation of "dimeric" Sav.<sup>210</sup> This "dimeric" Sav variant will facilitate mechanistic studies and the design of tailored and asymmetric scaffolds for chemical catalysis. In addition to the streptavidin-biotin technology, other protein-ligand systems should be used for novel protein-based organocatalytic enzymes, including the siderophore binding proteins<sup>182</sup> or coumarin binding albumins.<sup>211</sup>

#### 1.2.6.4 Monomeric streptavidin as host

The streptavidin-biotin technology was also employed to create artificial enzymes using a monomeric version of streptavidin (M-Sav) with high biotin affinity.<sup>181</sup> This engineered highly stable variant was created by rational design to overcome the lack of *in vivo* applications of a streptavidin monomer.<sup>212</sup> M-Sav was successfully applied to detect biotinylated ligands without target aggregation,<sup>213</sup> in fluorescent labelling,<sup>214</sup> structural studies on biotin-streptavidin affinity,<sup>215</sup> flow cytometry and ELISA.<sup>216</sup> Importantly, Rovis and co-worker exploited M-Sav for enantioselective catalysis using a rhodium-based biotinylated catalyst to achieve the asymmetric  $\delta$ -lactam synthesis (**Scheme 15**).<sup>181</sup>

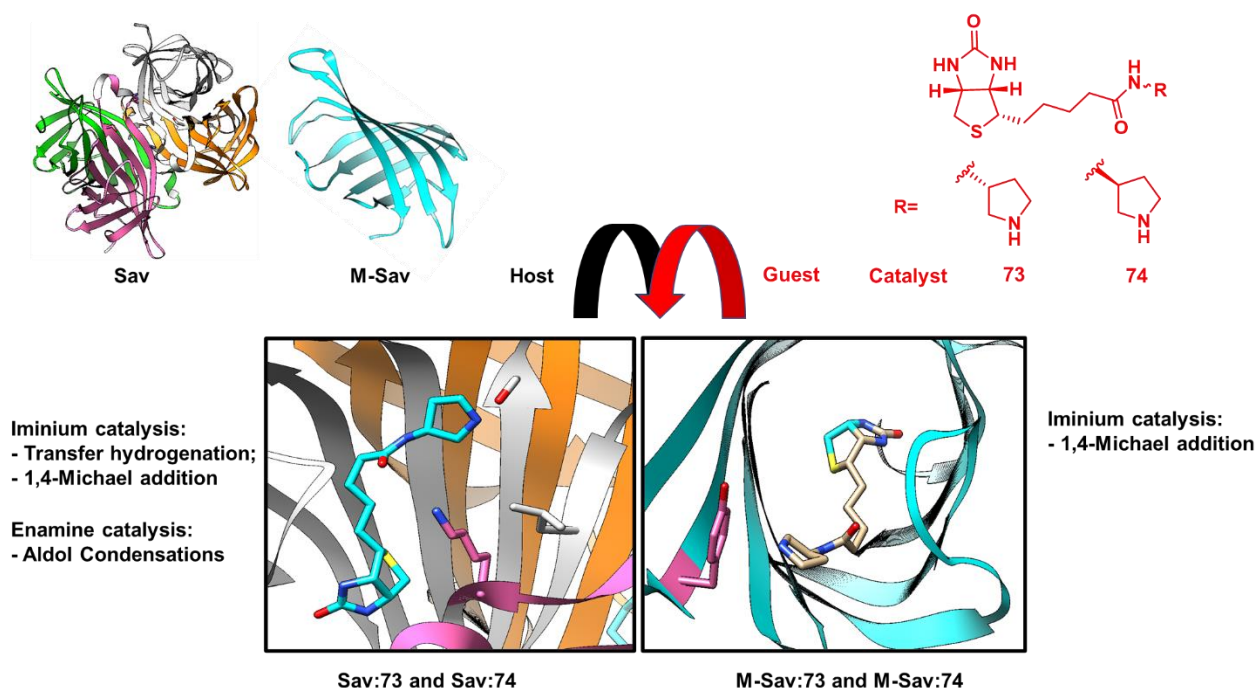


**Scheme 15.** Tandem C-H activation and [4+2] annulation reaction catalysed by wt M-Sav: Cp\*biotinRhCl.

In this report, the synthesis of  $\alpha,\beta$ -unsaturated- $\delta$ -lactams via a tandem C-H activation and [4+2] annulation reaction was described for 24 examples in yields as high as 99% and *ee* 97% under aqueous conditions at room temperature. Interestingly, the complex formed by M-Sav and the rhodium catalyst outperformed its well-known tetrameric version and the cofactor alone by 11–33 times. Moreover,  $\alpha,\beta$ -unsaturated- $\delta$ -lactams could be readily functionalised to achieve enantioenriched piperidines, which are common heterocycles found in pharmaceutically active compounds. This report laid the basis for the application of monomeric streptavidin as host for biocompatible organocatalysis.

### 1.3 Aim of the project

This work aims to create a family of streptavidin-based artificial enzymes able to mediate organocatalysis in a biocompatible environment. Inspired by previous work in our group,<sup>110</sup> the streptavidin-biotin technology was used to design organocatalytic artificial enzymes for iminium and enamine catalysis. In particular, two different proteins, tetrameric streptavidin (Sav) and its monomeric variant (M-Sav) were tested as hosts using the biotinylated organocatalyst **73** and **74** as ligands (**Fig. 16**). Subsequently, the goal was to examine (M-)Sav:**73** and (M-)Sav:**74** reaction profile, exploring transformations beyond the previously reported nitromethane addition.<sup>110</sup>



**Figure 16.** Creation of organocatalytic enzymes using a supramolecular approach.

The reactions of transfer hydrogenation (via iminium catalysis) and aldol condensations (via enamine catalysis) presented herein aim to set proof of concept for enabling biocompatible organocatalysis within an artificial enzyme. Furthermore, a thorough work to optimise the protein scaffolds was carried out to design artificial enzymes with improved activity and selectivity.

## Chapter 2: Monomeric streptavidin as host for iminium catalysis

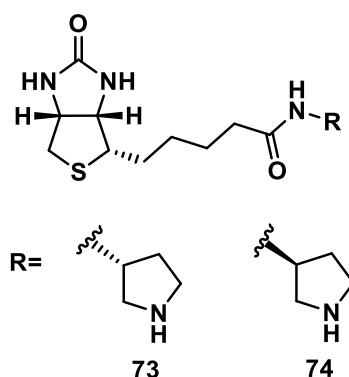
### 2.1 Introduction

Compared to other host-ligand combinations,<sup>105, 127, 178, 182, 189, 217-221</sup> the strept(avidin)-biotin technology still holds exceptional advantages.<sup>213</sup> In particular, two main features are essential to design artificial enzymes. First, the robust and specific non-covalent interaction between the strept(avidin) family proteins and biotin is crucial for incorporating synthetic catalysts.<sup>213</sup> Second, biotin's valeric acid motif can be conjugated with different molecules without altering the target molecule function (*i.e.* a catalyst) or disrupting any biological processes.<sup>213</sup> These unique characteristics facilitate diverse applications of the streptavidin-biotin technology in biology and chemistry.<sup>181, 213, 222-225</sup>

Regardless of the versatility of this strategy, other biotin-binding proteins can be employed to host biotinylated catalysts, including the monomeric and dimeric Sav.<sup>181, 210</sup> In an attempt to improve the reactivity of Sav-based artificial metalloenzymes for hosting a rhodium-catalysed asymmetric  $\delta$ -lactam synthesis (**Scheme 15**, see section 1.2.6.4),<sup>181</sup> a highly stable monomeric streptavidin variant (M-Sav) was used. M-Sav is an engineered hybrid of both rhizavidin and streptavidin with ability to bind biotin tightly ( $K_d \approx 10^{-9}$  M) and can be an appealing candidate for the generation of organocatalytic artificial enzymes.<sup>226</sup> This variant possesses an accessible active site, which can help the organocatalytic assembly tuning and analysis.<sup>181</sup> Monomeric streptavidin can be expressed as a stable and pure monomer without aggregating or forming tetramers (being a monomer does not cross-link the ligand).<sup>212, 215, 216, 227, 228</sup> More importantly, the lack of additional subunits in M-Sav can serve as a tool to understand whether subunit-subunit interactions are required to enable chemical catalysis in Sav-based artificial enzymes.<sup>229</sup> To this extent, we reasoned that monomeric streptavidin could serve as a host to create novel organocatalytic enzymes.

Previous work illustrated that iminium catalysis could be hosted within Sav.<sup>110</sup> In this chapter, the role of iminium catalysis using the more exposed monomeric scaffold was evaluated and compared to the results obtained using Sav:**73** assembly. Based on the previous assessment

obtained using Sav as host,<sup>110</sup> catalysts **73** and **74** were selected as ligands to be tethered to the protein core (**Fig. 17**).

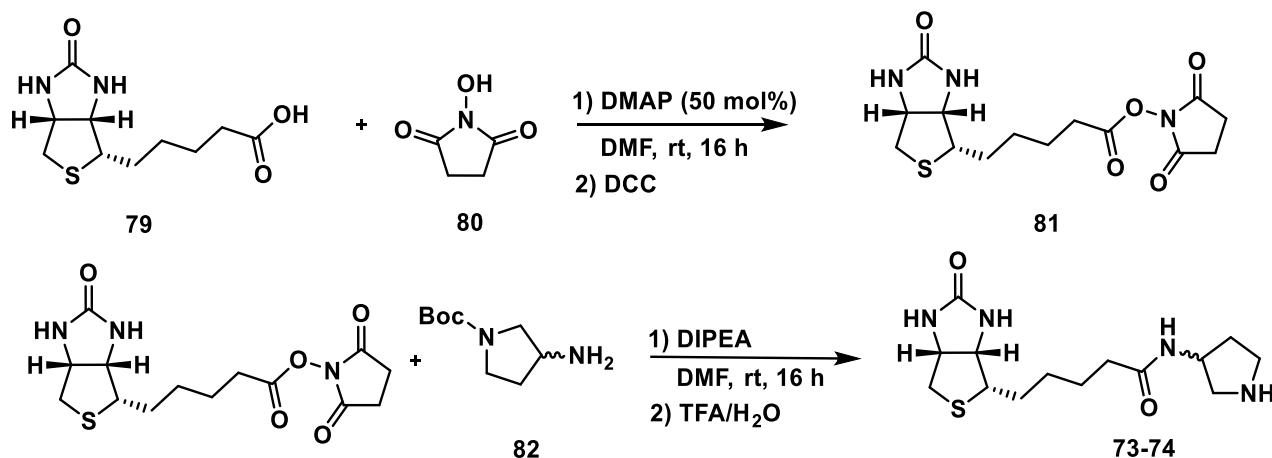


**Figure 17.** Biotinylated organocatalysts **73** and **74**.

The M-Sav-based organocatalytic artificial enzymes were created in two steps. Initially, the biotinylated organocatalysts **73** and **74** were chemically synthesised (see section 2.2). Then, the recombinant protein was expressed using a bacterial host, unfolded in denaturing conditions to facilitate the process of purification, and refolded in the presence of the two organocatalysts to generate M-Sav:**73** and M-Sav:**74** assemblies (see section 2.3). The incorporation of the guest into the host was verified by circular dichroism (CD). Also, the artificial enzymes' stability to temperature and the organic solvent was determined by using the same methodology (see section 2.4). The newly formed complexes M-Sav:**73** and M-Sav:**74** were tested for chemical catalysis, and a 1,4-Michael addition reaction was selected as a model reaction (see section 2.5). Eventually, by analysing M-Sav:**74** crystal structure (see section 2.6), previously obtained in our group, a series of point mutations on the protein scaffold were designed to improve the reactivity of the organocatalytic artificial enzyme and tested (see section 2.7).

## 2.2 Synthesis of organocatalysts **73** and **74**

The biotinylated organocatalysts **73** and **74** carrying a simple pyrrolidine motif linked to the valeric moiety of biotin were synthesised in a two-step procedure (**Scheme 16**).<sup>110</sup>



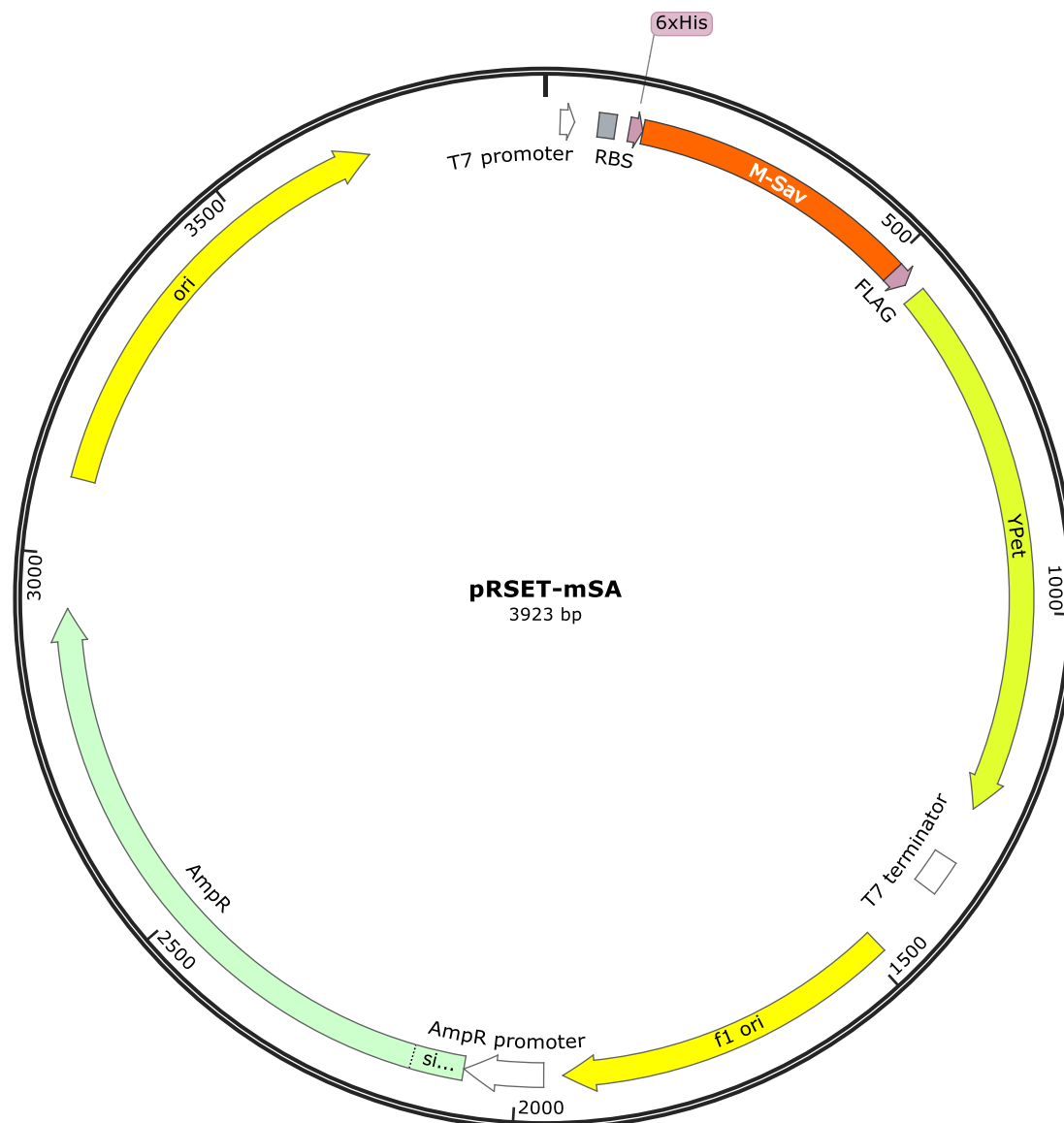
**Scheme 16.** Synthesis of biotinylated organocatalysts **73-74**.

The synthetic pathway started with a coupling reaction between the commercially available D-biotin (**79**) and *N*-hydroxy succinimide (**80**) using a catalytic amount of 4-dimethylamino pyridine (DMAP) and the coupling reagent *N,N*-Dicyclohexylcarbodiimide (DCC) to produce the activated ester **81**. Successively, the appropriate BOC-protected pyrrolidine derivative (*R/S*-**82**) was added to compound **81** in the presence of *N,N*-diisopropylethylamine (DIPEA). Further deprotection of the secondary amine using a 95:5 TFA:H<sub>2</sub>O mixture lead to biotinylated organocatalysts **73** and **74**. The structural assessment and the final purity were confirmed by <sup>1</sup>H- and <sup>13</sup>C-NMR spectroscopy and high-resolution mass spectrometry (HRMS).

### 2.3 Expression and purification of M-Sav

The second stage of creating M-Sav-based organocatalytic artificial enzymes focused on the expression and purification of the protein host. The *M-Sav* gene was expressed using an *Escherichia coli* (*E. coli*) system. The plasmid containing *M-Sav* was obtained as a gift from Sheldon Park's group (**Fig. 18**, pRSET-mSA, <http://n2t.net/addgene:39860>, RRID: Addgene\_39860),<sup>227</sup> and has the following amino acid sequence:

```
GSSHHHHHSQDLASAEAGITGTWYNQSGSTFTVTAGADGNLTGQYEN
RAQGTGCQNSPYTLTGRYNGTKLEWRVEWNNSTENCHSRTEWRGQYQG
GAEARINTQWNLTYEGLGSGPATEQGQDTFTKVKPSAASGSDYKDDDDK
```



**Figure 18.** pRSET-mSA plasmid.

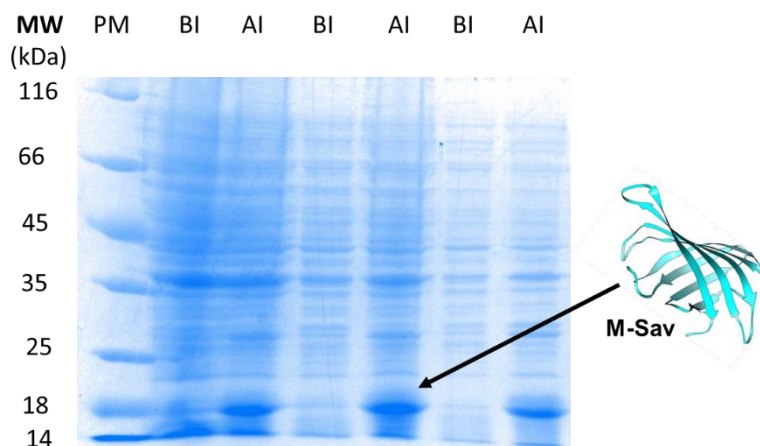
M-Sav has sequence similarities of both Sav (sequence identity of 55%, 67/75 amino acids) and rhizavidin (sequence identity of 57%, 67/115 amino acids).<sup>227</sup> The pRSET-mSA plasmid shows that both M-Sav and yellow fluorescent protein (YPet, 25 kDa) are delineated between the T7 promoter and T7 terminator regions, placing the expression of these two proteins under the direct control of the T7RNA polymerase. Moreover, considering the ampicillin resistance site (AmpR), a set working-concentration of 100  $\mu\text{g}/\text{mL}$  of ampicillin was added in all the cultures to exploit selective microbial resistance. Furthermore, the *M-Sav* gene encodes for a hexahistidine (6xHis) tag at the N terminal part of the backbone, to allow a selective purification of the protein by  $\text{Ni}^{2+}$ -NTA column and, a C-FLAG tag at the C terminal



side of the backbone, which could also aid M-Sav solubilisation in the early purification stages.<sup>227</sup>

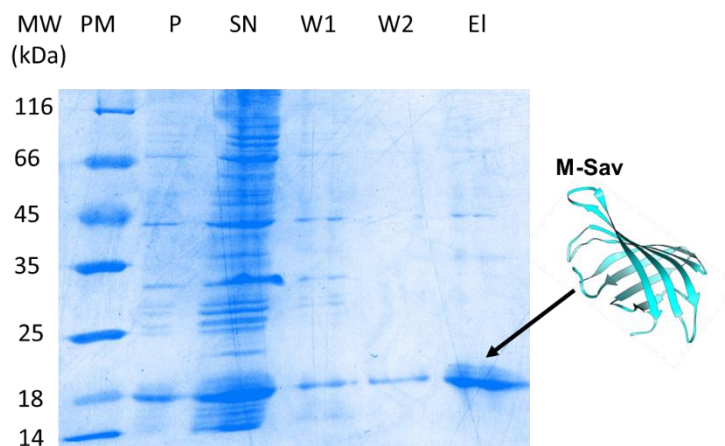
Initial attempts to transform *M-Sav* plasmid into a bacterial host were made using calcium competent BL21(DE3) pLysS cells. This bacterial strain was selected for its ability to allow high expression of proteins from any gene controlled by a T7 promoter and containing a ribosome binding site. Moreover, the pLysS plasmid carries the gene encoding for the T7 lysozyme, which lower the background expression level of target genes influenced by the T7 promoter. Simultaneously, it is not interfering with the level of expression achieved following induction by IPTG.<sup>230</sup> However, this strategy was not successful probably due to the toxicity of M-Sav for the host cells. Similar to all the variants deriving from (strept)avidin family, M-Sav possesses high affinity to biotin and can cause toxicity to cells after sequestering biotin from the cell environment.

In another approach, calcium competent BL21 AI cells, which are specifically designed for applications that require tight regulation and strong expression of toxic proteins, were tried for the expression. BL21 AI strains contain a chromosomal insertion of a gene encoding T7 RNA polymerase (T7RNAP) into the *araB* locus of the *araBAD* operon, placing T7 RNAP under the control of the L-arabinose-inducible *araBAD* promoter. Thus, BL21 AI can be helpful for the expression of genes that are toxic to other BL21 strains (such as BL21(DE3) pLysS).<sup>231</sup> *M-Sav* plasmid was transformed into these cells and grown at 37 °C for 16 h on LB agar plates containing a concentration of 100 µg/mL of ampicillin. After preparation and inoculation of the starter culture into a 1 L of LB medium containing 100 µg/mL ampicillin, the expression was carried out at 37 °C and 225 rpm to an OD<sub>600</sub> of 0.8–1.0 and induced with a final concentration of 0.5% w/v L-Arabinose. After growing the culture overnight at 200 rpm and 20 °C, the bacterial pellet harvested revealed expression of M-Sav as illustrated by SDS-PAGE analysis (**Fig. 19**, 15% w/v). Interestingly, the M-Sav band was observed around 18 kDa, which is different from the 15.7 kDa expected. This small difference can be attributed to the M-Sav charge state, which can create some interference when the protein is run in the SDS-PAGE.<sup>212</sup>



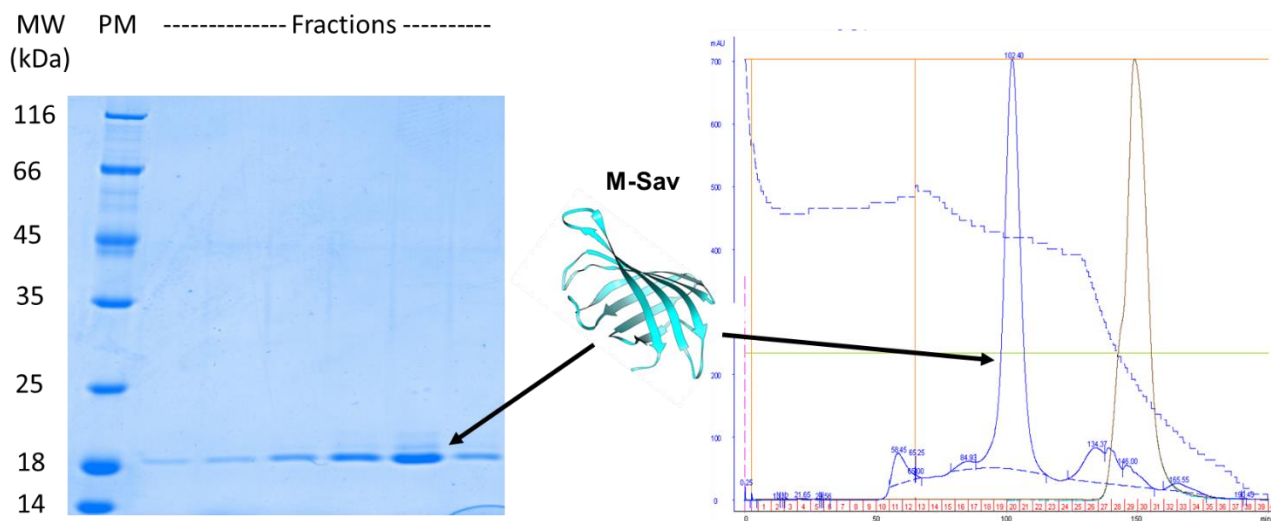
**Figure 19.** 15% w/v SDS-PAGE after expression showing M-Sav band around 18 kDa. MW= Molecular weight; PM= Protein Marker; BI= Before Induction; AI= After Induction.

Once the protein was successfully expressed, M-Sav was purified from other impurities under denaturing conditions. High concentrations of chaotropic agents, such as guanidium hydrochloride (GdnHCl) or urea, were added to disrupt the hydrophobic protein interactions, facilitating the loss of tertiary structure and the consequent solubilisation of most of the protein in the lysis buffer. Moreover, denaturation is also necessary to disrupt the biotin-Sav interaction, thereby removing all the biotin. Thus, the cell pellets were dissolved in a lysis buffer containing 6 M GdnHCl as a denaturing agent. As for the other buffer employed in this purification process, the pH of the solution was adjusted to 8.0. The lysis step was followed by sonication and centrifugation stages, where the soluble fraction, containing M-Sav, was filtered in a 0.22  $\mu\text{m}$  filter and incubated in a column containing a resin of  $\text{Ni}^{2+}$ -NTA on a bed of agarose beads for several h. The protein was then separated from other impurities through  $\text{Ni}^{2+}$ -NTA affinity to the 6xHis tag encoded in the *M-Sav* gene and eluted using a buffer with a high concentration of imidazole to displace the histidine-Ni interaction. The collected fractions were run on SDS-PAGE gel (**Fig. 20**).



**Figure 20.** M-Sav before and after Ni-column. MW= Molecular weight; PM= Protein Marker; P= Pellet; SN= Supernatant; W1 Wash 1; W2 Wash 2; EI= Elution.

The fractions carrying M-Sav were added drop by drop to an ice-cold refolding buffer containing the appropriate ligand (biotin or catalyst **73/74**) to reduce the GdnHCl concentration from 6 M to 1 M and allow the protein to recover the correct folding. At this stage, the organocatalytic artificial enzymes M-Sav:**73** and M-Sav:**74** were generated and were subject to a further round of purification using size exclusion chromatography (SEC) to remove imidazole and other impurities. This chromatographic technique discriminates proteins based on their molecular weight after being eluted into a resin having pores of different dimensions. Fractions containing M-Sav:ligand complex were subject to SDS-PAGE analysis (**Fig. 21**) to assess a final purity of more than 95%. M-Sav was assessed to be stable in aqueous solution, and it was stored at 4°C for several weeks without noticing aggregation or losing function (based on activity tests).<sup>227</sup>



**Figure 21.** M-Sav:ligand complex after size exclusion chromatography. MW= Molecular weight; PM= Protein Marker.

M-Sav expected molecular weight of 15730 kDa and purity were confirmed by HRMS (see 6.2.2.3). The non-covalent linkage between either biotin or biotinylated organocatalysts **73** and **74** could not be confirmed by HRMS and was subject to further analysis.

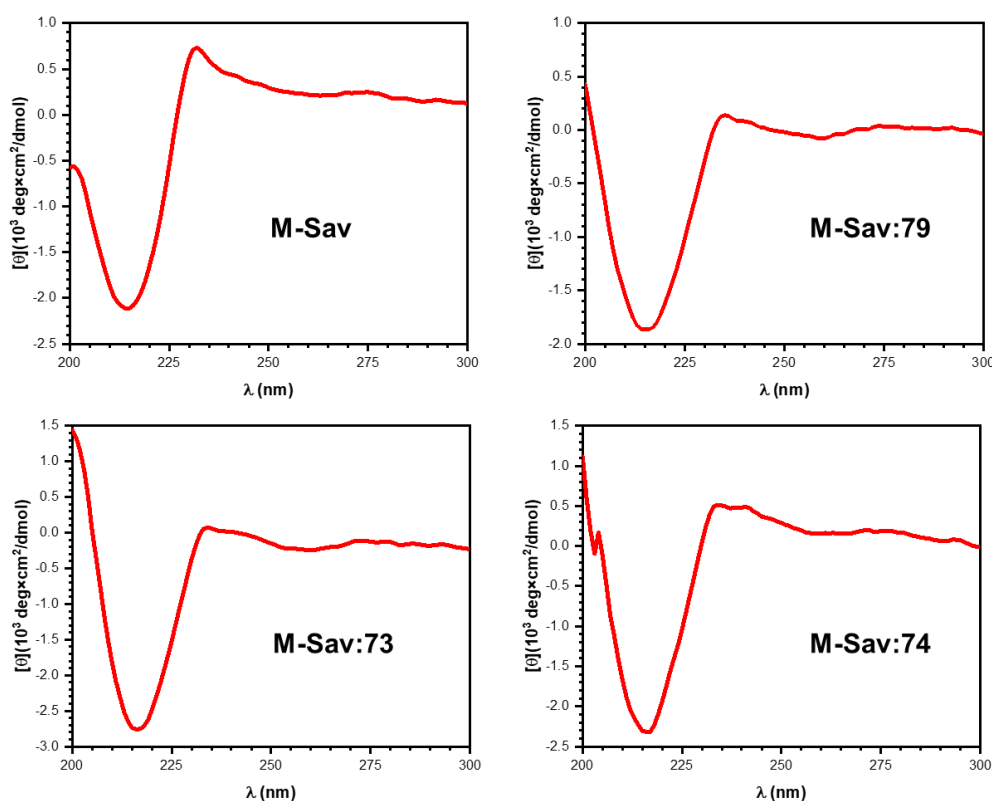
## 2.4 M-Sav:73 and M-Sav:74 stability

The formation of the organocatalytic artificial enzymes M-Sav:**73** and M-Sav:**74** was assessed using circular dichroism spectroscopy. This technique is based on the different absorption of left- and right-handed light (circularly polarised light) by optically active mediums or molecules. In the specific case of proteins or protein-based complexes, one can detect the temperature at which 50% of the protein is unfolded, the so-called melting temperature ( $T_m$ ), by detecting the change in the ellipticity signal. Protein can be stabilised when they form a supramolecular assembly with a ligand and increase the  $T_m$ .<sup>215, 229, 232</sup> A similar concept could be applied to M-Sav, where incorporation of either biotin (**79**) or catalyst **73/74** was expected to enhance the stability and indirectly confirm the formation of the complex. Therefore, the mean residue molar ellipticities ( $[\theta]$ , **Eq. 2**) of M-Sav, M-Sav:**79** and M-Sav: organocatalysts **73** and **74** were plotted vs the wavelength ( $\lambda$ ) (**Fig. 22**).

$$[\theta] = (\theta \cdot MRW) / (10 \cdot l \cdot C)$$

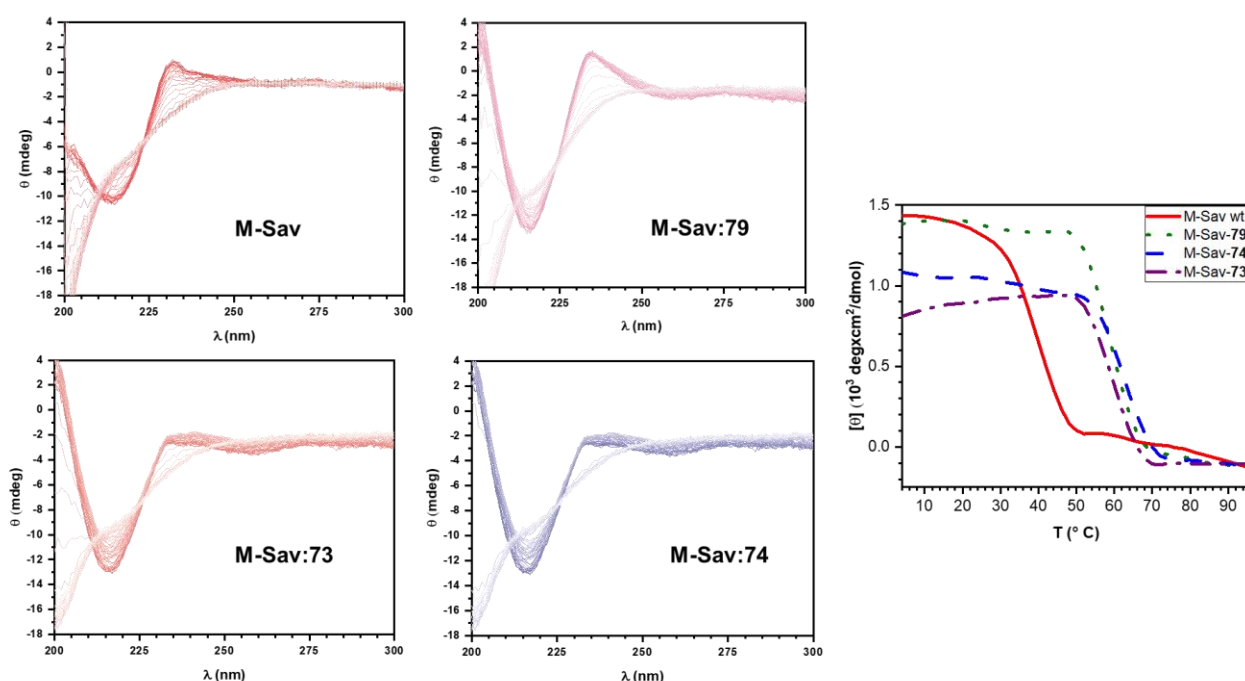
**Equation 2.** Mean residue molar ellipticity calculation. The unit of measure is  $\text{deg} \cdot \text{cm}^2 / \text{dmol}$ .  $\theta$  is the ellipticity (mdeg); MRW is the mean residue weight (g/mol) calculated from the protein MW (g/mol) divided by the number of amino acid minus 1;  $l$  is the path length of the cell (cm);  $C$  is the protein concentration in g/L.

The resulting spectra showed the absorption minimum at 216 nm, while the maximum absorption was observed at 233 nm. Although all the spectra have a similar trend, when M-Sav is not folded in the presence of any ligand, a distinct ramp is observed around the region 250-230 nm, indicating a difference in the protein conformation. As previously observed,<sup>227</sup> the circular dichroism spectrum shows the trend of a  $\beta$ -barrel protein (M-Sav has an 8-strand  $\beta$ -barrel conformation) with the typical broad minimum around 216 nm. This data is in line with the protein visual inspection using the X-ray structure of M-Sav scaffold (PDB: 4JNJ).



**Figure 22.** CD spectra of M-Sav (top left), M-Sav:79 (top right), M-Sav:73 (bottom left) and M-Sav:74 (bottom right).

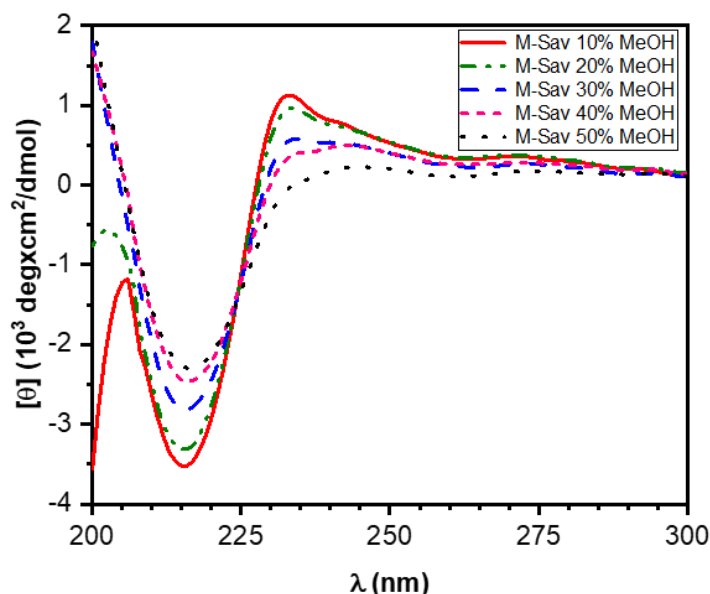
Variations in the  $[\theta]$  value during the  $T_m$  experiments were detected at the wavelength of 233 nm and selected for further assessment. The  $T_m$  of M-Sav alone, or in the presence of the three ligands, was measured in a range between 4 and 96 °C (**Fig. 23**). When 50  $\mu\text{M}$  of only M-Sav were dissolved in PBS (pH 7.4), the recorded  $T_m$  was assessed to be  $37.3 \pm 2.7$  °C. The  $T_m$  for M-Sav refolded in the presence of **79** was measured at  $59.1 \pm 0.5$  °C. This pattern shows a dramatic increase in the stability of the complex. An even more remarkable difference was found when the biotinylated organocatalysts **73** and **74** were used to replace biotin. The  $T_m$  of the complex M-Sav:**73** was measured at  $63.1 \pm 0.1$  °C, in line with the  $62.9 \pm 0.5$  °C detected for the assembly M-Sav:**74**.



**Figure 23.**  $T_m$  of M-Sav, M-Sav: **79**, M-Sav:**74** and M-Sav:**73**.

These data suggested the formation of a protein:organocatalyst complex and showed how the strong non-covalent interaction between M-Sav and **73/74** could stabilise the complex. Further efforts were made to measure the dissociation constant of the organocatalytic artificial enzymes. However, the complex formed by M-Sav and the azo-compound 2-(4-hydroxyphenylazo)benzoic acid (HABA), commonly used to measure  $K_d$  for tetrameric Sav: ligand assemblies, could not be displaced by compound **73/74**, indicating a tighter binding ability.<sup>233</sup> Other techniques to assess the binding affinity between protein and ligand were not explored in this report.

Furthermore, the stability of the organocatalytic enzymes in the presence of different concentrations of co-solvent was verified (**Fig. 24**). Among different organic solvents, methanol was chosen for its polarity and miscibility in aqueous solutions and its potential use as co-solvent for chemical catalysis. Interestingly, a substantial drop in the signal at 233 nm was observed at increasing concentration of co-solvent. Notably, concentrations higher than 20% seemed to interfere with the protein tertiary structure, suggesting an unfolding of M-Sav.

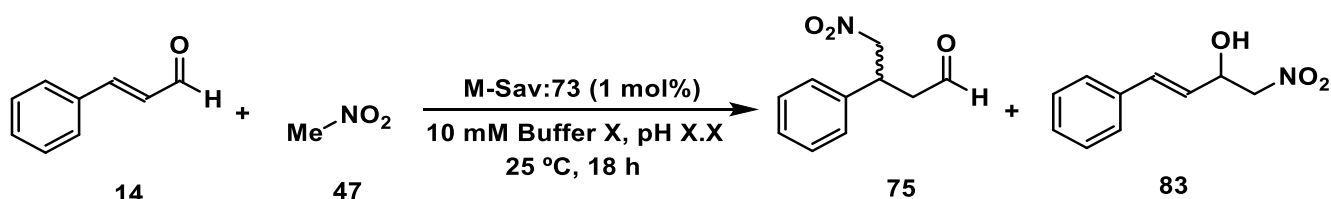


**Figure 24.** CD spectrum of M-Sav using different concentration of methanol: 10% (solid red line), 20% (dashed dotted green line), 30% (dashed blue line), 40% (short dashed red line), 50% (dotted black line).

## 2.5 Screening reactions

The organocatalytic artificial enzymes generated using M-Sav scaffold, and the biotinylated organocatalysts **73** and **74** were tested for iminium catalysis under biocompatible conditions. Inspired by previous work using Sav:**73** complex for iminium catalysis,<sup>110</sup> M-Sav:**73/74** assemblies were employed as catalysts for 1,4-Michael addition of nitromethane (**47**) to cinnamaldehyde (**14**). Conjugate additions, such as Michael additions, are a well-known class of organic transformations, which can be used to generate enantioselective  $\beta$ -functionalised carbonyls. Therefore, enabling 1,4-additions using organocatalysis in a biocompatible environment is highly desirable to allow potential chemical biology applications, such as synthesis of varieties bioactive molecules.<sup>5</sup> A thorough screening focusing on the variation of buffer, pH, co-solvent, and reaction time was performed to assess optimal conditions. Initially,

it was decided to employ only M-Sav:**73** assembly for screening, and further evaluate M-Sav:**74** complex when some optimised conditions were established (**Scheme 17**).



**Scheme 17.** Buffer screening for 1,4-Michael addition of **47** to **14**.

Initially, five buffers at a 10 mM concentration were investigated at three different pHs (**Table 2**). 1,4-Michael additions were tested at pH ranging from 7.0 to 8.0 to mimic physiological conditions. Reactions were run using 1 equivalent of the  $\alpha,\beta$ -unsaturated aldehyde **14** with a significant excess of the nitroalkane **47** for 18 h at 25 °C. Interestingly, using 1 mol% of M-Sav:**73** complex, the 1,4-addition product (**75**) was only detected in small quantity by  $^1\text{H-NMR}$  spectroscopy; meanwhile, the 1,2-addition side-product (**83**) was observed as a major adduct. After considering the high rate of formation of the adduct **83** compared to **75**, only Tris, KPi and PBS at pH 7.0 were considered for further analysis. However, the high background reaction observed using Tris and PBS limited their use for additional experiments. Thus, a 10 mM KPi solution at pH 7.0 was employed as a reaction medium for the next stages. On another note, some buffers showed to be ideal media for the formation of 1,2-addition product. Further experiments focused on the selective formation of product **83** where pursued, starting from the conditions obtained in **Table 2**.

**Table 2.** Buffer screening for 1,4-Michael addition of **47** to **14**.<sup>a</sup>

Buffer	pH	Conv. / % product <b>83</b> <sup>b</sup>	Conv. / % product <b>75</b> <sup>b</sup>
Tris	7.0	12 ± 2	7 ± 2
	7.5	21 ± 1	5 ± 1
	8.0	56 ± 4	5 ± 1
HEPES	7.0	7 ± 1	<1 ± 0
	7.5	66 ± 4	2 ± 0
	8.0	64 ± 5	2 ± 1
KPi	7.0	7 ± 1	4 ± 1
	7.5	39 ± 2	4 ± 1
	8.0	53 ± 6	3 ± 0



NaPi	7.0	10 ± 2	3 ± 1
	7.5	58 ± 1	<1 ± 0
	8.0	63 ± 5	3 ± 1
PBS	7.0	3 ± 0	3 ± 1
	7.5	13 ± 1	7 ± 0
	8.0	46 ± 2	2 ± 0
H <sub>2</sub> O	/	59 ± 3	2 ± 1

<sup>a</sup> Reactions were run using 1 eq. of **14** (3.3 μmol), 10 eq. of **47** (33 μmol), 1 mol% of M-Sav:**73** (33 nmol) in 500 μL of buffer 10 mM at 25 °C for 18 h. Shaking at 300 rpm. Values shown here are mean from triplicate.

<sup>b</sup> Estimated conversions were calculated integrating starting material and product peak by <sup>1</sup>H-NMR spectroscopy.

Driven by the desire to improve M-Sav:**73** catalytic performances, the relative strength of the buffer and the addition of a co-solvent were evaluated (**Table 3**). First, three different concentrations of potassium phosphate were tested, ranging from 10 to 50 mM. When KPi strength was increased to 25 mM, and 50 mM, there was no increase in the formation of product **75**. However, the unwanted adduct **83** was estimated at 14% and 10% respectively. Bearing in mind the poor solubility of cinnamaldehyde in the reaction mixture (the solubility of **14** in water is 1.1 g/L in normal conditions),<sup>234</sup> M-Sav:**73** catalytic activity was tested in the presence of different co-solvents, for a total of 50% of the final volume. First, ethyl acetate (EtOAc) and deuterated chloroform (CDCl<sub>3</sub>) were tested. Both aprotic solvents form a two-phase system, which was aimed to favour the binding between M-Sav:**73** and cinnamaldehyde at the interphase. However, in both cases, no product was observed. Second, the organocatalytic artificial enzyme was tested in the presence of 50% of acetonitrile (MeCN) or methanol (MeOH). Although both solvents are miscible with KPi, only the reaction in the presence of methanol leads to promising results. Indeed, a 3-fold increase in product **75** formations was observed using methanol as co-solvent, accompanied by the formation of a 13% of side-product **83**.

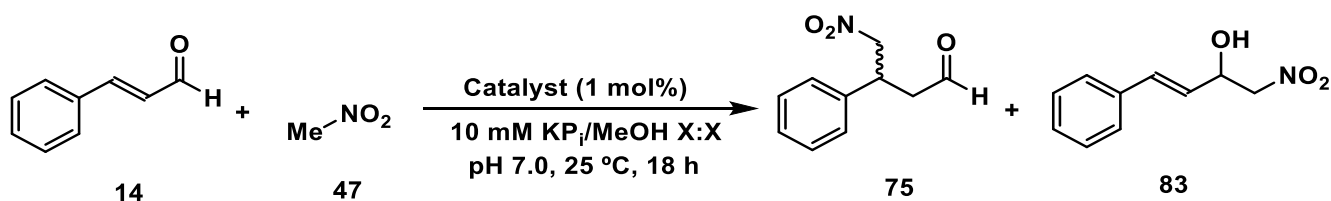
**Table 3.** Buffer strength and co-solvent screening for 1,4-Michael addition of **47** to **14**.<sup>a</sup>

Buffer and Molarity	Co-Solvent	Conv. / % product <b>83</b> <sup>b</sup>	Conv. / % product <b>75</b> <sup>b</sup>
KPi 10 mM	/	7 ± 1	4 ± 1
KPi 25 mM		14 ± 2	5 ± 1

KP <sub>i</sub> 50 mM		10 ± 1	5 ± 1
KP <sub>i</sub> 10 mM	EtOAc <sup>c</sup>	6 ± 1	3 ± 0
KP <sub>i</sub> 10 mM	CDCl <sub>3</sub> <sup>c</sup>	5 ± 2	<1 ± 0
KP <sub>i</sub> 10 mM	MeOH <sup>c</sup>	13 ± 2	21 ± 2
KP <sub>i</sub> 10 mM	MeCN <sup>c</sup>	4 ± 0	<1 ± 0

<sup>a</sup> Reactions were run using 1 eq. of **14** (3.3 μmol), 10 eq. of **47** (33 μmol), 1 mol% of M-Sav:**73** (33 nmol) in 500 μL of buffer 10 mM at 25 °C for 18 h, unless specified. Shaking at 300 rpm. Values shown here are mean from triplicate. <sup>b</sup> Estimated conversions were calculated integrating starting material and product peak by <sup>1</sup>H-NMR spectroscopy. <sup>c</sup> Reactions were run in 250 μL of buffer and 250 μL of co-solvent.

The addition of a substantial amount of methanol enhanced M-Sav:**73** activity. However, the estimated conversion was still considerably lower than expected. Based on these results, M-Sav:**74** assembly was also tested to verify whether organocatalyst **74** would be leading to the formation of a higher amount of product **75**. Thus, both catalyst **73** and **74** and the relative complexes with M-Sav were tested at different methanol concentrations (**Scheme 18**).



**Scheme 18.** Catalyst and concentration of methanol screening for 1,4-Michael addition of **47** to **14**.

Generally, cinnamaldehyde estimated conversion to product **75** did not exceed 21% (**Table 4**). With increasing concentration of methanol, M-Sav:**73** increased the formation of both adducts **75** and **83**, with the best hit observed at 50% methanol. When only the organocatalyst **73** was employed, 1,2-adduct and 1,4-product were formed in ratio 1:1. In this case, the best result detected in the presence of 50% of co-solvent. Surprisingly, M-Sav:**74** complex in the presence of 0-30% of methanol led to the formation of the expected β-branched carbonyl (**75**) in a higher amount than compound **83**. Notably, the best outcome was seen using 20% of methanol, where 20% of product **75** vs 7% of compound **83** were assessed. The control experiment using catalyst **74** led to a similar result, with slightly lower conversions. These results indicated M-Sav:**74** was a marginally better catalytic system than the equivalent assembly carrying catalyst **73**, especially with lower methanol concentrations. Eventually,

combining the results from the CD experiments reported in section 2.4 with these results, M-Sav:**74** was employed in the presence of 20% of methanol for further investigations.

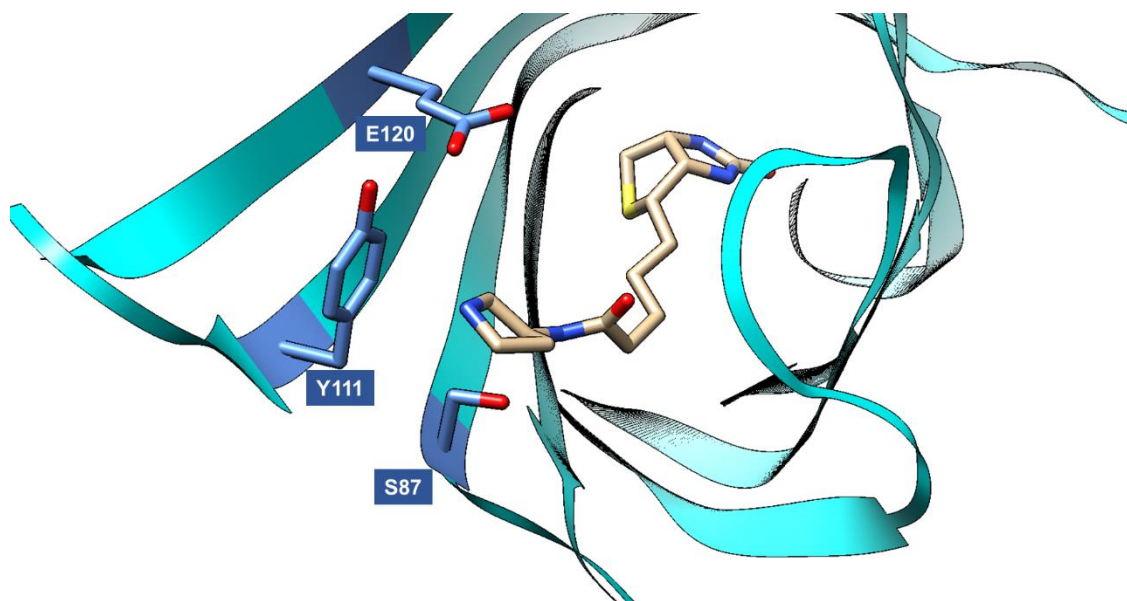
**Table 4.** Catalyst and methanol screening for 1,4-Michael addition of **47** to **14**.<sup>a</sup>

Catalyst	Methanol / %	Conv. / % product <b>83</b> <sup>b</sup>	Conv. / % product <b>75</b> <sup>b</sup>
M-Sav: <b>73</b>	0	7 ± 1	4 ± 1
	10	7 ± 0	9 ± 2
	20	9 ± 1	13 ± 0
	30	11 ± 1	15 ± 2
	40	13 ± 1	18 ± 2
	50	13 ± 1	21 ± 3
<b>73</b>	0	7 ± 0	3 ± 1
	10	6 ± 1	6 ± 2
	20	10 ± 1	12 ± 2
	30	14 ± 1	16 ± 3
	40	13 ± 0	19 ± 1
	50	13 ± 2	20 ± 2
M-Sav: <b>74</b>	0	8 ± 1	13 ± 2
	10	6 ± 1	16 ± 2
	20	7 ± 0	20 ± 1
	30	7 ± 2	17 ± 1
	40	8 ± 1	19 ± 2
	50	13 ± 0	18 ± 2
<b>74</b>	0	12 ± 1	4 ± 0
	10	5 ± 1	5 ± 1
	20	11 ± 2	12 ± 1
	30	8 ± 1	13 ± 1
	40	7 ± 1	13 ± 0
	50	7 ± 2	13 ± 1

<sup>a</sup> Reactions were run using 1 eq. of **14** (3.3 μmol), 10 eq. of **47** (33 μmol), 1 mol% of M-Sav:**73/74** (33 nmol) in 250-500 μL of KPi buffer 10 mM plus 0-250 μL of methanol at 25 °C for 18 h. Shaking at 300 rpm. Values shown here are mean from triplicate. <sup>b</sup> Estimated conversions were calculated integrating starting material and product peak by <sup>1</sup>H-NMR spectroscopy.

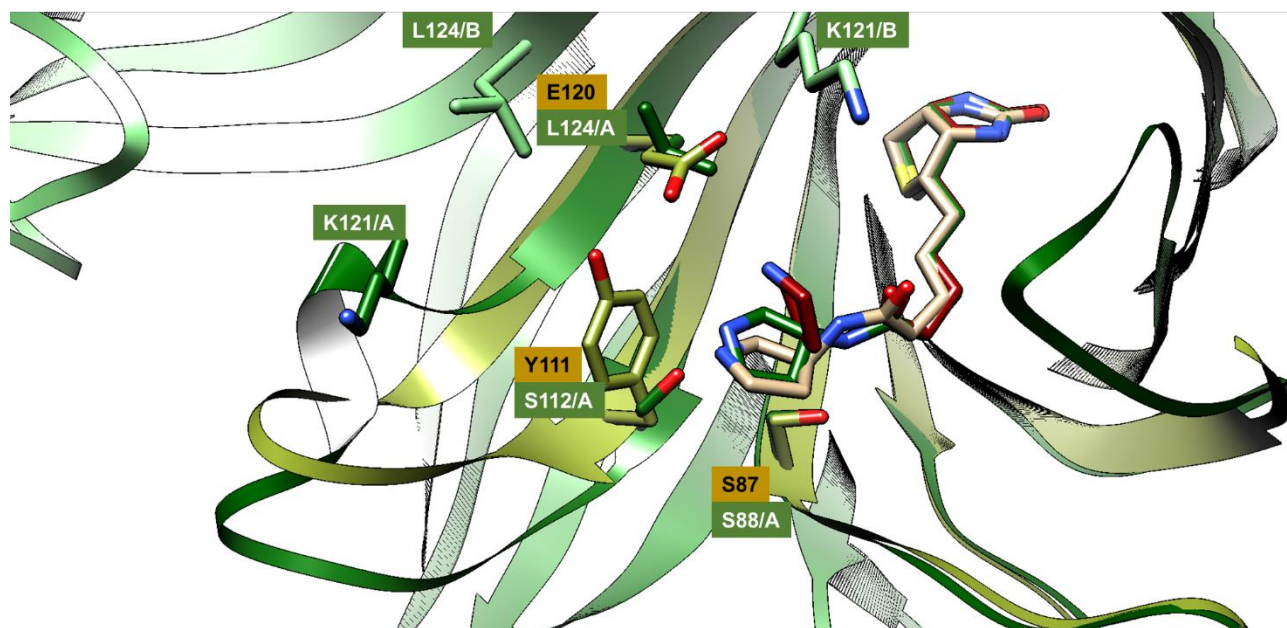
## 2.6 Analysis of M-Sav:74 crystal structure

To exploit the further possibility to enhance the reactivity by mutating the protein host, a thorough analysis of the M-Sav:**74** crystal structure (obtained in our group) was performed. By visual inspection, the first batch of residues located near catalyst **74**, and thus to the reaction centre, were identified as potential spots for mutations (**Fig. 25**). Residues E120, Y111, and S87 were selected for the second round of inspection. Other residues, such as T110, E112, T119 and Q121 are pointing in the active site opposite direction. Therefore, these amino acids were not considered for further analysis. First, by the alignment of Sav and M-Sav, the amino acid sequence was verified whether these residues were conserved in the two proteins and could play a similar role for iminium catalysis. This visual assessment shows only S87 is present in both monomeric and tetrameric (wt) structure, whereas E120 and Y111 correspond to leucine and serine, respectively.<sup>227</sup>



**Figure 25.** Cartoon overview of the crystal structure of M-Sav:**74** (PDB: TBA, 1.68 Å). Catalyst **74** is coloured in beige. In dark blue are identified critical residues for site-directed mutagenesis after visual inspection.

To further investigate the position of these three critical residues compared to the organocatalyst, the crystal structures of Sav:**73** (PDB: 6GH7), Sav:**74** (PDB: TBA) and M-Sav:**74** (PDB: TBA) were superimposed (**Fig.26**).



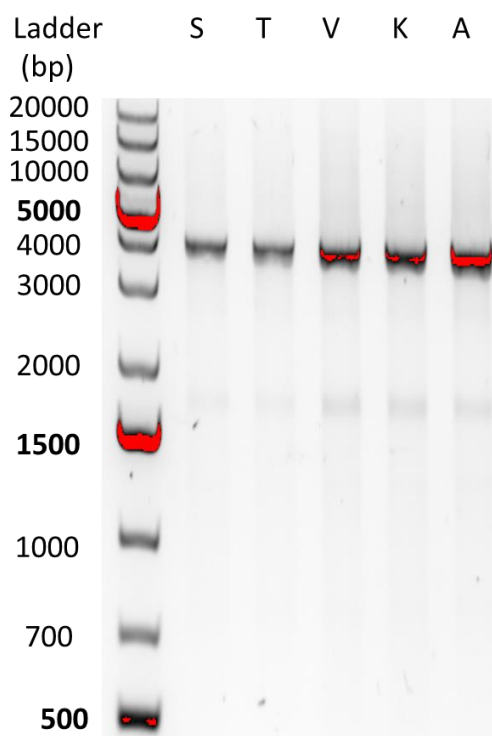
**Figure 26.** Cartoon overview of the crystal structure of Sav:**73** (PDB: 6GH7), Sav:**74** (PDB: TBA) and M-Sav:**74** (PDB: TBA). In green are highlighted residue from Sav:**73/74** (subunit A or B), whereas in ochre M-Sav:**74** residues. Catalyst **74** is coloured in red and beige, while catalyst **73** is coloured in green.

These three residues can be overlaid in both monomeric and tetrameric streptavidin. Assuming S87 plays a similar part in both scaffolds, modifications on E120 and Y111 can play a pivotal role in boosting iminium catalysis within the monomeric streptavidin environment. Furthermore, it is crucial to analyse the lack of a second subunit in the monomeric streptavidin. Indeed, K121 and L124 from both subunit A and B, are known to cover an essential part in tetrameric streptavidin-based iminium catalysis,<sup>110</sup> and they are located in the proximity of the catalytically active nitrogens of either catalysts **73** or **74**. In the case of monomeric streptavidin, both K121 and L124 deriving from the second subunit are missing, and this can be crucial to understand whether these residues are vital or not for iminium catalysis. Based on the initial screening results obtained from **Table 1, 2** and **3**, it can be assumed that the lack of subunit interactions might be one of the critical factors for the low catalytic efficiency of both M-Sav:**73** and M-Sav:**74** assemblies in catalysing 1,4-Michael additions.

## 2.7 Site-directed mutagenesis on Y111 residue

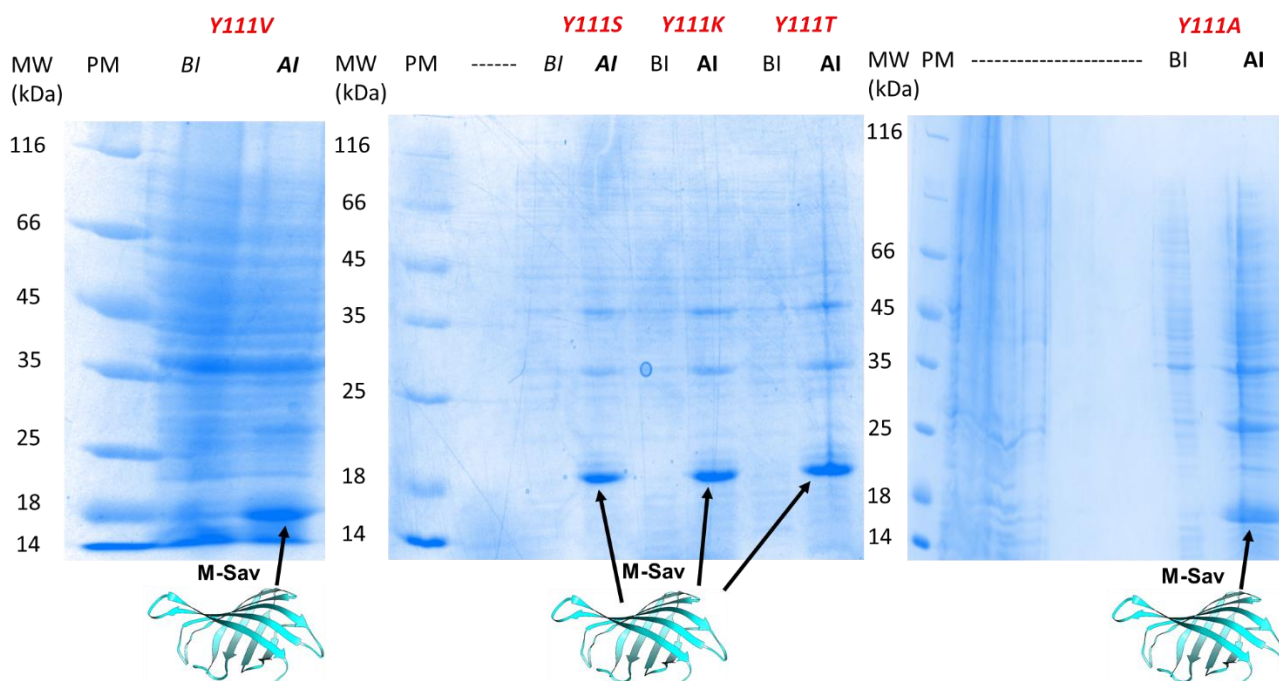
Among different genetic manipulation techniques, site-directed mutagenesis allows studying changes as an outcome of substituting one amino acid with another. In the M-Sav scaffold

specific case, this procedure was applied to generate M-Sav scaffolds bearing mutations on the vital amino acid Y111. For a different purpose, the role of Y111 in monomeric streptavidin-hosted catalysis was already evaluated for artificial metallo-enzymes.<sup>181</sup> Modification on E120 were described elsewhere and will not be part of this discussion (Manuscript in preparation). A series of variations on tyrosine 111, located at 4.31 Å from the catalytically active nitrogen of catalyst **74**, were selected to determine if steric or electronic factors would influence the performance of the artificial enzyme. Significantly, Y111 was mutated to serine, threonine, valine, lysine, and alanine. The serine mutation was designed to examine whether the removal of the  $\pi$ -H interaction between tyrosine-111 and catalyst **74** nitrogen was beneficial. In this case, the calculated H-bonding distance between serine and catalytic nitrogen (4.23 Å) would occur to be similar to the one observed with tyrosine. Bearing similar properties to serine, but being more sterically encumbered, the threonine variant was also created. Then, by replacing threonine with valine, Y111V mutation was introduced to examine how removing a hydrogen bond donor/receiver atom in that position would affect the catalysis. By modifying both steric and electronic properties, the lysine mutation Y111K was introduced to reduce the distance between residue and catalytically active nitrogen. On the opposite way, replacing tyrosine with alanine would explain if iminium catalysis is favoured or not by less bulky amino acids unable to provide a hydrogen bond. These mutations were introduced by site-directed mutagenesis polymerase chain reaction (PCR) using hot start (HS) DNA polymerase and accompanying buffers, dNTPs and primers mentioned in section 6.2.2.2. The mutants were constructed using the sequences reported in section 6.2.2.2 and confirmed by using the T7 promoter primer. After the PCR cycles, M-Sav mutants were checked by agarose gel, with an expected formation of a gene of 3923 base pairs (bp, **Fig. 27**).



**Figure 27.** Agarose gel for M-Sav mutants Y111S, Y111T, Y111V, Y111K and Y111A. The bands around 4000 bp confirm the *M-Sav* genes formation. S= serine; T= threonine; V= valine; K= lysine; A= alanine; bp= base pairs.

Successively, DNA was isolated by a gel extraction protocol and the double-stranded DNA plasmid containing the desired *M-Sav* mutations extracted. *M-Sav* genes were then sequenced and subjected to DNA purification procedure. Following the same protocol reported in section 6.2.2.1 for the *M-Sav* wt, the desired mutants were transformed into *E. coli* BL21 AI cells and expressed (**Fig. 28**). After the Ni-NTA column purification, the five mutants were refolded in the presence of catalyst **74** and subjected to further purification by size-exclusion chromatography.



**Figure 28.** SDS-PAGE of the expression for the Y111V, Y111S, Y111K, Y111T and Y111A M-Sav mutants. MW= Molecular weight; PM= Protein Marker; BI= Before Induction; AI= After Induction.

Eventually, these assemblies were tested for 1,4-Michael addition of nitromethane to cinnamaldehyde using the same conditions applied for M-Sav:**74** wt and using 20% methanol as co-solvent (**Table 5**). However, all five mutants led to an outcome similar to the one observed using M-Sav wt scaffold. The Y111S and Y111A variants showed comparable conversion to both main product **75** with an increase of side-product **83**. In contrast, the Y111V and Y111T mutants were disadvantageous for forming the expected main-product favouring the 1,2-addition product rather than the 1,4-adduct. Eventually, Y111K variants revealed a slight improvement in the performance for iminium catalysis.

**Table 5.** M-Sav mutants screening for 1,4-Michael addition of **47** to **14**.<sup>a</sup>

Catalyst	Conv. / % product <b>83</b> <sup>b</sup>	Conv. / % product <b>75</b> <sup>b</sup>
wt: <b>74</b>	7 ± 0	20 ± 1
Y111S: <b>74</b>	16 ± 2	20 ± 1
Y111T: <b>74</b>	20 ± 1	13 ± 0
Y111V: <b>74</b>	18 ± 3	10 ± 1
Y111K: <b>74</b>	15 ± 1	31 ± 3
Y111A: <b>74</b>	13 ± 2	20 ± 1



---

<sup>a</sup> Reactions were run using 1 eq. of **14** (3.3  $\mu$ mol), 10 eq. of **47** (33  $\mu$ mol), 1 mol% of M-Sav:**74** wt or mutants (33 nmol) in 400  $\mu$ L of buffer 10 mM plus 100  $\mu$ L of methanol at 25 °C for 18 h. Shaking at 300 rpm. Values shown here are mean from triplicate. <sup>b</sup> Estimated conversions were calculated integrating starting material and product peak by <sup>1</sup>H-NMR spectroscopy.

The data obtained from the activity test on the five mutants tested for iminium catalysis suggest modifications on the Y111 position do not significantly increase/decrease activity. Thus, considering that this set of amino acid bearing different electronic and steric properties was explored, this position might not be involved in the specific substrate recruitment for 1,4-Michael addition and might not be fundamental to stabilise the transition states formed during the reaction. However, as recently described by our group (manuscript in preparation), by modifying E120 residue to leucine, a significant increase in the formation of product **75** was detected (65% conversion). Also, in the same report, a double mutant E120L/Y111S was described and tested for 1,4-Michael addition leading to 43% conversion.

## 2.8 Conclusions

In this chapter, the first example of organocatalysis hosted within a monomeric streptavidin scaffold was reported. By non-covalent tethering, two biotinylated organocatalysts within monomeric streptavidin, the organocatalytic artificial enzymes M-Sav:**73** and M-Sav:**74** were generated. When tested for the 1,4-Michael addition of nitromethane to cinnamaldehyde under biocompatible conditions, these complexes could not perform iminium catalysis efficiently. Given these artificial enzymes novelty, detailed screening of reaction conditions was reported aiming to improve the estimated conversion to the desired 1,4-Michael adduct. Inspired by previous reports on Sav-based artificial enzymes,<sup>116, 235</sup> the M-Sav:**74** crystal structure was also examined, and three potential key residues (S87, Y111 and E120) were identified. By employing site-directed mutagenesis, five variants of the M-Sav scaffold bearing Y111 mutations were created and tested using organocatalyst **74** as a guest. This residue was assessed not to contribute for iminium catalysis providing only a marginal improvement on the catalytic efficiency. However, mutations on the E120 residue, performed in our group, revealed to be beneficial for improving organocatalysis within M-Sav scaffold.

Additional efforts are required to improve further the catalytic performance of M-Sav based artificial enzymes for iminium catalysis. Indeed, the protein scaffold could be further refined

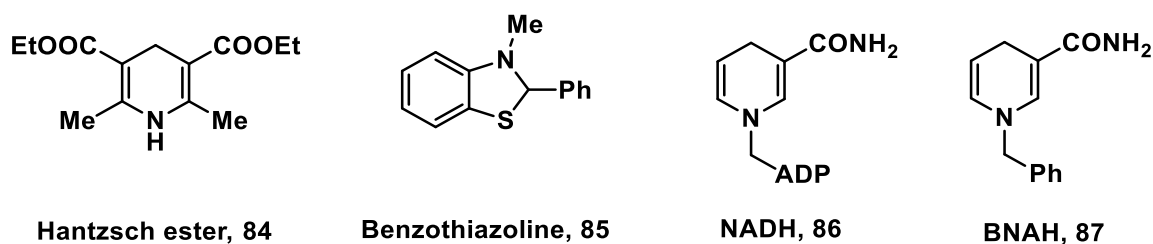
by using different techniques of genetic manipulations. On the one hand, site-directed mutagenesis can be employed to also exploit mutations on the key residues identified. On the other hand, directed evolution could generate random variants bearing mutations not accessible by visual inspections. Furthermore, either by accessing a modern library of biotinylated organocatalysts,<sup>110</sup> or by creating new sets, a series of catalysts different than **73/74** should be tested. This part of the dissertation aimed to set proof of concept for monomeric streptavidin-hosted iminium catalysis given this work innovation.

## Chapter 3: Tetrameric Streptavidin as Host for Iminium Catalysis

### 3.1 Introduction

The first part of this doctoral study has indicated that the tetrameric streptavidin is a better host for organocatalysis when **73** and **74** are employed. Hence, here we report the reaction of this protein-based catalytic system. Firstly, its ability to catalyse transfer hydrogenation was tested. Transfer hydrogenation reactions are chemical transformations involving the addition of hydrogen to a compound from a non-H<sub>2</sub> hydrogen source.<sup>236-240</sup> Transformations mediated by organocatalysts cover a considerable amount of the literature and complement many reactions found in nature. Often, combining secondary amine organocatalysts and Hantzsch esters (including compound **84**, **Fig. 29**), a class of biomimetic organoreductants, have produced remarkable results for transfer hydrogenations.<sup>65, 241</sup> Similarly, the non-biomimetic family of benzothiazolines (i. e. **85**) have also been reported as an efficient hydrogen source in the presence of secondary amine organocatalyst.<sup>242, 243</sup> Although being extremely useful and stable under the classic conditions applied in organocatalysis (high temperature and presence of organic solvents), these molecules have not been reported to function under biocompatible conditions.<sup>236, 242, 244</sup> Therefore, exploring hydrogen donors within a biocompatible environment represents an attractive opportunity to enable application in biology.<sup>193, 245</sup>

The most common ways to perform biocompatible transfer hydrogenations is by either using engineered enzymes as biocatalysts or employing proteins as host for chemical catalysis. In the first case, a top-down approach is used when existing enzymes are modified to function in the presence of non-natural substrates.<sup>246</sup> In these circumstances, the nicotinamide coenzymes NADPH and NADH (**86**) are regarded as the preferred hydrogen donors.<sup>246</sup> Alternatively, the synthetic biomimetics *N,N*-1,4-dihydrobenzyl nicotinamide (BNAH, **87**) has been used as a hydrogen source in different enzymes.<sup>247, 248</sup> Among these enzymes, ene-reductase,<sup>249, 250</sup> hydroxylases and glucose dehydrogenase<sup>251, 252</sup> have been reported to mediate transfer hydrogenations using BNAH.<sup>247</sup>



**Figure 29.** Synthetic and natural hydrogen sources employed for hydrogenations.

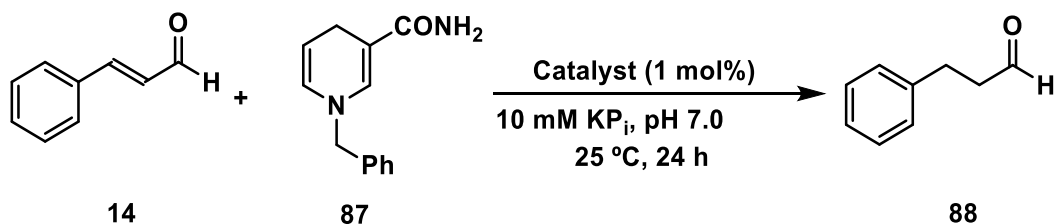
In the second case, when artificial enzymes are created by incorporating a chemical catalyst within a protein scaffold, a bottom-up approach is used. This strategy allows the design of artificial enzymes able to accept a wide range of substrates and cofactors with few restrictions.<sup>5, 50</sup> In this regard, transition-metal catalysts have been incorporated within protein scaffold to perform this reaction.<sup>65, 236, 253</sup> Among the different techniques applied to create protein-hosted chemical catalytic systems,<sup>5</sup> the streptavidin-biotin technology was used to design artificial enzymes able to mediate transfer hydrogenations.<sup>120, 221, 245</sup> Mainly, Sav-based systems were employed to mediate Ru and Ir-mediated transfer hydrogenation,<sup>218, 245</sup> including ones that use simple hydride donors.<sup>184, 254</sup> Even though Sav-based organocatalytic systems were developed,<sup>205, 219, 255-257</sup> examples transfer hydrogenations were not reported so far.

This chapter will describe our studies in enabling biocompatible transfer hydrogenations using the streptavidin-biotin technology. A family of organocatalytic artificial enzymes was prepared to combine the biotinylated organocatalyst **73** and **74** within Sav. These catalytic complexes were screened for the transfer hydrogenation from BNAH to cinnamaldehyde (see section 3.2) and several aromatic  $\alpha,\beta$ -unsaturated carbonyl (see section 3.3). Then, Sav:**73** complex was employed to reduce  $\beta$ -methylated  $\alpha,\beta$ -unsaturated carbonyls (synthesis in section 3.4) using BNAH as hydrogen donor (see section 3.5). Moreover, mechanistic studies on Sav-based transfer hydrogenations were also performed to improve the understanding of the mechanism of action (see section 3.7 and 3.8).

### 3.2 Screening reactions

The initial screening reactions to test the ability of Sav-based complexes to mediate the transfer hydrogenation was conducted using **14** and BNAH (**87**) in  $\text{KPi}$  buffer (10 mM, 10% methanol, pH 7.0) at room temperature and were assessed by  $^1\text{H-NMR}$  spectroscopy (**Scheme 19**). Compound **87** was synthesised following a known procedure.<sup>258</sup> The analytical

data and the synthetic pathway are reported in section 6. Estimated conversions were assessed using the method described in section 6.3.5.2.



**Scheme 19.** Reaction conditions screening for transfer hydrogenation from **87** to **14**.

When the reaction was performed in the absence of protein and catalysts, only 3 % of the reduced product was detected after 24 h incubation using two equivalents of BNAH (**Table 5, Entry 1**). By adding a catalytic amount (1 mol%) of either the biotinylated catalyst **73** or **74**, the estimated conversion was about 25% (**Entries 2-3**). Contrarily, the biotin-binding proteins, Sav and M-Sav, alone had negligible effects in catalysing hydride transfer (**Entries 4-5**). When both Sav and catalyst **73** were included (1:1.2 ratio of catalyst to protein) at 1-2 mol%, the estimated conversion was assessed to 77% and 95% respectively (**Entries 6-7**). Increasing the amount of hydrogen donor **87** to 5 equivalents in a 75:25 KP<sub>i</sub>: MeOH mixture enhanced the conversion up to 94% (**Entry 8**). Interestingly, when no shaking was applied to the reaction mixture, the product conversion decreased to 53% (**Entry 9**). Lastly, in agreement with the previous work in our group,<sup>110</sup> the conversion was lower when catalyst **74** was added to Sav (**Entry 10**). These outcomes indicate that Sav:**73** can mediate the transfer hydrogenation from **87** to **14** under biocompatible conditions.

Based on the experiments presented in the second chapter, the role of M-Sav as host for transfer hydrogenation was also probed. However, as for the 1,4-Michael addition, when M-Sav was used, the conversion for the transfer hydrogenation dropped, with 21% of product conversion by catalyst **73** and 10% by catalyst **74** (**Entries 11-12**). This observation suggests that iminium catalysis prefers a more shielded protein scaffold, and thus residues at the subunit interface of Sav are most likely crucial for the hydride transfer reaction. An investigation on how a change in the hydrogen donor affects the conversion rate was performed. When **87** was replaced with other compounds, such as the synthetic biomimetic known as Hantzsch ester (**84**) and the biological cofactor NADH (**86, Entries 13-14**), it was revealed that alternative hydrogen donors showed significantly lower conversion rate. Hantzsch ester **84** was predictably insoluble in the reaction mixture, and the low conversion

was expected. In contrast, NAD(P)H is highly preferred in most biological contexts recognised by enzymes for reactions. However, **86** did not work efficiently in the presence of Sav:**73** assembly. This result can be attributed to the bulkiness of **86**, which can cause steric hindrance with the Sav:**73** assembly. Indeed, the iminium intermediate formed by the aminocatalyst **73** and cinnamaldehyde might not be accessible to large molecules, such as **86**. Thus, it was confirmed that the Sav-based organocatalytic system prefers BNAH as a hydrogen donor for transfer hydrogenation reaction.

**Table 6.** Screening reaction for transfer hydrogenation from **87** to **14**.<sup>a</sup>

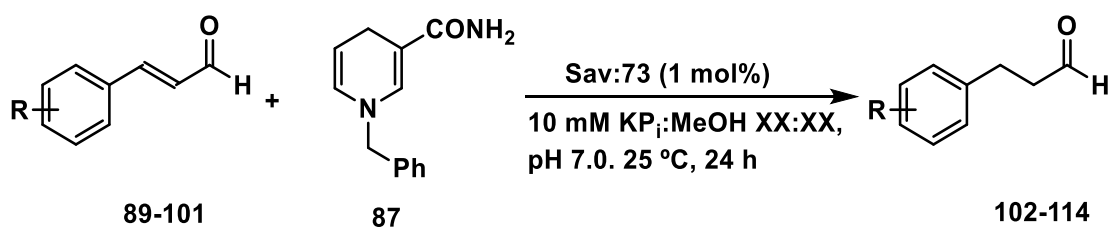
Entry	Host	Guest	H Source	Loading (mol%)	Conv. / % product <b>88</b> <sup>b</sup>
1	N.A.	N.A.	BNAH ( <b>87</b> )	N.A.	3
2	N.A.	<b>73</b>		1	26
3	N.A.	<b>74</b>		1	25
4	Sav	N.A.		1	5
5	M-Sav	N.A.		1	4
6	Sav	<b>73</b>		1	77
7	Sav	<b>73</b>		2	95
8	Sav	<b>73</b>		1	94 <sup>c</sup>
9	Sav	<b>73</b>		1	53 <sup>d</sup>
10	Sav	<b>74</b>		1	51
11	M-Sav	<b>73</b>		1	21
12	M-Sav	<b>74</b>		1	10
13	Sav	<b>73</b>	NADH ( <b>86</b> )	1	5
14	Sav	<b>73</b>	Hantzsch ( <b>84</b> )	1	0 <sup>e</sup>

<sup>a</sup> Conversion was determined by <sup>1</sup>H-NMR spectroscopic analysis. <sup>b</sup> Reactions performed in a mixture 90:10 KPi 10 mM:MeOH at pH 7.0 using 1 equivalent of **14** and 2 equivalents of **87**. <sup>c</sup> Reaction performed in a mixture 75:25 KPi 10 mM:MeOH at pH 7.0 using 1 equivalent of **14** and 5 equivalents of **87**. <sup>d</sup> 0 rpm, side-product observed <sup>e</sup> ppt observed. N.A. indicates not added.

### 3.3 Substrate scope for aromatic $\alpha,\beta$ -unsaturated aldehydes

Having determined the optimal condition for performing biocompatible organocatalytic hydride transfer within a Sav scaffold (**Table 6, Entry 8**), a pool of aromatic  $\alpha,\beta$ -unsaturated aldehydes were tested. Sav:**73** assembly showed significant substrate promiscuity towards

this class of compounds (**Scheme 20**). The aldehydes herein presented were synthesised following a known procedure reported in section 6.3.3.



**Scheme 20.** Sav:**73** tested for the transfer hydrogenation from **87** to aromatic  $\alpha,\beta$ -unsaturated aldehydes (**89-101**).

When substituents were inserted in *ortho* position on the aromatic ring, modest to excellent conversions were observed under biocompatible conditions. Sav:**73** was able to mediate the conversion of both *o*-fluoro (**89**) and *o*-bromo (**90**) derivatives into their hydrogenated counterparts for 90% and >99% respectively (**Table 7**, **Entries 1-2**). Although a modest 53% of conversion was found when the strong electron-withdrawing nitro group (**91**) was inserted in *ortho* (**Entry 3**), Sav:**73** was able to catalyse the full conversion of the *o*-tolyl (**92**) derivative (**Entry 4**). These outcomes indicate that the Sav-based assembly well-tolerated substitutions in the *ortho* position. Further experiments should be directed towards the insertion of bulky and electron-donating groups in the *ortho* position, such as the *tert*-butyl and the methoxy groups.

In contrast, the meta-substituted derivative produced conflicting results. When *m*-fluoro (**93**) and *m*-bromo (**94**) were employed as substrates good and modest conversions were observed, even if precipitation was detected (**Entries 5-6**, 77% and 45% respectively). Indeed, in both cases, precipitation can be the primary cause of these results. However, considering the C-Br bond length and the Br radius, steric repulsion between Sav scaffold and **94** might have taken place and limited the reduction process. When a methyl group was inserted in *meta*-position (**95**), the corresponding derivative was fully converted by Sav:**73** (**Entry 7**).

When cinnamaldehyde was added with halogens at the *para* position, Sav:**73** system leads to different results (**Entries 8-10**). For the conversion of the chloro (**96**) and fluoro (**97**) derivatives, up to >99% was observed, whereas *p*-bromo (**98**) substrate could only be converted up to 60%. Again, the bulkiness of the bromine atom could be a relevant parameter to consider for evaluating this result. A similar outcome was detected with an electron-

donating methoxy group (**99**) in *para*-position (**Entry 11**, 69% conversion). In this case, the methoxy group shares the lone pair with the aromatic ring, which is conjugated to the aldehyde moiety through the double bond, thus stabilising and reducing the reactivity of **99**. Instead, full conversion was also assessed for the *p*-nitro derivative (**Entry 12**). However, this happened only using 10% of co-solvent and 2 equivalents of BNAH, in line with the initial conditions tested using cinnamaldehyde (**Table 6, Entry 6**). Eventually, the *p*-tolyl derivative could be reduced with a 75% yield (**Entry 13**). Together, these observations suggest that the efficiency of hydride transfer using Sav:**73** complex is affected by the electrostatic properties of the substituents, and probably by steric effects as well (see bromine). Remarkably, it is one of the first examples of an organocatalytic artificial enzyme able to mediate transfer hydrogenation to several aromatic  $\alpha,\beta$ -unsaturated aldehydes. Additional experiments will be required to explore whether bulky and electron-donating groups are tolerated in *o*- and *m*-positions.

**Table 7.** Substrate scope for transfer hydrogenations from **87** to different  $\alpha,\beta$ -unsaturated aldehydes. <sup>a</sup>

Entry	Aldehyde (R)	Background <sup>b</sup>	Conv. / % product <b>102-114</b> <sup>b</sup>
1	<i>o</i> -F ( <b>89</b> )	5 ± 1	90 ± 2
2	<i>o</i> -Br ( <b>90</b> )	2 ± 0	>99 ± 3
3	<i>o</i> -NO <sub>2</sub> ( <b>91</b> )	2 ± 1	53 ± 1
4	<i>o</i> -CH <sub>3</sub> ( <b>92</b> )	5 ± 1	>99 ± 3
5	<i>m</i> -F ( <b>93</b> )	4 ± 0	77 <sup>c</sup> ± 2
6	<i>m</i> -Br ( <b>94</b> )	1 ± 0	45 <sup>c</sup> ± 4
7	<i>m</i> -CH <sub>3</sub> ( <b>95</b> )	4 ± 1	>99 ± 1
8	<i>p</i> -Cl ( <b>96</b> )	3 ± 0	94 ± 2
9	<i>p</i> -F ( <b>97</b> )	4 ± 1	>99 ± 2
10	<i>p</i> -Br ( <b>98</b> )	2 ± 0	60 ± 3
11	<i>p</i> -OCH <sub>3</sub> ( <b>99</b> )	3 ± 0	69 ± 1
12	<i>p</i> -NO <sub>2</sub> ( <b>100</b> )	4 ± 1	>99 <sup>d</sup> ± 2
13	<i>p</i> -CH <sub>3</sub> ( <b>101</b> )	5 ± 1	76 ± 1

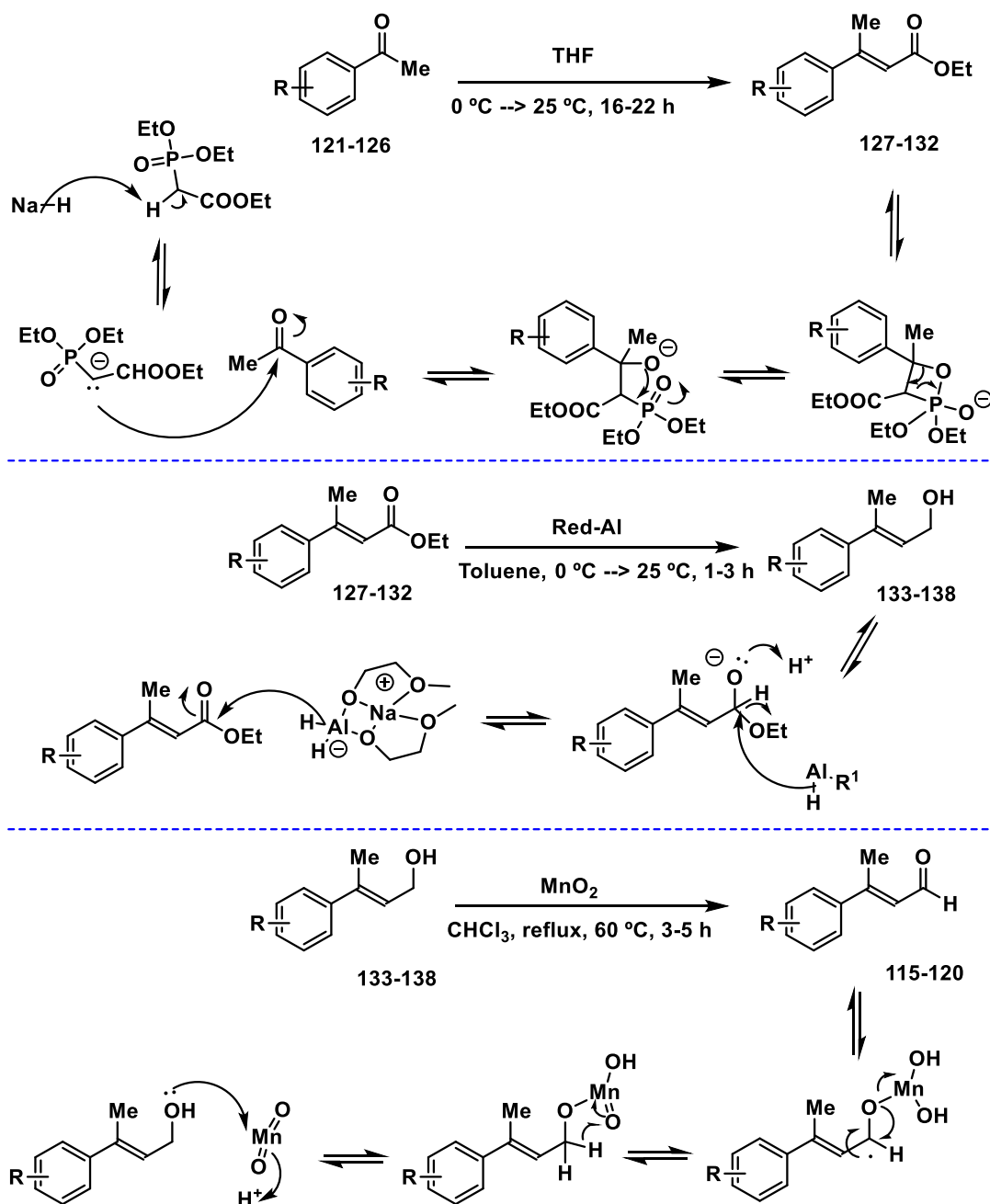
<sup>a</sup> Conversion was determined by <sup>1</sup>H-NMR integration. <sup>b</sup> Reaction performed in a mixture 75:25 KP<sub>i</sub> 10 mM:MeOH at pH 7.0 using 1 equivalent of aldehyde (**89-101**) and 5 equivalents of **87**. <sup>c</sup> ppt observed. <sup>d</sup> reaction performed in a mixture 9:1 KP<sub>i</sub> 10 mM:MeOH at pH 7.0 using 1 equivalent of aldehyde (**89-101**) and 2 equivalents of **87**.



### 3.4 Synthesis of aromatic $\beta$ -branched $\alpha,\beta$ -unsaturated aldehydes

Further tests to assess the promiscuity of Sav:73 complex were made after preparation of a family of derivatives bearing a methyl group in  $\beta$ -position (compounds **115-120**). These compounds were prepared by adapting a three-step pathway (**Scheme 21**, section 6.3.4).<sup>200</sup>,

259

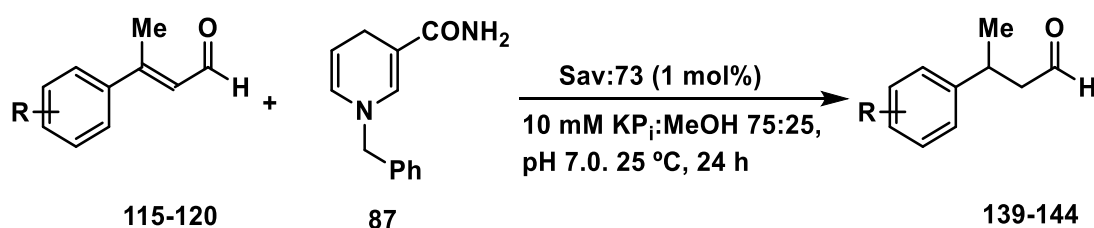


**Scheme 21.** Three-step procedures to afford  $\beta$ -methylated  $\alpha,\beta$ -unsaturated aldehydes (**115-120**) starting from acetophenone derivatives (**121-126**).

In the first step, a Horner–Wadsworth–Emmons (HWE) reaction was employed to obtain ethyl (*E*)-3-phenylbut-2-enoate (**127**) and derivatives (**128-132**).<sup>260, 261</sup> This transformation is a variation of the Wittig reaction and is used to produce mainly (*E*)-oriented olefins from carbonyls. Differently from the Wittig reaction, the phosphonium ylides are replaced by phosphonate-stabilised carbanions because of their higher nucleophilicity and the facility to remove the dialkylphosphate salt by-products by aqueous extraction.<sup>260</sup> In the early stages, the reaction proceeds by forming a stable phosphonate carbanion through the addition of sodium hydride (NaH) to ethyl phosphonacetate under anhydrous conditions. Then, the nucleophilic addition of the carbanion to the carbonyl group of acetophenone (**121**) and derivatives (**122-126**) defines the reaction rate.<sup>262</sup> In the last step, the dialkylphosphate is eliminated, leading to the  $\beta$ -methylated  $\alpha,\beta$ -unsaturated ester formation.<sup>262</sup> The (*E*)-stereoisomers of compounds **127-132** were isolated after extraction and purification by flash chromatography. By employing the strong reducing agent Red-Al<sup>®</sup> (sodium bis(2-methoxyethoxy)aluminum hydride solution),<sup>259</sup> the  $\beta$ -methylated  $\alpha,\beta$ -unsaturated esters **127-132** were converted to the corresponding alcohols **133-138** under anhydrous conditions. Once the full conversion from ester to alcohol was assessed by thin-layer chromatography (TLC), the resulting compounds were purified by aqueous extraction and directly employed in the next step. Alcohols **133-138** were combined with an excess of manganese dioxide (MnO<sub>2</sub>) in chloroform and were heated to reflux until the corresponding  $\beta$ -methylated  $\alpha,\beta$ -unsaturated aldehydes were generated. In this case, both aqueous work-out and flash chromatography were necessary to afford compounds **115-120**.

### 3.5 Substrate scope for aromatic $\beta$ -methylated $\alpha,\beta$ -unsaturated aldehydes

After isolating compounds **115-120**, Sav:**73** was tested to determine its promiscuity towards this substrates class (**Scheme 22**). The newly formed products **139-144** contain a chiral centre, but the formation of either the (*R*)- or the (*S*)-isomer was not assessed and will not be further discussed in this report.



**Scheme 22.** Sav:73 promiscuity towards  $\beta$ -methylated aromatic  $\alpha,\beta$ -unsaturated aldehydes for transfer hydrogenation from **87**.

By adopting the optimised conditions from **Table 6**,  $\beta$ -methylated derivatives **115-120** were hydrogenated using BNAH as a hydrogen donor (**Table 8**). When the unsubstituted derivatives (**115**) were employed, only 29% conversion was detected after 24 h of reaction (**Entry 1**). In this specific case, precipitation was observed when introducing 5 equivalents of BNAH. Thus, the reaction was conducted in the presence of 2 equivalents of **87** and 10% of methanol as co-solvent. With chlorine in the *para*-position (**116**), a slight increase in conversion was found, with this substrate being reduced for 40% (**Entry 2**). Compound **117** with fluorine in *para* lead to a conversion of 79%, showing modest to good promiscuity of Sav:73 towards *p*-halogenated substrates belonging to this family (**Entry 3**). Similarly to the non-methylated compound **97**, Sav:73 seems to tolerate substrates bearing *p*-F substitution. A dramatic decrease in Sav:73 activity was observed when *o*-, *m*-, *p*-methylated derivatives were tested (**Entry 4, 5 and 6**). Indeed, both *o*-tolyl (**118**) and *p*-tolyl (**120**) could not be converted into their equivalent reduced form for more than 18%. Similarly, the Sav:73 complex reduced only 56% of the *m*-tolyl (**119**) derivative under biocompatible conditions. The promising outcomes obtained by testing  $\beta$ -methylated compounds suggest that Sav:73 should be further evaluated to assess the enantioselectivity of the products belonging to this class. In particular, the substrate **117** can be taken as a model compound for further experiments. Additionally, research should be directed towards testing derivatives of this family bearing strong electron-withdrawing (*i.e.*  $-\text{NO}_2$ ), strong electron-donating (*i.e.*  $-\text{NMe}_2$ ) or bulky (*i.e.* Ph) groups in *para*.

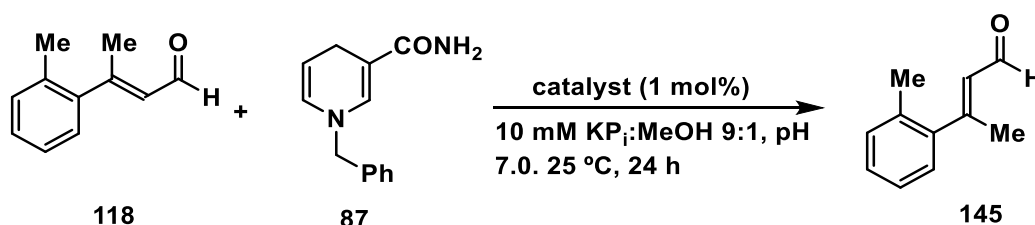
**Table 8.** Substrate scope for transfer hydrogenations from **87** to  $\beta$ -methylated  $\alpha,\beta$ -unsaturated aldehydes. <sup>a</sup>

Entry	Aldehyde (R)	Background <sup>b</sup>	Conv. / % product <b>139-144</b> <sup>b</sup>
1	H ( <b>115</b> )	1 $\pm$ 0	29 $\pm$ 3 <sup>c, e</sup>
2	<i>p</i> -Cl ( <b>116</b> )	2 $\pm$ 0	40 $\pm$ 4
3	<i>p</i> -F ( <b>117</b> )	1 $\pm$ 0	79 $\pm$ 5

4	<i>o</i> -CH <sub>3</sub> ( <b>118</b> )	1 ± 0	18 ± 1 <sup>d</sup>
5	<i>m</i> -CH <sub>3</sub> ( <b>119</b> )	2 ± 0	56 ± 1
6	<i>p</i> -CH <sub>3</sub> ( <b>120</b> )	1 ± 0	18 ± 2 <sup>c, e</sup>

<sup>a</sup> Conversion was determined by <sup>1</sup>H-NMR integration. <sup>b</sup> Reaction performed in a mixture 75:25 KP<sub>i</sub> 10 mM:MeOH at pH 7.0 using 1 equivalent of aldehyde (**115-120**) and 5 equivalents of **87**. <sup>c</sup> Reaction performed in a mixture 9:1 KP<sub>i</sub> 10 mM:MeOH at pH 7.0 using 1 equivalent of aldehyde (**115-120**) and 2 equivalents of **87**. <sup>d</sup> Isomerisation observed. <sup>e</sup> ppt observed.

Serendipitously, when Sav:**73** was initially tested for substrate **118** using 2 equivalents of BNAH and 10% methanol as co-solvent, the unexpected formation of 45% of the (*Z*)-isomer was revealed, with no conversion to product **145** observed (**Scheme 23**).



**Scheme 23.** Formation of the (*Z*)-isomer (**145**) of the substrate **118** using Sav:**73**.

Surprisingly, this phenomenon was observed only employing this substrate (**Table 9, Entry 1**). Then, it was investigated in which conditions the isomerisation of substrate **118** was taking place. In the absence of catalyst, neither the formation of product **142** nor isomerisation was observed (**Entry 2**). Similarly, in the presence of either catalyst **73** or Sav, the same pattern was confirmed (**Entries 3-4**). Eventually, by withdrawing BNAH from the reaction mixture in the presence of Sav:**73** assembly, no isomerisation was observed (**Entry 5**). This outcome indicates that the isomerisation of substrate **118** caused by Sav:**73** complex is BNAH-dependent. A plausible explanation of this phenomenon is that the cis-trans isomerism observed is due to the steric effect caused by the presence of BNAH. Considering this rearrangement was detected only for substrate **118**, the presence of two methyl groups in  $\beta$ - and *o*-positions plus BNAH seems to disfavour the (*E*)-isomer and to stabilise the (*Z*)-isomer. This example suggests it might be promising to explore the properties of Sav:**73** complex in catalysing isomerisation of  $\alpha,\beta$ -unsaturated carbonyls.

**Table 9.** Screening to determine the isomerisation conditions for substrate **118**.<sup>a</sup>

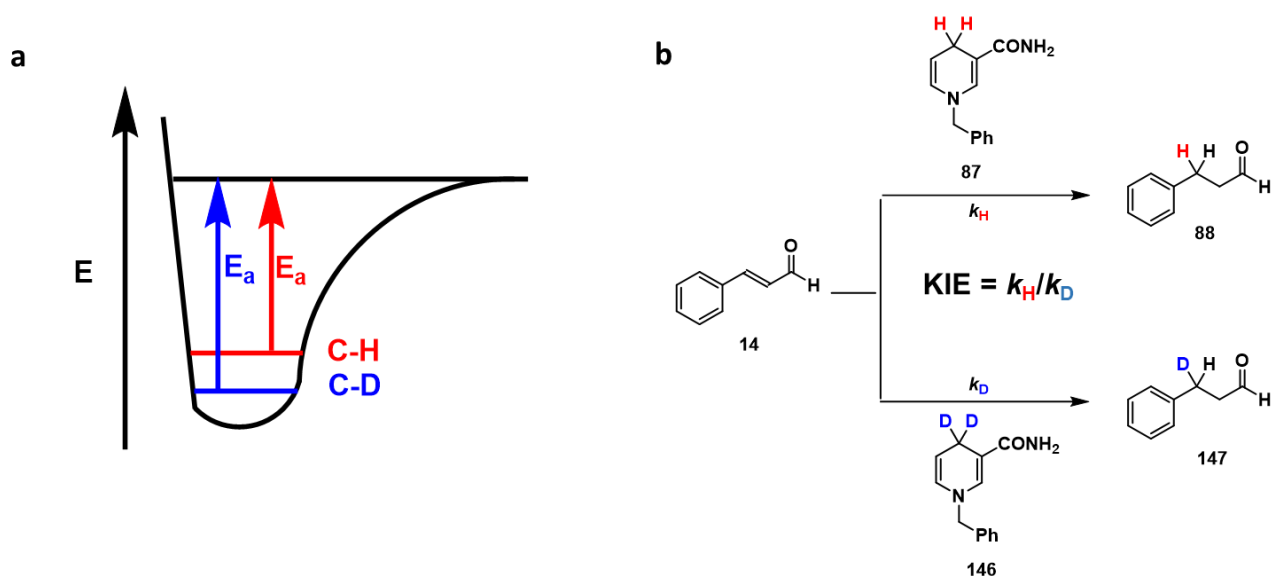
Entry	Catalyst	% ( <i>E</i> )-isomer ( <b>118</b> )	% ( <i>Z</i> )-isomer ( <b>145</b> )	Conv. / % product <b>142</b> <sup>b</sup>
1	Sav: <b>73</b>	55	45	N.A.

2	N.A.	>99	<1	N.A.
3	<b>73</b>	>99	<1	N.A.
4	Sav	>99	<1	N.A.
5	Sav: <b>73</b> <sup>c</sup>	95	5	N.A.

<sup>a</sup> Conversion was determined by <sup>1</sup>H-NMR integration. <sup>b</sup> Reaction performed in a mixture 9:1 KP<sub>i</sub> 10 mM:MeOH at pH 7.0 using 1 equivalent of **118** and 2 equivalents of **87**. <sup>c</sup> Reaction performed without using BNAH.

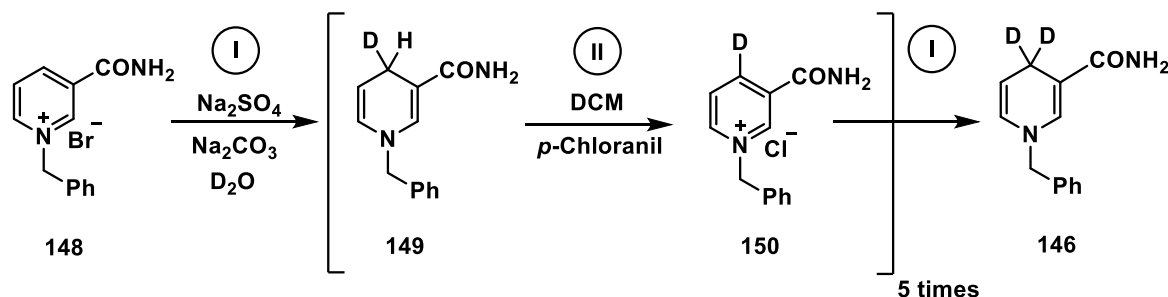
### 3.6 Synthesis of deuterated analogues for mechanistic studies

The reaction rate can sometimes be affected by replacing one atom of a reagent with its heavier/lighter counterpart (isotopologue). The bond between the compound and the heavy isotope has lower vibrational frequencies and higher energy of activation (for bond breaking) than the original bond (**Fig. 30a**). The heavier isotopologue will require more energetic input to reach the transition state of a reaction. Therefore, it will result in a slower reaction rate if the heavier isotope bond is involved in the rate-limiting step. This phenomenon, defined as kinetic isotope effect (KIE), is a quantum mechanical effect and can be useful to deduce mechanistic conclusions on chemical reactions. Thus, to gain knowledge on the mechanism of action for Sav-based transfer hydrogenations, kinetic isotope effect (KIE) studies can be used. By analysing the change in the rate of the reaction when the hydrogen (light,  $k_L$ ) located on the C-4 of BNAH is replaced by deuterium (heavy,  $k_H$ ), conclusions on the rate-limiting step of the reaction can be drawn (**Fig. 30b**).



**Figure 30.** **a**) Energy barriers involving C-H (light atom) and C-D (heavy atom) bonds. **b**) Employing KIE to define the rate-limiting step for Sav-based transfer hydrogenations.

The preparation of the BNAH analogue bearing deuterium in position 4 of the nicotinamide ring (*d*2-BNAH, **146**) was accomplished using a multiple-steps protocol starting from BNA<sup>+</sup> (**148**) (**Scheme 24**, see section 6.3.2).



**Scheme 24.** The synthetic pathway from oxidised BNA<sup>+</sup> (**148**) to *d*2-BNAH (**146**) involving 5 cycles of deuteration.

In the first step, BNA<sup>+</sup> was reduced following the procedure reported in section 6.3.1, although deuterated oxide (D<sub>2</sub>O) was employed as water replacement to provide deuterium to label position 4. Once the intermediate **149** was isolated, it was oxidised using *p*-chloranil to afford compound **150**. *d*2-BNAH was isolated after five more oxidation cycles (step II) and reductions (step I) were repeated, and the work-out followed each stage. The isotopic enrichment for compound **146** was confirmed to be >95% by both HRMS and <sup>1</sup>H-NMR (see section 6.3.2.2 and 6.3.2.3).

### 3.7 KIE studies for Sav-based transfer hydrogenation

After the synthesis and the purification stages, *d*2-BNAH was tested as a deuterium source for the transfer hydrogenation of cinnamaldehyde using the organocatalytic artificial enzyme Sav:**73** (**Scheme 25** and **Table 10**). The experiment was conducted using 2 equivalents of hydrogen/deuterium donor and 10% of methanol. Although KIE measurements are often taken at saturating conditions,<sup>263, 264</sup> the precipitation of either compound **14** or **87/146** was observed at high concentration and impeded to test the KIE in such saturated conditions. To calculate the KIE for Sav:**73** the conversion of the saturated product obtained using **87** was plotted versus the one measured using its deuterated analogue. In contrast to the 77% conversion of product **88** detected using BNAH (**Entry 1**), a mediocre 41% conversion was found when *d*2-BNAH was added as deuterium source (**Entry 2**). Thus, the calculated KIE value for Sav:**73** was 1.87 ± 0.03. A higher value of KIE, 2.16 ± 0.02, was observed when

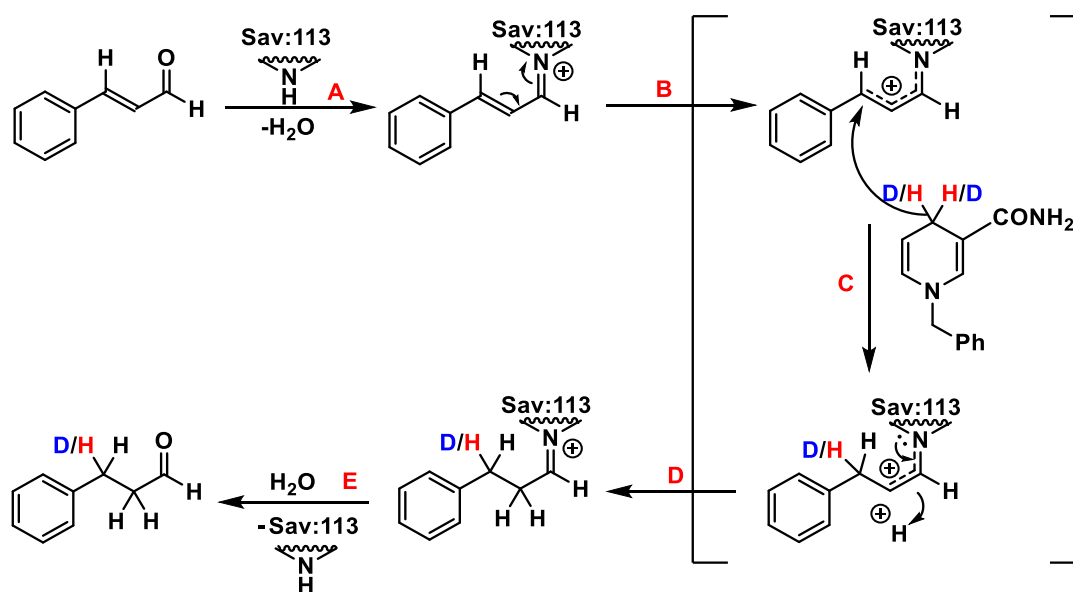
catalyst **73** was employed alone (**Entries 3-4**). Eventually, as a positive control, we determined the KIE of Jørgensen-Hayashi organocatalyst **23** under the biocompatible conditions (**Entries 5-6**). Although the catalyst **23** did not work efficiently in low methanol concentration, a KIE value of  $2.66 \pm 0.03$  could be isolated.

**Table 10.** KIE determination for Sav:**73** catalysed transfer hydrogenation.<sup>a</sup>

Entry	Catalyst	H/D Source	Conv. / % product <b>88/147</b> <sup>b</sup>	KIE <sup>c</sup>
1	Sav: <b>73</b>	BNAH	77	$1.87 \pm 0.03$
2		<i>d</i> 2-BNAH	41	
3	<b>73</b>	BNAH	13	$2.16 \pm 0.02$
4		<i>d</i> 2-BNAH	6	
5	<b>23</b>	BNAH	16	$2.66 \pm 0.03$
6		<i>d</i> 2-BNAH	6	

<sup>a</sup> Conversion was determined by <sup>1</sup>H-NMR integration. <sup>b</sup> Reaction performed in a mixture 9:1 KP; 10 mM:MeOH at pH 7.0 using 1 equivalent of **14** and 2 equivalents of **87/146**. <sup>c</sup> Experiments were performed in triplicate.

Analysis of the KIE values leads us to assume a primary kinetic isotope effect when Sav:**73** was employed. However, this value is lower than the ones found employing both organocatalysts **73** and **23**, indicating the protein assembly appears to facilitate the step of hydride transfer, probably by stabilising the transition state. Based on the proposed mechanism for iminium catalysed hydrogenations shown in **Scheme 25**, a primary KIE would suggest step C as the rate-limiting step. However, to further gain an insight into the mechanism of action and confirm the assumptions made, computational calculations, such as transition states energies, are required.



**Scheme 25.** Proposed transfer hydrogenation mechanism of action using Sav:73 complex.

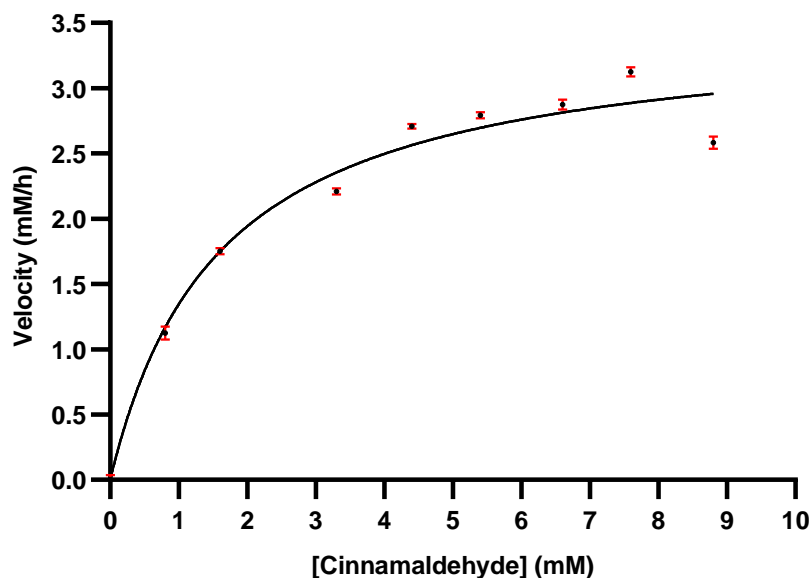
Finally, the KIE calculated value for Sav:73 is in line with what found for iminium catalysed transfer hydrogenation inside a self-assembled supramolecular capsule.<sup>253</sup> Within this macromolecular system the addition from Hantzsch ester (**84**) to the  $\alpha,\beta$ -unsaturated aldehyde **115** was detected to be  $1.90 \pm 0.05$ . The KIE values obtained by Sav:73 (KIE =  $1.87 \pm 0.03$ ) are comparable to the one of the capsule-organocatalyst system suggesting supramolecular interactions in both cases might attenuate the step of hydride transfer (Step C) in this reaction.

### 3.8 Kinetic measurement

The kinetic properties of the protein-based hydride transfer system were compared to those of other protein-based systems that could use simple hydride donors for reactions. The experiment was conducted varying concentration of cinnamaldehyde (**14**), although saturating conditions were not reached. It turned out that the streptavidin-hosted secondary amine Sav:73 manifested enzyme-like kinetic behaviours with the catalytic efficiency ( $k_{\text{cat}}/K_{\text{Mcinamaldehyde}}$ ) measured to be  $9.40 \pm 0.5 \text{ M}^{-1}\cdot\text{s}^{-1}$  at 25 °C (**Fig. 31**). In contrast,  $k_{\text{cat}}/K_{\text{MBNAH}}$  could not be measured, as conflicting results were obtained. The  $k_{\text{cat}}/K_{\text{M}}$  for flavopapain using BNAH (but not **14**) was reported to be  $5900 \text{ M}^{-1}\cdot\text{s}^{-1}$ ,<sup>136</sup> a significantly higher value than that of the organocatalytic Sav system; however, the hydride from BNAH was not used for synthesis in this case, but instead for converting hydrogen peroxide into water.<sup>136</sup> BNAH has also been used for aromatic hydroxylation, and the reduction of  $\alpha,\beta$ -unsaturated



carbonyl substrates with bimolecular reaction rate constant measured up to  $1.2 \times 10^4 \text{ M}^{-1}\cdot\text{s}^{-1}$  and  $1.9 \times 10^6 \text{ M}^{-1}\cdot\text{s}^{-1}$ .<sup>249, 252</sup> The kinetics of these systems that employed natural enzymes are noticeable. Nevertheless, the Sav:**73** system has not yet been engineered and offers significant flexibility in design.



$V_{\max}$	$k_{\text{cat}}$	$K_{\text{M}}$	$k_{\text{cat}}/K_{\text{M}}$
$3.5 \pm 0.5 \text{ mM}\cdot\text{h}^{-1}$	$46.9 \pm 0.3 \text{ h}^{-1}$	$1.5 \pm 0.7 \text{ mM}$	$30.1 \pm 0.5 \text{ mM}^{-1} \text{ h}^{-1}$ ( $9.4 \text{ M}^{-1}\cdot\text{s}^{-1}$ )

**Figure 31.** Kinetic evaluation of Sav:**73** complex for transfer hydrogenation from BNAH to cinnamaldehyde.

### 3.9 Conclusions

In summary, we have described the use of streptavidin as host for organocatalytic transfer hydrogenations. Sav:**73** was able to mediate the hydrogenation of a pool of aromatic  $\alpha,\beta$ -unsaturated aldehydes in a biocompatible environment. Excellent conversions could be achieved for several substrates, which are key intermediates in the synthesis of different pharmaceutical compounds.<sup>236</sup> KIE studies were employed to verify the role of the protein assembly in the mechanism of action and revealed that the protein facilitates the step of hydride transfer. Moreover, the Sav:**73** kinetics for the conversion of cinnamaldehyde into hydrocinnamaldehyde were determined. Further studies focusing on the reaction mechanisms and potential applications in cascade reactions are currently ongoing. Although Sav-based organocatalytic systems need additional efforts to be compared to the equivalent artificial metalloenzymes,<sup>116</sup> this chapter aimed to set a foundation for future protein-hosted

transfer hydrogenation applications via iminium catalysis in chemical and synthetic biology area.

## Chapter 4: Tetrameric Streptavidin as Host for Enamine Catalysis

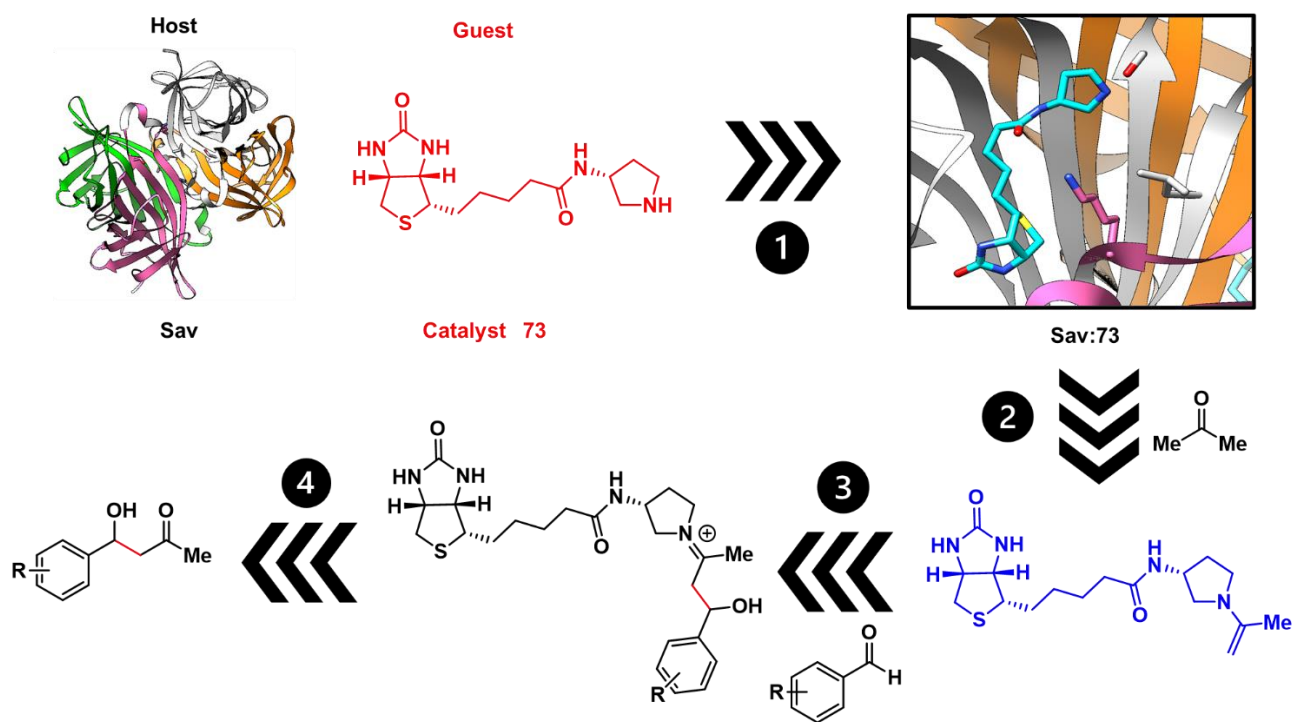
### 4.1 Introduction

In this chapter, Sav-based secondary amine organocatalytic system ability to perform enamine catalysis is presented.<sup>256</sup> Being one of the most popular and convenient ways to perform carbon-carbon bond formation, aldol addition is an attractive tool for chemical and synthetic biology research.<sup>50, 96, 265</sup> Among several applications, aldol reactions are useful for the chemo-enzymatic synthesis of chiral synthons and biologically active compounds.<sup>91, 266-271</sup> Aldol reactions also find an application for labelling biomolecules (DNA, RNA and protein).<sup>265, 272</sup> Several approaches have been developed to catalyse aldol addition,<sup>76, 108, 169, 266, 273, 274</sup> including employing the natural or artificial *de novo* aldolases. These are enzymes bearing a catalytically active lysine, which can mediate aldol addition through the formation of an enamine intermediate as a nucleophile for conjugation.<sup>117, 275</sup> Although *de novo* and naturally occurring aldolases possess excellent catalytic efficiency and quite remarkable promiscuity,<sup>111, 117, 125, 149, 156, 276-283</sup> they require substantial engineering efforts required to accept relevant substrates.<sup>117, 149</sup>

Alternatively, secondary amine organocatalysis can be used to perform aldol addition.<sup>28, 284, 285</sup> Generally, secondary amine-based catalysts tend to accept a broader range of substrates and are more nucleophilic than the primary amine counterparts.<sup>7</sup> It would be of fundamental relevance to enable secondary amine organocatalytic aldol reaction in a biological environment.<sup>5</sup> A simple solution is to incorporate catalytic amines within a protein scaffold as a tool to improve the biocompatibility of organocatalysis.<sup>5, 117, 176, 219, 286</sup> Protein-based systems employing the catalytically active N-terminal proline of 4-oxalocrotonate tautomerase (4-OT) and its variants have been used for stereoselective aldol addition.<sup>108, 169</sup> However, this system is limited to the use of N-terminal proline and modifications on the catalyst moiety, which could help improve the catalytical efficiency of the artificial enzyme (selectivity and reactivity), are not feasible.<sup>4, 11, 32-34, 37, 43, 287, 288</sup>

Different protein-based systems bearing secondary amine other than 4-OT can be used, including the streptavidin-biotin technology. As extensively exposed in the previous chapters, streptavidin can be used as the host for organocatalysis, in particular iminium catalysis. More

importantly, our group demonstrated that nucleophiles are accessible via organocatalysis using Sav scaffold.<sup>5, 110</sup> Thus, the possibility that Sav could be employed to host enantioselective organocatalytic aldol addition was suggested. In this section, stereoselective aldol addition between acetone and different benzaldehyde derivatives, obtained using only 1 mol% of Sav:**73** complex, will be discussed (**Fig. 32**). This work demonstrates that enamine catalysis, specifically aldol addition, can be successfully applied within the Sav scaffold by using the streptavidin-biotin technology.

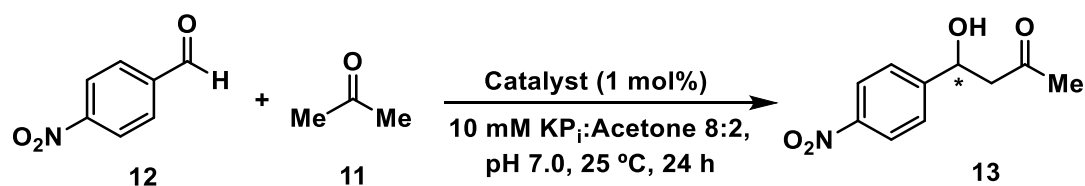


**Figure 32.** Generation of the organocatalytic artificial enzyme Sav:**73** (step 1), followed by the formation of the enamine intermediate (step 2), the attack to a benzaldehyde derivative (step 3) and release of the aldol addition product (step 4).

In the first part, a screening to assess the optimal conditions for the organocatalytic complex Sav:**73** was performed (see section 4.2). In the second part, several protein hosts were tested to increase the low enantioselectivity obtained using Sav:**73** (see section 4.3). Eventually, a pool of aromatic benzaldehydes was tested to assess Sav:**73** promiscuity towards this family of compounds (see section 4.4).

## 4.2 Screening for optimised conditions

The activity of Sav:**73** complex for enamine catalysis was initially evaluated through a series of screening tests for the aldol addition of acetone (**11**) to *p*-nitrobenzaldehyde (**12**). *p*-Nitrobenzaldehyde was initially used as it bears a reactive carbonyl group. It also does not contain any enolisable  $\alpha$ -hydrogen, whereas **11** was chosen as the nucleophile for its ability to act as both co-solvent and reactant (**Scheme 26**).



**Scheme 26.** Reaction conditions screening for aldol addition of **11** to **12**.

When no catalyst or protein was present, 17% of racemic product **13** was detected using a single equivalent of **12** in a mixture of buffer (KPi 10 mM at pH 7.0) and 20 vol% of **11** (>400 equivalent), as accessed by  $^1\text{H-NMR}$  spectroscopy (**Table 11**, **Entry 1**). By adding 1 mol% of the biotinylated organocatalyst **73**, the yield of product **13** was estimated to 36% (**Entry 2**). Interestingly, when Sav but not **73** was included, the estimated conversion was also slightly enhanced from 16% to 29% with an increasing amount of protein (0.1 mol%–1 mol%, **Entries 3–5**). In all these examples, no enantioselectivity was observed. To investigate whether aldol addition could be catalysed or not by the protein-host catalyst, Sav and ligand **73** (1:1 ratio) were added. Interestingly, a dramatic increase in the reaction yield (93%) was observed (**Entry 6**). Additionally, in the presence of Sav:**73**, the enantiomeric ratio (*er*) of *R* to *S* isomer of product **13** was assessed to be 33:67, thus indicating that stereoselective aldol addition occurs only when catalyst **73** binds to Sav (**Entries 6–8**). Akin to the previous report,<sup>110</sup> enantioselectivities were observed only when the protein scaffold was included, thereby adding evidence that the organocatalytic aldol addition occurs within Sav. To further increase the enantioselectivity, a series of reaction conditions were modified. No significant difference was observed when 1 mol% of the acid co-catalyst TFA was added, with the formation of 92% of **13** and 37:63 *er* (**Entry 9**).<sup>289-291</sup> By decreasing the reaction temperature to 10 °C, the reaction yield was dramatically reduced to 37%, and no improvement in the stereoselectivity was observed (**Entry 10**). Similarly, changing the amount of acetone or including polar co-solvents did not enhance either yield or enantioselectivity (**Entries 11-16**).

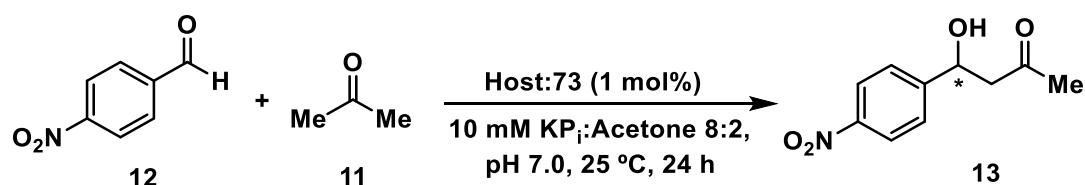
**Table 11.** Screening for assessing the best conditions to perform enamine-catalysed aldol addition.<sup>a</sup>

Entry	Catalyst	Acetone	Co-solvent	Loading (mol%)	Conv. / % product <b>13</b> <sup>b</sup>	<i>er</i> (R:S)
1	N.A.	20 vol%	N.A.	N.A.	17 ± 1	50:50
2	<b>73</b>			1	36 ± 2	50:50
3	Sav			0.1	16 ± 0	50:50
4	Sav			0.5	23 ± 2	50:50
5	Sav			1	29 ± 1	50:50
6	Sav: <b>73</b>			0.1	47 ± 3	38:62
7	Sav: <b>73</b>			0.5	79 ± 1	37:63
8	Sav: <b>73</b>			1	93 ± 0	37:63
9 <sup>c</sup>	Sav: <b>73</b>			1	92 ± 1	37:63
10 <sup>d</sup>	Sav: <b>73</b>			1	37 ± 3	34:66
11	Sav: <b>73</b>	5	25% MeOH	1	19 ± 4	33:67
12	Sav: <b>73</b>	5	25% ACN	1	12 ± 2	33:67
13	Sav: <b>73</b>	5	25% <i>i</i> -PrOH	1	1 ± 0	N.A.
14	Sav: <b>73</b>	10		1	5 ± 1	N.A.
15	Sav: <b>73</b>	20		1	9 ± 2	36:64
16	Sav: <b>73</b>	50		1	18 ± 1	33:67

<sup>a</sup> Conversion was determined by <sup>1</sup>H-NMR integration. <sup>b</sup> Reactions performed in a mixture 80:20 KPi 10 mM: Acetone at pH 7.0 using 1 equivalent of **12** at 25 °C for 24 h. <sup>c</sup> 1 mol% of TFA added. <sup>d</sup> Reaction runs at 10 °C. N.A. indicates not added.

### 4.3 Site-directed mutagenesis of the protein host

Modifications on the Sav scaffold were investigated to improve the stereoselectivity (**Scheme 27**) further. As discussed in section 2.6 and 2.7, selected variations on the protein backbone can enhance the catalytic efficiency of organocatalytic artificial enzymes without causing significant drawbacks in the binding ability.



**Scheme 27.** Aldol addition of **11** to **12** using different protein hosts.

In the specific case of Sav:**73** assembly, a combination of X-ray crystallography and molecular dynamics (MD) studies aided the identification of two “hot-spot” for mutagenesis.<sup>110</sup> Previous reports in our group revealed that Ser112 and Lys121 residues (see **Fig. 26**, section 2.6) are located close to the pyrrolidine motif of catalyst **73**. These residues were modified to verify whether the performance of the aldol addition reaction might be boosted (**Table 12**). These protein scaffolds were previously prepared, and the procedure of preparation can be found in the literature.<sup>256</sup> A short-length tetrameric streptavidin variant (T-rSav) was used to create these mutants.<sup>292</sup> T-rSav was tested for enamine catalysis in the presence of the aminocatalyst **73** showing 92% conversion of the product with a similar stereoselectivity (35:65) to what found with the native Sav scaffold (**Entry 2**). A second variant was created by modifying the residue Ser 112, positioned initially at a hydrogen-bonding distance to the pyrrolidine motif, to glutamate, a residue with substantial electronic differences. However, this mutant was found to poorly host aldol addition reaction, catalysing only the formation of 14% of product **13** with 39:61 *er* (**Entry 3**). Eventually, the Lys121 residue, which is located in close proximity to the tetrahedral intermediate formed between the aminocatalyst **73** and carbonyl groups, was replaced with the non-charged and small alanine. The newly formed K121A:**73** complex was successfully tested for aldol reaction and 89% of yield was detected (**Entry 4**). However, the enantioselectivity was assessed as 44:56, showing no improvement when compared to the original Sav:**73** complex. In general, the protein engineering efforts did not produce any enhancement in the Sav:**73** catalytic performance. Thus, further variation on the protein scaffold might be attempted to evaluate mutation on different protein residues (see L124 or S88). Also, it would be desirable to test different biotinylated organocatalysts.

**Table 12.** Screening for assessing the best conditions to perform enamine-catalysed aldol reactions. <sup>a</sup>

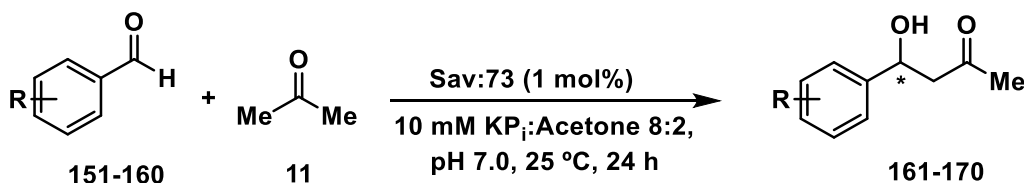
Entry	Catalyst	Conv. / % product <b>13</b> <sup>b</sup>	<i>er</i> ( <i>R</i> : <i>S</i> )
1	Sav: <b>73</b>	93 ± 0	33:67
2	T-rSav: <b>73</b>	92 ± 3	35:65
3	S112E: <b>73</b>	14 ± 2	39:61

4	K121A:73	89 ± 0	44:56
---	----------	--------	-------

<sup>a</sup> Conversion was determined by <sup>1</sup>H-NMR integration. <sup>b</sup> Reactions performed in a mixture 80:20 KPi 10 mM: Acetone at pH 7.0 using 1 equivalent of **12**, 20 vol% of **11**, 1 mol% of catalyst at 25 °C for 24 h.

#### 4.4 Substrate scope

Successively, the intriguing possibility to extend the innovative and fully biocompatible catalytic system Sav:73 to a broader scope of aromatic benzaldehydes was explored (**Scheme 28**).



**Scheme 28.** Aldol additions of benzaldehyde derivatives (**151-160**) to **11** using Sav:73.

First, aromatic aldehydes bearing the nitro group (-NO<sub>2</sub>) at different position of the aromatic ring were tested (**Table 13**). When the *o*-NO<sub>2</sub> derivative **151** was employed, the yield of the related product **161** decreased to 54% (**Entry 1**). Similarly, using *m*-nitrobenzaldehyde (**152**) Sav:73 led to the formation of only 22% of aldol addition product **162** with modest stereoselectivity (**Entry 2**). Therefore, the results obtained indicate that both *o*- and *m*-nitro derivatives are less reactive than the *p*-nitro counterpart, even though the enantiomeric ratio outcome for compound **162** is similar (**Entry 3**). When chlorine was added in the *ortho* position (**153**), the corresponding product **163** was detected in good yield (**Entry 4**). A similar yield was observed using *m*-chlorine substrate **154**, although the *er* dramatically decreased to 36:64 (**Entry 5**). Successively another class of halogenated derivatives was tested. A poor formation of aldol addition product was observed when *m*-bromine benzaldehyde **155** was reacted with **11** in the presence of Sav:73 (**Entry 6**). In this case, an *er* of 36:64 was assessed. When bromine was added in *para* (**156**), a 2-fold increase of the yield was observed (**Entry 7**). Similar to the *m*-derivative, the *p*-Br derivative product (**166**) was isolated with 40:60 *er*. When iodine was included in -meta (**157**), Sav:73 was not able to perform aldol addition more than 26%, with the *er* result in line with the one observed with other *meta*-substituted substrates (**Entry 8**). The addition of the electron-donating methoxy group in *ortho* (**158**) and *para* (**159**) position was not well-tolerated by Sav:73 complex, and the *er* of both product **168** and **169** was not determined (**Entries 9-10**). Eventually, the reactive substrate



pentafluoro benzaldehyde (**160**) was tested (**Entry 11**). In this case, the conversion to product **170** was quantitative. However, when no catalyst was employed, the conversion of **170** was assessed to 100% after the same amount of time (data not shown). When product **170** was isolated, an enantiomeric ratio of 36:64 was detected, suggesting that the reaction in the presence of Sav:**73** is faster than the background reaction.

On a marginal note, benzaldehyde was not included in these results due to difficulties to isolate the aldol product from the aqueous phase during work-out. Thus, a correct estimation of the reaction yield was not possible for this substrate.

Based on these results, it was possible to conclude that Sav:**73** assembly could mediate the formation of stereoselective aldol adducts under biocompatible conditions. When the artificial enzyme was added, the formation of *S*-enantiomer was always favoured over the *R*-enantiomer. These results confirmed the ability of Sav to form stereospecific intermediates, probably by creating a network of interactions that secure the position of the phenyl ring of the benzaldehyde derivatives into the protein scaffold. To confirm this hypothesis, further experiments using aliphatic aldehydes will be necessary.

**Table 13.** Benzaldehyde derivatives scope for aldol addition catalysed by Sav:**73** complex.<sup>a</sup>

Entry	Aldehyde (R)	Background reaction <sup>b</sup>	Conv. / % product <b>161-170</b> <sup>b</sup>	<i>er</i> ( <i>R</i> : <i>S</i> )
1	<i>o</i> -NO <sub>2</sub> ( <b>151</b> )	6 ± 2	54 ± 4	N.A.
2	<i>m</i> -NO <sub>2</sub> ( <b>152</b> )	2 ± 1	22 ± 1	31:69
3	<i>p</i> -NO <sub>2</sub> ( <b>12</b> )	17 ± 2	93 ± 0	33:67
4	<i>o</i> -Cl ( <b>153</b> )	4 ± 2	70 ± 2	N.A.
5	<i>m</i> -Cl ( <b>154</b> )	4 ± 1	67 ± 1	36:64
6	<i>m</i> -Br ( <b>155</b> )	6 ± 2	37 ± 1	36:64
7	<i>p</i> -Br ( <b>156</b> )	9 ± 0	70 ± 0	40:60
8	<i>m</i> -I ( <b>157</b> )	2 ± 0	26 ± 3	35:65
9	<i>o</i> -CH <sub>3</sub> ( <b>158</b> )	1 ± 0	17 ± 1	N.A.
10	<i>p</i> -CH <sub>3</sub> ( <b>159</b> )	<1 ± 0	<1 ± 0	N.A.
11	C <sub>6</sub> F <sub>5</sub> ( <b>160</b> )	100 ± 5	100 ± 2	36:64

<sup>a</sup> Conversion was determined by <sup>1</sup>H-NMR integration. <sup>b</sup> Reactions performed in a mixture 80:20 KPi 10 mM: Acetone at pH 7.0 using 1 equivalent of aldehydes **151-160**, 20 vol% of **11**, 1 mol% of Sav:**73** at 25 °C for 24 h. N.A. indicates not added.

## 4.5 Conclusions

In summary, we described the use of Sav as a host for organocatalytic aldol additions. For several substrates, Sav:**73** can mediate enamine catalysis leading from moderate to excellent reaction yields. The catalytic efficiency of Sav:**73** complex needs further improvement compared to other systems, such as ones catalysed by 4-OT,<sup>108, 169</sup> catalytic antibodies<sup>293</sup> and *de novo* retro-aldolases.<sup>117</sup> Therefore, Sav-based organocatalytic artificial enzymes require additional protein engineering efforts. Contrarily, to the other existing system, Sav:**73** and similar assemblies can be evolved and improved by modifying both the ligand (*i.e.* **73**) and the protein scaffold. In particular, further efforts should be dedicated to enhancing the modest enantioselectivity obtained to this point. The use of directed evolution techniques might be beneficial to isolate several variants of Sav able to boost the formation of stereospecific aldol adducts. Herein, it is described that Ser112 and Lys121 residues can be essential in dictating the reaction conversion and stereoselectivity, respectively. These residues will be subject to further investigations aiming to improve the performance of this Sav-hosted aldol addition reaction.

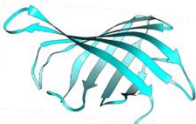
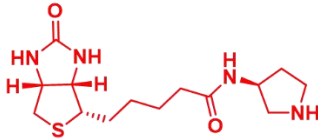
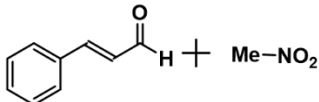

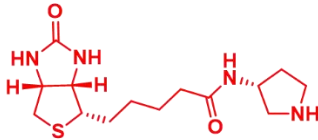
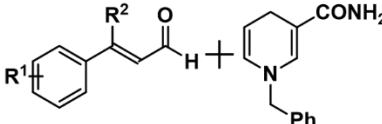

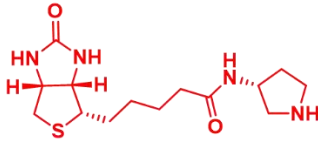
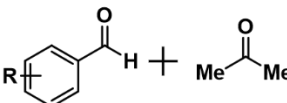
Although Sav:**73** complex was revealed to be promiscuous towards aromatic aldehydes, additional work is required to expand the substrate scope to ketones (*i.e.* cyclohexanone) and aliphatic aldehydes (linear and branched).

In conclusion, this chapter described a proof-of concept-study. In particular, this study shows that Sav-hosted organocatalytic aldol addition can be potentially applied with success in chemical and synthetic biology research in future.

## Chapter 5: Conclusion and future perspectives

### 5.1 Conclusion

This thesis aims to develop organocatalytic artificial enzymes for iminium and enamine catalysis under biocompatible conditions.<sup>5, 50</sup> Based on the previous works performed in our research group, the supramolecular approach built upon the streptavidin-biotin technology (Sav:**73**) is particularly fruitful.<sup>110</sup> In the first part of this work, two novel artificial enzymes, M-Sav:**73** and M-Sav:**74**, were created and tested for iminium catalysis (**Fig. 33**). In the second part, Sav:**73** was employed for iminium catalysed transfer hydrogenations, whereas in the last chapter enamine catalysis was performed using Sav:**73** complex.

Chapter (Protocol)	Host	Guest	Applied to
2 (Iminium catalysis)	 M-Sav	 Catalyst 74	1,4-Michael Addition 
3 (Iminium catalysis)	 Sav	 Catalyst 73	Transfer Hydrogenation 
4 (Enamine catalysis)	 Sav	 Catalyst 73	Aldol Addition 

**Figure 33.** Summary of the organocatalytic artificial enzymes presented in this work and their applications.

#### 5.1.1 Monomeric streptavidin-hosted 1,4-Michael addition

In the initial stages of this work, protein scaffold alternative to Sav was tested as host for iminium catalysis. A monomeric variant of streptavidin (M-Sav) was chosen for hosting 1,4-Michael additions of nitromethane to cinnamaldehyde. Compared to the tetrameric counterpart (Sav), M-Sav contains a more accessible active site and lacks subunit interactions. Therefore, testing the M-Sav scaffold for iminium catalysis could provide a useful

comparison to Sav for further artificial enzymes design. Initially, M-Sav was prepared by gene expression, purified and refolded in the presence of the biotinylated organocatalysts (**73** and **74**) to generate the complexes M-Sav:**73** and M-Sav:**74**. After characterising the newly formed artificial enzymes by CD spectroscopy, they were tested for iminium catalysis. Despite screening various conditions, low yield of the desired 1,4-Michael adduct was observed (20% conversion). Driven by the desire to improve the catalytic efficiency, the M-Sav:**74** crystal structure was examined and compared to the structures of Sav:**73** and Sav:**74**. Since M-Sav Y111 residue is close to aminocatalyst **74**, it was likely that this residue dictates how nitromethane approaches the iminium intermediate for the reaction. Through site-directed mutagenesis studies, five variants of the M-Sav scaffold bearing Y111 mutations were created and tested using organocatalyst **74** as a guest. The resulting variants did not lead to any significant improvement showing Y111 does not influence the catalytic efficiency of M-Sav:**73** and M-Sav:**74** complexes in this specific case. This outcome suggests that the Y111 residue might not be located in a crucial position to dictate how nitromethane approaches the iminium intermediate. Therefore, any modification on the steric/electronic properties of the residue 111 might not affect the formation of transition states or reaction intermediates.

In summary, this part of work showed that M-Sav catalytic efficiency is not comparable to the one of the tetrameric counterpart (Sav), implying the subunit interface is crucial for catalysis. It was reported that the protein subunits could dictate the orientation of the substrate and reaction stereoselectivity.<sup>110</sup> Indeed, molecular dynamics studies performed by our collaborators (Prof. Vicent Moliner and Dr Katarzyna Swiderek at Universitat Jaume I, Spain) suggest at least two Sav subunits contribute to the step of deprotonation of nitromethane. In the case of M-Sav, the lack of a second subunit might affect the efficiency of the deprotonation step. Furthermore, the formation of the 1,2-addition product seems to be favoured within M-Sav scaffold. In this case, the M-Sav active site could be too exposed and might not discriminate between the expected product and side-product.

### 5.1.2 Tetrameric streptavidin-hosted transfer hydrogenation

In the second part of this work (Chapter 3), streptavidin was reported as host for organocatalytic transfer hydrogenations. This part of the work aimed to expand the reaction repertoire of the Sav:**73** assembly using a well-known model reaction. Using only 1 mol %, Sav:**73** was able to mediate one of the first examples of organocatalytic transfer hydrogenation of a pool of aromatic  $\alpha,\beta$ -unsaturated aldehydes in a biocompatible

environment. Importantly, we demonstrated the use of the small biocompatible hydrogen donor BNAH within the organocatalytic artificial enzyme. In most cases, Sav:**73** could achieve excellent conversions for several substrates and demonstrated promiscuity for aromatic  $\alpha,\beta$ -unsaturated aldehydes. KIE studies were performed in an aim to analyse the mechanism of action of Sav-hosted transfer hydrogenation. It was revealed that the protein facilitates the step of hydrogen transfer, which was assumed as being the rate-limiting step because of the low KIE value. Eventually, the Sav:**73** kinetics for the conversion of cinnamaldehyde into hydrocinnamaldehyde were determined. It emerged that additional work of protein engineering is required to improve the catalytic efficiency of Sav:**73**. In summary, a proof-of-concept study was reported expanding the scope of iminium catalysed transformation available using artificial enzymes.

### 5.1.3 Tetrameric streptavidin-hosted aldol addition

The last part of this work aimed to verify whether Sav:**73** could host a different organocatalytic activation protocol other than iminium catalysis. Therefore, an enamine catalysed reaction was performed within an organocatalytic artificial enzyme.<sup>294</sup> In this proof-of-concept study, Sav:**73** was employed to mediate stereoselective aldol addition of acetone to several aromatic benzaldehydes achieving from moderate to excellent reaction yields. By using 1 mol% of catalyst enantiomeric ratios from 40:60 to 33:67 (*R:S*) were detected. For all the substrates tested, Sav:**73** favoured the formation of the *S* isomer. This preference can be explained by considering that the enamine intermediate between **73** and acetone is tightly bonded within the Sav cavity and possesses limited mobility within the protein scaffold. Thus, the benzaldehyde derivative orientation determines how the enamine intermediate attacks the electrophile, and therefore the product stereoselectivity. Lastly, we aimed to improve the stereoselectivity via a mutagenesis approach changing the scaffold of Sav. While modifications in position 112 and 121 significantly affect the reaction conversion and stereoselectivity, a variant that improves both the efficiency and selectivity could not be identified.

## 5.2 Future perspectives

To improve the design of the family of organocatalytic artificial enzymes presented herein, future directions and experimental designs are outlined in the following.

### 5.2.1 Monomeric streptavidin-hosted 1,4-Michael addition

The M-Sav scaffold has not proved to be ideal for hosting 1,4-Michael additions combined with catalysts **73** and **74**. Further refinement of the protein environment could be obtained using techniques of genetic manipulations. A straightforward solution is to modify single residues, as was done for Y111, by site-directed mutagenesis. The E120 residue showed promising results, and pursuing other modifications on this residue might substantially improve the catalytic efficiency. Moreover, it would be ideal to prepare mutants bearing modifications on the S87 residue to understand whether this residue is involved in the reaction. Alternatively, directed evolution could be employed to create a library of mutants. Screening systems based on colourimetric or fluorescent assays for 1,4-Michael addition have been previously developed and could be used for this purpose.<sup>111</sup>

In a different fashion, by inserting new classes of biotinylated organocatalysts within M-Sav, different organocatalytic activation protocol can be allowed within a biocompatible environment. On the one hand, thiourea-based biotinylated organocatalysts can be easily prepared (data not shown) and tested for improving the catalytic efficiency of M-Sav based systems using H-bonding organocatalysis. On the other hand, bulkier catalysts, such as metal-based catalysts reported within M-Sav,<sup>181</sup> have shown to be extremely active within the large scaffold of M-Sav. The development of bulky biotinylated organocatalysts, *i.e.* catalyst **23**, offers an attractive alternative in this aspect.

### 5.2.2 Tetrameric streptavidin-hosted transfer hydrogenations and aldol additions

The excellent results obtained using Sav:**73** complex for transfer hydrogenation could lead to further applications of this technology. To achieve that, the mechanism of the reaction within Sav scaffold should be completely identified. It would be desirable to prepare deuterated analogues for the different reaction steps and verify whether KIE is observed.

Furthermore, the Sav:**73** substrate scope is limited to aromatic  $\alpha,\beta$ -unsaturated aldehydes and  $\beta$ -methylated derivatives. The formation of the *S/R* enantiomer of the hydrogenated products has not been verified and should be added to the top-priority list. Furthermore, testing a variety of aliphatic and cyclic  $\alpha,\beta$ -unsaturated aldehydes or unreactive  $\alpha,\beta$ -unsaturated ketones class would help to establish the utility of the catalytic system.

For the aldol addition catalysed by Sav:**73**, the stereoselectivity can be further improved. The mutations proposed in this work were not successful, but changing S112 and K121 with different amino acids could help to design more competent variants.

Although Sav:**73** complex was revealed to be promiscuous towards aromatic aldehydes, additional work is required to expand the substrate scope to ketones (*i.e.* cyclohexanone) and aliphatic aldehydes (linear and branched).

At the moment, Sav:**73** assembly is not as efficient as other artificial enzyme employed for transfer hydrogenation and aldol addition.<sup>105, 116</sup> In particular, both activity and selectivity are far from optimal. Bringing these findings together with in-depth mechanistic studies, such as KIE and rational mutations, directed evolution should be used with appropriate screening reactions to speed up the process. Thus, site-directed mutagenesis and directed evolution can be employed to evolve the Sav scaffold. In particular, several reports have identified the S88, S112, K121, L124 residues to be crucial for chemical catalysis within Sav scaffold.<sup>105, 116</sup> of Sav mutants.

## Chapter 6: Experimental part

### 6.1 General information

#### 6.1.1 Chemistry

Reactions were performed in oven-dried glassware without precautions to exclude air. Reaction temperatures are stated as heating device temperature (e.g., oil bath, shaker, etc.), if not stated otherwise. Concentrations under reduced pressure were performed by rotary evaporation at 40 °C at the appropriated pressure, unless otherwise noted. Deionized water was obtained by a PURELAB® Option system (15 MΩ·cm, ELGA LabWater, High Wycombe, UK). Analytical and preparative thin-layer chromatography (TLC) was carried out with silica gel 60 F254 aluminium sheets (Merck KGaA, Darmstadt, Germany). Detection was carried out using UV light ( $\lambda = 254$  nm and 366 nm), followed by immersion in permanganate staining solution with subsequent development via careful heating with a heat gun. Flash column chromatography was performed using silica gel (pore size 60 Å, 0.040– 0.063 mm, Global Life Sciences Solutions USA LLC, Marlborough, USA). A 3510 benchtop pH Meter (VWR International, Radnor, USA) connected to a Universal pH electrode (VWR International, Radnor, USA) was used for the pH adjustment of buffers and reaction mixtures employing either 1.0 M or 0.1 M sodium hydroxide solution or hydrochloric acid. Shaking of the reactions (300 rpm) at 25 °C was achieved using a thermoshaker Mini shake lite (VWR International, Radnor, USA) or an Incubating Orbital Shaker (VWR International, Radnor, USA).  $^1\text{H}$ - and  $^{13}\text{C}$ -NMR spectra were recorded in  $\text{CDCl}_3$  or  $\text{DMSO-d}_6$  on Bruker Fourier 300, Ultrashield 400, or Ascend 500 instruments (Bruker Corporation, Billerica, USA). Chemical shifts are reported in parts per million (ppm) and are referenced to the residual solvent resonance as the internal standard ( $\text{CDCl}_3$ :  $\delta = 7.26$  ppm for  $^1\text{H}$ ;  $\text{DMSO}$ :  $\delta = 2.54$  ppm for  $^1\text{H}$ ). Data are reported as follows: chemical shift ( $\delta$ ), multiplicity (br s = broad singlet, s = singlet, d = doublet, dd = double doublet, td = triple doublet, t = triplet, dt = double triplet, q = quartet, p = pentet, sept = septet, br m = broad multiplet, m = multiplet, mc = centrosymmetric multiplet), coupling constants (Hz) and integration. Size exclusion chromatography was performed using a ÄKTA Purifier workstation (Global Life Sciences Solutions USA LLC, Marlborough, USA) system with the respective column mentioned in the detailed procedure. High resolution mass spectra (HRMS) were recorded on a *Waters LCT Premier* for ESI-(+) and APCI-(+) or a *Waters GCT Premier* (EI) system (Waters, Elstree, UK).



Cinnamaldehyde (**14**) for 1,4-Michael addition and transfer hydrogenation reactions with Sav and M-Sav was obtained commercially (Merck KGaA, Darmstadt, Germany) and was used without further purification. For all other reactions, **14** was washed with aqueous sodium bicarbonate solution (pH 8.3), dried over magnesium sulphate and stored under an inert atmosphere at  $-23\text{ }^{\circ}\text{C}$ . Nitromethane (**47**) for 1,4-Michael addition reaction was obtained commercially (Merck KGaA, Darmstadt, Germany) and was used without further purification. Diethyl 1,4-dihydro-2,6-dimethyl-3,5-pyridinedicarboxylate (Hantzsch ester, **84**), nicotinamide adenine dinucleotide (NADH, **86**), 3-phenyl propanal (**88**), (*E*)-3-(*p*-chlorophenyl) acrylaldehyde (**96**), (*E*)-3-(*p*-fluorophenyl) acrylaldehyde (**97**), (*E*)-3-(*p*-bromophenyl) acrylaldehyde (**98**), (*E*)-3-(*p*-methoxyphenyl) acrylaldehyde (**99**), (*E*)-3-(*p*-nitrophenyl) acrylaldehyde (**100**) and (*E*)-3-(*p*-tolyl) acrylaldehyde (**101**) are commercially available (Merck KGaA, Darmstadt, Germany) and were used without further purification.

*p*-Nitrobenzaldehyde (**12**) and acetone (**11**) for aldol addition reactions with Sav was obtained commercially (Merck KGaA, Darmstadt, Germany) and if necessary purified by washes with sodium bicarbonate pH 8.3, subsequent drying with magnesium sulphate and stored under an inert atmosphere at  $4\text{ }^{\circ}\text{C}$ . *o*-Nitrobenzaldehyde (**151**), *m*-nitrobenzaldehyde (**152**), *o*-chlorobenzaldehyde (**153**), *m*-chlorobenzaldehyde (**154**), *m*-bromobenzaldehyde (**155**), *p*-bromobenzaldehyde (**156**), *m*-iodobenzaldehyde (**157**), *o*-methoxybenzaldehyde (**158**), *p*-methoxybenzaldehyde (**159**) and pentafluorobenzaldehyde (**160**) are commercially available (Merck KGaA, Darmstadt, Germany) and were used without further purification.

All other solvents (Fischer Scientific, Waltham, USA) and reagents were obtained from commercial sources and used as received.

Tetrameric streptavidin (Sav), employed in Chapter 3 and 4, was obtained commercially (ProSpec-Tany TechnoGene Ltd., Ness-Ziona, Israel). Protein concentrations were determined using NanoDrop 2000/2000c Spectrophotometer (ThermoFischer UK, Loughborough, UK)

### 6.1.2 Circular dichroism experiments

The circular dichroism spectra were recorded on a Chirascan<sup>TM</sup> CD spectrophotometer (Applied Photophysics) with a temperature controller using a cuvette with a path length of 1

mm. A spectral bandwidth of 1 nm was used for data collection. M-Sav was dissolved in PBS buffer (pH 7.4) at a concentration of 50  $\mu\text{M}$  using 500  $\mu\text{M}$  of the appropriate ligand. Blank was prepared using 500  $\mu\text{M}$  of the proper ligand or using only the buffer. To induce heat denaturation, the temperature was increased from 4 to 96  $^{\circ}\text{C}$ , and the CD spectra were recorded between 200 and 300 nm for every 2  $^{\circ}\text{C}$  increments. Melting temperatures were recorded at 233 nm.<sup>227</sup> The CD measurement produced an ellipticity value (in mdeg), which was converted into the mean residue molar ellipticity ( $[\theta]$ , see **Eq. 2**, Chapter 2). Data for  $T_m$  were fitted using a dose-response function. The signal were plotted using Origin2019 (OriginLab Corporation One, Northampton, USA).

## 6.2 Monomeric streptavidin as host for iminium catalysis

### 6.2.1 Synthesis of catalyst 73 and 74

The synthesis of the biotinylated organocatalysts **73** and **74** (see **Scheme 16**, chapter 2). were carried out from a known procedure.<sup>110</sup>

#### 6.2.1.1 Synthesis of (+)-Biotin NHS ester 81

The (+)-Biotin NHS ester (**81**) was synthesised as follows: (+)-Biotin (**79**, 960 mg, 4.0 mmol, 1.0 eq), *N*-hydroxysuccinimide (**80**, NHS, 920 mg, 8.0 mmol, 2.0 eq), and 2-(dimethylamino)pyridine (DMAP, 24 mg, 0.2 mmol, 0.05 eq) were dissolved in dry DMF (40 mL) under inert atmosphere. The solution was cooled to 0  $^{\circ}\text{C}$  with an ice bath. Dicyclohexylcarbodiimide (DCC, 908 mg, 4.4 mmol, 1.1 eq) dissolved in 5 mL of dry DMF was then added dropwise. The reaction mixture was left stirring at room temperature overnight and formed precipitate was removed via vacuum filtration. Crude NHS ester was precipitated by the addition of  $\text{Et}_2\text{O}$ , collected by filtration, and washed with deionized water and  $\text{Et}_2\text{O}$ . The crude product was recrystallized from isopropanol, collected via filtration, and washed with  $\text{Et}_2\text{O}$  to afford the active ester as white solid after drying under fine vacuum (272 mg, 0.8 mmol, 20% yield).

**$^1\text{H-NMR}$  (400 MHz, DMSO- $d_6$ ),  $\delta$ :** 6.43 (s, 1H), 6.37 (s, 1H), 4.32 (mc, 1H), 4.13 (mc, 1H), 3.10 (mc, 1H), 2.87–2.78 (m, 5H), 2.67 (t,  $J = 7.3$  Hz, 1H), 2.58 (d,  $J = 12.6$  Hz, 1H), 1.71 – 1.28 (m, 6H) ppm. The analytical data have been found to be in good agreement with the reported data.<sup>110</sup>

### 6.2.1.2 Synthesis of catalyst 73

**81** (100 mg, 0.29 mmol, 1.0 eq) and (3*R*)-3-amino-1-Boc-pyrrolidine (**82a**, 64 mg, 0.29 mmol, 1.0 eq) were dissolved in 3 mL of dry DMF. Di-iso-propylethylamine (DIPEA, 106  $\mu$ L, 0.58 mmol, 2.0 eq) was added, and the reaction was allowed to proceed under stirring overnight at room temperature. The solvent was removed under reduced pressure at 80 °C. The residue was dissolved in a mixture of TFA:H<sub>2</sub>O (95:5, 5.0 mL) and stirred at room temperature for 1 h. Excess TFA was removed under reduced pressure, and the residue was dissolved in a minimal amount of H<sub>2</sub>O and lyophilized. The crude product was purified by preparative HPLC (Supelcosil C18 column, 25 cm x 21.2 mm, 12  $\mu$ m; gradient H<sub>2</sub>O:MeCN 99:1 to 50:50 over 30 min, 0.1% HCO<sub>2</sub>H, 10 mL·min<sup>-1</sup>, 20 °C,  $\lambda$ = 210 nm) and compound **73** was obtained as white solid (37 mg, 0.11 mmol, 41% yield).

**<sup>1</sup>H-NMR (400 MHz, D<sub>2</sub>O),  $\delta$** : 4.57 (dd,  $J$ = 7.8 and 4.9 Hz, 1H), 4.45–4.35 (m, 2H), 3.54 (dd,  $J$ = 12.5 and 7.0 Hz, 1H), 3.46–3.35 (m, 2H), 3.30 (dt,  $J$ = 9.6 and 4.1 Hz, 1H), 3.19 (dd,  $J$ = 12.5 and 4.9 Hz, 1H), 2.95 (dd,  $J$ = 13.1 and 4.9 Hz, 1H), 2.74 (d,  $J$ = 13.1 Hz, 1H), 2.38–2.27 (m, 1H), 2.23 (t,  $J$ = 7.2 Hz, 2H), 1.99 (td,  $J$ = 13.5 and 6.8 Hz, 1H), 1.76–1.47 (m, 4H), 1.45–1.31 (m, 2H) ppm.

**<sup>13</sup>C-NMR (100 MHz, D<sub>2</sub>O),  $\delta$** : 177.1, 170.9, 165.3, 62.0, 60.2, 55.3, 49.6, 48.6, 44.3, 39.6, 35.1, 29.4, 27.8, 27.6, 24.9 ppm.

**HRMS (ESI-+)**:  $m/z$ : calculated for C<sub>14</sub>H<sub>25</sub>N<sub>4</sub>O<sub>2</sub>S: 313.1698, [M+H]<sup>+</sup>; found: 313.1688.

The analytical data have been found to be in good agreement with the reported data.<sup>110</sup>

### 6.2.1.3 Synthesis of catalyst 74

Catalyst **74** was synthesised from compound **81** using the same procedure applied for catalyst **73**. (3*R*)-3-amino-1-Boc-pyrrolidine (**82a**) was replaced by the its enantiomer (3*S*)-3-amino-1-Boc-pyrrolidine (**82b**).

**<sup>1</sup>H-NMR (400 MHz, D<sub>2</sub>O),  $\delta$** : 4.57 (dd,  $J$ = 7.8 and 4.9 Hz, 1H), 4.45–4.35 (m, 2H), 3.54 (dd,  $J$ = 12.5 and 7.0 Hz, 1H), 3.46–3.35 (m, 2H), 3.30 (dt,  $J$ = 9.6 and 4.1 Hz, 1H), 3.19 (dd,  $J$ = 12.5 and 4.9 Hz, 1H), 2.95 (dd,  $J$ = 13.1 and 4.9 Hz, 1H), 2.74 (d,  $J$ = 13.1 Hz, 1H), 2.38–2.27 (m, 1H), 2.23 (t,  $J$ = 7.2 Hz, 2H), 1.99 (td,  $J$ = 13.5 and 6.8 Hz, 1H), 1.76–1.47 (m, 4H), 1.45–1.31 (m, 2H) ppm.

**<sup>13</sup>C-NMR (100 MHz, D<sub>2</sub>O), δ:** 177.1, 170.9, 165.3, 62.0, 60.2, 55.3, 49.6, 48.6, 44.3, 39.6, 35.1, 29.4, 27.8, 27.6, 24.9 ppm.

**HRMS (ESI(+)):** m/z: calculated for C<sub>14</sub>H<sub>25</sub>N<sub>4</sub>O<sub>2</sub>S: 313.1698, [M+H]<sup>+</sup>; found: 313.1688.

The analytical data have been found to be in good agreement with the reported data.<sup>110</sup>

## 6.2.2 Experimental details for the preparation and purification of M-Sav and mutants

### 6.2.2.1 Expression and Purification

Monomeric streptavidin (M-Sav) and relative mutants were expressed using an *E. coli* expression system with the following protocol. Plasmid pRSET-mSA (see chapter 2, **Fig. 18**) containing the desired *M-Sav* gene in a pRSET-A vector was transformed into calcium competent BL21 AI cells and grown for 16 h on LB agar plates containing 100 µg/mL ampicillin. A single colony from the plate was picked to inoculate a 5 mL LB culture overnight. The starter culture was diluted into 500 mL of LB medium containing 100 µg/mL ampicillin. The culture was grown at 37 °C and 225 rpm to an OD<sub>600</sub> of 0.8–1.0 and induced with a final concentration of 0.5 % w/v L-Arabinose. The culture was grown overnight at 20 °C. The pellet was harvested by centrifugation at 4000 rpm at 4 °C for 25 min, resuspended in 10 mL of wash buffer 1 (50 mM Tris-HCl, 100 mM NaCl, pH 8.0) and lysed via sonication (7 min, 5 s on, 10 s off). 10 mL of lysate buffer 2 (50 mM Tris-HCl, 100 mM NaCl, and 6 M GdnHCl, pH 8) were added to the suspension and left to dissolve incubating 3 h at 4 °C. The insoluble fraction was removed by centrifugation at 4000 rpm at 4 °C for 25 min, and the supernatant was mixed with 3 mL of Ni-NTA affinity resin for 6xHis affinity purification. After incubation at 25 °C for 1.5 h with occasional stirring, the resin was washed twice with 1.5 volumes of resin wash buffer 3 (50 mM Tris-HCl, 100 mM NaCl, 6 M GdnHCl, and 10 mM imidazole, pH 7.5). M-Sav was eluted with elution buffer 4 (3× 3.5 mL, 50 mM Tris-HCl, 150 mM NaCl, 6 M GdnHCl, and 300 mM imidazole, pH 8.0). Samples of the wash and elution fractions were collected and run on SDS-PAGE gel (15% w/v). The elution fractions were added drop by drop to 40 mL of ice-cold refolding buffer 5 (50 mM Tris-HCl, 150 mM NaCl, 0.3 mg/mL catalyst **73** or **74**, 0.2 mg/mL oxidized glutathione, and 1 mg/mL reduced glutathione) under rapid stirring to refold the protein. The precipitates were removed by centrifugation at 4000 rpm at 4 °C for 25 min. The refolded protein solution was concentrated to 5 mL using Amicon centrifugal concentrators with a 10 kDa cutoff. The concentrated protein solution was applied to size exclusion chromatography (Hi-Load<sup>TM</sup> column, Superdex 200 pg, 50 mM Tris-HCl, 150

mM NaCl, pH 8.0). Fractions containing protein (analysis by following 215, 255 and 280 nm UV traces) were collected, and the samples loaded on SDS-PAGE to check the purity of the protein (15% w/v). Fractions containing M-Sav were pooled, transferred to a centrifugal concentrator with a 10 kDa cutoff and the buffer was exchanged to 10 mM KPi, pH 7.0. Protein concentration was quantified by absorbance spectroscopy at 280 nm.

### 6.2.2.2 Site-directed mutagenesis

The mutations were introduced by site-directed mutagenesis PCR using PrimeStar HS DNA polymerase (Takara Bio Inc., Kusatsu, Japan) and the accompanying buffers, dNTPs and primers mentioned in **Table 14** below. For single mutants at Y111 the mentioned forward primers are used in conjunction with reverse primer and GGTCAGGTTCCACTGGTGTG. For all single mutants the following protocol was used:

#### Method 1

Initial denaturing: 3 min, 95 °C

33 cycles: 10 s, 98 °C

5 s, 63 °C

4 min, 72 °C

Final extension: 10 min, 72 °C

Hold: 4 °C

The mutant constructs were confirmed by DNA sequencing (Eurofins Genomics Germany GmbH, Ebersberg, Germany) using the T7 promoter primer (TAATACGACTCACTATAGG).

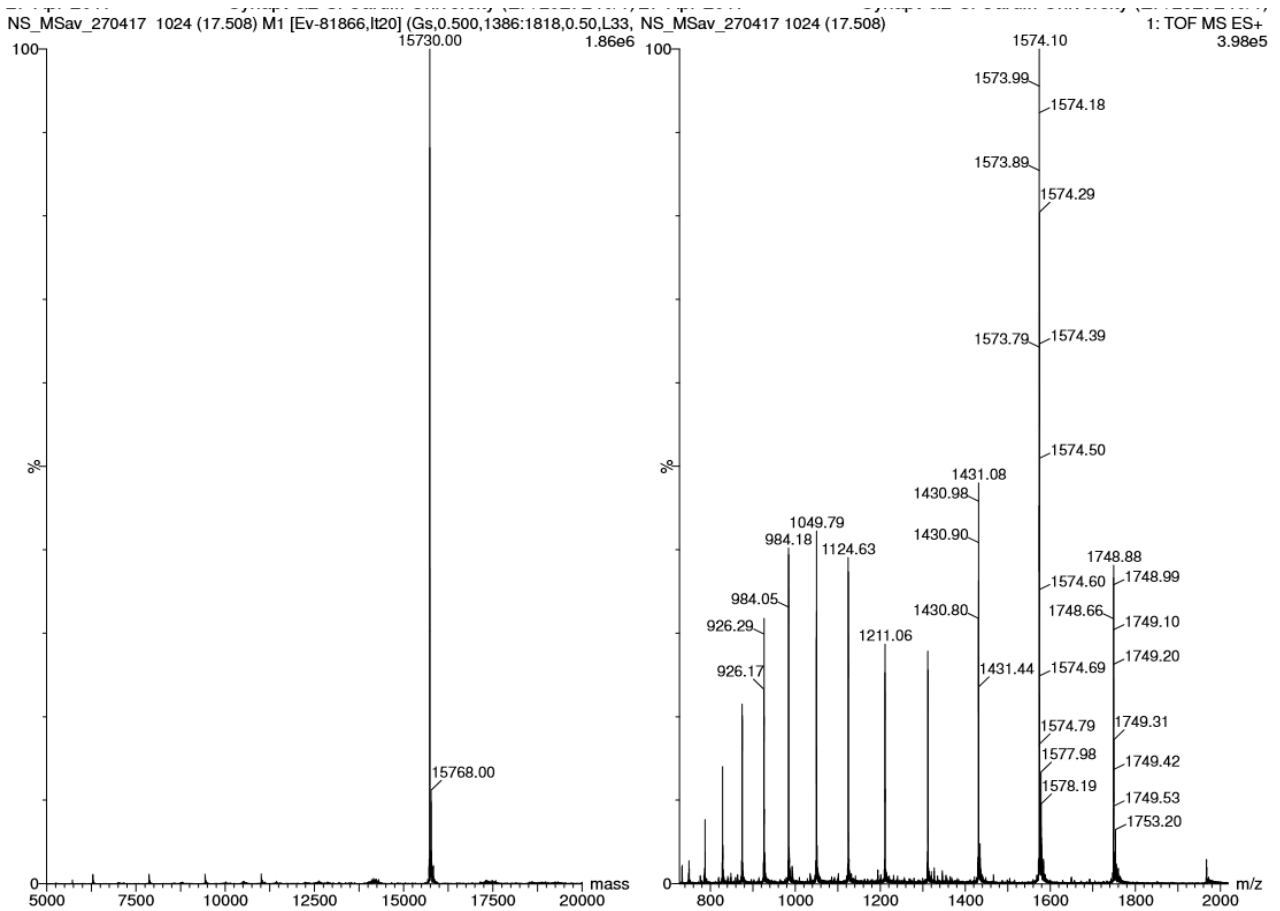
**Table 14.** List of primers used for the introduction of mutations in M-Sav at positions Y111.

Mutation	Primer (5' to 3')
Y111A	Forward CAGTGGAACCTGACC <b>GCG</b> GAAGGTGGTTCTGGTCCGGCGACCGAAC
Y111K	Forward CAGTGGAACCTGACC <b>AAA</b> GAAGGTGGTTCTGGTCCGGCGACCGAAC
Y111S	Forward

	CAGTGG AACCTGACC <b>AGC</b> GAAGGTGGTTCTGGTCCGGCGACCGAAC
Y111T	Forward CAGTGG AACCTGACC <b>ACC</b> GAAGGTGGTTCTGGTCCGGCGACCGAAC
Y111V	Forward CAGTGG AACCTGACC <b>GUG</b> GAAGGTGGTTCTGGTCCGGCGACCGAAC

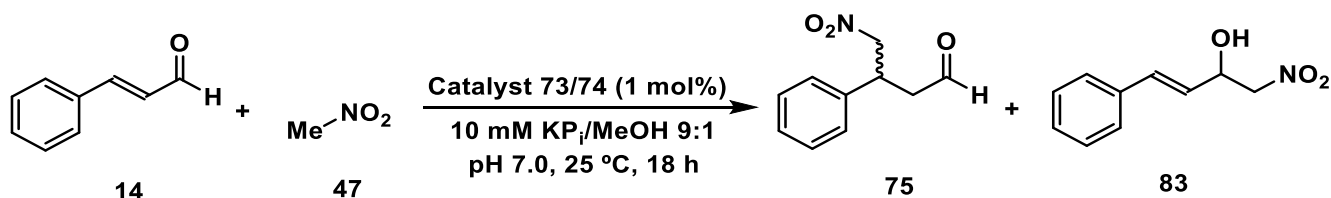
### 6.2.2.3 HRMS of M-Sav

Expected MW: 15730 Da. Observed MW: 15730 Da.



### 6.2.3 Experimental details for the 1,4-Michael addition activity screening

#### 6.2.3.1 General procedure for the <sup>1</sup>H-NMR based screening for yield determination



A stock solution of cinnamaldehyde (**14**, 1.33 M) and nitromethane (**47**, 6.61 M) were prepared and dissolved in methanol. In an 1.5 mL Eppendorf tube 0.5 mg (33 nmol, 1 mol %) of M-Sav were weighted and dissolved in 400  $\mu$ L  $KP_i$  pH 7.0. A stock solution of catalyst **73/74** (3.19 mM) was prepared and dissolved in  $KP_i$  pH 7.0 added to an 1.5 mL Eppendorf tube. An aliquot of the stock solution of **73/74** (10.3  $\mu$ L) was added to the Eppendorf tube. **47** (4.96  $\mu$ L, 33  $\mu$ mol, 10.00 eq) and **14** (2.48  $\mu$ L, 3.3  $\mu$ mol, 1.00 eq) were added and to the solution was added  $KP_i$  pH 7.0 up to 500  $\mu$ L. The mixture was homogenized by shaking at 500 rpm for 5 min at 25 °C and the mixture was shaken at 300 rpm at 25 °C for 18 h. DCM (500  $\mu$ L) was added and the biphasic mixture was shaken vigorously for 1 min. This operation was repeated three times and the organic phase collected and evaporated under vacuum. The crude of reaction was dissolved in  $CDCl_3$  and subject to <sup>1</sup>H-NMR.

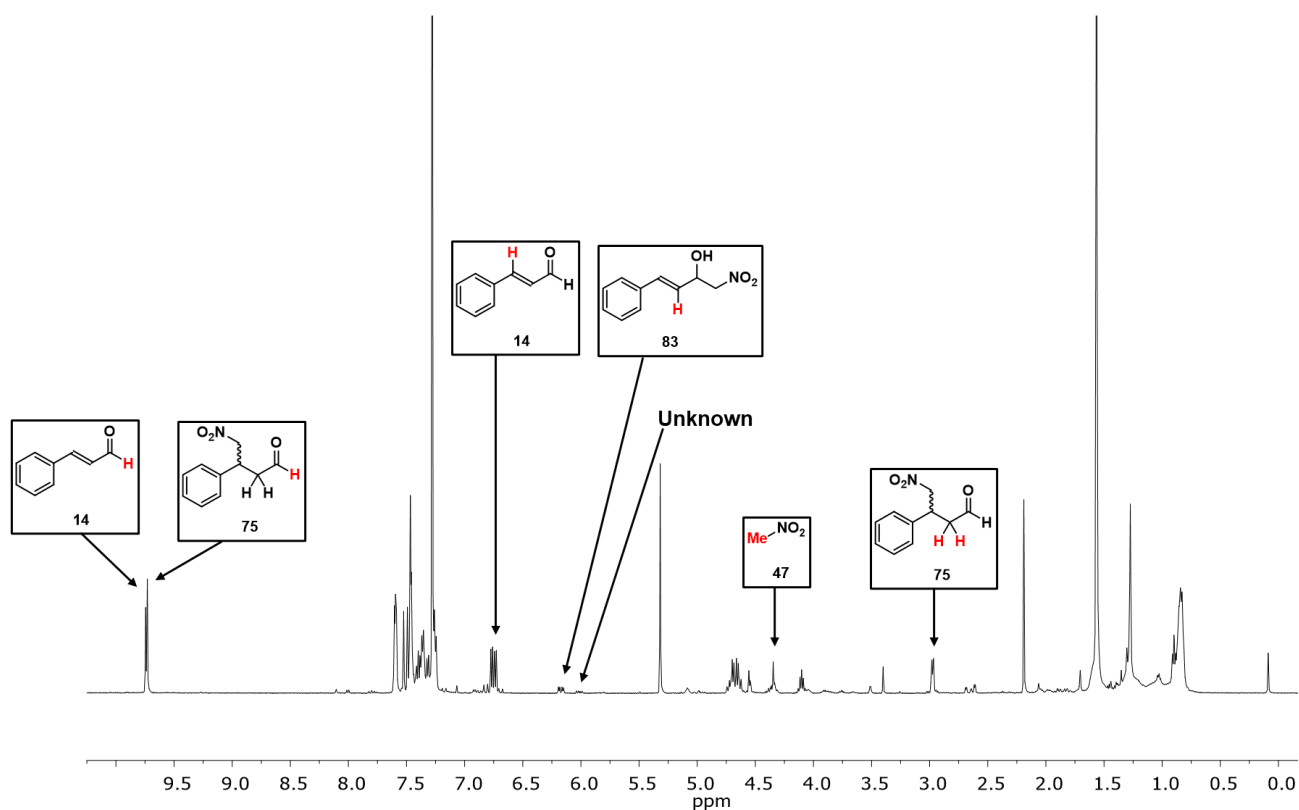
The same procedure was applied for the M-Sav mutants.

#### 6.2.3.2 <sup>1</sup>H-NMR based determination of the reaction conversion

The side-product (**83**, region between 6.5-6 ppm) and product (**75**, region between 2.5-3 ppm) conversions were estimated by measuring the integral ratio with **14** (region between 7-6.5 ppm) (**Fig. 34**). Initially, **83** conversion was estimated by integration of the **14** double bond (integrated as 1) and **83** double bond (integrated as 1). The remaining amount of **14** was used to calculate the conversion of **75**. The **75** conversion was estimated by integration of the **14** double bond (integrated as 1) and **75**  $CH_2$  protons (integrated as 2). The aldehydic peaks (region between 9-10 ppm) of both **75** and **14** could not be used for integration as they are overlapping. Also, a peak corresponding to an unknown compound was observed in

several spectra in the region between 6 and 6.25 ppm. The compound was not isolated but its peak was integrated as 1 and considered as side-product of the reaction.

It is important to note that in some cases the side-product **83** was formed in large amount and its other double bond peak at 6.75 ppm was interfering with the **14** double bond peak. In these unique situations, the cinnamaldehyde aldehydic peak (region 9.5-10 ppm) was taken as reference for the integration, although not corresponding to an extremely precise quantification.



**Figure 34.**  $^1\text{H-NMR}$  spectrum of M-Sav catalysed 1,4-Michael addition. Each compound (**14**, **47**, **75** and **83**) and relative peaks are reported in the black box. The proton used for integration are drawn in red.

## 6.2.4 $^1\text{H-NMR}$ determination for substrates and compounds

### 6.2.4.1 Isolation and characterisation of product **75**

Product **75** was isolated after reaction of **14** with **47** using M-Sav:**74** as catalyst.

$^1\text{H-NMR}$  (500 MHz,  $\text{CDCl}_3$ ),  $\delta$ : 9.71 (t,  $J = 1.0$  Hz, 1H), 7.38-7.20 (m, 5H), 4.68 (dd,  $J = 12.3$  and 7.1 Hz, 1H), 4.62 (dd,  $J = 12.6$  Hz and 7.7 Hz, 1H), 4.08 (quint,  $J = 7.3$  Hz, 1H), 2.96 (pt,  $J = 1.3$  Hz, 1H), 2.93 (pt,  $J = 1.2$  Hz, 1H)



The analytical data have been found to be in good agreement with the reported data.<sup>295</sup>

### 6.2.4.2 Isolation and characterisation of the side-product **83**

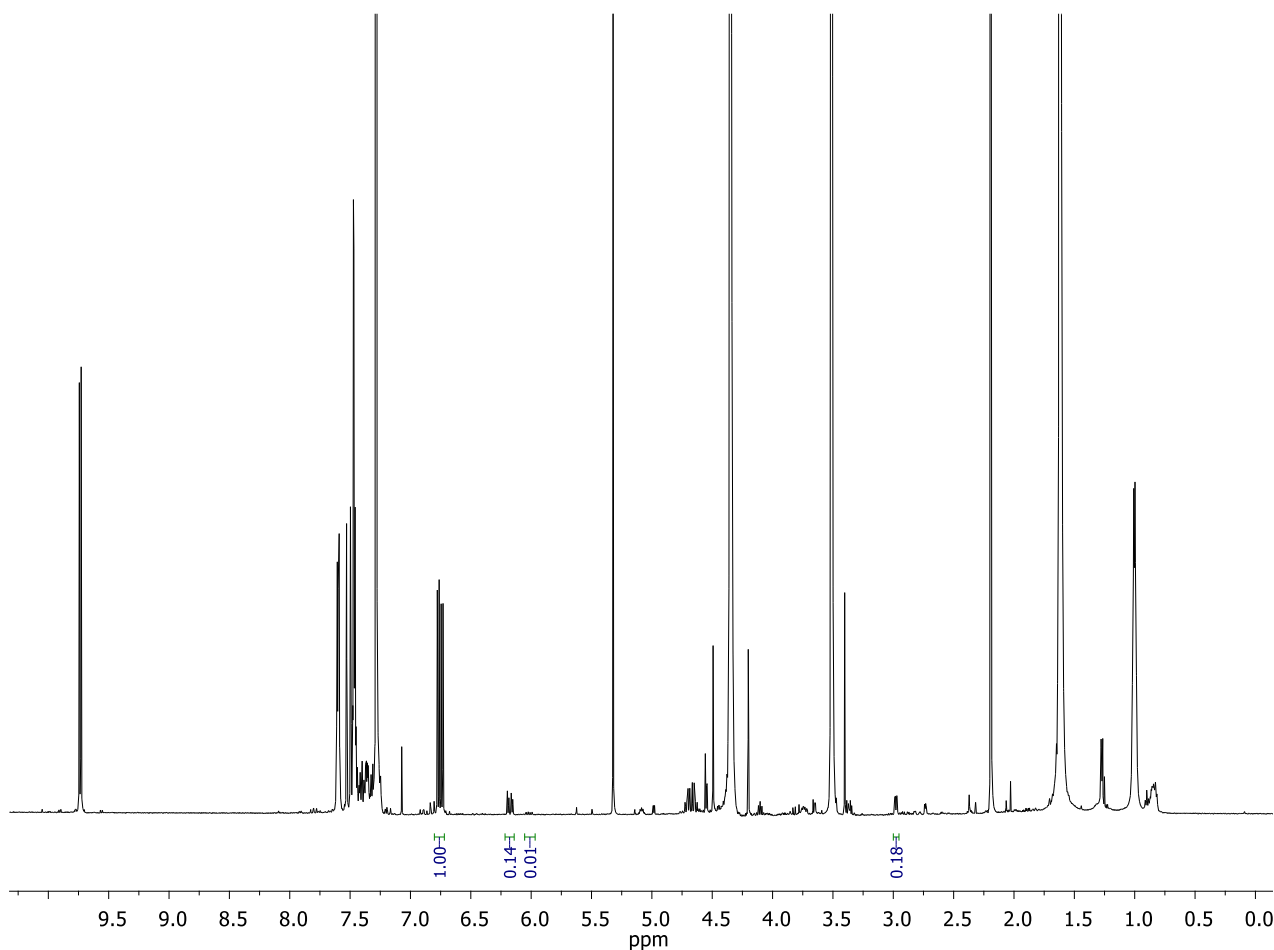
Product **83** was isolated after reaction of **14** with **47** using M-Sav:**74** as catalyst.

<sup>1</sup>H-NMR (500 MHz, CDCl<sub>3</sub>),  $\delta$ : 7.37-7.26 (m, 5H), 6.75 (dd,  $J$ = 16 and 1 Hz, 1H), 6.13 (dd,  $J$ = 16 and 6 Hz, 1H), 4.49-4.47 (m, 1H), 4.13-4.06 (m, 2H), 3.50 (bs, 1H) ppm.

The analytical data have been found to be in good agreement with the reported data.<sup>296</sup>

### 6.2.5 <sup>1</sup>H-NMR details for the activity screening of Table 2

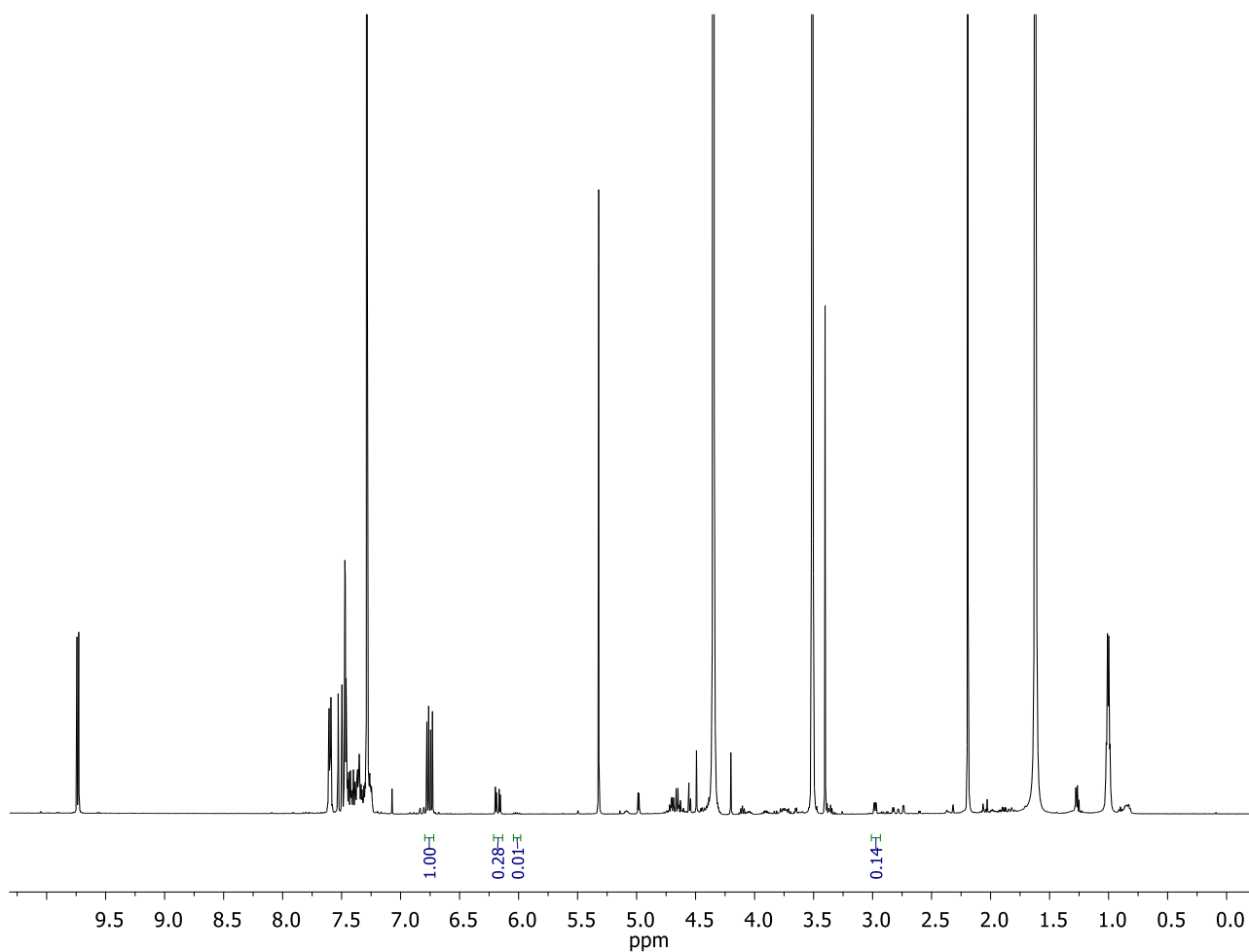
#### 6.2.5.1 Buffer screening for 1,4-Michael addition in Tris pH 7.0



Compound	Integration	% Conversion
<b>14</b> (Starting material)	1.00	80
<b>83</b> (Side-product)	0.14	12

Unknown side-product	0.01	<1
<b>75 (Product)</b>	0.18	7

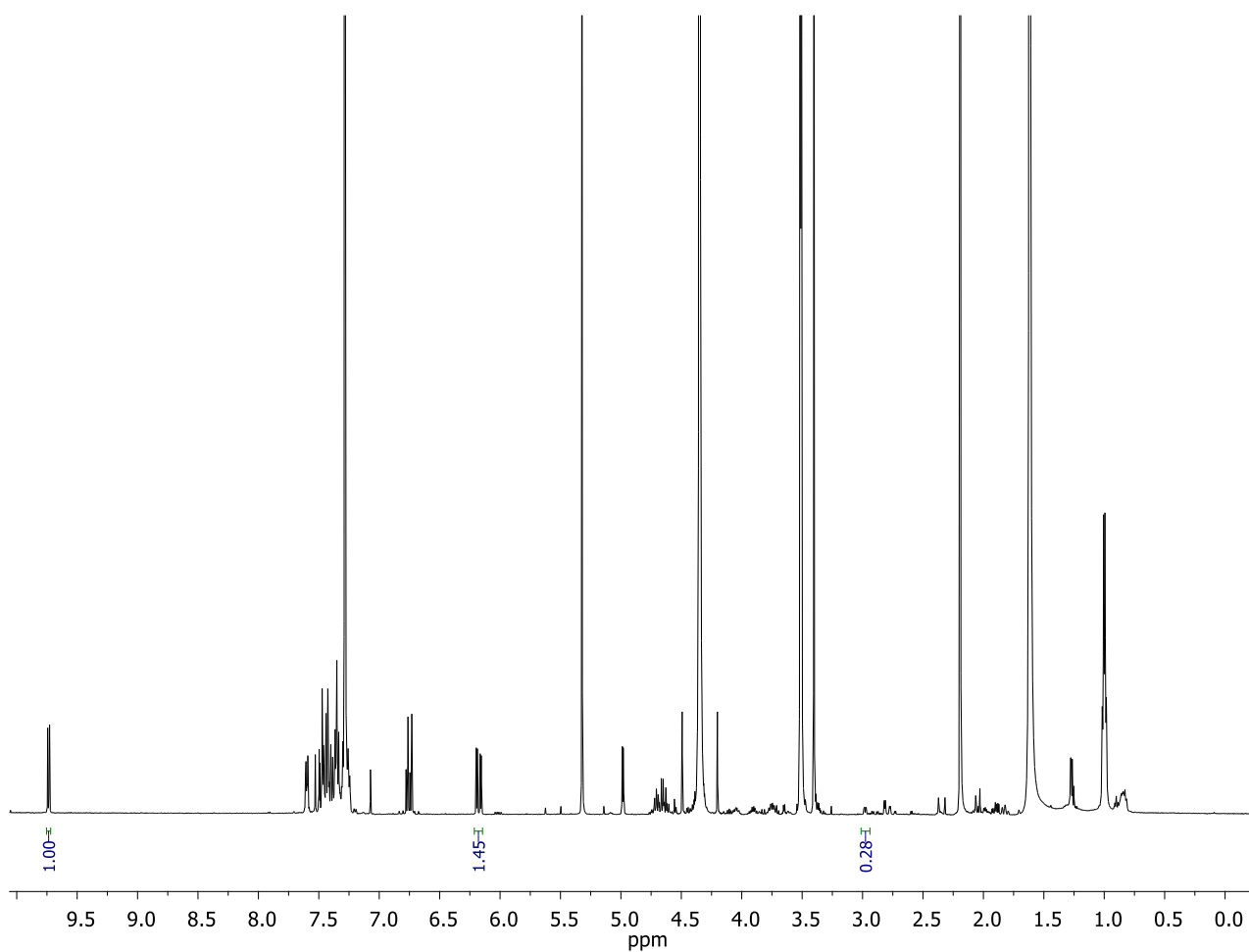
### 6.2.5.2 Buffer screening for 1,4-Michael addition in Tris pH 7.5



Compound	Integration	% Conversion
<b>14 (Starting material)</b>	1.00	74
<b>83 (Side-product)</b>	0.28	21
Unknown side-product	0.01	<1
<b>75 (Product)</b>	0.14	5

### 6.2.5.3 Buffer screening for 1,4-Michael addition in Tris pH 8.0

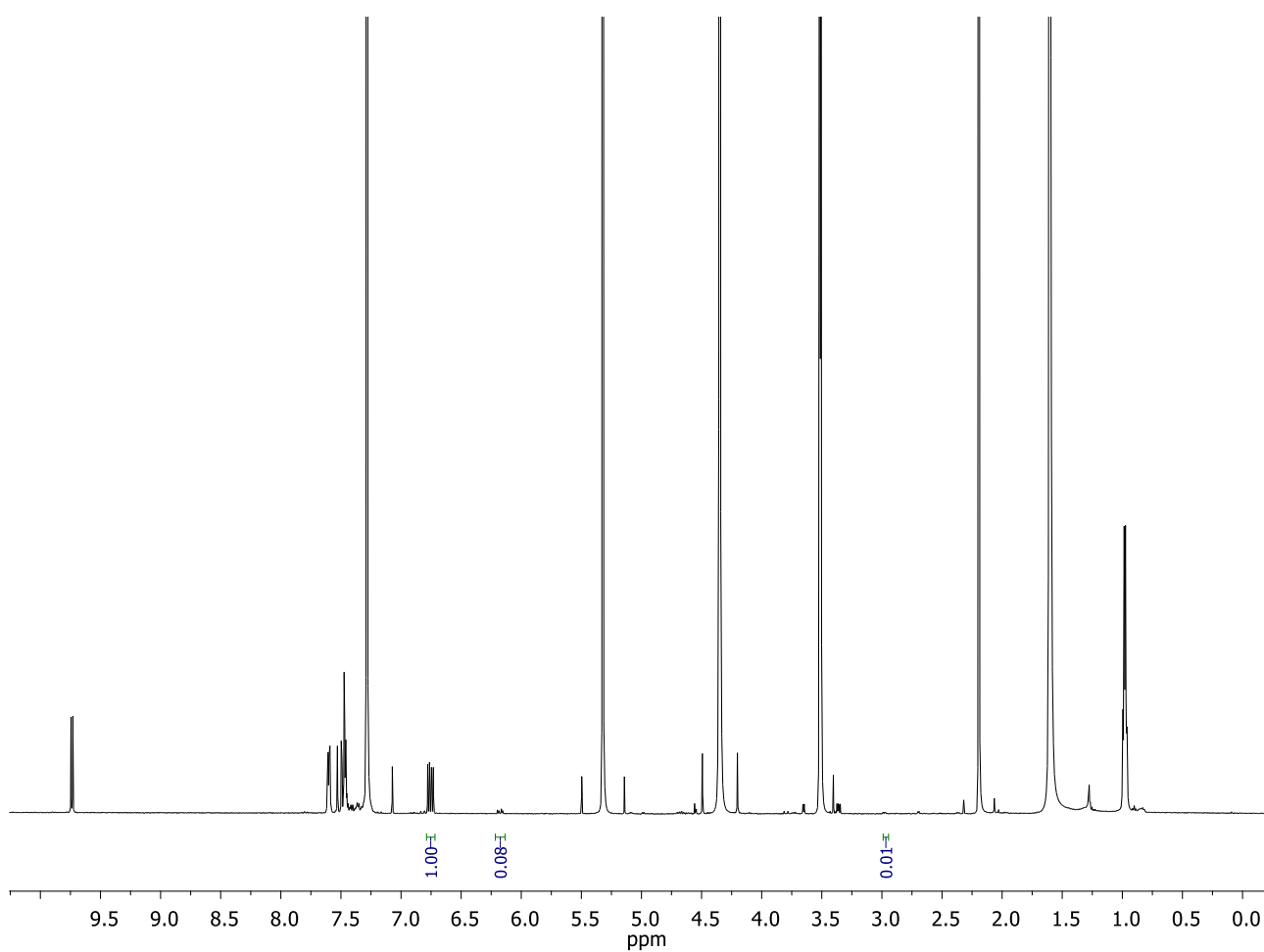
Cinnamaldehyde aldehydic peak (region 9.5-10 ppm) used as reference for the integration.



Compound	Integration	% Conversion
<b>14</b> (Starting material)	1.00	39
<b>83</b> (Side-product)	1.45	56
Unknown side-product	/	/

<b>75 (Product)</b>	0.28	5
---------------------	------	---

#### 6.2.5.4 Buffer screening for 1,4-Michael addition in HEPES pH 7.0

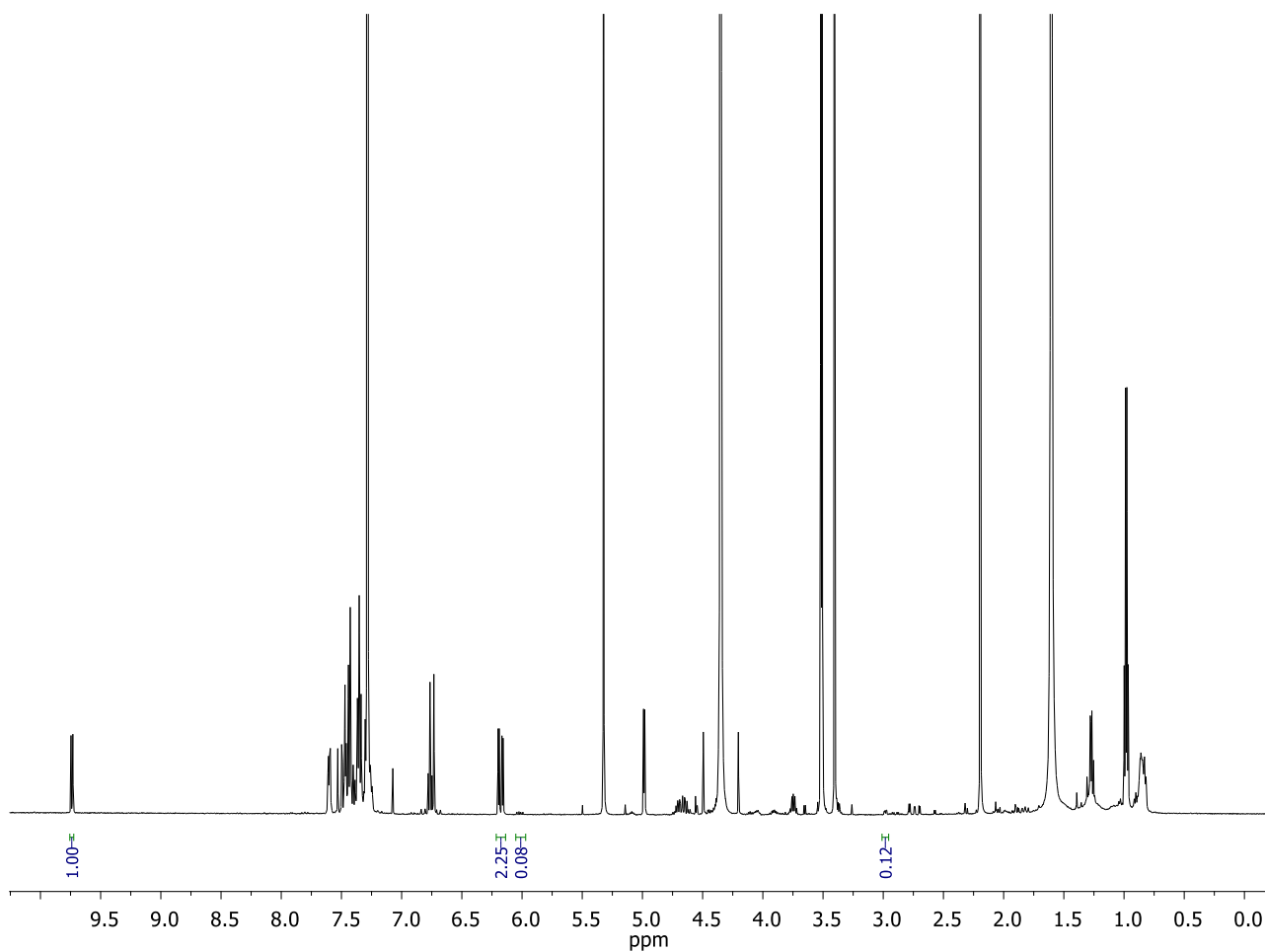


Compound	Integration	% Conversion
<b>14</b> (Starting material)	1.00	92
<b>83</b> (Side-product)	0.08	7
Unknown side-product	/	/

75 (Product)	0.01	<1
--------------	------	----

### 6.2.5.5 Buffer screening for 1,4-Michael addition in HEPES pH 7.5

Cinnamaldehyde aldehydic peak (region 9.5-10 ppm) used as reference for the integration.

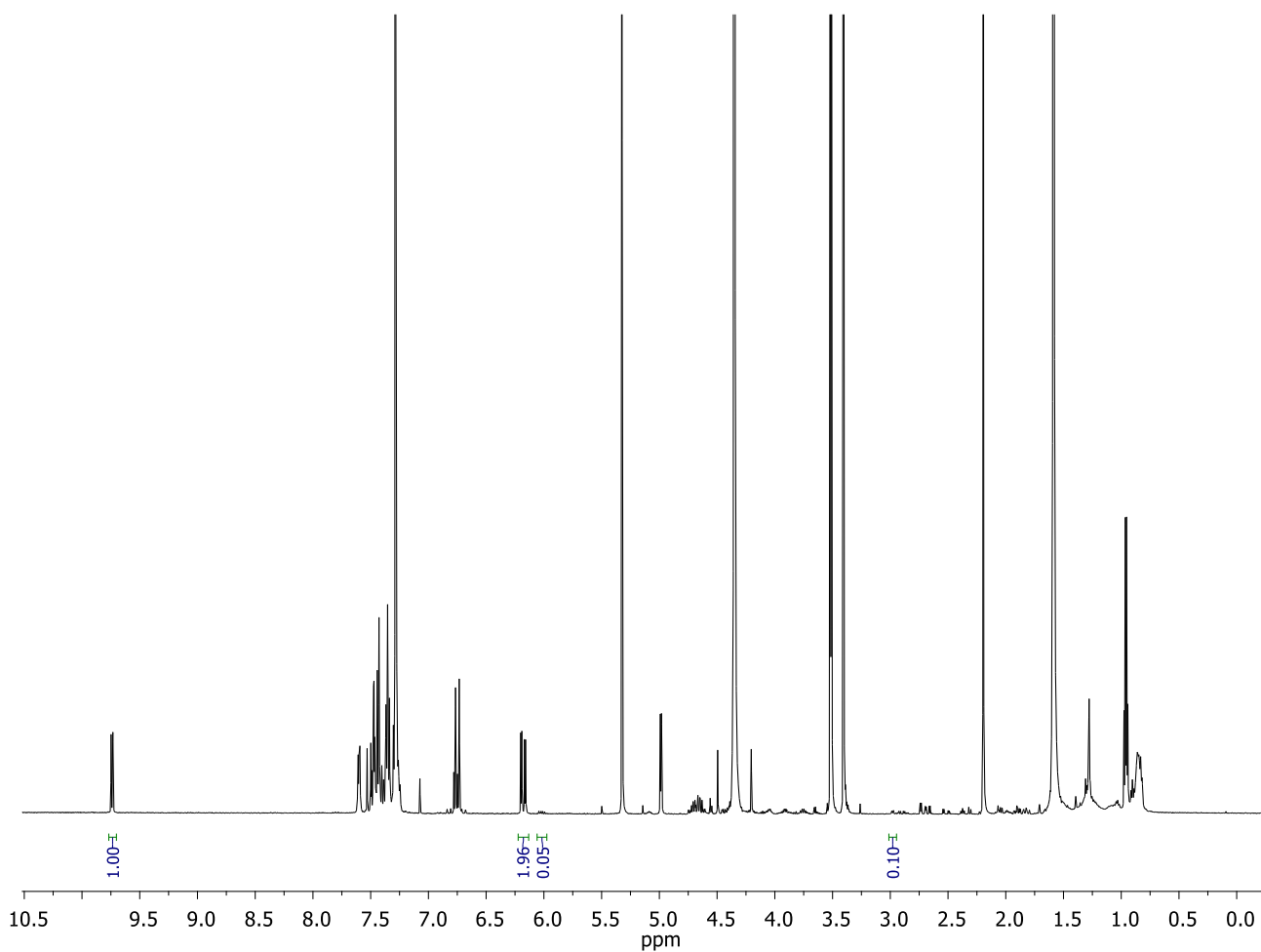


Compound	Integration	% Conversion
14 (Starting material)	1.00	27

<b>83</b> (Side-product)	2.25	66
Unknown side-product	0.08	5
<b>75</b> (Product)	0.12	2

### 6.2.5.6 Buffer screening for 1,4-Michael addition in HEPES pH 8.0

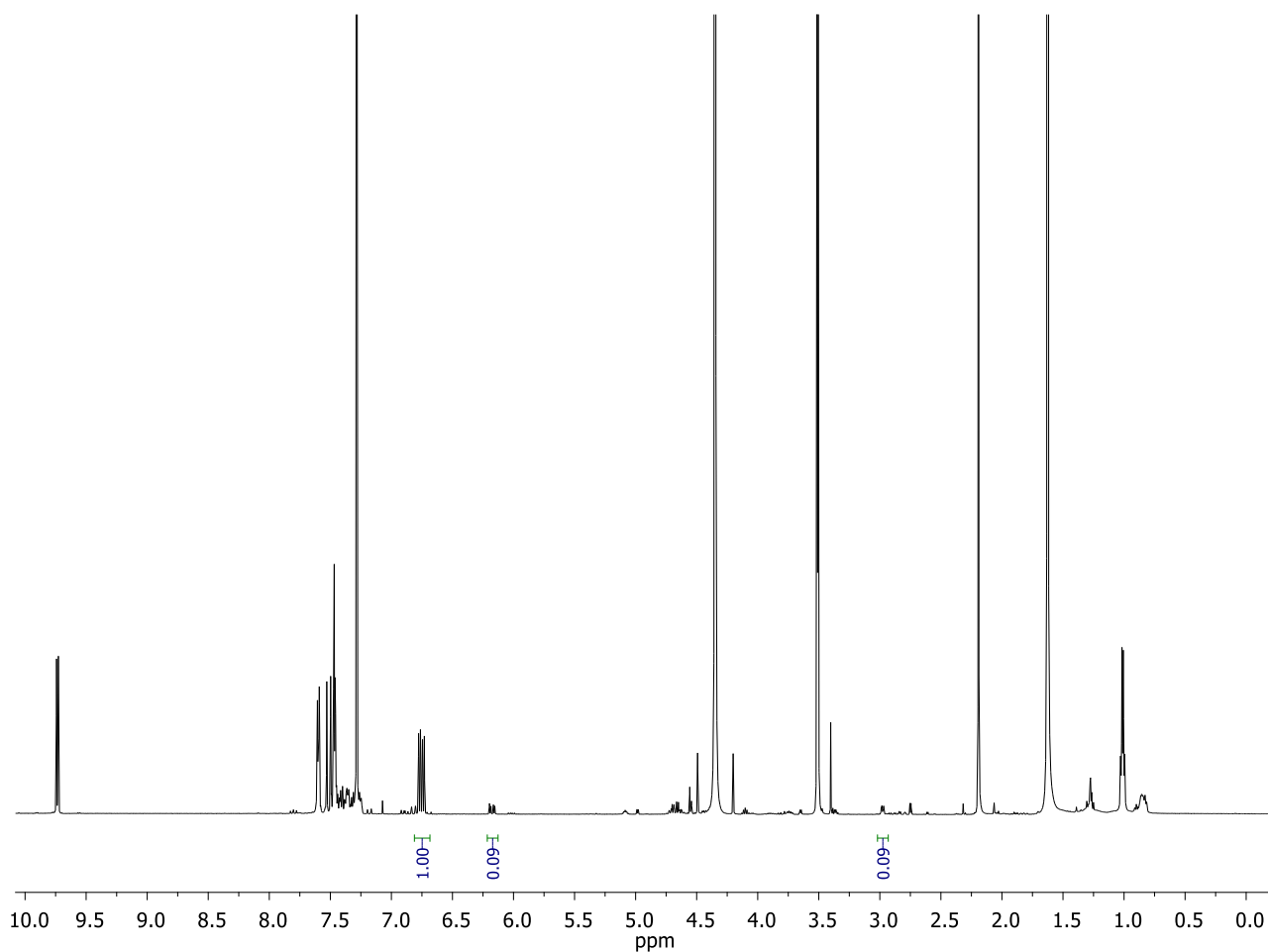
Cinnamaldehyde aldehydic peak (region 9.5-10 ppm) used as reference for the integration.



Compound	Integration	% Conversion
----------	-------------	--------------

<b>14</b> (Starting material)	1.00	31
<b>83</b> (Side-product)	1.95	64
Unknown side-product	0.05	3
<b>75</b> (Product)	0.10	2

### 6.2.5.7 Buffer screening for 1,4-Michael addition in KPi pH 7.0

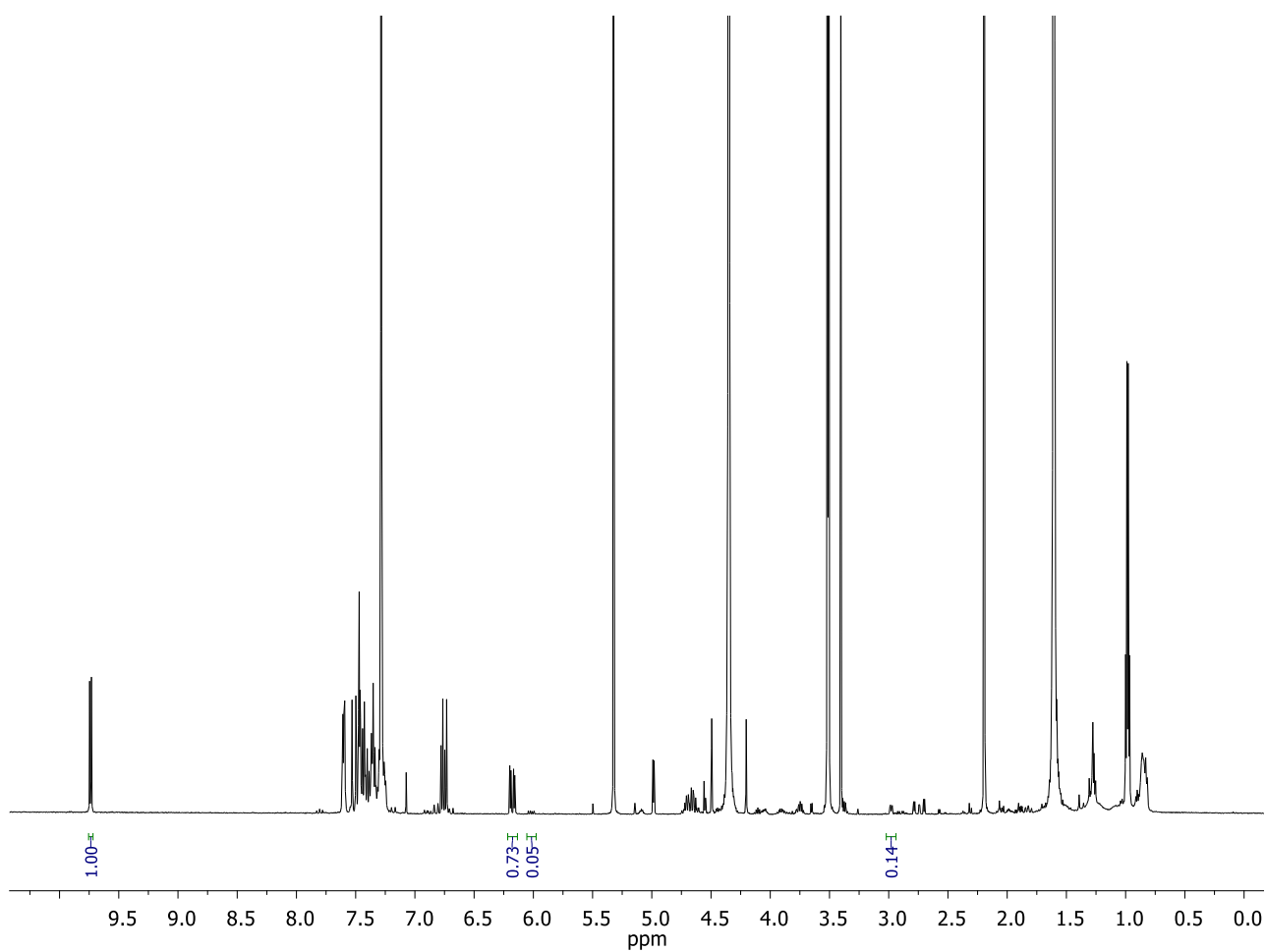


Compound	Integration	% Conversion
<b>14</b> (Starting material)	1.00	89

<b>83</b> (Side-product)	0.09	7
Unknown side-product	/	/
<b>75</b> (Product)	0.09	4

### 6.2.5.8 Buffer screening for 1,4-Michael addition in KPi pH 7.5

Cinnamaldehyde aldehydic peak (region 9.5-10 ppm) used as reference for the integration.

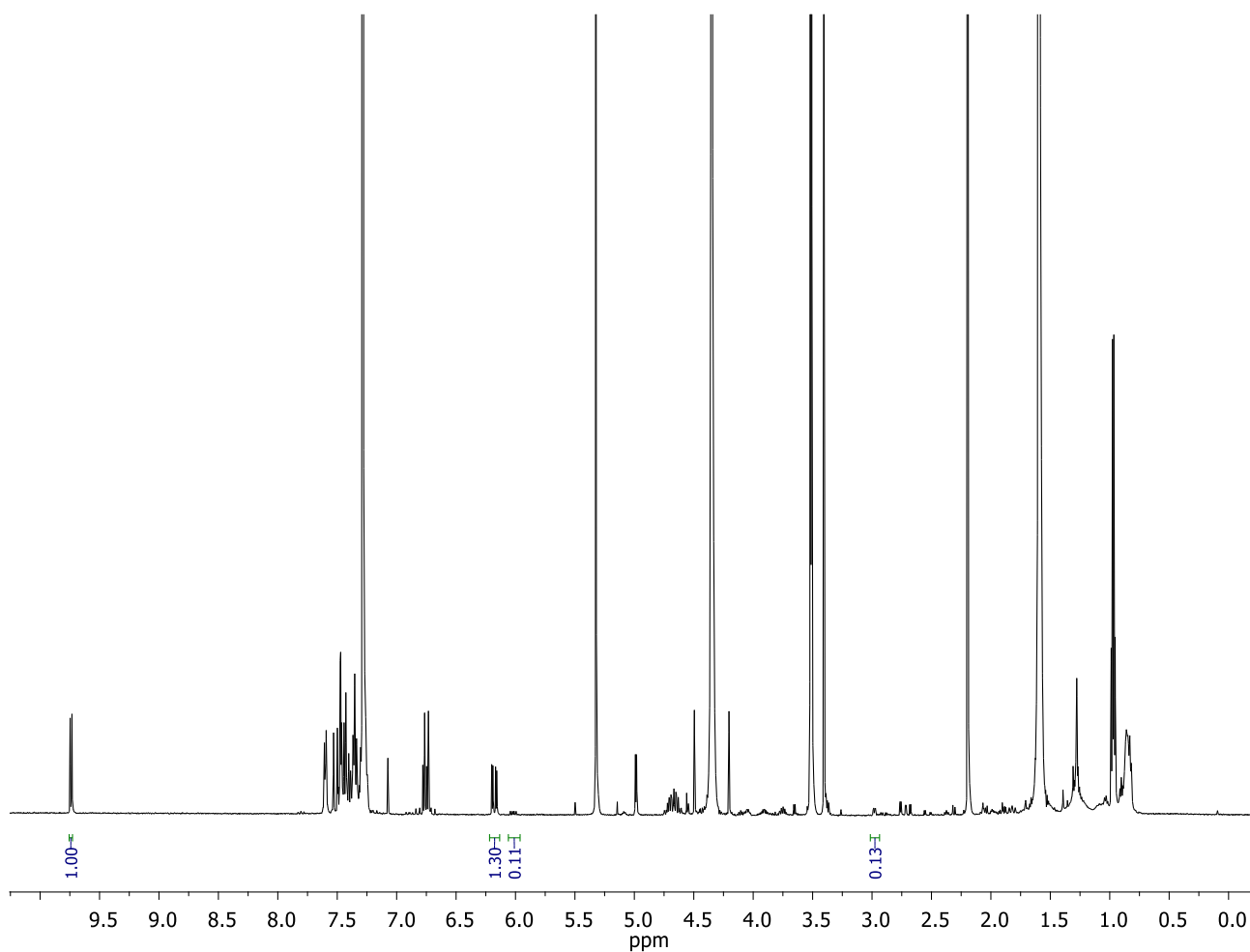




Compound	Integration	% Conversion
<b>14</b> (Starting material)	1.00	54
<b>83</b> (Side-product)	0.73	39
Unknown side-product	0.05	3
<b>75</b> (Product)	0.14	4

### 6.2.5.9 Buffer screening for 1,4-Michael addition in KP<sub>i</sub> pH 8.0

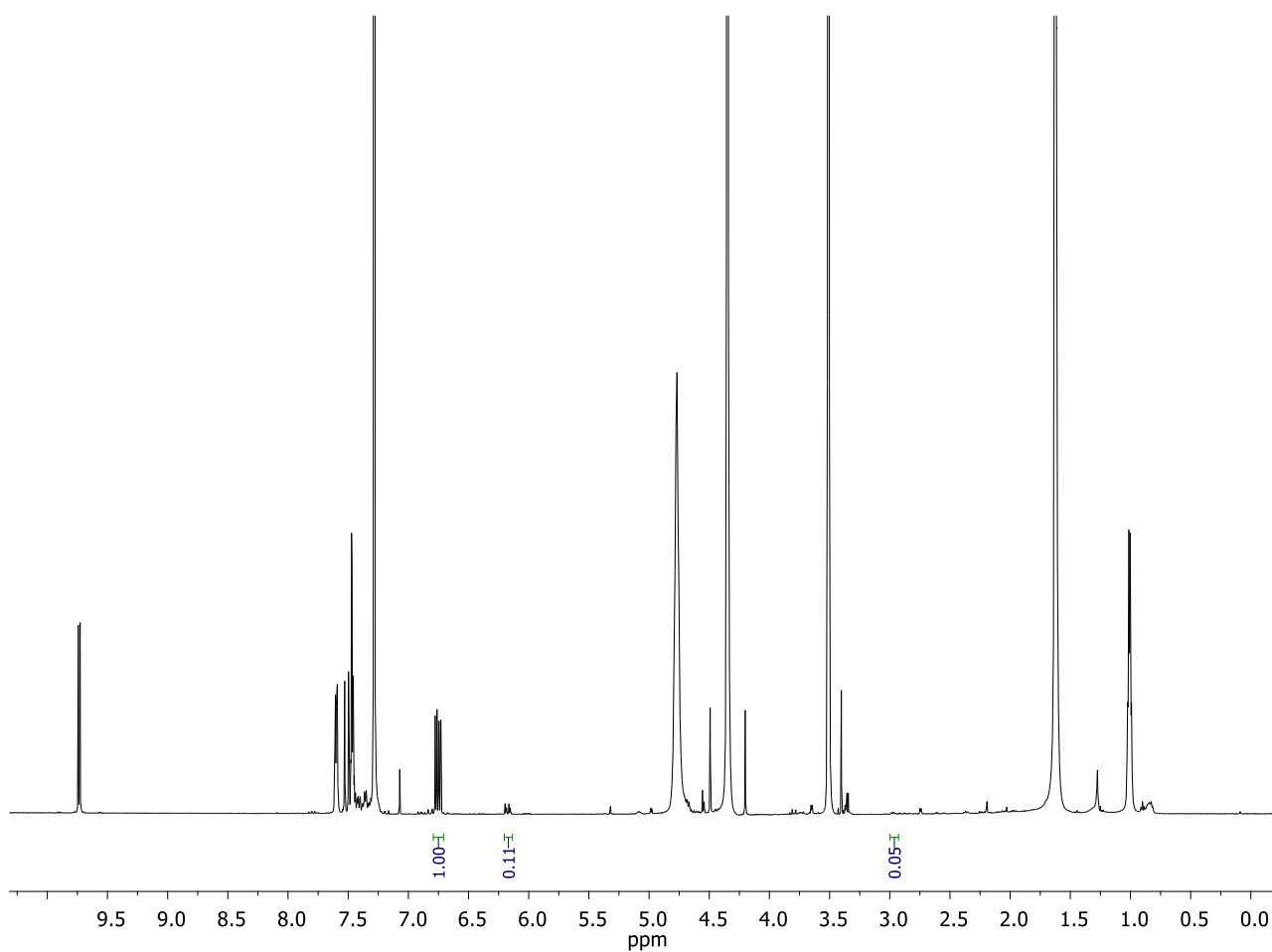
Cinnamaldehyde aldehydic peak (region 9.5-10 ppm) used as reference for the integration.



Compound	Integration	% Conversion
----------	-------------	--------------

<b>14</b> (Starting material)	1.00	36
<b>83</b> (Side-product)	1.30	53
Unknown side-product	0.11	8
<b>75</b> (Product)	0.13	3

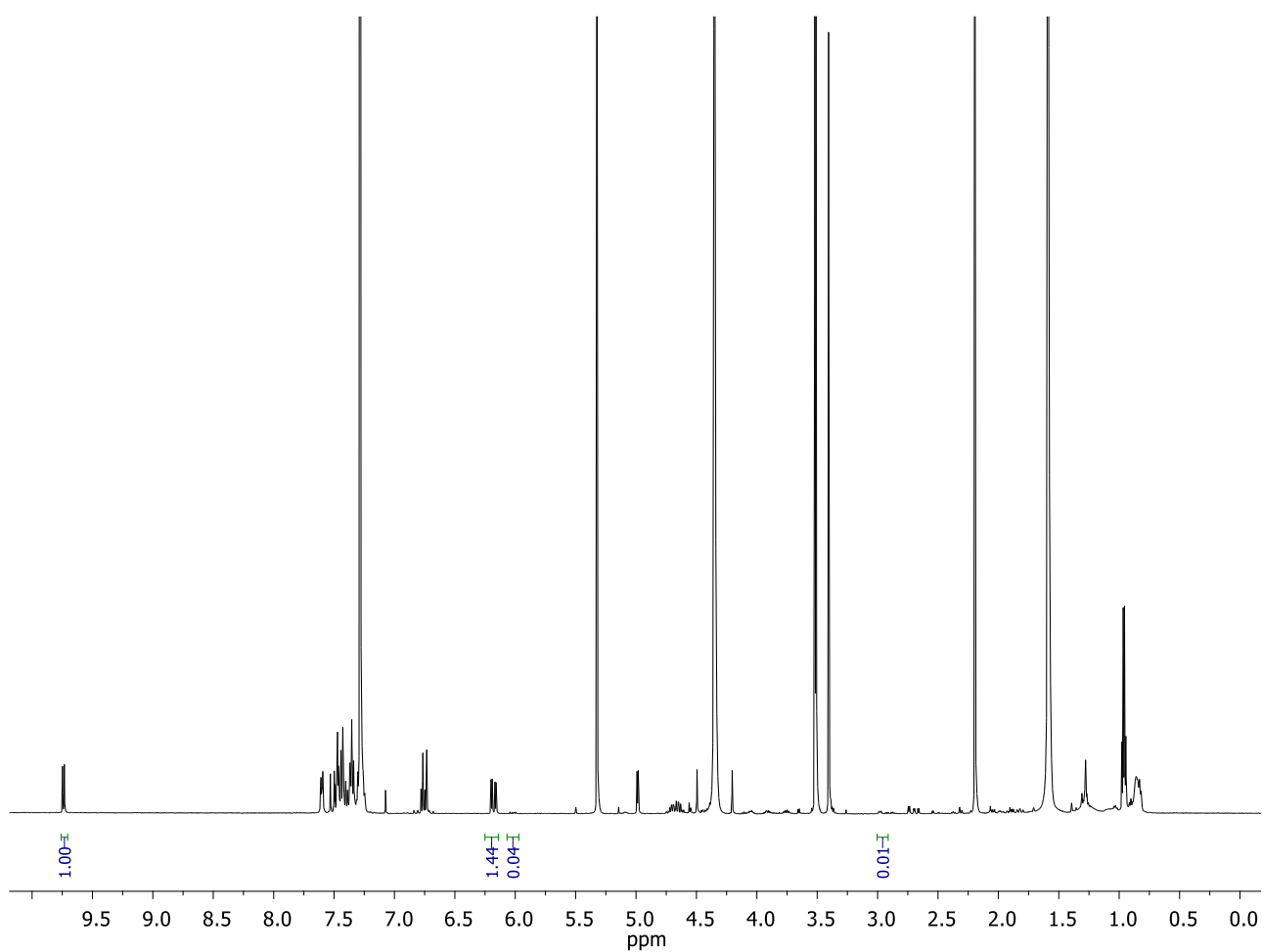
### 6.2.5.10 Buffer screening for 1,4-Michael addition in NaPi pH 7.0



Compound	Integration	% Conversion
<b>14</b> (Starting material)	1.00	87
<b>83</b> (Side-product)	0.11	10
Unknown side-product	/	/
<b>75</b> (Product)	0.05	3

### 6.2.5.11 Buffer screening for 1,4-Michael addition in NaP<sub>i</sub> pH 7.5

Cinnamaldehyde aldehydic peak (region 9.5-10 ppm) used as reference for the integration.

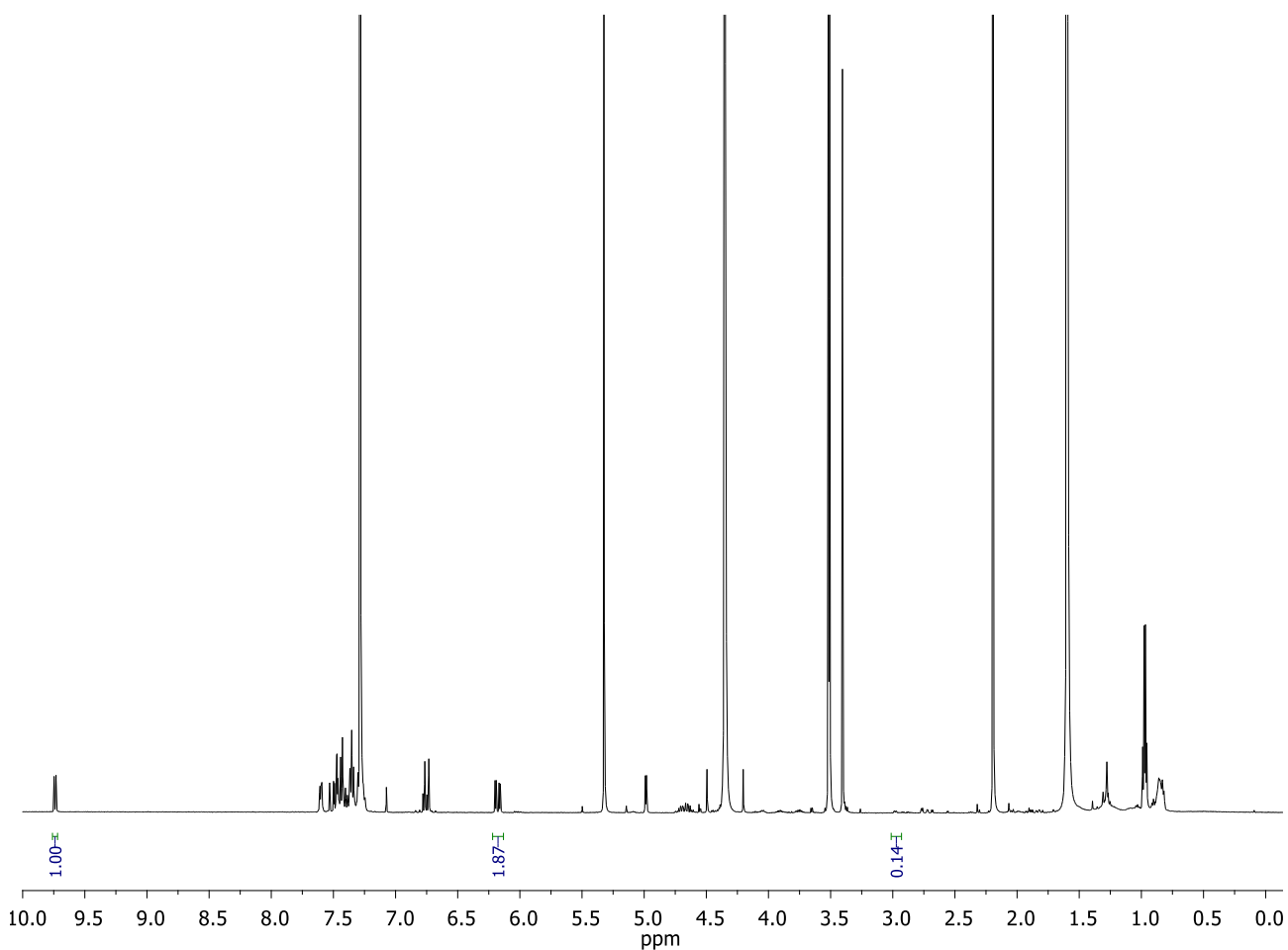


Compound	Integration	% Conversion
<b>14</b> (Starting material)	1.00	40
<b>83</b> (Side-product)	1.44	58
Unknown side-product	0.04	2

<b>75 (Product)</b>	0.01	<1
---------------------	------	----

### 6.2.5.12 Buffer screening for 1,4-Michael addition in NaP<sub>i</sub> pH 8.0

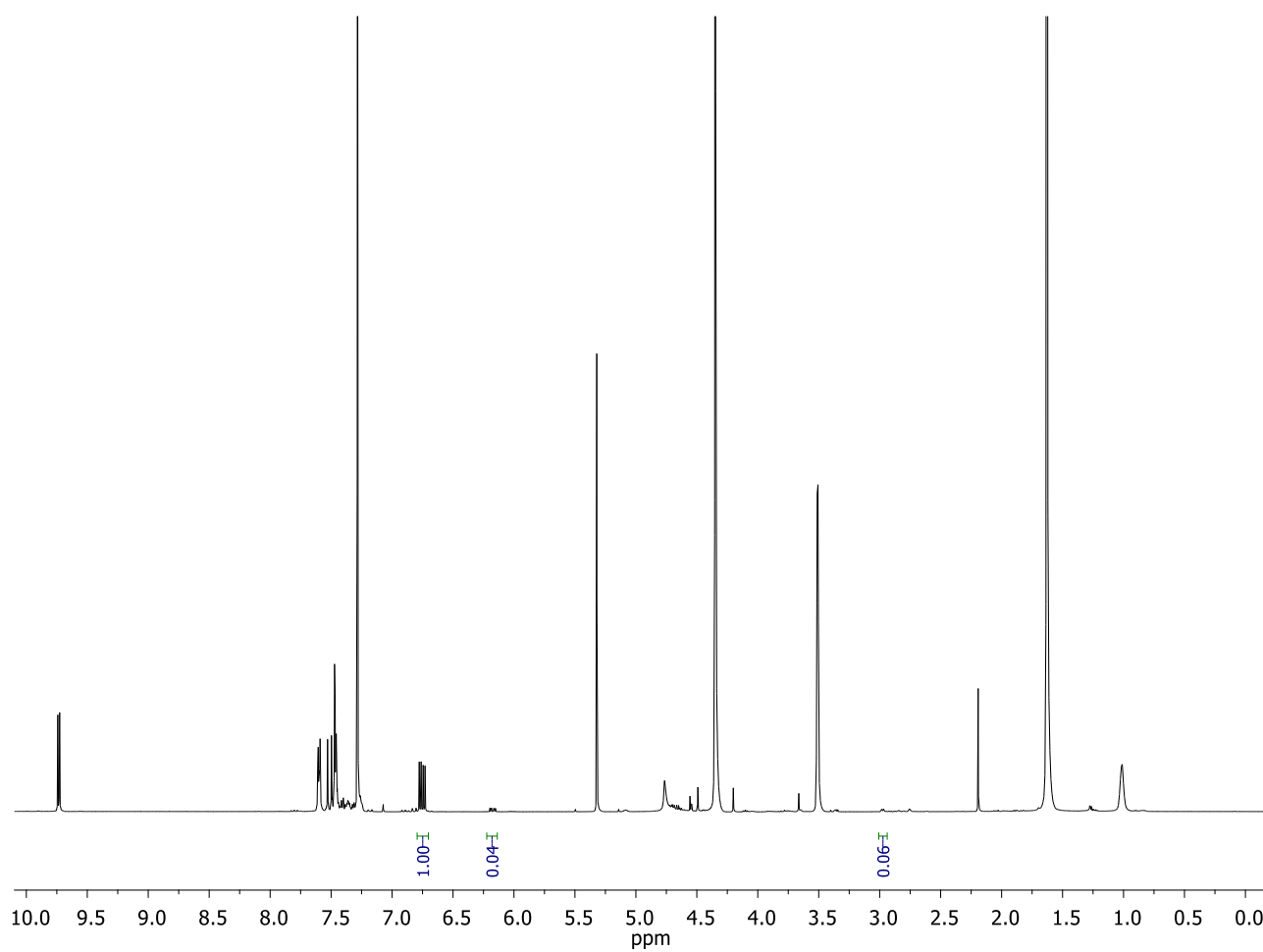
Cinnamaldehyde aldehydic peak (region 9.5-10 ppm) used as reference for the integration.



Compound	Integration	% Conversion
<b>14</b> (Starting material)	1.00	36
<b>83</b> (Side-product)	1.87	63
Unknown side-product	/	/

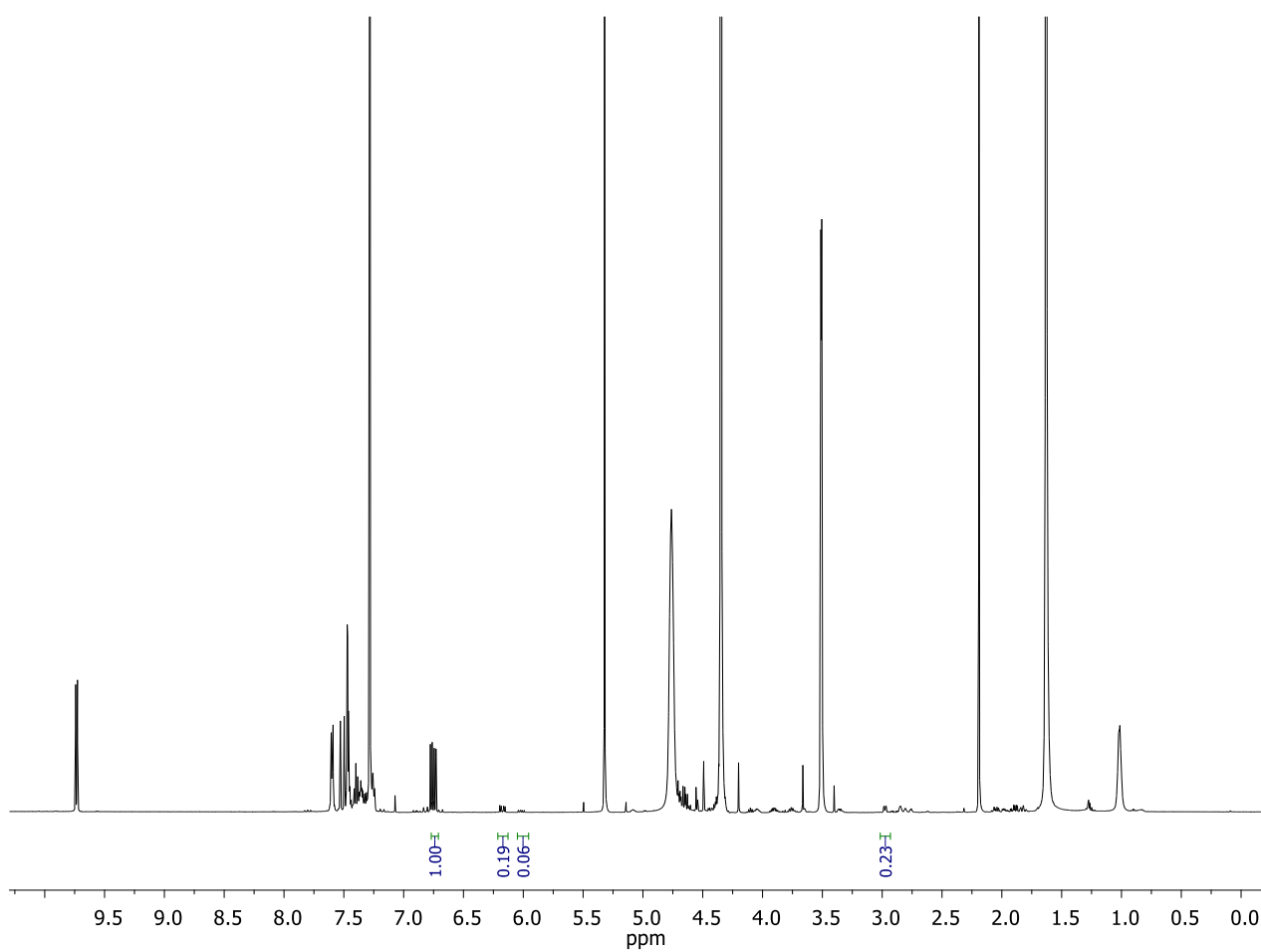
<b>75 (Product)</b>	0.14	3
---------------------	------	---

### 6.2.5.13 Buffer screening for 1,4-Michael addition in PBS pH 7.0



Compound	Integration	% Conversion
<b>14 (Starting material)</b>	1.00	94
<b>83 (Side-product)</b>	0.04	3
Unknown side-product	/	/
<b>75 (Product)</b>	0.06	3

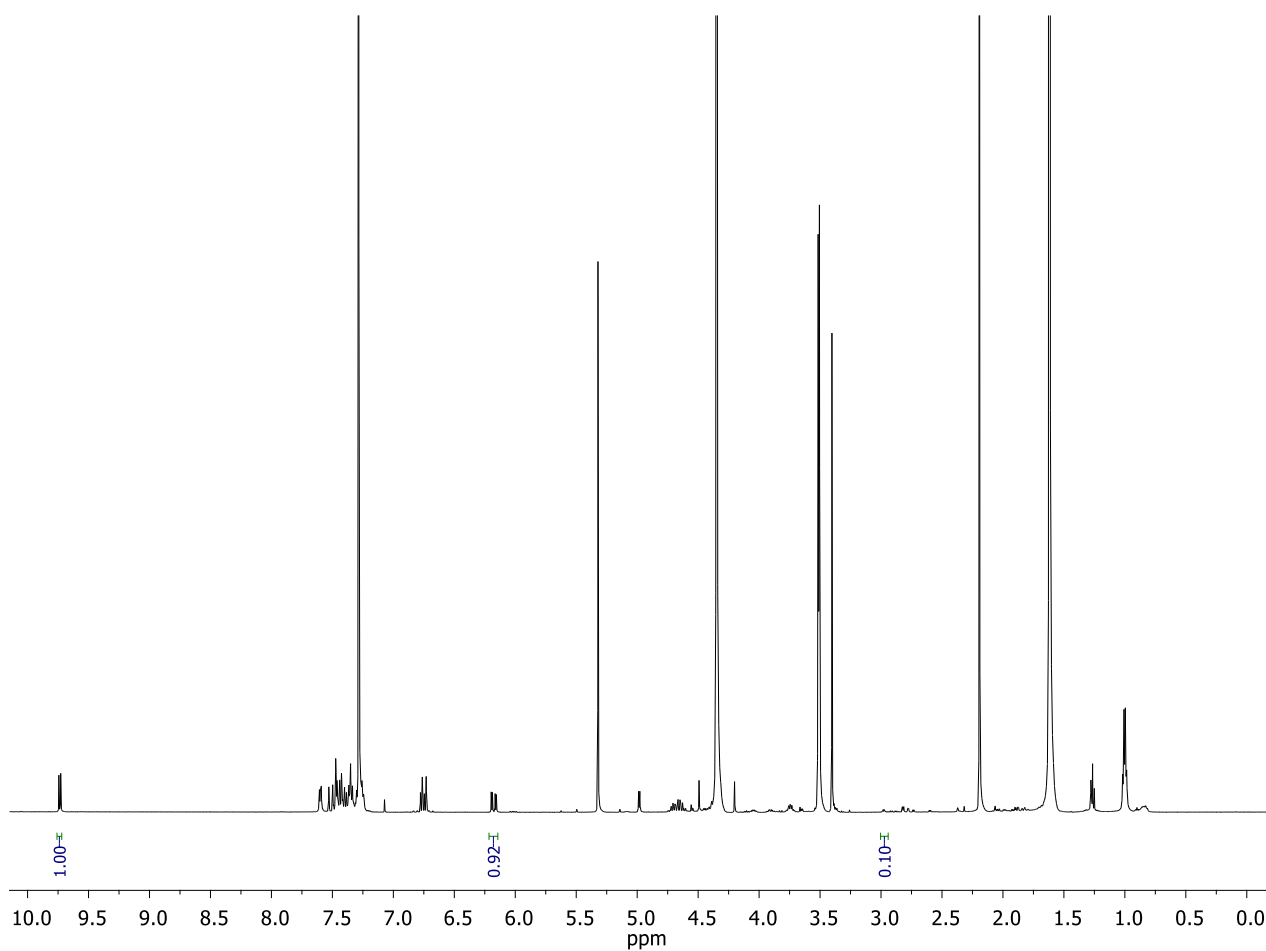
## 6.2.5.14 Buffer screening for 1,4-Michael addition in PBS pH 7.5



Compound	Integration	% Conversion
<b>14</b> (Starting material)	1.00	77
<b>83</b> (Side-product)	0.19	13
Unknown side-product	0.06	3
<b>75</b> (Product)	0.23	7

### 6.2.5.15 Buffer screening for 1,4-Michael addition in PBS pH 8.0

Cinnamaldehyde aldehydic peak (region 9.5-10 ppm) used as reference for the integration.

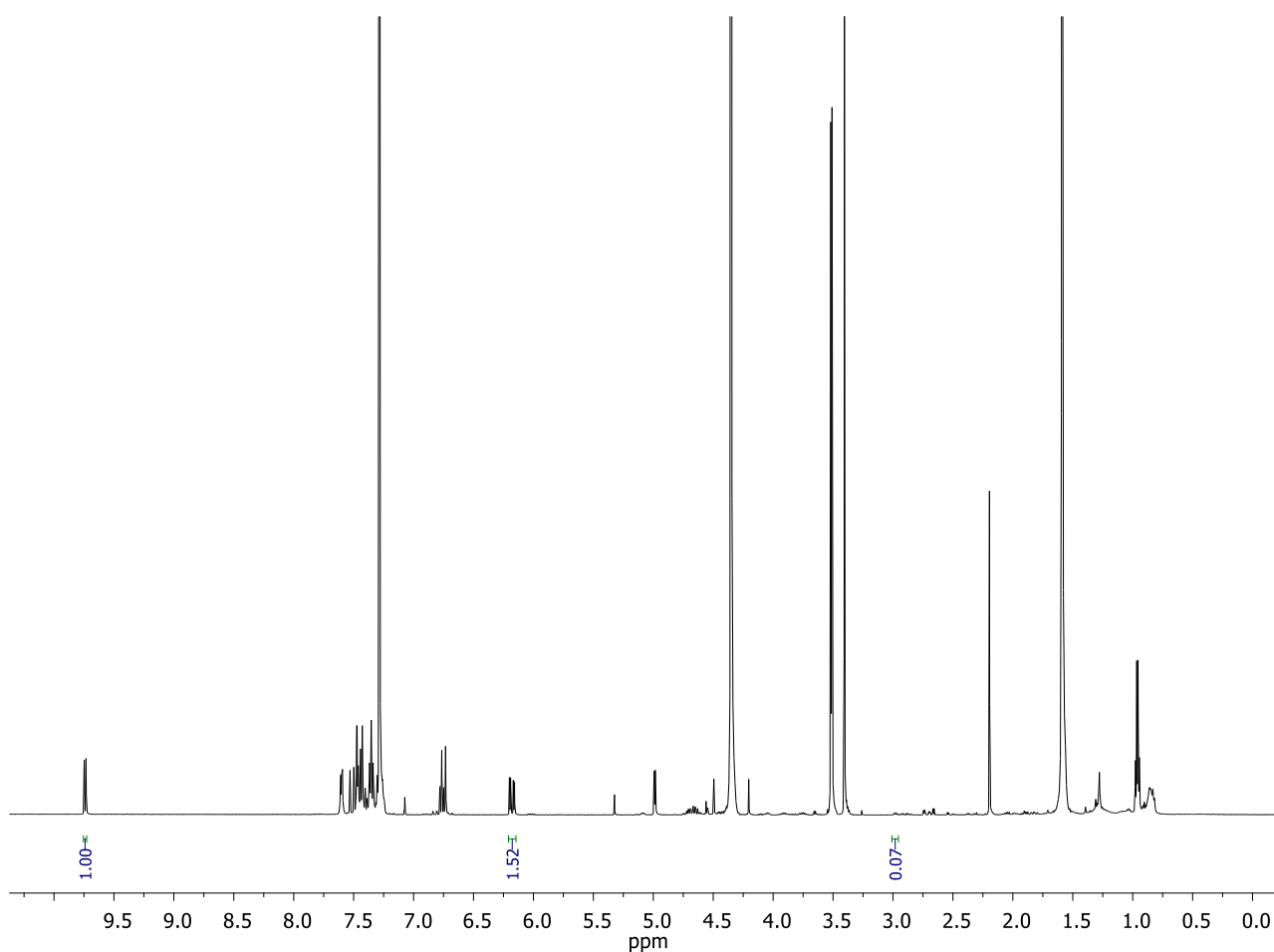


Compound	Integration	% Conversion
<b>14</b> (Starting material)	1.00	52
<b>83</b> (Side-product)	0.92	46
Unknown side-product	/	/

<b>75 (Product)</b>	0.10	2
---------------------	------	---

### 6.2.5.16 Buffer screening for 1,4-Michael addition in H<sub>2</sub>O

Cinnamaldehyde aldehydic peak (region 9.5-10 ppm) used as reference for the integration.

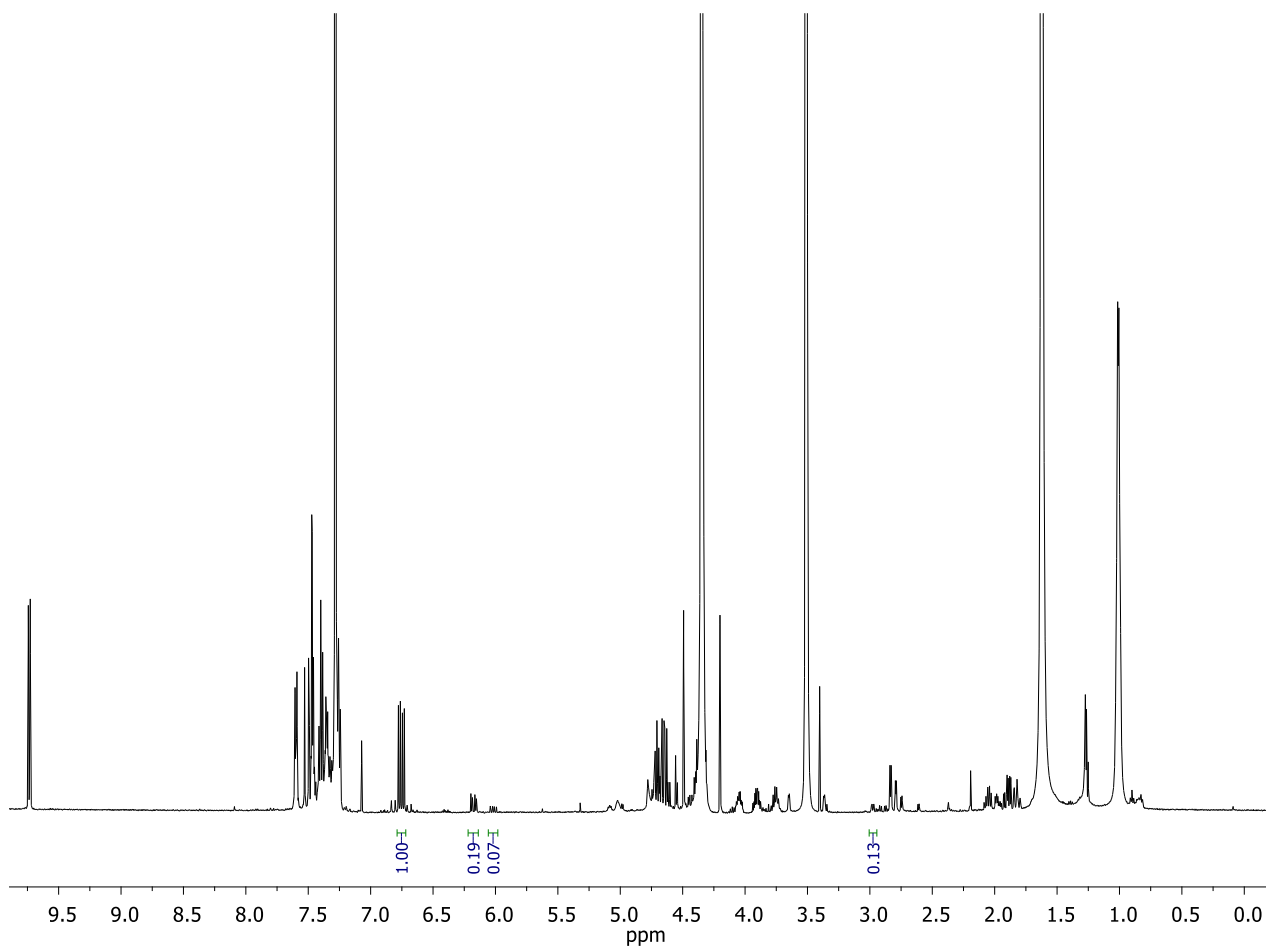


Compound	Integration	% Conversion
<b>14 (Starting material)</b>	1.00	39
<b>83 (Side-product)</b>	1.52	59
Unknown side-product	/	/
<b>75 (Product)</b>	0.07	2

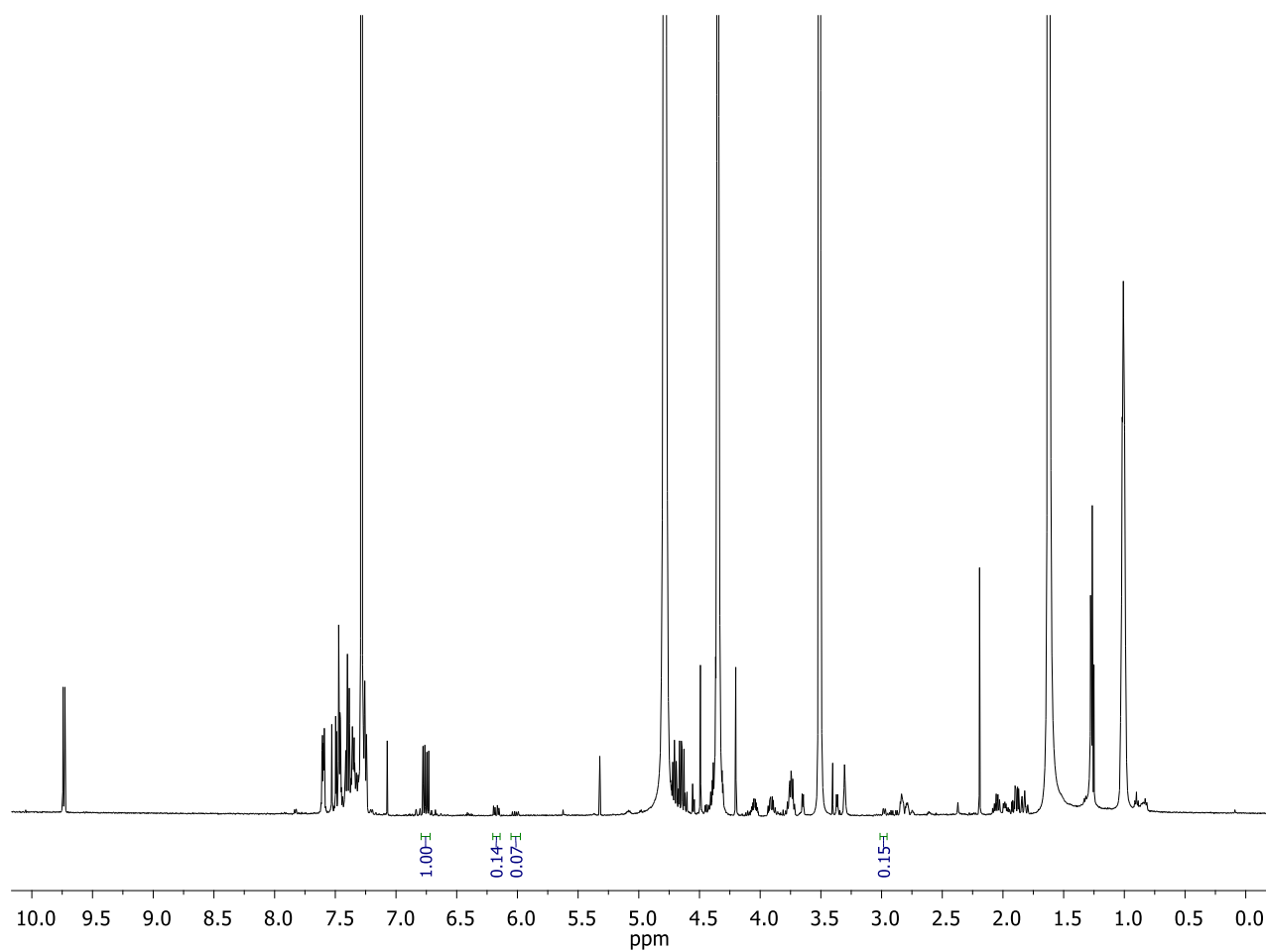


## 6.2.6 $^1\text{H-NMR}$ details for the activity screening of Table 3

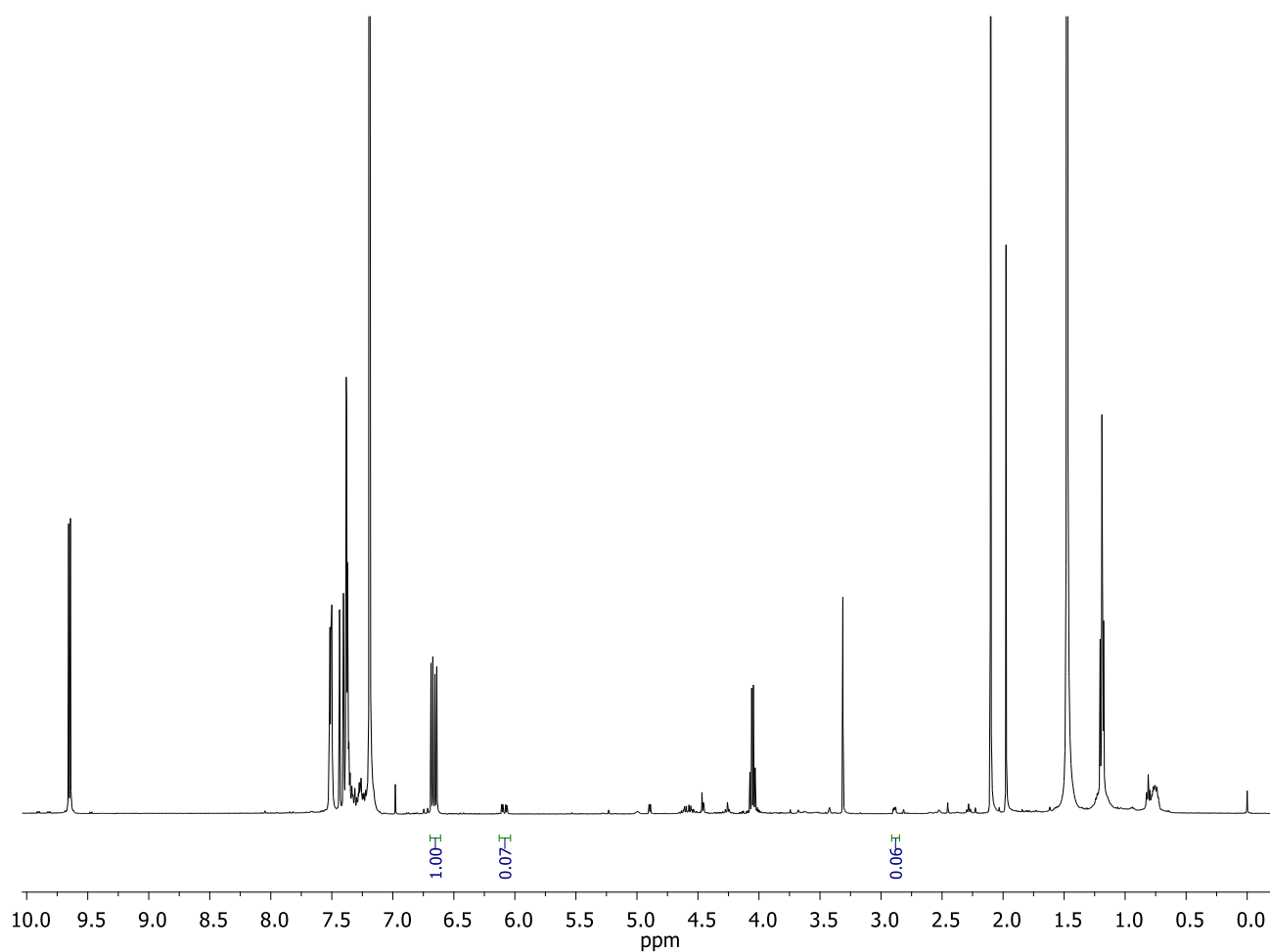
### 6.2.6.1 Buffer screening for 1,4-Michael addition in $\text{KPi}$ pH 7.0 25 mM



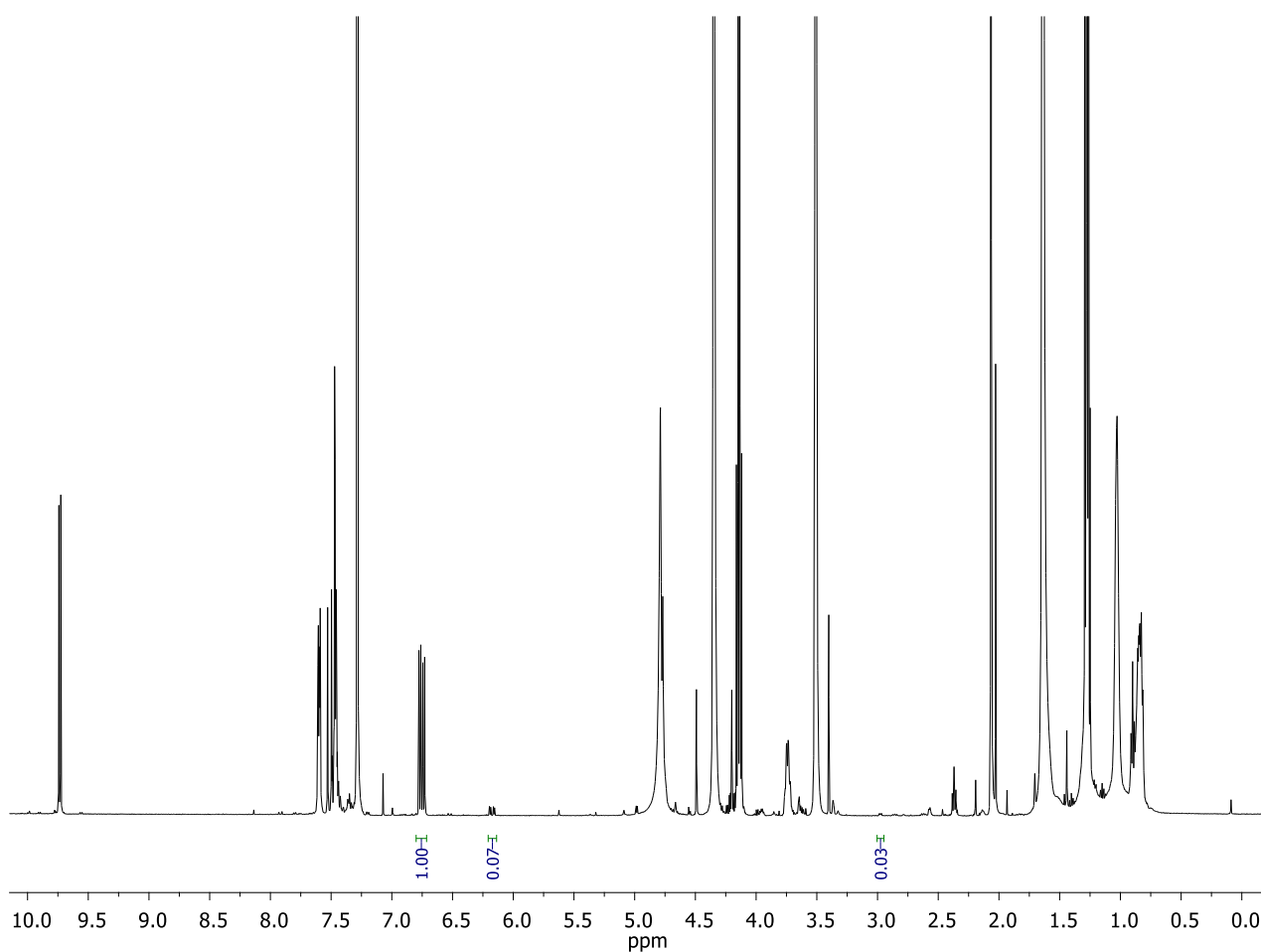
Compound	Integration	% Conversion
<b>14</b> (Starting material)	1.00	77
<b>83</b> (Side-product)	0.19	14
Unknown side-product	0.07	4
<b>75</b> (Product)	0.13	5

6.2.6.2 Buffer screening for 1,4-Michael addition in  $\text{KP}_i$  pH 7.0 50 mM

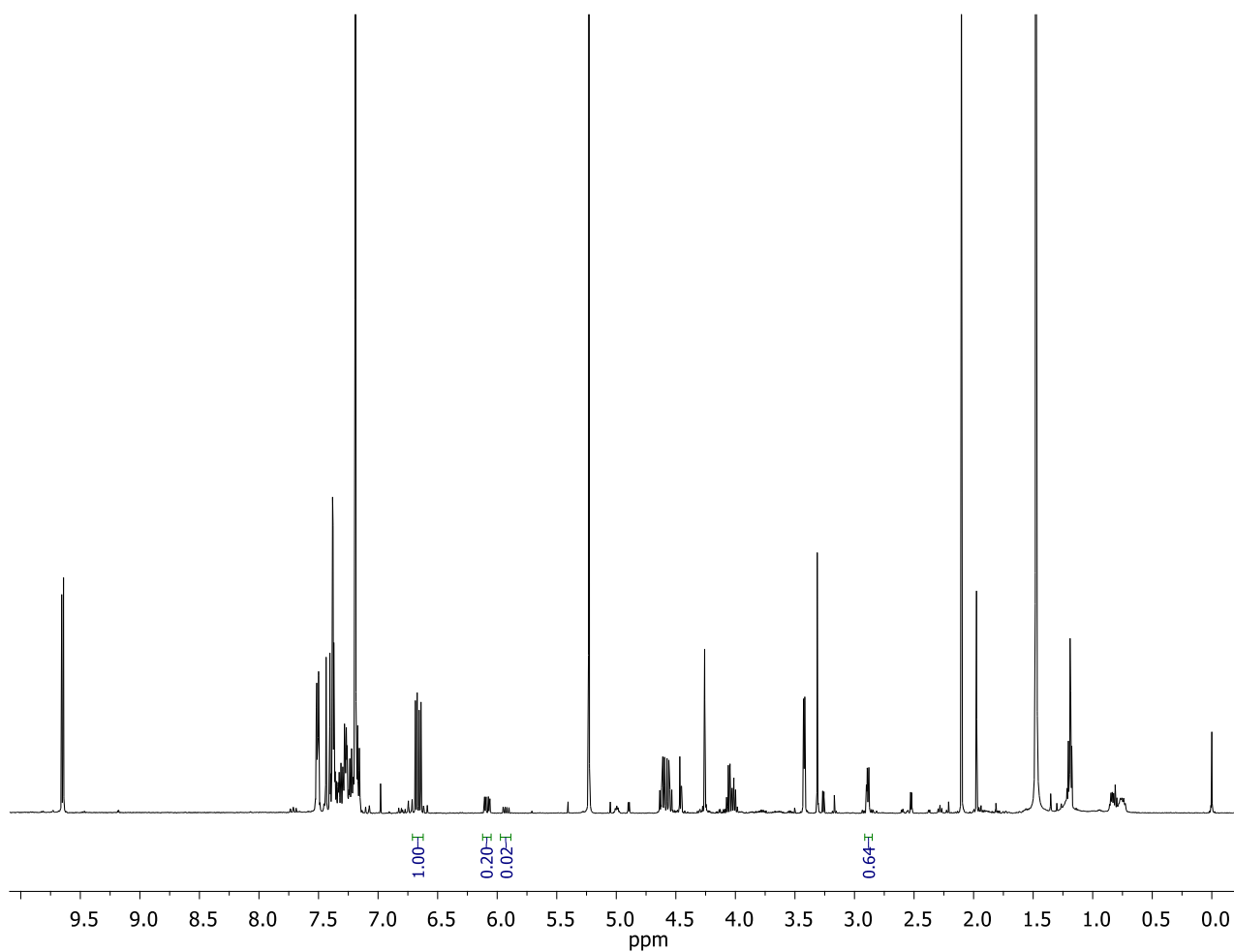
Compound	Integration	% Conversion
<b>14</b> (Starting material)	1.00	81
<b>83</b> (Side-product)	0.14	10
Unknown side-product	0.07	4
<b>75</b> (Product)	0.15	5

**6.2.6.3 Co-solvent screening for 1,4-Michael addition in 50% KPi pH 7.0 10 mM and 50% EtOAc**

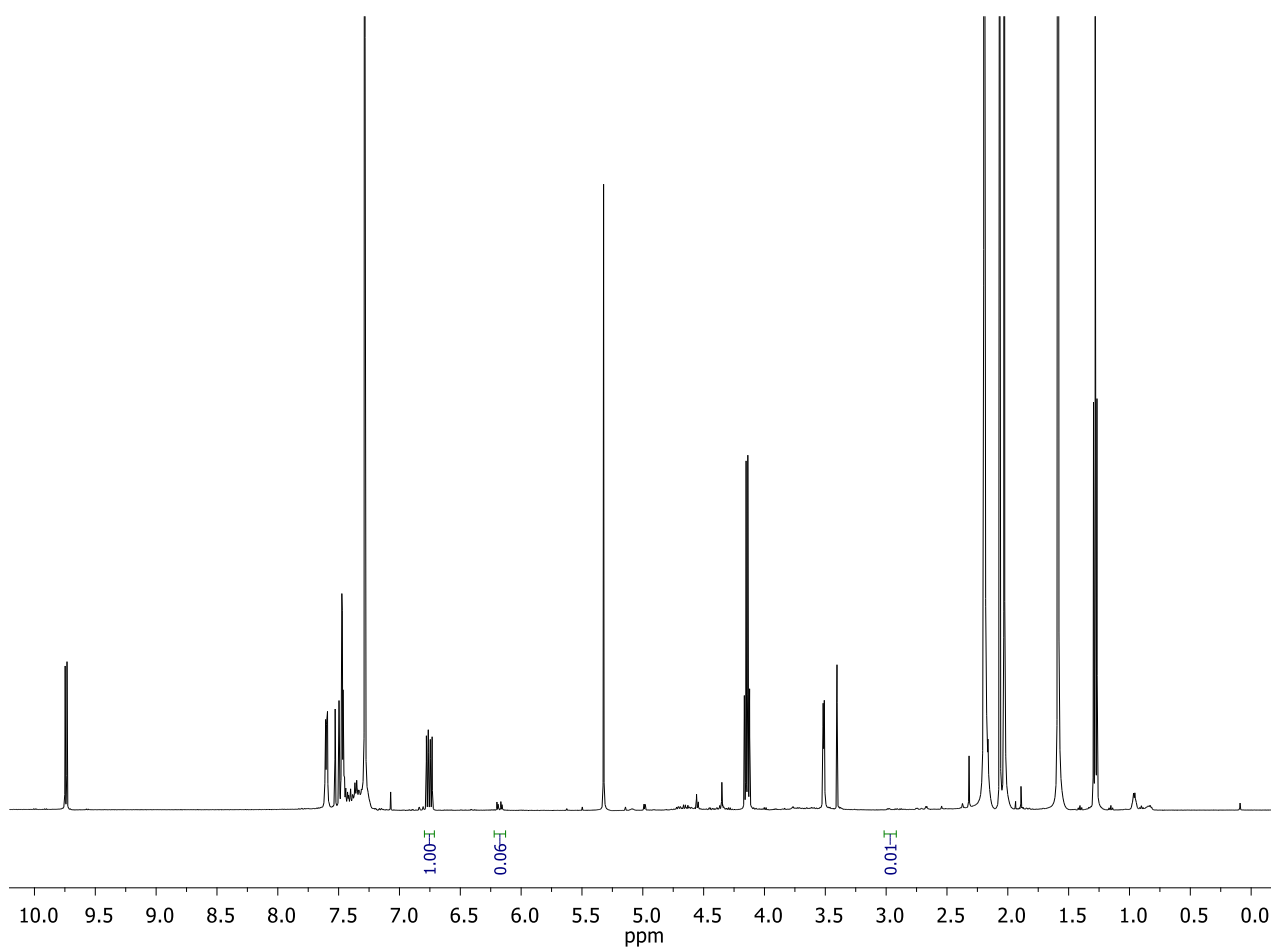
Compound	Integration	% Conversion
<b>14</b> (Starting material)	1.00	91
<b>83</b> (Side-product)	0.07	6
Unknown side-product	/	/
<b>75</b> (Product)	0.06	3

**6.2.6.4 Co-solvent screening for 1,4-Michael addition in 50% KP<sub>i</sub> pH 7.0 10 mM and 50% CDCl<sub>3</sub>**

Compound	Integration	% Conversion
<b>14</b> (Starting material)	1.00	95
<b>83</b> (Side-product)	0.07	5
Unknown side-product	/	/
<b>75</b> (Product)	0.03	<1

**6.2.6.5 Co-solvent screening for 1,4-Michael addition in 50% KPi pH 7.0 10 mM and 50% MeOH**

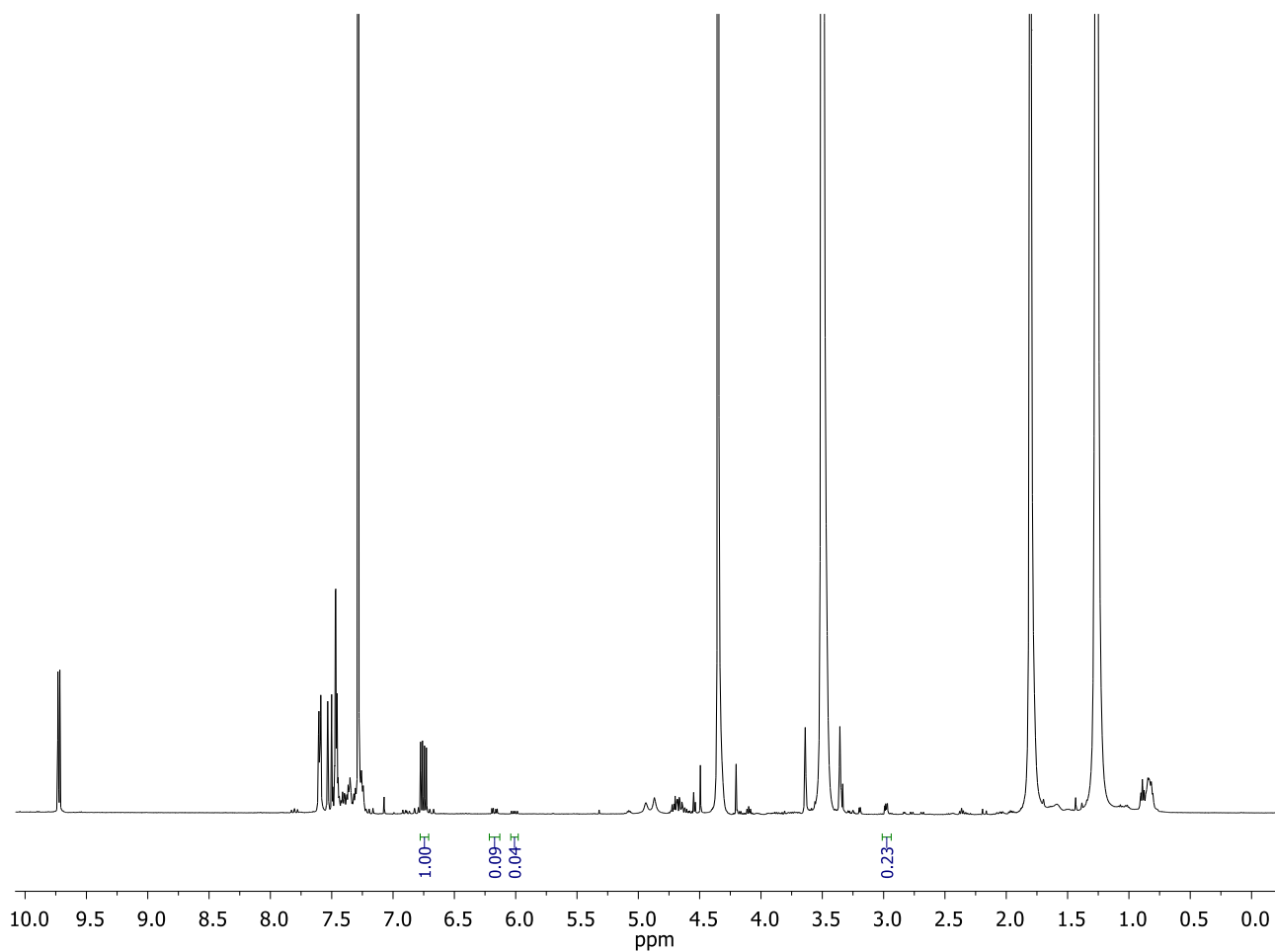
Compound	Integration	% Conversion
<b>14</b> (Starting material)	1.00	66
<b>83</b> (Side-product)	0.20	13
Unknown side-product	0.02	<1
<b>75</b> (Product)	0.64	21

**6.2.6.6 Co-solvent screening for 1,4-Michael addition in 50% KPi pH 7.0 10 mM and 50% MeCN**

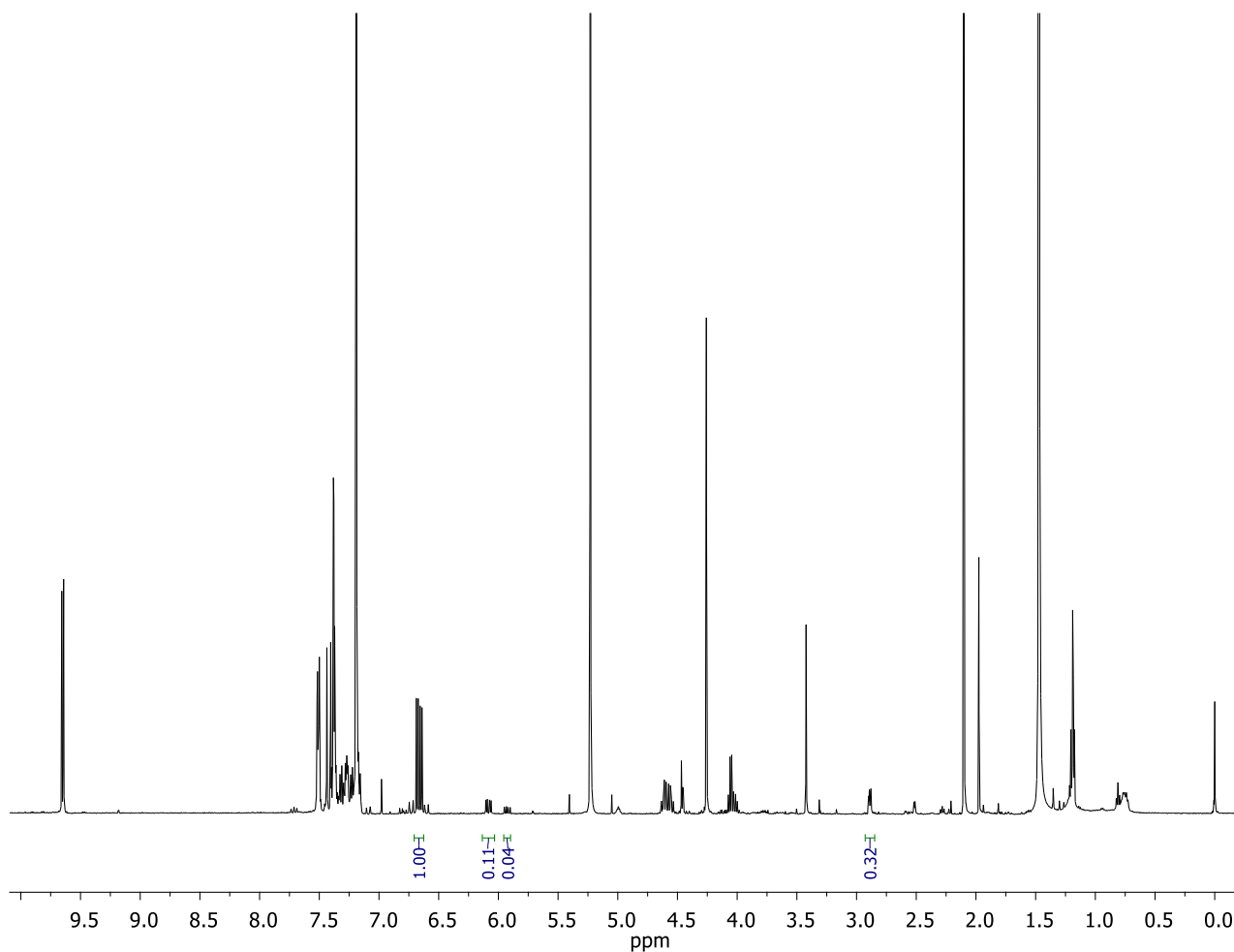
Compound	Integration	% Conversion
<b>14</b> (Starting material)	1.00	96
<b>83</b> (Side-product)	0.06	4
Unknown side-product	/	/
<b>75</b> (Product)	0.01	<1

## 6.2.7 <sup>1</sup>H-NMR details for the activity screening of Table 4

### 6.2.7.1 Buffer screening for 1,4-Michael addition in KP<sub>i</sub> pH 7.0 (10% MeOH) using M-Sav:73

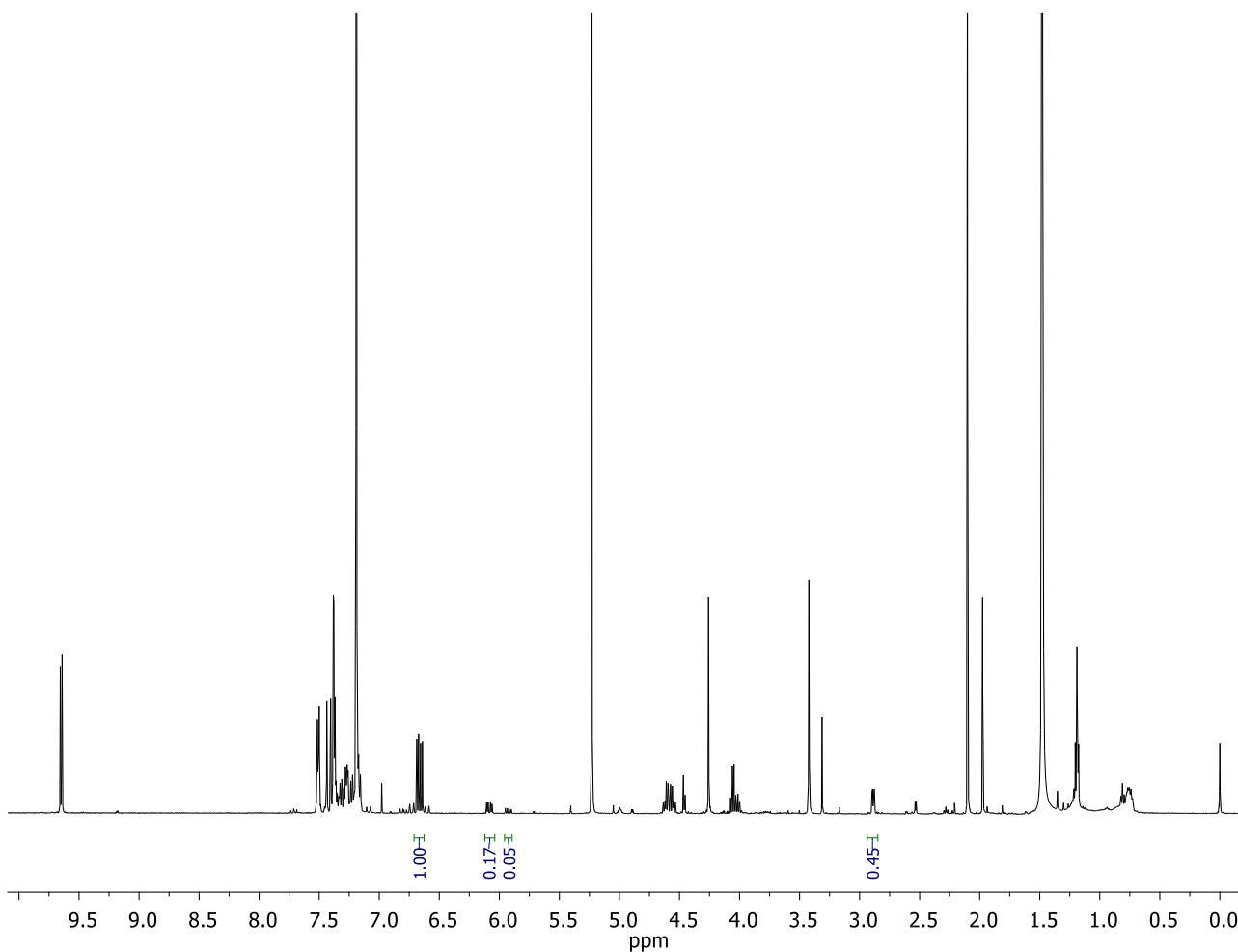


Compound	Integration	% Conversion
<b>14</b> (Starting material)	1.00	82
<b>83</b> (Side-product)	0.09	7
Unknown side-product	0.04	2
<b>75</b> (Product)	0.23	9

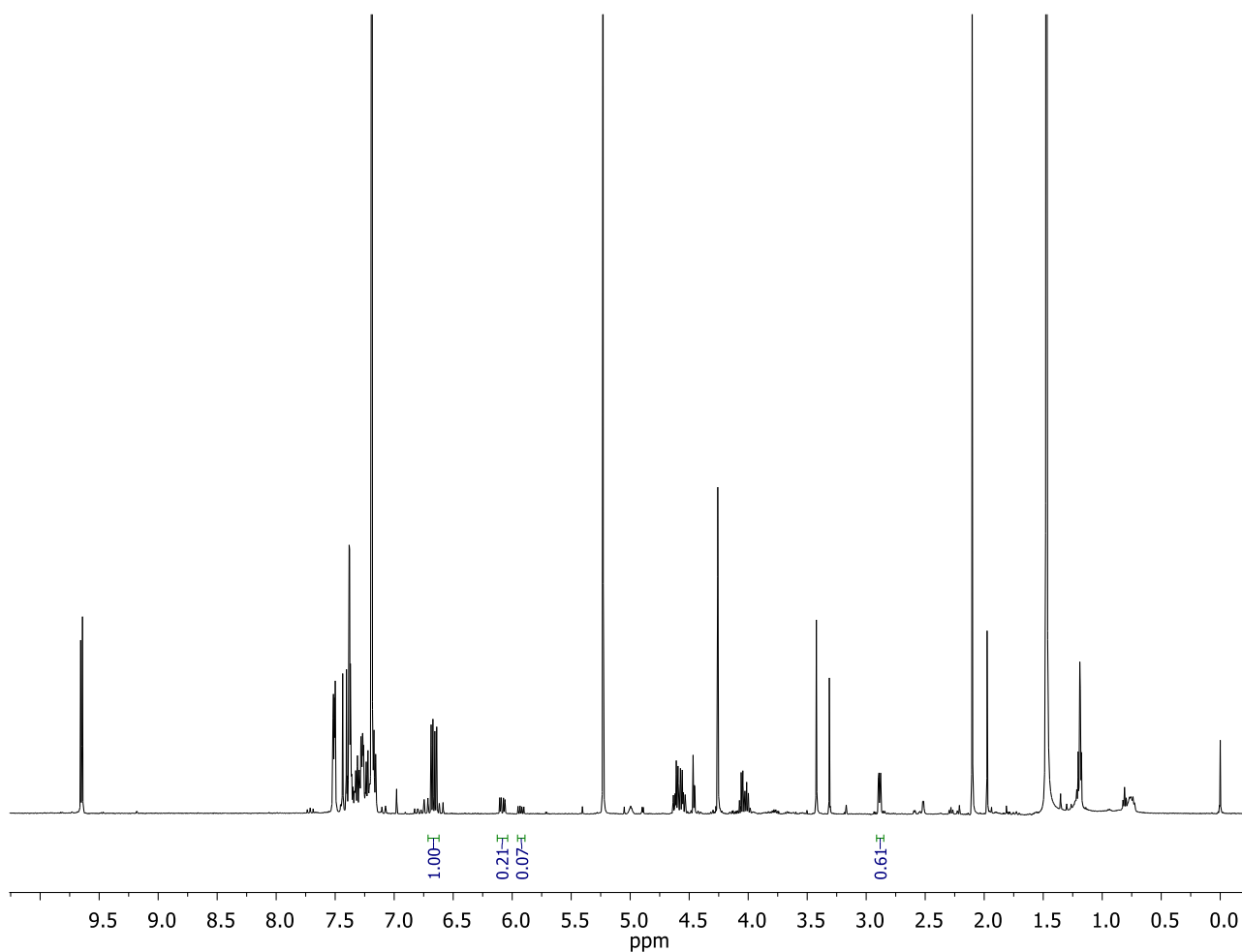
**6.2.7.2 Buffer screening for 1,4-Michael addition in KP<sub>i</sub> pH 7.0 (20% MeOH) using M-Sav:73**

Compound	Integration	% Conversion
<b>14</b> (Starting material)	1.00	77
<b>83</b> (Side-product)	0.11	9
Unknown side-product	0.04	2
<b>75</b> (Product)	0.32	13

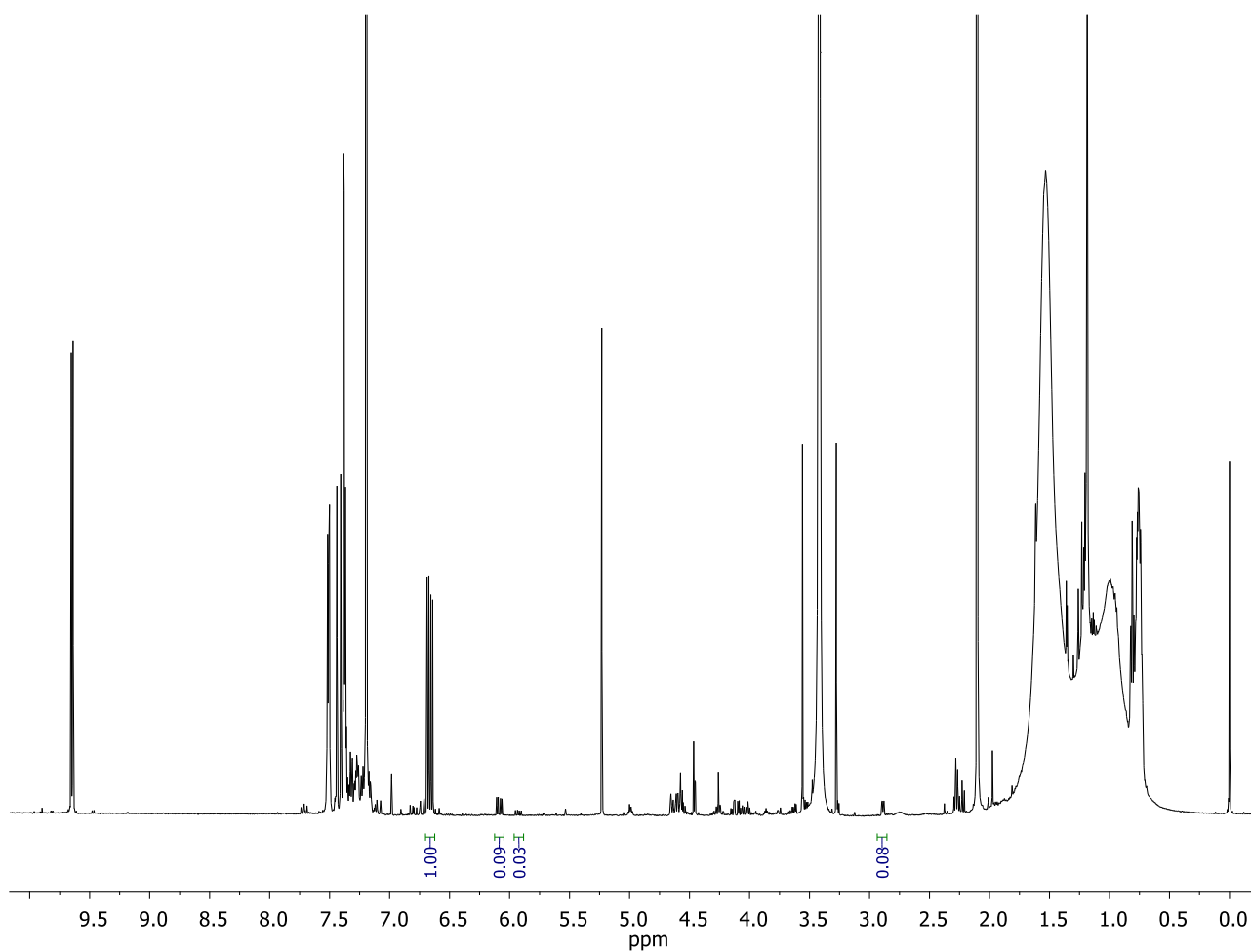


**6.2.7.3 Buffer screening for 1,4-Michael addition in KP<sub>i</sub> pH 7.0 (30% MeOH) using M-Sav:73**

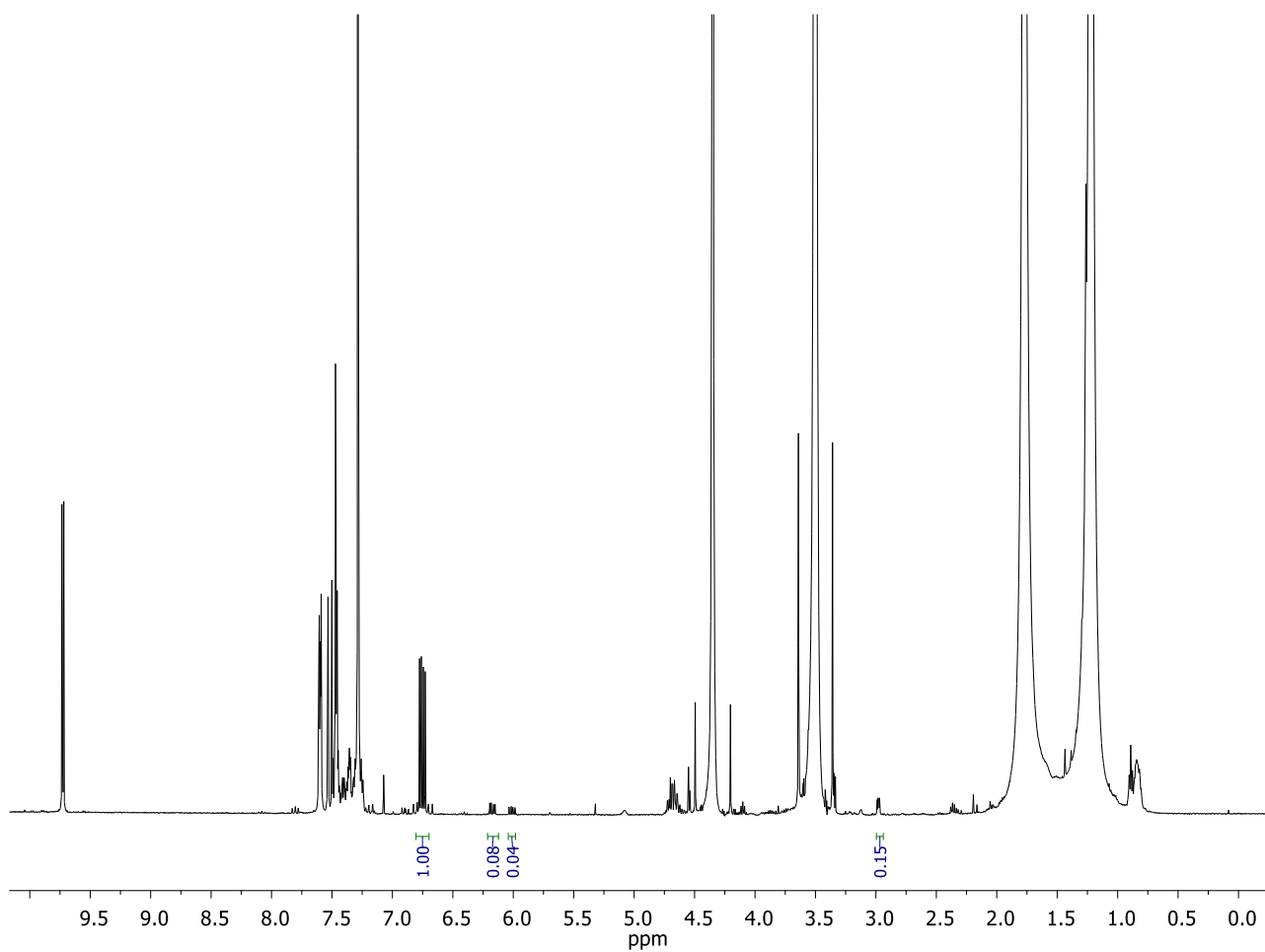
Compound	Integration	% Conversion
<b>14</b> (Starting material)	1.00	71
<b>83</b> (Side-product)	0.17	11
Unknown side-product	0.05	2
<b>75</b> (Product)	0.45	15

**6.2.7.4 Buffer screening for 1,4-Michael addition in KP<sub>i</sub> pH 7.0 (40% MeOH) using M-Sav:73**

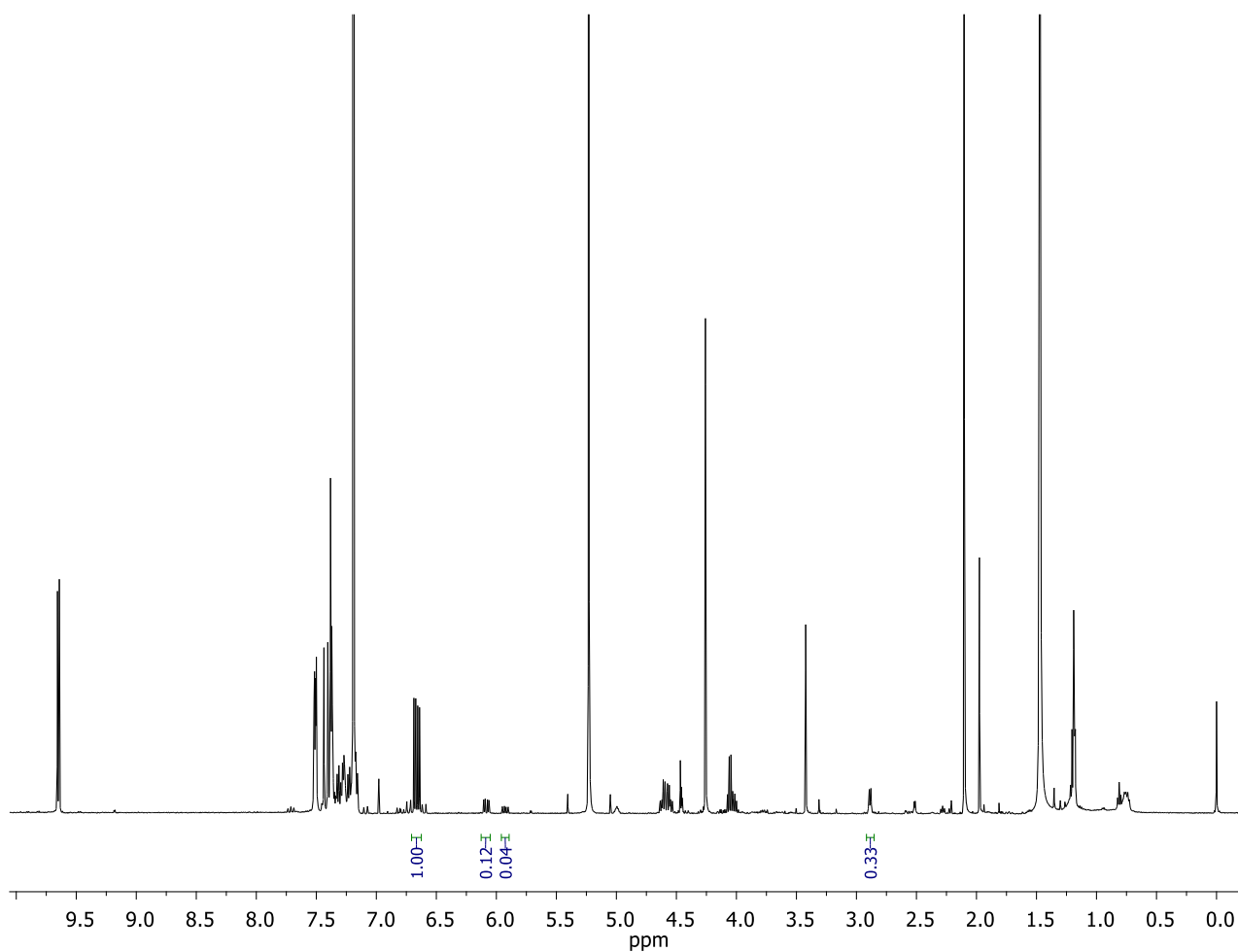
Compound	Integration	% Conversion
<b>14</b> (Starting material)	1.00	64
<b>83</b> (Side-product)	0.21	13
Unknown side-product	0.07	5
<b>75</b> (Product)	0.61	18

**6.2.7.5 Buffer screening for 1,4-Michael addition in KP<sub>i</sub> pH 7.0 (0% MeOH) using catalyst 73**

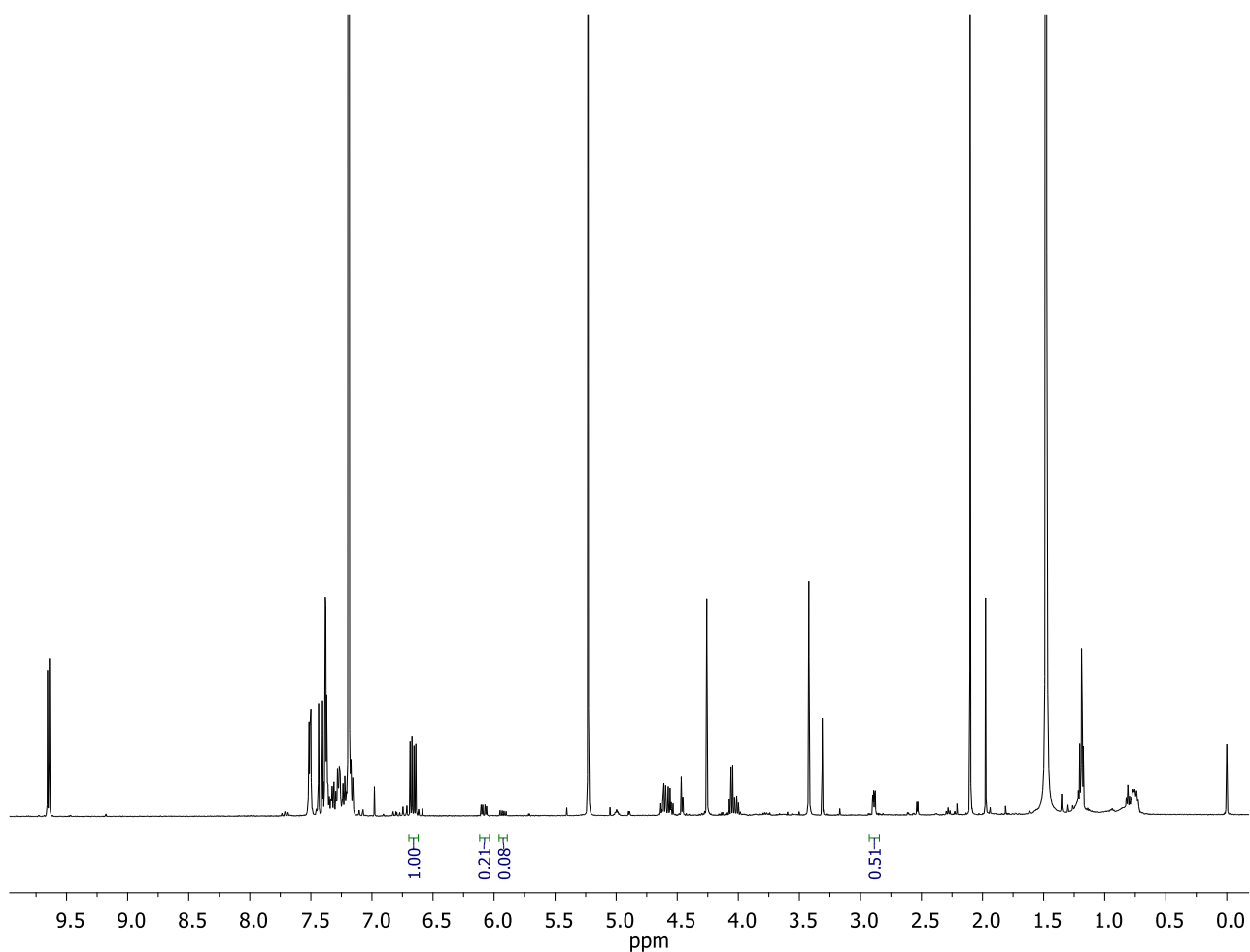
Compound	Integration	% Conversion
<b>14</b> (Starting material)	1.00	89
<b>83</b> (Side-product)	0.09	7
Unknown side-product	0.03	1
<b>75</b> (Product)	0.08	3

**6.2.7.6 Buffer screening for 1,4-Michael addition in KPi pH 7.0 (10% MeOH) using catalyst 73**

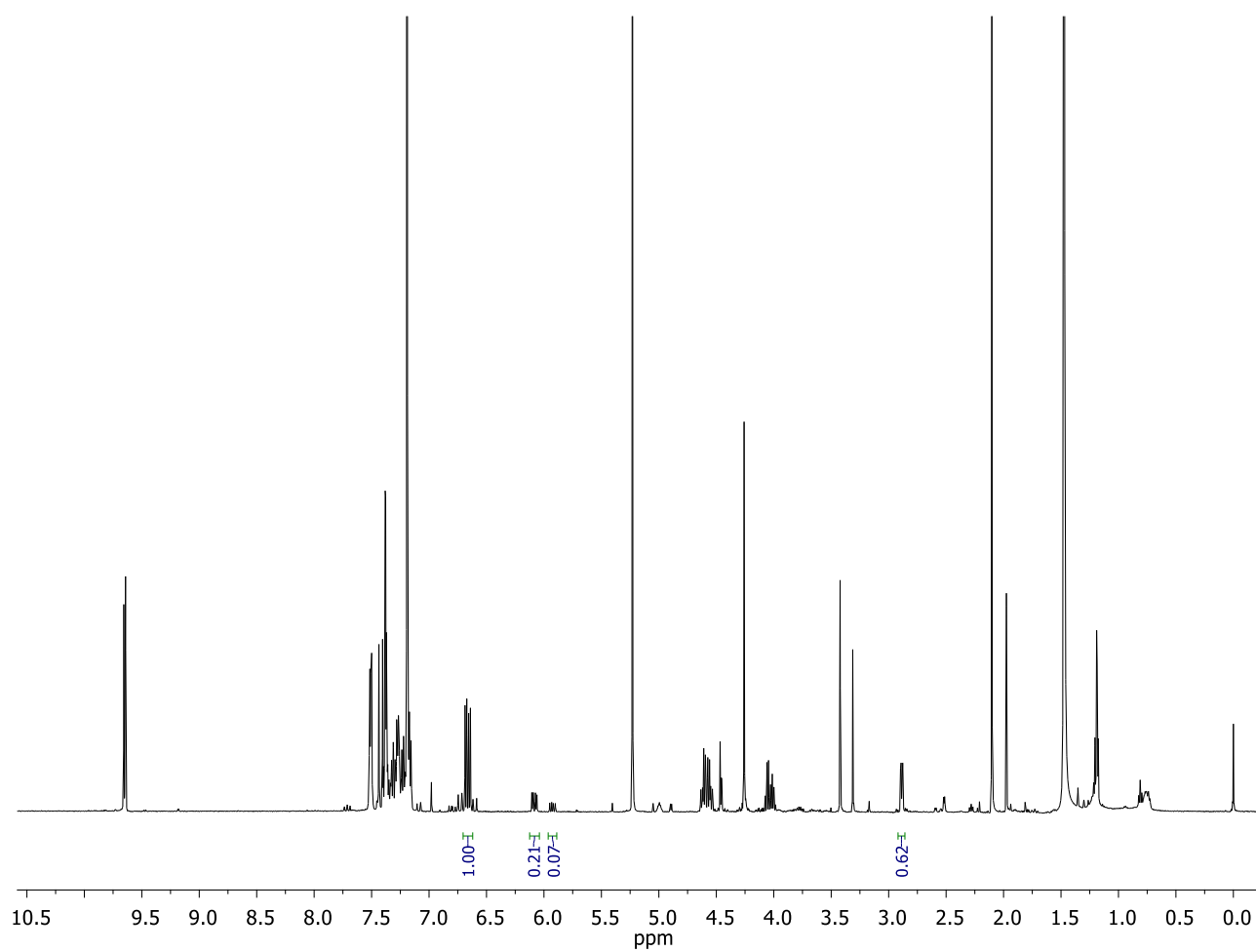
Compound	Integration	% Conversion
<b>14</b> (Starting material)	1.00	86
<b>83</b> (Side-product)	0.08	6
Unknown side-product	0.04	2
<b>75</b> (Product)	0.15	6

**6.2.7.7 Buffer screening for 1,4-Michael addition in KPi pH 7.0 (20% MeOH) using catalyst 73**

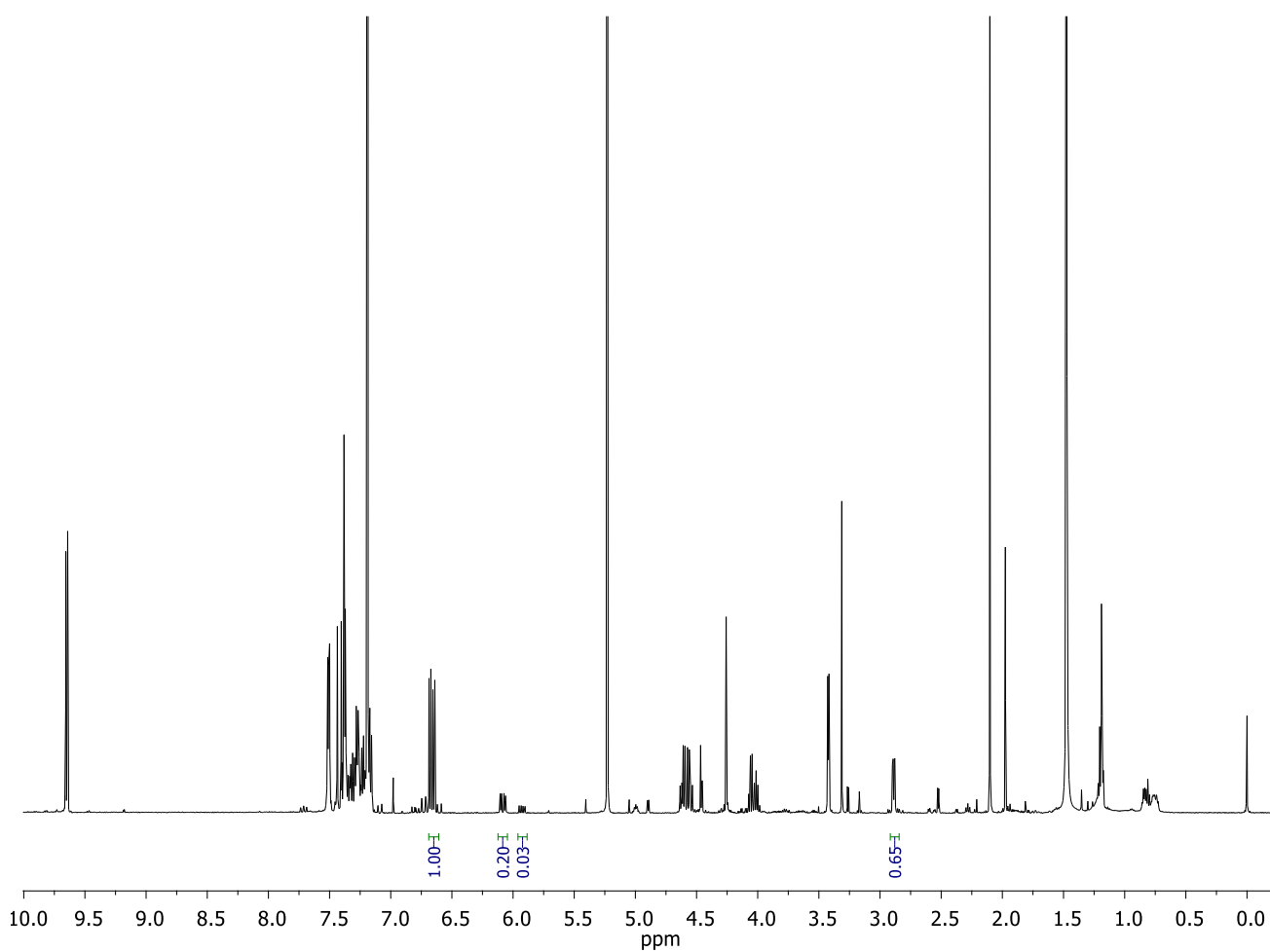
Compound	Integration	% Conversion
<b>14</b> (Starting material)	1.00	76
<b>83</b> (Side-product)	0.12	10
Unknown side-product	0.04	2
<b>75</b> (Product)	0.33	12

**6.2.7.8 Buffer screening for 1,4-Michael addition in KPi pH 7.0 (30% MeOH) using catalyst 73**

Compound	Integration	% Conversion
<b>14</b> (Starting material)	1.00	65
<b>83</b> (Side-product)	0.21	14
Unknown side-product	0.08	5
<b>75</b> (Product)	0.51	16

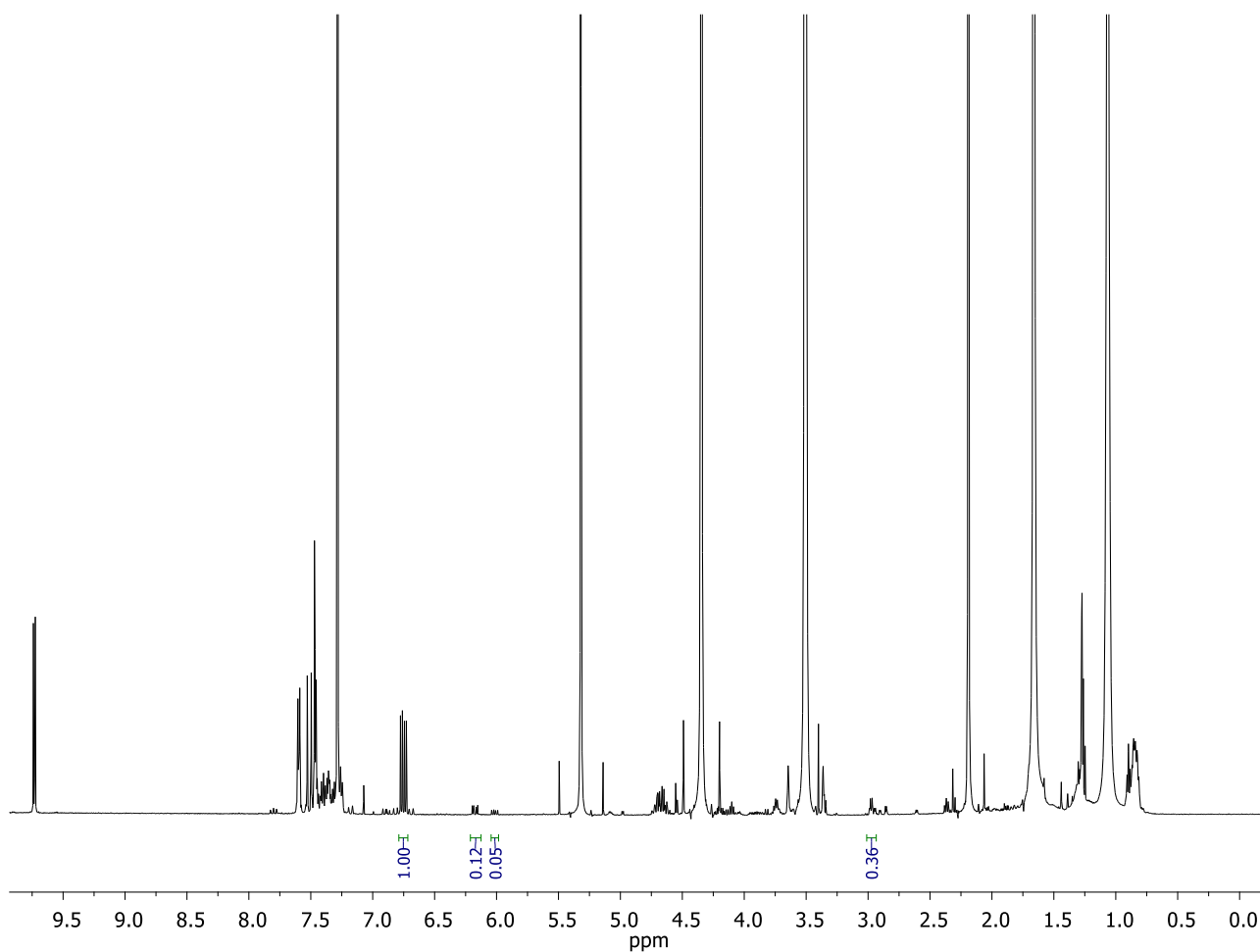
**6.2.7.9 Buffer screening for 1,4-Michael addition in KPi pH 7.0 (40% MeOH) using catalyst 73**

Compound	Integration	% Conversion
<b>14</b> (Starting material)	1.00	63
<b>83</b> (Side-product)	0.21	13
Unknown side-product	0.07	5
<b>75</b> (Product)	0.62	19

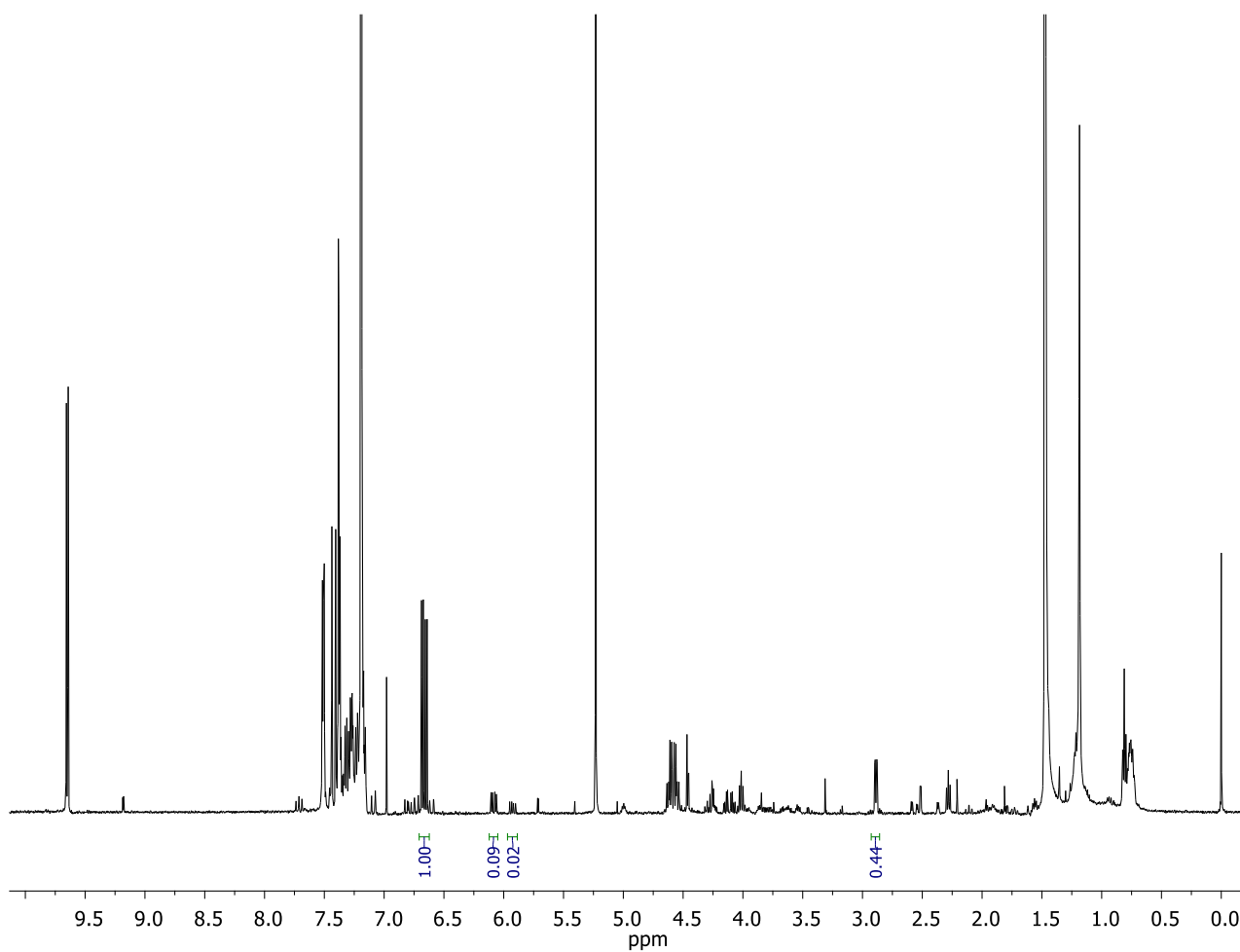
**6.2.7.10 Buffer screening for 1,4-Michael addition in KPi pH 7.0 (50% MeOH) using catalyst 73**

Compound	Integration	% Conversion
<b>14</b> (Starting material)	1.00	66
<b>83</b> (Side-product)	0.20	13
Unknown side-product	0.03	1
<b>75</b> (Product)	0.65	20

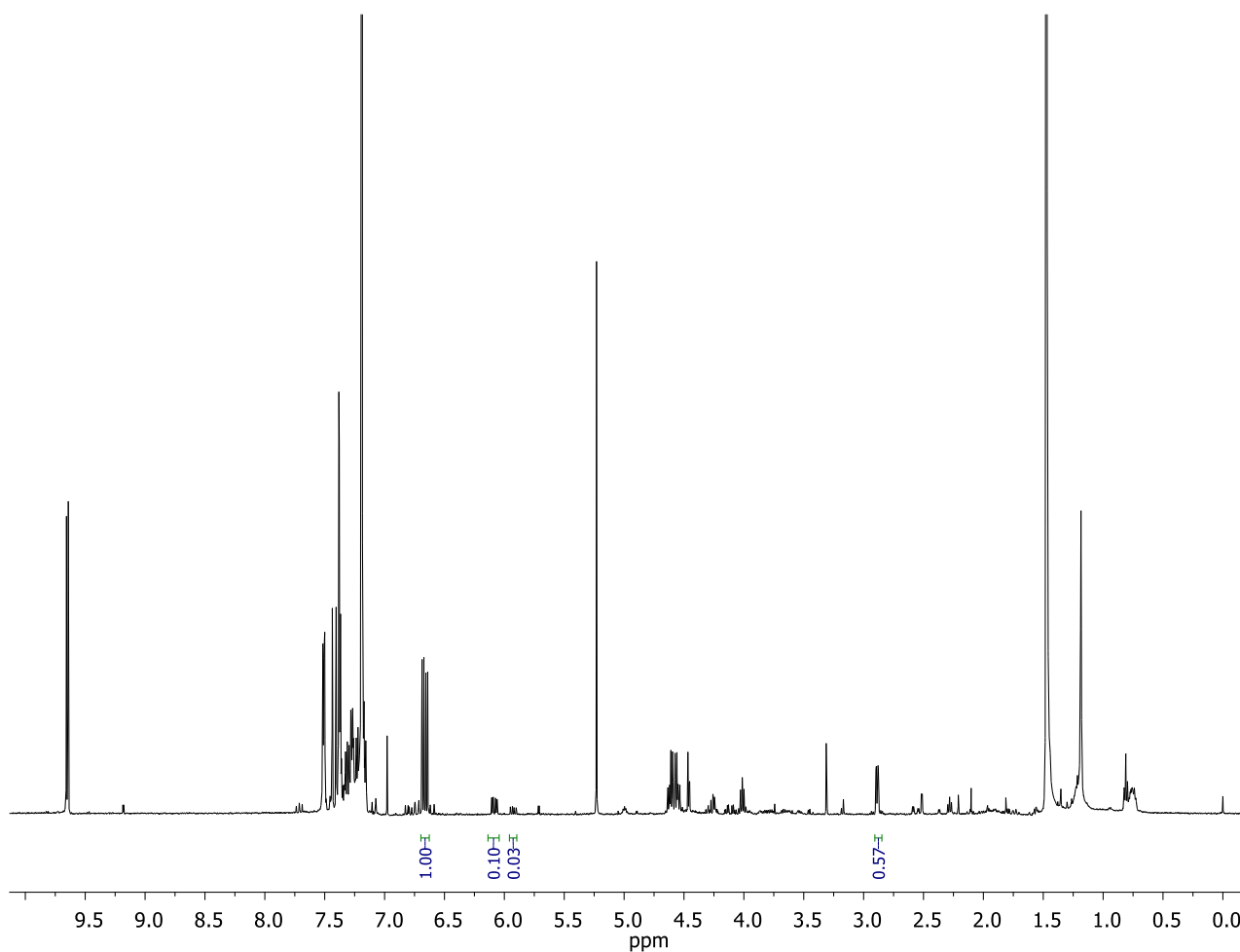


**6.2.7.11 Buffer screening for 1,4-Michael addition in KPi pH 7.0 (0% MeOH) using M-Sav:74**

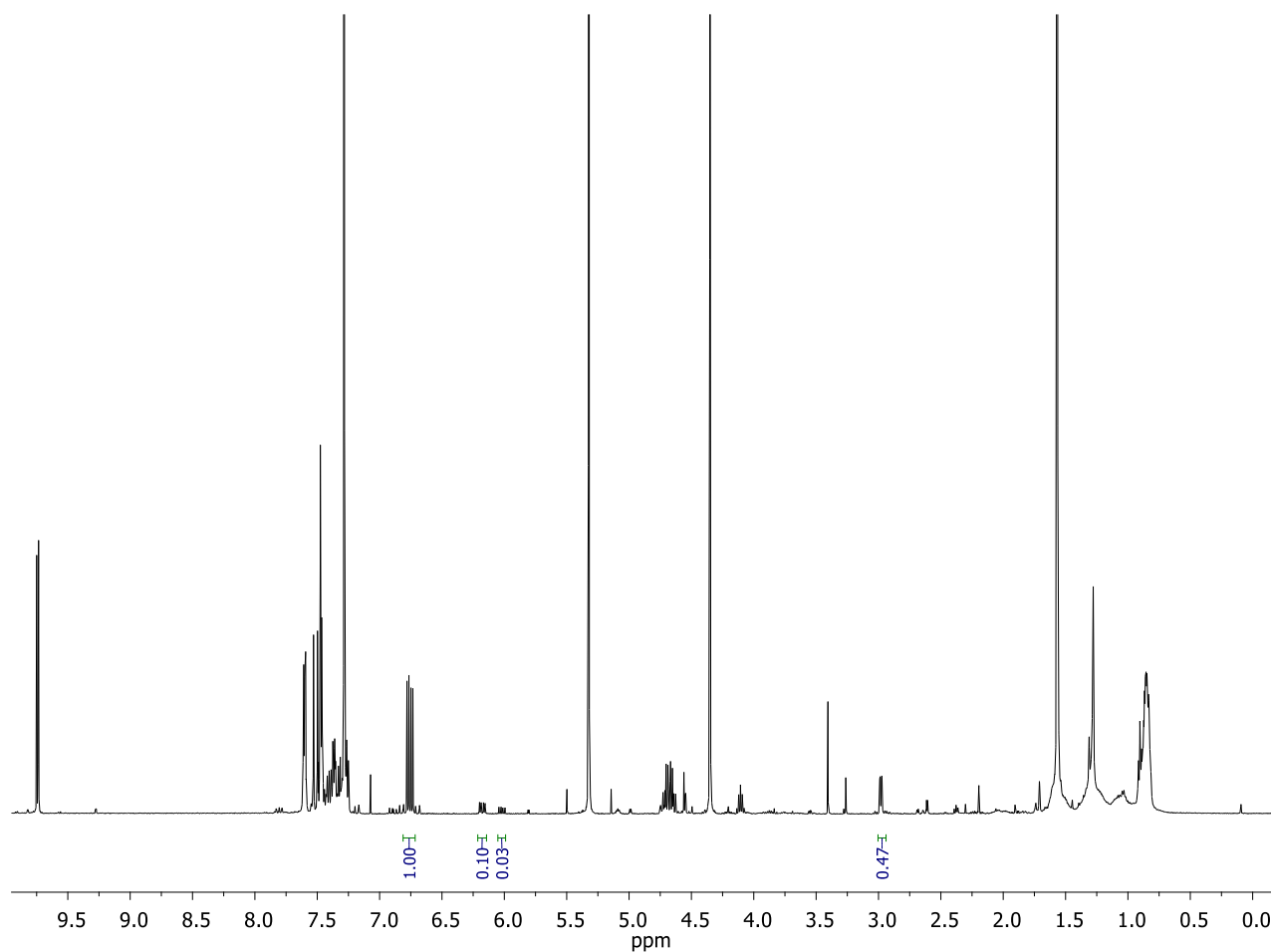
Compound	Integration	% Conversion
<b>14</b> (Starting material)	1.00	76
<b>83</b> (Side-product)	0.12	8
Unknown side-product	0.05	3
<b>75</b> (Product)	0.36	13

**6.2.7.12 Buffer screening for 1,4-Michael addition in KP<sub>i</sub> pH 7.0 (10% MeOH) using M-Sav:74**

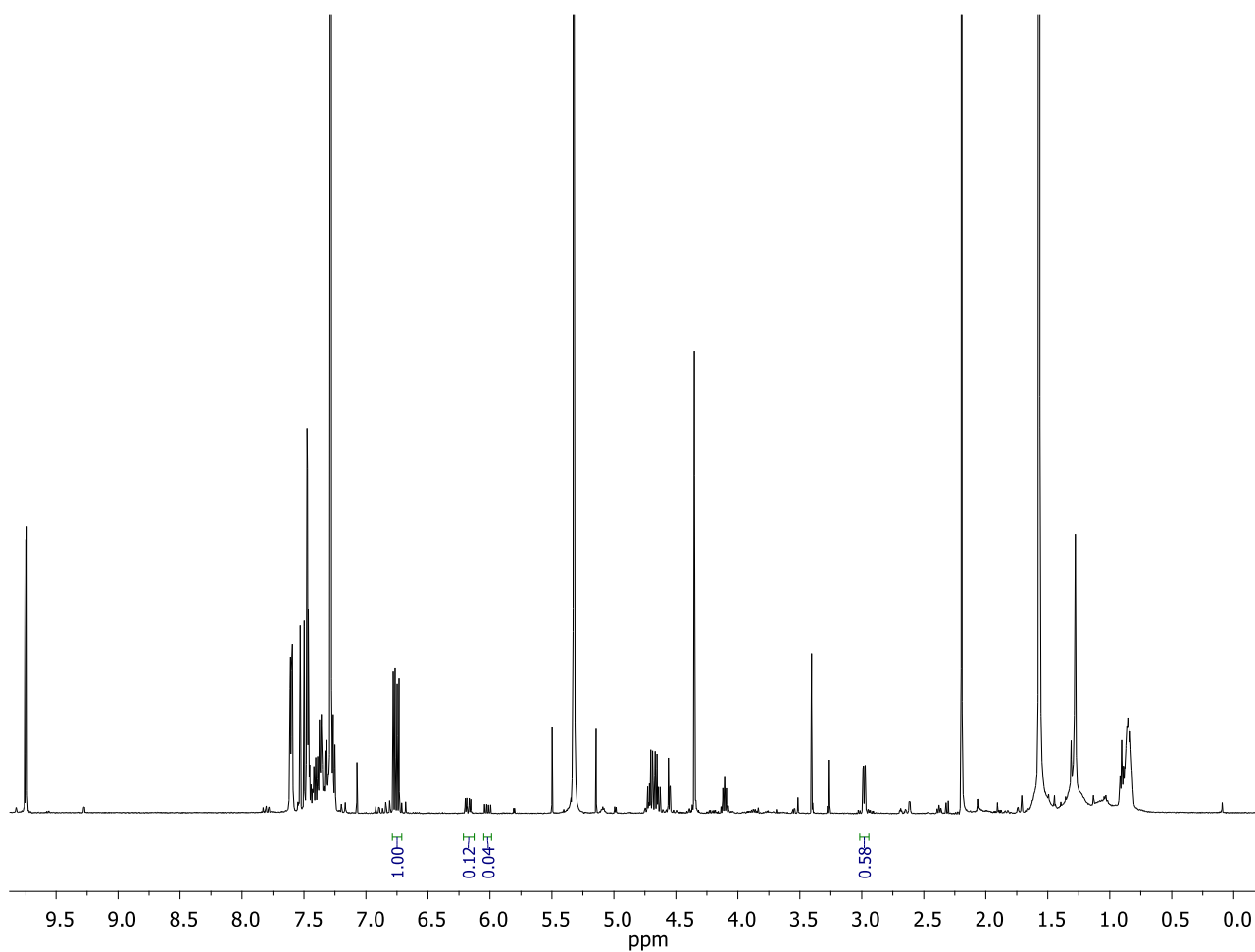
Compound	Integration	% Conversion
<b>14</b> (Starting material)	1.00	78
<b>83</b> (Side-product)	0.09	6
Unknown side-product	0.02	<1
<b>75</b> (Product)	0.44	16

**6.2.7.13 Buffer screening for 1,4-Michael addition in KP<sub>i</sub> pH 7.0 (20% MeOH) using M-Sav:74**

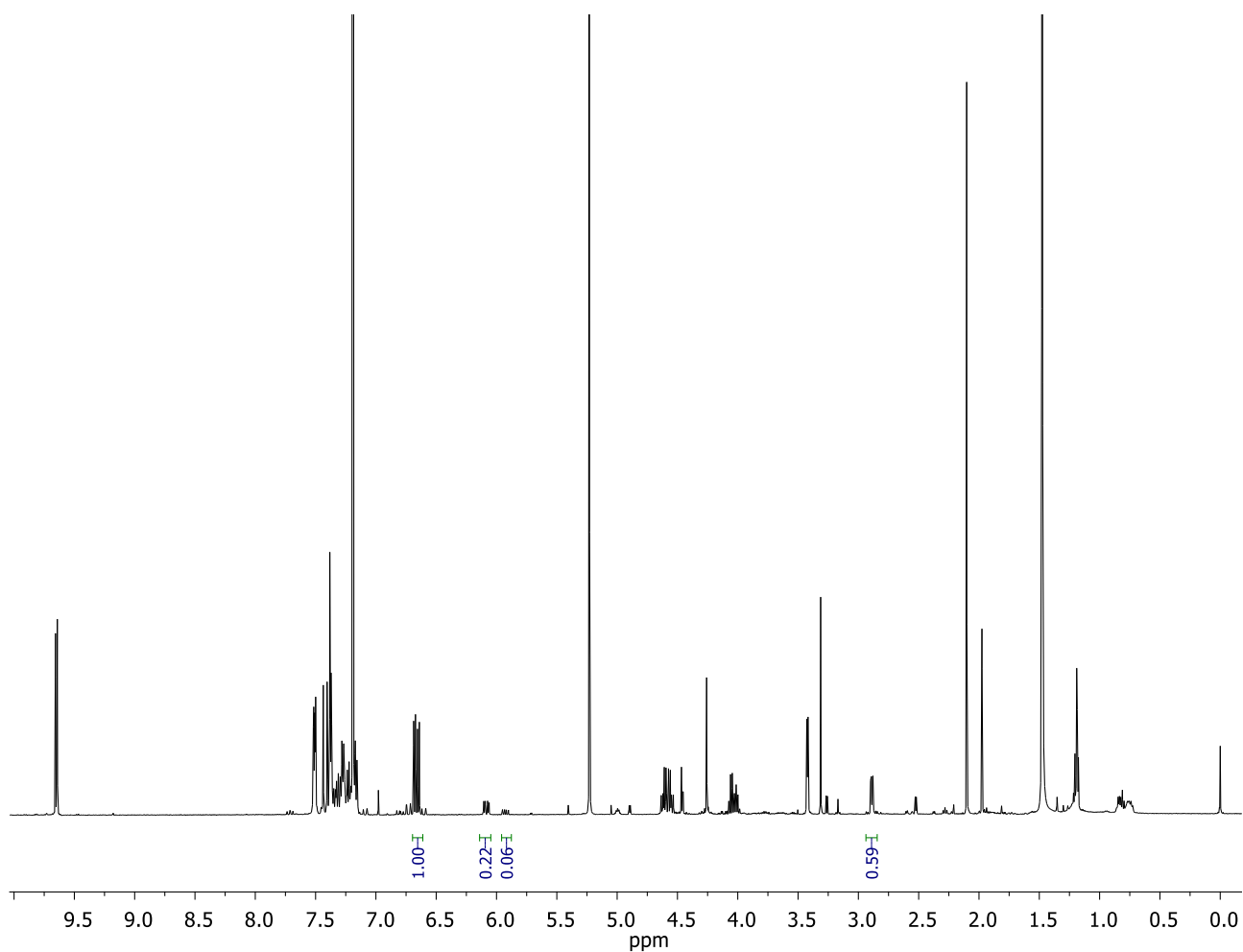
Compound	Integration	% Conversion
<b>14</b> (Starting material)	1.00	73
<b>83</b> (Side-product)	0.10	7
Unknown side-product	0.03	1
<b>75</b> (Product)	0.57	20

**6.2.7.14 Buffer screening for 1,4-Michael addition in KP<sub>i</sub> pH 7.0 (30% MeOH) using M-Sav:74**

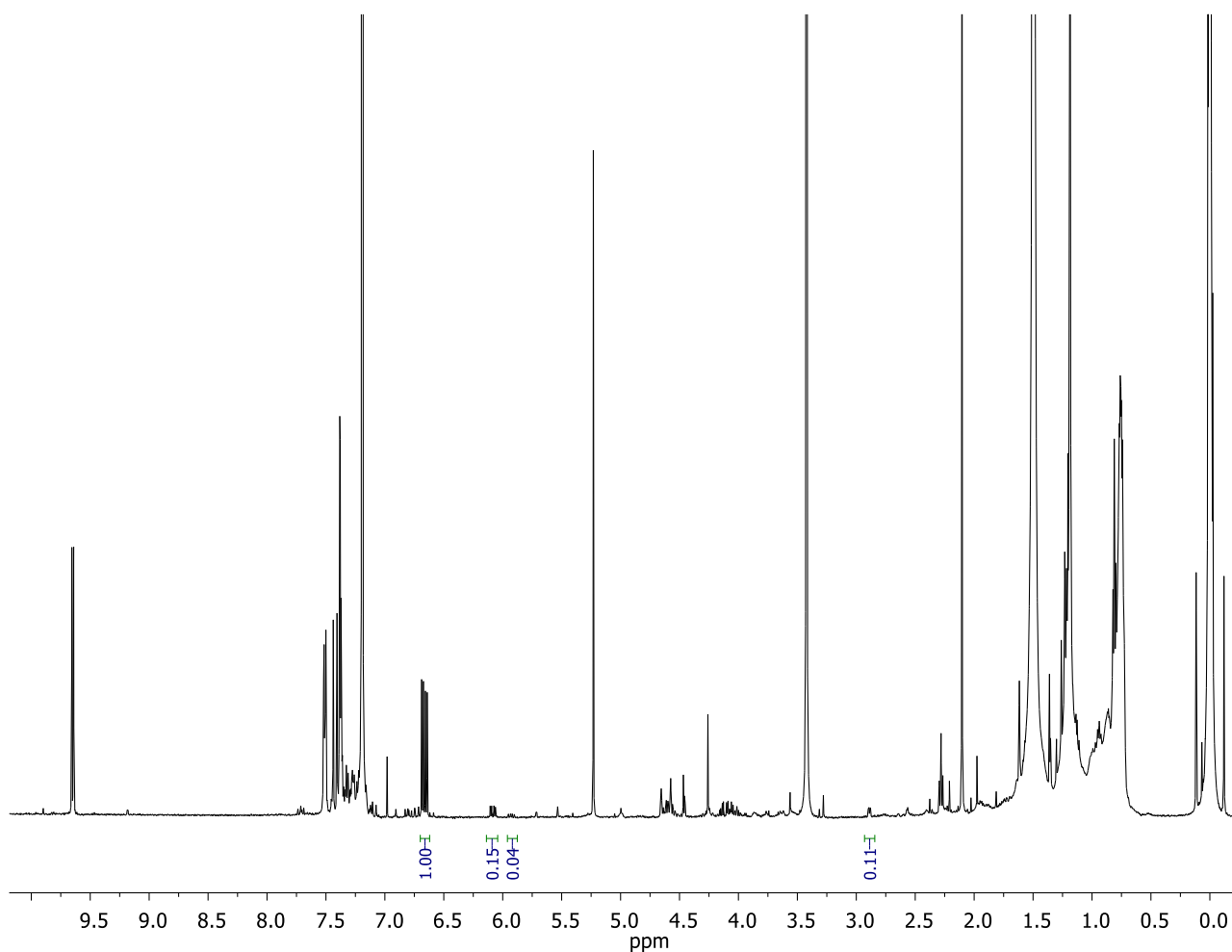
Compound	Integration	% Conversion
<b>14</b> (Starting material)	1.00	75
<b>83</b> (Side-product)	0.10	7
Unknown side-product	0.03	1
<b>75</b> (Product)	0.47	17

**6.2.7.15 Buffer screening for 1,4-Michael addition in KP<sub>i</sub> pH 7.0 (40% MeOH) using M-Sav:74**

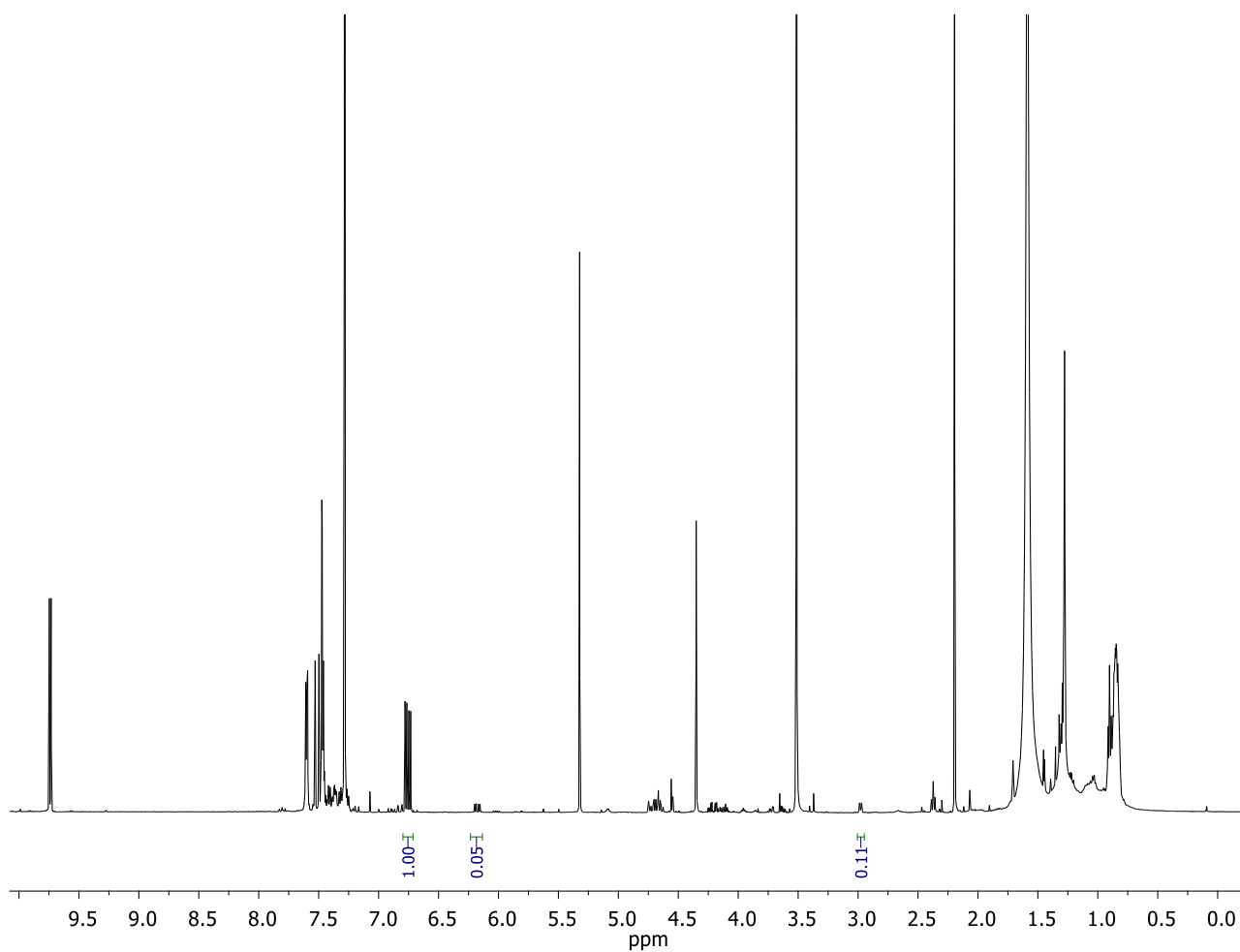
Compound	Integration	% Conversion
<b>14</b> (Starting material)	1.00	71
<b>83</b> (Side-product)	0.12	8
Unknown side-product	0.04	2
<b>75</b> (Product)	0.58	19

**6.2.7.16 Buffer screening for 1,4-Michael addition in KP<sub>i</sub> pH 7.0 (50% MeOH) using M-Sav:74**

Compound	Integration	% Conversion
<b>14</b> (Starting material)	1.00	65
<b>83</b> (Side-product)	0.22	13
Unknown side-product	0.06	4
<b>75</b> (Product)	0.59	18

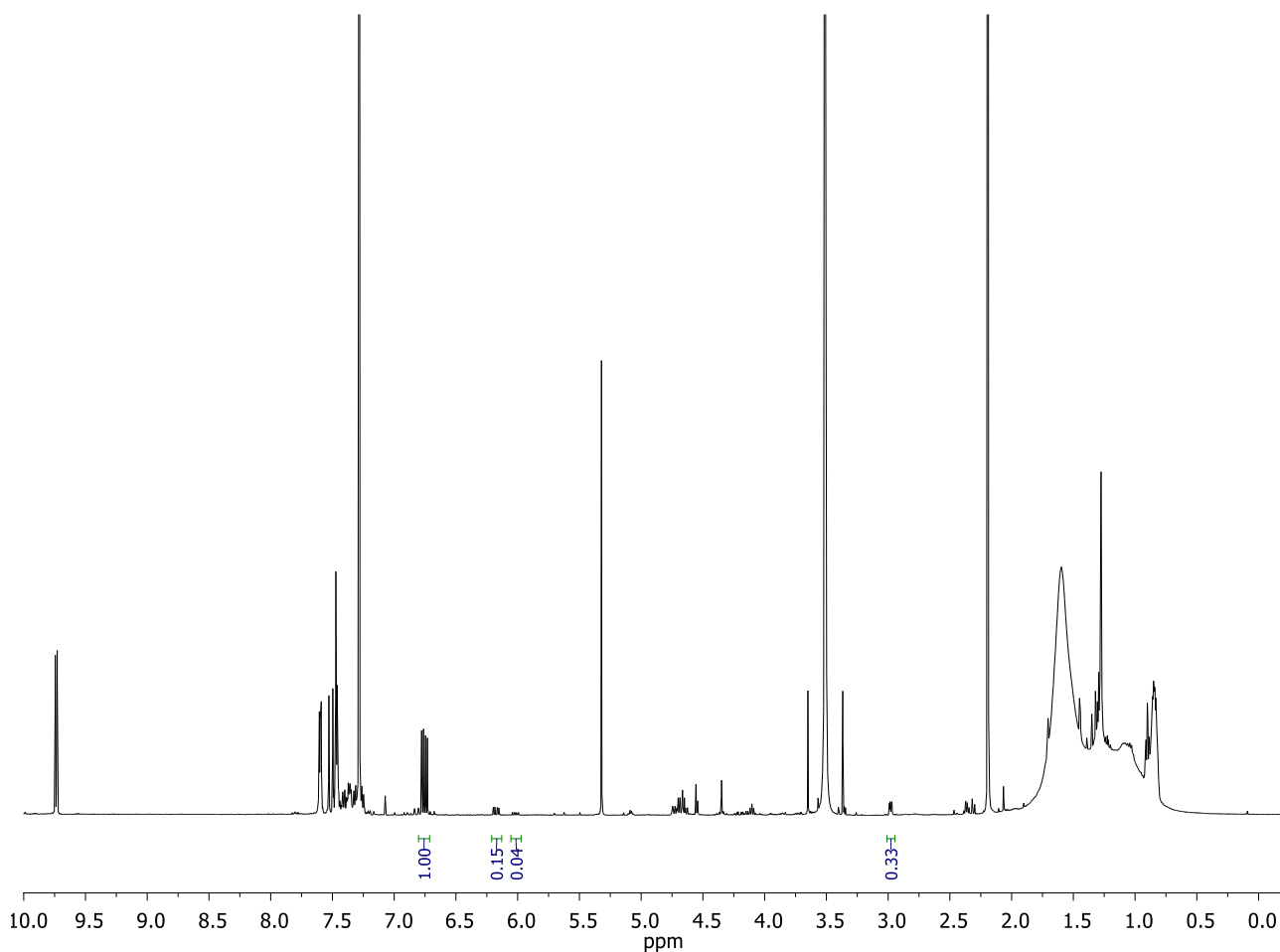
**6.2.7.17 Buffer screening for 1,4-Michael addition in KP<sub>i</sub> pH 7.0 (0% MeOH) using catalyst 74**

Compound	Integration	% Conversion
<b>14</b> (Starting material)	1.00	82
<b>83</b> (Side-product)	0.15	12
Unknown side-product	0.04	2
<b>75</b> (Product)	0.11	4

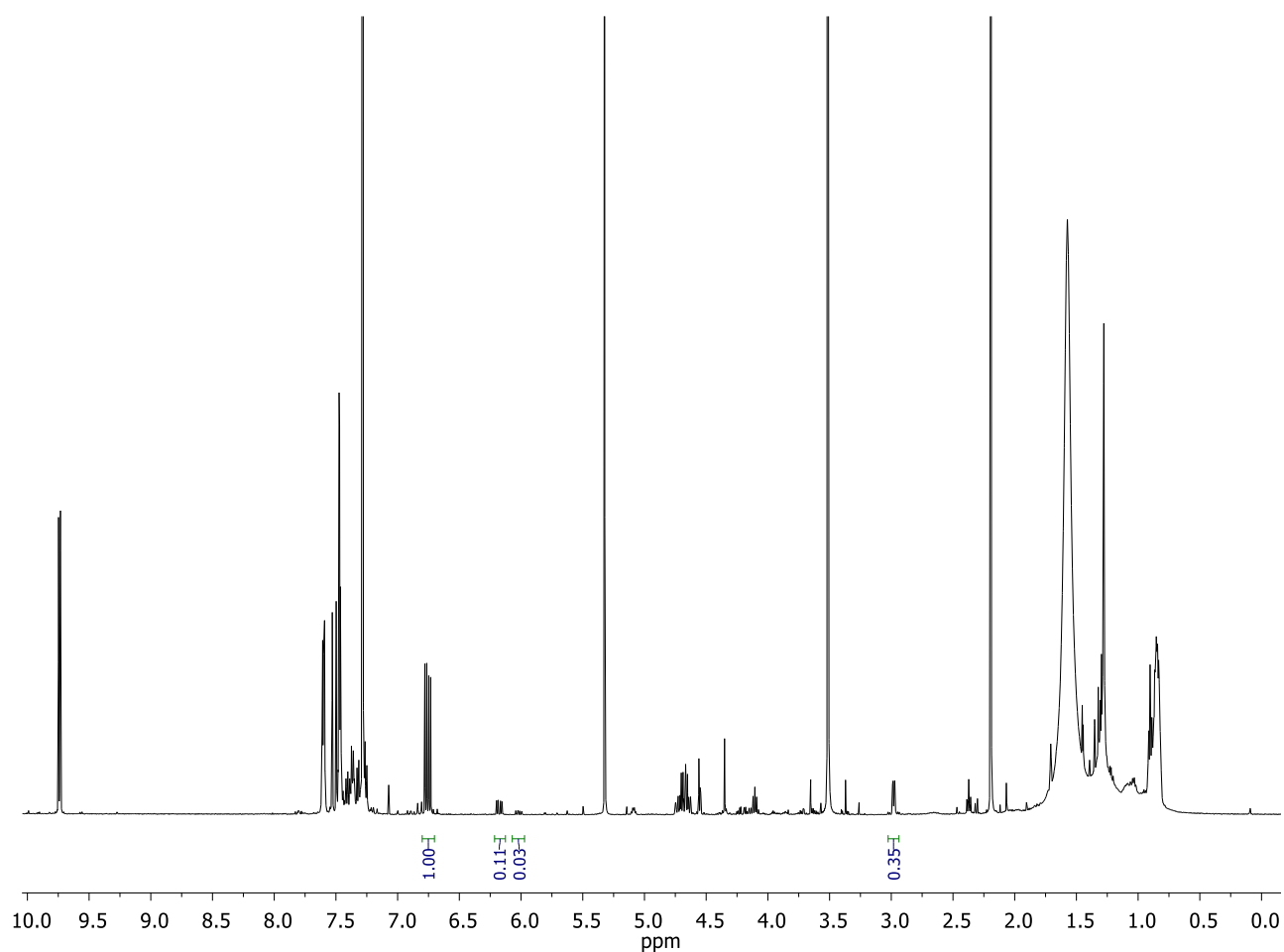
**6.2.7.18 Buffer screening for 1,4-Michael addition in KPi pH 7.0 (10% MeOH) using catalyst 74**

Compound	Integration	% Conversion
<b>14</b> (Starting material)	1.00	90
<b>83</b> (Side-product)	0.05	5
Unknown side-product	/	/
<b>75</b> (Product)	0.11	5

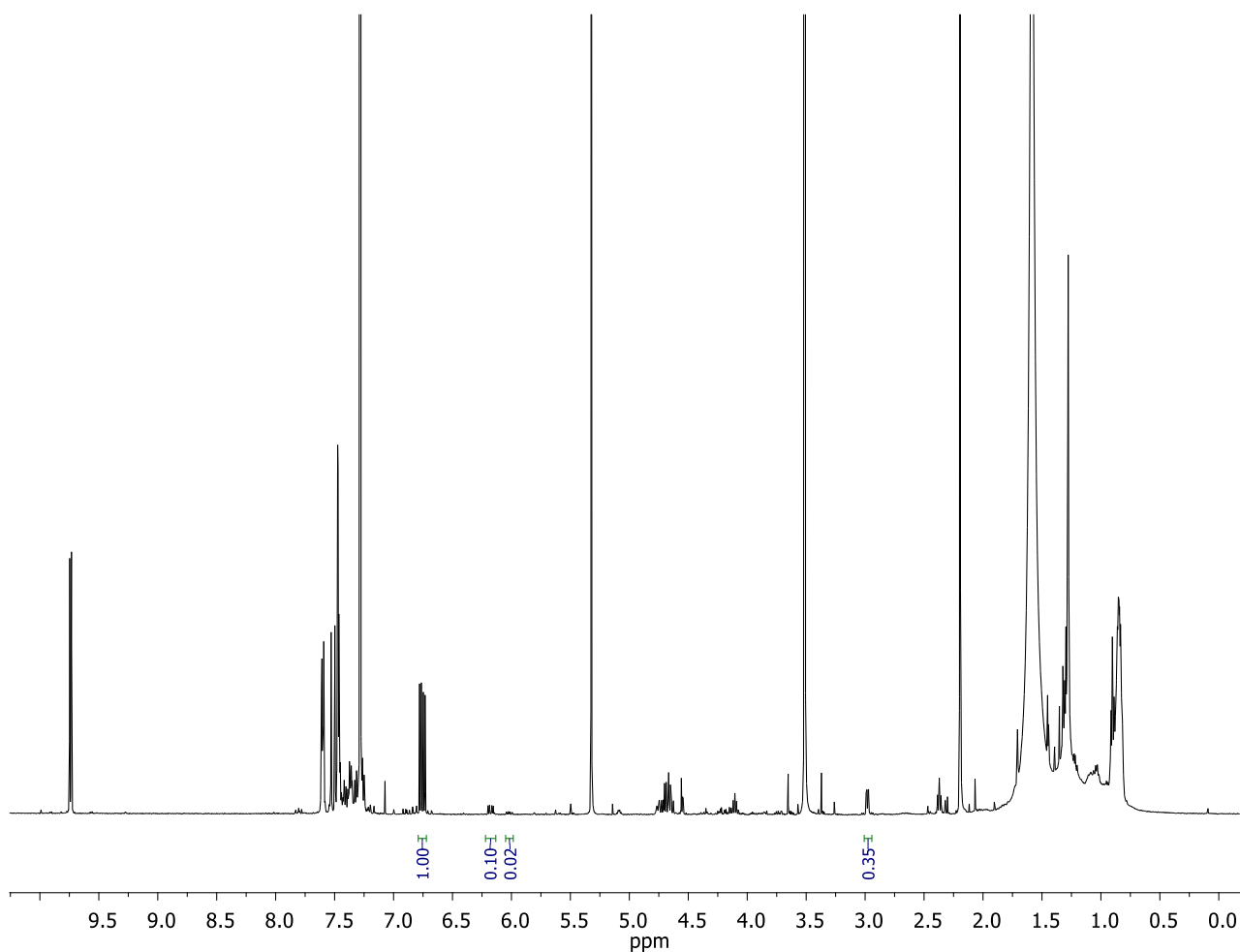


**6.2.7.19 Buffer screening for 1,4-Michael addition in KPi pH 7.0 (20% MeOH) using catalyst 74**

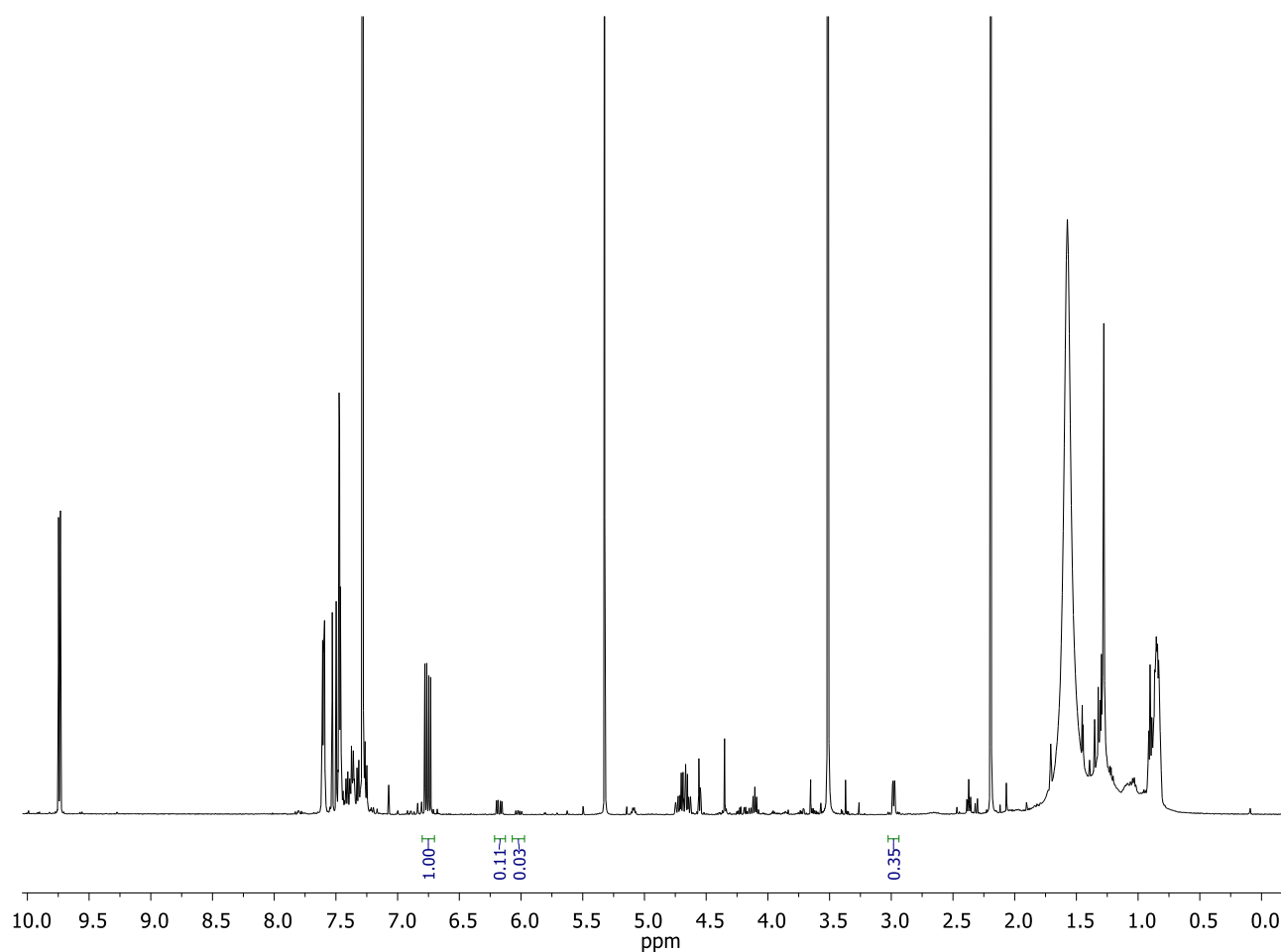
Compound	Integration	% Conversion
<b>14</b> (Starting material)	1.00	75
<b>83</b> (Side-product)	0.15	11
Unknown side-product	0.04	2
<b>75</b> (Product)	0.33	12

**6.2.7.20 Buffer screening for 1,4-Michael addition in KPi pH 7.0 (30% MeOH) using catalyst 74**

Compound	Integration	% Conversion
<b>14</b> (Starting material)	1.00	78
<b>83</b> (Side-product)	0.11	8
Unknown side-product	0.03	1
<b>75</b> (Product)	0.35	13

**6.2.7.21 Buffer screening for 1,4-Michael addition in KP<sub>i</sub> pH 7.0 (40% MeOH) using catalyst 74**

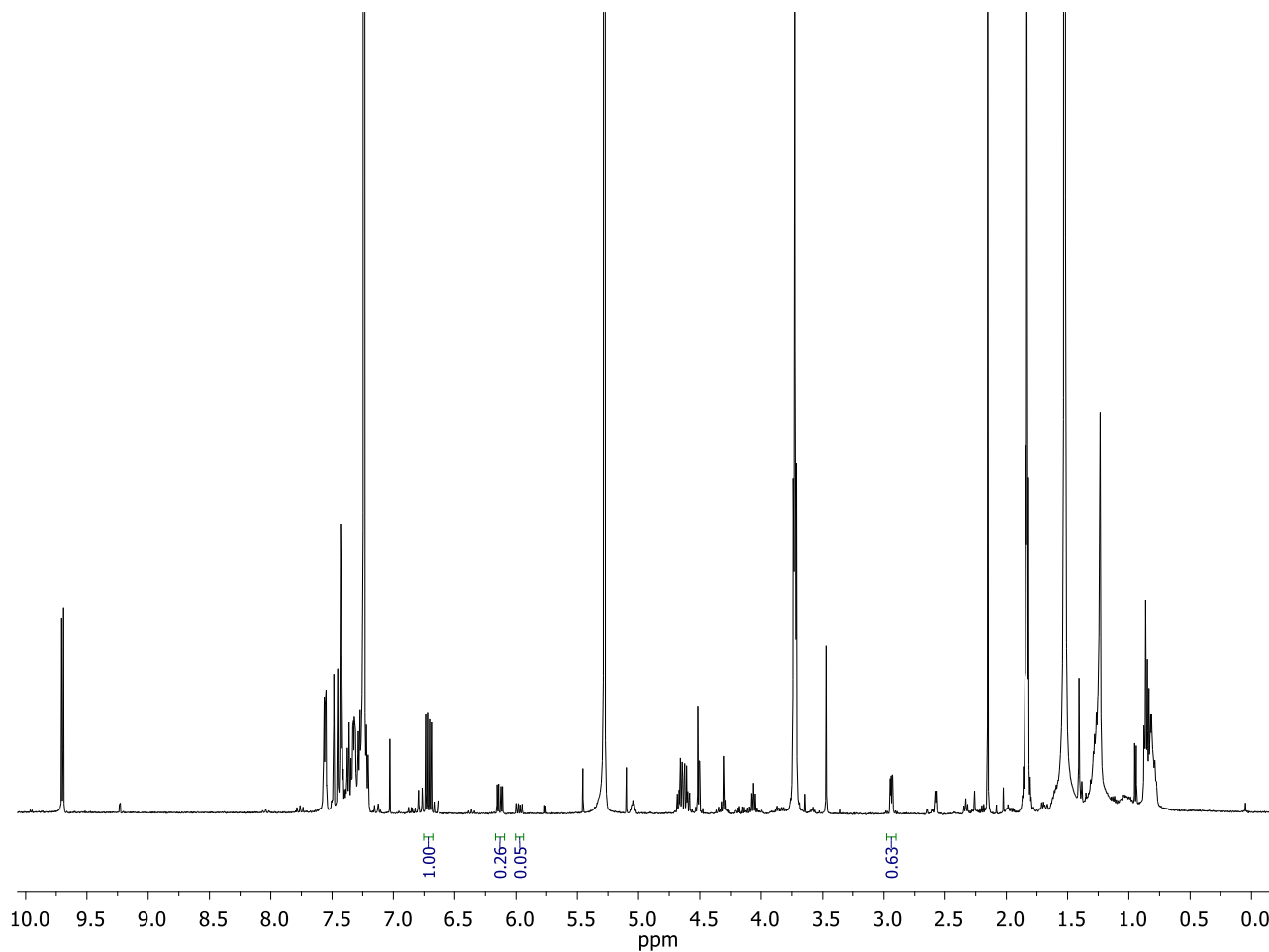
Compound	Integration	% Conversion
<b>14</b> (Starting material)	1.00	80
<b>83</b> (Side-product)	0.10	7
Unknown side-product	0.02	<1
<b>75</b> (Product)	0.35	13

**6.2.7.22 Buffer screening for 1,4-Michael addition in KPi pH 7.0 (50% MeOH) using catalyst 74**

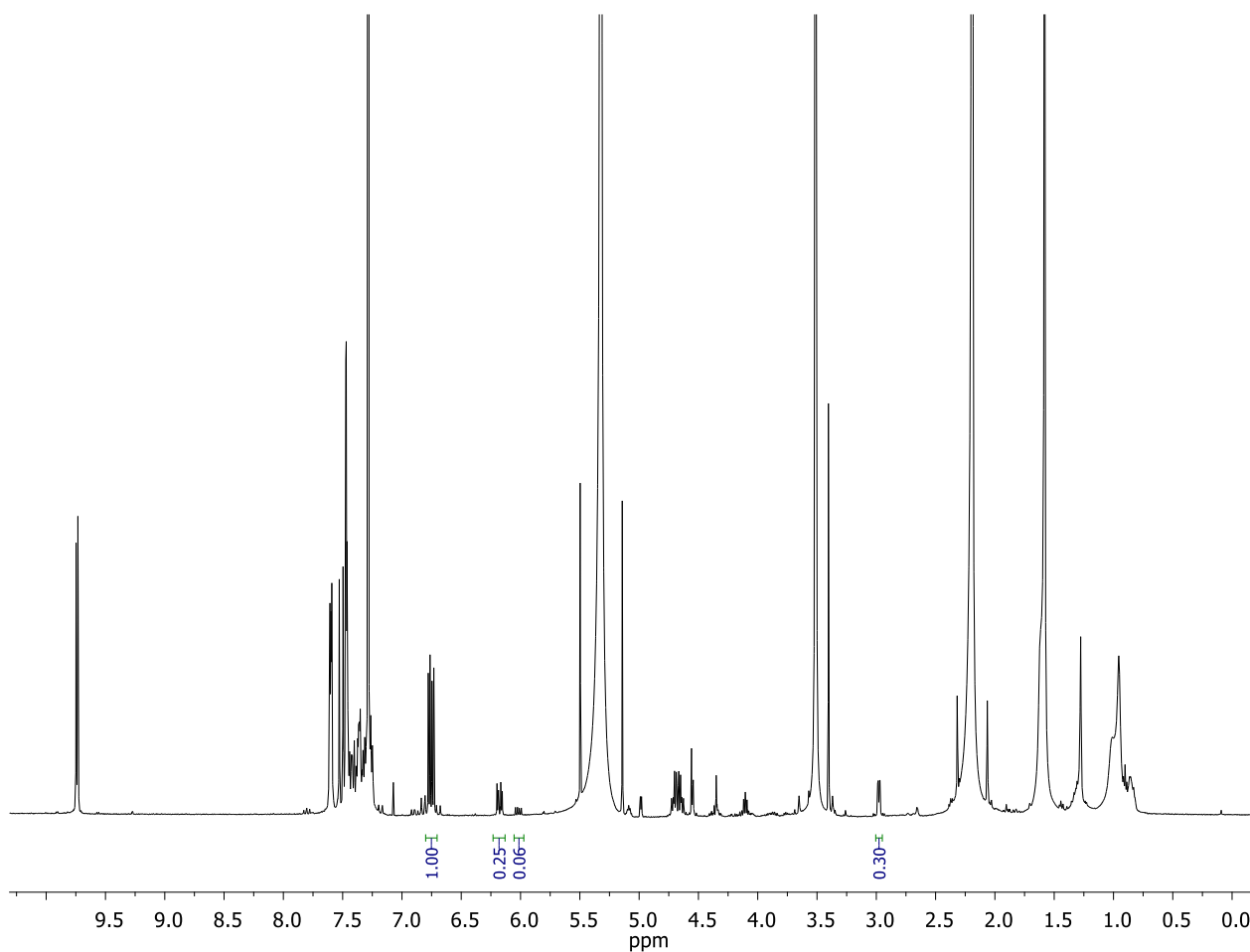
Compound	Integration	% Conversion
<b>14</b> (Starting material)	1.00	79
<b>83</b> (Side-product)	0.11	7
Unknown side-product	0.03	1
<b>75</b> (Product)	0.35	13

## 6.2.8 $^1\text{H-NMR}$ details for the activity screening of Table 5

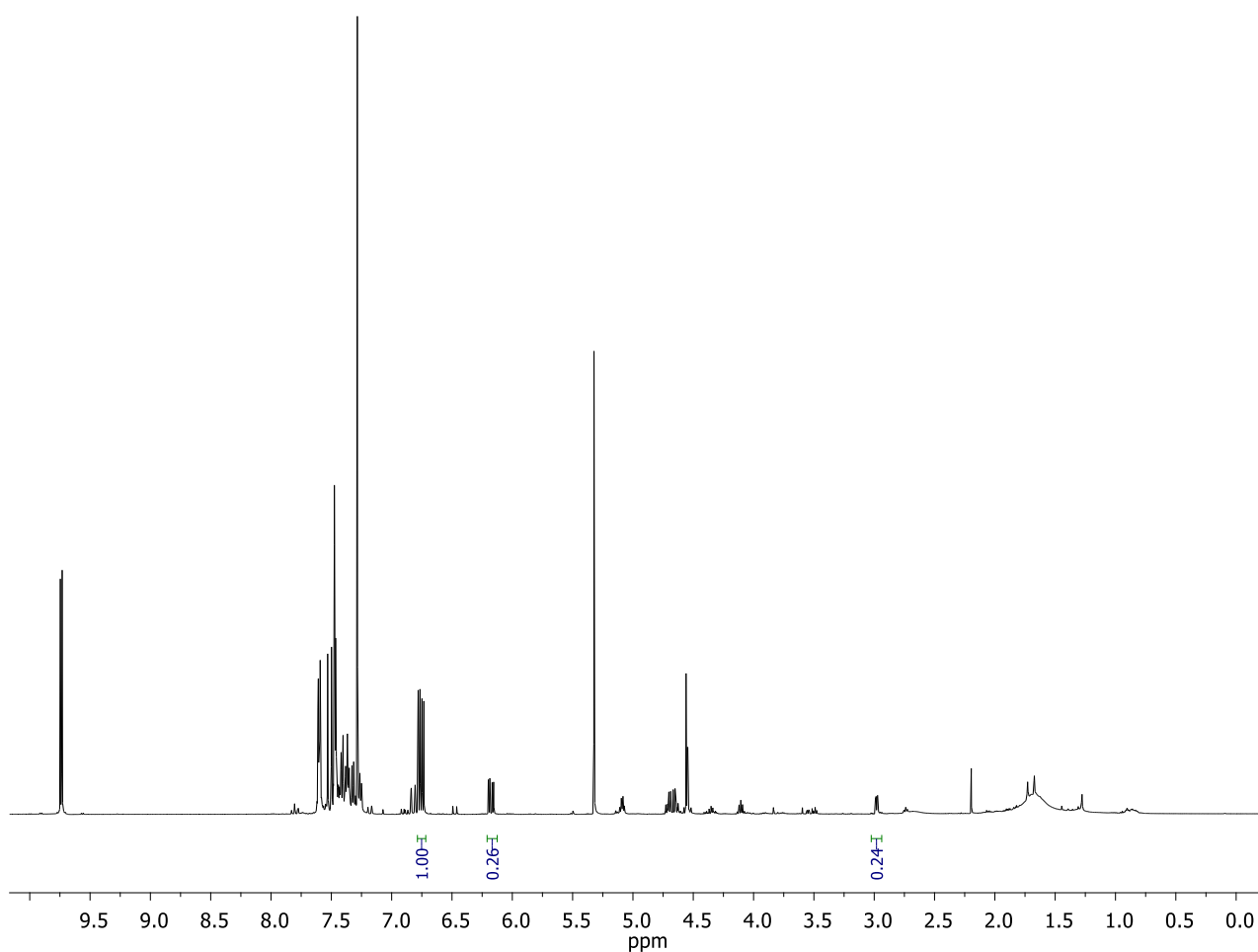
### 6.2.8.1 Buffer screening for 1,4-Michael addition in $\text{KPi}$ pH 7.0 (20% MeOH) using Y111S:74



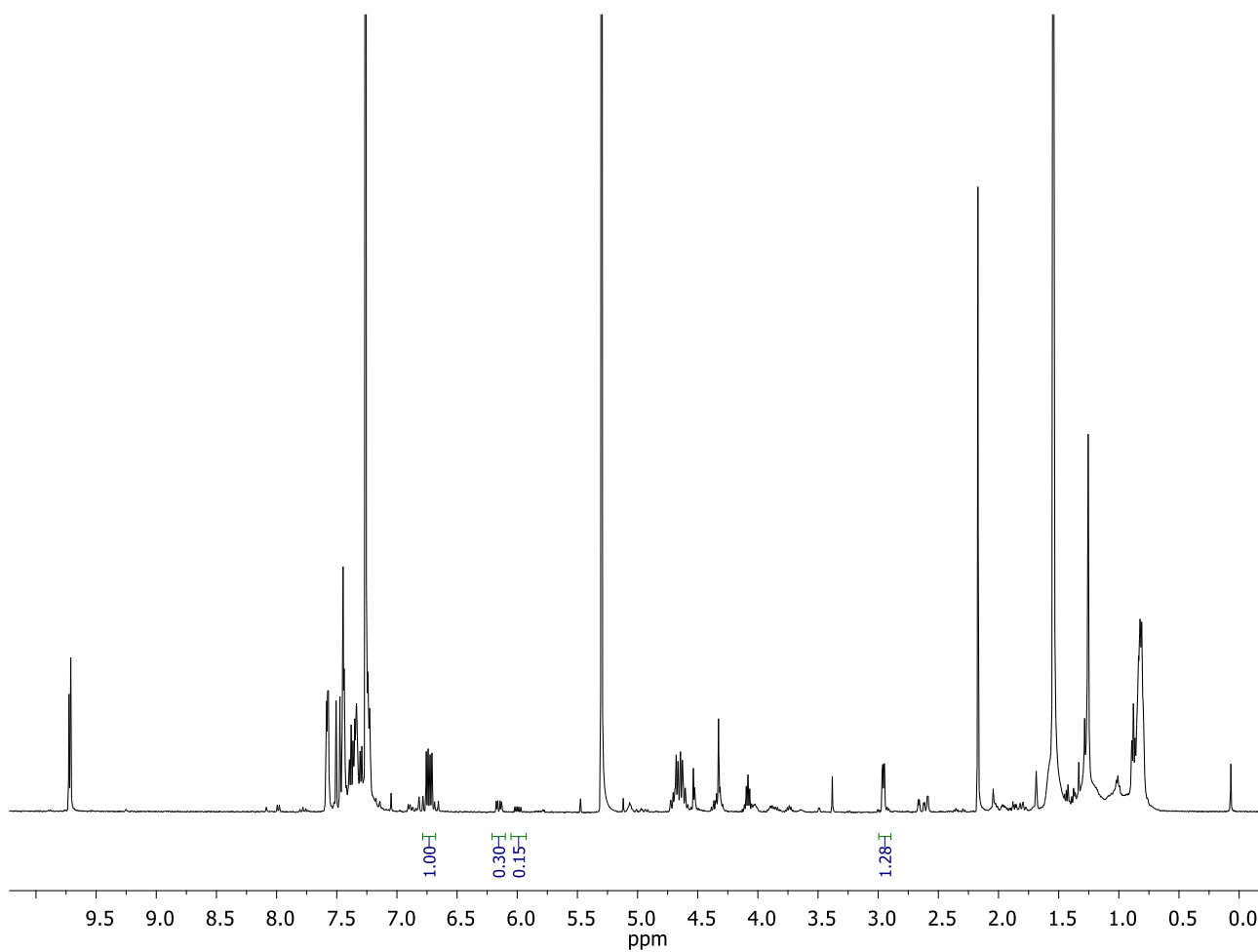
Compound	Integration	% Conversion
<b>14</b> (Starting material)	1.00	62
<b>83</b> (Side-product)	0.26	16
Unknown side-product	0.05	2
<b>75</b> (Product)	0.63	20

**6.2.8.2 Buffer screening for 1,4-Michael addition in KPi pH 7.0 (20% MeOH) using Y111T:74**

Compound	Integration	% Conversion
<b>14</b> (Starting material)	1.00	64
<b>83</b> (Side-product)	0.25	20
Unknown side-product	0.06	3
<b>75</b> (Product)	0.30	13

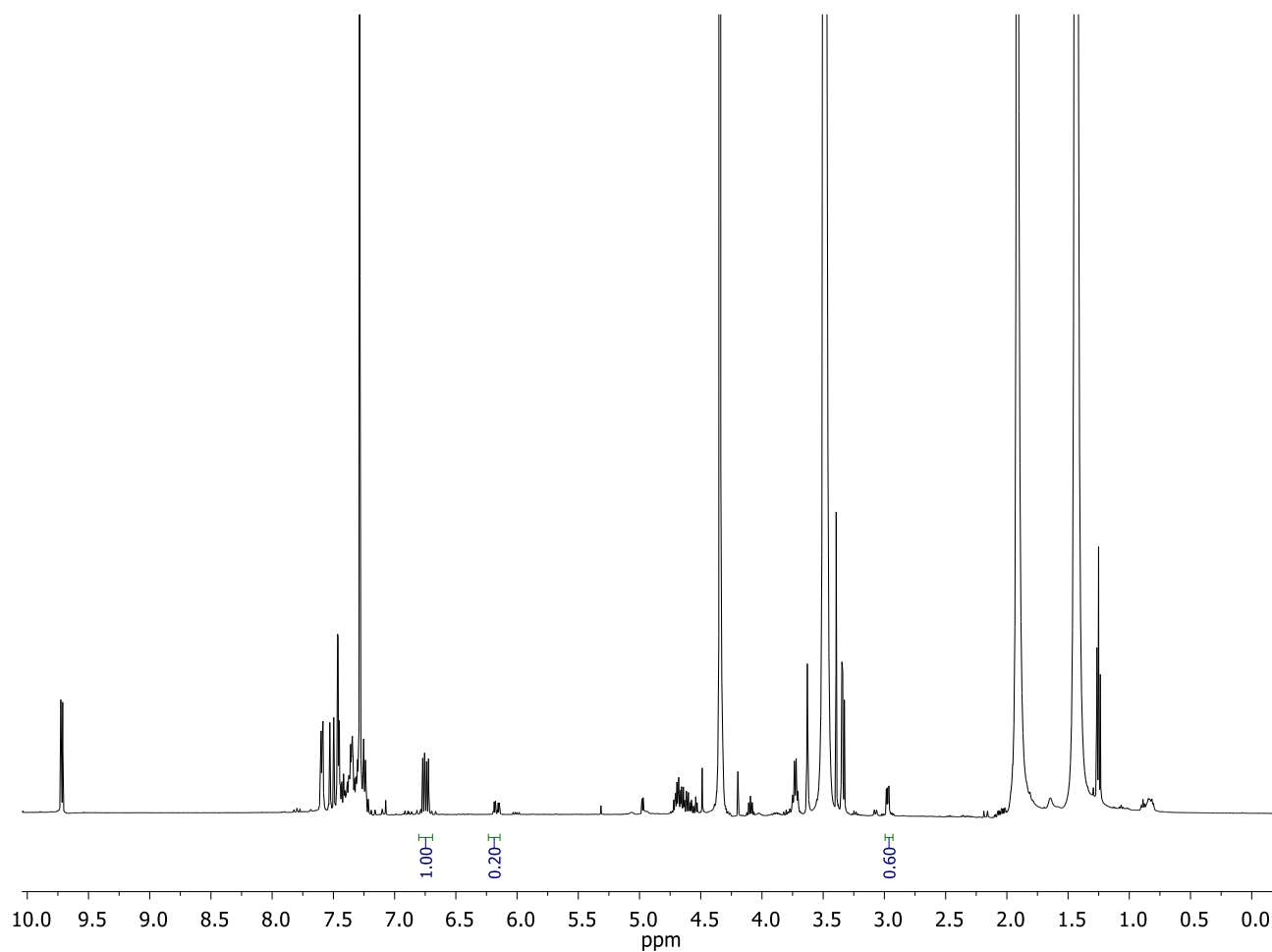
**6.2.8.3 Buffer screening for 1,4-Michael addition in KPi pH 7.0 (20% MeOH) using Y111V:74**

Compound	Integration	% Conversion
<b>14</b> (Starting material)	1.00	72
<b>83</b> (Side-product)	0.26	18
Unknown side-product	/	/
<b>75</b> (Product)	0.24	10

**6.2.8.4 Buffer screening for 1,4-Michael addition in KPi pH 7.0 (20% MeOH) using Y111K:74**

Compound	Integration	% Conversion
<b>14</b> (Starting material)	1.00	42
<b>83</b> (Side-product)	0.30	15
Unknown side-product	0.15	12
<b>75</b> (Product)	1.28	31



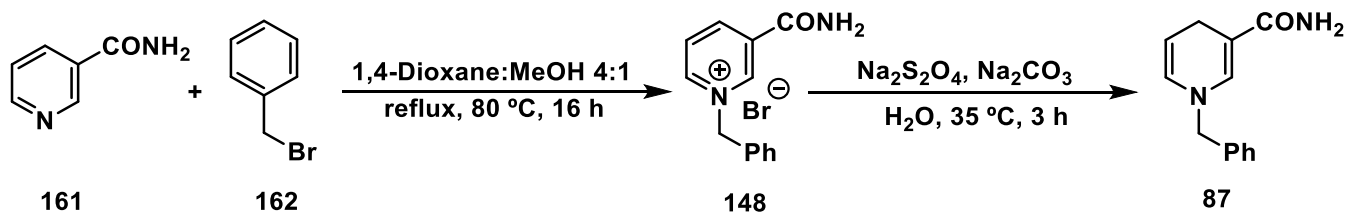
**6.2.8.5 Buffer screening for 1,4-Michael addition in KPi pH 7.0 (20% MeOH) using Y111A:74**

Compound	Integration	% Conversion
<b>14</b> (Starting material)	1.00	67
<b>83</b> (Side-product)	0.20	13
Unknown side-product	/	/
<b>75</b> (Product)	0.60	20

## 6.3 Tetrameric streptavidin as host for iminium catalysis

### 6.3.1 Synthesis of BNAH

The synthesis of BNAH (**87**) was carried out in a two-step synthetic pathway.<sup>258, 297</sup>



#### 6.3.1.1 Synthesis of *N*-benzyl-3-carbamoylpyridinium bromide (**148**, BNA<sup>+</sup>)

Nicotinamide (**161**, 4.8 g, 1 eq., 40 mmol) was dissolved in 100 mL of 1,4-dioxane-methanol (4:1), and benzyl bromide (**162**, 4.75 mL, 1 eq., 40 mmol) was added. The reaction mixture was refluxed at 80 °C for 16 h, after which time a precipitate was observed. This solution was cooled and 1,4-dioxane (50 mL) was added to further precipitate the final product. After filtration, the precipitate was washed with 1,4-dioxane (3x50 mL) and *N*-benzyl-3-carbamoylpyridinium bromide was obtained (**148**, 6.35 g, 74.48% yield).

<sup>1</sup>H-NMR (500 MHz, D<sub>2</sub>O), δ: 9.39 (s, 1H), 9.10 (d, *J* = 6.25 Hz, 1H), 8.94 (d, *J* = 8 Hz, 1H), 8.22 (t, *J* = 6 Hz, 1H), 7.55 (m, 5H), 5.94 (s, 2H) ppm. The analytical data is in accordance with literature.<sup>298, 299</sup>

#### 6.3.1.2 Synthesis of *N*-benzyl-1,4-dihydropyridin-3(1H)-carboxamide (**87**, BNAH)

Under nitrogen atmosphere, the bromide salt of 1-benzyl-3-carbamoylpyridinium bromide (**148**, 1.06 g, 5.00 mmol) was dissolved in distilled water (100 mL) and sodium hydrogen carbonate (2.10 g, 5 eq., 25.00 mmol) was added. Sodium dithionite (4.35 g, 5 eq., 25.00 mmol) was then added portion-wise and the reaction mixture was stirred at room temperature for 3 h in the dark. During this time, the solution turned from orange to yellow and a yellow product precipitated. The solid was filtered, washed with cold distilled water (3x50 mL) and dried over phosphorus pentoxide under vacuum to afford a bright to allow solid (**87**, 1.00 g, 93.43% yield).

$^1\text{H-NMR}$  (400 MHz,  $\text{CDCl}_3$ ),  $\delta$ : 7.35-7.30 (m, 5H), 7.16 (d,  $J= 1.6$  Hz, 1H), 5.74 (dq,  $J= 8, 3.5$  Hz, 1H), 5.11 (s br, 2 H), 4.75 (dt,  $J= 8, 3.5$  Hz, 1H), 4.29 (s, 2H), 3.18 (dd,  $J= 3.3, 1.6$  Hz, 2H) ppm. The analytical data is in accordance with literature.<sup>298, 299</sup>

### 6.3.2 Synthesis of *d*2-BNAH

The synthesis of *d*2-BNAH (**87**) was carried out in a two-step synthetic pathway repeated for 5 times (reported here and in chapter 3, **Scheme 24**).<sup>297</sup> In each cycle (step I+II) the hydrogens in position 4 in the nicotinamide ring of compound **146** were isotopically enriched in the following way:

Starting point: 100% H (Compound **148**)

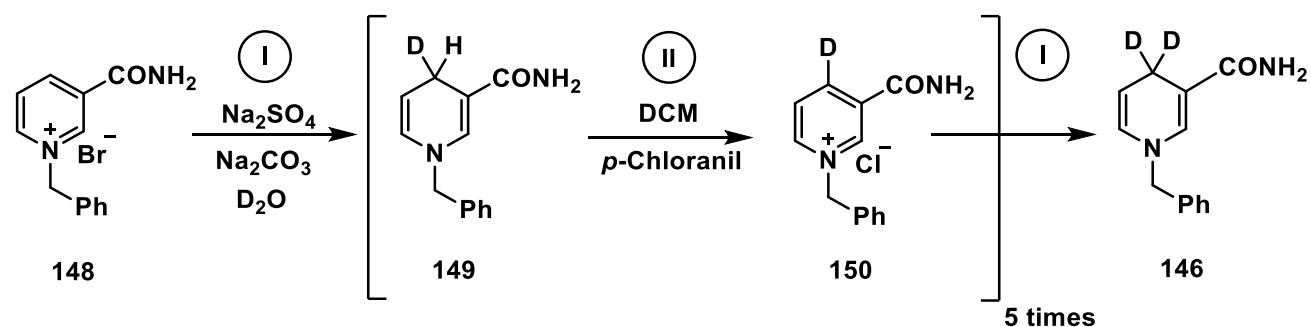
1<sup>st</sup> cycle: 50% D, 50% H

2<sup>nd</sup> cycle: 75% D, 25% H

3<sup>rd</sup> cycle: 87.5% D, 12.5% H

4<sup>th</sup> cycle: 93.75% D, 6.75% H

5<sup>th</sup> cycle: 96.88% D, 3.12% H



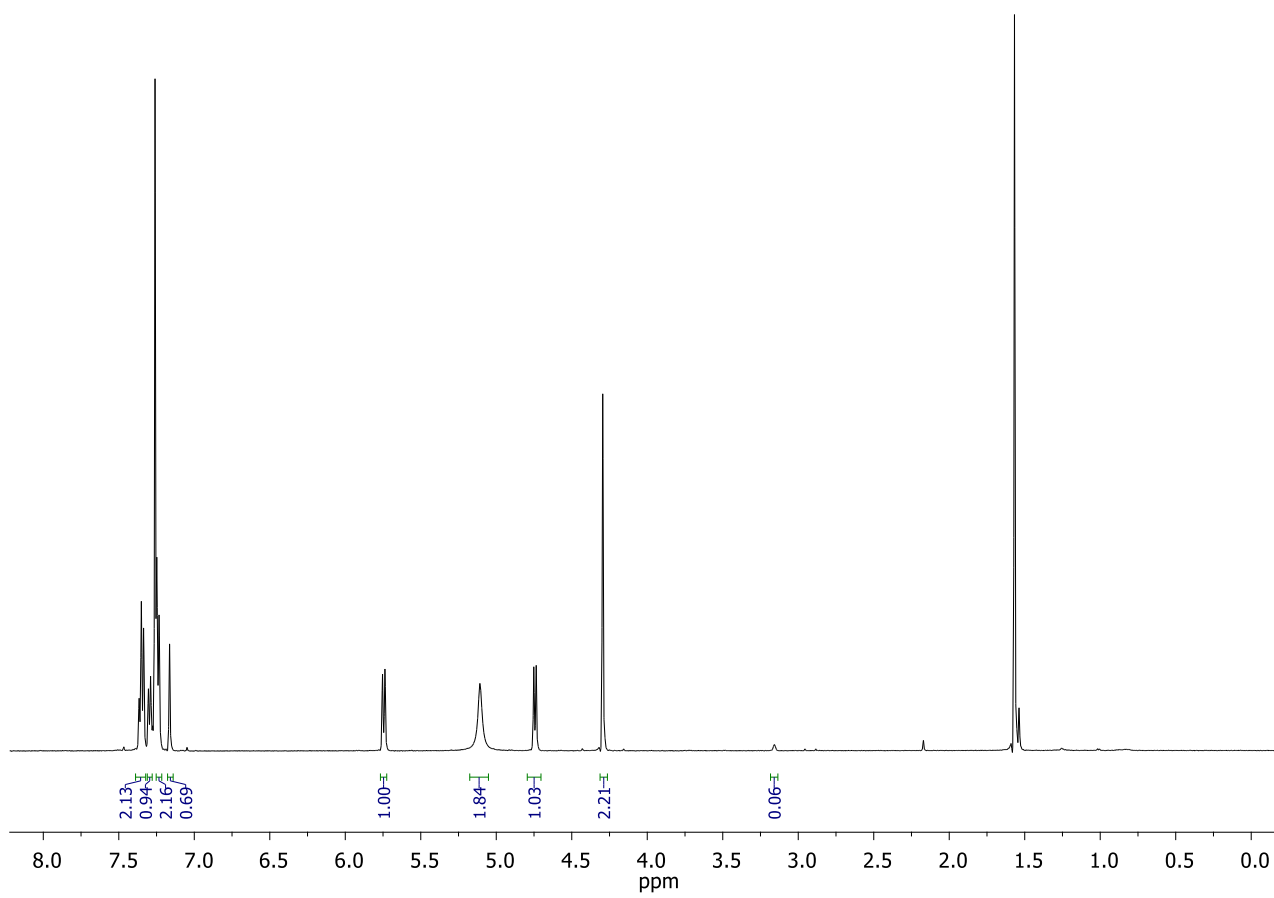
#### 6.3.2.1 Synthesis of 1-benzyl-1,4-dihydropyridine-4,4-*d*2-3-carboxamide (**146**, *d*2-BNAH)

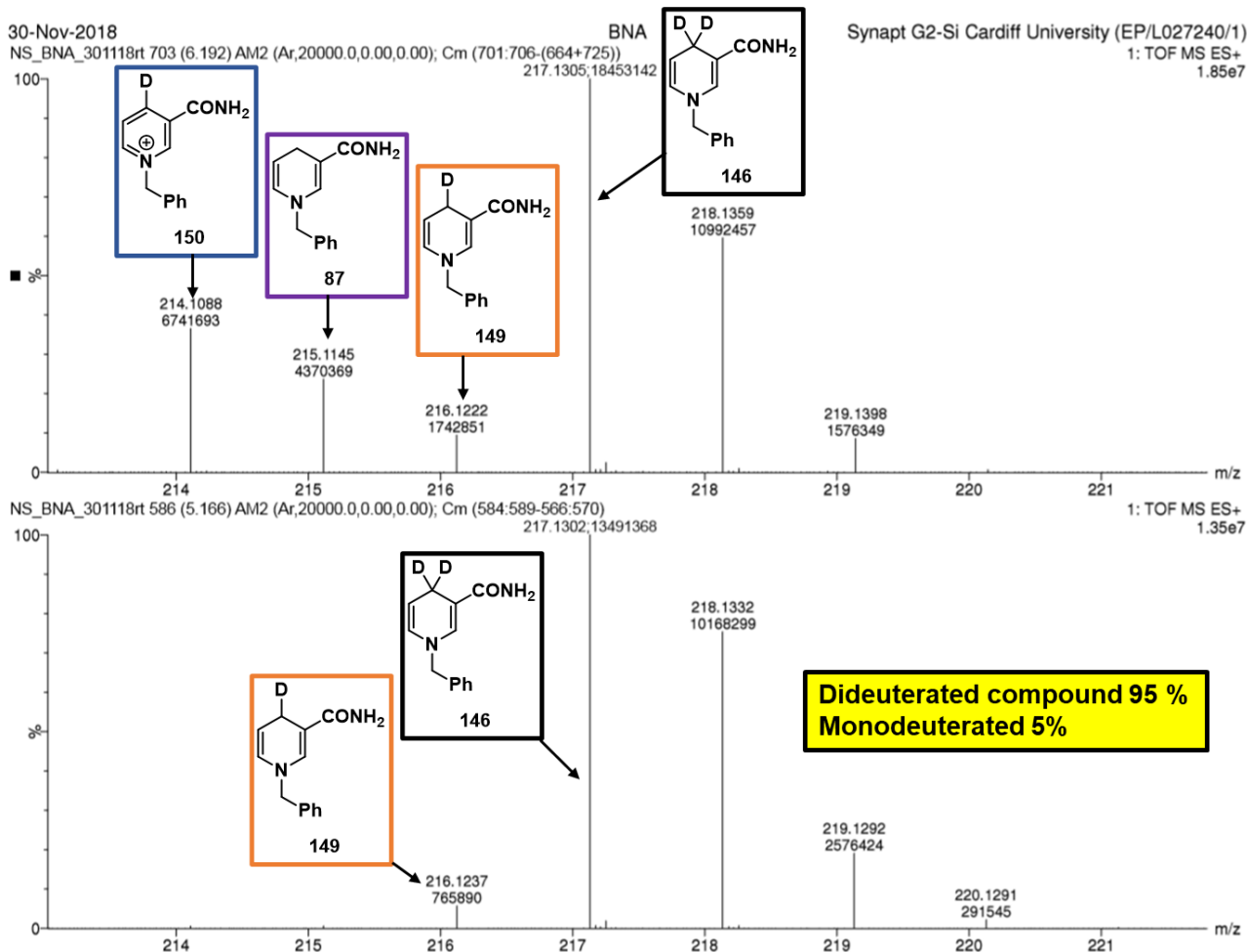
*N*-benzyl-3-carbamoylpyridinium bromide (**148**, 1.1 g, 4.4 mmol) was dissolved in 20 mL of deuterium oxide to which sodium carbonate (1.4 g, 13 mmol) was added. Sodium dithionite (2.58 g, 14.8 mmol) was added in small portions over time and the reaction was heated to 45 °C. After 15 min of stirring at 45 °C the reaction mixture was left to cool at room temperature,

and the yellow precipitate was filtered, washed with cold distilled water and dried over phosphorus pentoxide to afford a bright yellow solid powder (**149**, 920 mg, 88% yield).

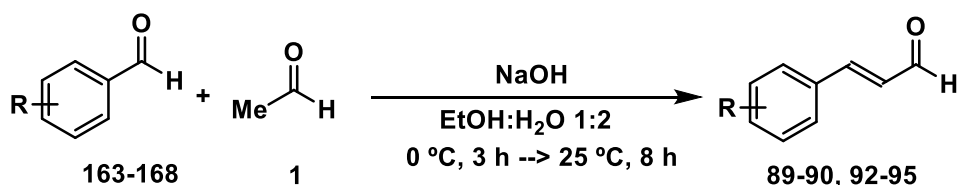
The obtained compound **149** (920 mg, 4.2 mmol) was dissolved in 10 mL dichloromethane to which a solution of chloranil (1.1 g, 4.4 mmol) in DCM (20 mL) was slowly added at 0 °C while stirring. 1 M HCl (100 mL) was then added. The aqueous phase was washed three times with ethyl acetate and evaporated under vacuum. The solid obtained was recrystallised from absolute ethanol to afford an off white solid product (**150**, 900 g, 84% yield). The oxidised product was reduced following the same procedure as above. A total of five reductions and four oxidations were performed to finally obtain compound **146**, which was recrystallised from absolute ethanol and distilled water (1:4) afford a bright yellow solid powder (400 mg, 42% overall yield).

**<sup>1</sup>H-NMR (500 MHz, CDCl<sub>3</sub>)**,  $\delta$ : 7.35-7.30 (m, 5H), 7.16 (d,  $J$ = 1.6 Hz, 1H), 5.74 (dq,  $J$ = 8, 3.5 Hz, 1H), 5.11 (s br, 2 H), 4.75 (dt,  $J$ = 8, 3.5 Hz, 1H), 4.29 (s, 2H) ppm. The analytical data is in accordance with literature.<sup>297</sup> The <sup>1</sup>H-NMR spectrum confirmed **146** was 97.5% deuterated at C-4. However, the isotopic label was confirmed by HRMS, which showed a 95% of deuteration at C-4 (see section 6.3.2.3).

6.3.2.2  $^1\text{H}$ -NMR spectrum of  $d_2$ -BNAH

6.3.2.3 HRMS of *d*<sup>2</sup>-BNAH6.3.3 Synthesis of the  $\alpha,\beta$ -unsaturated aldehydes **89-90** and **92-95**

The aromatic  $\alpha,\beta$ -unsaturated aldehydes **89-90** and **92-95** were synthesised using a general procedure based on a one-step aldol condensation.



To a solution of sodium hydroxide (416 mg, 0.62 eq., 10.4 mmol) in a mixture of ethanol (6 mL) and distilled water (12 mL) was added the aldehyde (**163-168**, 2 g, 1 eq.). The mixture was stirred at 0 °C for 10 min. Then 40% acetaldehyde (**1**, 1.8 mL, 2 eq., 33.2 mmol) was added dropwise to the mixture over 3 h at the same temperature. Stirring was continued for

8 h at room temperature. The resulting solution was extracted with diethyl ether (3x20 mL), then the combined organic layer was washed with water (30 mL) and brine (30 mL) and dried over MgSO<sub>4</sub>. The solution was concentrated under vacuum and purified by flash chromatography on silica gel (EtOPet: EtOAc 100:0 → 90:10) to afford a yellow oil (2.16 g, 89.5% yield).

#### 6.3.3.1 <sup>1</sup>H-NMR assignment for (*E*)-3-(*o*-fluoro) acrylaldehyde (89)

<sup>1</sup>H-NMR (500 MHz, CDCl<sub>3</sub>), δ: 9.74 (d, *J* = 7.8 Hz, 1H), 7.67 (d, *J* = 16 Hz, 1H), 7.61 (td, *J* = 7.5, 1.8 Hz, 1H), 7.45 (m, 1H), 7.23 (td, *J* = 7.3, 1.5 Hz, 1H), 7.16 (m, 1H), 6.81 (dd, *J* = 15.8, 9 Hz, 1H) ppm. The analytical data is in accordance with literature.<sup>300</sup>

#### 6.3.3.2 <sup>1</sup>H-NMR assignment for (*E*)-3-(*o*-bromo) acrylaldehyde (90)

<sup>1</sup>H-NMR (500 MHz, CDCl<sub>3</sub>), δ: 9.70 (d, *J* = 7.7 Hz, 1H), 7.83 (d, *J* = 15.8 Hz, 1H), 7.59 (dt, *J* = 8.3, 2.3 Hz, 2H), 7.30 (t, *J* = 7.5 Hz, 1H), 7.21 (m, 1H), 6.60 (dd, *J* = 15.8, 9 Hz, 1H) ppm. The analytical data is in accordance with literature.<sup>301, 302</sup>

#### 6.3.3.3 <sup>1</sup>H-NMR assignment for (*E*)-3-(*o*-tolyl) acrylaldehyde (92)

<sup>1</sup>H-NMR (500 MHz, CDCl<sub>3</sub>), δ: 9.73 (d, *J* = 7.5 Hz, 1H), 7.78 (d, *J* = 16.5 Hz, 1H), 7.59 (d, *J* = 7.8 Hz, 1H), 7.37-7.22 (m, 3H), 6.67 (dd, *J* = 16.5, 8 Hz, 1H), 2.48 (s, 3H) ppm. The analytical data is in accordance with literature.<sup>301</sup>

#### 6.3.3.4 <sup>1</sup>H-NMR assignment for (*E*)-3-(*m*-fluoro) acrylaldehyde (93)

<sup>1</sup>H-NMR (500 MHz, CDCl<sub>3</sub>), δ: 9.72 (d, *J* = 7.4 Hz, 1H), 7.46-7.23 (m, 4H), 7.15 (t, *J* = 9.2 Hz, 1H), 6.70 (dd, *J* = 15.8, 9 Hz, 1H) ppm. The analytical data is in accordance with literature.<sup>303</sup>

#### 6.3.3.5 <sup>1</sup>H-NMR assignment for (*E*)-3-(*m*-bromo) acrylaldehyde (94)

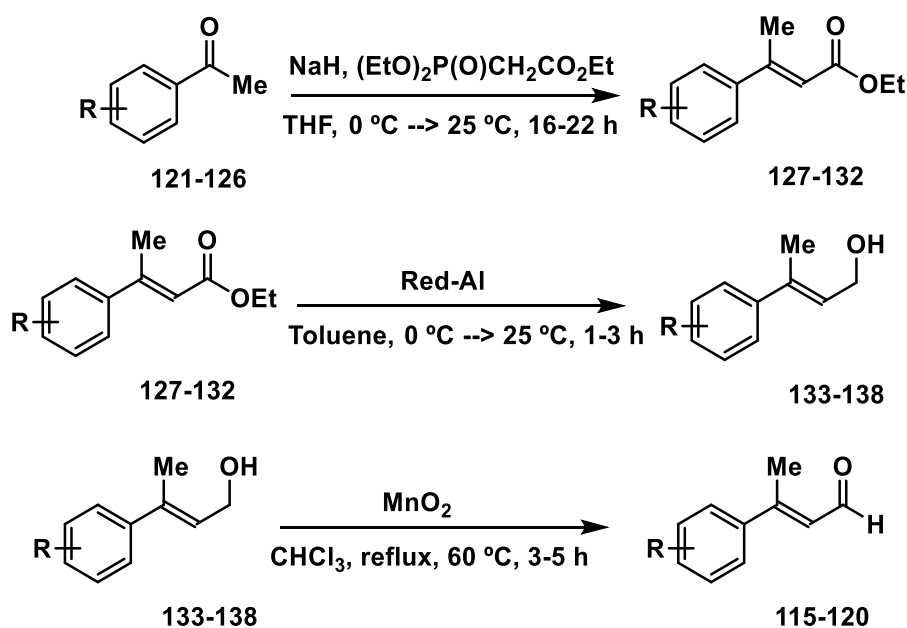
<sup>1</sup>H-NMR (500 MHz, CDCl<sub>3</sub>), δ: 9.73 (d, *J* = 7.7 Hz, 1H), 7.72 (t, *J* = 1.9 Hz, 1H), 7.58 (dt, *J* = 8.3, 1.5 Hz, 1H), 7.51 (dt, 7.8, 1.5 Hz, 1H), 7.42 (d, *J* = 16 Hz, 1H), 7.33 (t, *J* = 8.5 Hz, 1H), 6.72 (dd, *J* = 15.8, 9 Hz, 1H) ppm. The analytical data is in accordance with literature.<sup>304</sup>

### 6.3.3.6 $^1\text{H-NMR}$ assignment for (*E*)-3-(*m*-tolyl) acrylaldehyde (**95**)

$^1\text{H-NMR}$  (500 MHz,  $\text{CDCl}_3$ ),  $\delta$ : 9.60 (d,  $J = 7.9$  Hz, 1H), 7.35 (d,  $J = 16$  Hz, 1H), 7.28 (m, 2H), 7.23 (t,  $J = 7.8$  Hz, 1H), 7.16 (m, 1H), 6.62 (dd,  $J = 16.5, 8$  Hz, 1H), 2.30 (s, 3H) ppm.<sup>300</sup>

### 6.3.4 Synthesis of the $\beta$ -branched $\alpha,\beta$ -unsaturated aldehydes **115-120**

The aromatic  $\alpha,\beta$ -unsaturated aldehydes bearing a methyl group in  $\beta$ -position (compounds **115-120**) were prepared by adapting a three-steps pathway previously reported (reported here and in chapter 3, **Scheme 21**).<sup>200, 259</sup>



#### 6.3.4.1 Synthesis of compounds **127-132**

To a suspension of sodium hydride ( $\text{NaH}$ , 1 g, 60% dispersion in mineral oil, 25 mmol, 1.25 eq.) in anhydrous THF (50 mL) was added dropwise triethyl phosphonoacetate (5 mL, 5.6 g, 25 mmol, 1.25 equiv) over 15 min at  $0\text{ }^\circ\text{C}$ . After 30 min, acetophenone or its derivatives (**121-126**, 2.36 mL, 2.4 g, 20.0 mmol, 1 equiv) was added to the reaction mixture, which was then allowed to warm to room temperature. The reaction was allowed to run overnight and its completion was confirmed by TLC control. The reaction mixture was cooled to  $0\text{ }^\circ\text{C}$ , quenched by the addition of sat. aq. Ammonium chloride ( $\text{NH}_4\text{Cl}$ , 50 mL) and extracted with diethyl ether (3x50 mL). The combined organic phases were washed with brine (2x50 mL), dried over  $\text{MgSO}_4$ , filtered and concentrated under vacuum. The crude product was purified



by flash column chromatography (hexane: EtOAc = 30:1 → 20:1 or 20:1 → 10:1) to yield compounds **127-132** (yield between 80-85%) as a colorless/yellow oils.

#### 6.3.4.2 <sup>1</sup>H-NMR assignment for ethyl (*E*)-3-phenylbut-2-enoate (**127**)

<sup>1</sup>H-NMR (500 MHz, CDCl<sub>3</sub>), δ: 7.60-7.40 (m, 5H), 6.15 (s, 1H), 4.25 (q, *J* = 7.1 Hz, 2H), 2.60 (s, 3H), 1.35 (t, *J* = 7.1 Hz, 3H). The analytical data is in accordance with literature.<sup>305</sup>

#### 6.3.4.3 <sup>1</sup>H-NMR assignment for ethyl (*E*)-3-(*p*-chlorophenyl) but-2-enoate (**128**)

<sup>1</sup>H-NMR (500 MHz, CDCl<sub>3</sub>), δ: 7.46-7.30 (m, 4H), 6.10 (s, 1H), 4.27 (q, *J* = 7.1 Hz, 2H), 2.55 (s, 3H), 1.30 (t, *J* = 7.1 Hz, 3H). The analytical data is in accordance with literature.<sup>306</sup>

#### 6.3.4.4 <sup>1</sup>H-NMR assignment for ethyl (*E*)-3-(*p*-fluorophenyl) but-2-enoate (**129**)

<sup>1</sup>H-NMR (500 MHz, CDCl<sub>3</sub>), δ: 8.22 (d, *J* = 8.5 Hz, 2H), 7.61 (d, *J* = 8.5 Hz, 2H), 6.18 (s, 1H), 4.23 (q, *J* = 7.1 Hz, 2H), 2.58 (s, 3H), 1.30 (t, *J* = 7.1 Hz, 3H). The analytical data is in accordance with literature.<sup>307</sup>

#### 6.3.4.5 <sup>1</sup>H-NMR assignment for ethyl (*E*)-3-(*o*-tolyl) but-2-enoate (**130**)

<sup>1</sup>H-NMR (500 MHz, CDCl<sub>3</sub>), δ: 7.25-7.10 (m, 4H), 6.15 (s, 1H), 4.21 (q, *J* = 7.1 Hz, 2H), 2.55 (s, 3H), 2.41 (s, 3H), 1.31 (t, *J* = 7.1 Hz, 3H). The analytical data is in accordance with literature.<sup>308</sup>

#### 6.3.4.6 <sup>1</sup>H-NMR assignment for ethyl (*E*)-3-(*m*-tolyl) but-2-enoate (**131**)

<sup>1</sup>H-NMR (500 MHz, CDCl<sub>3</sub>), δ: 7.31-7.14 (m, 4H), 6.11 (s, 1H), 4.23 (q, *J* = 7.1 Hz, 2H), 2.57 (s, 3H), 2.37 (s, 3H), 1.32 (t, *J* = 7.1 Hz, 3H). The analytical data is in accordance with literature.<sup>308</sup>

#### 6.3.4.7 <sup>1</sup>H-NMR assignment for ethyl (*E*)-3-(*p*-tolyl) but-2-enoate (**132**)

<sup>1</sup>H-NMR (500 MHz, CDCl<sub>3</sub>), δ: 7.40-7.17 (m, 4H), 6.14 (s, 1H), 4.22 (q, *J* = 7.1 Hz, 2H), 2.56 (s, 3H), 2.38 (s, 3H), 1.32 (t, *J* = 7.1 Hz, 3H). The analytical data is in accordance with literature.<sup>306</sup>

#### 6.3.4.8 Synthesis of compounds 133-138

To a stirred solution of aldehydes **127-132** (2.3 g, 12.1 mmol, 1.00 equiv) in anhydrous toluene (15 mL) at 0 °C was added dropwise Red-Al (60 wt% solution in toluene, 4.5 mL, 4.7 g, 14 mmol, 1.2 equiv). The mixture was stirred for 15 min at 0 °C and then allowed to warm to room temperature. The completion of the reaction was confirmed by TLC after 2-4 h. The reaction mixture was cooled to 0 °C, diluted with diethyl ether (50 mL), quenched by the addition of 1 M HCl (50 mL) and extracted with diethyl ether (3x50 mL). The combined organic phases were washed with brine (2x50 mL), dried over MgSO<sub>4</sub>, filtered and concentrated under vacuum. The crude products **133-138** were not subject to further purifications and used directly for the next step.

#### 6.3.4.9 Synthesis of compounds 115-120

To a stirred solution of crude products **133-138** (981 mg, 4.3 mmol, 1.00 equiv) in chloroform (20 mL) was added manganese dioxide (MnO<sub>2</sub>, 1.88 g, 21.5 mmol, 5.00 equiv) in one portion. The mixture was warmed to 60 °C. After 3 h, the completion of the reaction was confirmed by TLC. After cooling to room temperature, the mixture was filtered through a pad of celite using diethyl ether to wash away impurities. The filtrate was concentrated under vacuum. The crude product was purified by flash column chromatography (hexane: EtOAc = 10:1 → 5:1 or 5:1 → 3:1) to yield compound **115-120** (yields between 60-40 %) as oils.

#### 6.3.4.10 <sup>1</sup>H-NMR assignment for (*E*)-3-phenylbut-2-enal (**115**)

<sup>1</sup>H-NMR (500 MHz, CDCl<sub>3</sub>), δ: 10.13 (d, *J* = 7.5 Hz, 1H), 7.49-7.19 (m, 5H), 6.34 (dd, *J* = 16.5 and 8 Hz, 1H), 2.53 (s, 3H) ppm. The analytical data is in accordance with literature.<sup>309, 310</sup>

#### 6.3.4.11 <sup>1</sup>H-NMR assignment for (*E*)-3-(*p*-chlorophenyl) but-2-enal (**116**)

<sup>1</sup>H-NMR (500 MHz, CDCl<sub>3</sub>), δ: 10.17 (d, *J* = 7.8 Hz, 1H), 7.86 (d, *J* = 12 Hz, 1H), 7.44 (m, 3H), 6.36 (d, *J* = 7.8 Hz, 1H), 2.55 (s, 3H) ppm. The analytical data is in accordance with literature.<sup>309</sup>

### 6.3.4.12 <sup>1</sup>H-NMR assignment for (*E*)-3-(*p*-fluororophenyl) but-2-enal (117)

<sup>1</sup>H-NMR (500 MHz, CDCl<sub>3</sub>), δ: 10.07 (d, *J* = 7.8 Hz, 1H), 7.45 (dd, *J* = 8.9 and 1.4 Hz, 2H), 7.01 (td, *J* = 8.6 and 1.4 Hz, 2H), 6.26 (dd, *J* = 7.8 and 1.4 Hz, 1H), 2.46 (s, 3H) ppm. The analytical data is in accordance with literature.<sup>309</sup>

### 6.3.4.13 <sup>1</sup>H-NMR assignment for (*E*)-3-(*o*-tolyl) but-2-enal (118)

<sup>1</sup>H-NMR (500 MHz, CDCl<sub>3</sub>), δ: 10.17 (d, *J* = 7.8 Hz, 1H), 7.23 (dd, *J* = 8.9 and 1.4 Hz, 2H), 7.10 (td, *J* = 8.6 and 1.4 Hz, 2H), 5.95 (dd, *J* = 7.8 and 1.4 Hz, 1H), 2.47 (s, 3H), 2.31 (s, 3H) ppm. The analytical data is in accordance with literature.<sup>309</sup>

### 6.3.4.14 <sup>1</sup>H-NMR assignment for (*E*)-3-(*m*-tolyl) but-2-enal (119)

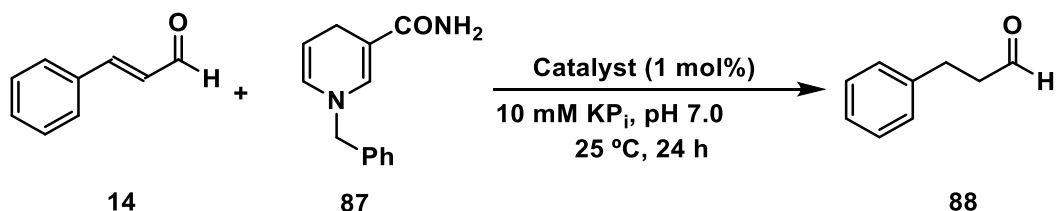
<sup>1</sup>H-NMR (500 MHz, CDCl<sub>3</sub>), δ: 10.11 (d, *J* = 7.8 Hz, 1H), 7.28-7.16 (m, 4H), 6.31 (dd, *J* = 7.8 and 1.4 Hz, 1H), 2.50 (s, 3H), 2.31 (s, 3H) ppm. The analytical data is in accordance with literature.<sup>309</sup>

### 6.3.4.15 <sup>1</sup>H-NMR assignment for (*E*)-3-(*p*-tolyl) but-2-enal (120)

<sup>1</sup>H-NMR (500 MHz, CDCl<sub>3</sub>), δ: 10.07 (d, *J* = 7.8 Hz, 1H), 7.36 (dd, *J* = 8.9 and 1.4 Hz, 2H), 7.12 (td, *J* = 8.6 and 1.4 Hz, 2H), 6.30 (dd, *J* = 7.8 and 1.4 Hz, 1H), 2.46 (s, 3H), 2.29 (s, 3H) ppm. The analytical data is in accordance with literature.<sup>309</sup>

## 6.3.5 Experimental details for the transfer hydrogenation activity screening

### 6.3.5.1 General procedure for the <sup>1</sup>H-NMR based screening for yield determination

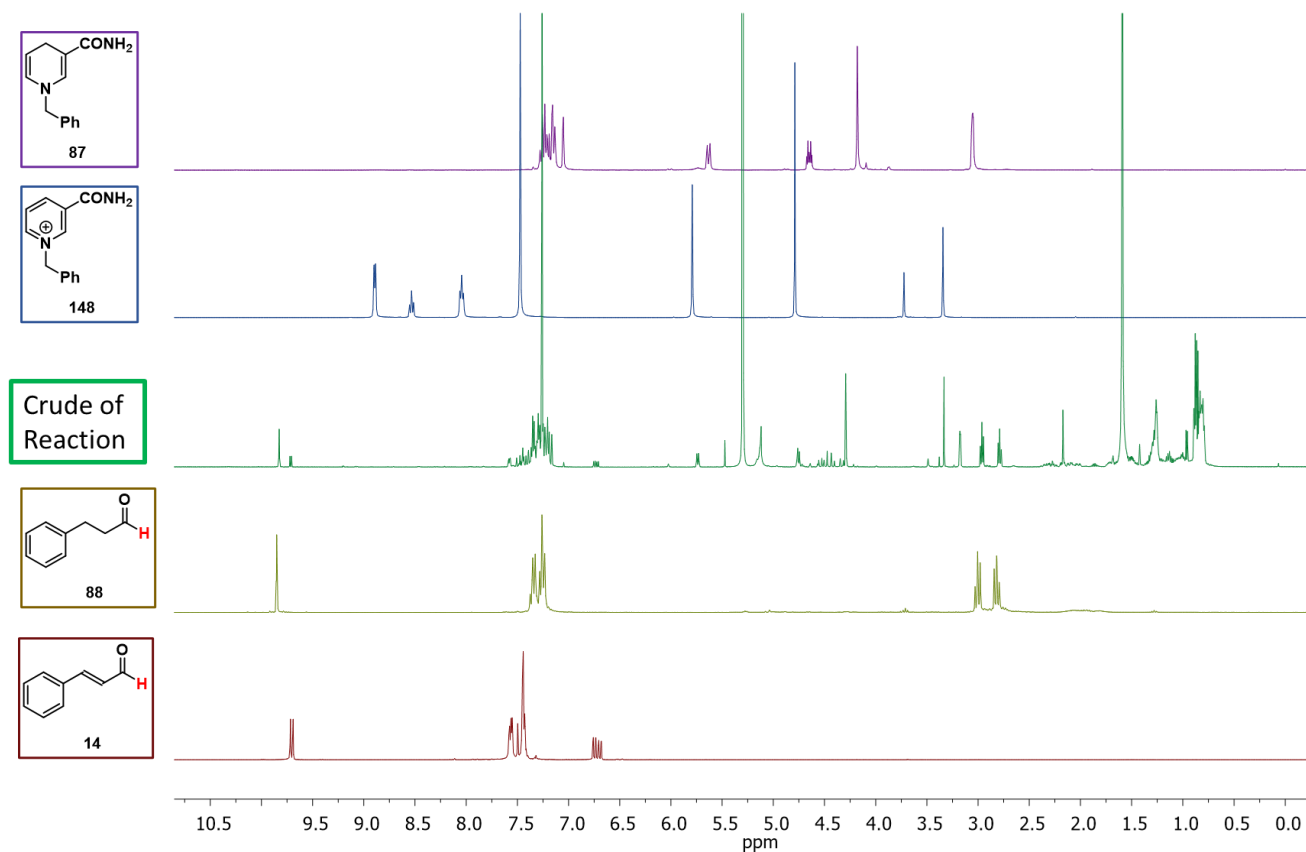


To the respective **Sav:73/74** or **M-Sav:73/74** solution (250 μL, 2.32 mg/mL, 33 nmol catalytic sites, 1.2 mol%, 10 mM KPi buffer, pH 7.0), 44.2 μL of BNAH stock solution (0.38 M in MeOH,

16.5  $\mu\text{mol}$ , 5.0 eq.), 2.5  $\mu\text{L}$  of cinnamaldehyde stock solution (1.33 M in MeOH, 3.3  $\mu\text{mol}$ , 1.0 eq.) and 78.27  $\mu\text{L}$  MeOH were added. The Eppendorf tube was placed in a Falcon tube, which was placed inside an incubating shaker (300 rpm, 25  $^{\circ}\text{C}$ ). After 24 h, DCM (500  $\mu\text{L}$ ) and water (500  $\mu\text{L}$ ) were added, and the phases were separated. The aqueous phase was extracted (2  $\times$  500  $\mu\text{L}$  DCM), and the organic phases were combined. The volatiles were removed under reduced pressure, the residue was taken up in 700  $\mu\text{L}$   $\text{CDCl}_3$ , and transferred to an NMR tube. This was directly subjected to  $^1\text{H-NMR}$  analysis (See section 3.2). Each **Sav:73/74** or **M-Sav:73/74** catalysis were run in triplicates. This procedure was also applied for the aldehydes (**89-120**) screening. For those reactions where 5 equivalents of BNAH and 25% methanol were employed, adjustment in the calculation of BNAH and Sav stock solutions were made.

#### 6.3.5.2 $^1\text{H-NMR}$ based determination of the reaction conversion

The conversion was estimated by integration of the substrate (red box, **doublet**) and the product (yellow box, **singlet**) aldehydic peaks (region between 9-10 ppm) (**Fig. 35**). Formation of the product was also confirmed by the presence of the  $\text{H}_\alpha$  and  $\text{H}_\beta$  peaks (yellow box, region between 2.5-3.5 ppm). Exemplary of the crude of reaction for the reduction of cinnamaldehyde (**14**) to hydrocinnamaldehyde (**88**) in presence of BNAH (**87**) is shown in the green spectrum. The same methodology was applied to calculate the estimated conversion for all the other substrates (**89-120**).

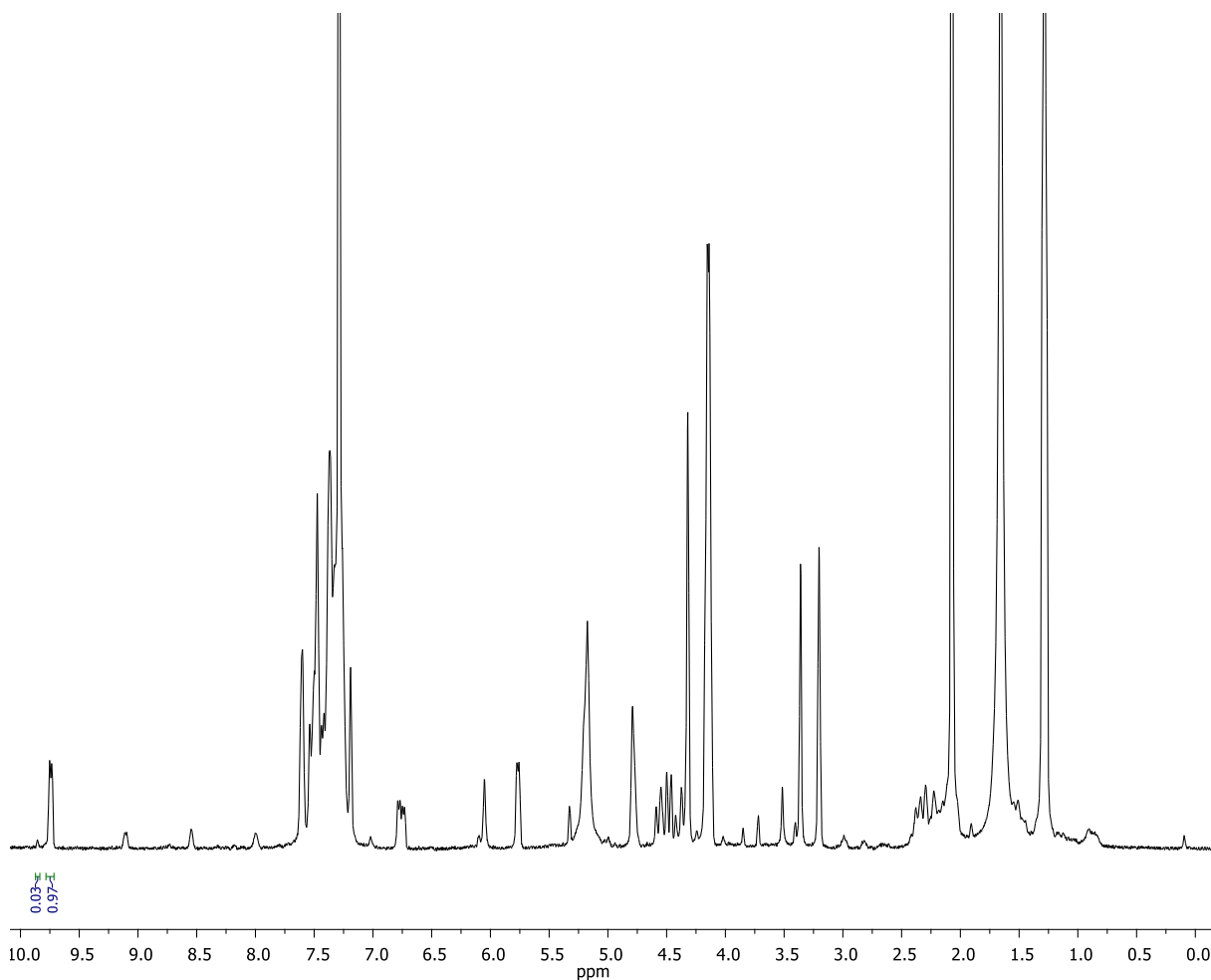


**Figure 35.** <sup>1</sup>H-NMR spectrum of Sav catalysed transfer hydrogenation. In each row are reported the spectrum of the pure compounds **87**, **148**, **88** and **14**. In the middle is reported an exemplary of crude of reaction

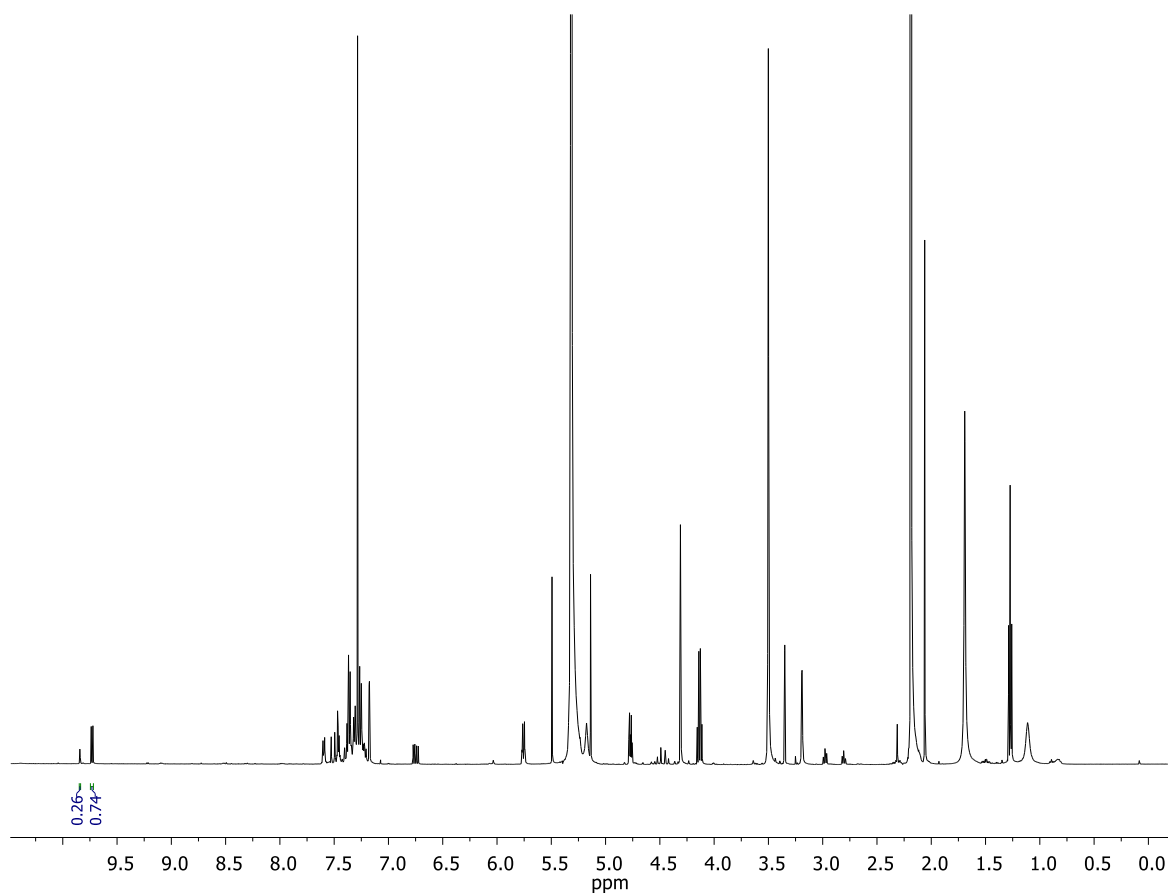
### 6.3.6 <sup>1</sup>H-NMR details for the activity screening of Table 6

The estimated conversion of cinnamaldehyde (**14**) into hydrocinnamaldehyde (**88**) is calculated after integration of the product peak at 9.85 ppm with the substrate peak at 9.72 ppm. The spectroscopic data of **88** are the following: <sup>1</sup>H-NMR (500 MHz, CDCl<sub>3</sub>), δ: 9.85 (t, *J* = 1.4 Hz, 1 H), 7.40-7.20 (m, 5H), 3.00 (t, *J* = 7.5 Hz, 2 H), 2.82 (t, *J* = 7.5 Hz, 2 H) ppm. These data matched those reported in the literature.<sup>311</sup> Traces of the oxidised version of BNAH (BNA<sup>+</sup>, **148**) can be observed and confirmed by stacking the spectra of BNA<sup>+</sup> and of the crude of reaction.

#### 6.3.6.1 Catalyst screening for transfer hydrogenation using no catalyst

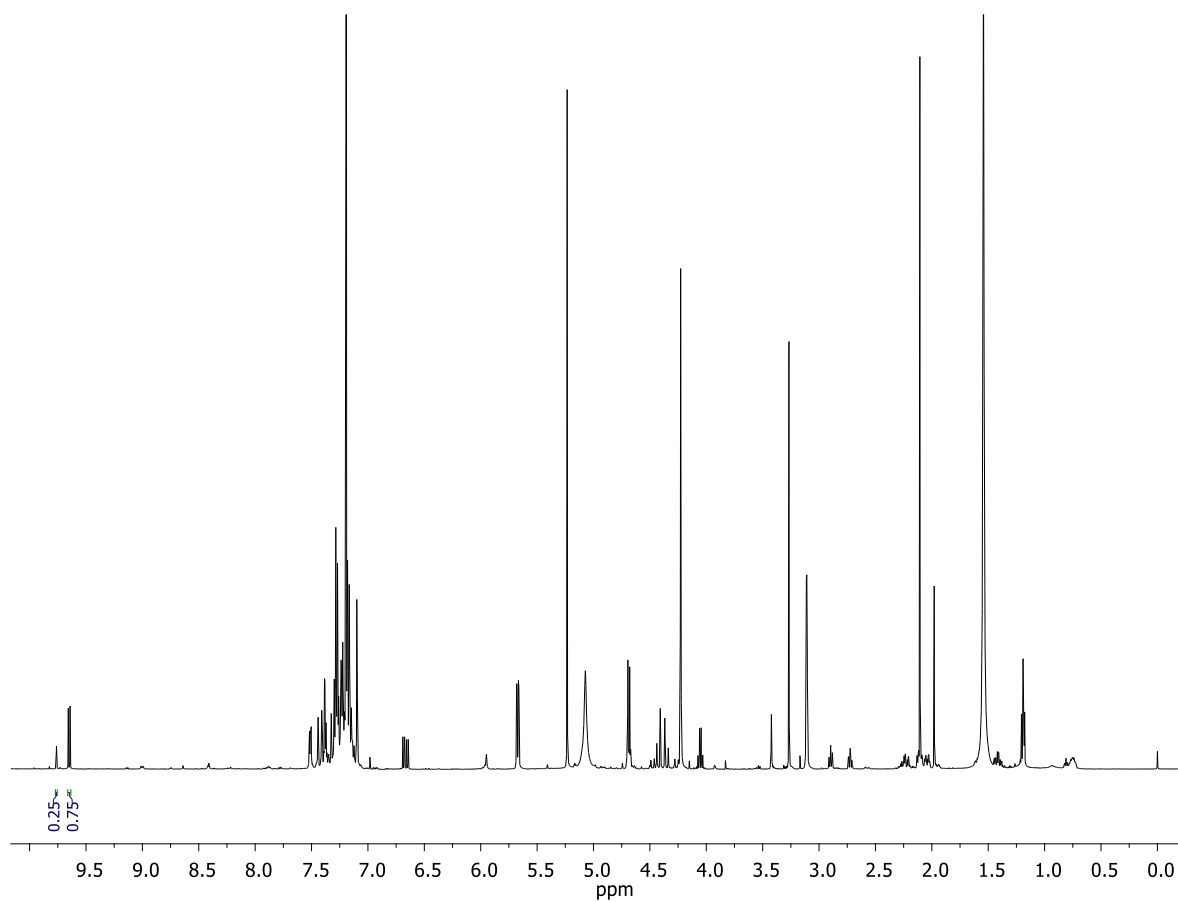


Compound	Integration	% Conversion
<b>14</b> (Starting material)	0.97	97
<b>88</b> (Product)	0.03	3

**6.3.6.2 Catalyst screening for transfer hydrogenation using catalyst 73**

Compound	Integration	% Conversion
<b>14</b> (Starting material)	0.74	74
<b>88</b> (Product)	0.26	26

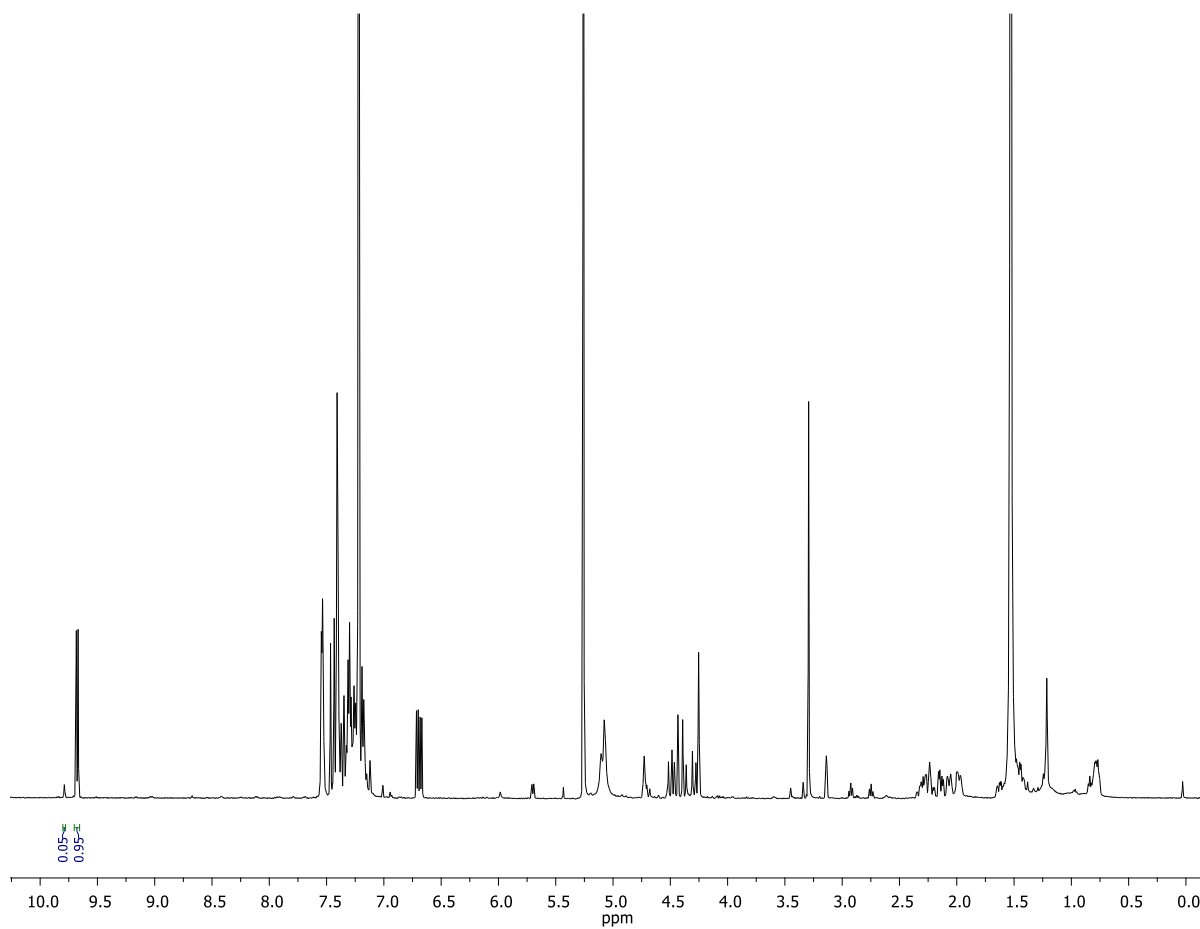
## 6.3.6.3 Catalyst screening for transfer hydrogenation using catalyst 74



Compound	Integration	% Conversion
<b>14</b> (Starting material)	0.75	75
<b>88</b> (Product)	0.25	25

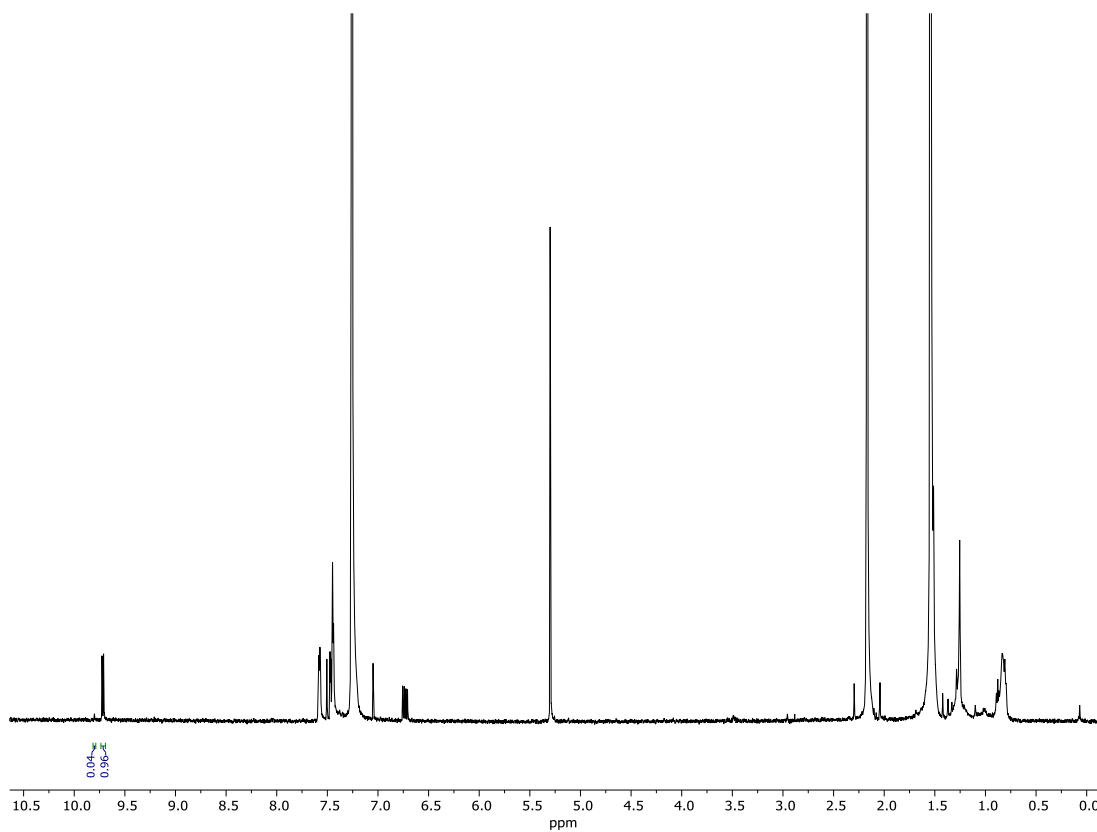


## 6.3.6.4 Catalyst screening for transfer hydrogenation using Sav



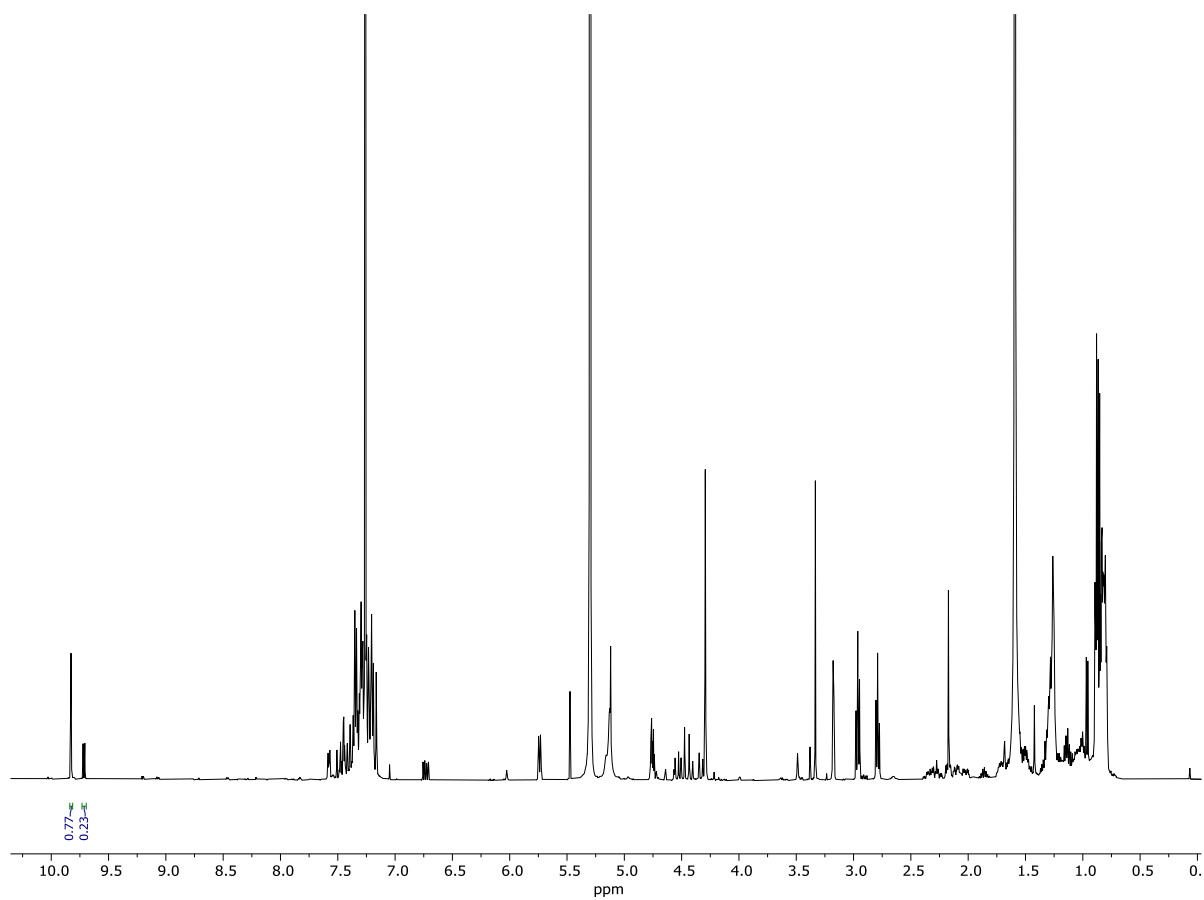
Compound	Integration	% Conversion
<b>14</b> (Starting material)	0.95	95
<b>88</b> (Product)	0.05	5

## 6.3.6.5 Catalyst screening for transfer hydrogenation using M-Sav

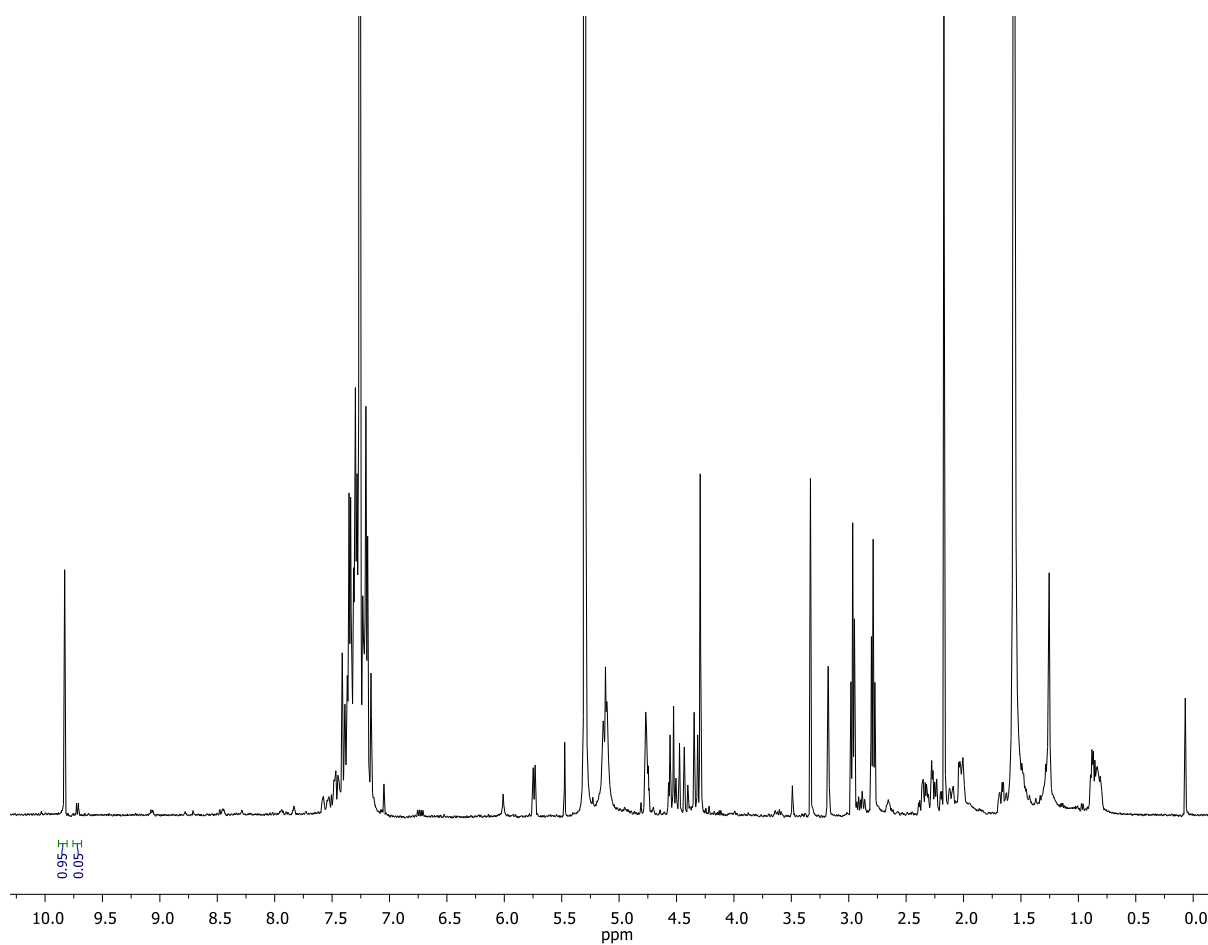


Compound	Integration	% Conversion
<b>14</b> (Starting material)	0.96	96
<b>88</b> (Product)	0.04	4

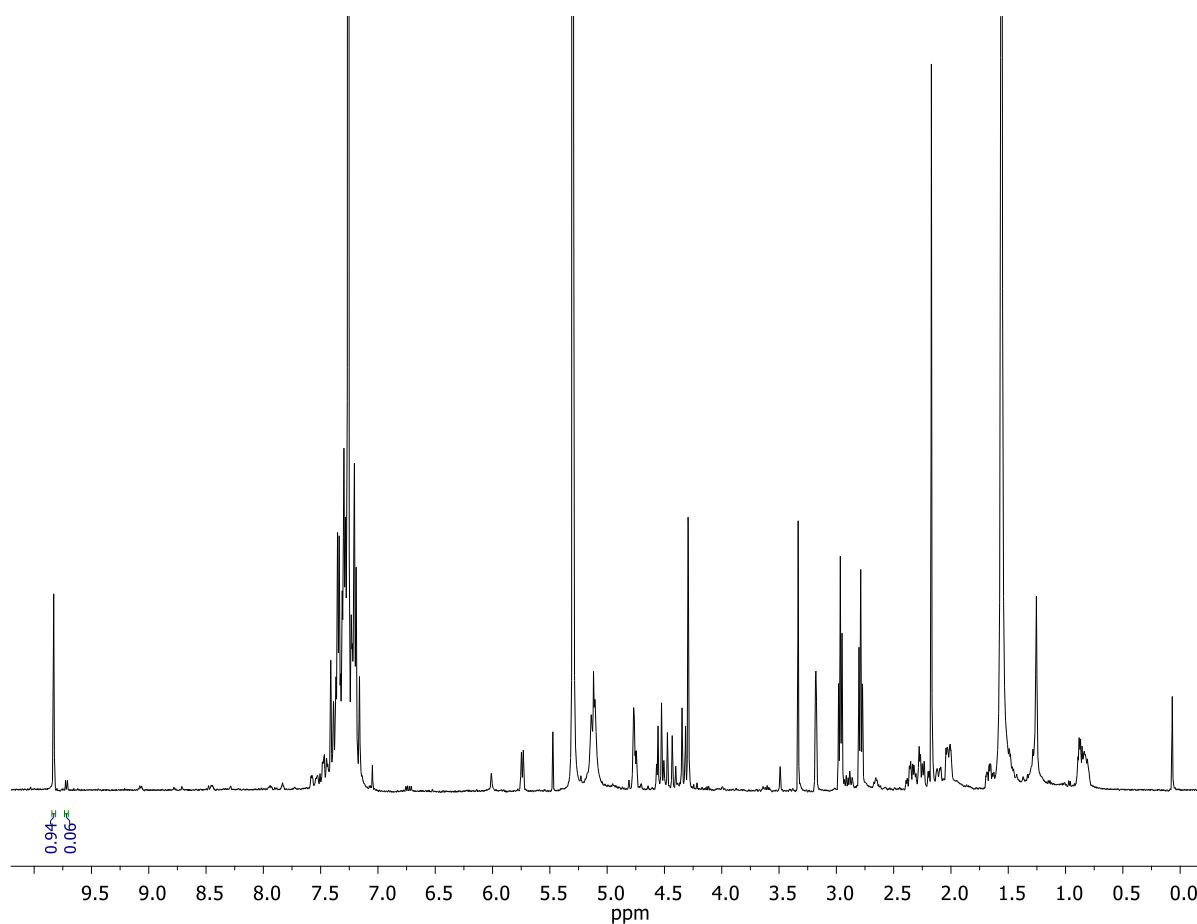
## 6.3.6.6 Catalyst screening for transfer hydrogenation using Sav:73



Compound	Integration	% Conversion
<b>14</b> (Starting material)	0.23	23
<b>88</b> (Product)	0.77	77

**6.3.6.7 Catalyst screening for transfer hydrogenation using Sav:73 (2 mol%)**

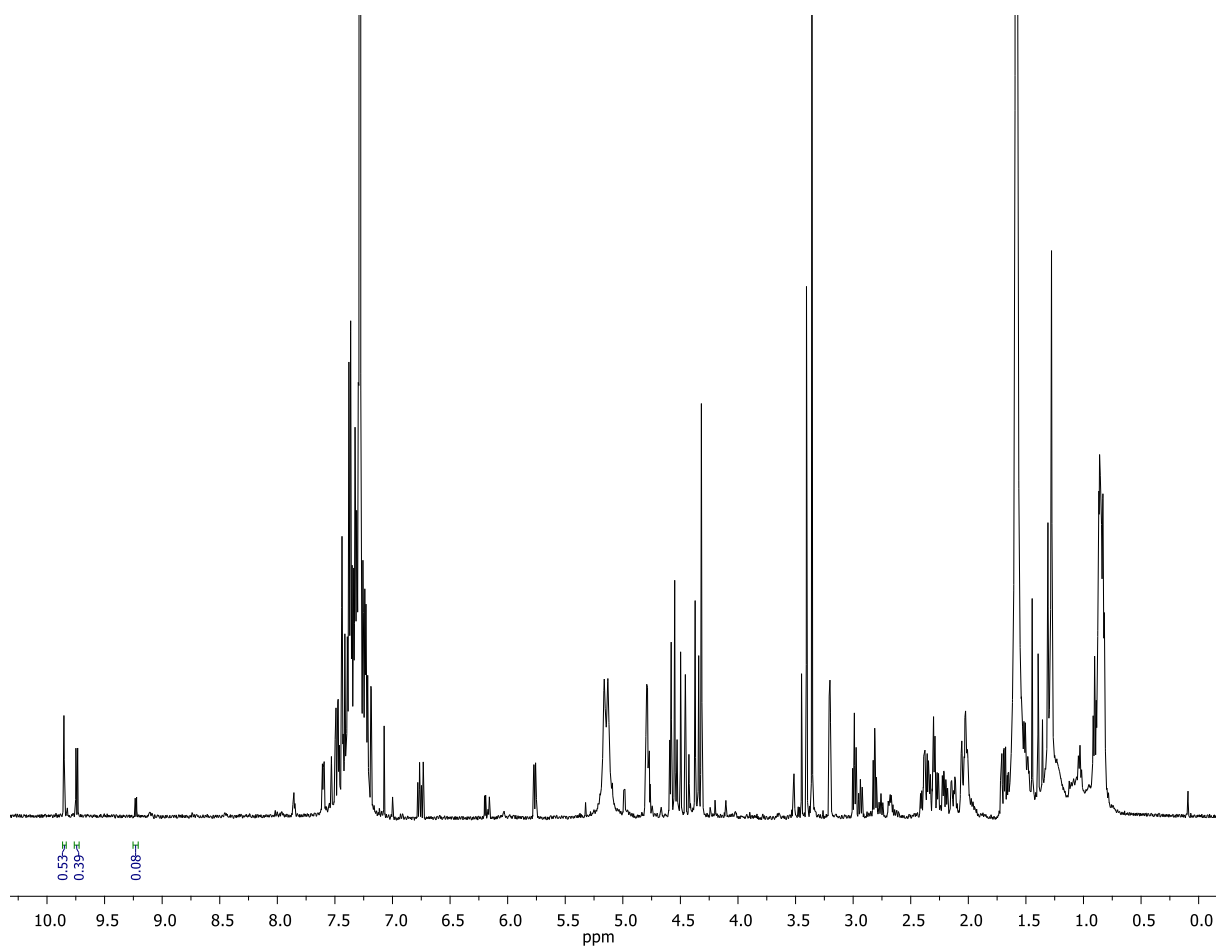
Compound	Integration	% Conversion
<b>14</b> (Starting material)	0.05	5
<b>88</b> (Product)	0.95	95

**6.3.6.8 Catalyst screening for transfer hydrogenation using Sav:73 (5 equivalents BNAH, 25% MeOH)**

Compound	Integration	% Conversion
<b>14</b> (Starting material)	0.06	6
<b>88</b> (Product)	0.94	94

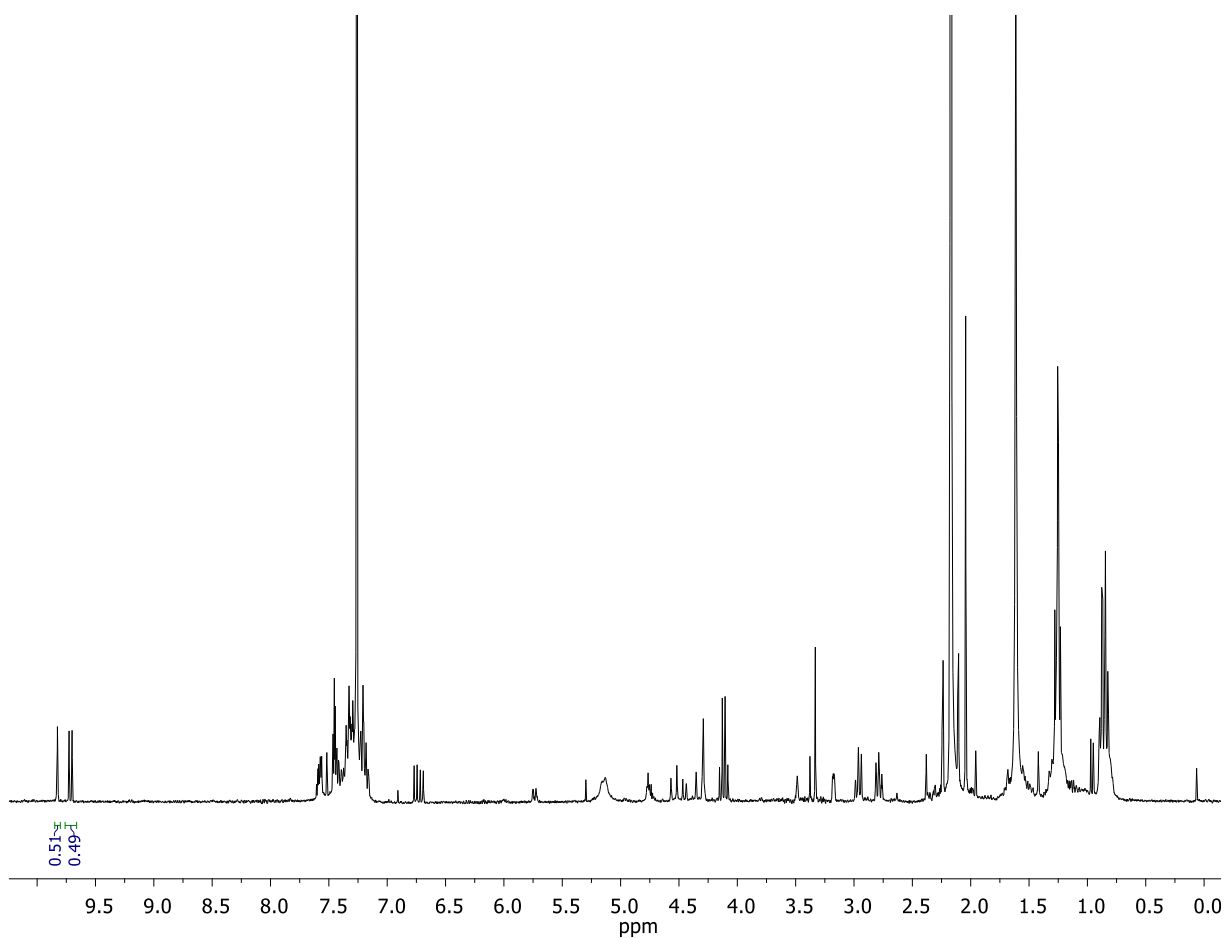
**6.3.6.9 Catalyst screening for transfer hydrogenation using Sav:73, no shaking (0 rpm)**

Formation of an unidentified side-product was observed around 9.25 ppm. The peak around 9.25 ppm resembles the characteristic doublet of an aldehyde, thus the peak was assumed to refer to a single H. Therefore, the estimated conversion of this reaction was made by a ratio between the aldehydic peaks of the starting material **14**, product **88** and this side-product.



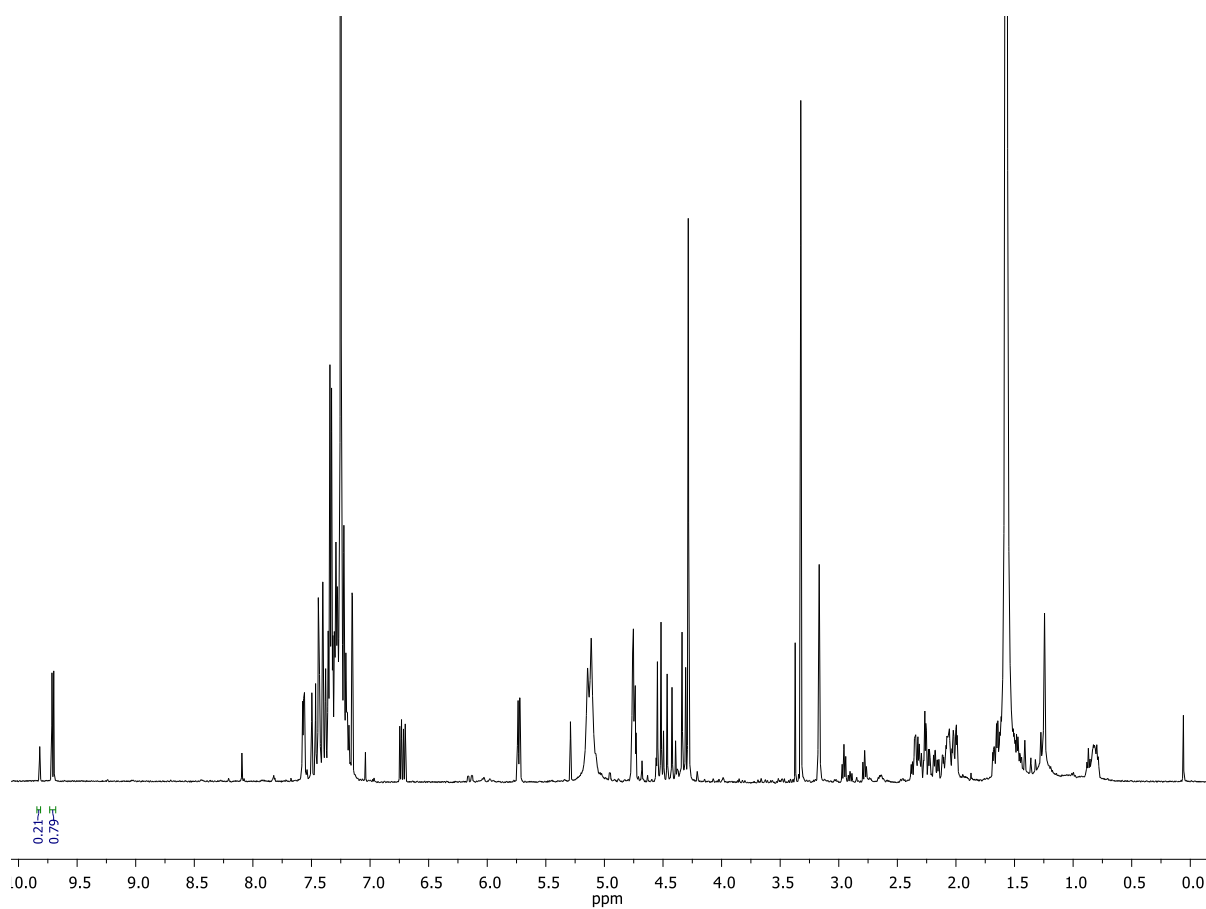
Compound	Integration	% Conversion
<b>14</b> (Starting material)	0.39	39
Unknown side-product	0.08	8
<b>88</b> (Product)	0.53	53

## 6.3.6.10 Catalyst screening for transfer hydrogenation using Sav:74



Compound	Integration	% Conversion
<b>14</b> (Starting material)	0.49	49
<b>88</b> (Product)	0.51	51

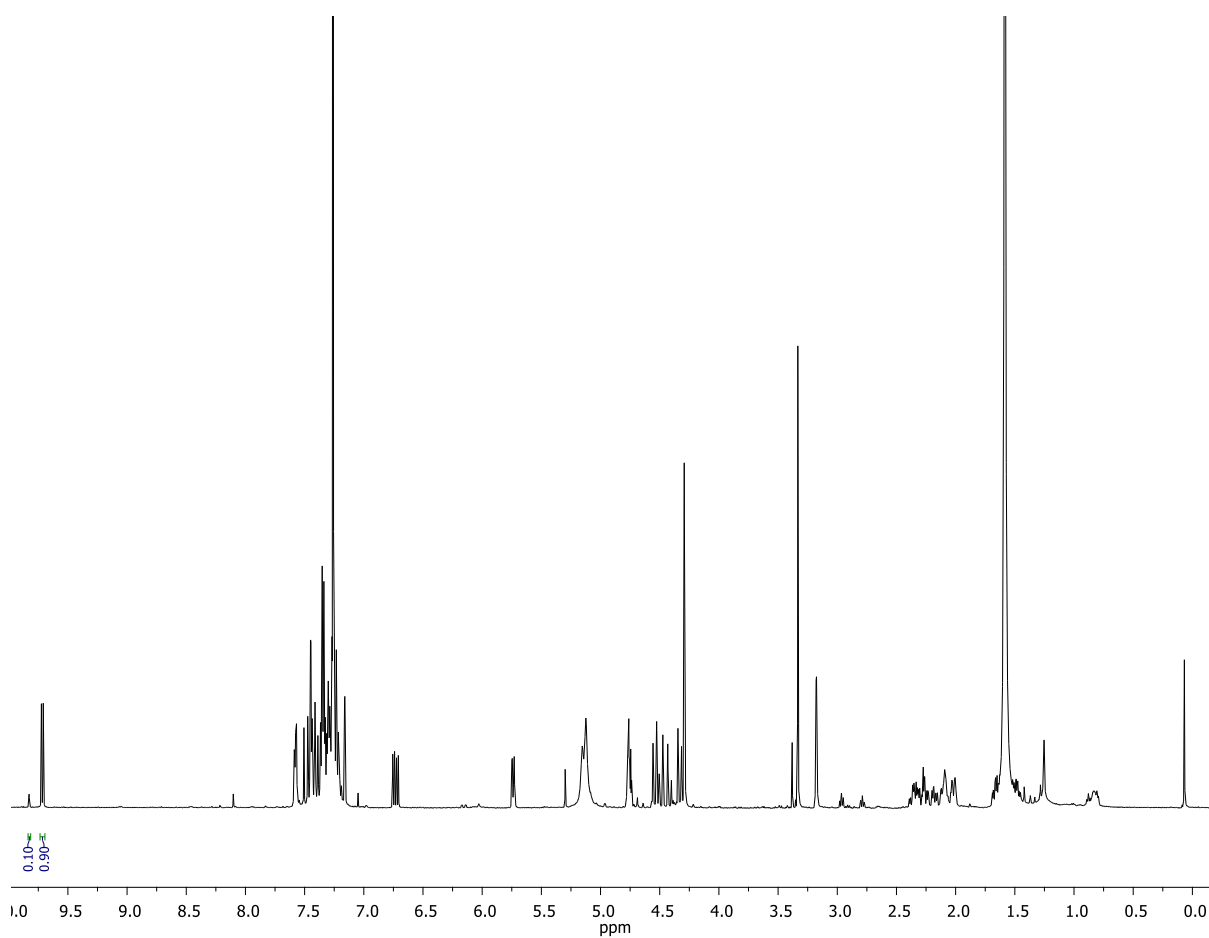
## 6.3.6.11 Catalyst screening for transfer hydrogenation using M-Sav:73



Compound	Integration	% Conversion
<b>14</b> (Starting material)	0.79	79
<b>88</b> (Product)	0.21	21

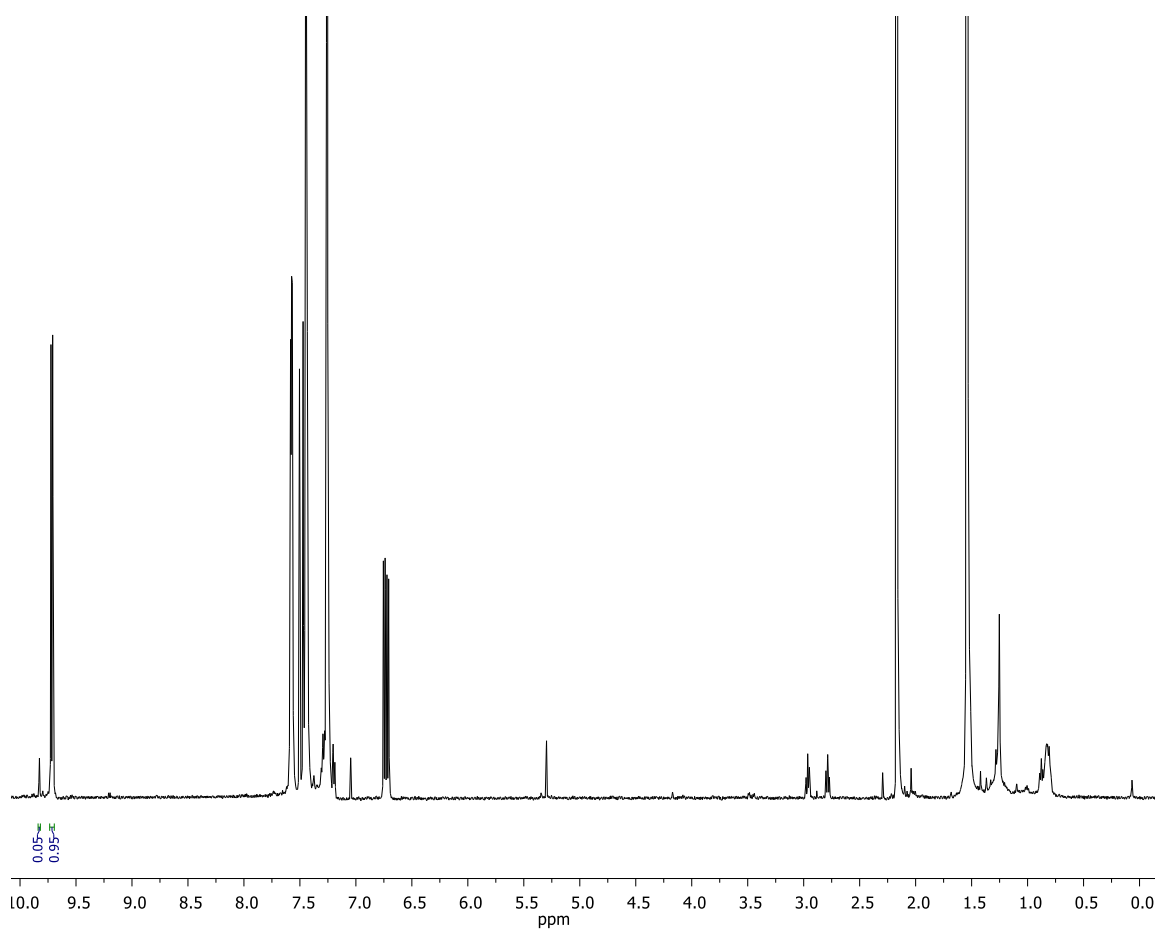


## 6.3.6.12 Catalyst screening for transfer hydrogenation using M-Sav:74

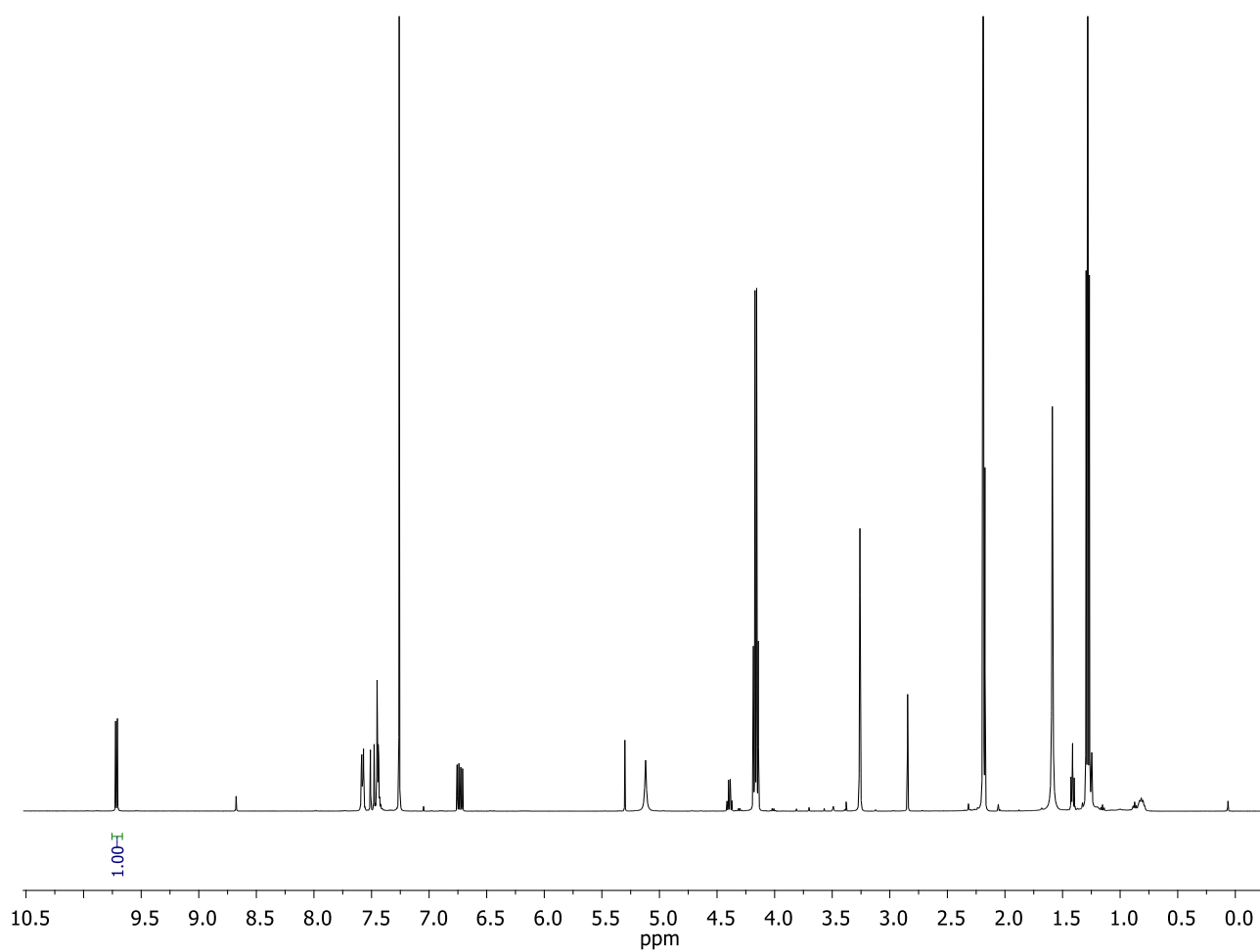


Compound	Integration	% Conversion
<b>14</b> (Starting material)	0.90	90
<b>88</b> (Product)	0.10	10

## 6.3.6.13 Catalyst screening for transfer hydrogenation using Sav:73 and NADH (86)



Compound	Integration	% Conversion
<b>14</b> (Starting material)	0.95	95
<b>88</b> (Product)	0.05	5

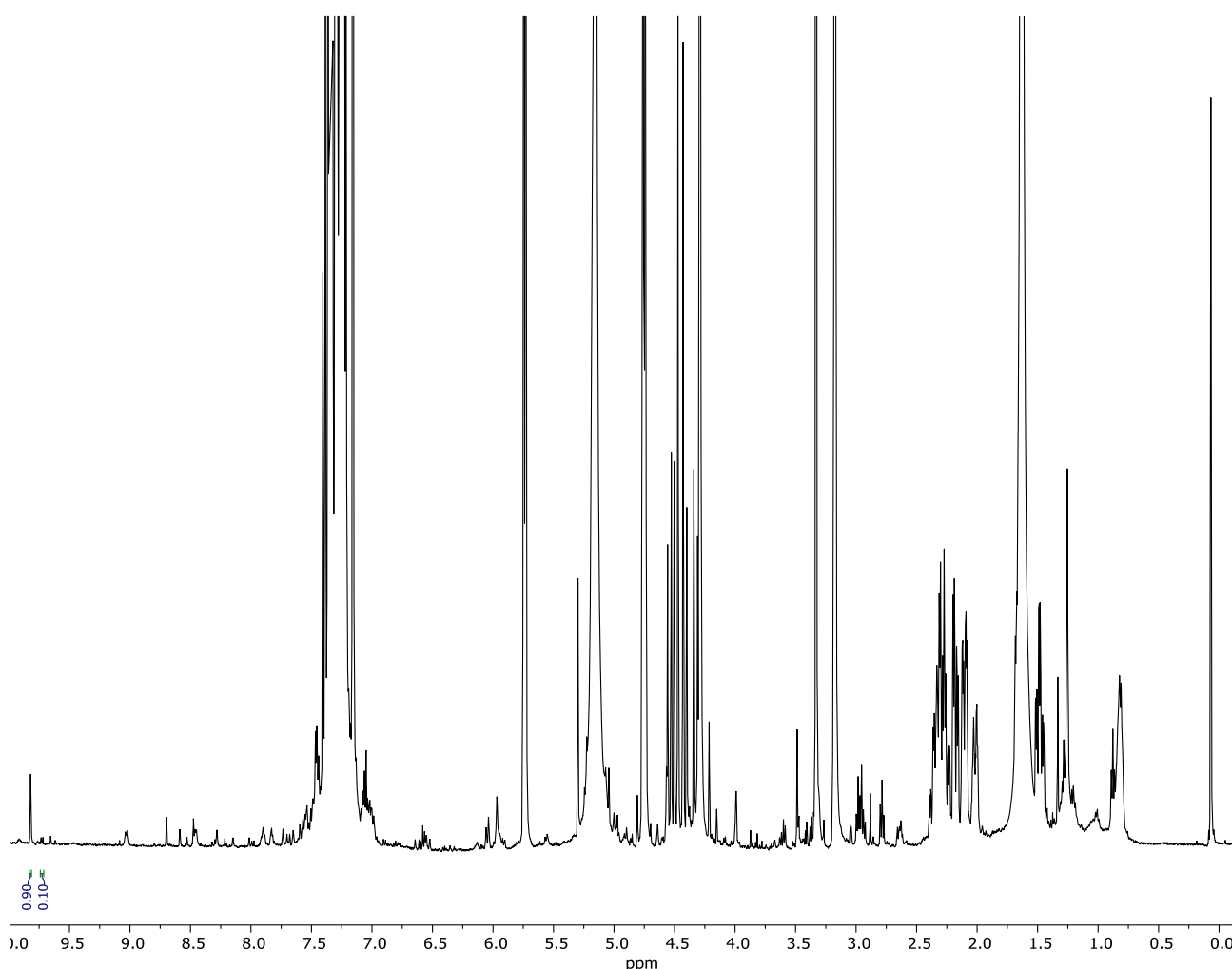
**6.3.6.14 Catalyst screening for transfer hydrogenation using Sav:73 and Hantzsch ester (84)**

Compound	Integration	% Conversion
<b>14</b> (Starting material)	1.00	100
<b>88</b> (Product)	/	/

### 6.3.7 <sup>1</sup>H-NMR details for the activity screening of Table 7

#### 6.3.7.1 Transfer hydrogenation to (*E*)-3-(*o*-fluorophenyl) acrylaldehyde

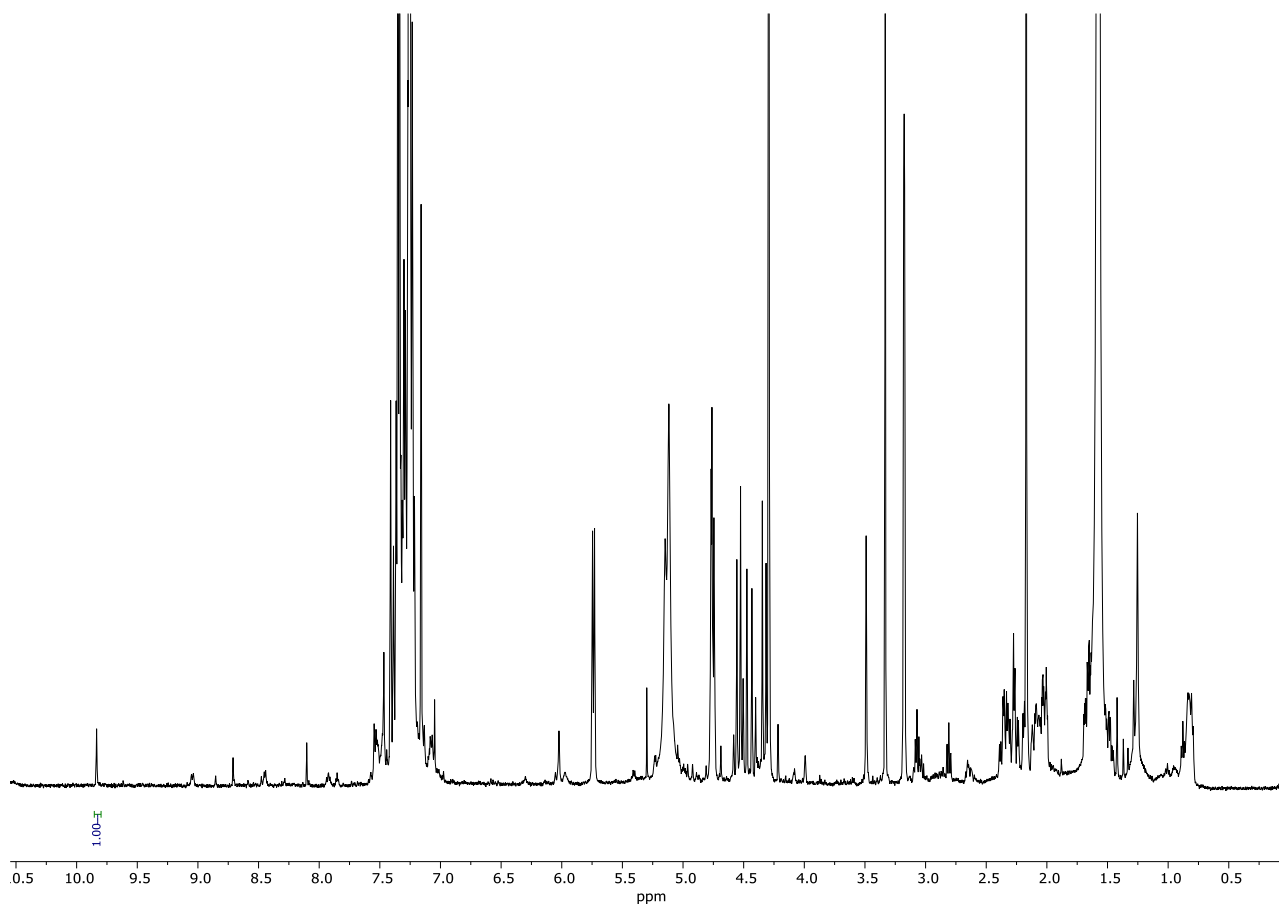
The estimated conversion of **89** into 3-(*o*-fluorophenyl) propanal (**102**) is calculated after integration of the product peak at 9.75 ppm with the substrate peak at 9.65 ppm. The spectroscopic data of **102** are the following: <sup>1</sup>H-NMR (500 MHz, CDCl<sub>3</sub>), δ: 9.75 (t, *J* = 1.3 Hz, 1 H), 7.25-7.18 (m, 2H), 7.09-7.03 (m, 2H), 2.97 (t, *J* = 7.5 Hz, 2 H), 2.79-2.76 (t, *J* = 7.5 Hz, 2 H) ppm. These data matched those reported in the literature. The spectroscopic data of **102** matched those reported in the literature.<sup>312</sup>



Compound	Integration	% Conversion
<b>89</b> (Starting material)	0.10	10
<b>102</b> (Product)	0.90	90

### 6.3.7.2 Transfer hydrogenation to (*E*)-3-(*o*-bromophenyl) acrylaldehyde

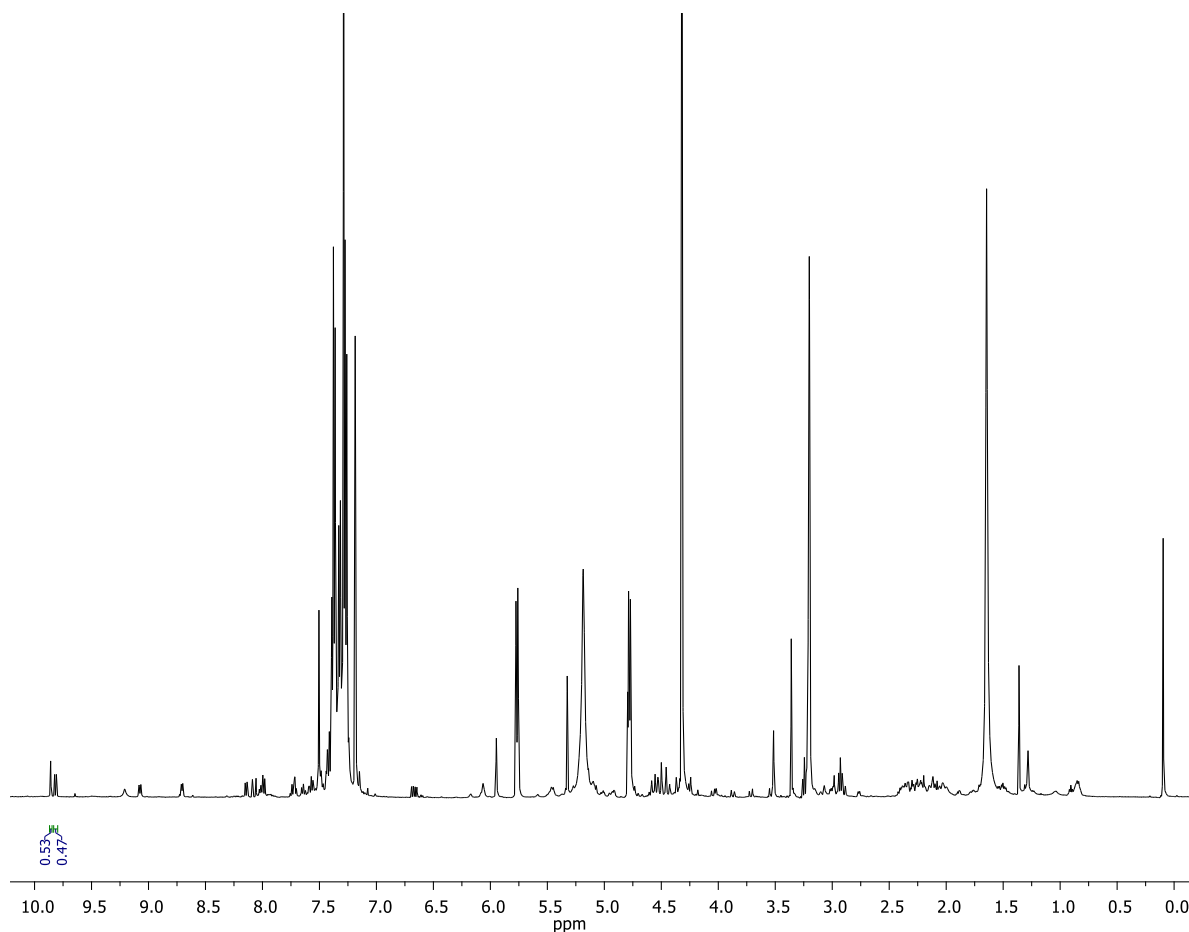
The estimated conversion of **90** into 3-(*o*-bromophenyl) propanal (**103**) is calculated after integration of the product peak at 9.76 ppm with the substrate peak at 9.70 ppm. The spectroscopic data of **103** are the following:  $^1\text{H-NMR}$  (500 MHz,  $\text{CDCl}_3$ ),  $\delta$ : 9.76 (t,  $J = 1.3$  Hz, 1 H), 7.55-7.50 (m, 2H), 7.28-7.15 (m, 2H), 3.05 (t,  $J = 7.5$  Hz, 2 H), 2.81 (t,  $J = 7.5$  Hz, 2 H) ppm. These data matched those reported in the literature.<sup>313</sup>



Compound	Integration	% Conversion
<b>90</b> (Starting material)	/	/
<b>103</b> (Product)	1.00	100

### 6.3.7.3 Transfer hydrogenation to (*E*)-3-(*o*-nitrophenyl) acrylaldehyde

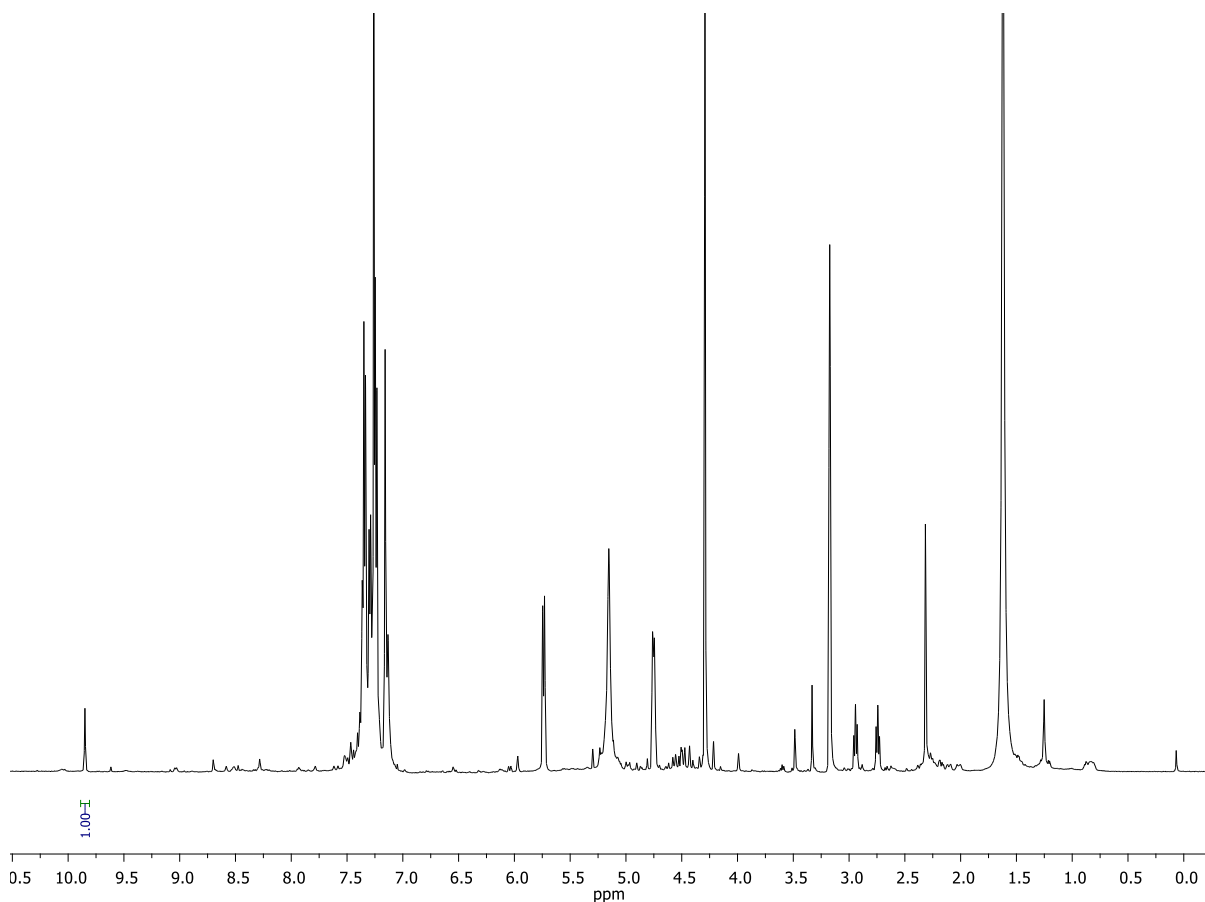
The estimated conversion of **91** into 3-(*o*-nitrophenyl) propanal (**104**) is calculated after integration of the product peak at 9.79 ppm with the substrate peak at 9.75 ppm. The spectroscopic data of **104** are the following:  $^1\text{H-NMR}$  (500 MHz,  $\text{CDCl}_3$ ),  $\delta$ : 9.79 (t,  $J= 1.3$  Hz, 1 H), 8.00 (d,  $J= 8.0$  Hz, 1H), 7.61 (d,  $J= 8.0$  Hz, 1H), 7.48-7.40 (m, 2H), 3.20 (t,  $J= 7.5$  Hz, 2 H), 2.95 (t,  $J= 7.5$  Hz, 2 H) ppm. These data matched those reported in the literature.<sup>314</sup>



Compound	Integration	% Conversion
<b>91</b> (Starting material)	0.47	47
<b>104</b> (Product)	0.53	53

### 6.3.7.4 Transfer hydrogenation to (*E*)-3-(*o*-tolyl) acrylaldehyde

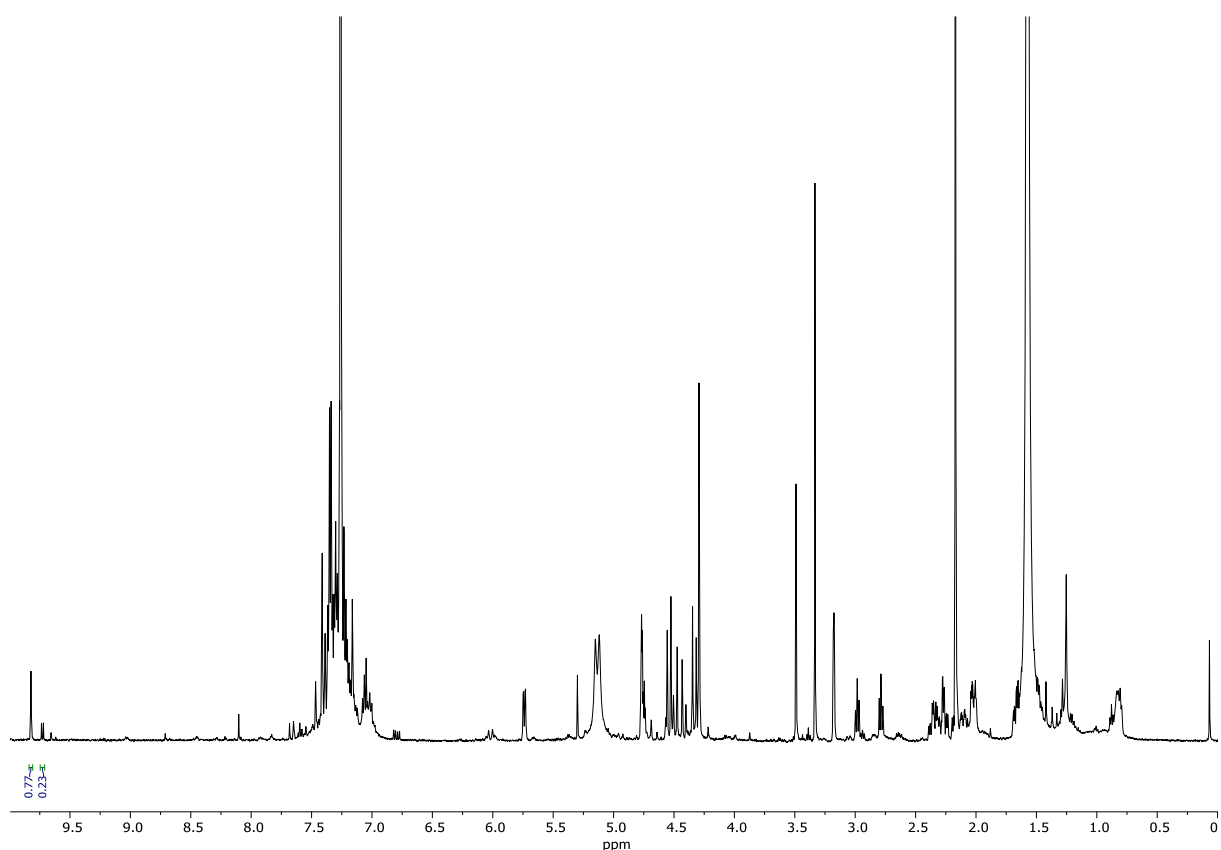
The estimated conversion of **92** into 3-(*o*-tolyl) propanal (**105**) is calculated after integration of the product peak at 9.82 ppm with the substrate peak at 9.73 ppm. The spectroscopic data of **105** are the following:  $^1\text{H-NMR}$  (500 MHz,  $\text{CDCl}_3$ ),  $\delta$ : 9.82 (t,  $J = 1.3$  Hz, 1 H), 7.30 (t,  $J = 8.0$  Hz, 2H), 7.15-7.10 (m, 2H), 3.01 (t,  $J = 7.5$  Hz, 2 H), 2.81 (t,  $J = 7.5$  Hz, 2 H), 2.27 (s, 3H) ppm. These data matched those reported in the literature.<sup>315</sup>



Compound	Integration	% Conversion
<b>92</b> (Starting material)	/	/
<b>105</b> (Product)	1.00	100

### 6.3.7.5 Transfer hydrogenation to (*E*)-3-(*m*-fluorophenyl) acrylaldehyde

The estimated conversion of (*E*)-3-(*m*-fluorophenyl) acrylaldehyde (**93**) into 3-(*m*-fluorophenyl) propanal (**106**) is calculated after integration of the product peak at 9.75 ppm with the substrate peak at 9.65 ppm. The spectroscopic data of **106** are the following: **<sup>1</sup>H-NMR (500 MHz, CDCl<sub>3</sub>)**,  $\delta$ : 9.75 (t,  $J$  = 1.3 Hz, 1 H), 7.25-7.22 (m, 1H), 7.01-6.91 (m, 3H), 2.95 (t,  $J$  = 7.5 Hz, 2 H), 2.80 (t,  $J$  = 7.5 Hz, 2 H) ppm. These data matched those reported in the literature.<sup>316</sup>

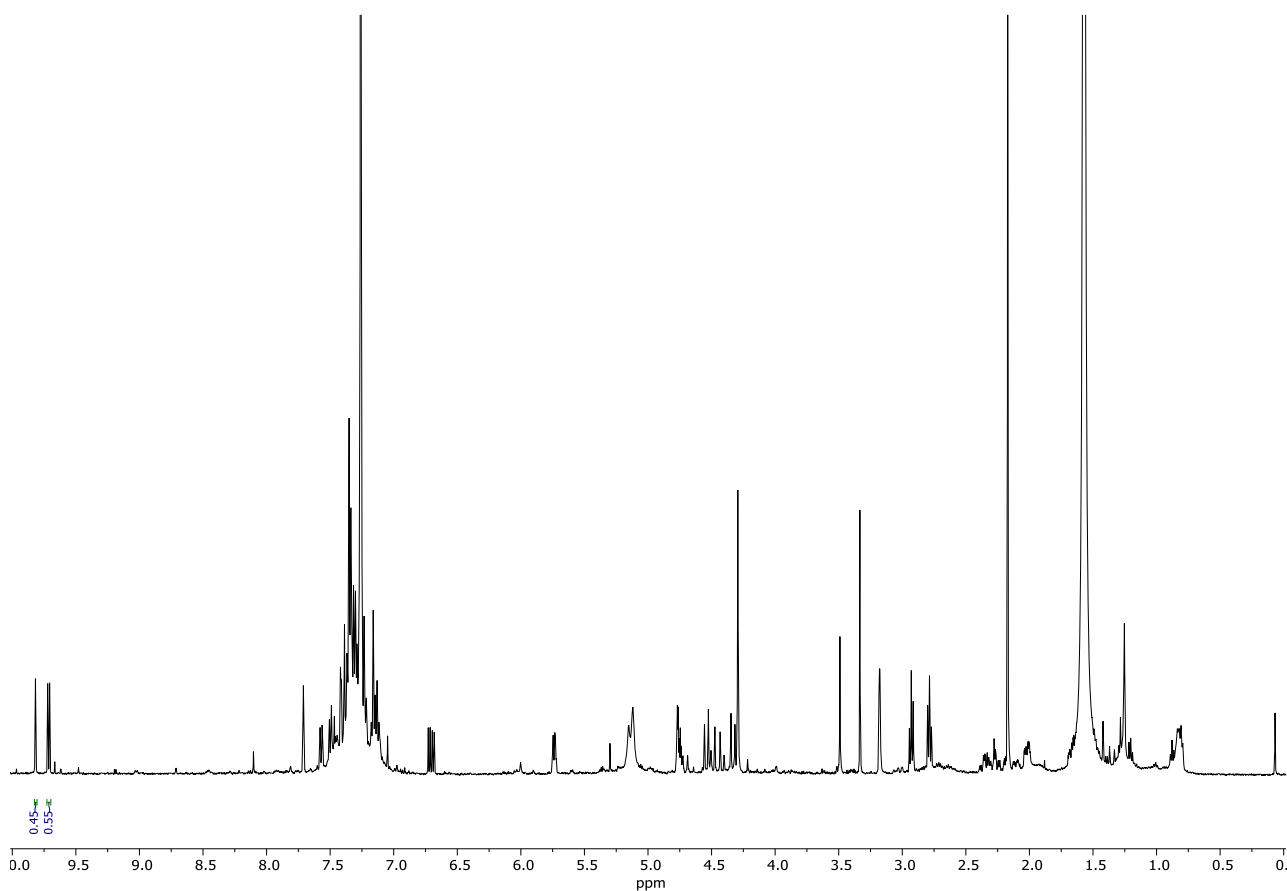


Compound	Integration	% Conversion
<b>93</b> (Starting material)	0.23	23
<b>106</b> (Product)	0.77	77



### 6.3.7.6 Transfer hydrogenation to (*E*)-3-(*m*-bromophenyl) acrylaldehyde

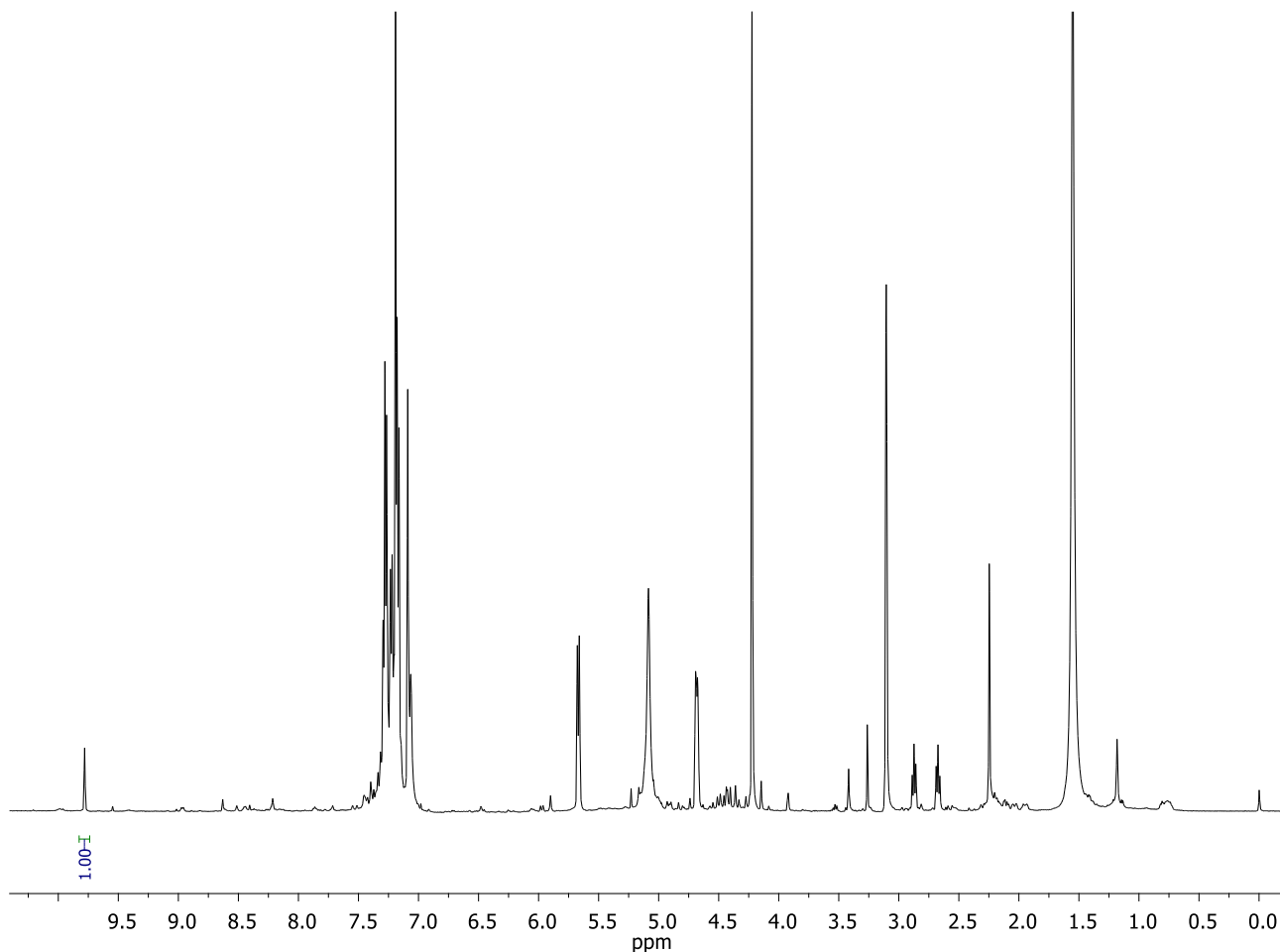
The estimated conversion of (*E*)-3-(*m*-bromophenyl) acrylaldehyde (**94**) into 3-(*m*-bromophenyl) propanal (**107**) is calculated after integration of the product peak at 9.74 ppm with the substrate peak at 9.64 ppm. The spectroscopic data of **107** are the following: **<sup>1</sup>H-NMR (500 MHz, CDCl<sub>3</sub>)**,  $\delta$ : 9.74 (t,  $J$  = 1.3 Hz, 1 H), 7.34-7.26 (m, 2H), 7.18-7.10 (m, 2H), 2.93 (t,  $J$  = 7.5 Hz, 2 H), 2.77 (t,  $J$  = 7.5 Hz, 2 H) ppm. These data matched those reported in the literature.<sup>317</sup>



Compound	Integration	% Conversion
<b>94</b> (Starting material)	0.55	55
<b>107</b> (Product)	0.45	45

### 6.3.7.7 Transfer hydrogenation to (*E*)-3-(*m*-tolyl) acrylaldehyde

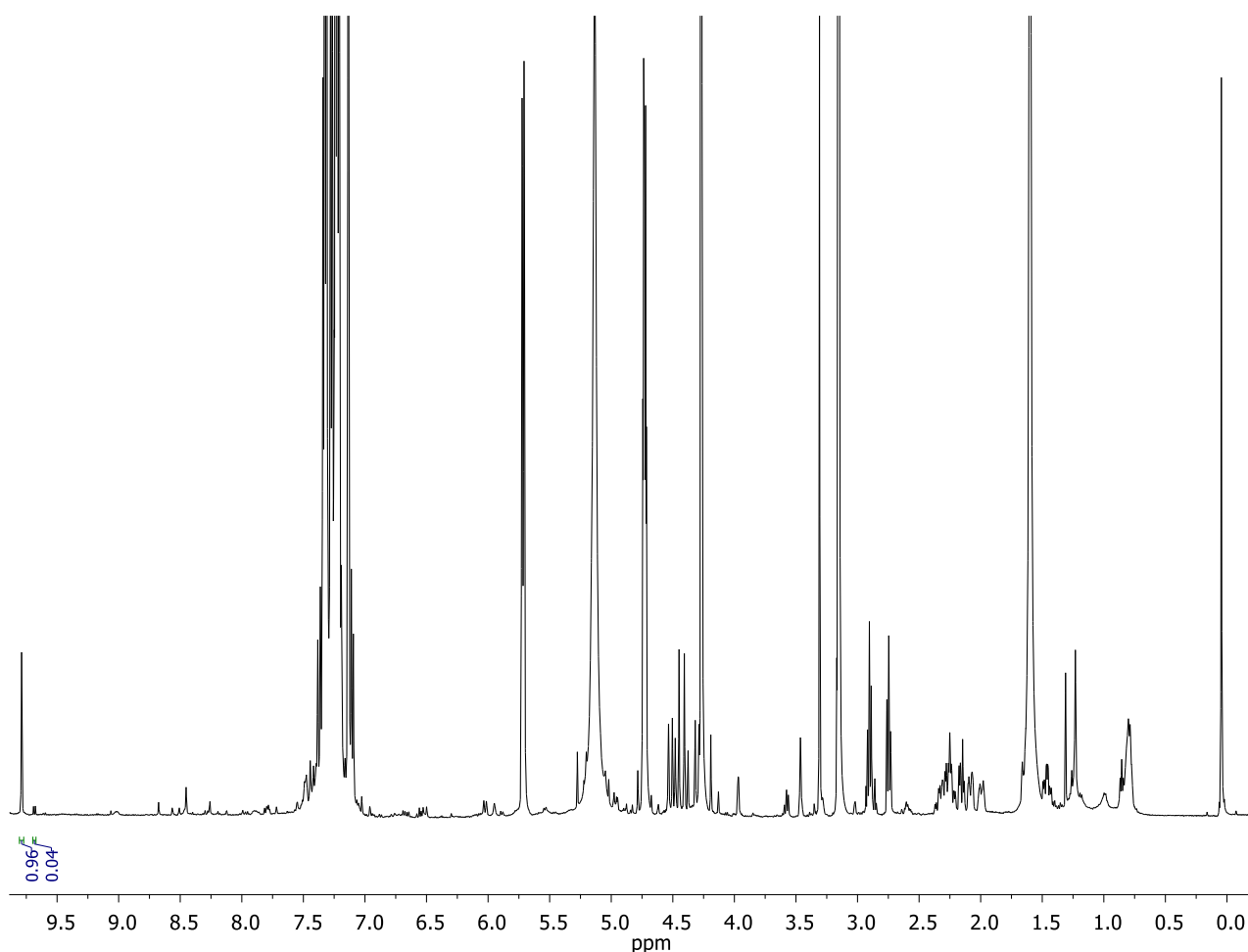
The estimated conversion of (*E*)-3-(*m*-tolyl) acrylaldehyde (**95**) into 3-(*m*-tolyl) propanal (**108**) is calculated after integration of the product peak at 9.78 ppm with the substrate peak at 9.60 ppm. The spectroscopic data of **108** are the following:  $^1\text{H-NMR}$  (500 MHz,  $\text{CDCl}_3$ ),  $\delta$ : 9.78 (t,  $J = 1.3$  Hz, 1 H), 7.32-7.28 (m, 2H), 7.19-7.15 (m, 2H), 2.89 (t,  $J = 7.5$  Hz, 2 H), 2.70 (t,  $J = 7.5$  Hz, 2 H), 2.22 (s, 3 H) ppm. These data matched those reported in the literature.<sup>317</sup>



Compound	Integration	% Conversion
<b>95</b> (Starting material)	/	/
<b>108</b> (Product)	1.00	100

### 6.3.7.8 Transfer hydrogenation to (*E*)-3-(*p*-chlorophenyl) acrylaldehyde

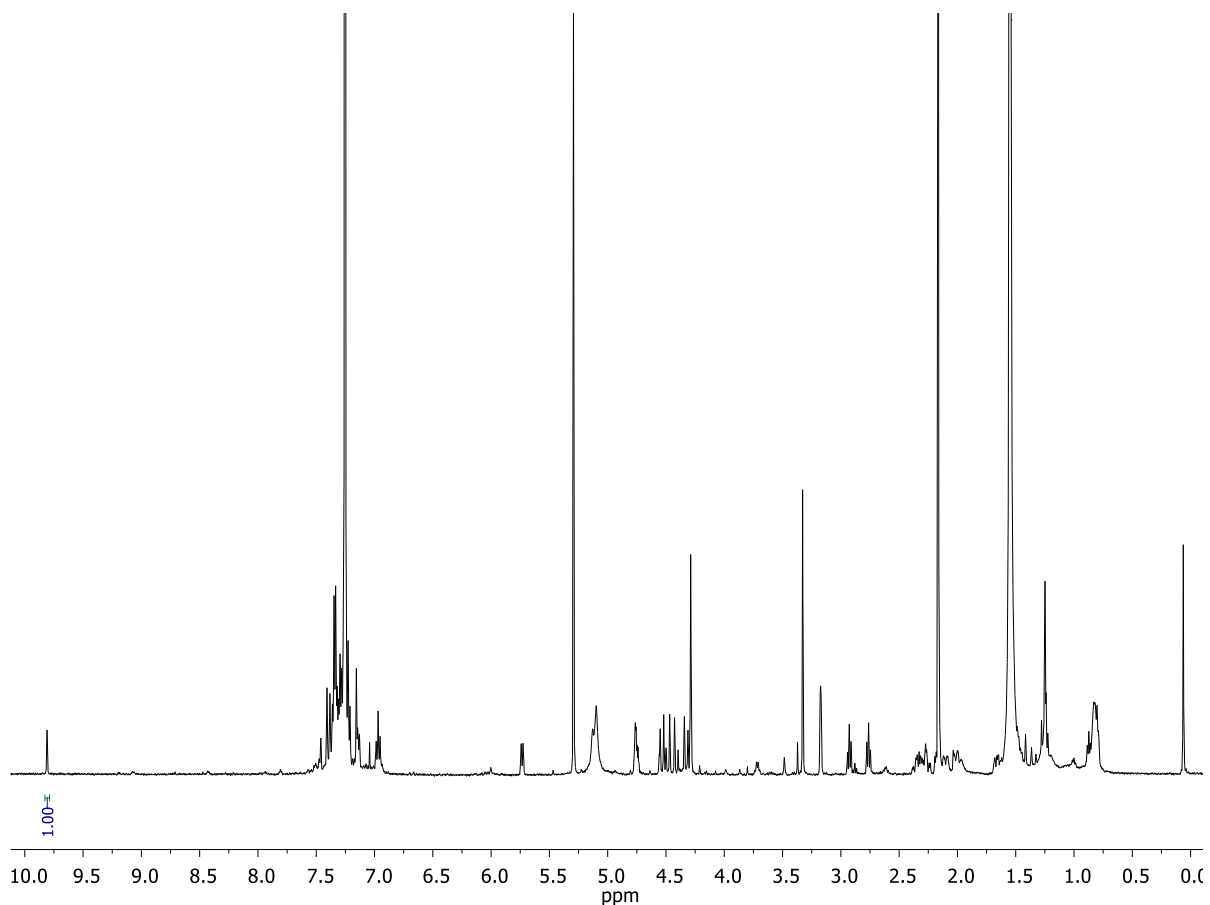
The estimated conversion of (*E*)-3-(*p*-chlorophenyl) acrylaldehyde (**96**) into 3-(*p*-chlorophenyl) propanal (**109**) is calculated after integration of the product peak at 9.81 ppm with the substrate peak at 9.63 ppm. The spectroscopic data of **109** are the following: **<sup>1</sup>H-NMR (500 MHz, CDCl<sub>3</sub>)**,  $\delta$ : 9.81 (t,  $J$  = 1.3 Hz, 1 H), 7.28-7.23 (m, 2H), 7.15-7.10 (m, 2H), 2.92 (t,  $J$  = 7.5 Hz, 2 H), 2.79-2.74 (t,  $J$  = 7.5 Hz, 2 H) ppm. These data matched those reported in the literature.<sup>318</sup>



Compound	Integration	% Conversion
<b>96</b> (Starting material)	0.04	4
<b>109</b> (Product)	0.96	96

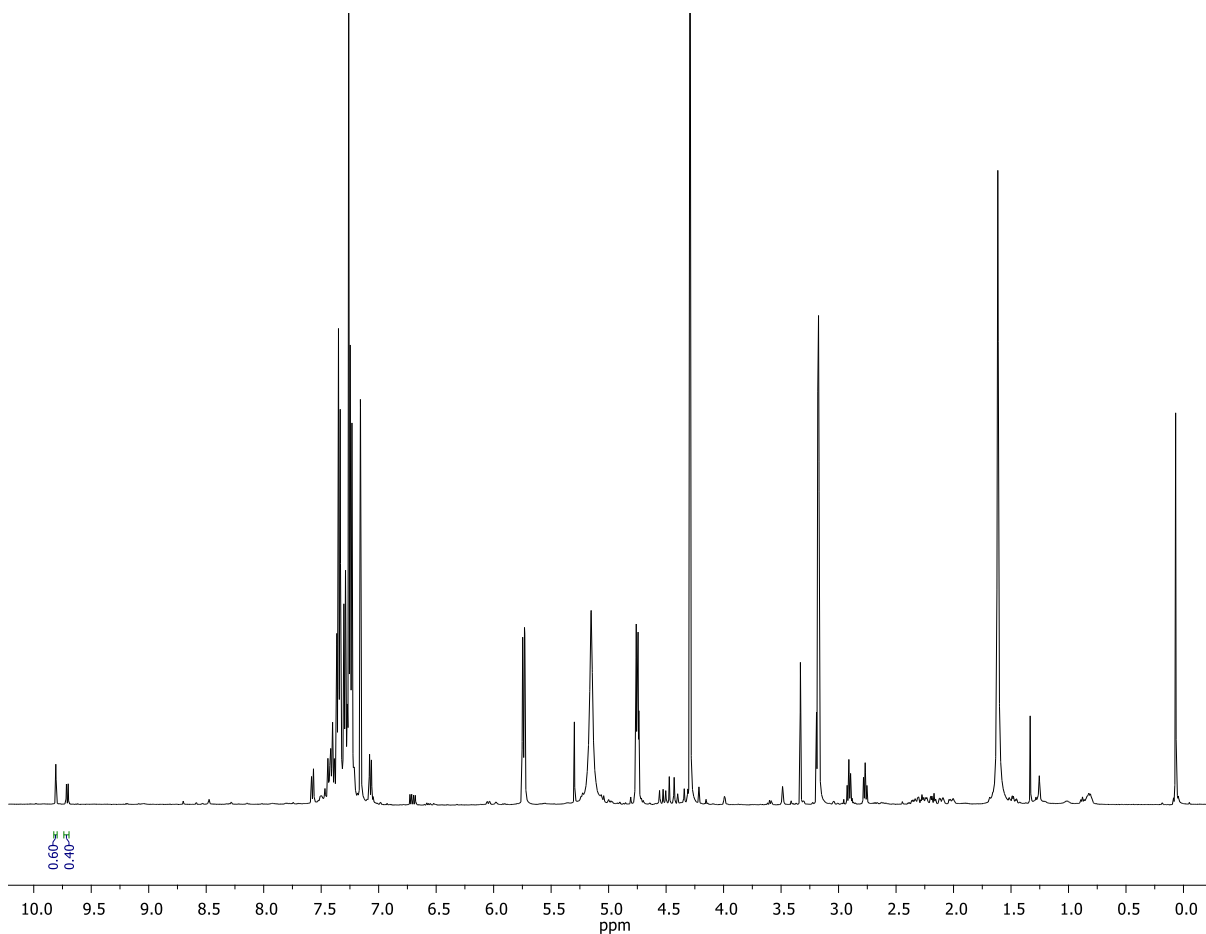
### 6.3.7.9 Transfer hydrogenation to (*E*)-3-(*p*-fluorophenyl) acrylaldehyde

The estimated conversion of (*E*)-3-(*p*-fluorophenyl) acrylaldehyde (**97**) into 3-(*p*-fluorophenyl) propanal (**110**) is calculated after integration of the product peak at 9.80 ppm with the substrate peak at 9.63 ppm. The spectroscopic data of **110** are the following: **<sup>1</sup>H-NMR (500 MHz, CDCl<sub>3</sub>)**, δ: 9.80 (t, *J*= 1.3 Hz, 1 H), 7.17-7.11 (m, 2H), 7.00-6.93 (m, 2H), 2.92 (t, *J*= 7.5 Hz, 2 H), 2.76 (t, *J*= 7.5 Hz, 2 H) ppm.<sup>319</sup>



### 6.3.7.10 Transfer hydrogenation to (*E*)-3-(*p*-bromophenyl) acrylaldehyde

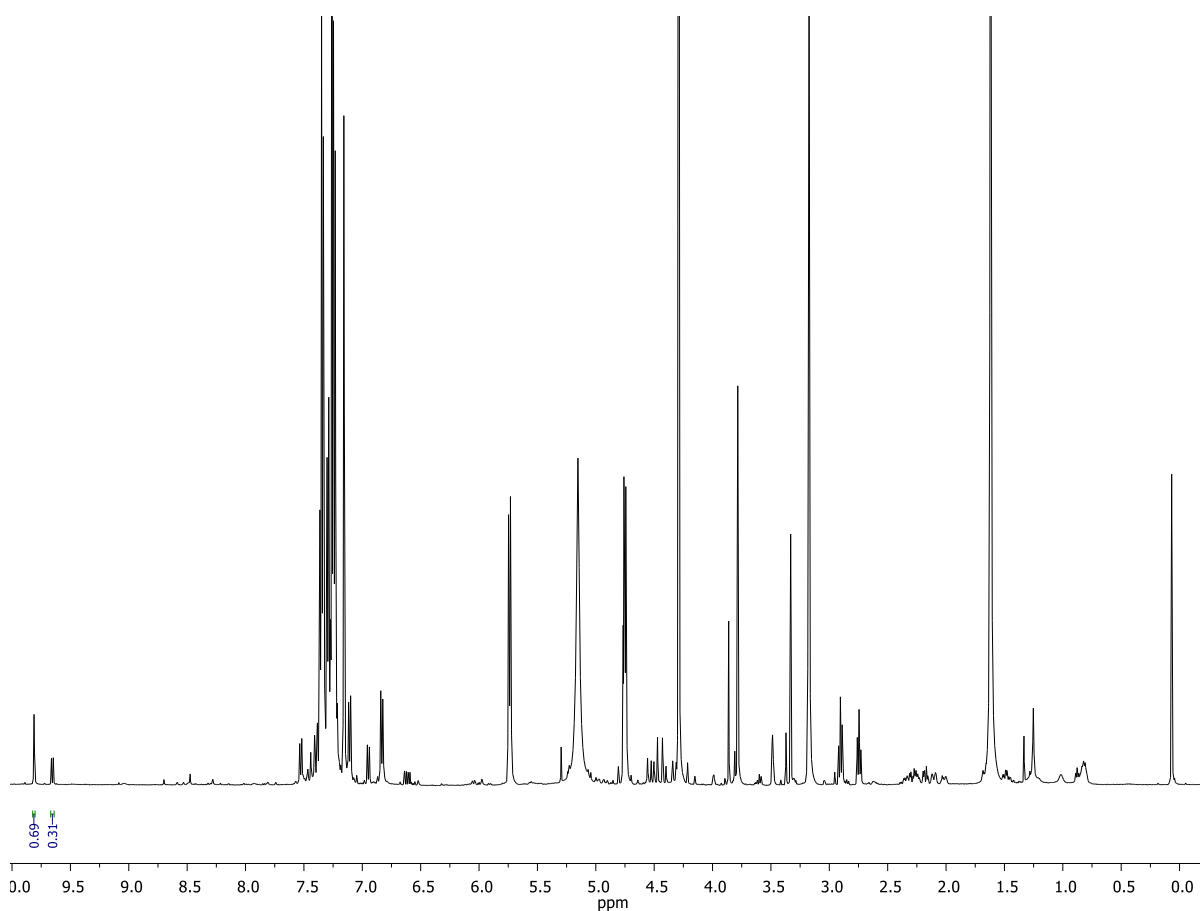
The estimated conversion of (*E*)-3-(*p*-bromophenyl) acrylaldehyde (**98**) into 3-(*p*-bromophenyl) propanal (**111**) is calculated after integration of the product peak at 9.81 ppm with the substrate peak at 9.65 ppm. The spectroscopic data of **111** are the following: **<sup>1</sup>H-NMR (500 MHz, CDCl<sub>3</sub>), δ**: 9.81 (t, *J*= 1.5 Hz, 1H), 7.41 (m, 2H), 7.07 (m, 2H), 2.91 (t, *J*= 7.4 Hz, 2H), 2.77 (t, *J*= 7.3 Hz, 2H) ppm. These data matched those reported in the literature.<sup>320</sup>



Compound	Integration	% Conversion
<b>98</b> (Starting material)	0.40	40
<b>111</b> (Product)	0.60	60

### 6.3.7.11 Transfer hydrogenation to (*E*)-3-(*p*-methoxyphenyl) acrylaldehyde

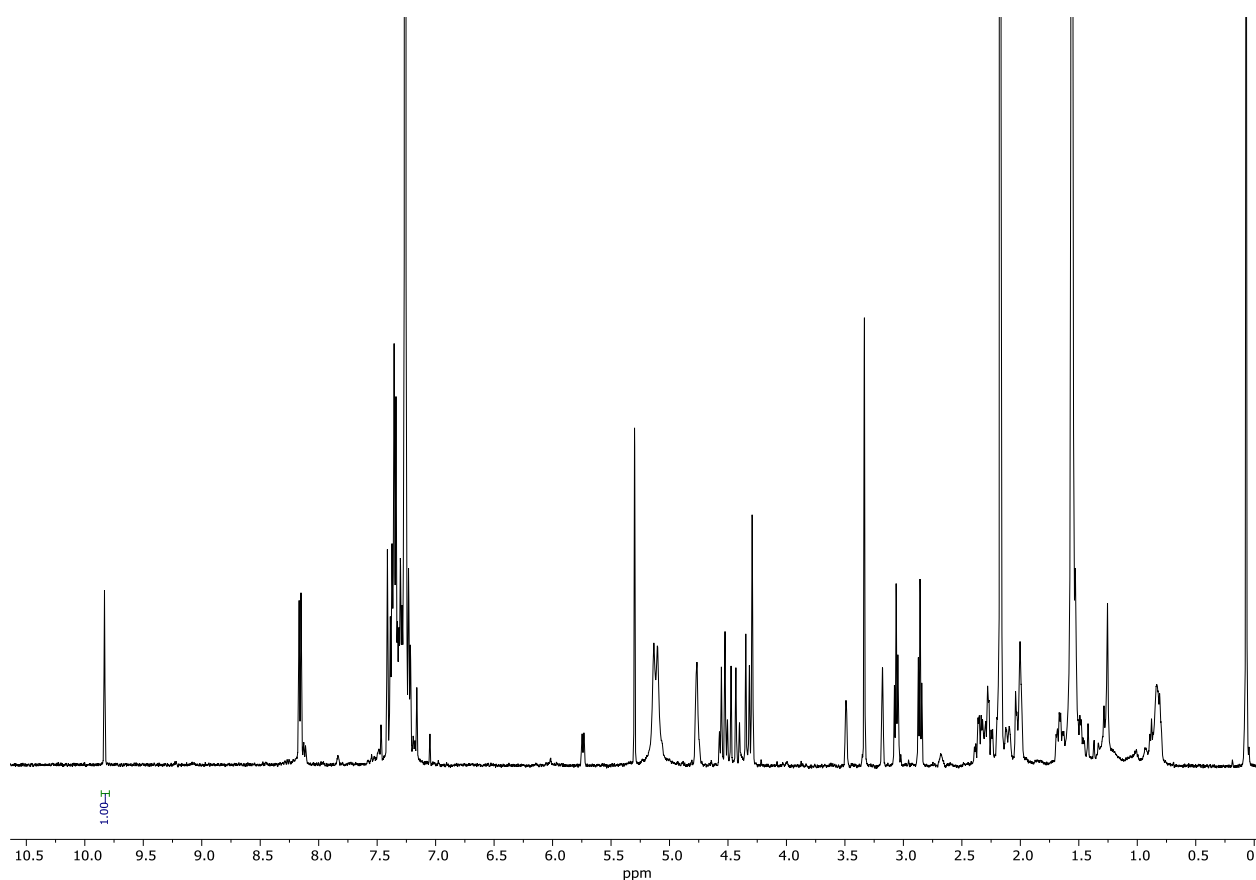
The estimated conversion of (*E*)-3-(*p*-methoxyphenyl) acrylaldehyde (**99**) into 3-(*p*-methoxyphenyl) propanal (**112**) is calculated after integration of the product peak at 9.84 ppm with the substrate peak at 9.68 ppm. The spectroscopic data of **112** are the following: **<sup>1</sup>H-NMR (500 MHz, CDCl<sub>3</sub>)**,  $\delta$ : 9.84 (t,  $J$  = 1.5 Hz, 1 H), 7.14-7.09 (m, 2H), 6.86-6.81 (m, 2H), 3.79 (s, 3H), 2.91 (t,  $J$  = 7.5 Hz, 2 H), 2.78-2.72 (t,  $J$  = 7.5 Hz, 2 H) ppm. These data matched those reported in the literature.<sup>318, 319</sup>



Compound	Integration	% Conversion
<b>99</b> (Starting material)	0.31	31
<b>112</b> (Product)	0.69	69

### 6.3.7.12 Transfer hydrogenation to (*E*)-3-(*p*-nitrophenyl) acrylaldehyde

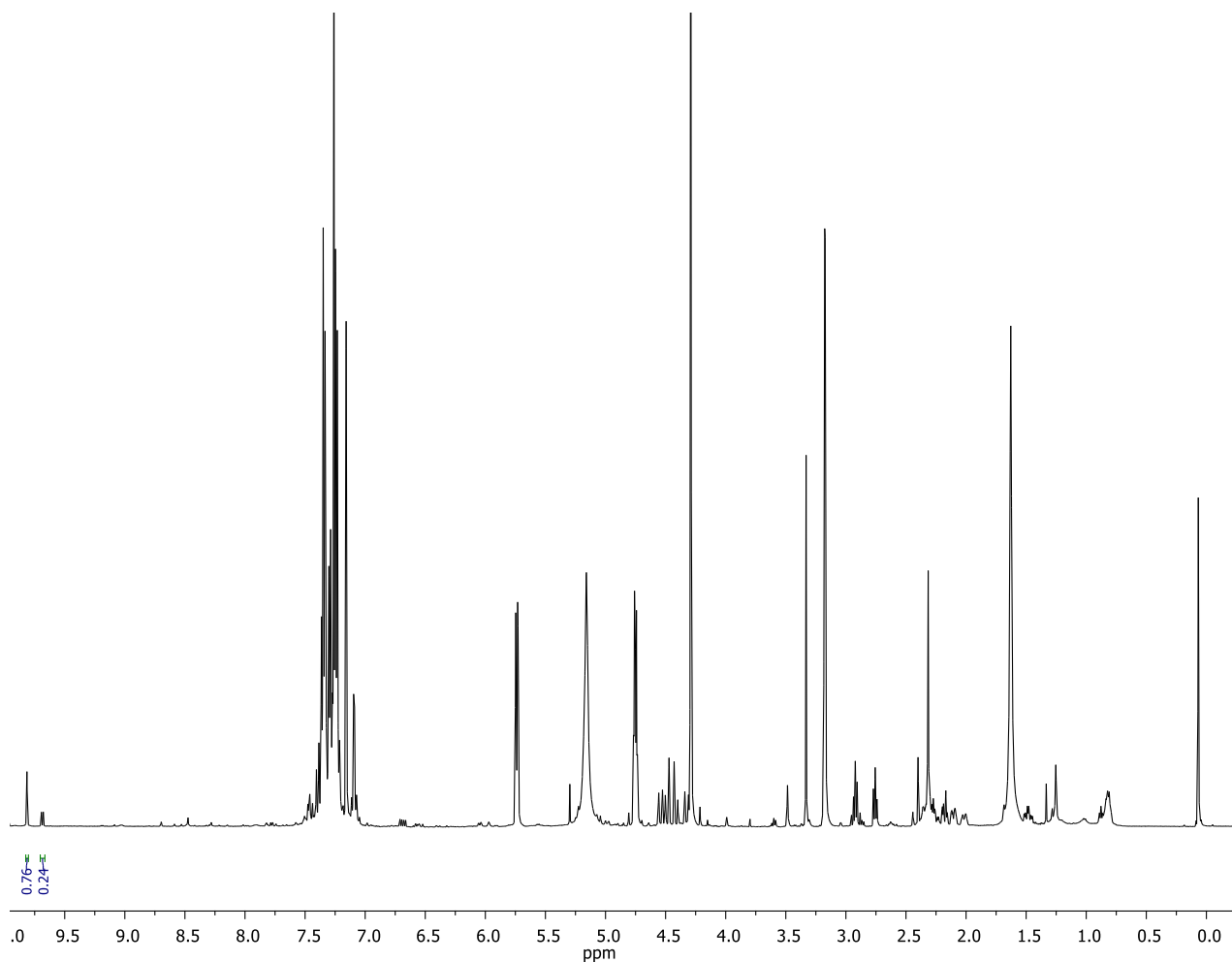
The estimated conversion of (*E*)-3-(*p*-nitrophenyl) acrylaldehyde (**100**) into 3-(*p*-nitrophenyl) propanal (**113**) is calculated after integration of the product peak at 9.84 ppm with the substrate peak at 9.81 ppm. The spectroscopic data of **113** are the following: **<sup>1</sup>H-NMR (500 MHz, CDCl<sub>3</sub>)**,  $\delta$ : 9.84 (t,  $J = 1.5$  Hz, 1 H), 8.15 (m, 2H), 7.37 (m, 2H), 3.07 (t,  $J = 7.5$  Hz, 2 H), 2.87 (t,  $J = 7.5$  Hz, 2 H), 2.78-2.72 (t,  $J = 7.5$  Hz, 2 H) ppm. These data matched those reported in the literature.<sup>321</sup>



Compound	Integration	% Conversion
<b>100</b> (Starting material)	/	/
<b>113</b> (Product)	1.00	100

### 6.3.7.13 Transfer hydrogenation to (*E*)-3-(*p*-tolyl) acrylaldehyde

The estimated conversion of (*E*)-3-(*p*-tolyl) acrylaldehyde (**101**) into 3-(*p*-tolyl) propanal (**114**) is calculated after integration of the product peak at 9.81 ppm with the substrate peak at 9.72 ppm. The spectroscopic data of **114** are the following:  $^1\text{H-NMR}$  (500 MHz,  $\text{CDCl}_3$ ),  $\delta$ : 9.81 (t,  $J = 1.5$  Hz, 1 H), 7.09 (m, 4H), 2.86 (t,  $J = 7.5$  Hz, 2 H), 2.69 (t,  $J = 7.5$  Hz, 2 H), 2.31 (s, 3H) ppm. These data matched those reported in the literature.<sup>321, 322</sup>



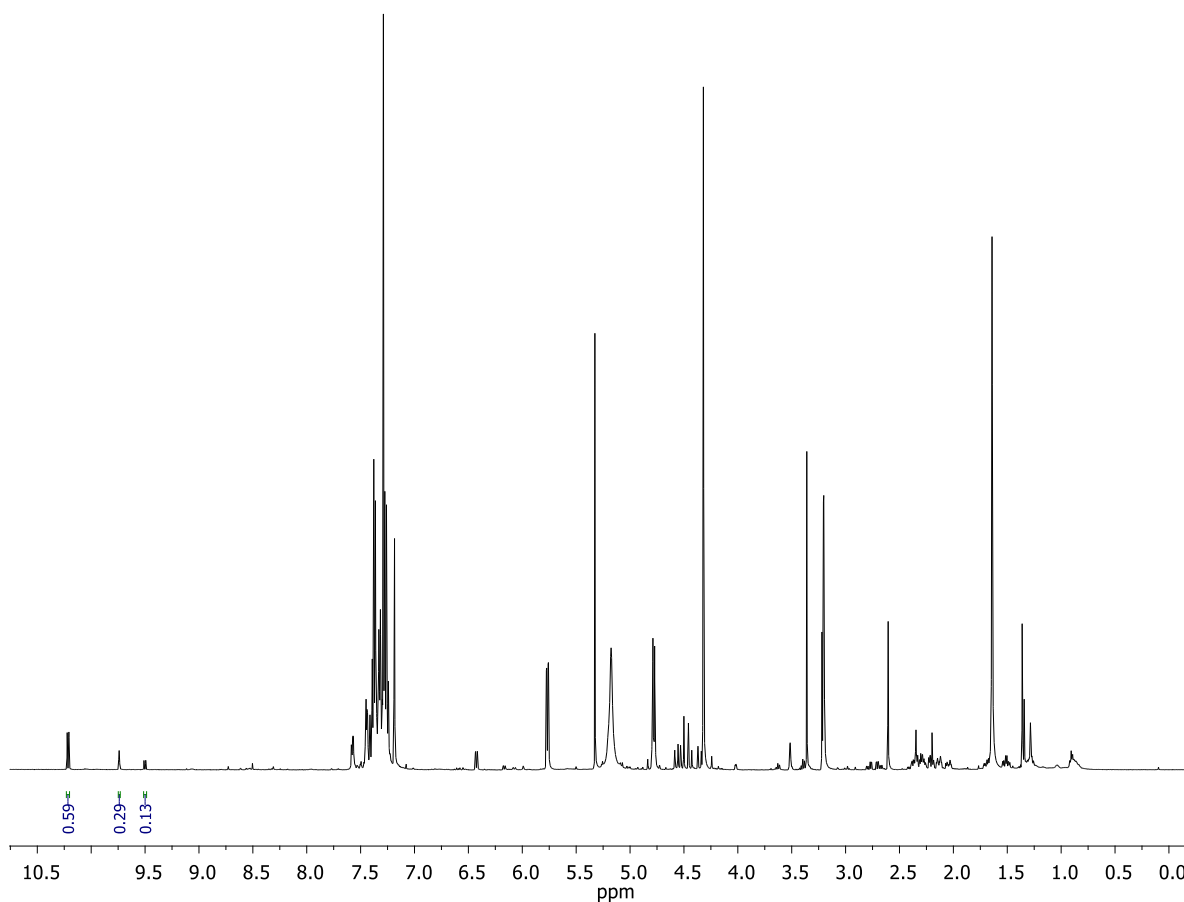
Compound	Integration	% Conversion
<b>101</b> (Starting material)	0.24	24
<b>114</b> (Product)	0.76	76



### 6.3.8 <sup>1</sup>H-NMR details for the activity screening of Table 8

#### 6.3.8.1 Transfer hydrogenation to (*E*)-3-phenylbut-2-enal

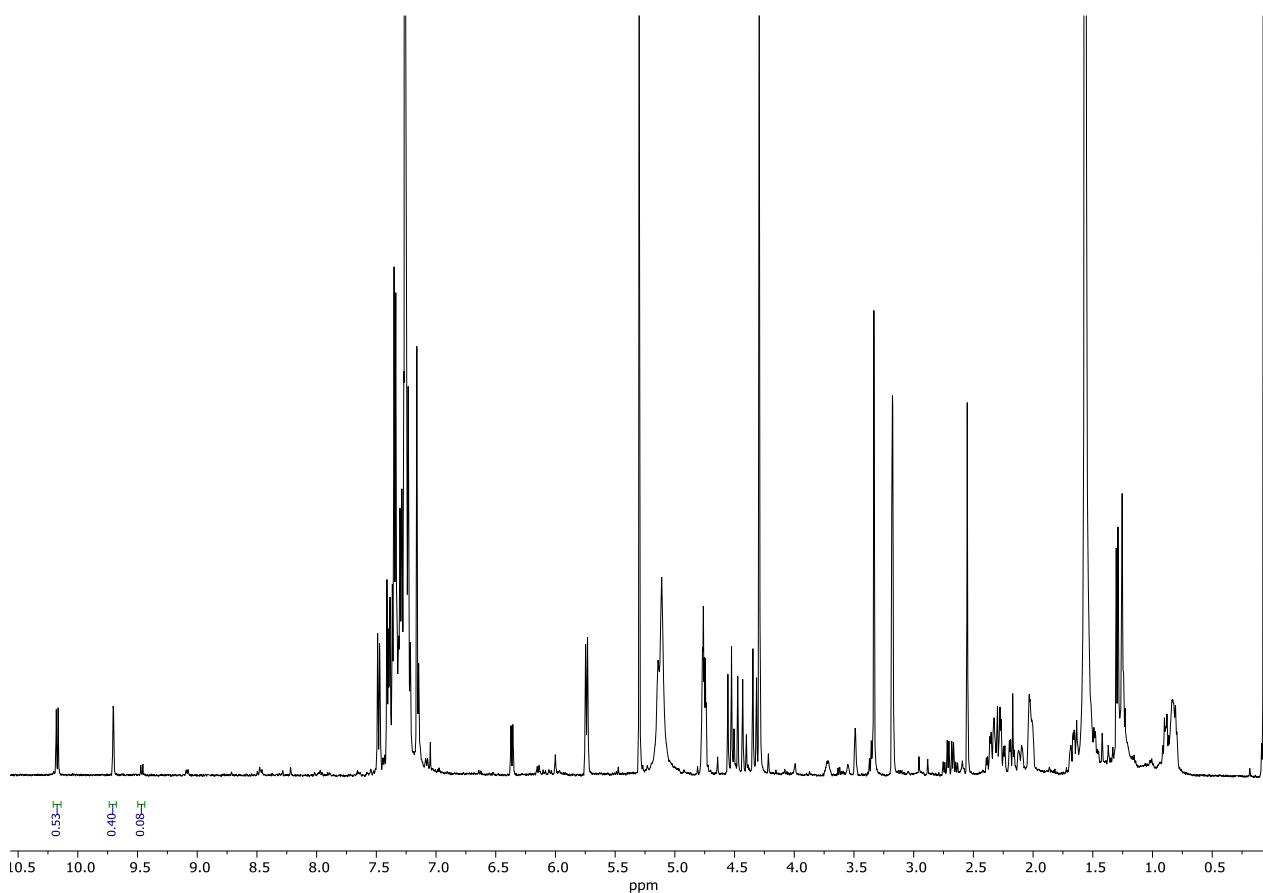
The estimated conversion of (*E*)-3-phenylbut-2-enal (**115**) into 3-phenylbutanal (**139**) is calculated after integration of the product peak at 9.74 ppm with the substrate peak at 10.13 ppm. Formation of side-product (*Z*)-3-phenylbut-2-enal (**139a**) at 9.50 ppm was observed. The spectroscopic data of **139** are the following: <sup>1</sup>H-NMR (500 MHz, CDCl<sub>3</sub>), δ: 9.74 (t, *J*= 2.0 Hz, 1H), 7.35-7.28 (m, 2H), 7.26-7.18 (m, 3H), 3.35-3.31 (m, 1H), 2.74 (ddd, *J*= 16.5, 7.2 and 2.0 Hz, 1H), 2.68 (ddd, *J*= 16.5, 7.2 and 2.0 Hz, 1H), 1.31 (d, *J*= 7.0 Hz, 3H). These data matched those reported in the literature.<sup>318, 323</sup>



Compound	Integration	% Conversion
<b>115</b> (Starting material)	0.59	59
<b>139a</b> (Side-product)	0.13	13
<b>139</b> (Product)	0.29	29

### 6.3.8.2 Transfer hydrogenation to (*E*)-3-(*p*-chlorophenyl) but-2-enal

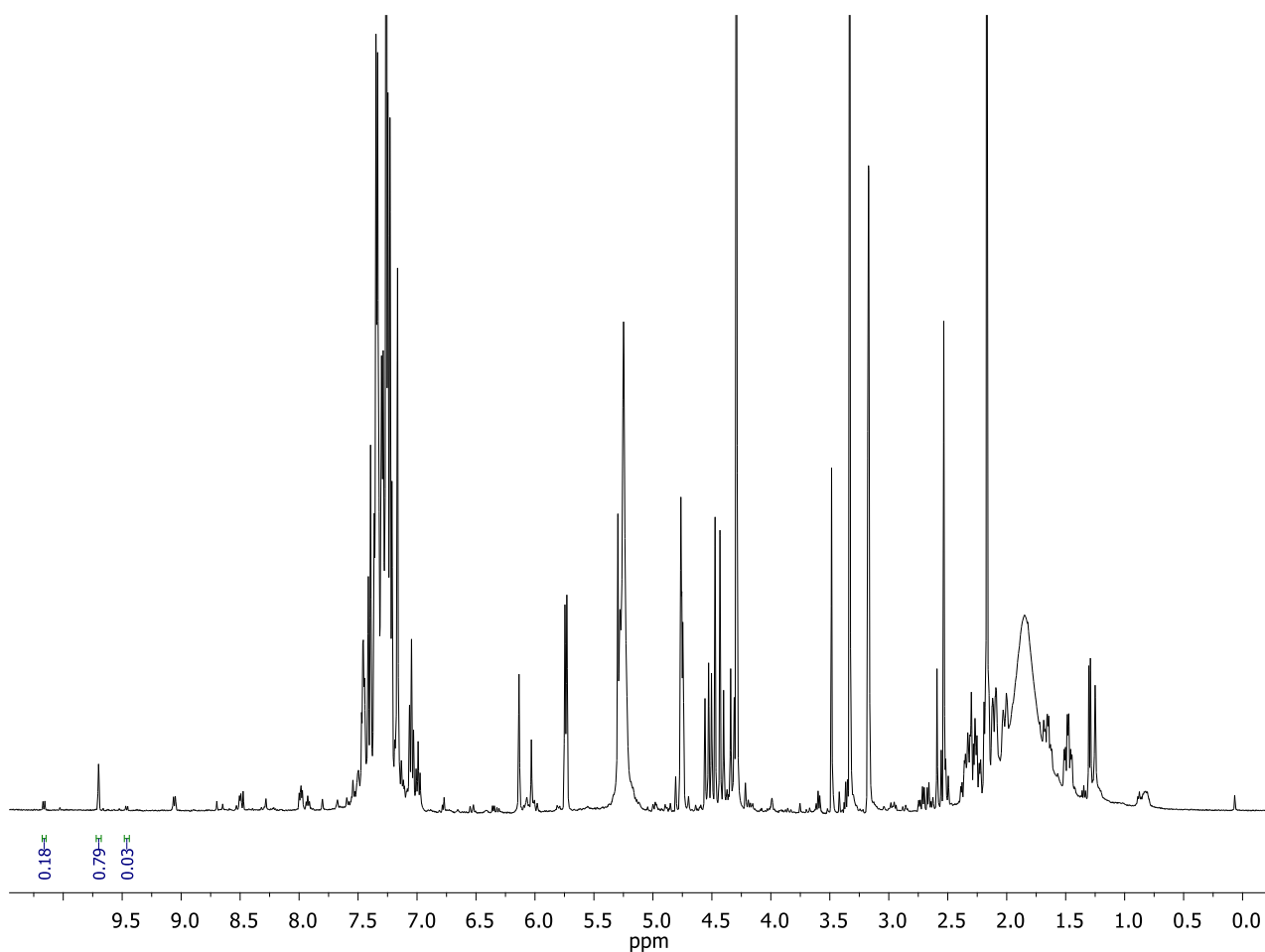
The estimated conversion of (*E*)-3-(*p*-chlorophenyl) but-2-enal (**116**) into 3-(*p*-chlorophenyl) butanal (**140**) is calculated after integration of the product peak at 9.67 ppm with the substrate peak at 10.17 ppm. Formation of side-product (*Z*)-3-(*p*-chlorophenyl) but-2-enal (**140a**) at 9.43 ppm was observed. The spectroscopic data of **140** are the following: **<sup>1</sup>H-NMR (500 MHz, CDCl<sub>3</sub>)**,  $\delta$ : 9.67 (t,  $J$ = 2.0 Hz, 1H), 7.28-7.23 (m, 2H), 7.16-7.11 (m, 2H), 3.36-3.28 (m, 1H), 2.73 (ddd,  $J$ = 16.9, 7.0 and 1.8 Hz, 1H), 2.65 (ddd,  $J$ = 16.9, 7.5 and 2.0 Hz, 1H), 1.29 (d,  $J$ = 7.0 Hz, 3H). These data matched those reported in the literature.<sup>318</sup>



Compound	Integration	% Conversion
<b>116</b> (Starting material)	0.53	53
<b>140a</b> (Side-product)	0.08	8
<b>140</b> (Product)	0.40	40

### 6.3.8.3 Transfer hydrogenation to (*E*)-3-(*p*-fluorophenyl) but-2-enal

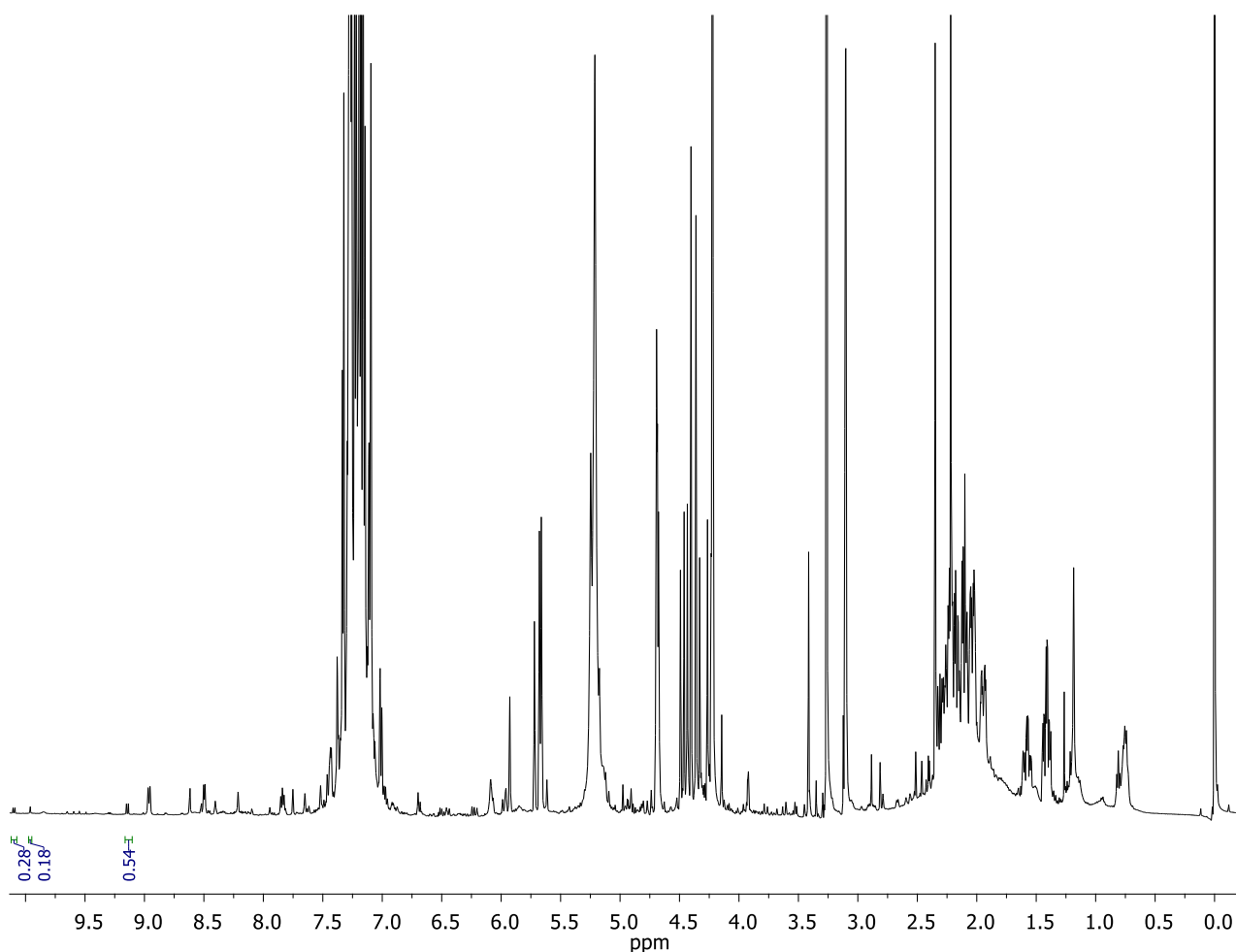
The estimated conversion of (*E*)-3-(*p*-fluorophenyl) but-2-enal (**117**) into 3-(*p*-fluorophenyl) butanal (**141**) is calculated after integration of the product peak at 9.68 ppm with the substrate peak at 10.07 ppm. Formation of side-product (*Z*)-3-(*p*-fluorophenyl) but-2-enal (**141a**) at 9.44 ppm was observed. The spectroscopic data of **141** are the following:  $^1\text{H-NMR}$  (500 MHz,  $\text{CDCl}_3$ ),  $\delta$ : 9.68 (t,  $J = 2.0$  Hz, 1H), 7.20-7.16 (m, 2H), 7.04-6.98 (m, 2H), 3.36-3.31 (m, 1H), 2.71 (ddd,  $J = 16.9, 7.0$  and  $1.8$  Hz, 1H), 2.64 (ddd,  $J = 16.9, 7.5$  and  $2.0$  Hz, 1H), 1.30 (d,  $J = 7.0$  Hz, 3H). These data matched those reported in the literature.<sup>324</sup>



Compound	Integration	% Conversion
<b>117</b> (Starting material)	0.18	18
<b>141a</b> (Side-product)	0.03	3
<b>141</b> (Product)	0.79	79

### 6.3.8.4 Transfer hydrogenation to (*E*)-3-(*o*-tolyl) but-2-enal

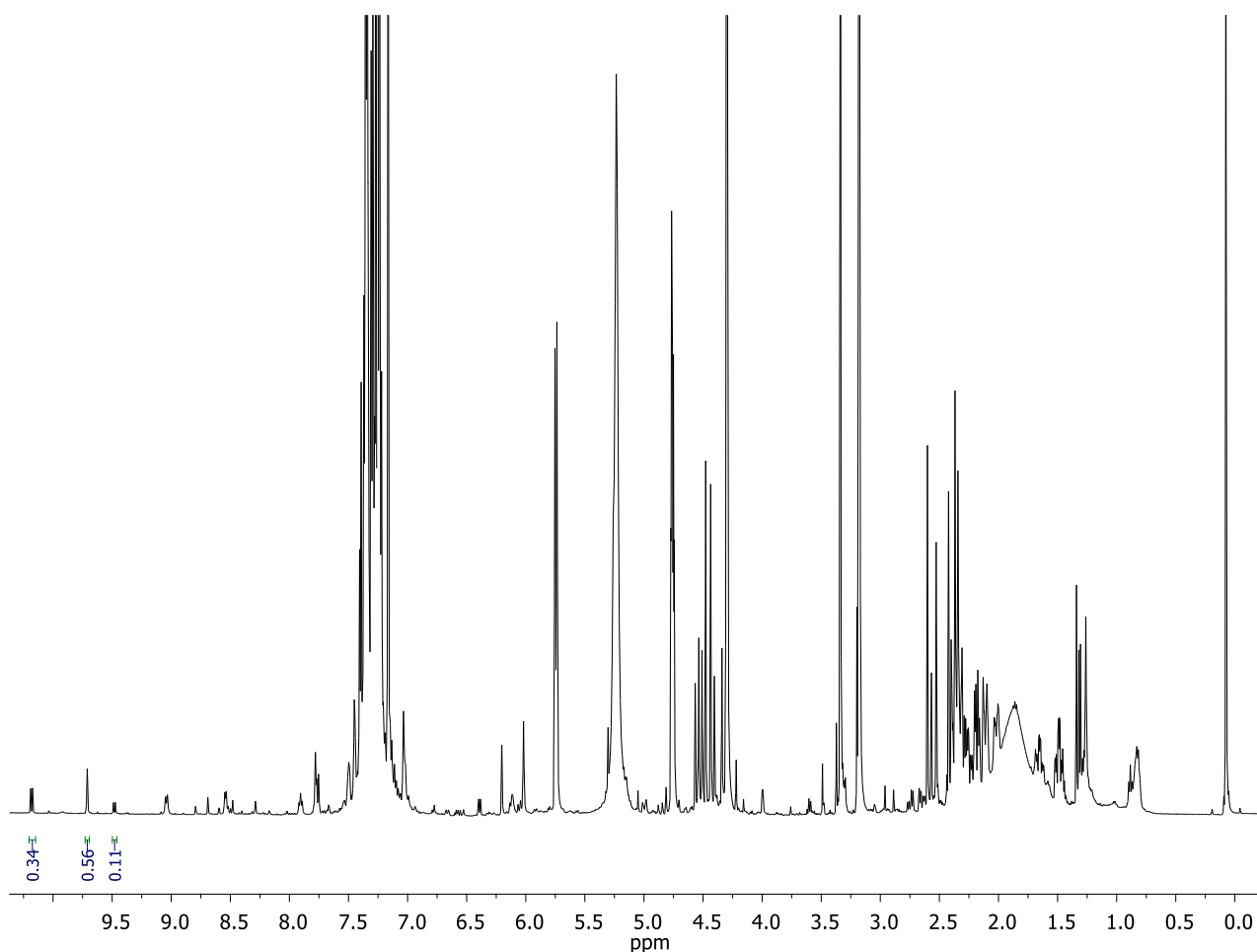
The estimated conversion of (*E*)-3-(*o*-tolyl) but-2-enal (**118**) into 3-(*o*-tolyl) butanal (**142**) is calculated after integration of the substrate peak at 10.17 ppm with the side-product (*Z*)-3-(*o*-tolyl) but-2-enal (**142a**) peak at 9.14 ppm was observed. The spectroscopic data of **142** are the following:  $^1\text{H-NMR}$  (500 MHz,  $\text{CDCl}_3$ ),  $\delta$ : 9.71 (t,  $J = 2.0$  Hz, 1H), 7.23-7.14 (m, 2H), 7.10-7.05 (m, 2H), 3.65-3.54 (m, 1H), 2.80 (ddd,  $J = 16.9, 7.0$  and  $1.8$  Hz, 1H), 2.64 (ddd,  $J = 16.9, 7.5$  and  $2.0$  Hz, 1H), 2.37 (s, 3H), 1.27 (d,  $J = 7.0$  Hz, 3H). These data matched those reported in the literature.<sup>324</sup>



Compound	Integration	% Conversion
<b>118</b> (Starting material)	0.28	28
<b>142a</b> (Side-product)	0.54	54
<b>142</b> (Product)	0.19	19

### 6.3.8.5 Transfer hydrogenation to (*E*)-3-(*m*-tolyl) but-2-enal

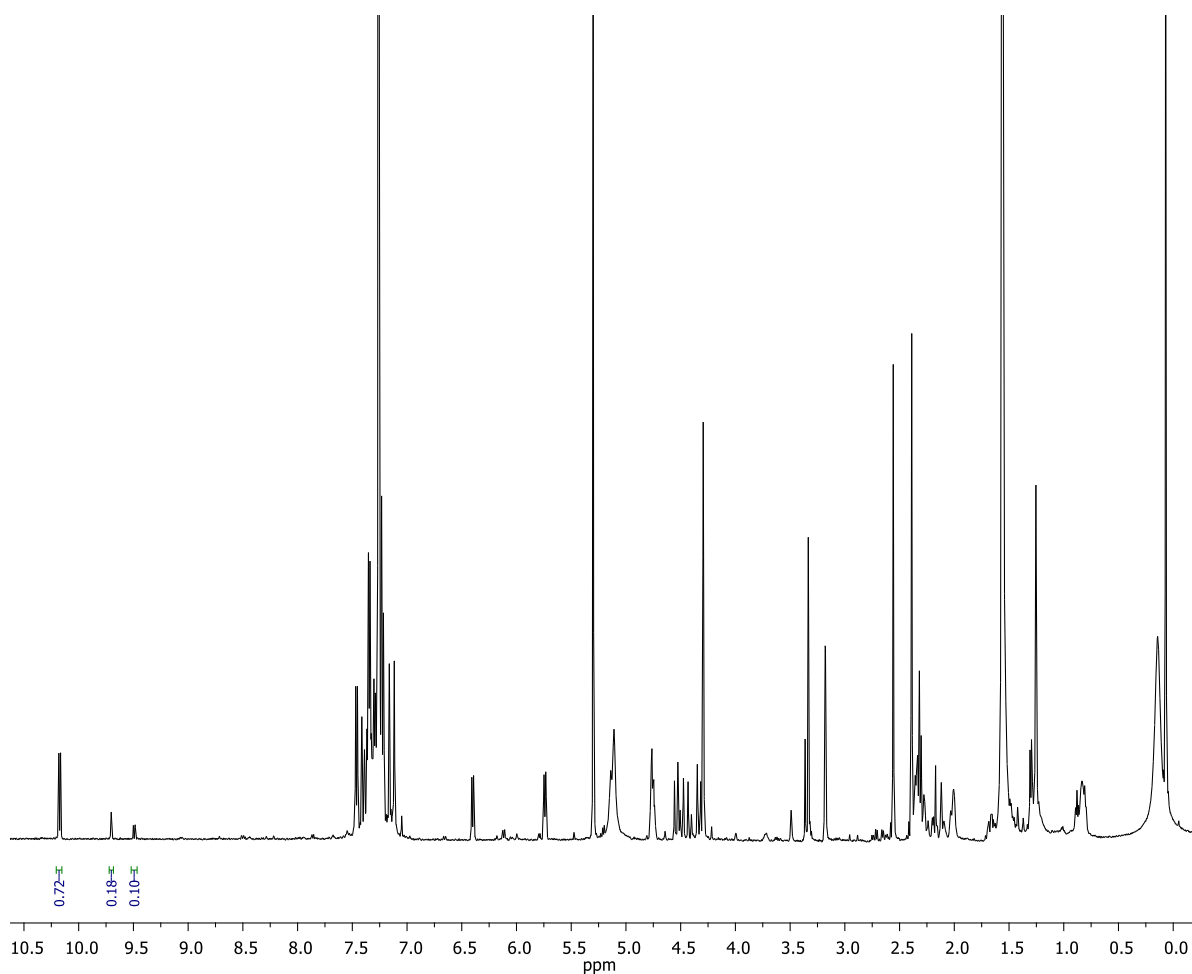
The estimated conversion of (*E*)-3-(*m*-tolyl) but-2-enal (**119**) into 3-(*m*-tolyl) butanal (**143**) is calculated after integration of the product peak at 9.68 ppm with the substrate peak at 10.15 ppm. Formation of side-product (*Z*)-3-(*m*-tolyl) but-2-enal (**143a**) at 9.44 ppm was observed. The spectroscopic data of **143** are the following:  $^1\text{H-NMR}$  (500 MHz,  $\text{CDCl}_3$ ),  $\delta$ : 9.68 (t,  $J=2.0$  Hz, 1H), 7.25-7.16 (m, 2H), 7.08-7.01 (m, 2H), 3.42-3.31 (m, 1H), 2.78 (ddd,  $J=16.9, 7.0$  and 1.8 Hz, 1H), 2.61 (ddd,  $J=16.9, 7.5$  and 2.0 Hz, 1H), 2.33 (s, 3H), 1.30 (d,  $J=7.0$  Hz, 3H). These data matched those reported in the literature.<sup>324</sup>



Compound	Integration	% Conversion
<b>119</b> (Starting material)	0.34	34
<b>143a</b> (Side-product)	0.11	11
<b>143</b> (Product)	0.56	56

### 6.3.8.6 Transfer hydrogenation to (*E*)-3-(*p*-tolyl) but-2-enal

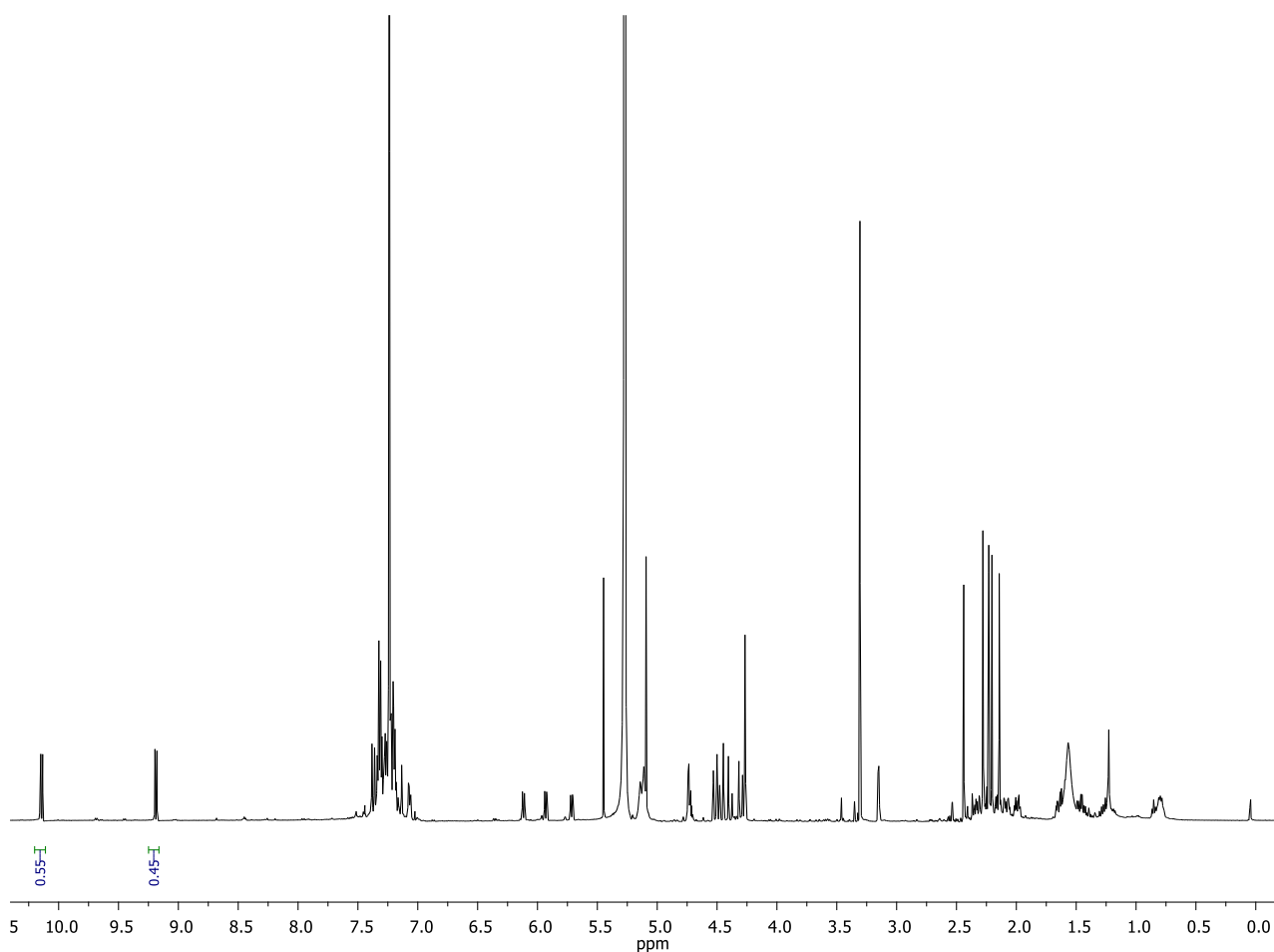
The estimated conversion of (*E*)-3-(*p*-tolyl) but-2-enal (**120**) into 3-(*p*-tolyl) butanal (**144**) is calculated after integration of the product peak at 9.70 ppm with the substrate peak at 10.07 ppm. Formation of side-product (*Z*)-3-(*p*-tolyl) but-2-enal (**144a**) at 9.48 ppm was observed. The spectroscopic data of **144** are the following:  $^1\text{H-NMR}$  (500 MHz,  $\text{CDCl}_3$ ),  $\delta$ : 9.70 (t,  $J=2.0$  Hz, 1H), 7.18-7.06 (m, 4H), 3.39-3.32 (m, 1H), 2.73 (ddd,  $J=16.5, 7.0$  and 1.9 Hz, 1H), 2.66 (ddd,  $J=16.5, 7.6$  and 2.2 Hz, 1H), 2.36 (s, 3H), 1.31 (d,  $J=7.0$  Hz, 3H). These data matched those reported in the literature.<sup>318</sup>



Compound	Integration	% Conversion
<b>120</b> (Starting material)	0.72	72
<b>144a</b> (Side-product)	0.10	10
<b>144</b> (Product)	0.18	18

### 6.3.9 $^1\text{H-NMR}$ details for the activity screening of Table 9

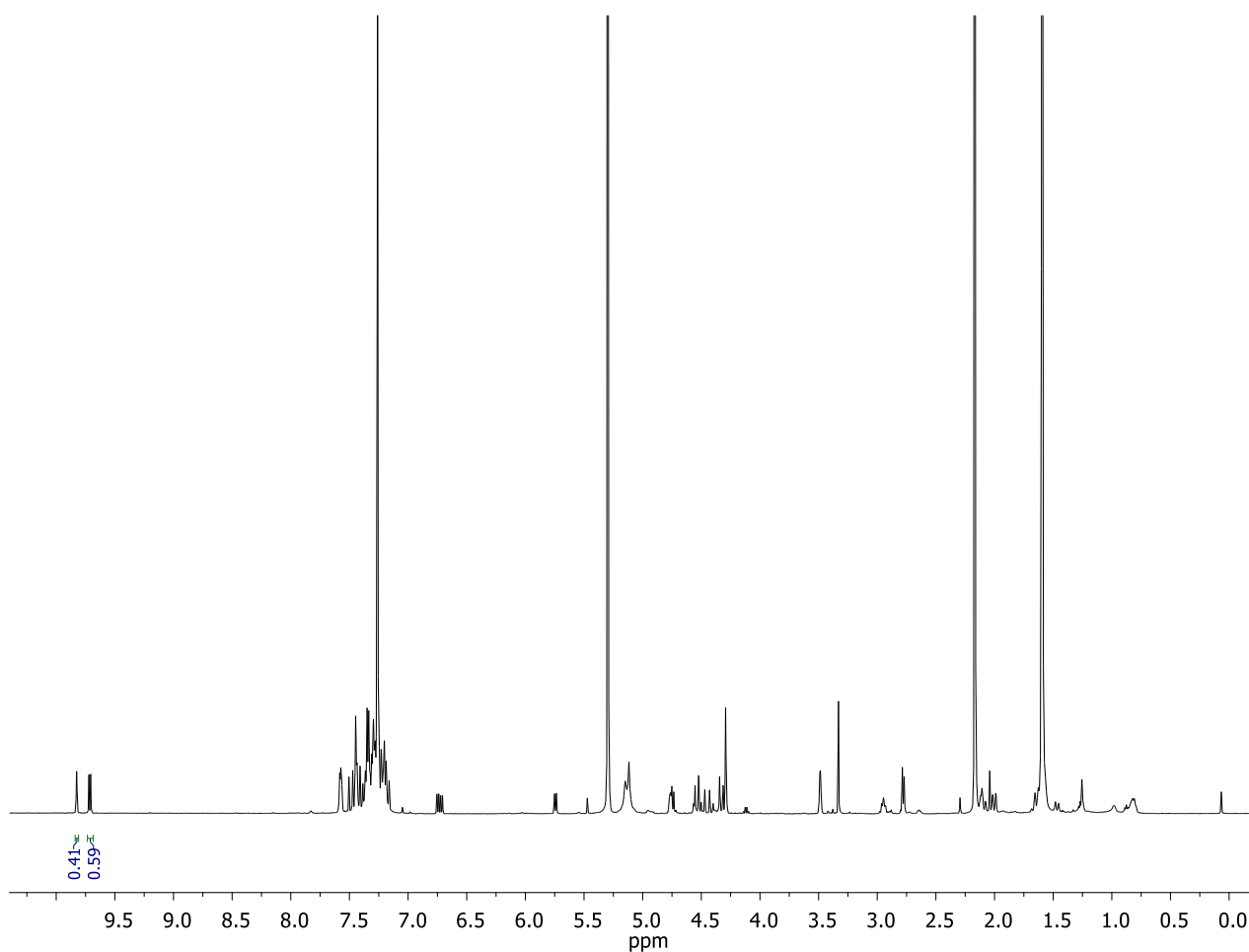
#### 6.3.9.1 Transfer hydrogenation to (*E*)-3-(*o*-tolyl) but-2-enal in presence of BNAH



Compound	Integration	% Conversion
<b>118</b> (Starting material)	0.55	55
<b>142a</b> (Side-product)	0.45	45
<b>142</b> (Product)	/	/

### 6.3.10 $^1\text{H-NMR}$ details for the activity screening of Table 10

#### 6.3.10.1 Transfer hydrogenation to cinnamaldehyde in presence of *d2*-BNAH



Compound	Integration	% Conversion
<b>14</b> (Starting material)	0.59	59
<b>17</b> (Product)	0.41	41



### 6.3.11 Michaelis-Menten kinetics for the reaction between 14 and 87

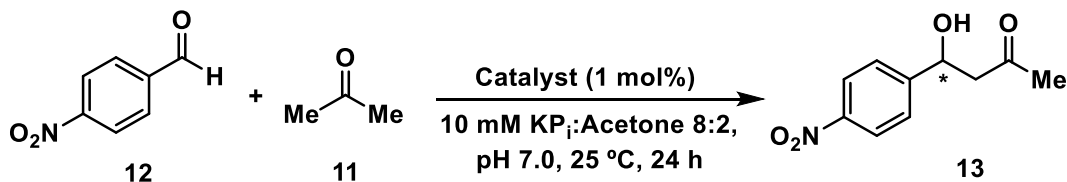
#### 6.3.11.1 Procedure for the kinetic assessment

The pseudo-first order kinetic assessment for the transfer hydrogenation of BNAH (**87**) to cinnamaldehyde (**14**) was setup following the procedure reported in the section 6.3.5.1. Reaction were stopped after 24 h, and the estimated conversion was assessed by <sup>1</sup>H-NMR spectroscopy. Cinnamaldehyde was used at the following concentrations: 0, 0.8, 1.6, 3.3, 4.4, 5.5, 6.6, 7.7 and 8.8 mM. BNAH concentration was maintained constant at 20 mM, meanwhile 0.076 mM of Sav:**73** complex were employed.

$V_{\max}$	$k_{\text{cat}}$	$K_M$	$k_{\text{cat}} / K_M$
$3.5 \pm 0.5 \text{ mM}\cdot\text{h}^{-1}$	$46.9 \pm 0.3 \text{ h}^{-1}$	$1.5 \pm 0.7 \text{ mM}$	$30.1 \pm 0.5 \text{ mM}^{-1} \text{ h}^{-1} (9.4 \text{ M}^{-1}\cdot\text{s}^{-1})$

## 6.4 Tetrameric streptavidin as host for enamine catalysis

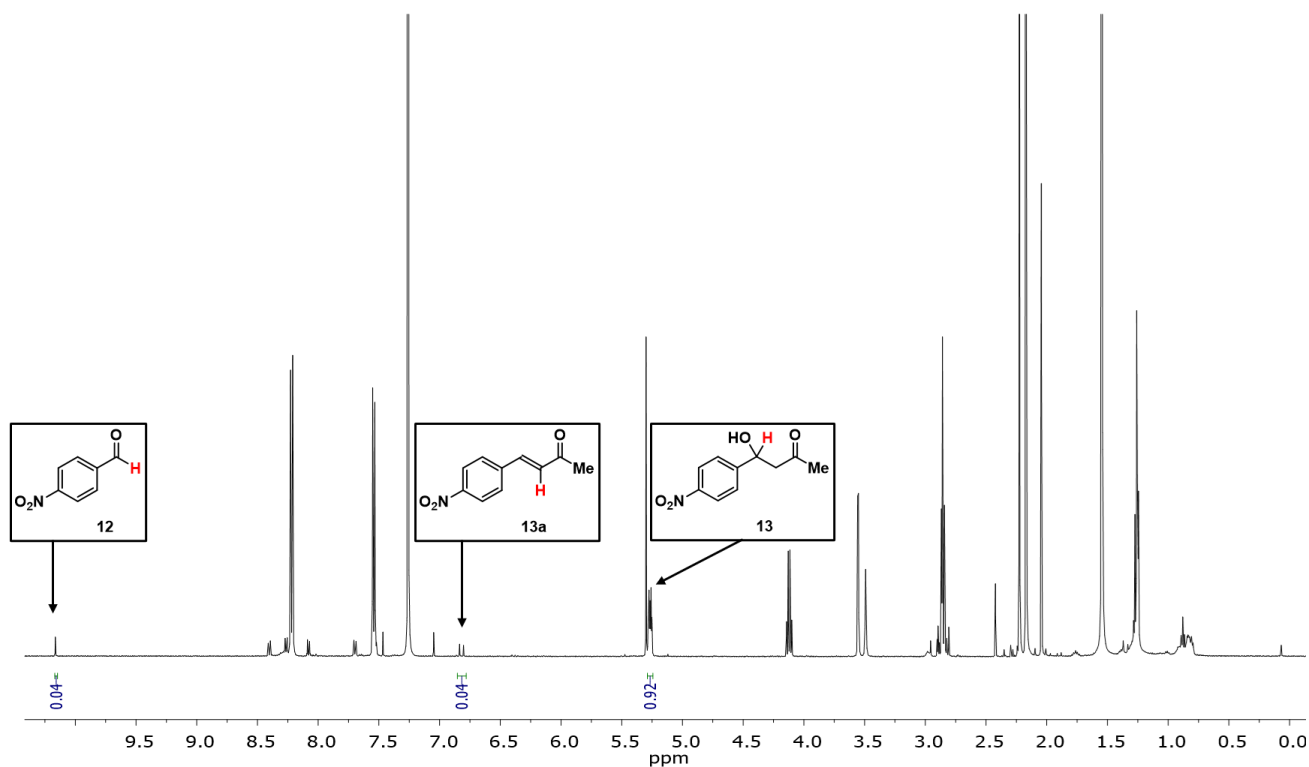
### 6.4.1 General procedure for the $^1\text{H-NMR}$ based screening for yield determination



A stock solution of catalyst **73** (0.50 mg, 1.59  $\mu\text{mol}$ ) was prepared dissolving the catalyst in 1 mL of  $\text{KPi}$  (pH 7.0, 10 mM) into a 1.5 mL Eppendorf tube. *p*-Nitrobenzaldehyde (**12**, 20 mg, 132.3  $\mu\text{mol}$ ) was dissolved in 1 mL of acetone (**11**) to create a stock solution. Sav (0.58 mg, 1 mol%, 33 nmol) was weighted into a 1.5 mL Eppendorf tube and dissolved in 379.2  $\mu\text{L}$  of  $\text{KPi}$  (pH 7.0, 10 mM). An aliquot of 20.8  $\mu\text{L}$  (1 mol%) of the catalyst stock solution was added to the Sav Eppendorf tube. Subsequently, an aliquot of 24.9  $\mu\text{L}$  (1 eq.) of the *p*-nitrobenzaldehyde stock solution was added to the Eppendorf tube. An amount of 75.1  $\mu\text{L}$  of acetone was added to reach a final acetone volume of 100  $\mu\text{L}$ . The mixture was shaken at 300 rpm at 25 °C for 24 h. The mixture was extracted with  $\text{CH}_2\text{Cl}_2$  (3 $\times$ 500  $\mu\text{L}$ ) and the organic phase evaporated under reduced pressure. The crude of reaction was dissolved in  $\text{CDCl}_3$  (620  $\mu\text{L}$ ) and subjected to  $^1\text{H-NMR}$  analysis. This procedure was applied for all the aldehydes (**151-160**) screened.

### 6.4.2 $^1\text{H-NMR}$ based determination of the reaction conversion

The product conversion was estimated by measuring the integral ratio between the starting material aldehydic peak (**Fig. 40**, region of the  $^1\text{H}$  spectrum between 9-10 ppm), the elimination product (if formed, region of the  $^1\text{H}$  spectrum between 6-7 ppm) and the  $\text{ArCH(OH)CH}_2$  peak of the product (region of the  $^1\text{H}$  spectrum between 5-6 ppm).



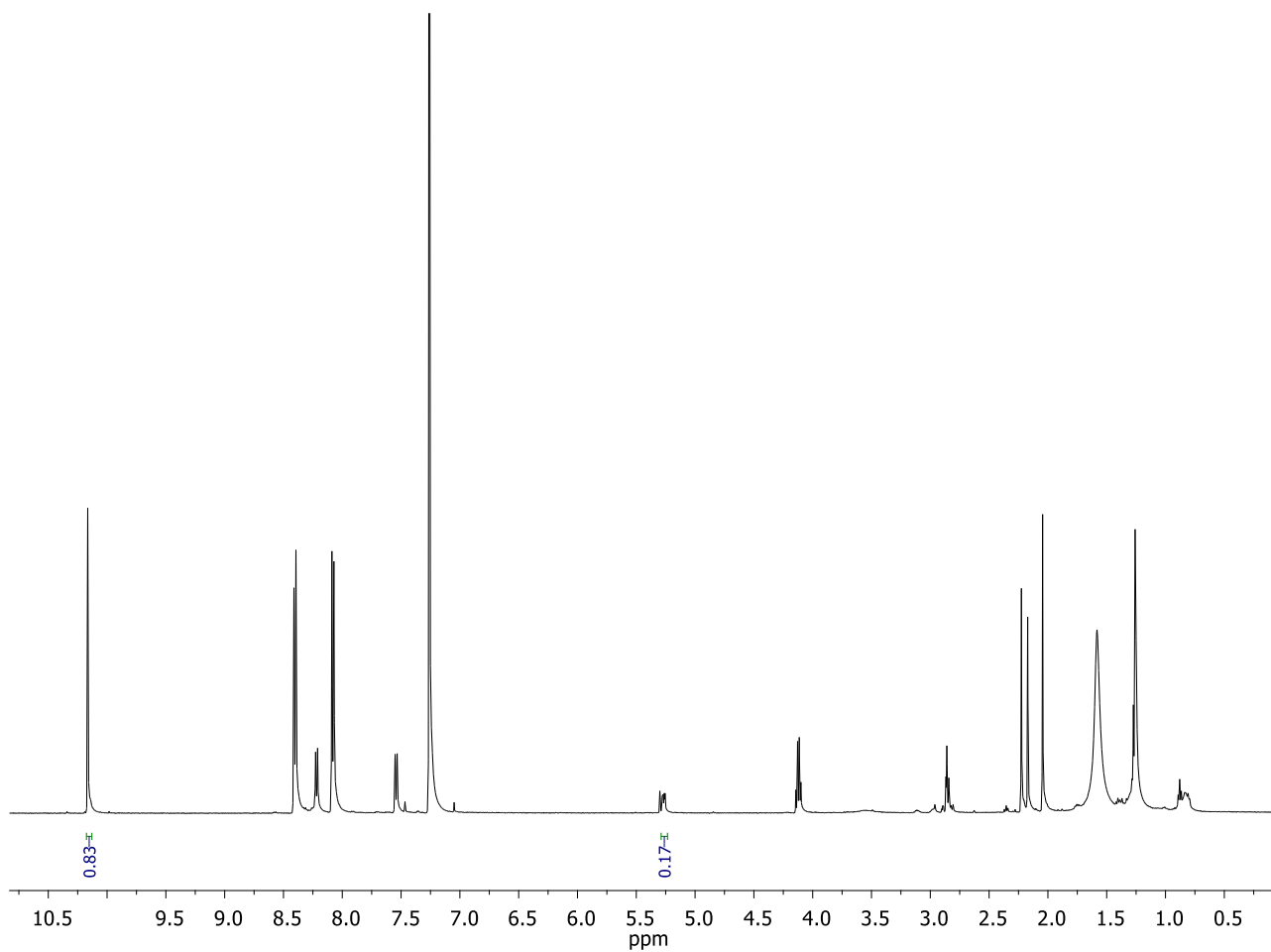
**Figure 36.** <sup>1</sup>H-NMR spectrum of Sav catalysed aldol addition. For the addition of acetone to *p*-nitrobenzaldehyde, each compound (**11**, **13** and **13a**) and relative peaks are reported in the black box. The proton used for integration are drawn in red.

### 6.4.3 <sup>1</sup>H-NMR details for the activity screening of Table 11

The estimated conversion of *p*-nitrobenzaldehyde (**12**) into 4-hydroxy-4-(*p*-nitrophenyl) butan-2-one (**13**) is calculated after integration of the product peak at 5.26 ppm with the substrate peak at 10.15 ppm. Formation of side-product (*E*)-4-(*p*-nitrophenyl) but-3-en-2-one (**13a**) at 6.81 ppm was observed. The spectroscopic data of **13** are the following: **<sup>1</sup>H-NMR (500 MHz, CDCl<sub>3</sub>), δ:** 8.20 (d, *J* = 8.8 Hz, 2H), 7.53 (d, *J* = 8.8 Hz, 2H), 5.26 (m, 1H), 3.61 (br s, 1H), 2.85 (m, 2H), 2.22 (s, 3H) ppm. These data matched those reported in the literature.<sup>294</sup>

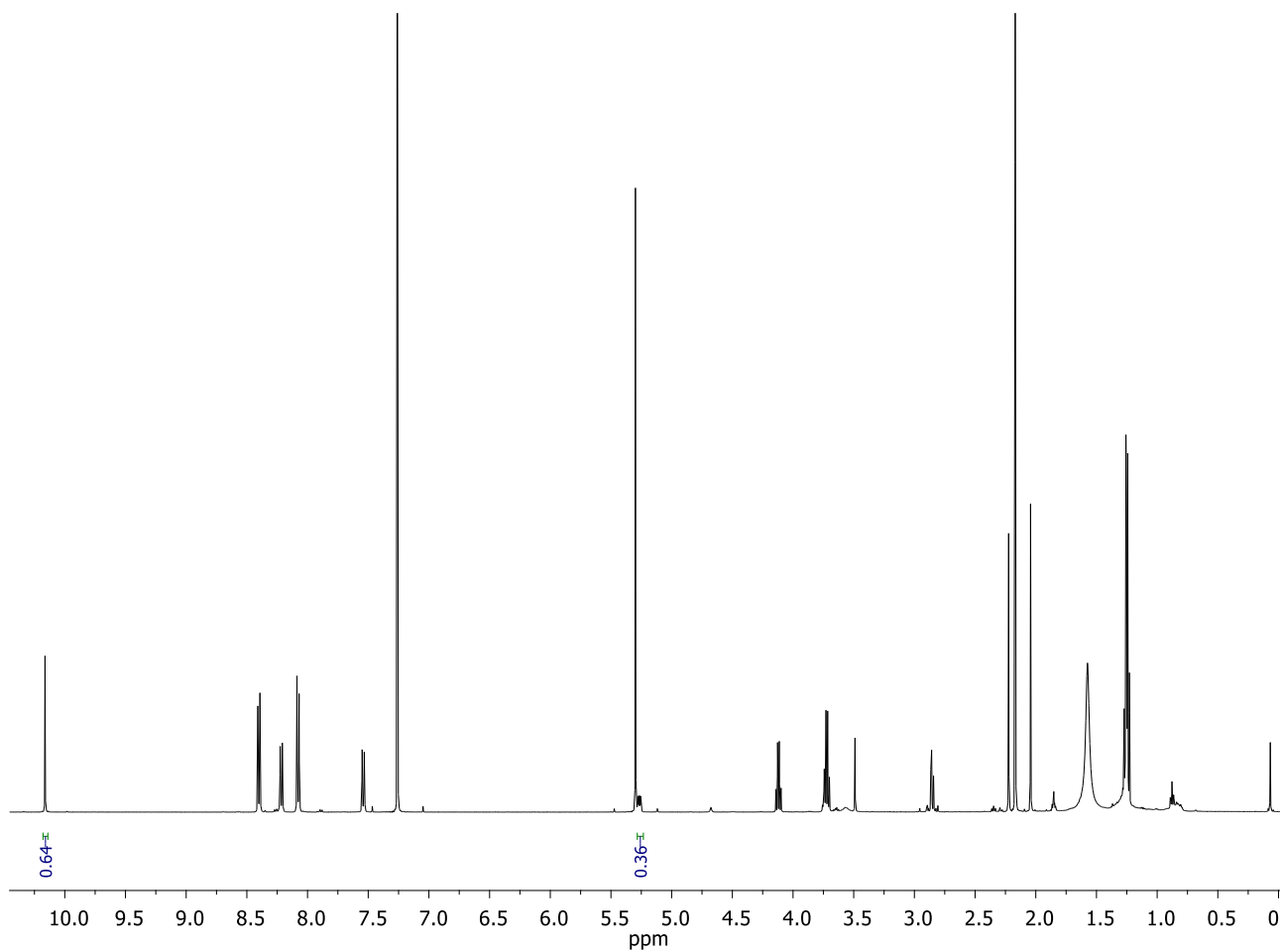
325

## 6.4.3.1 Catalyst screening for aldol additions using no catalyst

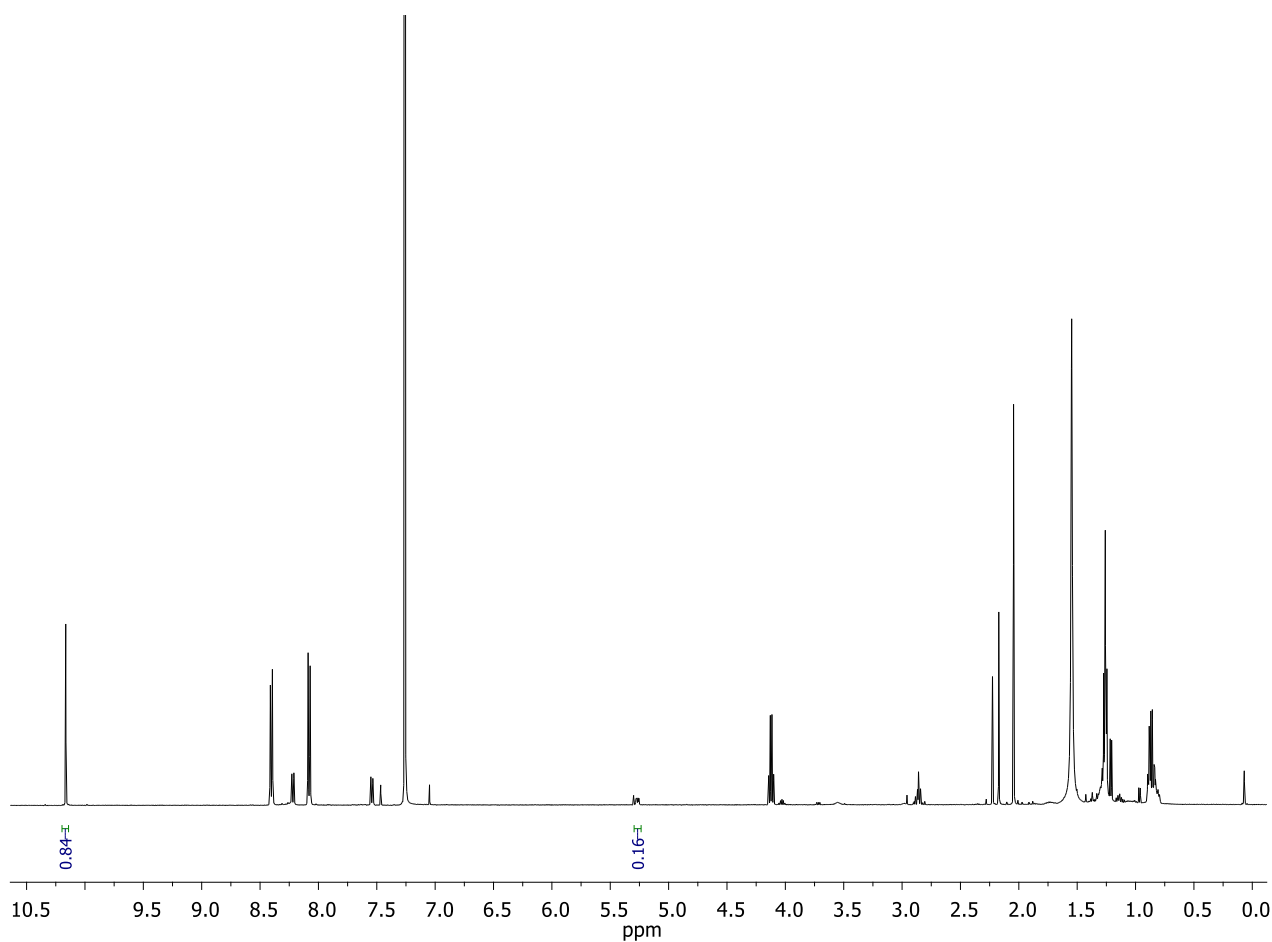


Compound	Integration	% Conversion
<b>11</b> (Starting material)	0.83	83
<b>13</b> (Product)	0.17	17

## 6.4.3.2 Catalyst screening for aldol additions using catalyst 73

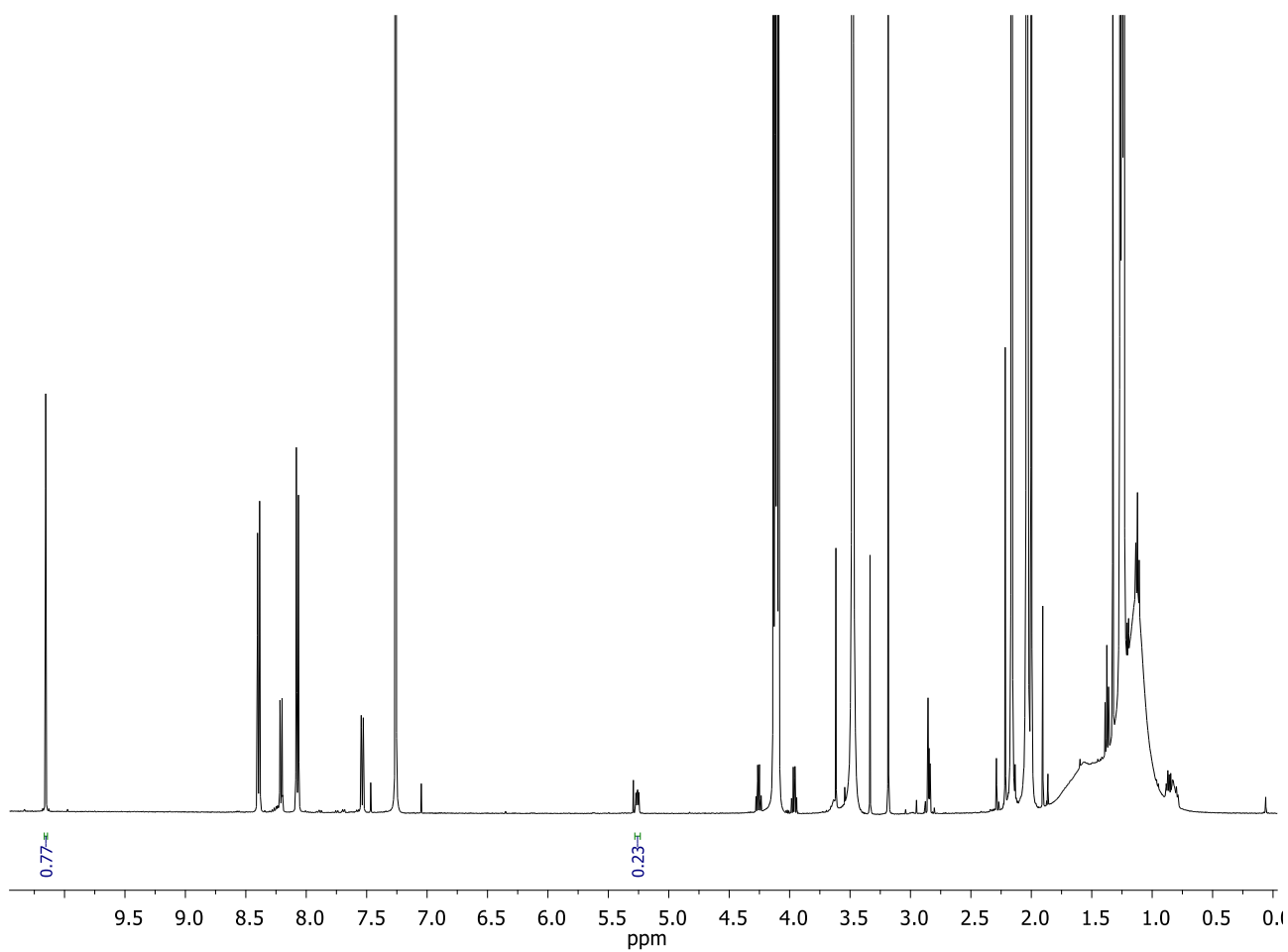


Compound	Integration	% Conversion
<b>11</b> (Starting material)	0.64	64
<b>13</b> (Product)	0.36	36

**6.4.3.3 Catalyst screening for aldol additions using Sav (0.1 mol%)**

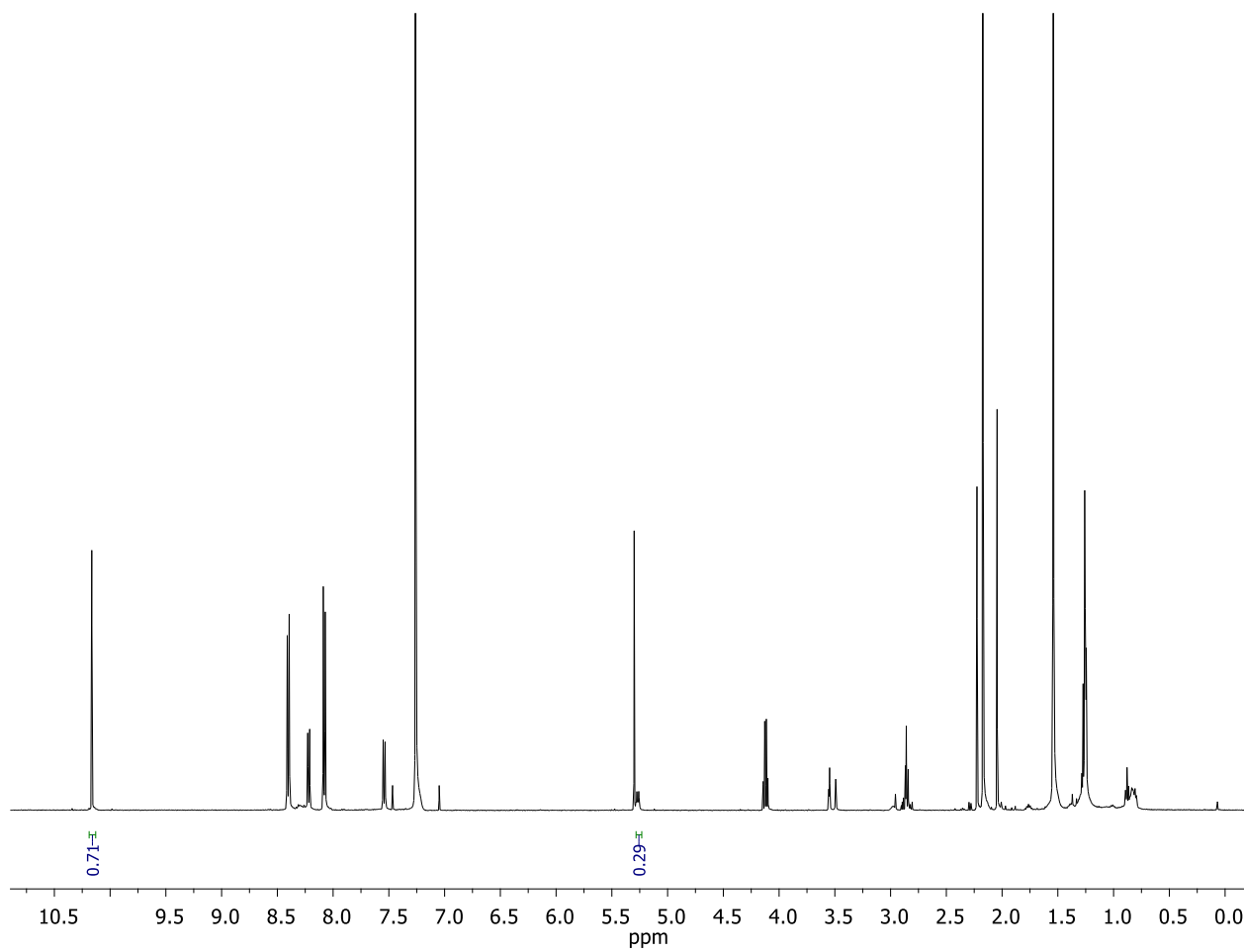
Compound	Integration	% Conversion
<b>11</b> (Starting material)	0.84	84
<b>13</b> (Product)	0.16	16

## 6.4.3.4 Catalyst screening for aldol additions using Sav (0.5 mol%)



Compound	Integration	% Conversion
<b>11</b> (Starting material)	0.77	77
<b>13</b> (Product)	0.23	23

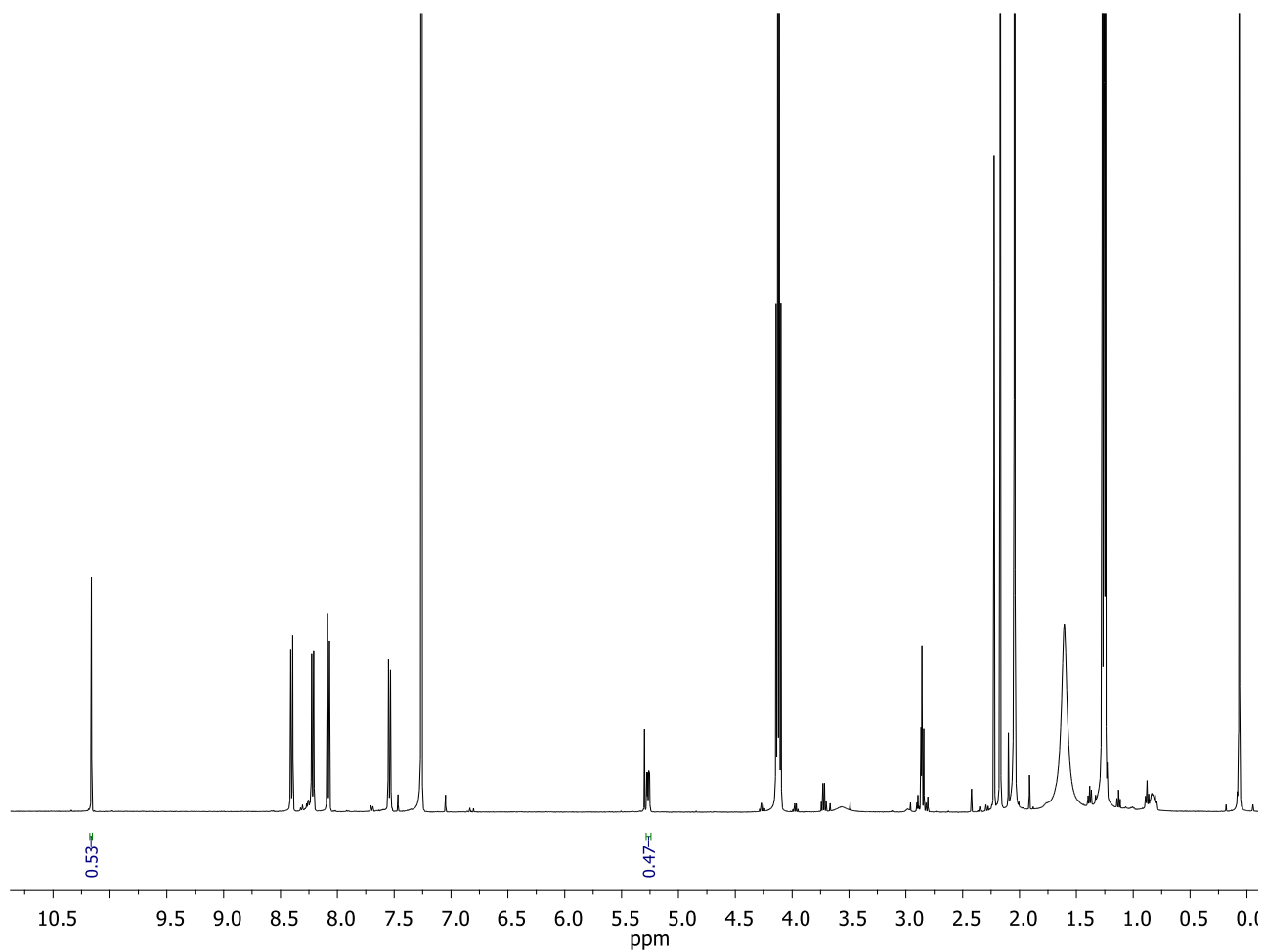
## 6.4.3.5 Catalyst screening for aldol additions using Sav (1 mol%)



Compound	Integration	% Conversion
<b>11</b> (Starting material)	0.71	71
<b>13</b> (Product)	0.29	29

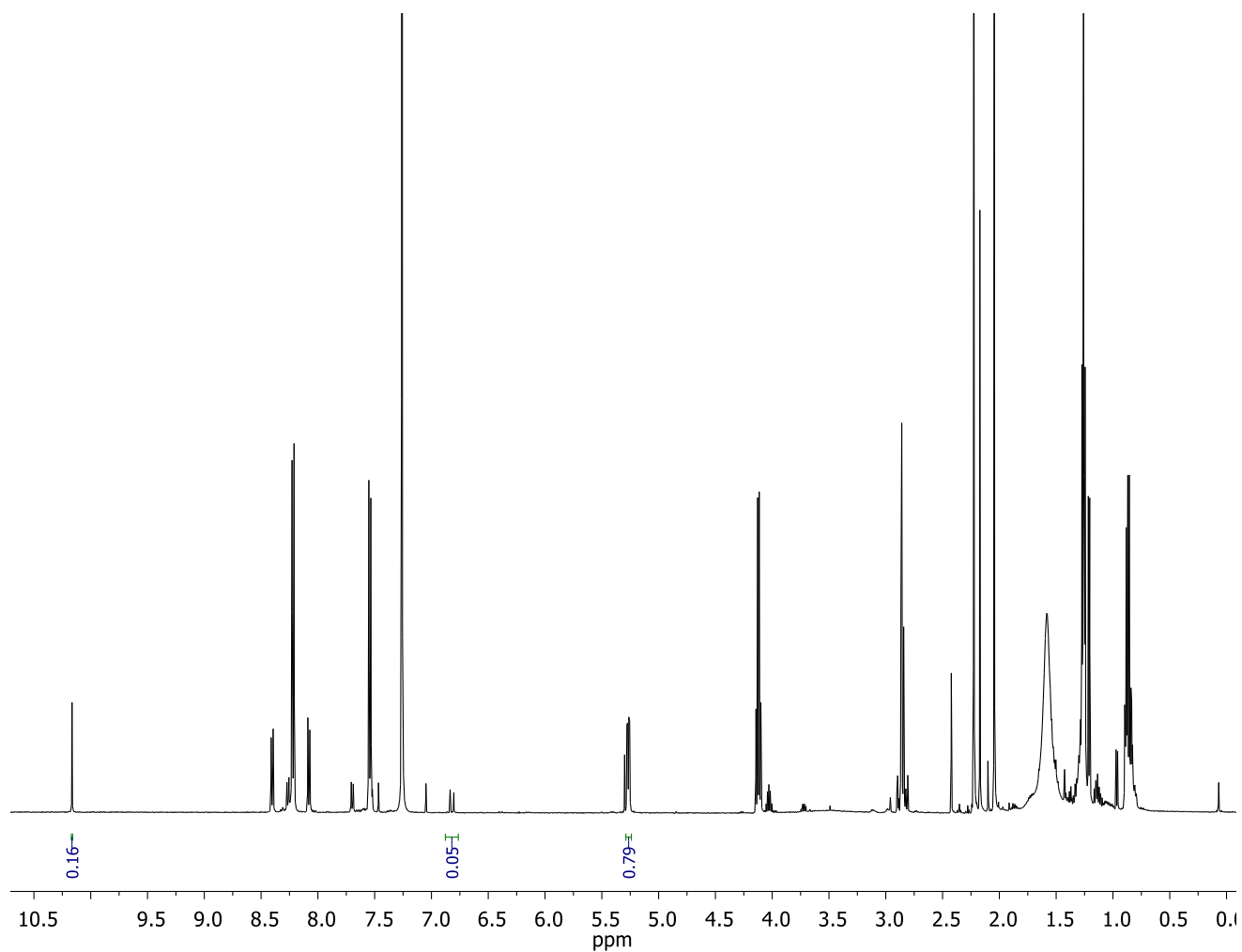


## 6.4.3.6 Catalyst screening for aldol additions using Sav:73 (0.1 mol%)



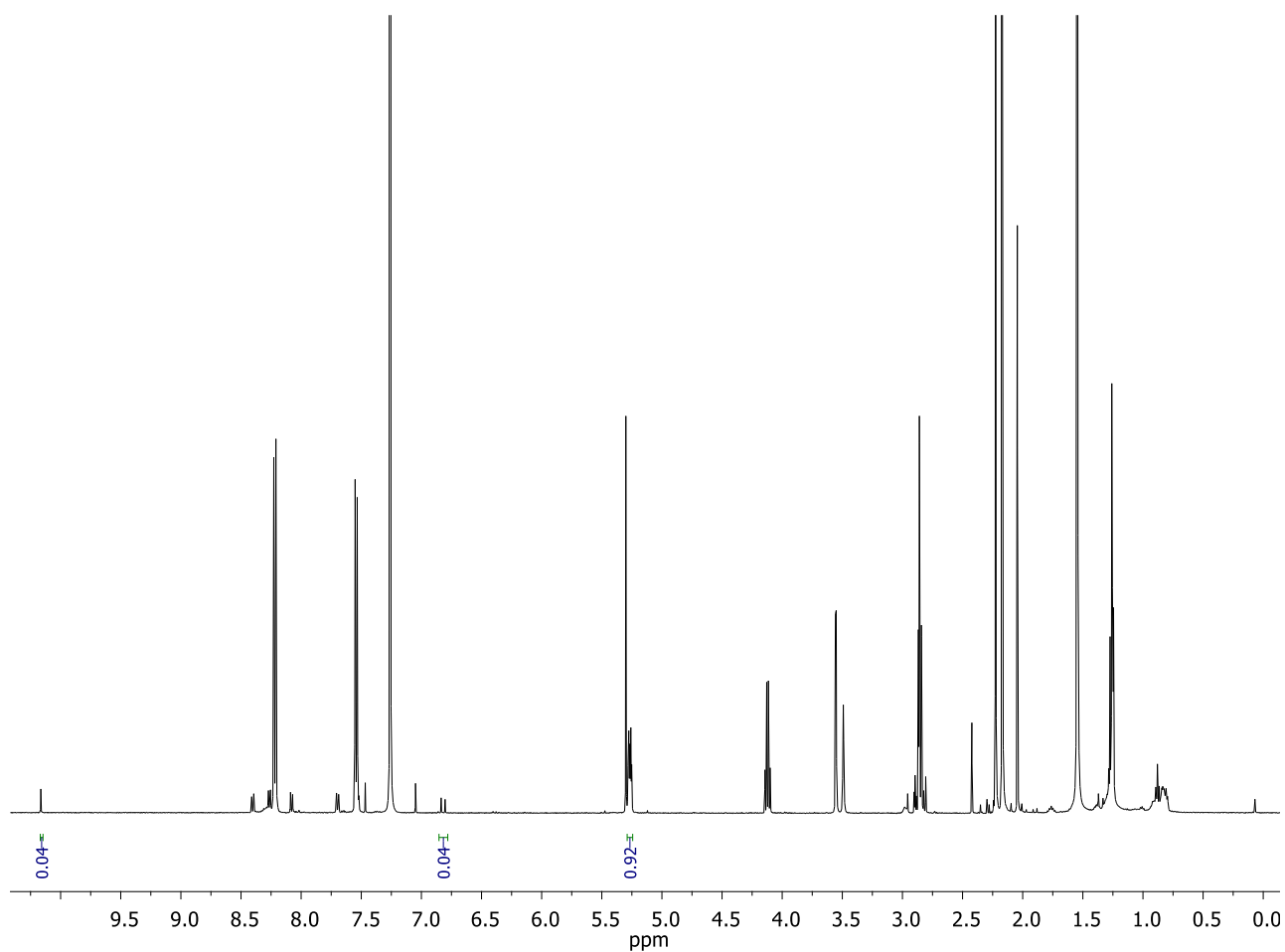
Compound	Integration	% Conversion
<b>11</b> (Starting material)	0.53	53
<b>13</b> (Product)	0.47	47

## 6.4.3.7 Catalyst screening for aldol additions using Sav:73 (0.5 mol%)



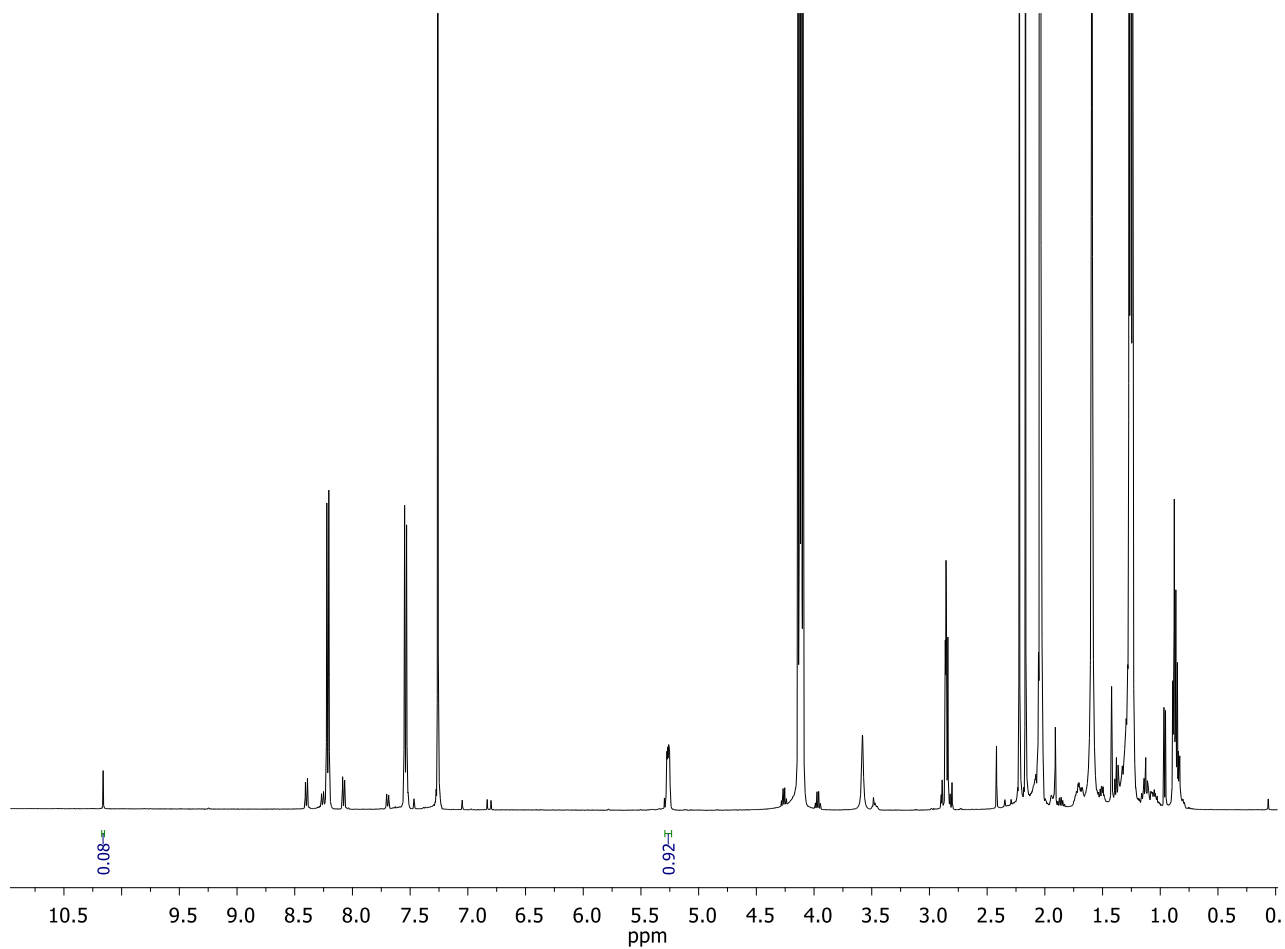
Compound	Integration	% Conversion
<b>11</b> (Starting material)	0.16	16
<b>13a</b> (Side-product)	0.05	5
<b>13</b> (Product)	0.79	79

## 6.4.3.8 Catalyst screening for aldol additions using Sav:73 (1 mol%)



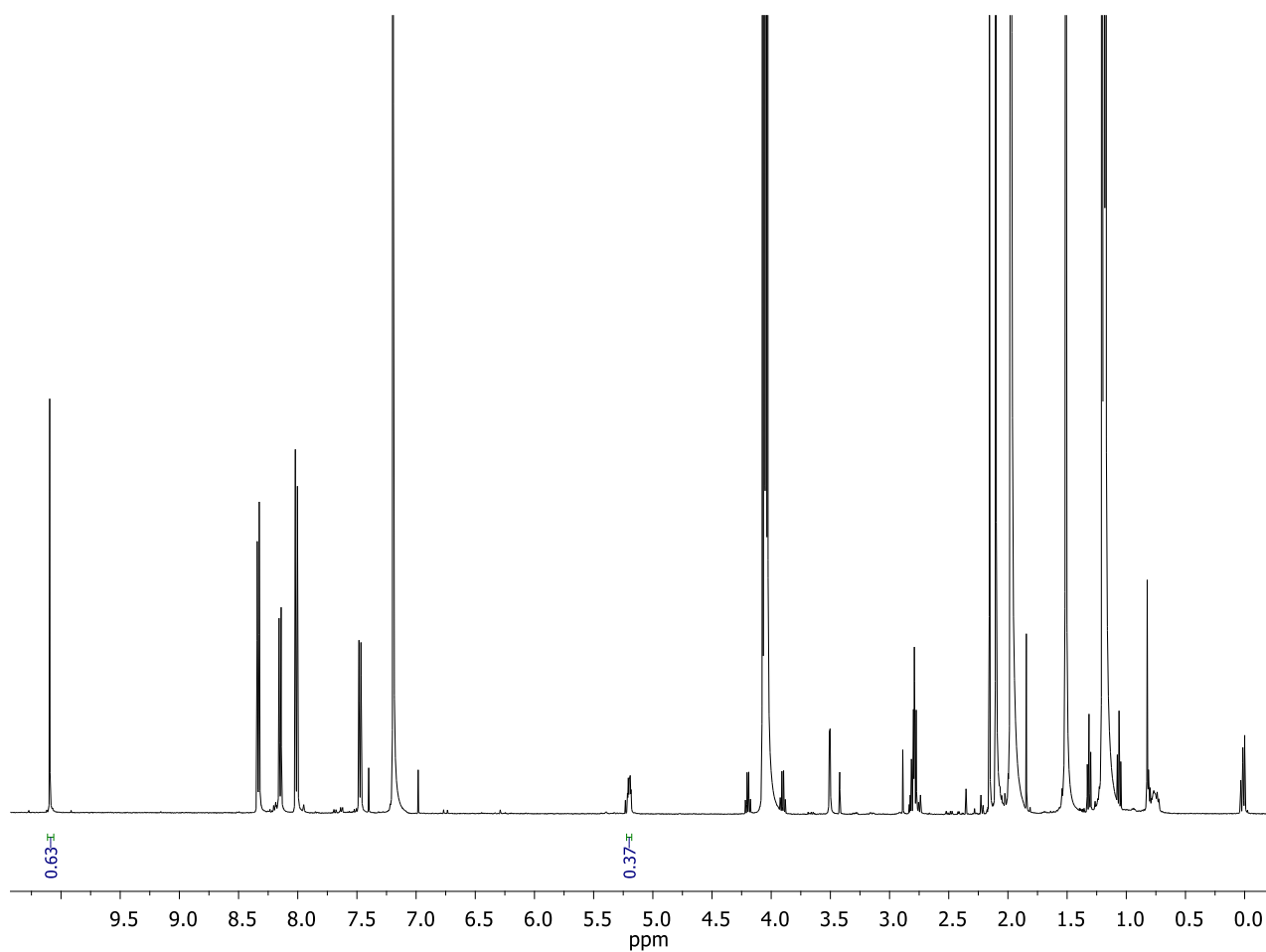
Compound	Integration	% Conversion
<b>11</b> (Starting material)	0.04	4
<b>13a</b> (Side-product)	0.04	4
<b>13</b> (Product)	0.92	92

## 6.4.3.9 Catalyst screening for aldol additions using Sav:73 (1 mol%) and 1 mol% of TFA

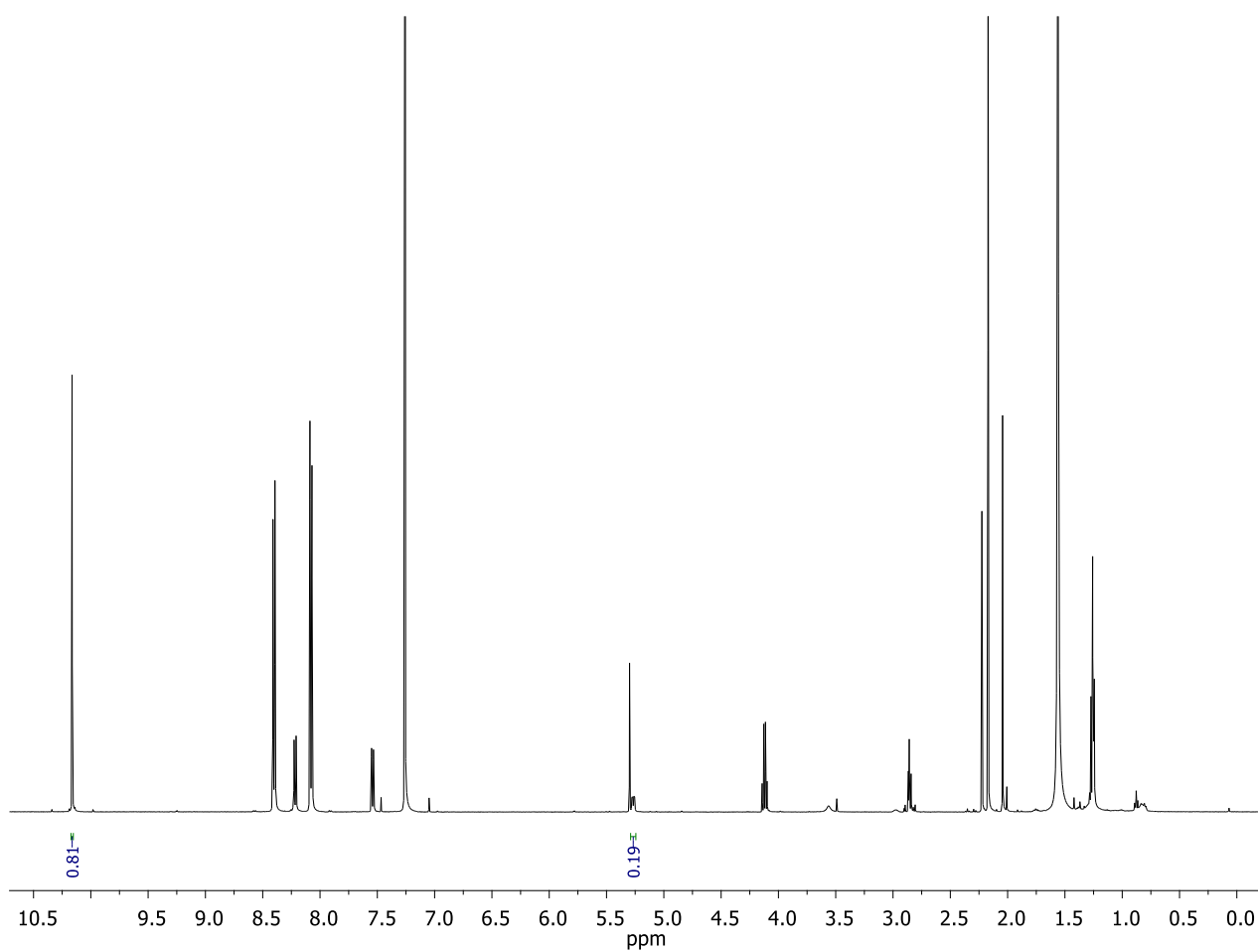


Compound	Integration	% Conversion
<b>11</b> (Starting material)	0.08	8
<b>13</b> (Product)	0.92	92

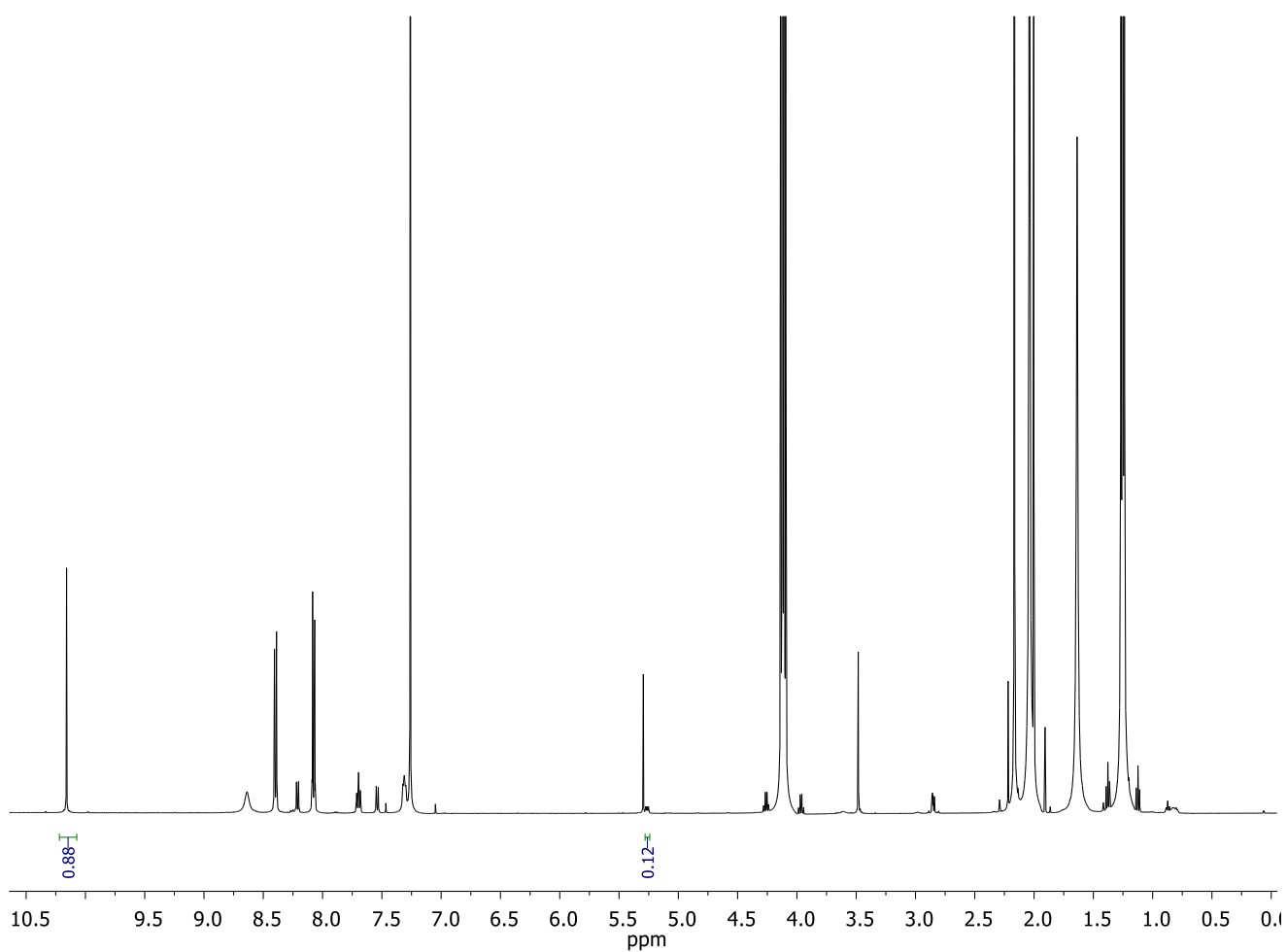
## 6.4.3.10 Catalyst screening for aldol additions using Sav:73 (1 mol%) at 10 °C



Compound	Integration	% Conversion
<b>11</b> (Starting material)	0.63	63
<b>13</b> (Product)	0.37	37

**6.4.3.11 Catalyst screening for aldol additions using Sav:73 (5 equivalents of acetone and 25% methanol)**

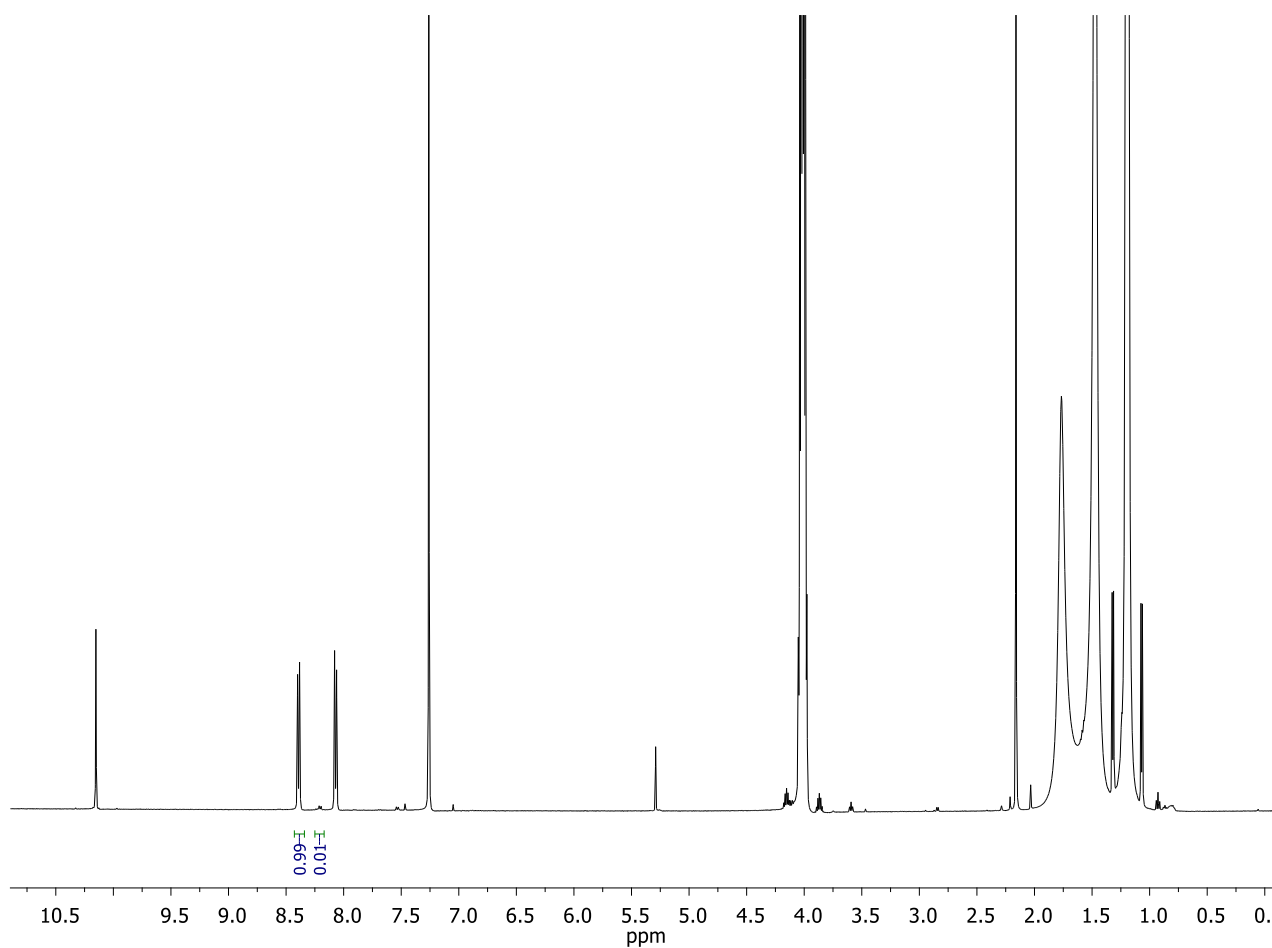
Compound	Integration	% Conversion
<b>11</b> (Starting material)	0.81	81
<b>13</b> (Product)	0.19	19

**6.4.3.12 Catalyst screening for aldol additions using Sav:73 (5 equivalents of acetone and 25% acetonitrile)**

Compound	Integration	% Conversion
<b>11</b> (Starting material)	0.88	88
<b>13</b> (Product)	0.12	12

**6.4.3.13 Catalyst screening for aldol additions using Sav:73 (5 equivalents of acetone and 25% iso-propanol)**

Integrations of starting material and product was performed using the aromatic peaks as standard.

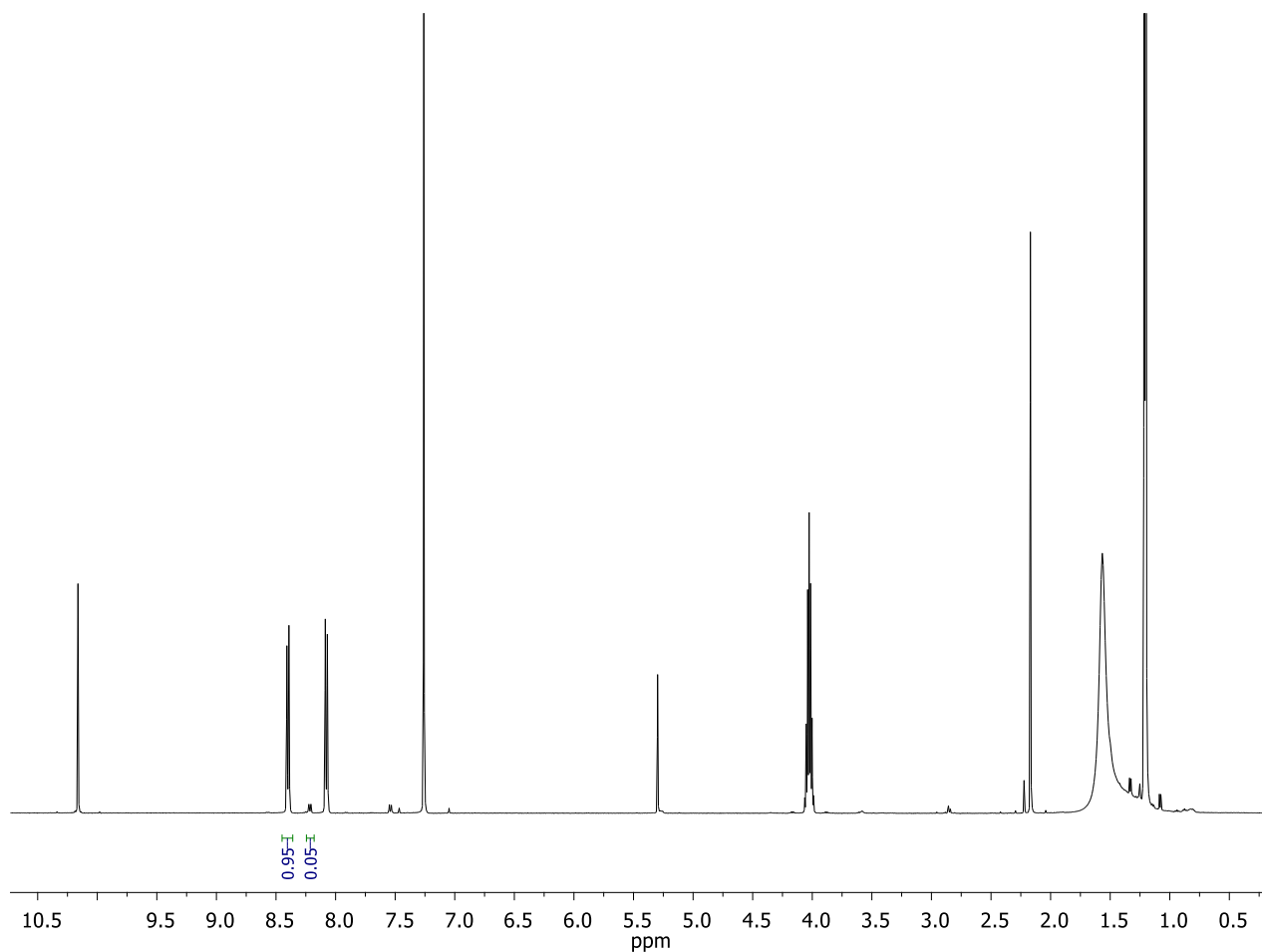


Compound	Integration	% Conversion
<b>11</b> (Starting material)	0.99	99
<b>13</b> (Product)	0.01	1

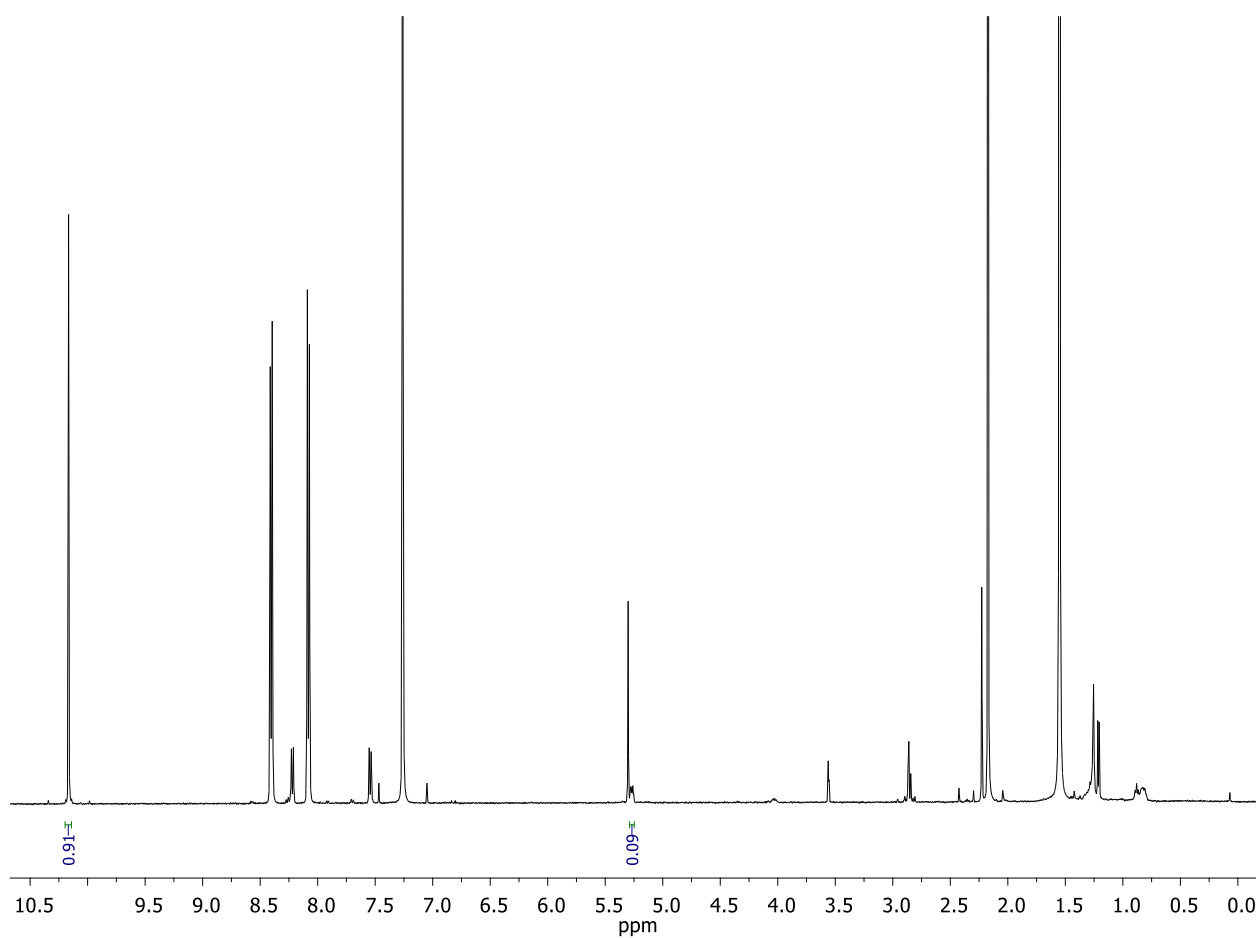


**6.4.3.14 Catalyst screening for aldol additions using Sav:73 (10 equivalents of acetone and 25% iso-propanol)**

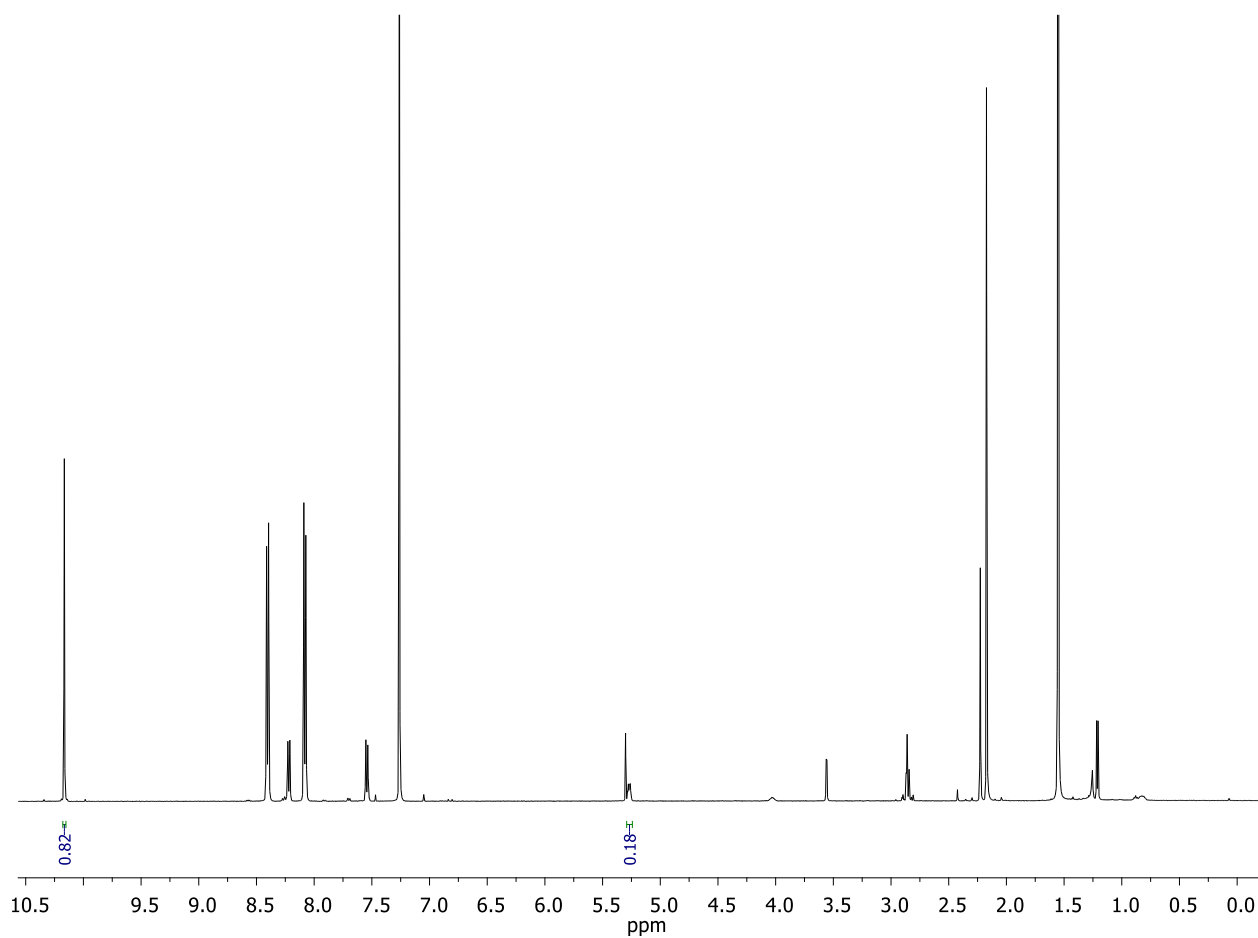
Integrations of starting material and product has been made using the aromatic peaks as standard.



Compound	Integration	% Conversion
<b>11</b> (Starting material)	0.95	95
<b>13</b> (Product)	0.05	5

**6.4.3.15 Catalyst screening for aldol additions using Sav:73 (20 equivalents of acetone and 25% iso-propanol)**

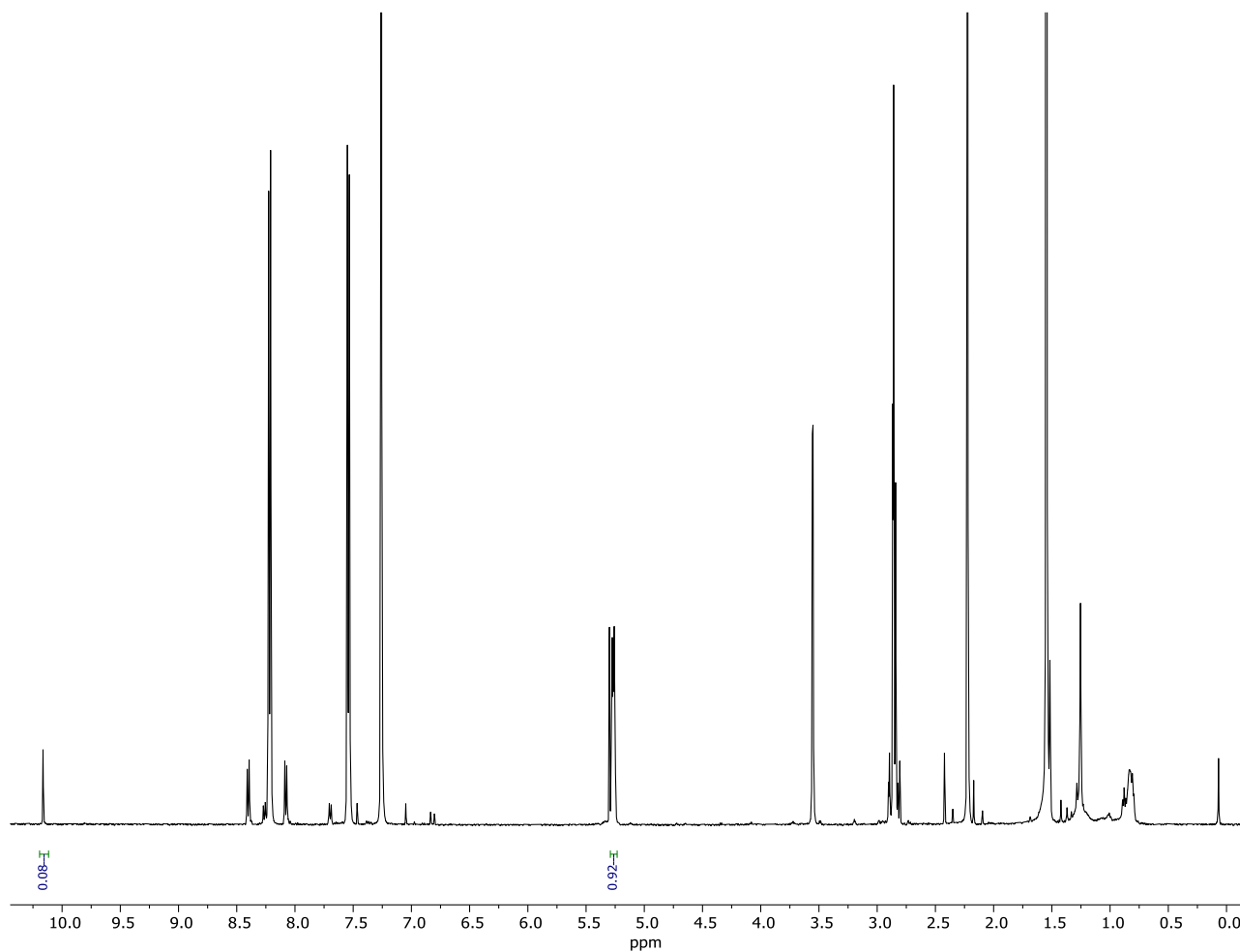
Compound	Integration	% Conversion
<b>11</b> (Starting material)	0.91	91
<b>13</b> (Product)	0.09	9

**6.4.3.16 Catalyst screening for aldol additions using Sav:73 (50 equivalents of acetone and 25% iso-propanol)**

Compound	Integration	% Conversion
<b>11</b> (Starting material)	0.82	82
<b>13</b> (Product)	0.18	18

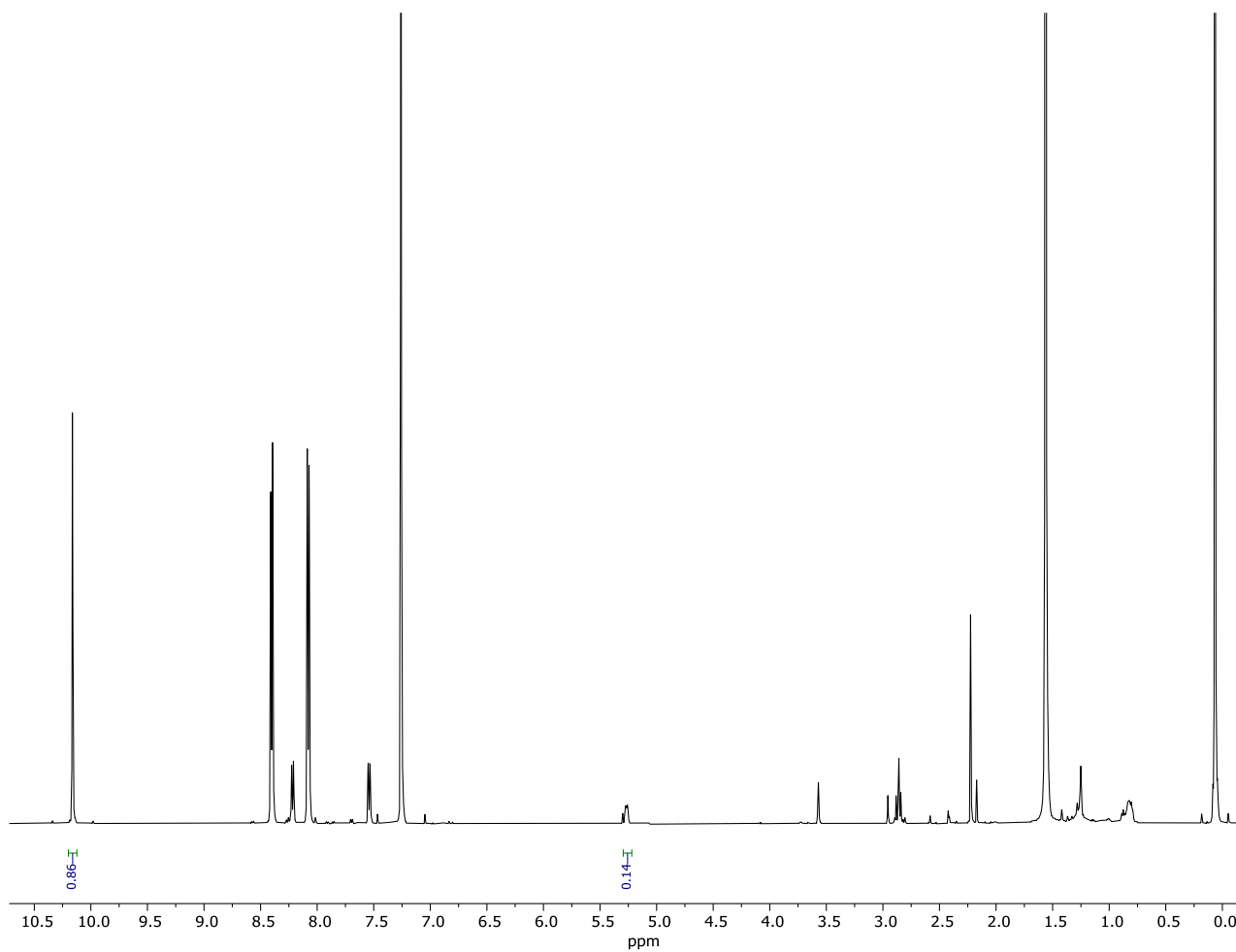
#### 6.4.4 $^1\text{H-NMR}$ details for the activity screening of Table 12

##### 6.4.4.1 Catalyst screening for aldol additions using T-rSav:73 as catalyst



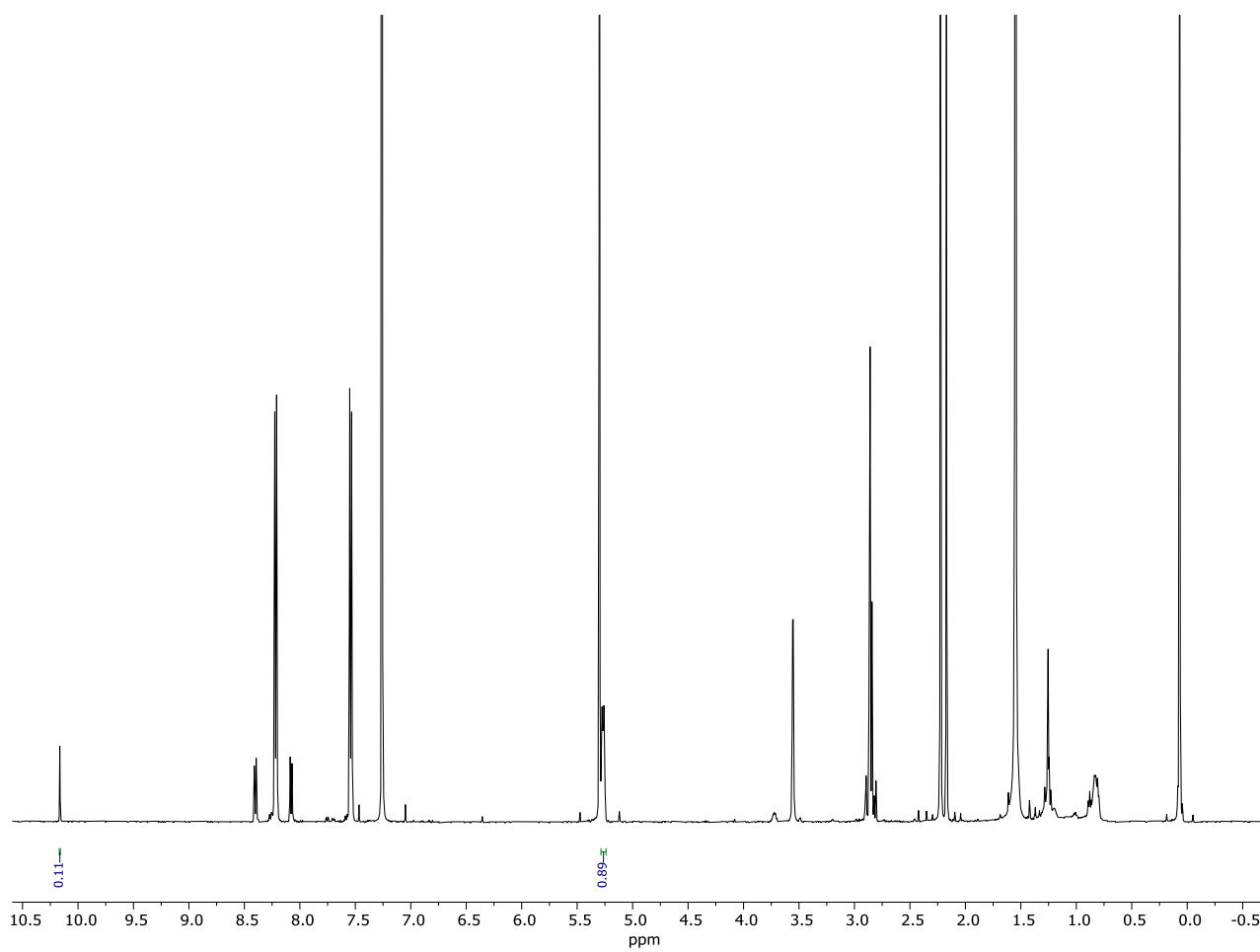
Compound	Integration	% Conversion
<b>11</b> (Starting material)	0.08	8
<b>13</b> (Product)	0.92	92

## 6.4.4.2 Catalyst screening for aldol additions using S112E:73 as catalyst



Compound	Integration	% Conversion
<b>11</b> (Starting material)	0.86	86
<b>13</b> (Product)	0.14	14

## 6.4.4.3 Catalyst screening for aldol additions using K121A:73 as catalyst

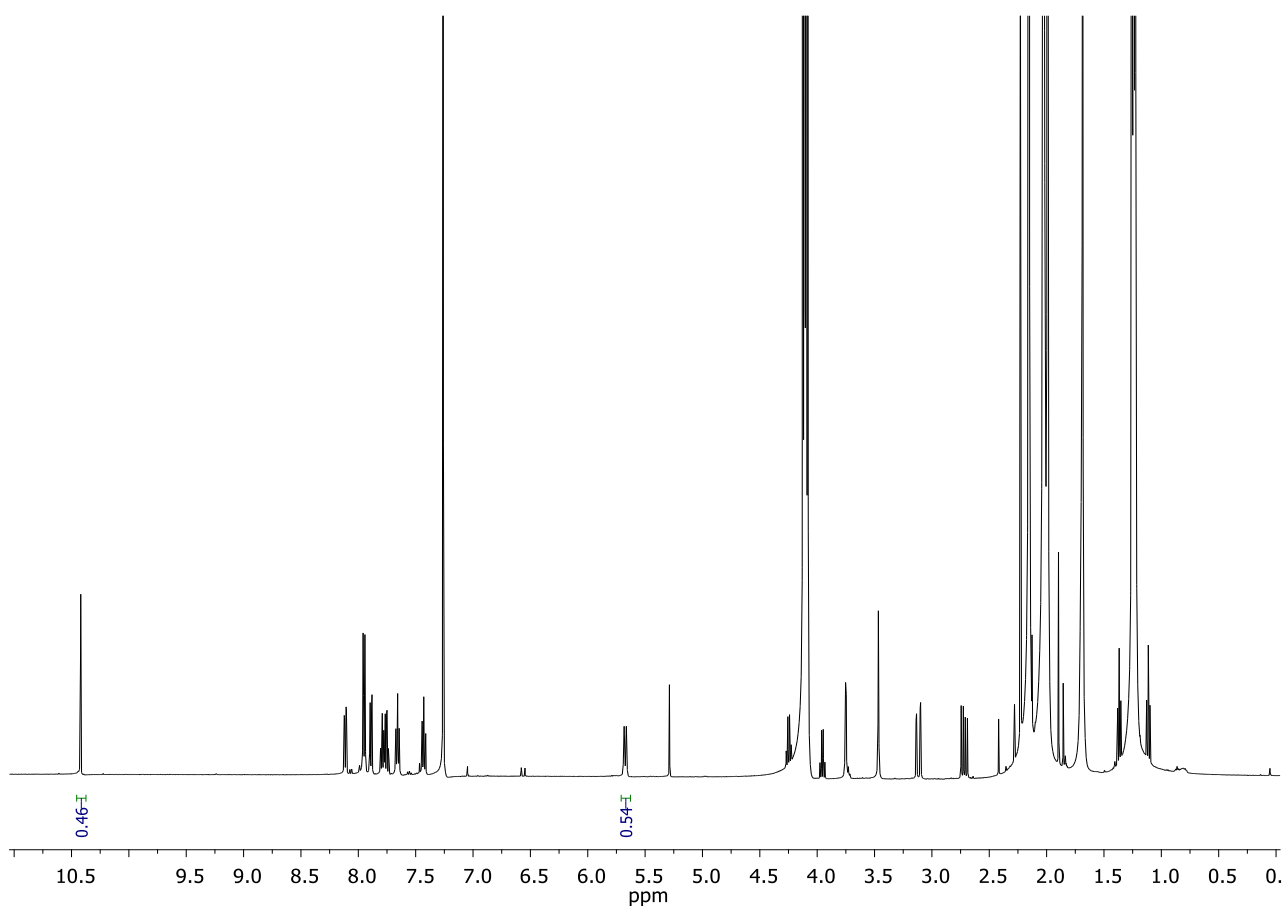


Compound	Integration	% Conversion
<b>11</b> (Starting material)	0.11	11
<b>13</b> (Product)	0.89	89

## 6.4.5 $^1\text{H-NMR}$ details for the activity screening of Table 13

### 6.4.5.1 Catalyst screening for aldol additions using *o*-nitrobenzaldehyde as substrate

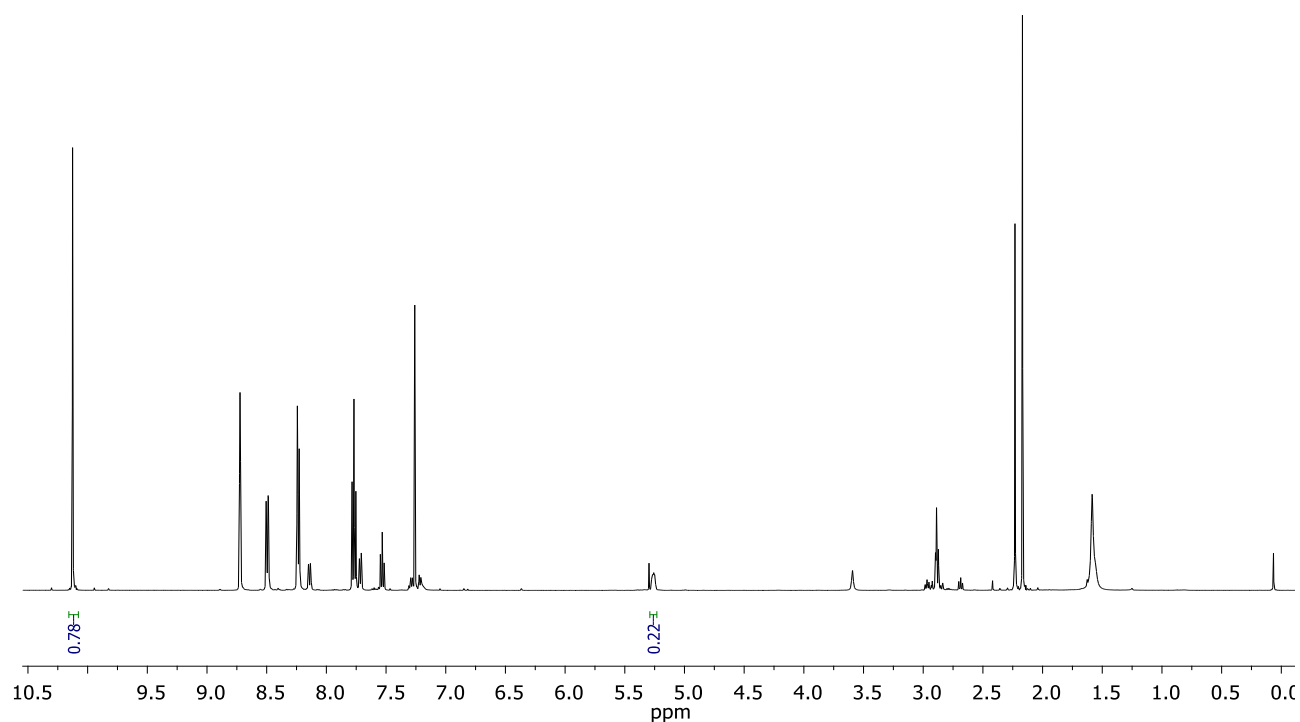
The estimated conversion of *o*-nitrobenzaldehyde (**151**) into 4-hydroxy-4-(*o*-nitrophenyl) butan-2-one (**161**) is calculated after integration of the product peak at 5.68 ppm with the substrate peak at 10.44 ppm. The spectroscopic data of **161** are the following:  $^1\text{H-NMR}$  (500 MHz,  $\text{CDCl}_3$ ),  $\delta$ : 7.96 (d,  $J=8.0$  Hz, 1H), 7.89 (d,  $J=8.0$  Hz, 1H), 7.68 (t,  $J=7.5$  Hz, 1H), 7.45 (t,  $J=7.5$  Hz, 1H), 5.68 (m, 1H), 3.12 (br s, 1H), 2.75 (m, 2H), 2.25 (s, 3H) ppm. These data matched those reported in the literature.<sup>326</sup>



Compound	Integration	% Conversion
<b>151</b> (Starting material)	0.46	46
<b>161</b> (Product)	0.54	54

### 6.4.5.2 Catalyst screening for aldol additions using *m*-nitrobenzaldehyde as substrate

The estimated conversion of *m*-nitrobenzaldehyde (**152**) into 4-hydroxy-4-(*m*-nitrophenyl) butan-2-one (**162**) is calculated after integration of the product peak at 5.26 ppm with the substrate peak at 10.12 ppm. The spectroscopic data of **162** are the following: **<sup>1</sup>H-NMR (500 MHz, CDCl<sub>3</sub>)**, δ: 8.24 (d, *J*= 8.0 Hz, 1H), 8.12 (d, *J*= 8.0 Hz, 1H), 7.71 (t, *J*= 7.5 Hz, 1H), 7.55 (t, *J*= 7.5 Hz, 1H), 5.26 (m, 1H), 3.65 (br s, 1H), 2.91 (m, 2H), 2.24 (s, 3H) ppm. These data matched those reported in the literature.<sup>326</sup>

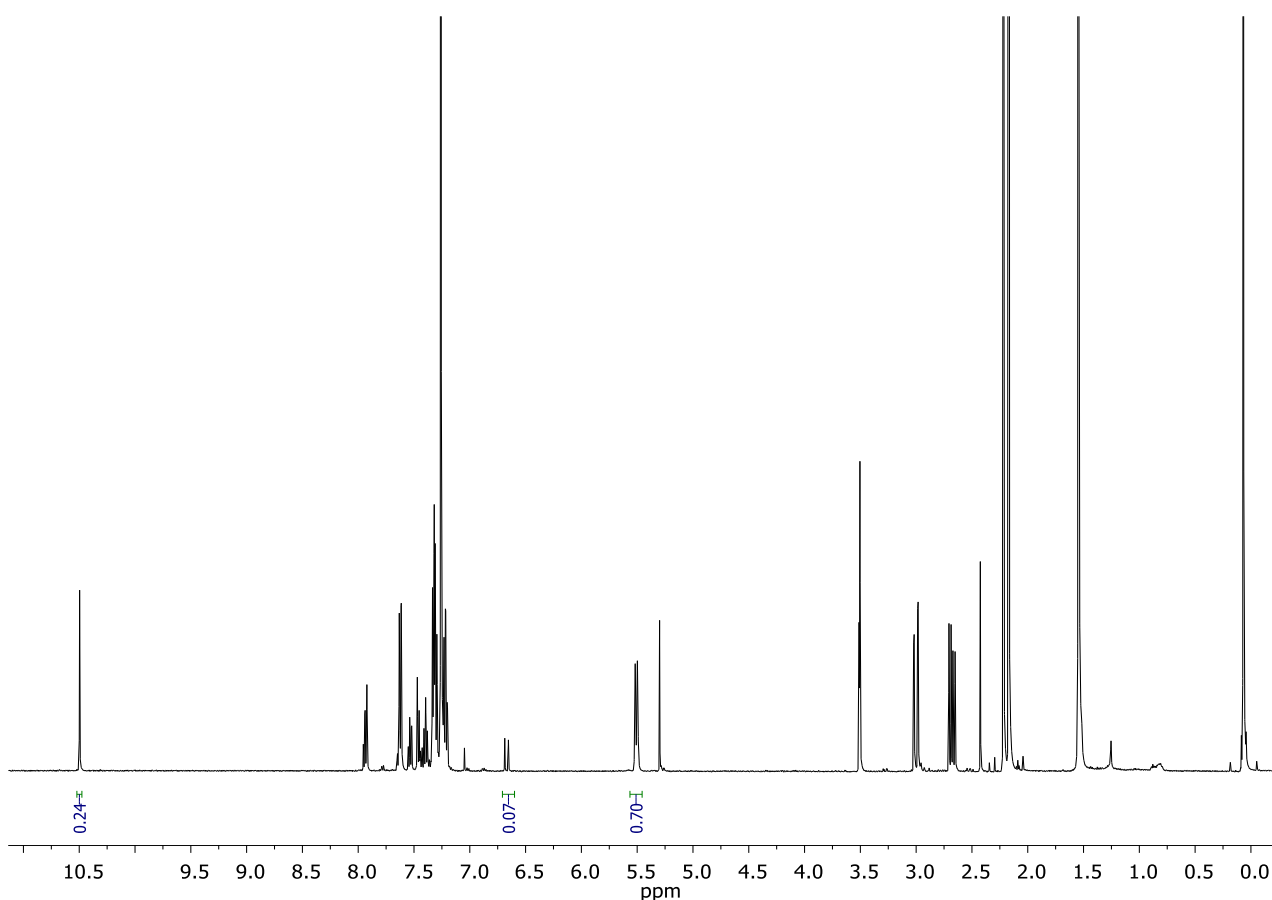


Compound	Integration	% Conversion
<b>152</b> (Starting material)	0.78	78
<b>162</b> (Product)	0.22	22



### 6.4.5.3 Catalyst screening for aldol additions using *o*-chlorobenzaldehyde as substrate

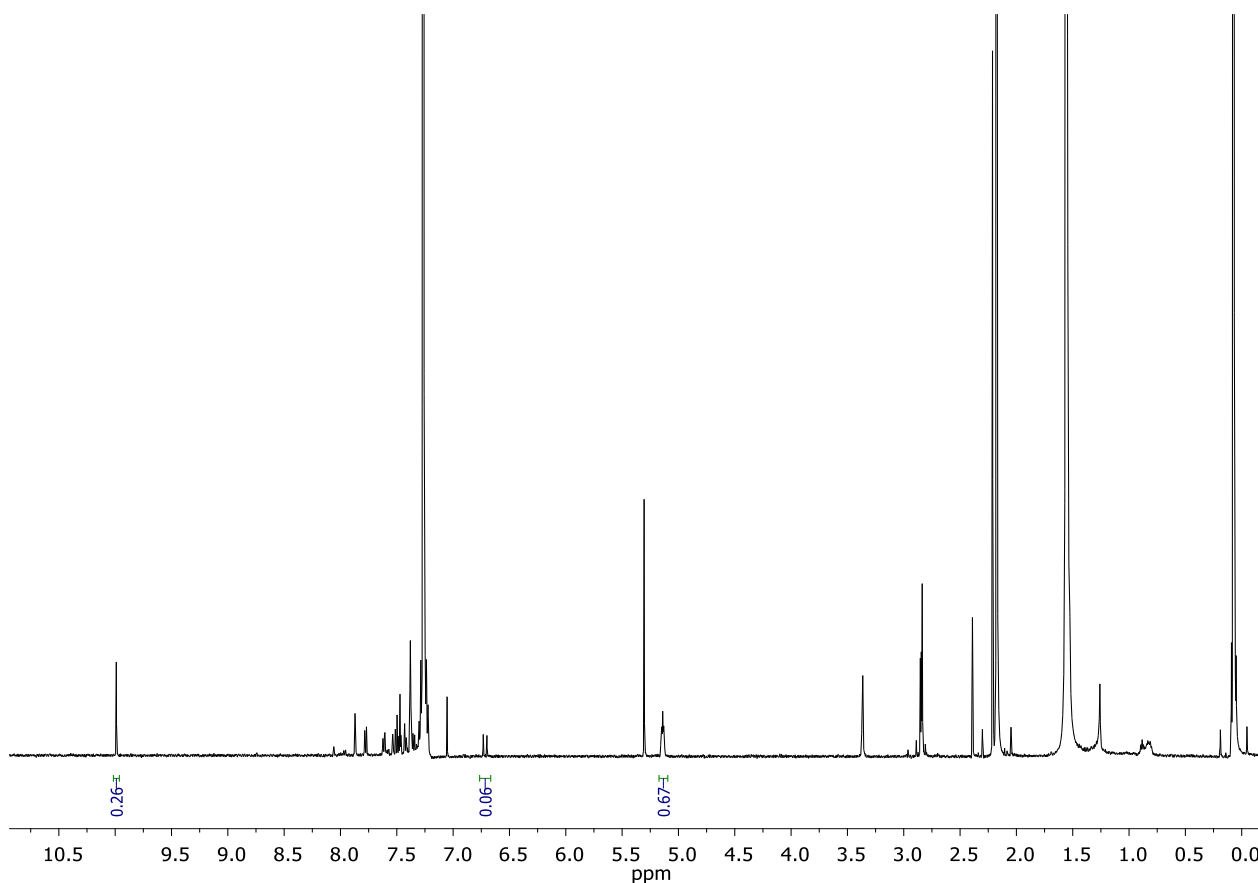
The estimated conversion of *o*-chlorobenzaldehyde (**153**) into 4-hydroxy-4-(*o*-chlorophenyl) butan-2-one (**163**) is calculated after integration of the product peak at 5.51 ppm with the substrate peak at 10.50 ppm. Formation of side-product (*E*)-4-(*o*-chlorophenyl) but-3-en-2-one (**163a**) at 6.68 ppm was observed. The spectroscopic data of **163** are the following: **<sup>1</sup>H-NMR (500 MHz, CDCl<sub>3</sub>)**,  $\delta$ : 7.90 (d,  $J$ = 8.0 Hz, 1H), 7.64 (d,  $J$ = 8.0 Hz, 1H), 7.41 (t,  $J$ = 7.5 Hz, 1H), 7.32 (t,  $J$ = 7.5 Hz, 1H), 5.51 (m, 1H), 3.08 (br s, 1H), 2.62 (m, 2H), 2.39 (s, 3H) ppm. These data matched those reported in the literature.<sup>326</sup>



Compound	Integration	% Conversion
<b>153</b> (Starting material)	0.24	23
<b>163a</b> (Side-product)	0.07	7
<b>163</b> (Product)	0.70	70

#### 6.4.5.4 Catalyst screening for aldol additions using *m*-chlorobenzaldehyde as substrate

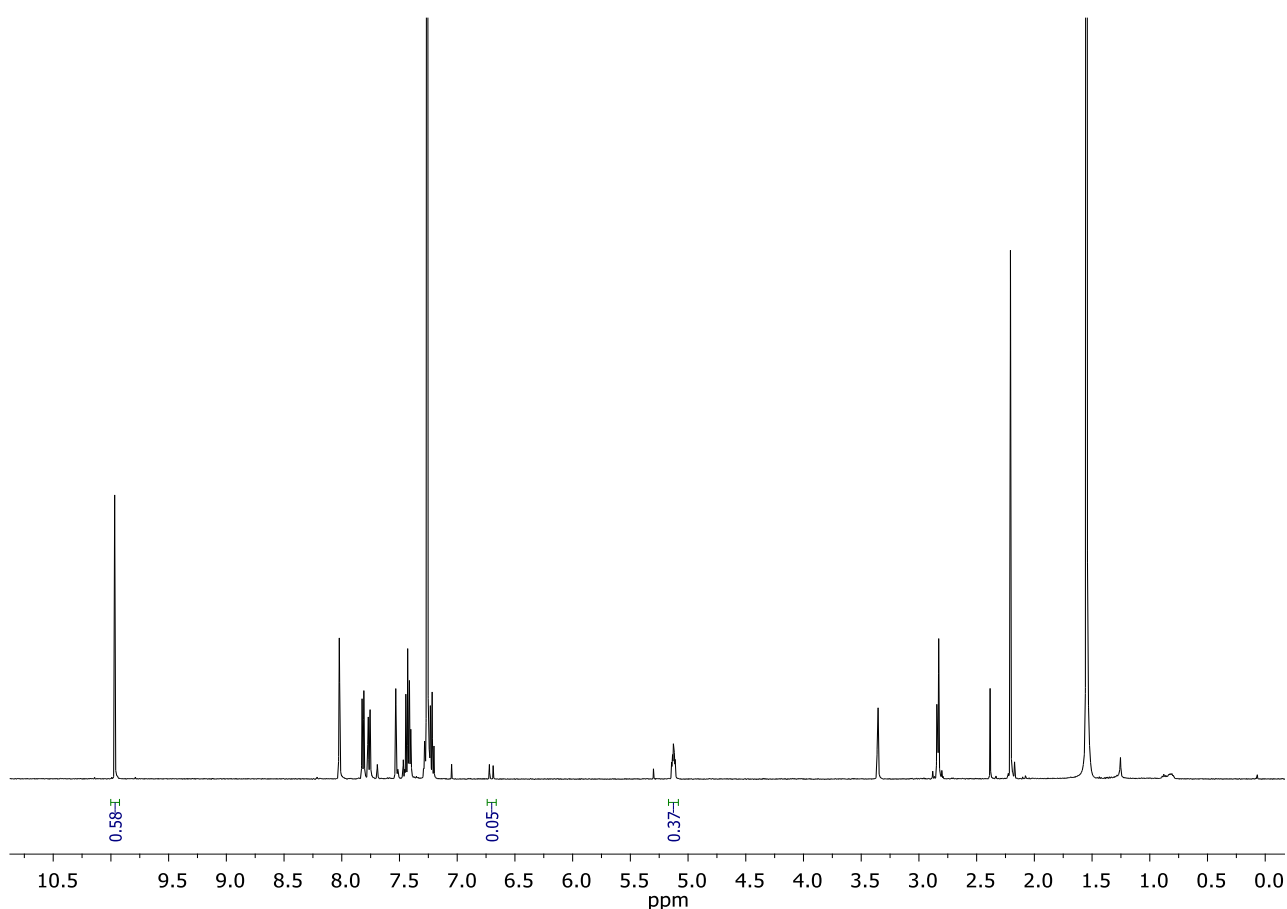
The estimated conversion of *m*-chlorobenzaldehyde (**154**) into 4-hydroxy-4-(*m*-chlorophenyl) butan-2-one (**164**) is calculated after integration of the product peak at 5.13 ppm with the substrate peak at 9.98 ppm. Formation of side-product (*E*)-4-(*m*-chlorophenyl) but-3-en-2-one (**164a**) at 6.71 ppm was observed. The spectroscopic data of **164** are the following: **<sup>1</sup>H-NMR (500 MHz, CDCl<sub>3</sub>)**,  $\delta$ : 7.33 (m, 1H), 7.25-7.16 (m, 3H), 5.13 (m, 1H), 3.36 (br s, 1H), 2.84 (m, 2H), 2.17 (s, 3H) ppm. These data matched those reported in the literature.<sup>267</sup>



Compound	Integration	% Conversion
<b>154</b> (Starting material)	0.26	27
<b>164a</b> (Side-product)	0.06	6
<b>164</b> (Product)	0.67	67

### 6.4.5.5 Catalyst screening for aldol additions using *m*-bromobenzaldehyde as substrate

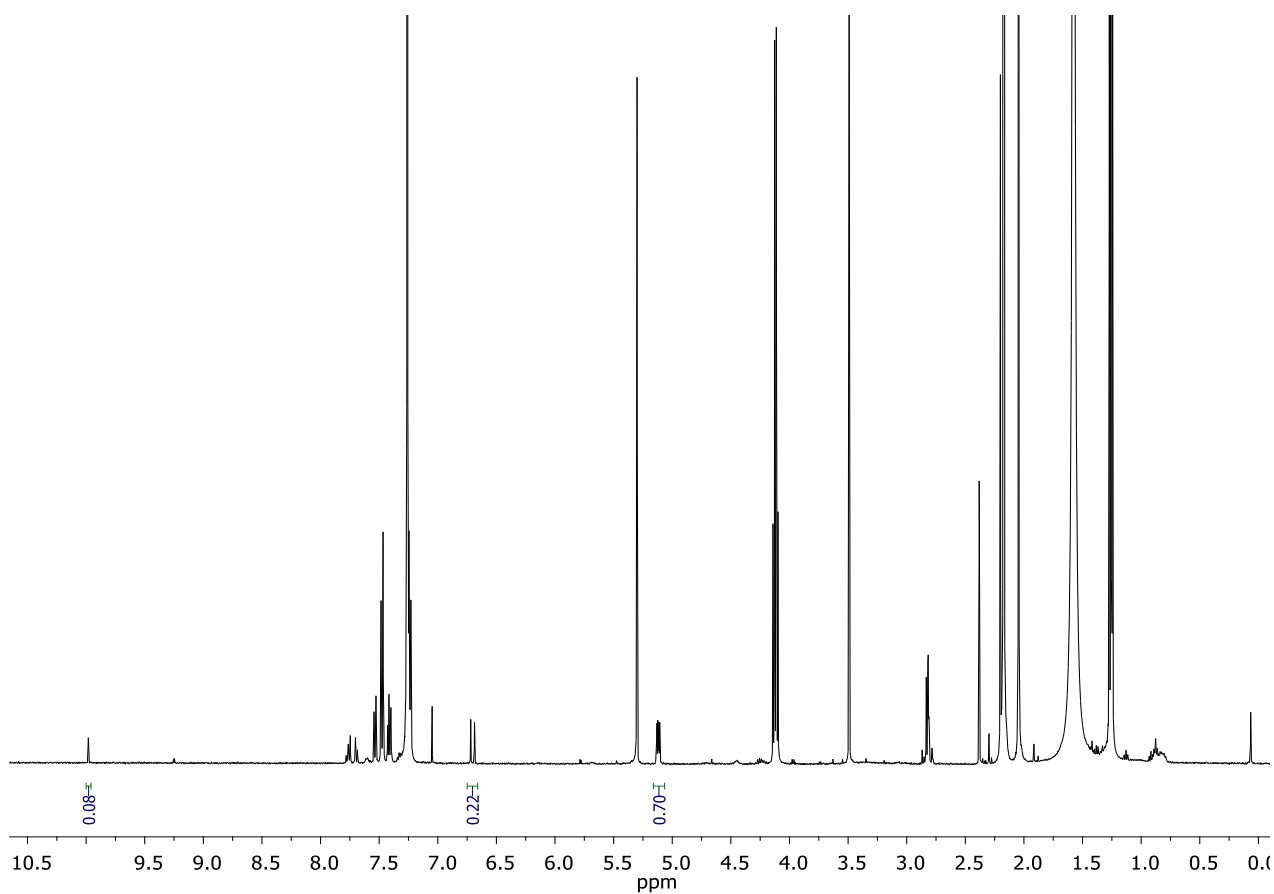
The estimated conversion of *m*-bromobenzaldehyde (**155**) into 4-hydroxy-4-(*m*-bromophenyl) butan-2-one (**165**) is calculated after integration of the product peak at 5.13 ppm with the substrate peak at 9.97 ppm. Formation of side-product (*E*)-4-(*m*-bromophenyl) but-3-en-2-one (**165a**) at 6.70 ppm was observed. The spectroscopic data of **165** are the following: **<sup>1</sup>H-NMR (500 MHz, CDCl<sub>3</sub>), δ: 7.44 (m, 1H), 7.33-7.30 (m, 1H), 7.24-7.15 (m, 2H), 5.13 (m, 1H), 3.36 (br s, 1H), 2.83 (m, 2H), 2.19 (s, 3H) ppm.** These data matched those reported in the literature.<sup>327</sup>



Compound	Integration	% Conversion
<b>155</b> (Starting material)	0.58	58
<b>165a</b> (Side-product)	0.05	5
<b>165</b> (Product)	0.37	37

#### 6.4.5.6 Catalyst screening for aldol additions using *p*-bromobenzaldehyde as substrate

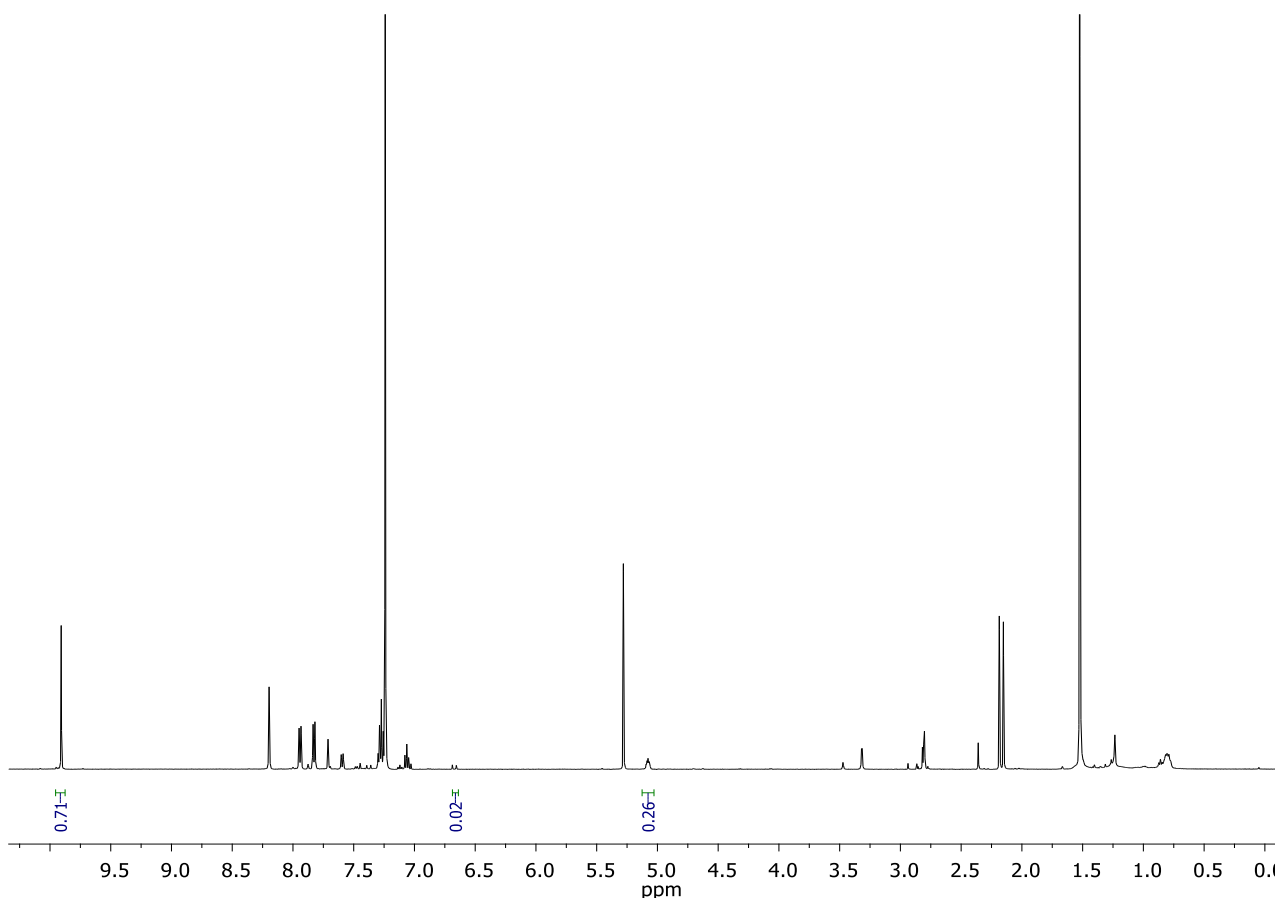
The estimated conversion of *p*-bromobenzaldehyde (**156**) into 4-hydroxy-4-(*p*-bromophenyl) butan-2-one (**166**) is calculated after integration of the product peak at 5.12 ppm with the substrate peak at 9.98 ppm. Formation of side-product (*E*)-4-(*p*-bromophenyl) but-3-en-2-one (**166a**) at 6.70 ppm was observed. The spectroscopic data of **166** are the following: **<sup>1</sup>H-NMR (500 MHz, CDCl<sub>3</sub>)**,  $\delta$ : 7.45 (d,  $J$ = 8.5 Hz, 2H), 7.24 (d,  $J$ = 8.5 Hz, 2H), 5.12 (m, 1H), 2.82 (m, 2H), 2.20 (s, 3H). These data matched those reported in the literature.<sup>328</sup>



Compound	Integration	% Conversion
<b>156</b> (Starting material)	0.08	8
<b>166a</b> (Side-product)	0.22	22
<b>166</b> (Product)	0.70	70

### 6.4.5.7 Catalyst screening for aldol additions using *m*-iodobenzaldehyde as substrate

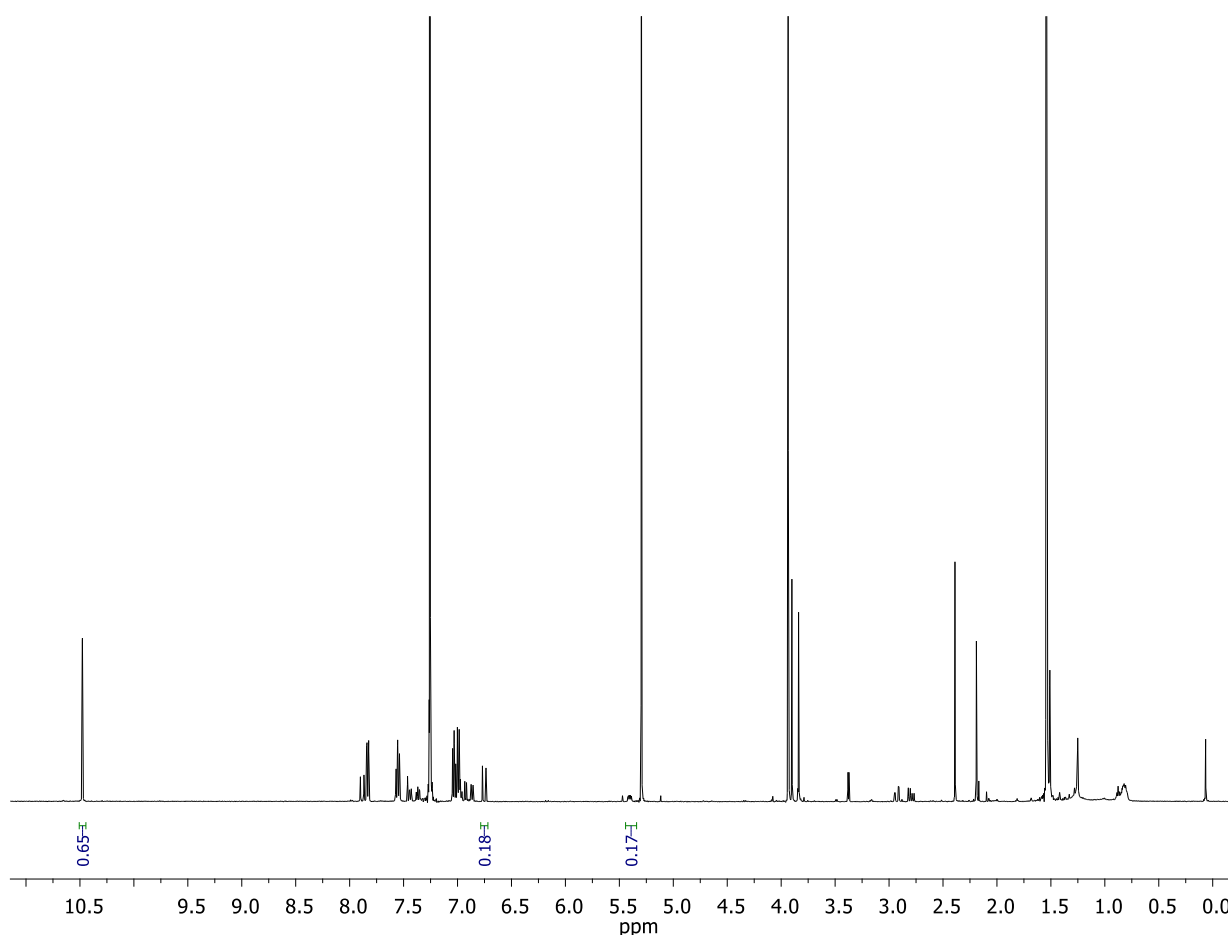
The estimated conversion of *m*-iodobenzaldehyde (**157**) into 4-hydroxy-4-(*m*-iodophenyl) butan-2-one (**167**) is calculated after integration of the product peak at 5.10 ppm with the substrate peak at 9.93 ppm. Formation of side-product (*E*)-4-(*m*-iodophenyl) but-3-en-2-one (**167a**) at 6.69 ppm was observed. The spectroscopic data of **167** are the following: **<sup>1</sup>H-NMR (500 MHz, CDCl<sub>3</sub>)**,  $\delta$ : 7.72 (d,  $J = 8.0$  Hz, 1H), 7.61 (d,  $J = 8.0$  Hz, 1H), 7.29 (m, 1H), 7.08 (m, 2H), 5.10 (m, 1H), 3.34 (br s, 1H), 2.83 (m, 2H), 2.21 (s, 3H) ppm. These data matched those reported in the literature.<sup>285</sup>



Compound	Integration	% Conversion
<b>157</b> (Starting material)	0.71	71
<b>167a</b> (Side-product)	0.02	2
<b>167</b> (Product)	0.26	26

### 6.4.5.8 Catalyst screening for aldol additions using *o*-methoxybenzaldehyde as substrate

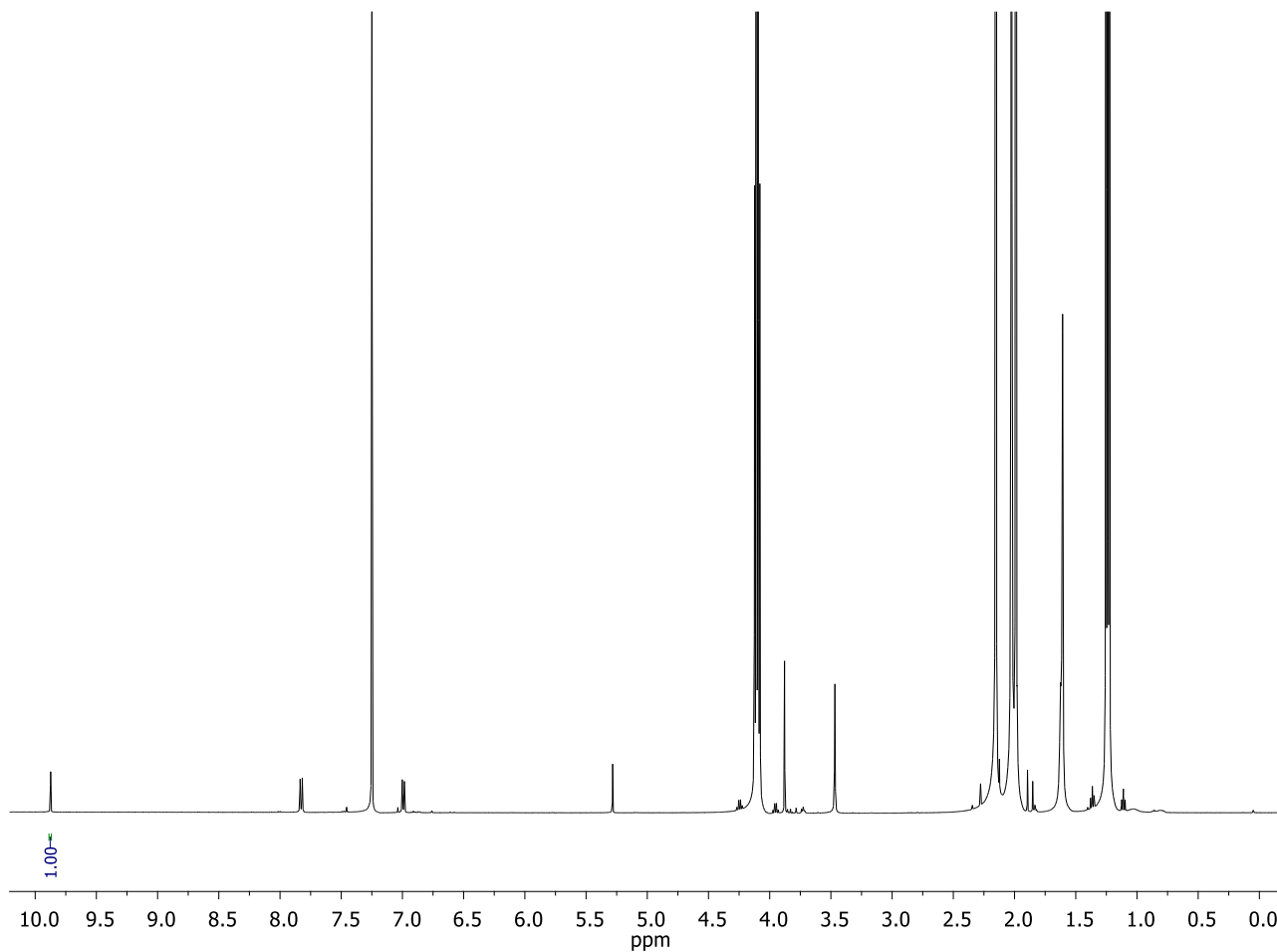
The estimated conversion of *o*-methoxybenzaldehyde (**158**) into 4-hydroxy-4-(*o*-methoxyphenyl) butan-2-one (**168**) is calculated after integration of the product peak at 5.41 ppm with the substrate peak at 10.45 ppm. Formation of side-product (*E*)-4-(*o*-methoxyphenyl) but-3-en-2-one (**168a**) at 6.75 ppm was observed. The spectroscopic data of **168** are the following:  $^1\text{H-NMR}$  (500 MHz,  $\text{CDCl}_3$ ),  $\delta$ : 7.44 (d,  $J = 8$  Hz, 1H), 7.25 (t,  $J = 8$  Hz, 1H), 6.97 (t,  $J = 8$  Hz, 1H), 6.86 (d,  $J = 8$  Hz, 1H), 5.41 (m, 1H), 3.82 (s, 3H), 3.61 (br s, 1H), 2.90-2.75 (m, 2H), 2.17 (s, 3H) ppm. These data matched those reported in the literature.<sup>329</sup>



Compound	Integration	% Conversion
<b>158</b> (Starting material)	0.65	65
<b>168a</b> (Side-product)	0.18	18
<b>168</b> (Product)	0.17	17

### 6.4.5.9 Catalyst screening for aldol additions using *p*-methoxybenzaldehyde as substrate

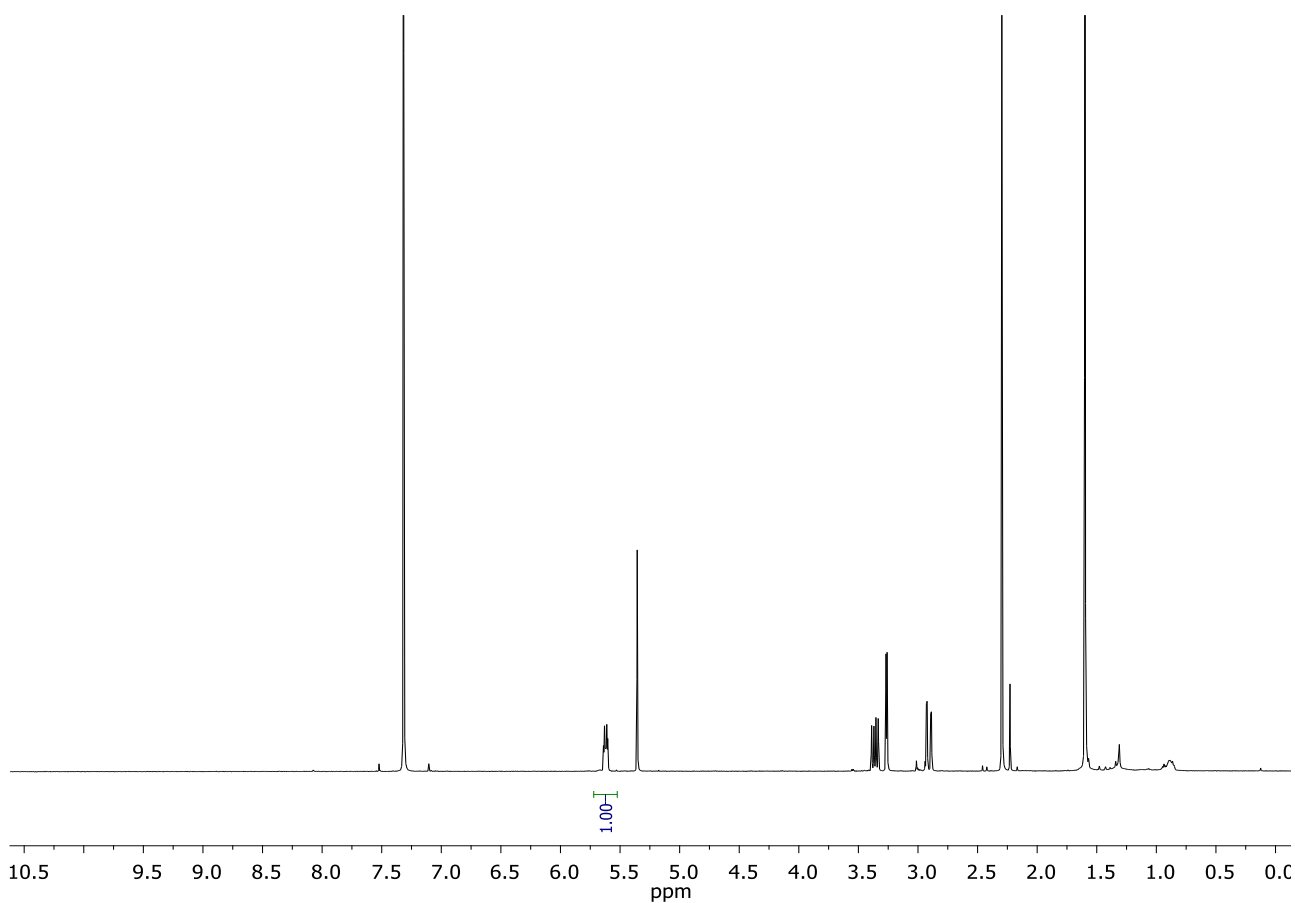
The estimated conversion of *p*-methoxybenzaldehyde (**159**) into 4-hydroxy-4-(*p*-methoxyphenyl) butan-2-one (**169**) is calculated after integration of the substrate peak at 9.88 ppm. Neither the product nor the side-product (*E*)-4-(*p*-methoxyphenyl) but-3-en-2-one (**169a**) were observed.



Compound	Integration	% Conversion
<b>159</b> (Starting material)	1.00	100
<b>169</b> (Product)	/	/

#### 6.4.5.10 Catalyst screening for aldol additions using pentafluorobenzaldehyde as substrate

The estimated conversion of pentafluorobenzaldehyde (**160**) into 4-hydroxy-4-(perfluorophenyl) butan-2-one (**170**) is calculated after integration of the product peak at 5.57 ppm. The spectroscopic data of **170** are the following:  $^1\text{H-NMR}$  (500 MHz,  $\text{CDCl}_3$ ),  $\delta$ : 5.57 (m, 1H), 3.31 (dd,  $J= 18.0$  and  $9.5$  Hz, 1H), 3.21 (d,  $J= 4.5$  Hz, 1H), 2.86 (m, 2H), 2.24 (s, 3H) ppm. These data matched those reported in the literature.<sup>330</sup>



Compound	Integration	% Conversion
<b>160</b> (Starting material)	/	/
<b>170</b> (Product)	1.00	100



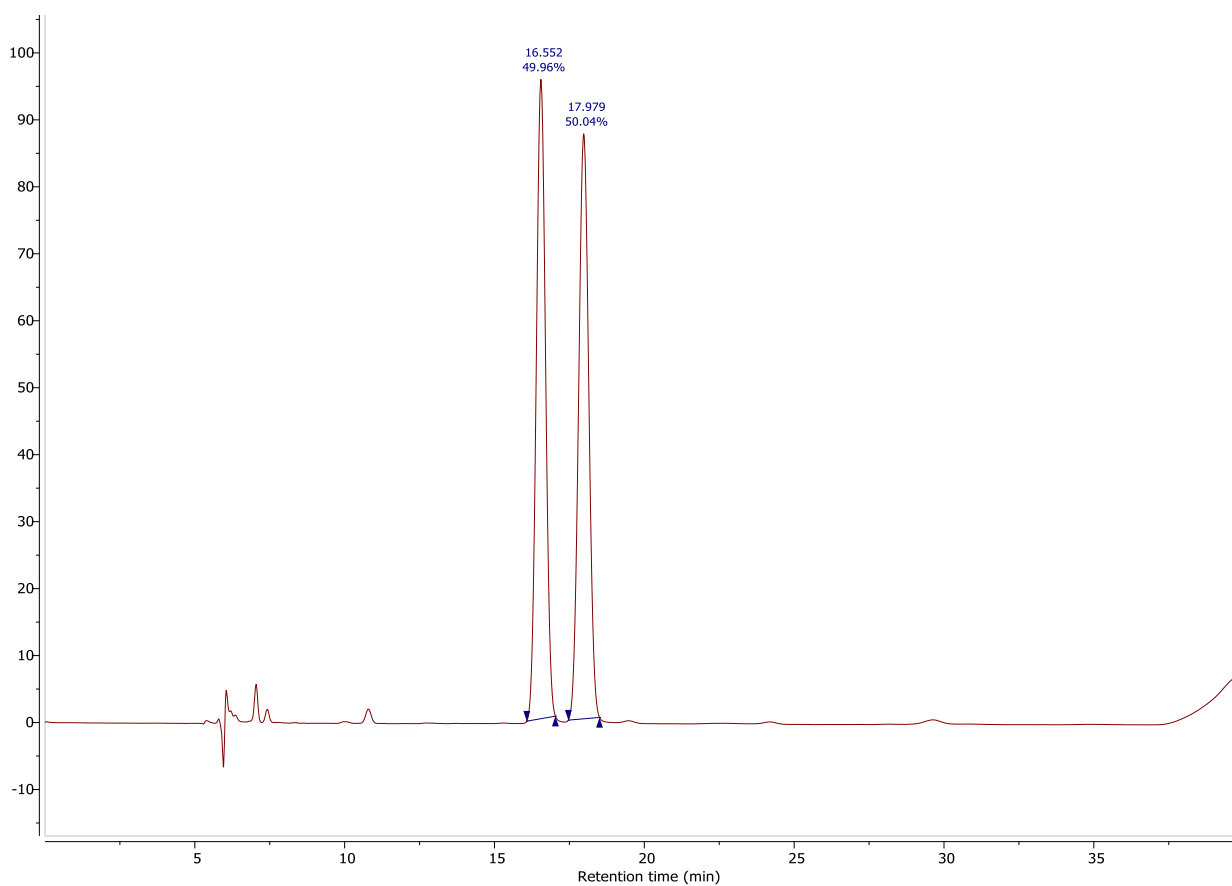
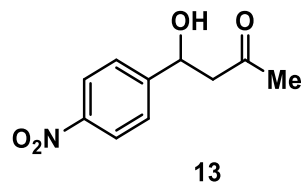
## 6.4.5 Chiral HPLC data of activity and selectivity screening

### 6.4.5.1 Chiral HPLC data for Table 11

Analytical chiral HPLC analysis of product **13** was performed on a 1260 Infinity Quaternary LC system (Agilent Technologies, Santa Clara, USA) using a Lux Amylose-1 column (Phenomenex, Torrance, USA), 4.6 mm × 250 mm (0.5 mL/min, 25 °C, n-hexane/isopropanol 75:25, 50 min). Slight variations on the retention time are due to the change of the column guard throughout the measurements. The peaks were assigned using signal at 280 nm.<sup>294</sup>

### 6.4.5.1.1 Racemate of 13

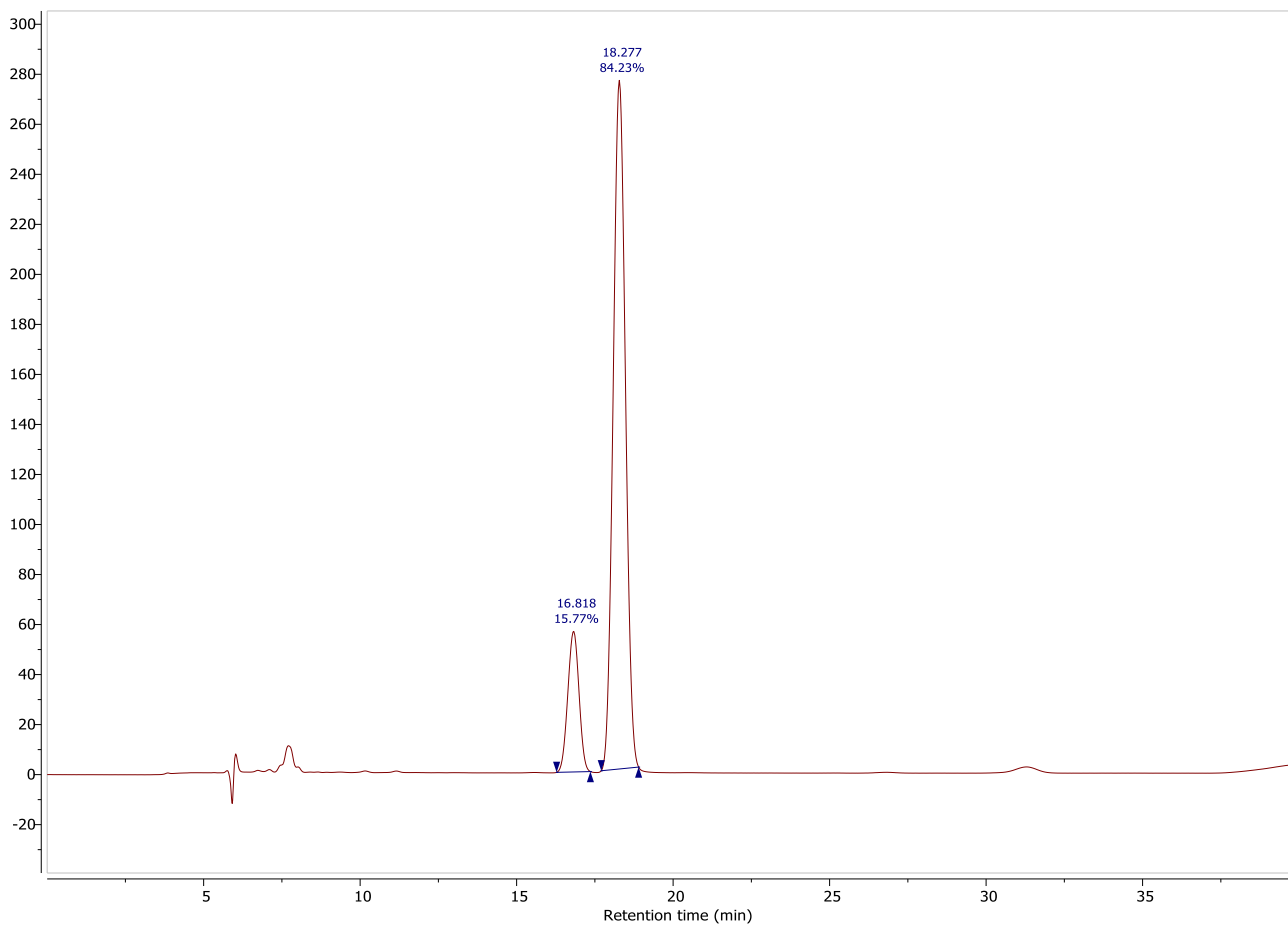
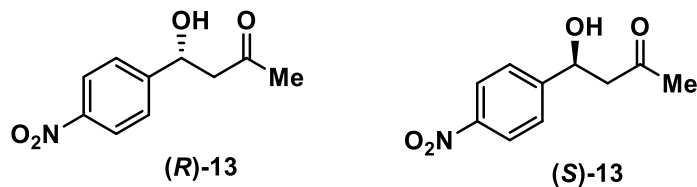
Racemic samples of **13** were obtained following a known procedure, using piperidine as catalyst.



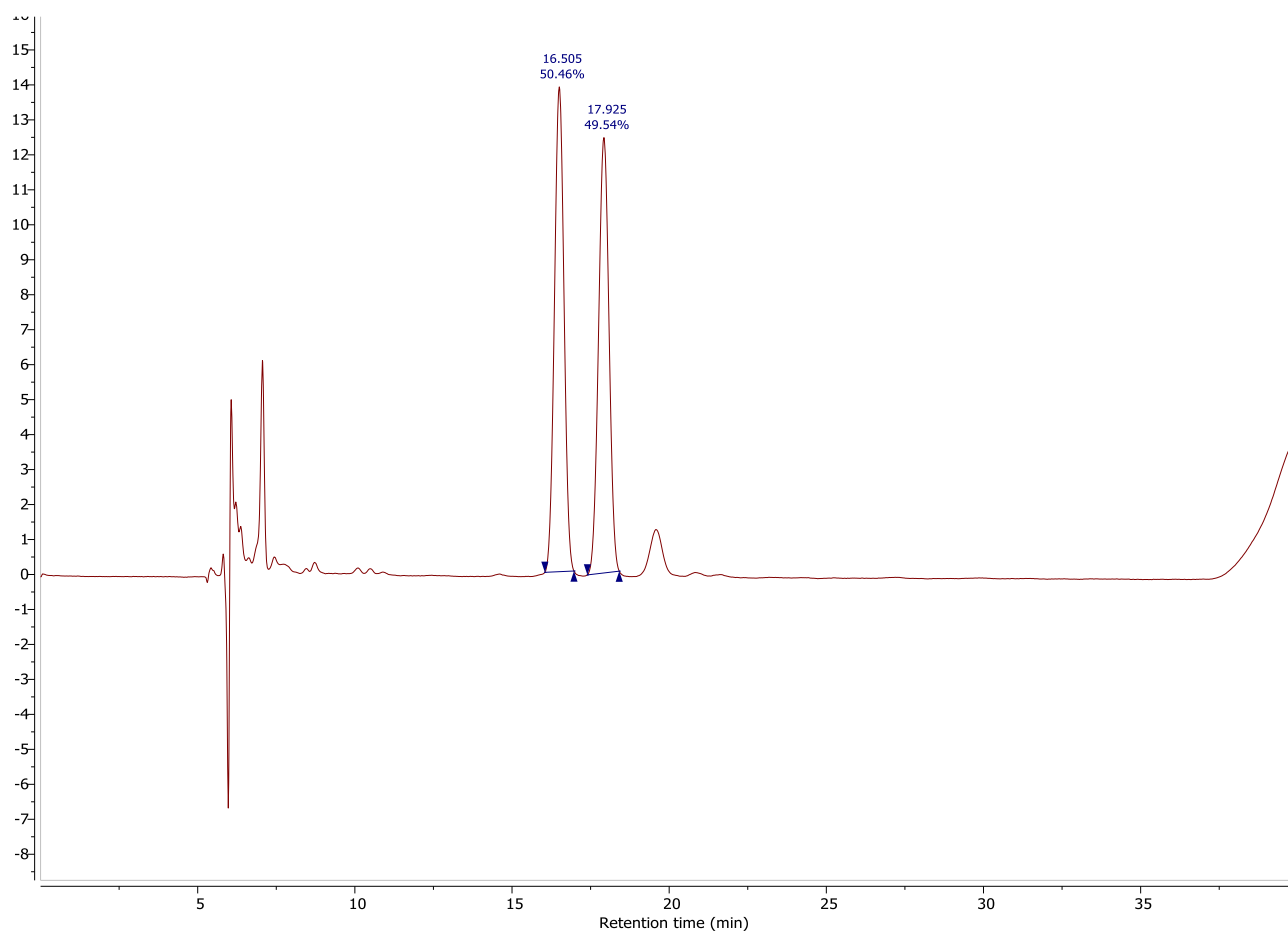
Entry	Retention time (min)	Peak Area (%)
1 ( <i>R</i> -enantiomer)	16.5	50.0
2 ( <i>S</i> -enantiomer)	18.0	50.0

## 6.4.5.1.2 L-proline

The absolute stereochemistry of **13** was assigned after running the sample obtained using L-Proline as catalyst.

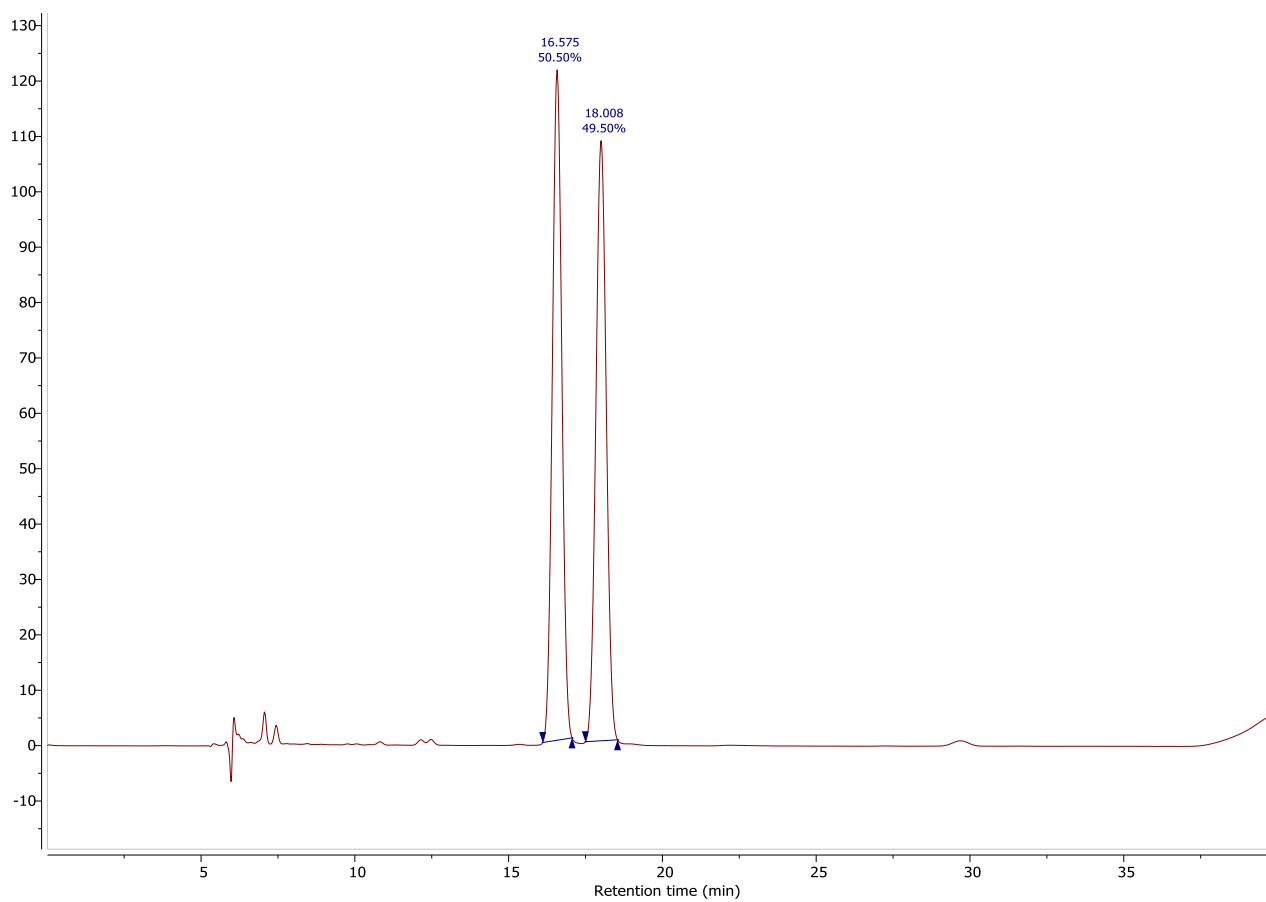


Entry	Retention time (min)	Peak Area (%)
1 ( <i>R</i> -enantiomer)	16.8	15.7
2 ( <i>S</i> -enantiomer)	18.3	84.3

**6.4.5.1.3 Catalyst 73 (1 mol%)**

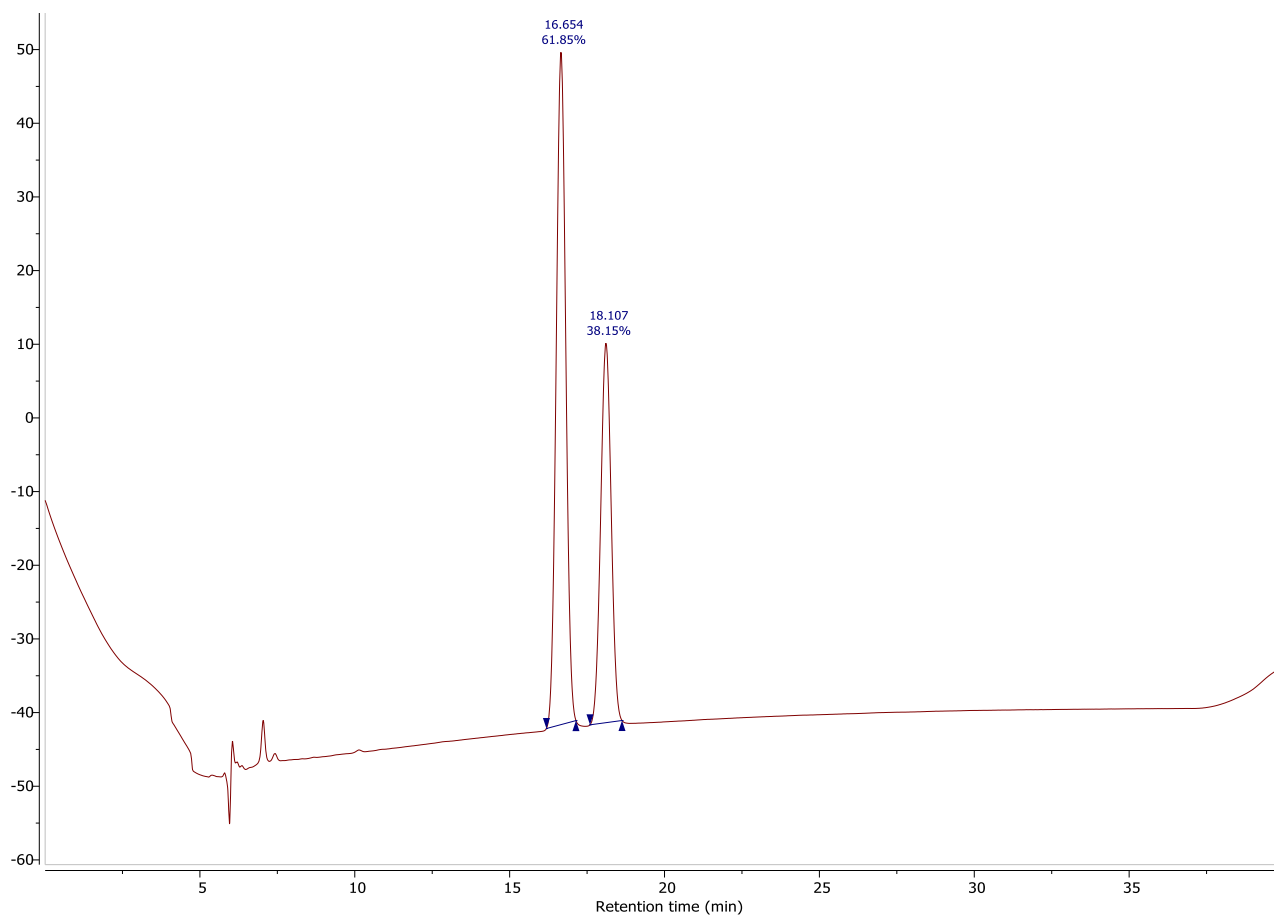
Entry	Retention time (min)	Peak Area (%)
1 ( <i>R</i> -enantiomer)	16.5	50.5
2 ( <i>S</i> -enantiomer)	17.9	49.5

## 6.4.5.1.4 Sav (1 mol%)



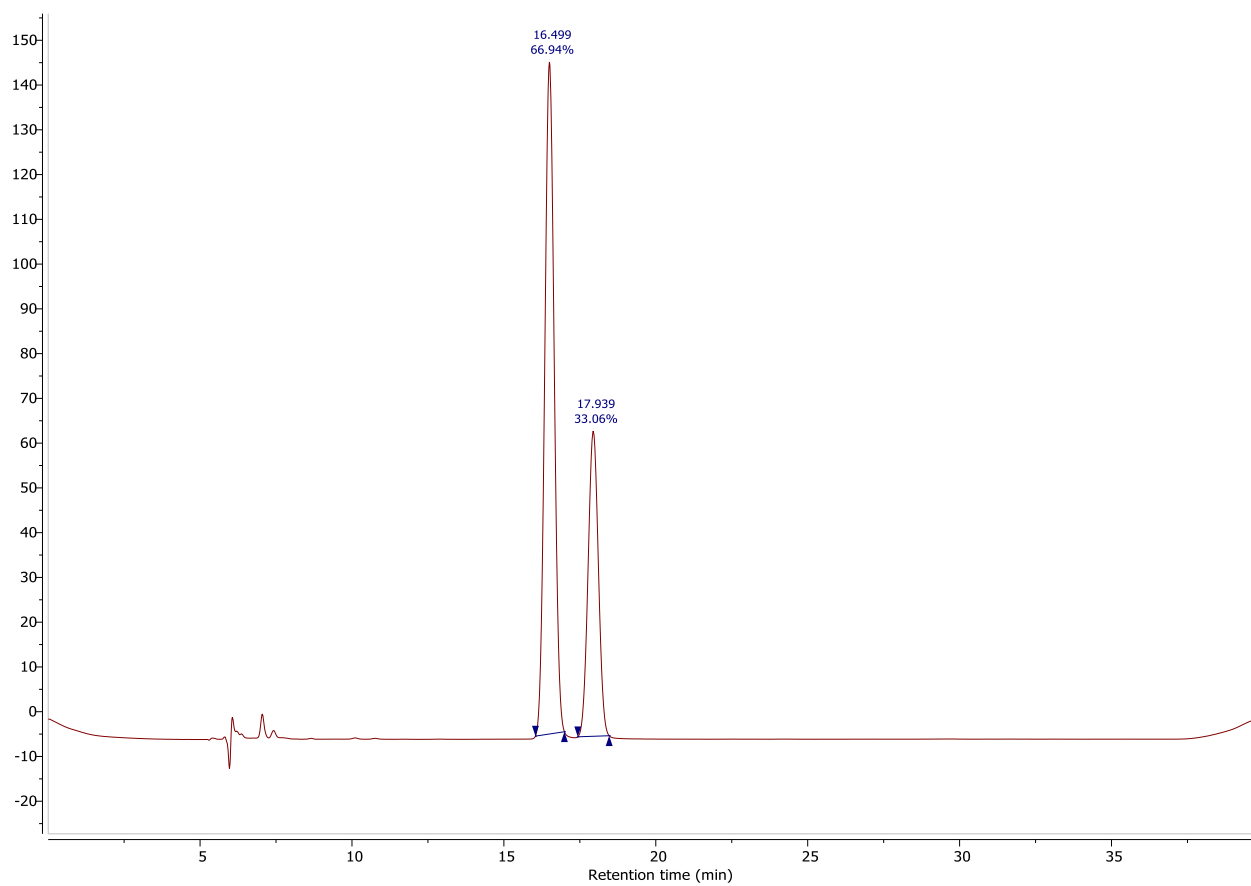
Entry	Retention time (min)	Peak Area (%)
1 ( <i>R</i> -enantiomer)	16.5	50.5
2 ( <i>S</i> -enantiomer)	18.0	49.5

## 6.4.5.1.5 Sav:1 (0.1 mol%)



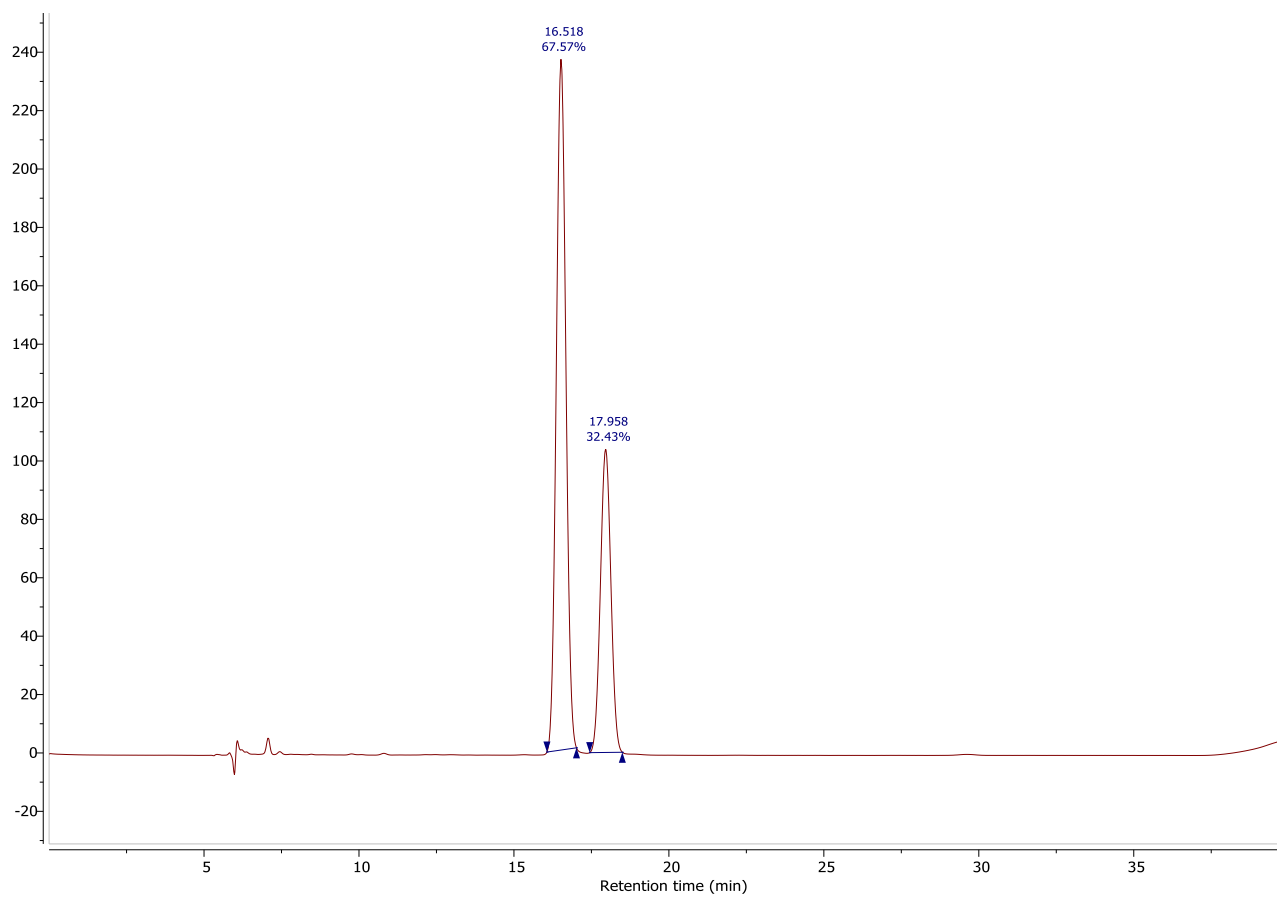
Entry	Retention time (min)	Peak Area (%)
1 ( <i>R</i> -enantiomer)	16.6	61.9
2 ( <i>S</i> -enantiomer)	18.1	38.1

## 6.4.5.1.6 Sav:1 (0.5 mol%)



Entry	Retention time (min)	Peak Area (%)
1 ( <i>R</i> -enantiomer)	16.5	67.0
2 ( <i>S</i> -enantiomer)	17.9	33.0

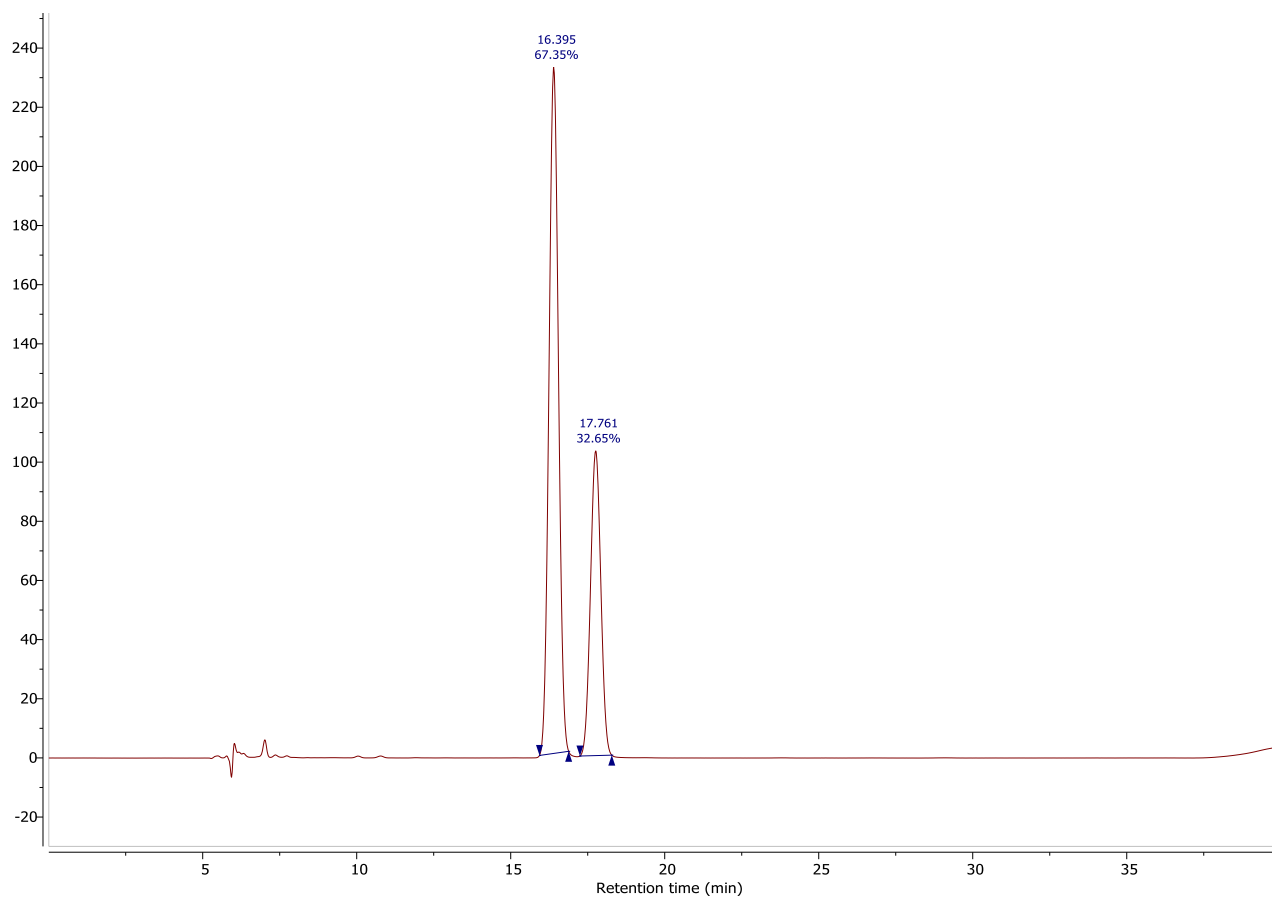
## 6.4.5.1.7 Sav:1 (1 mol%)



Entry	Retention time (min)	Peak Area (%)
1 ( <i>R</i> -enantiomer)	16.5	67.6
2 ( <i>S</i> -enantiomer)	17.9	32.4

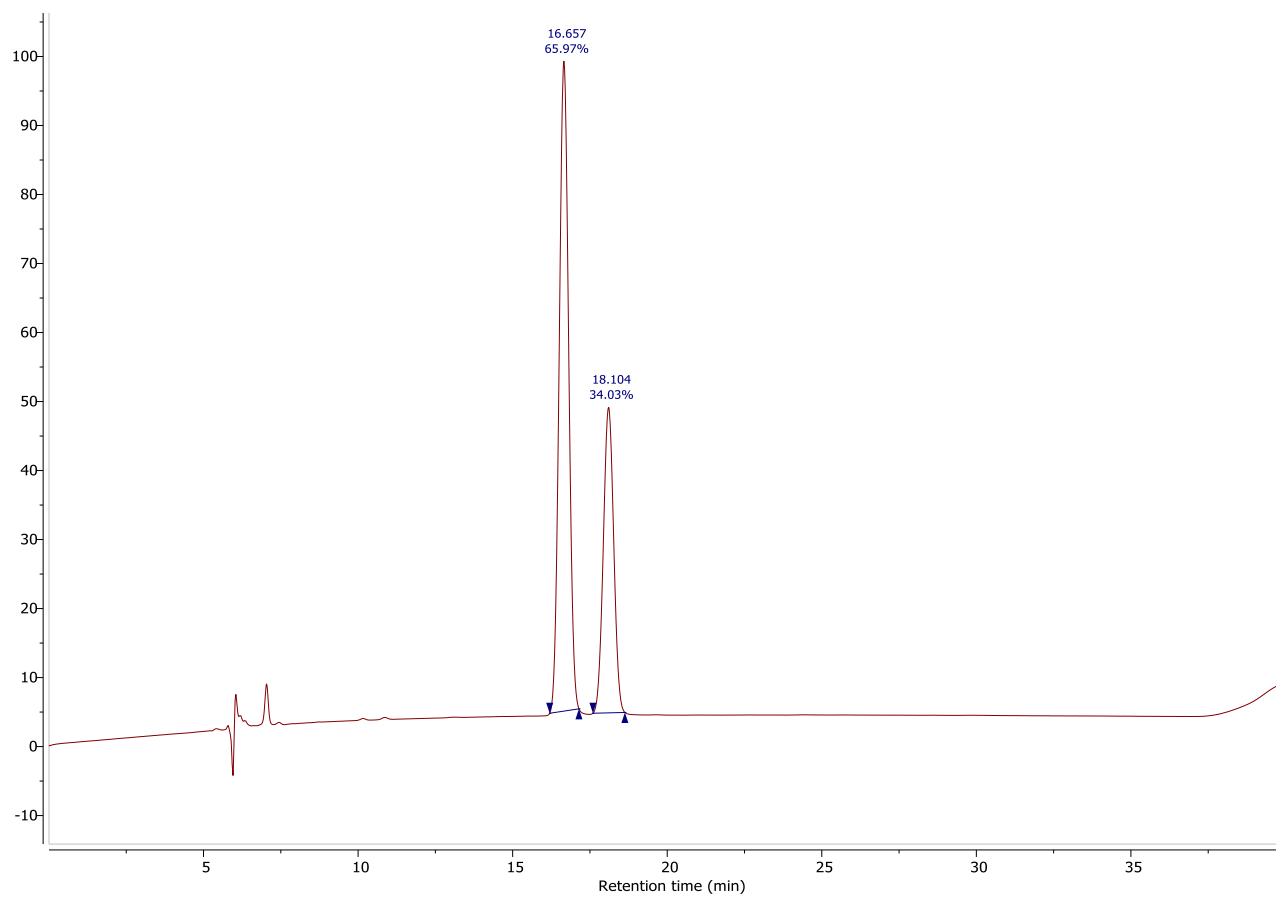


## 6.4.5.1.8 Sav:1 (1 mol%) and TFA (1 mol%)



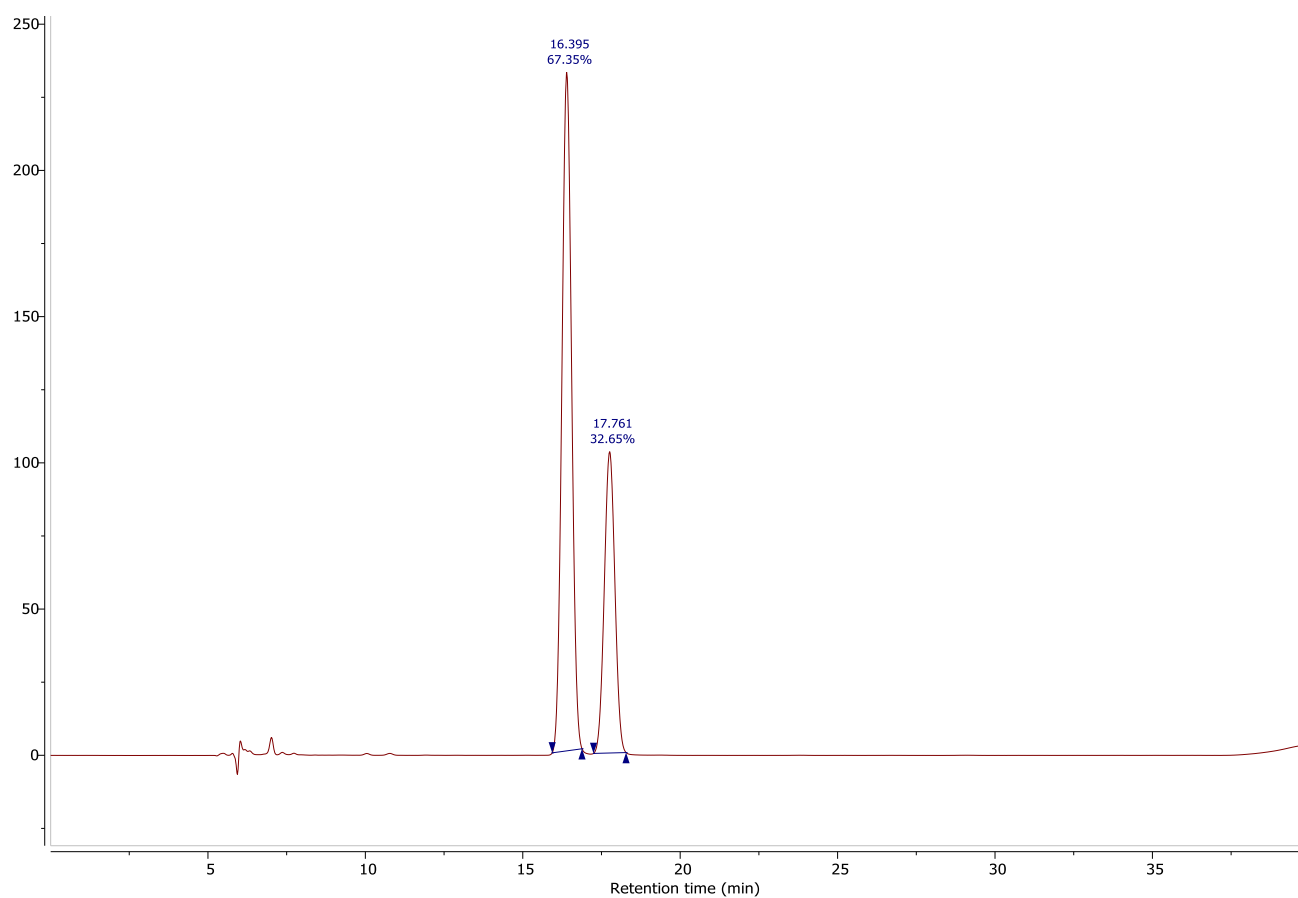
Entry	Retention time (min)	Peak Area (%)
1 ( <i>R</i> -enantiomer)	16.4	67.4
2 ( <i>S</i> -enantiomer)	17.8	32.6

## 6.4.5.1.9 Sav:1 (1 mol%) at 10 °C



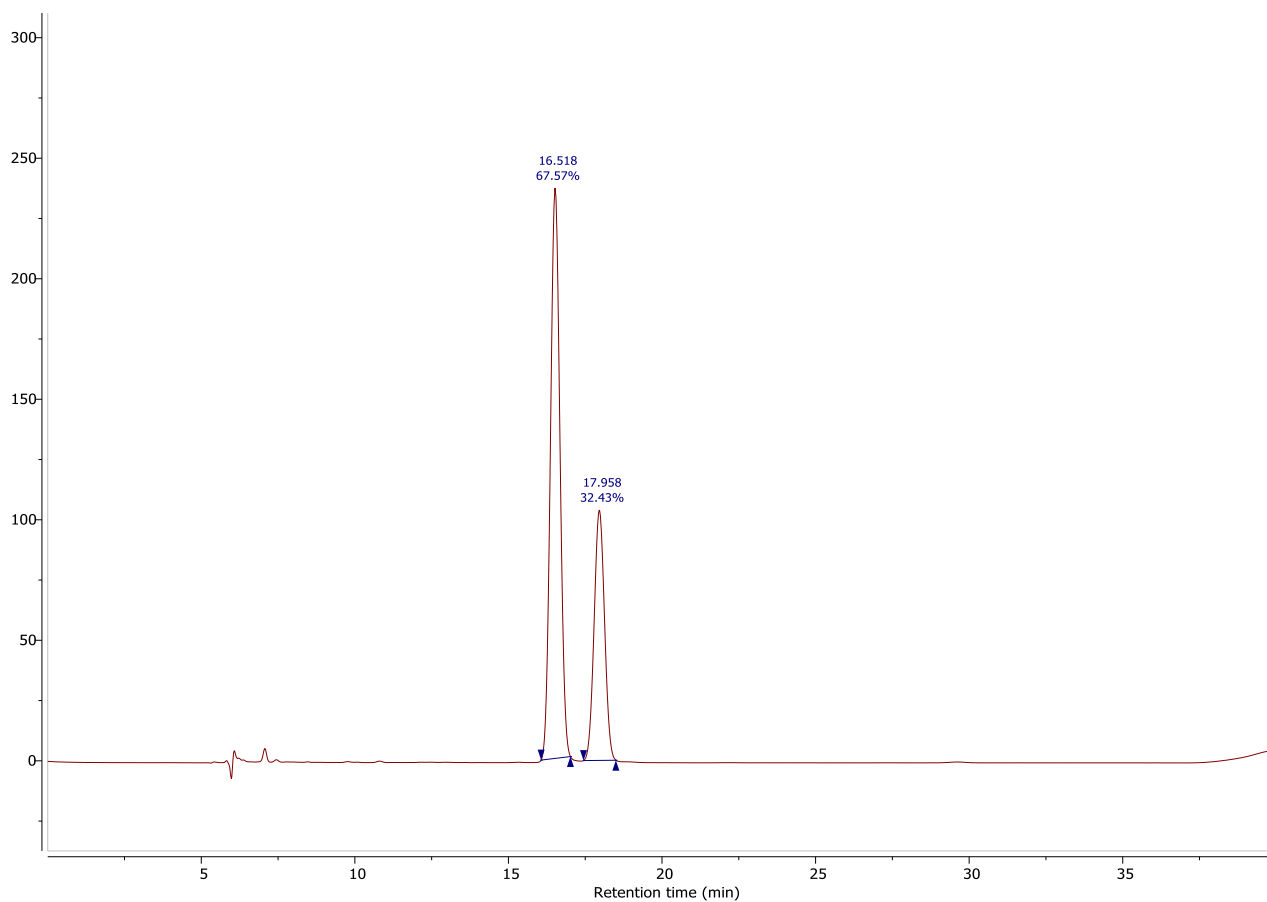
Entry	Retention time (min)	Peak Area (%)
1 ( <i>R</i> -enantiomer)	16.6	66.0
2 ( <i>S</i> -enantiomer)	18.1	34.0

## 6.4.5.1.10 Sav:1 (5 equivalents of acetone and 25% methanol)



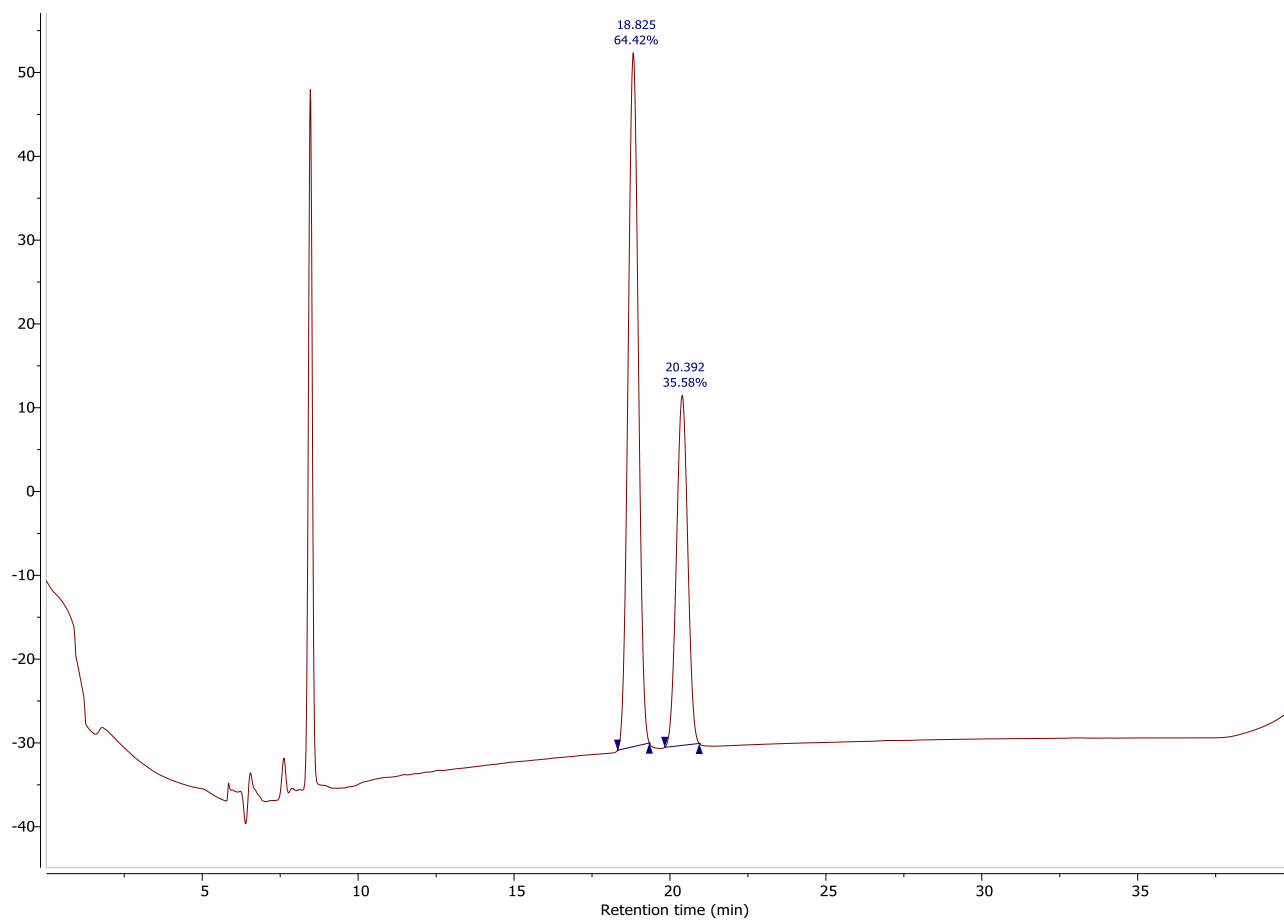
Entry	Retention time (min)	Peak Area (%)
1 ( <i>R</i> -enantiomer)	16.4	67.4
2 ( <i>S</i> -enantiomer)	17.8	32.6

## 6.4.5.1.11 Sav:1 (5 equivalents of acetone and 25% acetonitrile)



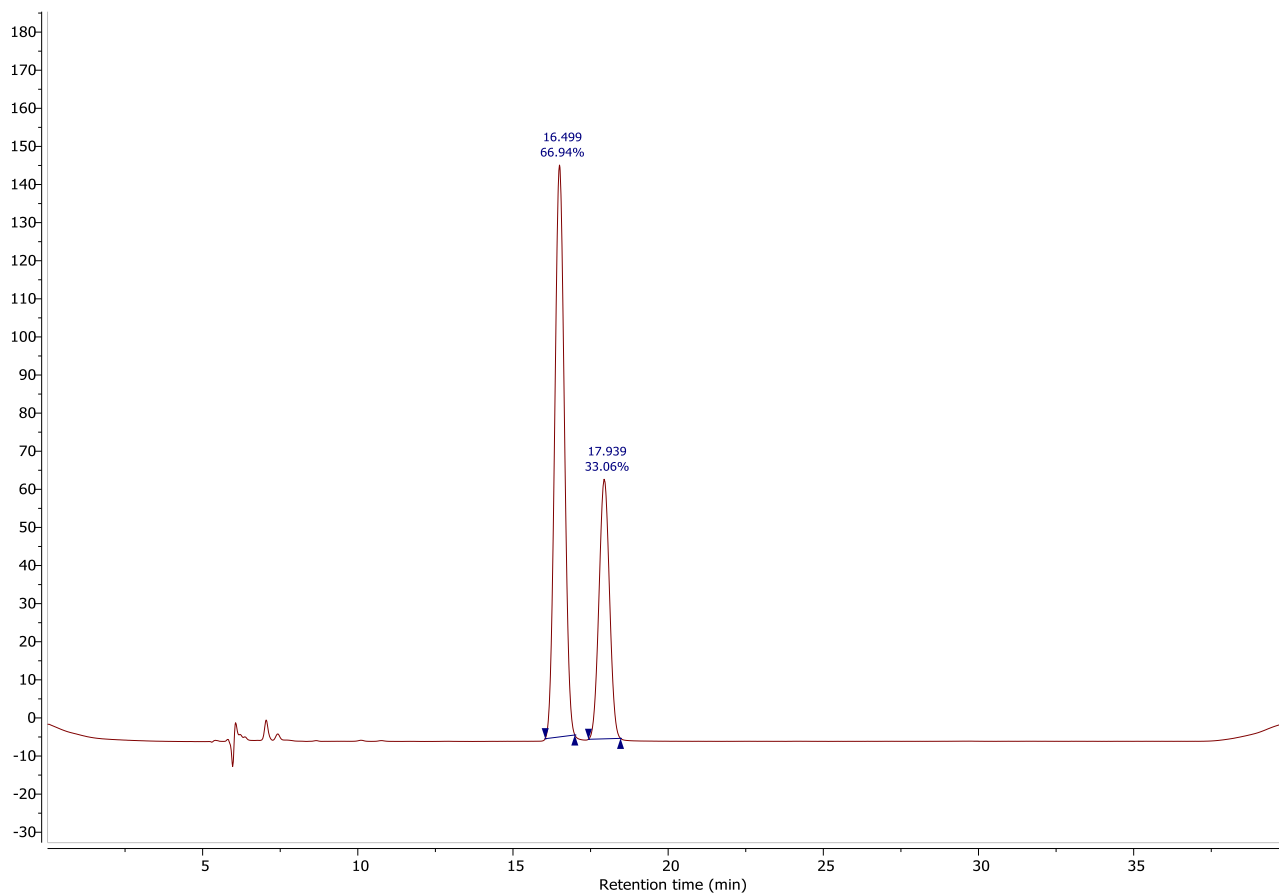
Entry	Retention time (min)	Peak Area (%)
1 ( <i>R</i> -enantiomer)	16.5	67.6
2 ( <i>S</i> -enantiomer)	17.9	32.4

## 6.4.5.1.12 Sav:1 (5 equivalents of acetone and 25% iso-propanol)



Entry	Retention time (min)	Peak Area (%)
1 ( <i>R</i> -enantiomer)	18.8	64.4
2 ( <i>S</i> -enantiomer)	20.4	35.6

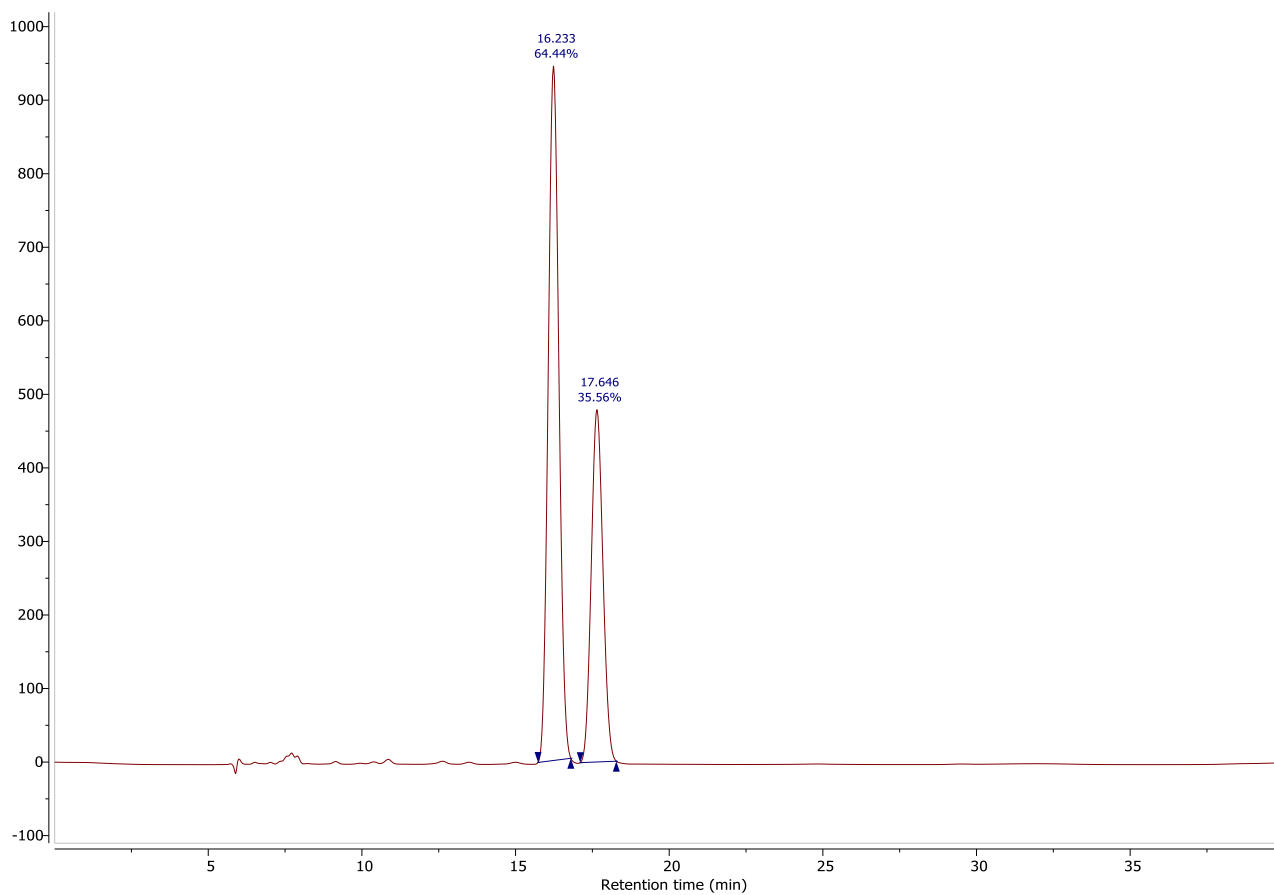
## 6.4.5.1.13 Sav:1 (50 equivalents of acetone and 25% iso-propanol)



Entry	Retention time (min)	Peak Area (%)
1 ( <i>R</i> -enantiomer)	16.4	66.9
2 ( <i>S</i> -enantiomer)	17.9	33.1

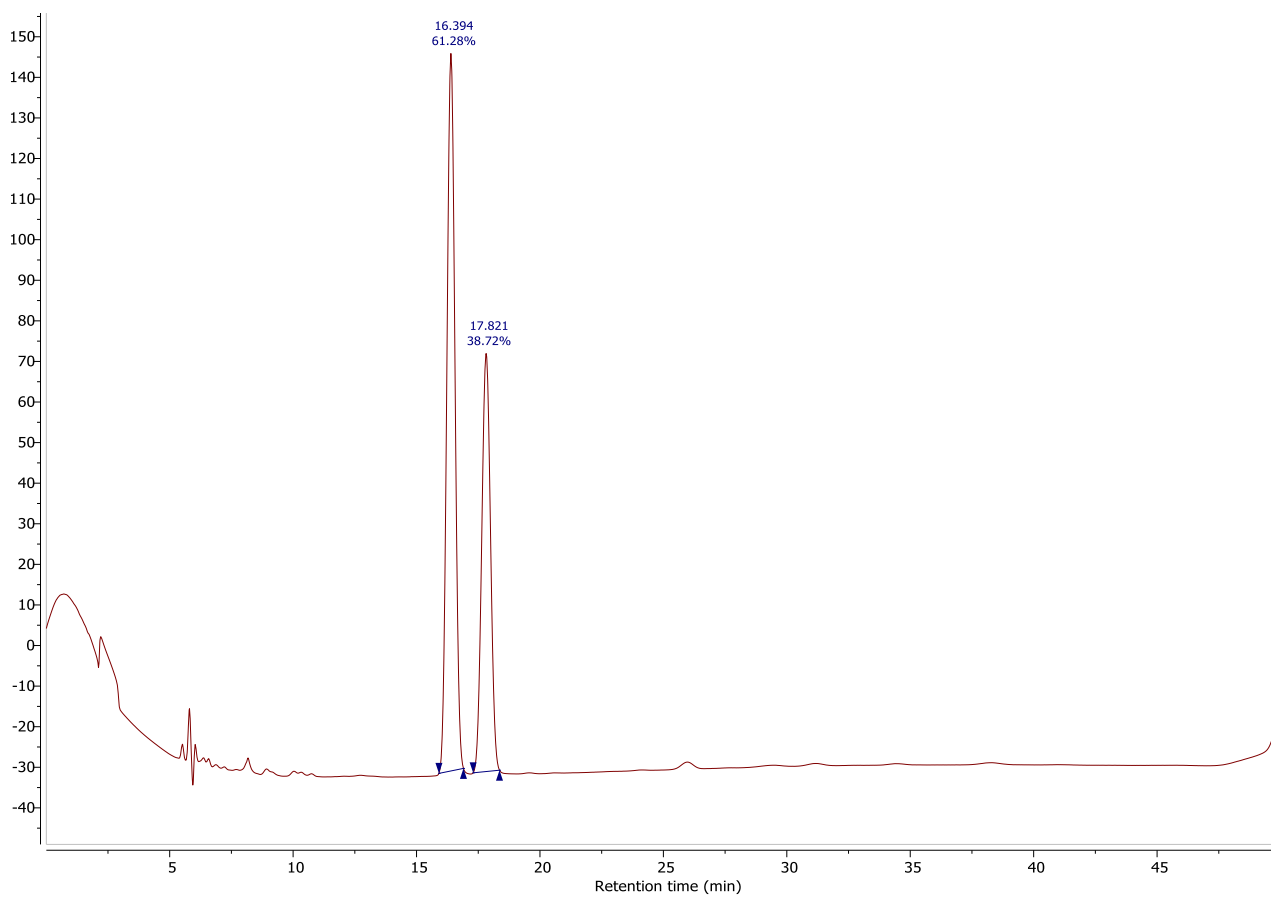
### 6.4.5.2 Chiral HPLC data for Table 12

#### 6.4.5.2.1 T-rSav:73



Entry	Retention time (min)	Peak Area (%)
1 ( <i>R</i> -enantiomer)	16.2	64.4
2 ( <i>S</i> -enantiomer)	17.6	35.6

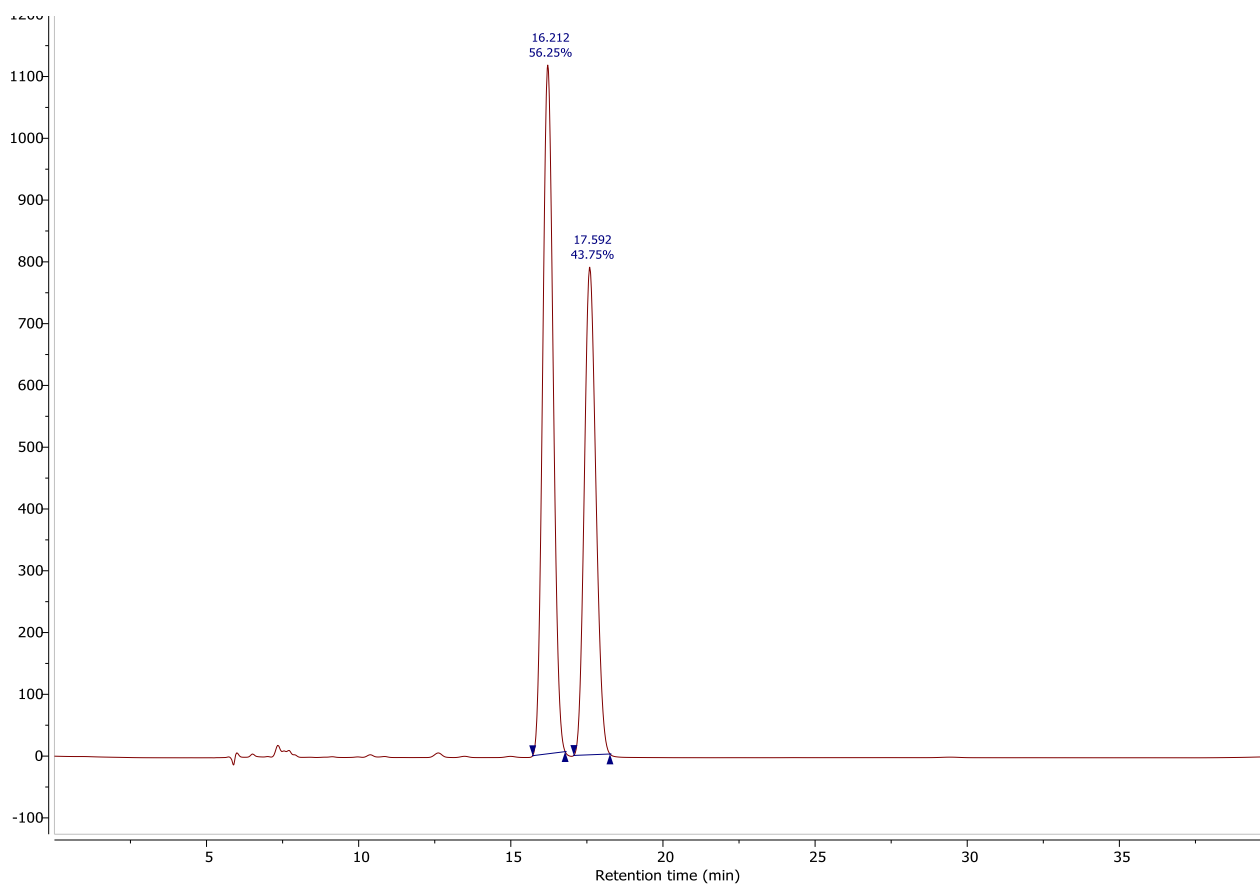
## 6.4.5.2.2 S112E:73



Entry	Retention time (min)	Peak Area (%)
1 ( <i>R</i> -enantiomer)	16.4	61.3
2 ( <i>S</i> -enantiomer)	17.8	38.7



## 6.4.5.2.3 K121A:73

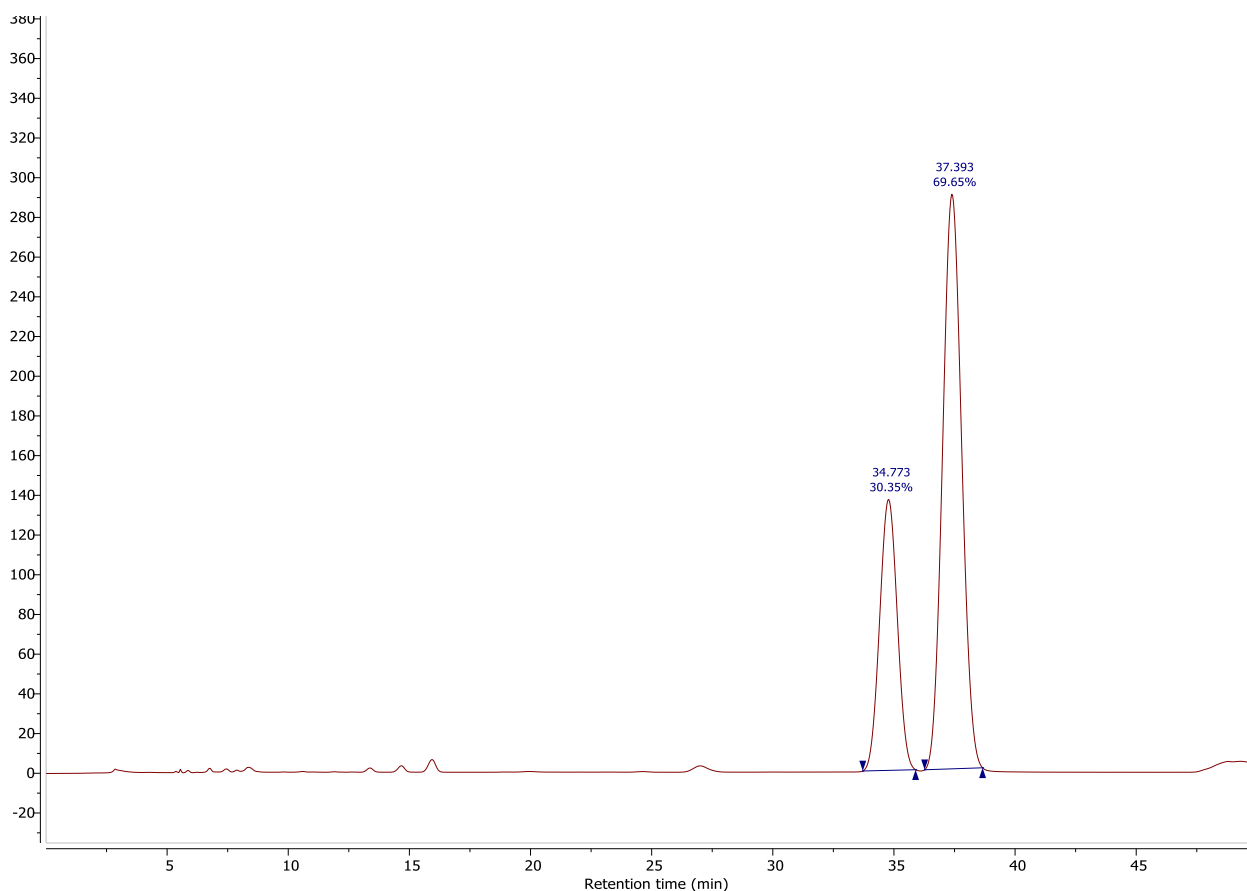


Entry	Retention time (min)	Peak Area (%)
1 ( <i>R</i> -enantiomer)	16.2	56.2
2 ( <i>S</i> -enantiomer)	17.6	43.8

### 6.4.5.3 Chiral HPLC data for Table 13

#### 6.4.5.3.1 (*S/R*)-4-hydroxy-4-(*m*-nitrophenyl) butan-2-one

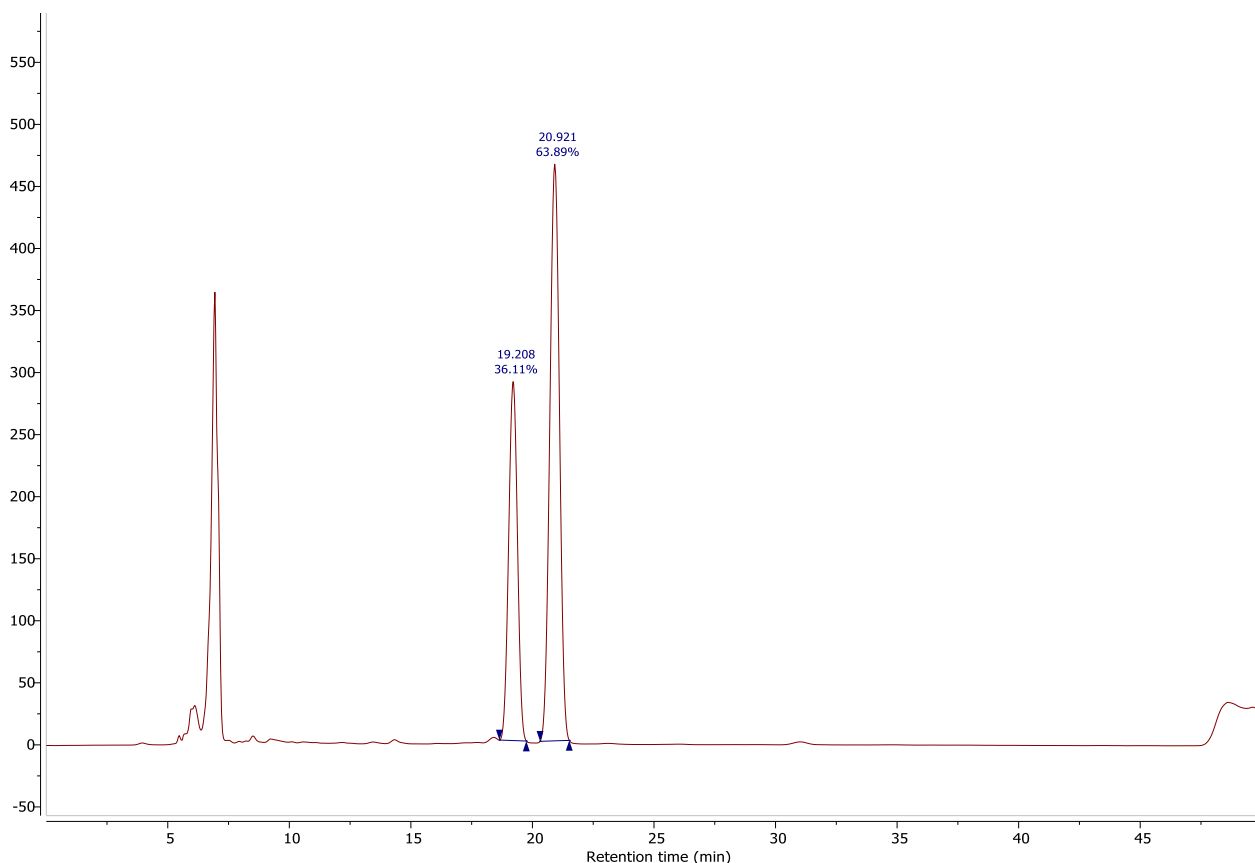
Analytical chiral HPLC analysis of product **162** was performed on an *Agilent Technologies 1260 Infinity Quaternary* LC system using a *Phenomenex Lux Amylose-1* column, 4.6 mm × 250 mm (0.5 mL/min, 25 °C, *n*-hexane/*iso*-propanol 90:10, 50 min). The peaks were assigned using signal at 280 nm. The absolute stereochemistry of **162** was assigned after running the sample obtained using L-proline as catalyst.



Entry	Retention time (min)	Peak Area (%)
1 ( <i>R</i> -enantiomer)	34.8	30.4
2 ( <i>S</i> -enantiomer)	37.4	69.6

### 6.4.5.3.2 (*S/R*)-4-hydroxy-4-(*m*-chlorophenyl) butan-2-one

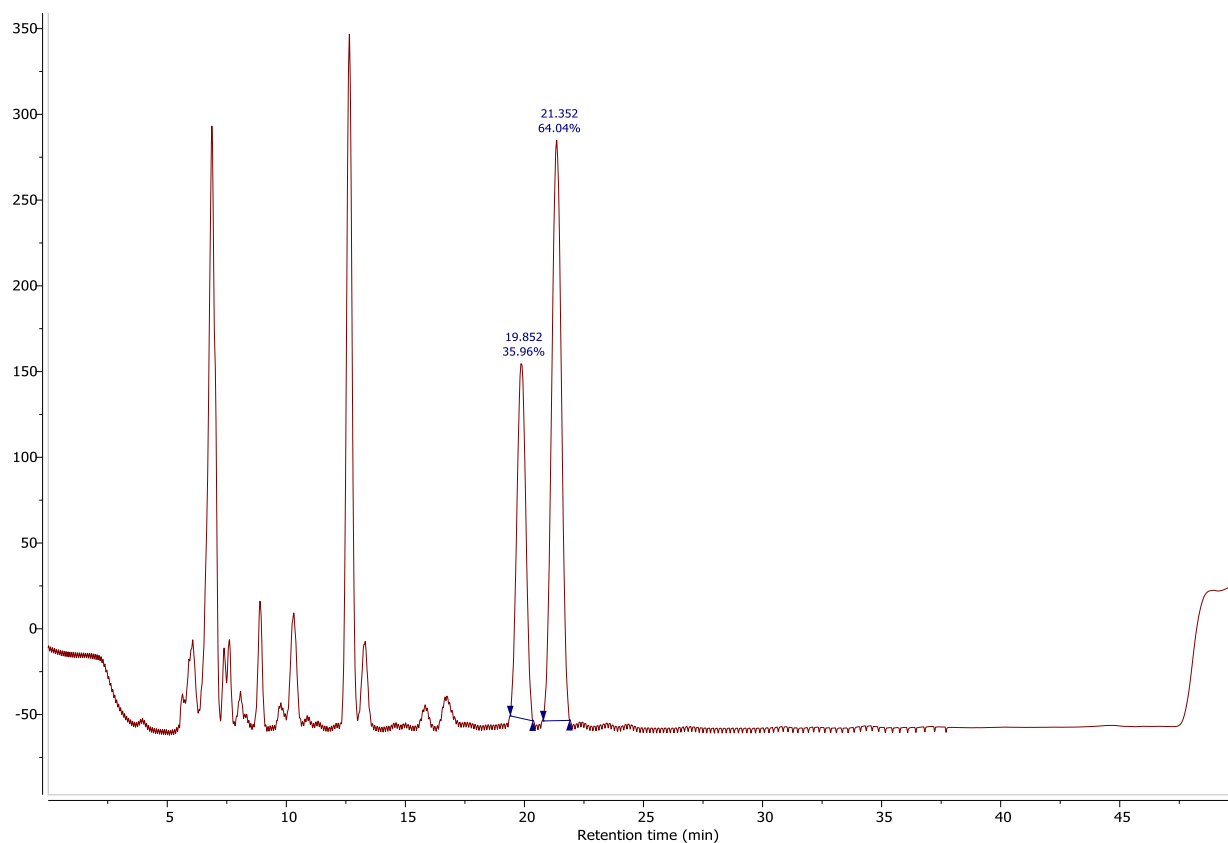
Analytical chiral HPLC analysis of product **164** was performed on an *Agilent Technologies 1260 Infinity Quaternary* LC system using a *Phenomenex Lux Amylose-1* column, 4.6 mm × 250 mm (0.5 mL/min, 25 °C, *n*-hexane/*iso*-propanol 90:10, 50 min). The peaks were assigned using signal at 254 nm. The absolute stereochemistry of **164** was assigned after running the sample obtained using L-proline as catalyst.



Entry	Retention time (min)	Peak Area (%)
1 ( <i>R</i> -enantiomer)	19.2	36.1
2 ( <i>S</i> -enantiomer)	20.9	63.9

### 6.4.5.3.3 (*S/R*)-4-hydroxy-4-(*m*-bromophenyl) butan-2-one

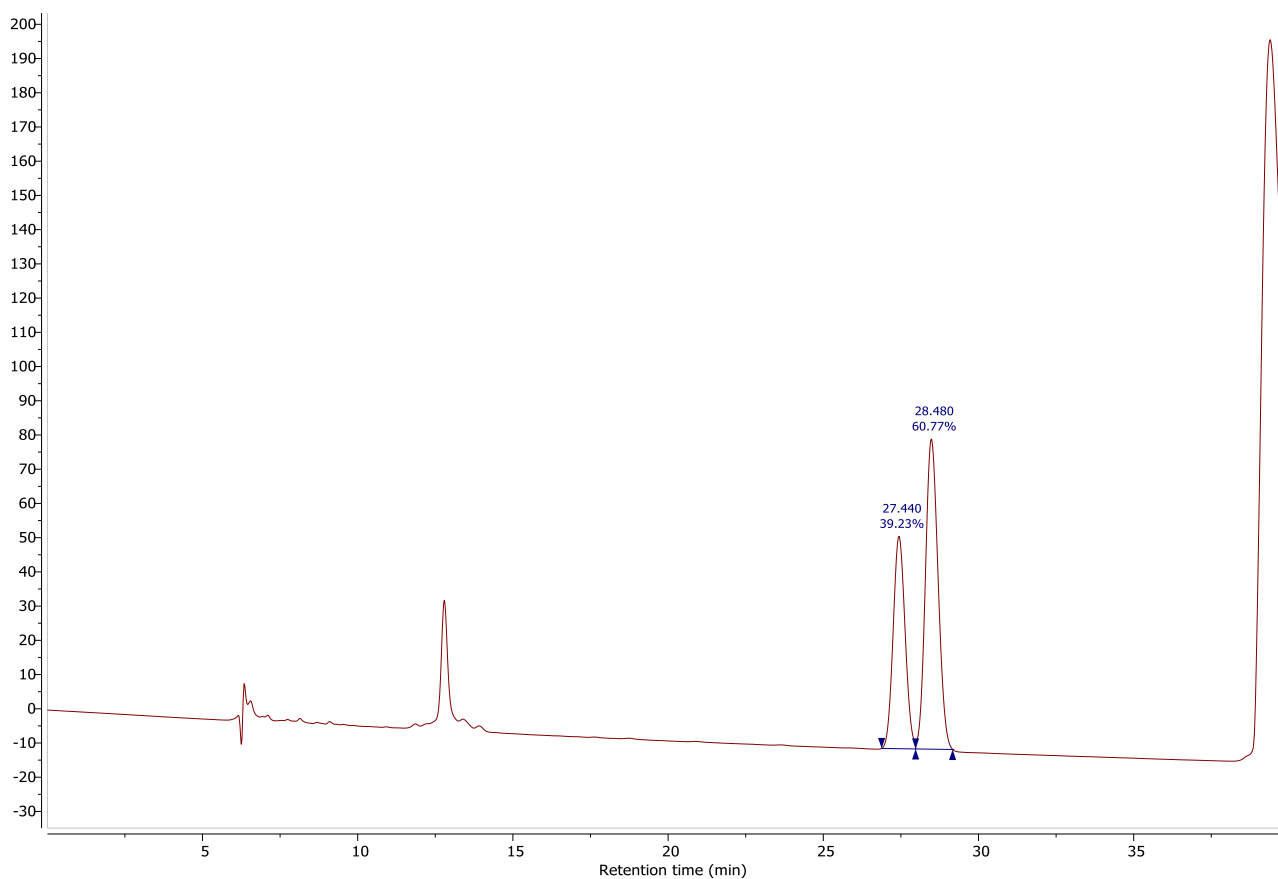
Analytical chiral HPLC analysis of product **165** was performed on an *Agilent Technologies 1260 Infinity Quaternary* LC system using a *Phenomenex Lux Amylose-1* column, 4.6 mm x 250 mm (0.5 mL/min, 25 °C, *n*-hexane/*iso*-propanol 90:10, 50 min). The peaks were assigned using signal at 254 nm. The absolute stereochemistry of **165** was assigned after running the sample obtained using L-proline as catalyst.



Entry	Retention time (min)	Peak Area (%)
1 ( <i>R</i> -enantiomer)	19.8	36.0
2 ( <i>S</i> -enantiomer)	21.3	64.0

**6.4.5.3.4 (S/R)-4-hydroxy-4-(p-bromophenyl) butan-2-one**

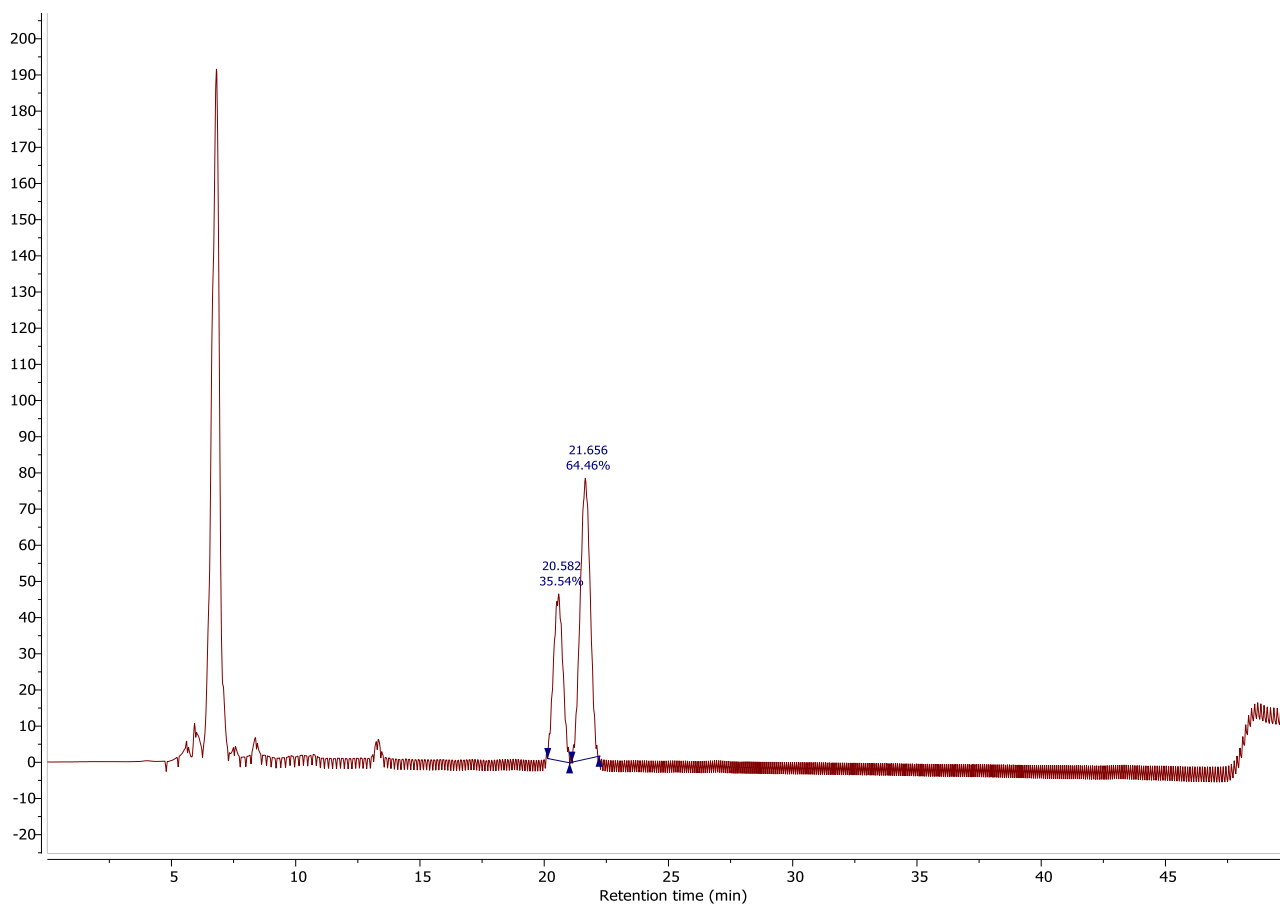
Analytical chiral HPLC analysis of product **166** was performed on an *Agilent Technologies 1260 Infinity Quaternary* LC system using a *Daicel ChiralPak® IE* column, 4.6 mm x 250 mm (0.5 mL/min, 25 °C, *n*-hexane/*iso*-propanol 93:7, 40 min). The peaks were assigned using signal at 254 nm. The absolute stereochemistry of **166** was assigned after running the sample obtained using L-proline as catalyst.



Entry	Retention time (min)	Peak Area (%)
1 ( <i>R</i> -enantiomer)	27.4	39.2
2 ( <i>S</i> -enantiomer)	28.4	60.8

#### 6.4.5.3.5 (*S/R*)-4-hydroxy-4-(*m*-iodophenyl) butan-2-one

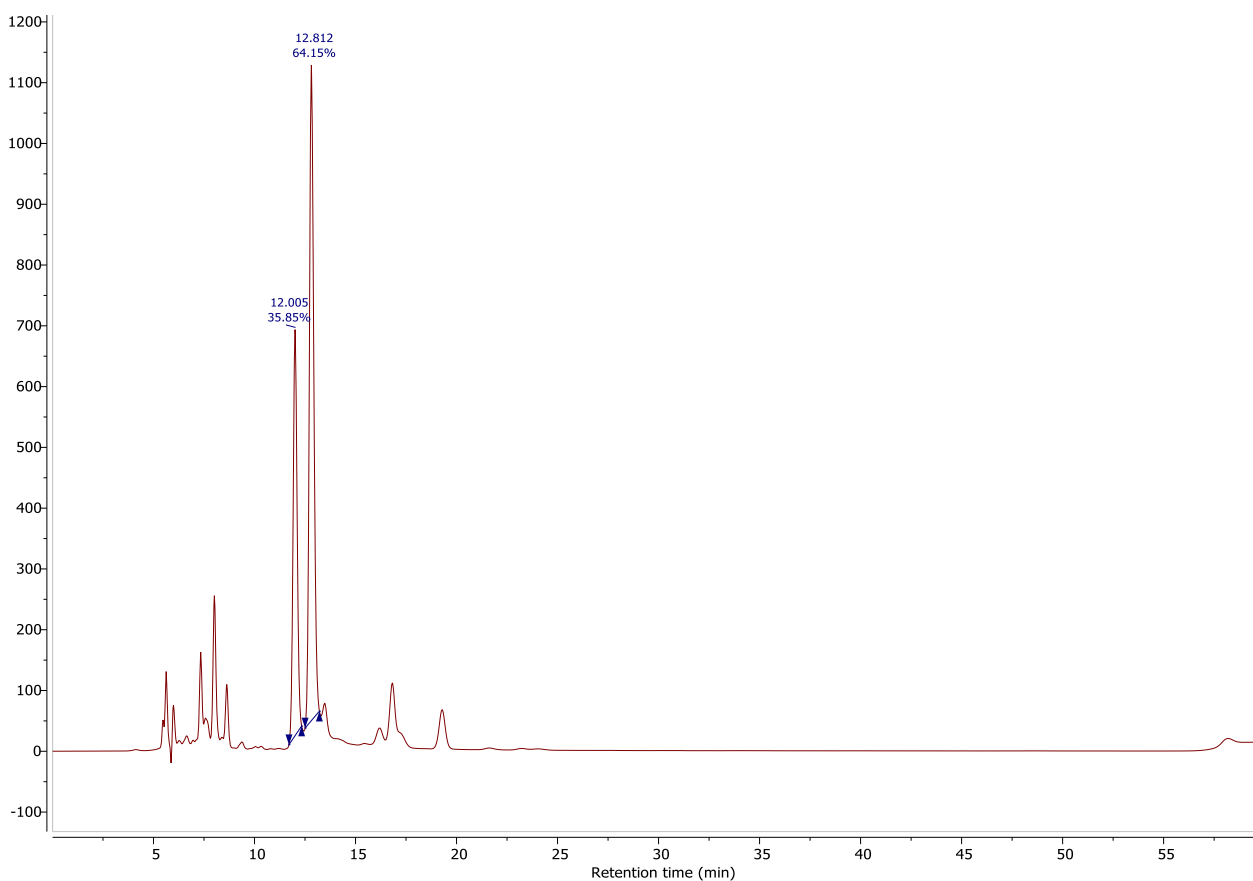
Analytical chiral HPLC analysis of product **167** was performed on an *Agilent Technologies 1260 Infinity Quaternary* LC system using a *Phenomenex Lux Amylose-1* column, 4.6 mm x 250 mm (0.5 mL/min, 25 °C, *n*-hexane/*iso*-propanol 90:10, 50 min). The peaks were assigned using signal at 254 nm. The absolute stereochemistry of **167** was assigned after running the sample obtained using L-proline as catalyst.



Entry	Retention time (min)	Peak Area (%)
1 ( <i>R</i> -enantiomer)	20.5	35.5
2 ( <i>S</i> -enantiomer)	21.6	64.5

#### 6.4.5.3.6 (*S/R*)-4-hydroxy-4-(perfluorophenyl) butan-2-one

Analytical chiral HPLC analysis of product **170** was performed on an *Agilent Technologies 1260 Infinity Quaternary* LC system using a *Phenomenex Lux Cellulose-1* column, 4.6 mm x 250 mm (0.5 mL/min, 25 °C, *n*-hexane/*iso*-propanol 85:15, 50 min). The peaks were assigned using signal at 214 nm. The absolute stereochemistry of **170** was assigned after running the sample obtained using L-proline as catalyst.



Entry	Retention time (min)	Peak Area (%)
1 ( <i>R</i> -enantiomer)	12.0	35.8
2 ( <i>S</i> -enantiomer)	12.8	64.2

## 6.5 References

1. J. Wisniak, *Edu. Quím.*, 2010, **21**, 60-69.
2. A. D. McNaught and A. Wilkinson, *Compendium of Chemical Terminology* Wiley, Oxford, 2<sup>nd</sup> edn., 1997.
3. A. Svante, *Z. Phys. Chem.*, 1889, **4U**, 96-116.
4. Y.-Q. Zou, F. M. Hörmann and T. Bach, *Chem. Soc. Rev.*, 2018, **47**, 278-290.
5. A. R. Nödling, N. Santi, T. L. Williams, Y.-H. Tsai and L. Y. P. Luk, *RSC Adv.*, 2020, **10**, 16147-16161.
6. M. P. van der Helm, B. Klemm and R. Eelkema, *Nature Reviews Chemistry*, 2019, **3**, 491-508.
7. V. G. Oliveira, M. F. C. Cardoso and L. S. M. Forezi, *Catalysts*, 2018, **8**.
8. F. R. Bisogno, M. G. López-Vidal and G. de Gonzalo, *Adv. Synth. Catal.*, 2017, **359**, 2026-2049.
9. C. Jimeno, *Org. Biomol. Chem.*, 2016, **14**, 6147-6164.
10. M. Nielsen, D. Worgull, T. Zweifel, B. Gschwend, S. Bertelsen and K. A. Jørgensen, *Chem. Commun.*, 2011, **47**, 632-649.
11. D. W. MacMillan, *Nature*, 2008, **455**, 304-308.
12. H. Kolbe, *Justus Liebigs Ann. Chem.*, 1860, **113**, 125-127.
13. Z. G. Hajos and D. R. Parrish, *J. Org. Chem.*, 1974, **39**, 1615-1621.
14. Z. G. Hajos and D. R. Parrish, *J. Org. Chem.*, 1974, **39**, 1612-1615.
15. B. List, *Tetrahedron*, 2002, **58**, 5573-5590.
16. U. Eder, G. Sauer and R. Wiechert, *Angew. Chem., Int. Ed.*, 1971, **10**, 496-497.
17. M. S. Sigman and E. N. Jacobsen, *J. Am. Chem. Soc.*, 1998, **120**, 4901-4902.
18. E. J. Corey and M. J. Grogan, *Org. Lett.*, 1999, **1**, 157-160.
19. Y. Tu, Z.-X. Wang and Y. Shi, *J. Am. Chem. Soc.*, 1996, **118**, 9806-9807.
20. D. Yang, Y.-C. Yip, M.-W. Tang, M.-K. Wong, J.-H. Zheng and K.-K. Cheung, *J. Am. Chem. Soc.*, 1996, **118**, 491-492.
21. S. E. Denmark, Z. Wu, C. M. Crudden and H. Matsuhashi, *J. Org. Chem.*, 1997, **62**, 8288-8289.
22. S. J. Miller, G. T. Copeland, N. Papaioannou, T. E. Horstmann and E. M. Ruel, *J. Am. Chem. Soc.*, 1998, **120**, 1629-1630.
23. D. P. Curran and L. H. Kuo, *Tetrahedron Lett.*, 1995, **36**, 6647-6650.
24. D. P. Curran and L. H. Kuo, *J. Org. Chem.*, 1994, **59**, 3259-3261.
25. J. Hine, S. M. Linden and V. M. Kanagasabapathy, *J. Am. Chem. Soc.*, 1985, **107**, 1082-1083.
26. T. R. Kelly, P. Meghani and V. S. Ekkundi, *Tetrahedron Lett.*, 1990, **31**, 3381-3384.
27. H. Stetter, R. Y. RÄMsch and H. Kuhlmann, *Synthesis*, 1976, **1976**, 733-735.
28. B. List, R. A. Lerner and C. F. Barbas, *J. Am. Chem. Soc.*, 2000, **122**, 2395-2396.
29. K. A. Ahrendt, C. J. Borths and D. W. C. MacMillan, *J. Am. Chem. Soc.*, 2000, **122**, 4243-4244.
30. G. J. Reyes-Rodríguez, N. M. Rezayee, A. Vidal-Albalat and K. A. Jørgensen, *Chem. Rev.*, 2019, **119**, 4221-4260.
31. B. Matos Paz, H. Jiang and K. A. Jørgensen, *Chem. Eur. J.*, 2015, **21**, 1846-1853.
32. K. L. Jensen, G. Dickmeiss, H. Jiang, Ł. Albrecht and K. A. Jørgensen, *Acc. Chem. Res.*, 2012, **45**, 248-264.
33. S. Bertelsen and K. A. Jørgensen, *Chem. Soc. Rev.*, 2009, **38**, 2178-2189.
34. E. N. Jacobsen and D. W. C. MacMillan, *Proc. Natl. Acad. Sci. U. S. A.*, 2010, **107**, 20618.
35. A. G. Doyle and E. N. Jacobsen, *Chem. Rev.*, 2007, **107**, 5713-5743.



36. D. W. C. MacMillan, *Nature*, 2008, **455**, 304-308.
37. A. Erkkilä, I. Majander and P. M. Pihko, *Chem. Rev.*, 2007, **107**, 5416-5470.
38. S. Bertelsen, M. Marigo, S. Brandes, P. Dinér and K. A. Jørgensen, *J. Am. Chem. Soc.*, 2006, **128**, 12973-12980.
39. Z.-J. Jia, H. Jiang, J.-L. Li, B. Gschwend, Q.-Z. Li, X. Yin, J. Grouleff, Y.-C. Chen and K. A. Jørgensen, *J. Am. Chem. Soc.*, 2011, **133**, 5053-5061.
40. J. Stiller, P. H. Poulsen, D. C. Cruz, J. Dourado, R. L. Davis and K. A. Jørgensen, *Chem. Sci.*, 2014, **5**, 2052-2056.
41. X. Tian, Y. Liu and P. Melchiorre, *Angew. Chem., Int. Ed.*, 2012, **51**, 6439-6442.
42. T. D. Beeson, A. Mastracchio, J.-B. Hong, K. Ashton and D. W. C. MacMillan, *Science*, 2007, **316**, 582.
43. S. Mukherjee, J. W. Yang, S. Hoffmann and B. List, *Chem. Rev.*, 2007, **107**, 5471-5569.
44. M. Tavakolian, S. Vahdati-Khajeh and S. Asgari, *ChemCatChem*, 2019, **11**, 2943-2977.
45. K. L. Jensen, G. Dickmeiss, H. Jiang, L. Albrecht and K. A. Jørgensen, *Acc. Chem. Res.*, 2012, **45**, 248-264.
46. A. Watson and D. MacMillan, in *Catalytic Asymmetric Synthesis, 3rd Edition*, 2010, pp. 39-57.
47. A. Erkkilä, I. Majander and P. M. Pihko, *Chem. Rev.*, 2007, **107**, 5416-5470.
48. A. C. Kinsman and M. A. Kerr, *J. Am. Chem. Soc.*, 2003, **125**, 14120-14125.
49. M. G. Banwell, D. A. S. Beck and A. C. Willis, *ArkiVoc*, 2006, **163**, 163-174.
50. M. P. van der Helm, B. Klemm and R. Eelkema, *Nat. Rev. Chem.*, 2019, **3**, 491-508.
51. M. Marigo, T. C. Wabnitz, D. Fielenbach and K. A. Jørgensen, *Angew. Chem., Int. Ed.*, 2005, **44**, 794-797.
52. Y. Hayashi, H. Gotoh, T. Hayashi and M. Shoji, *Angew. Chem., Int. Ed.*, 2005, **44**, 4212-4215.
53. B. S. Donslund, T. K. Johansen, P. H. Poulsen, K. S. Halskov and K. A. Jørgensen, *Angew. Chem., Int. Ed.*, 2015, **54**, 13860-13874.
54. S. Bertelsen and K. A. Jørgensen, *Chem. Soc. Rev.*, 2009, **38**, 2178-2189.
55. N. A. Paras and D. W. C. MacMillan, *J. Am. Chem. Soc.*, 2001, **123**, 4370-4371.
56. P. Breistein, S. Karlsson and E. Hedenström, *Tetrahedron: Asymmetry*, 2006, **17**, 107-111.
57. J.-W. Xie, L. Yue, D. Xue, X.-L. Ma, Y.-C. Chen, Y. Wu, J. Zhu and J.-G. Deng, *Chem. Commun.*, 2006, 1563-1565.
58. M. T. Hechavarria Fonseca and B. List, *Angew. Chem., Int. Ed.*, 2004, **43**, 3958-3960.
59. J. F. Austin and D. W. C. MacMillan, *J. Am. Chem. Soc.*, 2002, **124**, 1172-1173.
60. N. A. Paras and D. W. C. MacMillan, *J. Am. Chem. Soc.*, 2002, **124**, 7894-7895.
61. D. Madec, F. Mingoia, C. Macovei, G. Maitro, G. Giambastiani and G. Poli, *Eur. J. Org. Chem.*, 2005, **2005**, 552-557.
62. R. M. Wilson, W. S. Jen and D. W. C. MacMillan, *J. Am. Chem. Soc.*, 2005, **127**, 11616-11617.
63. S. P. Brown, N. C. Goodwin and D. W. C. MacMillan, *J. Am. Chem. Soc.*, 2003, **125**, 1192-1194.
64. W. Wang, H. Li and J. Wang, *Org. Lett.*, 2005, **7**, 1637-1639.
65. S. G. Ouellet, J. B. Tuttle and D. W. C. MacMillan, *J. Am. Chem. Soc.*, 2005, **127**, 32-33.
66. S. Hanessian and V. Pham, *Org. Lett.*, 2000, **2**, 2975-2978.
67. N. Utsumi, H. Zhang, F. Tanaka and C. F. Barbas lii, *Angew. Chem. Int. Ed.*, 2007, **46**, 1878-1880.

68. B.-C. Hong, M.-F. Wu, H.-C. Tseng and J.-H. Liao, *Org. Lett.*, 2006, **8**, 2217-2220.
69. D. B. Ramachary, K. Anebuselvy, N. S. Chowdari and C. F. Barbas, *The Journal of Organic Chemistry*, 2004, **69**, 5838-5849.
70. M. Marigo, J. Franzén, T. B. Poulsen, W. Zhuang and K. A. Jørgensen, *J. Am. Chem. Soc.*, 2005, **127**, 6964-6965.
71. V. Terrasson, A. van der Lee, R. Marcia de Figueiredo and J. M. Campagne, *Chem.: Eur. J.*, 2010, **16**, 7875-7880.
72. R. Rios, H. Sundén, J. Vesely, G.-L. Zhao, P. Dzedzic and A. Córdova, *Adv. Synth. Catal.*, 2007, **349**, 1028-1032.
73. J. Vesely, I. Ibrahim, G.-L. Zhao, R. Rios and A. Córdova, *Angew. Chem., Int. Ed.*, 2007, **46**, 778-781.
74. B. S. Vachan, M. Karuppasamy, P. Vinoth, S. Vivek Kumar, S. Perumal, V. Sridharan and J. C. Menéndez, *Advanced Synthesis & Catalysis*, 2019, **0**.
75. C. Jimeno, *Org. Biomol. Chem.*, 2016, **14**, 6147-6164.
76. R. J. Spears, R. L. Brabham, D. Budhadev, T. Keenan, S. McKenna, J. Walton, J. A. Brannigan, A. M. Brzozowski, A. J. Wilkinson, M. Plevin and M. A. Fascione, *Chem. Sci.*, 2018, **9**, 5585-5593.
77. I. Drienovská, C. Mayer, C. Dulson and G. Roelfes, *Nat. Chem.*, 2018, **10**, 946-952.
78. Y. Qin, L. Zhu and S. Luo, *Chem. Rev.*, 2017, **117**, 9433-9520.
79. Y. B. Wang and B. Tan, *Acc. Chem. Res.*, 2018, **51**, 534-547.
80. S. Y. Jang, D. P. Murale, A. D. Kim and J. S. Lee, *ChemBioChem*, 2019, **20**, 1498-1507.
81. J. Lou, F. Liu, C. D. Lindsay, O. Chaudhuri, S. C. Heilshorn and Y. Xia, *Adv. Mater.*, 2018, **30**, 1705215.
82. G. Liang, H. Ren and J. Rao, *Nat. Chem.*, 2010, **2**, 54-60.
83. H. Ren, F. Xiao, K. Zhan, Y. P. Kim, H. Xie, Z. Xia and J. Rao, *Angew. Chem., Int. Ed.*, 2009, **48**, 9658-9662.
84. D. W. MacMillan, *Nature*, 2008, **455**, 304-308.
85. T. D. Beeson and D. W. C. MacMillan, *J. Am. Chem. Soc.*, 2005, **127**, 8826-8828.
86. S. G. Ouellet, J. B. Tuttle and D. W. MacMillan, *J. Am. Chem. Soc.*, 2005, **127**, 32-33.
87. W. Notz, F. Tanaka and C. F. Barbas III, *Acc. Chem. Res.*, 2004, **37**, 580-591.
88. O. V. Serdyuk, C. M. Heckel and S. B. Tsogoeva, *Org. Biomol. Chem.*, 2013, **11**, 7051-7071.
89. Y. Zhao, Y. Cotelle, L. Liu, J. Lopez-Andarias, A. B. Bornhof, M. Akamatsu, N. Sakai and S. Matile, *Acc. Chem. Res.*, 2018, **51**, 2255-2263.
90. R. J. Spears and M. A. Fascione, *Org. Biomol. Chem.*, 2016, **14**, 7622-7638.
91. M. Heidlindemann, G. Rulli, A. Berkessel, W. Hummel and H. Gröger, *ACS Catal.*, 2014, **4**, 1099-1103.
92. G. Rulli, N. Duangdee, K. Baer, W. Hummel, A. Berkessel and H. Gröger, *Angew. Chem., Int. Ed.*, 2011, **50**, 7944-7947.
93. K. Baer, M. Krausser, E. Burda, W. Hummel, A. Berkessel and H. Gröger, *Angew. Chem., Int. Ed.*, 2009, **48**, 9355-9358.
94. E. M. Sletten and C. R. Bertozzi, *Angew. Chem., Int. Ed.*, 2009, **48**, 6974-6998.
95. A. Mondal, S. Bhowmick, A. Ghosh, T. Chanda and K. C. Bhowmick, *Tetrahedron: Asymmetry*, 2017, **28**, 849-875.
96. S. Bhowmick, A. Mondal, A. Ghosh and K. C. Bhowmick, *Tetrahedron: Asymmetry*, 2015, **26**, 1215-1244.
97. Y.-Q. Yu and Z.-L. Wang, *J. Chin. Chem. Soc.*, 2013, **60**, 288-292.
98. L. Burroughs, M. E. Vale, J. A. R. Gilks, H. Forintos, C. J. Hayes and P. A. Clarke, *Chem. Commun.*, 2010, **46**, 4776-4778.

99. A. Seingeot, Y. Charmasson, M. Attolini and M. Maffei, *Heteroat. Chem.*, 2017, **28**, e21352.
100. W. W. Y. Leong, X. Chen and Y. R. Chi, *Green Chem.*, 2013, **15**, 1505-1508.
101. J. Yan, R. Sun, K. Shi, K. Li, L. Yang and G. Zhong, *J. Org. Chem.*, 2018, **83**, 7547-7552.
102. N. Mase, Y. Nakai, N. Ohara, H. Yoda, K. Takabe, F. Tanaka and C. F. Barbas III, *J. Am. Chem. Soc.*, 2006, **128**, 734-735.
103. G. Zhong, R. A. Lerner and C. F. Barbas III, *Angew. Chem., Int. Ed.*, 1999, **38**, 3738-3741.
104. B. S. Vachan, M. Karuppasamy, P. Vinoth, S. V. Kumar, S. Perumal, V. Sridharan and J. C. Menendez, *Adv. Synth. Catal.*, 2020, **362**, 87-110.
105. F. Schwizer, Y. Okamoto, T. Heinisch, Y. Gu, M. M. Pellizzoni, V. Lebrun, R. Reuter, V. Kohler, J. C. Lewis and T. R. Ward, *Chem. Rev.*, 2018, **118**, 142-231.
106. T. Heinisch and T. R. Ward, *Acc. Chem. Res.*, 2016, **49**, 1711-1721.
107. Y. Cotelle, V. Lebrun, N. Sakai, T. R. Ward and S. Matile, *ACS Cent. Sci.*, 2016, **2**, 388-393.
108. M. Rahimi, E. M. Geertsema, Y. Miao, J. Y. van der Meer, T. van den Bosch, P. de Haan, E. Zandvoort and G. J. Poelarends, *Org. Biomol. Chem.*, 2017, **15**, 2809-2816.
109. E. Zandvoort, E. M. Geertsema, B. J. Baas, W. J. Quax and G. J. Poelarends, *Angew. Chem., Int. Ed.*, 2012, **51**, 1240-1243.
110. A. R. Nödling, K. Świderek, R. Castillo, J. W. Hall, A. Angelastro, L. C. Morrill, Y. Jin, Y.-H. Tsai, V. Moliner and L. Y. P. Luk, *Angew. Chem., Int. Ed.*, 2018, **57**, 12478-12482.
111. X. Garrabou, D. S. Macdonald, B. I. M. Wicky and D. Hilvert, *Angew. Chem., Int. Ed.*, 2018, **57**, 5288-5291.
112. X. Garrabou, D. S. Macdonald and D. Hilvert, *Chem. - Eur. J.*, 2017, **23**, 6001-6003.
113. X. Garrabou, R. Verez and D. Hilvert, *J. Am. Chem. Soc.*, 2017, **139**, 103-106.
114. X. Garrabou, B. I. Wicky and D. Hilvert, *J. Am. Chem. Soc.*, 2016, **138**, 6972-6974.
115. X. Garrabou, T. Beck and D. Hilvert, *Angew. Chem., Int. Ed.*, 2015, **54**, 5609-5612.
116. H. J. Davis and T. R. Ward, *ACS Cent. Sci.*, 2019, **5**, 1120-1136.
117. C. Zeymer and D. Hilvert, *Annu. Rev. Biochem.*, 2018, **87**, 131-157.
118. C. Mayer, C. Dulson, E. Reddem, A. W. H. Thunnissen and G. Roelfes, *Angew. Chem., Int. Ed.*, 2019, **58**, 2083-2087.
119. L. Li, C. Li, Z. Zhang and E. Alexov, *J. Chem. Theory Comput.*, 2013, **9**, 2126-2136.
120. A. D. Liang, J. Serrano-Plana, R. L. Peterson and T. R. Ward, *Acc. Chem. Res.*, 2019, **52**, 585-595.
121. M. Hesticová, T. Heinisch, L. Alonso-Cotchico, J. D. Maréchal, P. Vidossich and T. R. Ward, *Angew. Chem., Int. Ed.*, 2018, **57**, 1863-1868.
122. G. Roelfes, *Acc. Chem. Res.*, 2019, **52**, 545-556.
123. Y. Wang, J. Chen and Z. Kang, *Biochemistry*, 2019, **58**, 1451-1453.
124. V. Vaissier Welborn and T. Head-Gordon, *Chem. Rev.*, 2019, **119**, 6613-6630.
125. H. Kries, R. Blomberg and D. Hilvert, *Curr. Opin. Chem. Biol.*, 2013, **17**, 221-228.
126. C. Trindler and T. R. Ward, in *Effects of Nanoconfinement on Catalysis*, ed. R. Poli, Springer International Publishing, Cham, 2017, ch. 49, pp. 49-82.
127. M. M. Pellizzoni, F. Schwizer, C. W. Wood, V. Sabatino, Y. Cotelle, S. Matile, D. N. Woolfson and T. R. Ward, *ACS Catal.*, 2018, **8**, 1476-1484.
128. K. Akagawa and K. Kudo, *Acc. Chem. Res.*, 2017, **50**, 2429-2439.
129. M. D. Toscano, K. J. Woycechowsky and D. Hilvert, *Angew. Chem., Int. Ed.*, 2007, **46**, 3212-3236.
130. E. T. Kaiser and D. S. Lawrence, *Science*, 1984, **226**, 505-511.

131. D. Qi, C. M. Tann, D. Haring and M. D. Distefano, *Chem. Rev.*, 2001, **101**, 3081-3111.
132. D. Häring, E. Schüler, W. Adam, C. R. Saha-Möller and P. Schreier, *J. Org. Chem.*, 1999, **64**, 832-835.
133. K. E. Neet and D. E. Koshland, Jr., *Proc. Natl. Acad. Sci. U. S. A.*, 1966, **56**, 1606-1611.
134. Z. P. Wu and D. Hilvert, *J. Am. Chem. Soc.*, 1990, **112**, 5647-5648.
135. Z. P. Wu and D. Hilvert, *J. Am. Chem. Soc.*, 1989, **111**, 4513-4514.
136. H. L. Levine, Y. Nakagawa and E. T. Kaiser, *Biochem. Biophys. Res. Commun.*, 1977, **76**, 64-70.
137. C. J. Suckling and L.-M. Zhu, *Bioorg. Med. Chem. Lett.*, 1993, **3**, 531-534.
138. H. Kuang, M. L. Brown, R. R. Davies, E. C. Young and M. D. Distefano, *J. Am. Chem. Soc.*, 1996, **118**, 10702-10706.
139. T. L. Williams, A. R. Nödling, Y. H. Tsai and L. Y. P. Luk, *Wellcome Open Res.*, 2018, **3**, 107.
140. S. Mao, Z. Dong, J. Liu, X. Li, X. Liu, G. Luo and J. Shen, *J. Am. Chem. Soc.*, 2005, **127**, 11588-11589.
141. J. C. Maza, D. L. V. Bader, L. Xiao, A. M. Marmelstein, D. D. Brauer, A. M. ElSohly, M. J. Smith, S. W. Krska, C. A. Parish and M. B. Francis, *J. Am. Chem. Soc.*, 2019, **141**, 3885-3892.
142. C. B. Rosen and M. B. Francis, *Nat. Chem. Biol.*, 2017, **13**, 697-705.
143. P. G. Isenegger and B. G. Davis, *J. Am. Chem. Soc.*, 2019, **141**, 8005-8013.
144. B. Bhushan, Y. A. Lin, M. Bak, A. Phanumartwiwath, N. Yang, M. K. Bilyard, T. Tanaka, K. L. Hudson, L. Lercher, M. Stegmann, S. Mohammed and B. G. Davis, *J. Am. Chem. Soc.*, 2018, **140**, 14599-14603.
145. S. R. G. Galan, J. R. Wickens, J. Dadova, W.-L. Ng, X. Zhang, R. A. Simion, R. Quinlan, E. Pires, R. S. Paton, S. Caddick, V. Chudasama and B. G. Davis, *Nat. Chem. Biol.*, 2018, **14**, 955-963.
146. A. Dumas, L. Lercher, C. D. Spicer and B. G. Davis, *Chem. Sci.*, 2015, **6**, 50-69.
147. M. Morais, N. Forte, V. Chudasama and J. R. Baker, in *Bioconjugation: Methods and Protocols*, eds. S. Massa and N. Devoogdt, Springer New York, New York, NY, 2019, ch. 15, pp. 15-24.
148. J. N. deGruyter, L. R. Malins and P. S. Baran, *Biochemistry*, 2017, **56**, 3863-3873.
149. D. Hilvert, *Annu. Rev. Biochem.*, 2013, **82**, 447-470.
150. A. Zanghellini, L. Jiang, A. M. Wollacott, G. Cheng, J. Meiler, E. A. Althoff, D. Röthlisberger and D. Baker, *Protein. Sci.*, 2006, **15**, 2785-2794.
151. A. Leaver-Fay, M. Tyka, S. M. Lewis, O. F. Lange, J. Thompson, R. Jacak, K. W. Kaufman, P. D. Renfrew, C. A. Smith, W. Sheffler, I. W. Davis, S. Cooper, A. Treuille, D. J. Mandell, F. Richter, Y.-E. A. Ban, S. J. Fleishman, J. E. Corn, D. E. Kim, S. Lyskov, M. Berrondo, S. Mentzer, Z. Popović, J. J. Havranek, J. Karanicolas, R. Das, J. Meiler, T. Kortemme, J. J. Gray, B. Kuhlman, D. Baker and P. Bradley, in *Methods in Enzymology*, eds. M. L. Johnson and L. Brand, Academic Press, 2011, vol. 487, ch. 545, pp. 545-574.
152. D. J. Tantillo, C. Jiangang and K. N. Houk, *Curr. Opin. Chem. Biol.*, 1998, **2**, 743-750.
153. M. Merski and B. K. Shoichet, *Proc. Natl. Acad. Sci. U. S. A.*, 2012, **109**, 16179-16783.
154. D. Röthlisberger, O. Khersonsky, A. M. Wollacott, L. Jiang, J. DeChancie, J. Betker, J. L. Gallaher, E. A. Althoff, A. Zanghellini, O. Dym, S. Albeck, K. N. Houk, D. S. Tawfik and D. Baker, *Nature*, 2008, **453**, 190-195.
155. C. Zeymer, R. Zschoche and D. Hilvert, *J. Am. Chem. Soc.*, 2017, **139**, 12541-12549.
156. R. Obexer, S. Studer, L. Giger, D. M. Pinkas, M. G. Grütter, D. Baker and D. Hilvert, *ChemCatChem*, 2014, **6**, 1043-1050.

157. L. Giger, S. Caner, R. Obexer, P. Kast, D. Baker, N. Ban and D. Hilvert, *Nat. Chem. Biol.*, 2013, **9**, 494-498.
158. L. Jiang, E. A. Althoff, F. R. Clemente, L. Doyle, D. Röthlisberger, A. Zanghellini, J. L. Gallaher, J. L. Betker, F. Tanaka, C. F. Barbas III, D. Hilvert, K. N. Houk, B. L. Stoddard and D. Baker, *Science*, 2008, **319**, 1387-1391.
159. E. A. Althoff, L. Wang, L. Jiang, L. Giger, J. K. Lassila, Z. Wang, M. Smith, S. Hari, P. Kast, D. Herschlag, D. Hilvert and D. Baker, *Protein. Sci.*, 2012, **21**, 717-726.
160. S. Bjelic, L. G. Nivón, N. Çelebi-Ölçüm, G. Kiss, C. F. Rosewall, H. M. Lovick, E. L. Ingalls, J. L. Gallaher, J. Seetharaman, S. Lew, G. T. Montelione, J. F. Hunt, F. E. Michael, K. N. Houk and D. Baker, *ACS Chem. Biol.*, 2013, **8**, 749-757.
161. J. Lazic, J. Spasic, D. Francuski, Z. Tokic-Vujosevic, J. Nikodinovic-Runic, V. Maslak and L. Djokic, *J. Serb. Chem. Soc.*, 2016, **81**.
162. T. K. Harris, R. M. Czerwinski, W. H. Johnson, Jr., P. M. Legler, C. Abeygunawardana, M. A. Massiah, J. T. Stivers, C. P. Whitman and A. S. Mildvan, *Biochemistry*, 1999, **38**, 12343-12357.
163. E. A. Burks, C. D. Fleming, A. D. Mesezar, C. P. Whitman and S. D. Pegan, *Biochemistry*, 2010, **49**, 5016-5027.
164. E. Zandvoort, B.-J. Baas, W. J. Quax and G. J. Poelarends, *ChemBioChem*, 2011, **12**, 602-609.
165. E. M. Geertsema, Y. Miao, P. G. Tepper, P. de Haan, E. Zandvoort and G. J. Poelarends, *Chem. - Eur. J.*, 2013, **19**, 14407-14410.
166. Y. Miao, E. M. Geertsema, P. G. Tepper, E. Zandvoort and G. J. Poelarends, *ChemBioChem*, 2013, **14**, 191-194.
167. C. Guo, M. Saifuddin, T. Saravanan, M. Sharifi and G. J. Poelarends, *ACS Catal.*, 2019, **9**, 4369-4373.
168. E. Zandvoort, E. M. Geertsema, W. J. Quax and G. J. Poelarends, *ChemBioChem*, 2012, **13**, 1274-1277.
169. M. Saifuddin, C. Guo, L. Biewenga, T. Saravanan, S. J. Charnock and G. J. Poelarends, *ACS Catal.*, 2020, **10**, 2522-2527.
170. L. Biewenga, T. Saravanan, A. Kunzendorf, J. Y. van der Meer, T. Pijning, P. G. Tepper, R. van Merkerk, S. J. Charnock, A. W. H. Thunnissen and G. J. Poelarends, *ACS Catal.*, 2019, **9**, 1503-1513.
171. T. Narancic, J. Radivojevic, P. Jovanovic, D. Francuski, M. Bigovic, V. Maslak, V. Savic, B. Vasiljevic, K. E. O'Connor and J. Nikodinovic-Runic, *Bioresour. Technol.*, 2013, **142**, 462-468.
172. L. Djokic, J. Spasic, S. Jeremic, B. Vasiljevic, O. Prodanovic, R. Prodanovic and J. Nikodinovic-Runic, *Bioprocess. Biosyst. Eng.*, 2015, **38**, 2389-2395.
173. J. Radivojevic, G. Minovska, L. Senerovic, K. O'Connor, P. Jovanovic, V. Savic, Z. Tokic-Vujosevic, J. Nikodinovic-Runic and V. Maslak, *RSC Adv.*, 2014, **4**, 60502-60510.
174. A. R. Nödling, L. A. Spear, T. L. Williams, L. Y. P. Luk and Y.-H. Tsai, *Essays Biochem.*, 2019, **63**, 237-266.
175. J. W. Chin, S. W. Santoro, A. B. Martin, D. S. King, L. Wang and P. G. Schultz, *J. Am. Chem. Soc.*, 2002, **124**, 9026-9027.
176. R. B. Leveson-Gower, C. Mayer and G. Roelfes, *Nat. Rev. Chem.*, 2019, **3**, 687-705.
177. J. Bos, W. R. Browne, A. J. Driessen and G. Roelfes, *J. Am. Chem. Soc.*, 2015, **137**, 9796-9799.
178. Z. Zhou and G. Roelfes, *Nat. Catal.*, 2020, **3**, 289-294.
179. A. J. Burke, S. L. Lovelock, A. Frese, R. Crawshaw, M. Ortmayer, M. Dunstan, C. Levy and A. P. Green, *Nature*, 2019, **570**, 219-223.

180. J. W. Chin, *Nature*, 2017, **550**, 53-60.
181. I. S. Hassan, A. N. Ta, M. W. Danneman, N. Semakul, M. Burns, C. H. Basch, V. N. Dippon, B. R. McNaughton and T. Rovis, *J. Am. Chem. Soc.*, 2019, **141**, 4815-4819.
182. D. J. Raines, J. E. Clarke, E. V. Blagova, E. J. Dodson, K. S. Wilson and A.-K. Duhme-Klair, *Nat. Catal.*, 2018, **1**, 680-688.
183. F. W. Monnard, E. S. Nogueira, T. Heinisch, T. Schirmer and T. R. Ward, *Chem. Sci.*, 2013, **4**, 3269-3274.
184. T. R. Ward, *Acc. Chem. Res.*, 2011, **44**, 47-57.
185. M. T. Reetz, J. J. Peyralans, A. Maichele, Y. Fu and M. Maywald, *Chem. Commun.*, 2006, 4318-4320.
186. T. Heinisch, F. Schwizer, B. Garabedian, E. Csibra, M. Jeschek, J. Vallapurackal, V. B. Pinheiro, P. Marliere, S. Panke and T. R. Ward, *Chem. Sci.*, 2018, **9**, 5383-5388.
187. M. Jeschek, R. Reuter, T. Heinisch, C. Trindler, J. Klehr, S. Panke and T. R. Ward, *Nature*, 2016, **537**, 661-665.
188. A. Zocchi, N. Humbert, T. Berta and T. R. Ward, *Chimia*, 2003, **57**, 589-592.
189. M. E. Wilson and G. M. Whitesides, *J. Am. Chem. Soc.*, 1978, **100**, 306-307.
190. L. Olshansky, R. Huerta-Lavorie, A. I. Nguyen, J. Vallapurackal, A. Furst, T. D. Tilley and A. S. Borovik, *J. Am. Chem. Soc.*, 2018, **140**, 2739-2742.
191. C.-C. Lin, C.-W. Lin and A. S. C. Chan, *Tetrahedron: Asymmetry*, 1999, **10**, 1887-1893.
192. J. Bos, W. R. Browne, A. J. Driessen and G. Roelfes, *J. Am. Chem. Soc.*, 2015, **137**, 9796-9799.
193. J. G. Rebelein, Y. Cotelle, B. Garabedian and T. R. Ward, *ACS Catal.*, 2019, **9**, 4173-4178.
194. J. Zhao, A. Kajetanowicz and T. R. Ward, *Org. Biomol. Chem.*, 2015, **13**, 5652-5655.
195. F. W. Monnard, T. Heinisch, E. S. Nogueira, T. Schirmer and T. R. Ward, *Chem. Commun.*, 2011, **47**, 8238-8240.
196. Q. Raffy, R. Ricoux, E. Sansiaume, S. Pethe and J.-P. Mahy, *J. Mol. Catal. A: Chem.*, 2010, **317**, 19-26.
197. E. Sansiaume, R. Ricoux, D. Gori and J.-P. Mahy, *Tetrahedron: Asymmetry*, 2010, **21**, 1593-1600.
198. E. Girgenti, R. Ricoux and J.-P. Mahy, *Tetrahedron*, 2004, **60**, 10049-10058.
199. L. Rondot, E. Girgenti, F. Oddon, C. Marchi-Delapierre, A. Jorge-Robin and S. Ménage, *J. Mol. Catal. A: Chem.*, 2016, **416**, 20-28.
200. T. M. Brauer, Q. Zhang and K. Tiefenbacher, *J. Am. Chem. Soc.*, 2017, **139**, 17500-17507.
201. T. M. Brauer, Q. Zhang and K. Tiefenbacher, *Angew. Chem., Int. Ed.*, 2016, **55**, 7698-7701.
202. R. E. Dawson, A. Hennig, D. P. Weimann, D. Emery, V. Ravikumar, J. Montenegro, T. Takeuchi, S. Gabutti, M. Mayor, J. Mareda, C. A. Schalley and S. Matile, *Nat. Chem.*, 2010, **2**, 533-538.
203. Y. Zhao, Y. Domoto, E. Orentas, C. Beuchat, D. Emery, J. Mareda, N. Sakai and S. Matile, *Angew. Chem., Int. Ed.*, 2013, **52**, 9940-9943.
204. Y. Zhao, Y. Cotelle, A.-J. Avestro, N. Sakai and S. Matile, *J. Am. Chem. Soc.*, 2015, **137**, 11582-11585.
205. Y. Zhao, C. Beuchat, Y. Domoto, J. Gajewy, A. Wilson, J. Mareda, N. Sakai and S. Matile, *J. Am. Chem. Soc.*, 2014, **136**, 2101-2111.
206. A. J. Neel, M. J. Hilton, M. S. Sigman and F. D. Toste, *Nature*, 2017, **543**, 637-646.
207. M. Giese, M. Albrecht and K. Rissanen, *Chem. Commun.*, 2016, **52**, 1778-1795.

208. L. Liu, Y. Cotelle, J. Klehr, N. Sakai, T. R. Ward and S. Matile, *Chem. Sci.*, 2017, **8**, 3770-3774.
209. Y. Cotelle, S. Benz, A.-J. Avestro, T. R. Ward, N. Sakai and S. Matile, *Angew. Chem., Int. Ed.*, 2016, **55**, 4275-4279.
210. S. Wu, Y. Zhou, J. G. Rebelein, M. Kuhn, H. Mallin, J. Zhao, N. V. Igareta and T. R. Ward, *J. Am. Chem. Soc.*, 2019, **141**, 15869-15878.
211. S. Eda, I. Nasibullin, K. Vong, N. Kudo, M. Yoshida, A. Kurbangalieva and K. Tanaka, *Nat. Catal.*, 2019, **2**, 780-792.
212. K. H. Lim, H. Huang, A. Pralle and S. Park, *Biochemistry*, 2011, **50**, 8682-8691.
213. Q. Le, V. Nguyen and S. Park, *Applied Microbio. & Biotech.*, 2019, **103**, 7355-7365.
214. C. M. Dundas, D. Demonte and S. J. A. M. a. B. Park, *Appl. Microbiol. Biotechnol.*, 2013, **97**, 9343-9353.
215. D. Demonte, C. M. Dundas and S. Park, *Appl. Microbiol. Biotechnol.*, 2014, **98**, 6285-6295.
216. A. Kroetsch, B. Chin, V. Nguyen, J. Gao and S. Park, *Applied Microbio. & Biotech.*, 2018, **102**, 10079-10089.
217. A. D. Liang, J. Serrano-Plana, R. L. Peterson and T. R. Ward, *Acc. Chem. Res.*, 2019, **52**, 585-595.
218. Y. Okamoto, R. Kojima, F. Schwizer, E. Bartolami, T. Heinisch, S. Matile, M. Fussenegger and T. R. Ward, *Nat. Commun.*, 2018, **9**, 1943.
219. Y. Zhao, Y. Cotelle, L. Liu, J. López-Andarias, A.-B. Bornhof, M. Akamatsu, N. Sakai and S. Matile, *Acc. Chem. Res.*, 2018, **51**, 2255-2263.
220. Y. Cotelle, V. Lebrun, N. Sakai, T. R. Ward and S. Matile, *ACS Cent. Sci.*, 2016, **2**, 388-393.
221. M. Hesticova, T. Heinisch, L. Alonso-Cotchico, J. D. Marechal, P. Vidossich and T. R. Ward, *Angew. Chem., Int. Ed.*, 2018, **57**, 1863-1868.
222. I. Chamma, M. Letellier, C. Butler, B. Tessier, K.-H. Lim, I. Gauthereau, D. Choquet, J.-B. Sibarita, S. Park, M. Sainlos and O. Thoumine, *Nat. Commun.*, 2016, **7**, 10773.
223. T. Terai, M. Kohno, G. Boncompain, S. Sugiyama, N. Saito, R. Fujikake, T. Ueno, T. Komatsu, K. Hanaoka, T. Okabe, Y. Urano, F. Perez and T. Nagano, *J. Am. Chem. Soc.*, 2015, **137**, 10464-10467.
224. C. M. Csizmar, J. R. Petersburg, A. Hendricks, L. A. Stern, B. J. Hackel and C. R. Wagner, *Bioconjugate Chem.*, 2018, **29**, 1291-1301.
225. X.-Y. Tang, Y. Sun, A. Zhang, G.-L. Hu, W. Cao, D.-H. Wang, B. Zhang and H. Chen, *BMJ Open*, 2016, **6**, e013904.
226. K. H. Lim, H. Huang, A. Pralle and S. Park, *Biochemistry*, 2011, **50**, 8682-8691.
227. K. H. Lim, H. Huang, A. Pralle and S. Park, *Biotechnol. Bioeng.*, 2013, **110**, 57-67.
228. D. Demonte, E. J. Drake, K. H. Lim, A. M. Gulick and S. Park, *Proteins*, 2013, **81**, 1621-1633.
229. D. DeMonte, E. J. Drake, K. H. Lim, A. M. Gulick and S. Park, *Proteins*, 2013, **81**, 1621-1633.
230. F. W. Studier and B. A. Moffatt, *Journal of Molecular Biology*, 1986, **189**, 113-130.
231. O. H. Laitinen, K. J. Airene, V. P. Hytönen, E. Peltomaa, A. J. Mähönen, T. Wirth, M. M. Lind, K. A. Mäkelä, P. I. Toivanen, D. Schenkwein, T. Heikura, H. R. Nordlund, M. S. Kulomaa and S. Ylä-Herttuala, *Nucleic Acids Res.*, 2005, **33**, e42-e42.
232. C. M. Dundas, D. Demonte and S. Park, *Appl. Microbiol. Biotechnol.*, 2013, **97**, 9343-9353.
233. S. Repo, T. A. Paldanius, Vesa P. Hytönen, T. K. M. Nyholm, Katrin K. Halling, J. Huuskonen, Olli T. Pentikäinen, K. Rissanen, J. P. Slotte, T. T. Airene, T. A.

- Salminen, Markku S. Kulomaa and Mark S. Johnson, *Chem. Biol.*, 2006, **13**, 1029-1039.
234. W. Si, J. Gong, C. Chanas, S. Cui, H. Yu, C. Caballero and R. M. Friendship, *J. Appl. Microbiol.*, 2006, **101**, 1282-1291.
235. F. Schwizer, Y. Okamoto, T. Heinisch, Y. Gu, M. M. Pellizzoni, V. Lebrun, R. Reuter, V. Köhler, J. C. Lewis and T. R. Ward, *Chemical Reviews*, 2018, **118**, 142-231.
236. D. Wang and D. Astruc, *Chem. Rev.*, 2015, **115**, 6621-6686.
237. G. Brieger and T. J. Nestruck, *Chem. Rev.*, 1974, **74**, 567-580.
238. R. A. W. Johnstone, A. H. Wilby and I. D. Entwistle, *Chem. Rev.*, 1985, **85**, 129-170.
239. S. Gladiali and E. Alberico, *Chem. Soc. Rev.*, 2006, **35**, 226-236.
240. C. Wang, X. Wu and J. Xiao, *Chem. Asian J.*, 2008, **3**, 1750-1770.
241. J. W. Yang, M. T. Hechavarria Fonseca and B. List, *Angew. Chem., Int. Ed.*, 2004, **43**, 6660-6662.
242. J. Wang and Y.-G. Zhou, *Homogeneous Hydrogenation with Non-Precious Catalysts*, 2019, 261-284.
243. C. Zhu, K. Saito, M. Yamanaka and T. Akiyama, *Acc. Chem. Res.*, 2015, **48**, 388-398.
244. C. Zheng and S.-L. You, *Chem. Soc. Rev.*, 2012, **41**, 2498-2518.
245. J. Zhao, J. G. Rebelein, H. Mallin, C. Trindler, M. M. Pellizzoni and T. R. Ward, *J. Am. Chem. Soc.*, 2018, **140**, 13171-13175.
246. E. Tassano and M. Hall, *Chem. Soc. Rev.*, 2019, **48**, 5596-5615.
247. C. E. Paul, E. Churakova, E. Maurits, M. Girhard, V. B. Urlacher and F. Hollmann, *Bioorg. Med. Chem.*, 2014, **22**, 5692-5696.
248. N. Falcone, Z. She, J. Syed, A. Lough and H.-B. Kraatz, *ChemBioChem*, 2019, **20**, 838-845.
249. T. Knaus, C. E. Paul, C. W. Levy, S. de Vries, F. G. Mutti, F. Hollmann and N. S. Scrutton, *J. Am. Chem. Soc.*, 2016, **138**, 1033-1039.
250. C. E. Paul, S. Gargiulo, D. J. Opperman, I. Lavandera, V. Gotor-Fernández, V. Gotor, A. Taglieber, I. W. C. E. Arends and F. Hollmann, *Org. Lett.*, 2013, **15**, 180-183.
251. C. Nowak, A. Pick, P. Lommes and V. Sieber, *ACS Catal.*, 2017, **7**, 5202-5208.
252. A. Guarneri, A. H. Westphal, J. Leertouwer, J. Lunsonga, M. C. R. Franssen, D. J. Opperman, F. Hollmann, W. J. H. van Berkel and C. E. Paul, *ChemCatChem*, 2020, **12**, 1368-1375.
253. T. M. Bräuer, Q. Zhang and K. Tiefenbacher, *J. Am. Chem. Soc.*, 2017, **139**, 17500-17507.
254. T. Heinisch and T. R. Ward, *Acc. Chem. Res.*, 2016, **49**, 1711-1721.
255. Y. Cotelle, V. Lebrun, N. Sakai, T. R. Ward and S. Matile, *ACS Cent. Sci.*, 2016, **2**, 388-393.
256. S. Nicolò, M. L. Christian and L. L. Y. Pan., *Molecules*, 2020, **25**.
257. A. R. Nodling, K. Swiderek, R. Castillo, J. W. Hall, A. Angelastro, L. C. Morrill, Y. Jin, Y. H. Tsai, V. Moliner and L. Y. P. Luk, *Angew. Chem., Int. Ed.*, 2018, **57**, 12478-12482.
258. L. C. Wilkins, N. Santi, L. Y. P. Luk and R. L. Melen, *Philos. Trans. A Math. Phys. Eng. Sci.*, 2017, **375**, 20170009.
259. T. M. Bräuer, Q. Zhang and K. Tiefenbacher, *Angew. Chem., Int. Ed.*, 2016, **55**, 7698-7701.
260. W. S. Wadsworth Jr, *Organic Reactions*, 2005, 73-253.
261. W. S. Wadsworth and W. D. Emmons, *J. Am. Chem. Soc.*, 1961, **83**, 1733-1738.
262. G. Lefèbvre and J. Seyden-Penne, *J. Chem. Soc. D*, 1970, 1308-1309.
263. A. Geddes, C. E. Paul, S. Hay, F. Hollmann and N. S. Scrutton, *J. Am. Chem. Soc.*, 2016, **138**, 11089-11092.



264. T. Wymore, *ChemBioChem*, 2009, **10**, 2541-2541.
265. T. S. Howard, R. D. Cohen, O. Nwajobi, Z. P. Muneeswaran, Y. E. Sim, N. N. Lahankar, J. T. H. Yeh and M. Raj, *Org. Lett.*, 2018, **20**, 5344-5347.
266. L. Schober, S. Ratnam, Y. Yamashita, N. Adebar, M. Pieper, A. Berkessel, V. Hessel and H. Gröger, *Synthesis*, 2019, **51**, 1178-1184.
267. G. Rulli, N. Duangdee, K. Baer, W. Hummel, A. Berkessel and H. Gröger, *Angew. Chem. Int. Ed.*, 2011, **50**, 7944-7947.
268. C. G. Avila-Ortiz, M. Pérez-Venegas, J. Vargas-Caporali and E. Juaristi, *Tetrahedron Lett.*, 2019, **60**, 1749-1757.
269. S. Kamo, S. Maruo, K. Kuramochi and K. Tsubaki, *Tetrahedron*, 2015, **71**, 3478-3484.
270. Varun, Sonam and R. Kakkar, *Med. Chem. Commun.*, 2019, **10**, 351-368.
271. K. Baer, M. Kraußer, E. Burda, W. Hummel, A. Berkessel and H. Gröger, *Angew. Chem., Int. Ed.*, 2009, **48**, 9355-9358.
272. B. Samanta, J. Seikowski and C. Höbartner, *Angew. Chem. Int. Ed.*, 2016, **55**, 1912-1916.
273. R. Roldán, K. Hernandez, J. Joglar, J. Bujons, T. Parella, I. Sánchez-Moreno, V. Hélaine, M. Lemaire, C. Guérard-Hélaine, W.-D. Fessner and P. Clapés, *ACS Catal.*, 2018, **8**, 8804-8809.
274. Y. Yamashita, T. Yasukawa, W.-J. Yoo, T. Kitanosono and S. Kobayashi, *Chem. Soc. Rev.*, 2018, **47**, 4388-4480.
275. R. Obexer, A. Godina, X. Garrabou, P. R. E. Mittl, D. Baker, A. D. Griffiths and D. Hilvert, *Nat. Chem.*, 2016, **9**, 50.
276. S. Bjelic, Y. Kipnis, L. Wang, Z. Pianowski, S. Vorobiev, M. Su, J. Seetharaman, R. Xiao, G. Kornhaber, J. F. Hunt, L. Tong, D. Hilvert and D. Baker, *J. Mol. Biol.*, 2014, **426**, 256-271.
277. L. Giger, S. Caner, R. Obexer, P. Kast, D. Baker, N. Ban and D. Hilvert, *Nat. Chem. Biol.*, 2013, **9**, 494-498.
278. X. Garrabou, D. S. Macdonald and D. Hilvert, *Chemistry*, 2017, **23**, 6001-6003.
279. X. Garrabou, R. Verez and D. Hilvert, *J. Am. Chem. Soc.*, 2017, **139**, 103-106.
280. X. Garrabou, B. I. Wicky and D. Hilvert, *J. Am. Chem. Soc.*, 2016, **138**, 6972-6974.
281. X. Garrabou, T. Beck and D. Hilvert, *Angew. Chem., Int. Ed.*, 2015, **54**, 5609-5612.
282. S. Studer, D. A. Hansen, Z. L. Pianowski, P. R. E. Mittl, A. Debon, S. L. Guffy, B. S. Der, B. Kuhlman and D. Hilvert, *Science*, 2018, **362**, 1285.
283. C. Zeymer, R. Zschoche and D. Hilvert, *Journal of the American Chemical Society*, 2017, **139**, 12541-12549.
284. N. Mase, Y. Nakai, N. Ohara, H. Yoda, K. Takabe, F. Tanaka and C. F. Barbas, *J. Am. Chem. Soc.*, 2006, **128**, 734-735.
285. M. Raj, Vishnumaya, S. K. Ginotra and V. K. Singh, *Org. Lett.*, 2006, **8**, 4097-4099.
286. C. Guo, M. Saifuddin, T. Saravanan, M. Sharifi and G. J. Poelarends, *ACS Catal.*, 2019, **9**, 4369-4373.
287. B. S. Donslund, T. K. Johansen, P. H. Poulsen, K. S. Halskov and K. A. Jørgensen, *Angew. Chem., Int. Ed.*, 2015, **54**, 13860-13874.
288. K. Anebousevly, K. S. Shruthi and D. B. Ramachary, *Eur. J. Org. Chem.*, 2017, **2017**, 5460-5483.
289. J. Gao, S. Bai, Q. Gao, Y. Liu and Q. Yang, *Chem. Commun.*, 2011, **47**, 6716-6718.
290. D. Gryko, M. Zimnicka and R. Lipiński, *J. Org. Chem.*, 2007, **72**, 964-970.
291. R. L. Sutar and N. N. Joshi, *Synth. Commun.*, 2014, **44**, 352-360.
292. T. Sano, W. M. Pandori, X. Chen, L. C. Smith and R. C. Cantor, *J. Biol. Chem.*, 1995, **270**, 28204-28209.

293. G. Zhong, R. A. Lerner and I. C. Barbas, *Angew. Chem., Int. Ed.*, 1999, **38**, 3738-3741.
294. S. Nicolò, M. C. Louis. and L. Y. P. Louis., *Molecules*, 2020, **25**.
295. I. Mager and K. Zeitler, *Org. Lett.*, 2010, **12**, 1480-1483.
296. Y. Xiong, F. Wang, X. Huang, Y. Wen and X. Feng, *Chem. Eur. J.*, 2007, **13**, 829-833.
297. A. Geddes, C. E. Paul, S. Hay, F. Hollmann and N. S. Scrutton, *J. Am. Chem. Soc.*, 2016, **138**, 11089-11092.
298. C. E. Paul, E. Churakova, E. Maurits, M. Girhard, V. B. Urlacher and F. Hollmann, *Bioorganic & medicinal chemistry*, 2014, **22**, 5692-5696.
299. C. E. Paul, S. Gargiulo, D. J. Opperman, I. Lavandera, V. Gotor-Fernández, V. Gotor, A. Taglieber, I. W. C. E. Arends and F. Hollmann, *Organic letters.*, 2013, **15**, 180-183.
300. G. Battistuzzi, S. Cacchi and G. Fabrizi, *Org. Lett.*, 2003, **5**, 777-780.
301. T.-S. Jiang and J.-H. Li, *Chemical Communications*, 2009, 7236-7238.
302. S.-Y. Zhang, Y.-Q. Tu, C.-A. Fan, M. Yang and F.-M. Zhang, *Tetrahedron Letters*, 2009, **50**, 4178-4181.
303. H. Dong, M. Shen, J. E. Redford, B. J. Stokes, A. L. Pumphrey and T. G. Driver, *Organic letters.*, 2007, **9**, 5191-5194.
304. E. Kim, M. Koh, B. J. Lim and S. B. Park, *J. Am. Chem. Soc.*, 2011, **133**, 6642-6649.
305. T. Maji, A. Karmakar and O. Reiser, *J. Org. Chem.*, 2011, **76**, 736-739.
306. J. B. Metternich and R. Gilmour, *J. Am. Chem. Soc.*, 2015, **137**, 11254-11257.
307. X. Zhang, Q. Chen, R. Song, J. Xu, W. Tian, S. Li, Z. Jin and Y. R. Chi, *ACS Catal.*, 2020, **10**, 5475-5482.
308. A. Guzman-Martinez and A. H. Hoveyda, *J. Am. Chem. Soc.*, 2010, **132**, 10634-10637.
309. T. M. Bräuer, Q. Zhang and K. Tiefenbacher, *Journal of the American Chemical Society*, 2017, **139**, 17500-17507.
310. A. Song, X. Zhang, X. Song, X. Chen, C. Yu, H. Huang, H. Li and W. Wang, *Angew. Chem., Int. Ed.*, 2014, **53**, 4940-4944.
311. A. Gangjee, Y. Qiu and R. L. Kisliuk, *J. Heterocyclic Chem.*, 2004, **41**, 941-946.
312. T. I. Houjeiry, S. L. Poe and D. T. McQuade, *Org. Lett.*, 2012, **14**, 4394-4397.
313. E. E. Stache, A. B. Ertel, T. Rovis and A. G. Doyle, *ACS Catal.*, 2018, **8**, 11134-11139.
314. J. A. Ferreira Ramos, C. S. Araújo, T. J. Nagem and J. G. Taylor, *J. Heterocyclic Chem.*, 2015, **52**, 54-58.
315. J.-H. Lee, S. C. Shin, S. H. Seo, Y. H. Seo, N. Jeong, C.-W. Kim, E. E. Kim and G. Keum, *Bioorg. Med. Chem. Lett.*, 2017, **27**, 237-241.
316. M. A. Cinelli, H. Li, G. Chreifi, P. Martásek, L. J. Roman, T. L. Poulos and R. B. Silverman, *J. Med. Chem.*, 2014, **57**, 1513-1530.
317. Y. Shang, X. Jie, K. Jonnada, S. N. Zafar and W. Su, *Nat. Commun.*, 2017, **8**, 2273.
318. W. Ren, W. Chang, J. Dai, Y. Shi, J. Li and Y. Shi, *J. Am. Chem. Soc.*, 2016, **138**, 14864-14867.
319. P. Mahto, N. K. Rana, K. Shukla, B. G. Das, H. Joshi and V. K. Singh, *Org. Lett.*, 2019, **21**, 5962-5966.
320. A. B. Sanford, T. A. Thane, T. M. McGinnis, P.-P. Chen, X. Hong and E. R. Jarvo, *J. Am. Chem. Soc.*, 2020, **142**, 5017-5023.
321. D. T. Payne, Y. Zhao and J. S. Fossey, *Sci. Rep.*, 2017, **7**, 1720.
322. B. Qin, X. Xiao, X. Liu, J. Huang, Y. Wen and X. Feng, *J. Org. Chem.*, 2007, **72**, 9323-9328.
323. R. Umeda, Y. Takahashi, T. Yamamoto, H. Iseki, I. Osaka and Y. Nishiyama, *J. Organomet. Chem.*, 2018, **877**, 92-101.

324. C. You, S. Li, X. Li, J. Lan, Y. Yang, L. W. Chung, H. Lv and X. Zhang, *J. Am. Chem. Soc.*, 2018, **140**, 4977-4981.
325. M. Hosseini, N. Stiasni, V. Barbieri and C. O. Kappe, *J. Org. Chem.*, 2007, **72**, 1417-1424.
326. Y. Zhang, H. Koizumi, S. Inagaki and Y. Kubota, *Catal. Commun.*, 2015, **69**, 92-96.
327. T. Maity, D. Saha, S. Das and S. Koner, *Eur. J. Inorg. Chem.*, 2012, **2012**, 4914-4920.
328. D. Singappuli-Arachchige, T. Kobayashi, Z. Wang, S. J. Burkhov, E. A. Smith, M. Pruski and I. I. Slowing, *ACS Catal.*, 2019, **9**, 5574-5582.
329. P. Barrulas, M. Benaglia and A. J. Burke, *Tetrahedron: Asymmetry*, 2014, **25**, 923-935.
330. H. Liu, G. Li, Y.-w. Wang, S. Zhang and Z. Tang, *Synlett*, 2018, **29**, 560-565.




 Cite this: *RSC Adv.*, 2020, 10, 16147



Received 17th February 2020

Accepted 25th March 2020

DOI: 10.1039/d0ra01526a

[rsc.li/rsc-advances](http://rsc.li/rsc-advances)

## Enabling protein-hosted organocatalytic transformations

 Alexander R. Nödling,  Nicolò Santi,  Thomas L. Williams, Yu-Hsuan Tsai   
 and Louis Y. P. Luk \*

In this review, the development of organocatalytic artificial enzymes will be discussed. This area of protein engineering research has underlying importance, as it enhances the biocompatibility of organocatalysis for applications in chemical and synthetic biology research whilst expanding the catalytic repertoire of enzymes. The approaches towards the preparation of organocatalytic artificial enzymes, techniques used to improve their performance (selectivity and reactivity) as well as examples of their applications are presented. Challenges and opportunities are also discussed.

### Introduction

#### Biocompatible organocatalysis

Serving as a major tool for asymmetric chemical transformations,<sup>1–3</sup> organocatalysis has now matured to a point where its bio-orthogonality can be exploited for important chemical and synthetic biology applications. Catalysts such as imidazolidinone,<sup>4–6</sup> proline,<sup>7</sup> thiourea,<sup>8</sup> and anion- $\pi$ <sup>9</sup> derivatives have been used to mediate reactions that have no parallel in nature. Provided its bio-orthogonality, organocatalysis can be used in biological contexts for valuable chemical and biological applications.<sup>10–17</sup> For instance, organocatalysts can serve to mediate labelling of biomolecules,<sup>11,12</sup> analogous to existing approaches that use metals for reactions.<sup>18–20</sup> Also, it is worth

considering to merge organocatalysis and biocatalysis for the production of chiral synthons in a one-pot and atom economic fashion.<sup>13–17</sup> However, there are only a few examples where organocatalysts function along with biomolecules or under biological conditions. In fact, taking into account the aqueous reaction medium, physiological pH (near 7.4) and temperature (near 37 °C),<sup>20</sup> many of the reported organocatalysts do not function under biocompatible conditions.<sup>8,10,17,21–31</sup> These boundaries vastly narrow the number of organocatalytic reactions applicable and, in response, efforts have been made to overcome limitations related to biocompatibility.<sup>17,32,33</sup>

#### The use of proteins to host organocatalysts

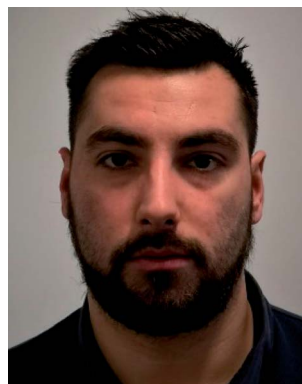
To enhance the biocompatibility of organocatalysis, biomolecules including DNA, RNA and proteins can be used to host the reactions.<sup>34–44</sup> Among them, proteins are particularly suitable. Most proteins can be made recombinantly, correctly folded in

School of Chemistry, Cardiff University, Main Building, Cardiff, CF10 3AT, UK. E-mail: [lukly@cardiff.ac.uk](mailto:lukly@cardiff.ac.uk)



*Alexander R. Nödling is a Post-doctoral Research Associate in the groups of Louis Luk and Yu-Hsuan Tsai. He was born in Frankenthal, Germany, in 1986. He obtained his Diploma in Chemistry at the Philipps-Universität Marburg (2011), and his Dr rer. nat. (2016) under the guidance of Gerhard Hilt with a focus on QSAR of Lewis acid catalysis. His rising interest in tackling biological questions led*

*to his current position at Cardiff University. His current research focuses on artificial enzyme design and biomolecule delivery.*



*Nicolò Santi was born in Vignola, Italy, in 1992. He received his MSc degree in Medicinal Chemistry from Università degli studi di Modena e Reggio Emilia (UNIMORE, 2016). During this time, he spent 7 months at Cardiff University under the supervision of Fabrizio Pertusati working on the preparation of phosphonamides (ProTides) as potential antiviral compounds. In 2017,*

*he began his postgraduate studies at Cardiff University under the supervision of Louis Luk. His research includes the design and optimisation of organocatalytic artificial enzymes.*

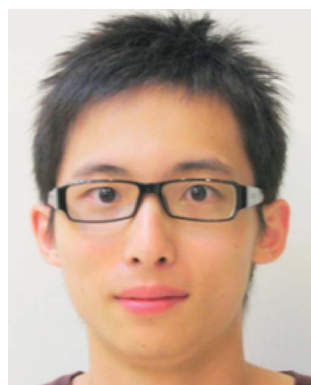


an aqueous environment under physiological conditions and are thus inherently biocompatible. Yet, the outer surfaces and interior of most proteins possess relatively low dielectric constants, which are similar to those found in many organic solvents.<sup>45</sup> Consequently, proteins can provide a microenvironment that can stabilise the transition state during chemical transformation.<sup>34,46,47</sup> Furthermore, superior to most organic solvents, proteins are inherently chiral – the scaffold where the catalytic motif is located can be modelled and/or genetically modified for improved selectivity.<sup>48</sup> Most importantly, the protein host can be further refined by laboratory evolution, which has become increasingly facile as molecular cloning and screening techniques have become user-friendly.<sup>49,50</sup> In contrast, it is relatively difficult to incorporate such “evolvability” in traditional catalyst design.<sup>34,36,48,49,51–54</sup> To this end, the creation of genetically encoded protein scaffolds is a promising avenue to develop biocompatible stereoselective organocatalytic reactions.<sup>36,55</sup>



*Thomas L. Williams graduated from the University of South Wales with a BSc in Forensic Science (2012) followed by a MSc in Forensic and Analytical Science (2014). He joined Cardiff University as an analytical technician specialising in mass spectrometry of proteins and peptides (2014). Thomas then joined the research groups of Louis Luk and Yu-Hsuan Tsai as a PhD student in Chemical Biology (2015). His*

*research focuses on designing and characterising artificial enzymes using advanced synthetic biology techniques.*



*Yu-Hsuan Tsai is a Lecturer in the Cardiff School of Chemistry. He obtained his BSc at the National Taiwan University (2006), MSc at the ETH Zurich (2008), and Dr rer. nat. at the Freie Universität Berlin (2012). He was a graduate student under the guidance of Peter H. Seeberger at the ETH Zurich and Max Planck Institute of Colloids and Interfaces, and a post-doctoral researcher in the*

*group of Jason W. Chin at the MRC Laboratory of Molecular Biology. Since 2015 he has become an independent researcher in Cardiff. His research focuses on developing tools to study and control protein functions.*

## Artificial organocatalytic enzymes

The term “artificial enzyme” has been widely used for any macromolecular complex designed to catalyse chemical reactions.<sup>54</sup> Herein, we describe artificial enzymes as protein-based systems that have been genetically or chemically altered, repurposed or designed *de novo* to catalyse a reaction. While contemporary artificial enzyme design is mainly focused on metallo-enzymes or redesign of reaction-promiscuous natural enzymes,<sup>49,56</sup> we set the scope of this review to the development of artificial organocatalytic enzymes based on recombinant proteins. These enzymes were categorised based on their design (Table 1). We will describe relevant examples of each strategy and the success in their approach. Engineering of natural cofactors in their native enzymes will be briefly discussed.<sup>17,32</sup>

## Chemical modification

### Site-selective chemical modification of proteins

Prior to the onset of modern molecular biology technologies, proteins were often chemically modified to purposefully alter their activity.<sup>77–79</sup> Initially, modified enzymes were made by single atom replacement. Serine protease subtilisin was converted to its cysteine equivalent by a three-step chemical protocol (tosylation, followed by replacement with thioacetate and hydrolysis).<sup>80</sup> The resulting “thiol-subtilisin” could hydrolyse activated aryl substituted ester bonds. However, this cysteine variant lost its protease activity and was found to be 100-fold less active than the parental enzyme towards activated esters, despite the higher nucleophilicity of the free thiol.<sup>81,82</sup> In another study, selenosubtilisin was created by converting the active site serine residue into selenocysteine.<sup>57,58,83</sup> The selenium-containing protein was shown to be a reductase; alkyl peroxides could be converted to their alcohol equivalents under the action of this modified enzyme using thiophenol as a source of oxidant (Fig. 1a).<sup>57</sup> The artificial enzyme exhibits reaction rates comparable to those of natural enzymes. While

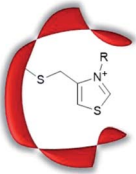
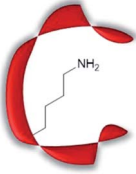
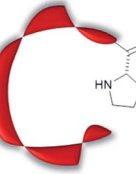
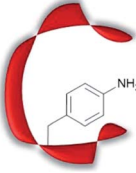
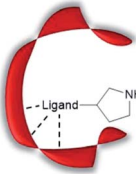


*Louis YP Luk is a Lecturer at the School of University of Cardiff University. He obtained his BSc in Chemistry and Microbiology & Immunology at the University of British Columbia. He obtained his PhD in the same university under the supervisor of Martin E. Tanner, followed by post-doctoral studies in the laboratories of Stephen BH Kent at the University of Chicago and Rudolf K. Allemann at Cardiff*

*University. Louis became a University Research Fellow in 2015 and was recently tenured at Cardiff University. Combining his training in enzymology and peptide chemistry, Louis' current research focuses on artificial enzyme design and protein bioconjugation chemistry.*



Table 1 Advantages and disadvantages of the five approaches used for performing organocatalysis in a protein scaffold

Systems	Features	Advantages	Potential challenges	Reactions tested
<b>Covalent modification</b>				
	Site-selective modification with catalytically active motifs	Relative ease of preparation; quick screening of different catalytic moieties possible	Site-specific labelling can be challenging	Reduction; <sup>57,58</sup> cyclisation; <sup>59</sup> reductive amination; <sup>60</sup> C–C bond formation <sup>61</sup>
<b>De novo design/laboratory evolution</b>				
	Computational design of active site, creating "theozyme"	High probability to create a novel active site as a consequence of precise design, and hence screening time is minimised	Mechanistic and structural knowledge needed; knowledge in computational chemistry needed	(Retro-)aldol reaction; <sup>62–68</sup> Henry reaction; <sup>41</sup> Knoevenagel condensation; <sup>24,43</sup> conjugate addition <sup>40,42,44</sup>
<b>Enzyme bearing N-terminal proline</b>				
	Use of substrate promiscuous N-terminal proline	No need of chemical modification or computer modelling	Limited to secondary amine organocatalysis at the N-terminal position; is it very easy to generate protein with N-terminal Pro recombinantly	Conjugate addition; <sup>38,69–71</sup> intramolecular and intermolecular aldol condensation <sup>37,72,73</sup>
<b>Genetic code expansion</b>				
	Genetic incorporation of an unnatural amino acid which bears (part of the) catalytically active motif	Wide selection of catalytically active amino acids; no chemical protein modification needed	Recombinant expression might be low yielding	Ester hydrolysis; <sup>74</sup> oxime/hydrazone conjugation <sup>50,75</sup>
<b>Supramolecular scaffold</b>				
	Binding of a ligand bearing catalytically active motifs	Many catalytically active moieties can be attached; enable quick screening of different catalytic moieties	Limited to proteins with high affinity ligand(s)	Conjugate addition; <sup>39</sup> decarboxylative Michael addition; <sup>36,55</sup> domino aldol-Michael reaction <sup>76</sup>

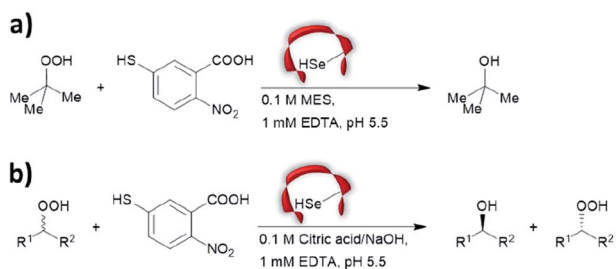


Fig. 1 Selenosubtilisin catalyses the reduction of (a) *tert*-butyl hydroperoxide and (b) secondary alkyl hydroperoxide. MES = 2-(*N*-morpholino)ethanesulfonic acid, EDTA = ethylenediaminetetraacetic acid.

mechanistic insights are not available, the selenosubtilisin displays an inverted enantioselectivity in the kinetic resolution of racemic peroxides when compared to the native enzymes (Fig. 1b).<sup>58</sup>

Cysteine, due to its nucleophilic nature, is most frequently modified with cofactors for the creation of new organocatalytic artificial enzymes. An artificial oxidoreductase was created by linking the catalytically active cysteine residue of the protease papain to flavins. Using oxygen for oxidation, the resulting "flavopapain" was able to oxidise NADH and its derivatives at a rate 50-fold higher than that by flavin alone (Fig. 2a).<sup>84</sup> Similarly, the natural cofactor thiamine was introduced to papain.



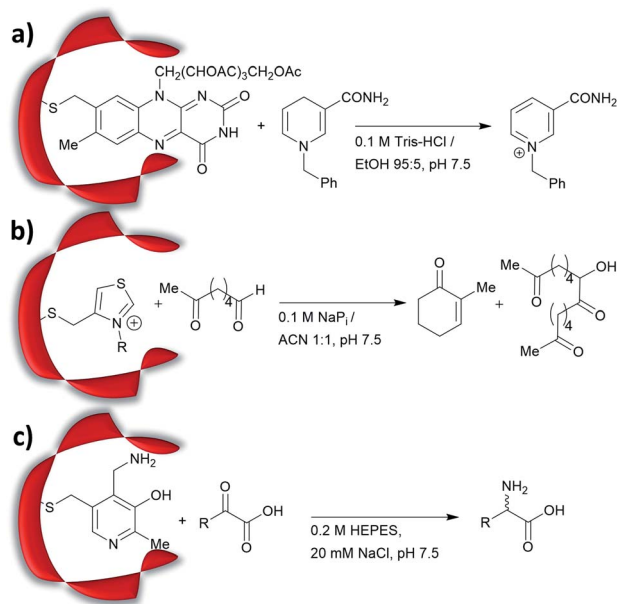


Fig. 2 Artificial enzymes created by covalent modification of cofactors: (a) artificial flavopapain used for the oxidation of BNAH; (b) artificial thiazolopapain for C–C bond formation; and (c) artificial ALBP–pyridoxamine for enantioselective reductive amination. Tris = tris(hydroxymethyl)aminomethane, HEPES = (4-(2-hydroxyethyl)-1-piperazine-ethanesulfonic acid), ALBP = adipocyte lipid binding protein.

The resulting “thiazolopapain” was one of the early artificial enzymes that can mediate C–C bond formation.<sup>59</sup> Nevertheless, activity was suboptimal, as the model cyclisation reaction of 6-oxo heptanal required six days to reach completion with a significant portion of substrate transformed in dimerisation byproduct (Fig. 2b). A third cofactor, pyridoxamine, was used to label the adipocyte lipid binding protein.<sup>60</sup> The pyridoxamine protein complex could successfully mediate the production of a wide range of amino acids with modest to excellent enantioselectivity with enantiomeric excess (ee) up to 94% (Fig. 2c).

Recently, an alternative labelling strategy based on the metabolism of carbapenems by penicillin binding proteins was developed.<sup>61</sup> In this work, secondary amine containing penicillin derivatives were anchored to beta-lactamase and the covalently modified protein was employed in a conjugate addition of nitromethane to cinnamaldehyde, giving moderate yields and low enantioselectivities (20–27%, e.r.  $\approx$  55 : 45).

These studies lay the foundations for the future development of protein-hosted organocatalysis.<sup>57,84,85</sup> Chemical methodologies for protein labelling have vastly diversified and improved in recent years, showing fine-tuned reactivity and biocompatibility with labelling achieved within live cells.<sup>86–94</sup> One can anticipate that efficient artificial enzymes can be made by adapting these novel technologies.

## De novo design/laboratory evolution

### Development of *de novo* enzymes

The increase in computational power and applicable software, including Rosetta and ORBIT,<sup>95</sup> has accelerated the

development of *de novo* enzyme design.<sup>96,97</sup> The first stage of *de novo* enzyme design is the *in silico* generation of a “theozyme,” a theoretical arrangement of side chain residues and bioavailable molecules (water and ions) that can stabilise the rate-limiting transition state(s) of a chosen reaction.<sup>98</sup> This assembly of theozyme is subsequently transformed into an experimentally tangible protein structure through evaluations based on calculated parameters (*e.g.* geometry and energy) by screening of available protein structures available in repositories.<sup>49,95</sup> Eventually, the best options are recombinantly produced for characterisations. The initial *de novo* enzymes are typically inefficient and are not selective. Thus, laboratory evolution is used to enhance both catalytic activity and reaction profile. This pathway led to the formation of a highly competent and promiscuous *de novo* Kemp eliminase,<sup>99,100</sup> retro-aldolases (RA)<sup>40,43,44,63,65–68</sup> and Diels–Alderases.<sup>52,101</sup> Here, we will focus on retro-aldolases which bear a catalytically active lysine for iminium and enamine catalysis.

Retro-aldolases are a class of *de novo* designed enzymes capable of catalysing retro-aldol reactions *via* formation of an iminium intermediate.<sup>68</sup> Retro-aldolases have been created from a theozyme that is able to mediate cleavage of the fluorogenic compound methodol (**1**, Fig. 3).<sup>68</sup> The reaction was selected to allow for facile screening as the retro-aldol product naphthaldehyde (**2**) is fluorescent.

The most effective theozyme in terms of rate enhancement in the recombinantly produced protein contains a catalytically active lysine residue within a hydrophobic binding pocket and a strategically positioned water molecule that helps mediating formation of the Schiff base intermediate.<sup>68</sup> Interestingly, this artificially designed network was found to be catalytically more active than those made based on naturally found proton shuffle networks. Computational tools, such as RosettaMatch,<sup>96</sup> were recruited to dock the theozyme into a protein scaffold, creating a suitable host for the artificial active site.

Indole-3-glycerol phosphate synthase,<sup>102</sup> a TIM-barrel protein fold, was identified for hosting the theozyme. Further adjustment of the residues surrounding the transition state was made using RosettaDesign, which among other purposes enables optimisation of residue interactions around the active site.<sup>103</sup> Among these active models, the variant RA95.0 with the catalytically active lysine at position 210 (apparent  $pK_a = 8.1$ , Fig. 4) was identified as the most promising candidate. Experimentally, RA95.0 is able to mediate cleavage of methodol (**1**)

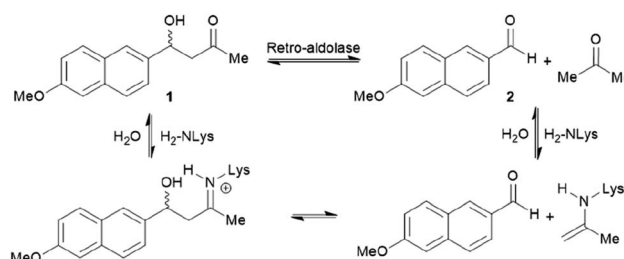


Fig. 3 Net reaction of methodol (**1**) cleavage catalysed by the *de novo* designed retro-aldolases and important intermediates.





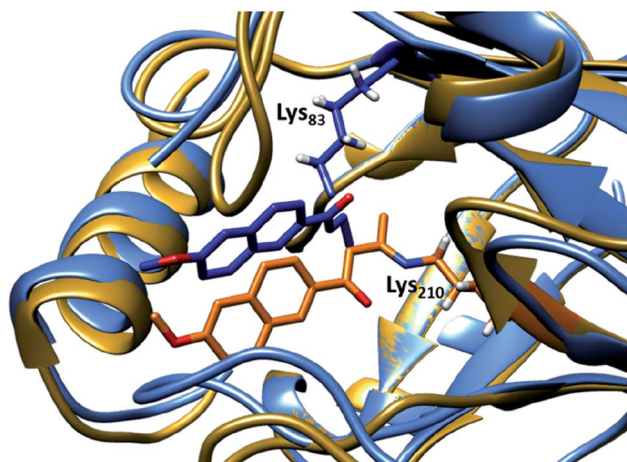


Fig. 4 Overlay of crystal structures of the first retro-aldolase RA95.0 (gold & orange, PDB: 4A29), in which Lys210 is responsible for forming the Schiff base intermediate with a 1,3-diketone inhibitor and the evolved variant RA95.5-8 (light & dark blue, PDB: 5AN7) that carries a novel catalytically active Lys83 (in complex with a 1,3-diketone inhibitor).

with catalytic efficiency ( $k_{\text{cat}}/K_{\text{M}}$ ) of  $\sim 0.19 \text{ M}^{-1} \text{ s}^{-1}$  and selectivity for *S* over *R* (2.3 : 1).<sup>66,67</sup> To create an enzyme with improved performance, regions at and around the active site of RA95.0 were subjected to iterative cassette mutagenesis, a form of saturation mutagenesis where pre-synthesised and mutated DNA strands are inserted into the gene by restriction enzyme digest and ligation.<sup>104</sup> By combining mutations of the most active single variants, a highly improved variant RA95.5, which has six mutations in total, showed 73-fold increase in catalytic efficiency when compared to RA95.0 ( $k_{\text{cat}}/K_{\text{M}} = 14 \text{ M}^{-1} \text{ s}^{-1}$  with 3 : 1 *R*-to-*S* selectivity). Crystallographic studies revealed that the T83K mutation in RA95.5 created a second reaction centre, in addition to Lys210, both capable of forming Schiff base intermediates. This finding indicated that the active site underwent restructuring, and further refinement was needed (see below).<sup>66,67</sup> In particular, the replacement of T83K mutation shifted the  $\text{pK}_{\text{a}}$  of Lys210 to 7.6, to which the authors attributed the improved performance.

Additional laboratory evolution studies of the entire gene (error-prone PCR and DNA shuffling) created the variant RA95.5-5 that has an additional six mutations (compared to RA95.5) and demonstrated significantly improved activity (>20-fold,  $k_{\text{cat}}/K_{\text{M}} = 320 \text{ M}^{-1} \text{ s}^{-1}$ , and selectivity 5 : 1 *R* over *S*). Crystallographic studies illustrated that Lys83 transformed into the only reaction centre for the methodol (**1**) cleavage, indicating that there is a switch in location of the residue responsible for catalysis.<sup>66</sup> Restructuring of the active site was likely unpredictable during the initial design, highlighting that randomness is a key element during the evolution of an efficient enzyme. Finally, a last three rounds of laboratory evolution yielded the variant RA95.5-8 (Fig. 4), which contains substitutions at both the active site and distal positions, and its catalytic efficiency ( $k_{\text{cat}}/K_{\text{M}}$ ) was measured to be  $850 \text{ M}^{-1} \text{ s}^{-1}$ .<sup>66</sup>

## Aldolase evolution

Showcasing the power of ultra-high throughput screening methods, microfluidic fluorescence-activated droplet sorters (FADS) were used to further improve the performance of the retro-aldolase. The resulting variant RA95.5-8F displayed 13 mutations and a 30-fold higher activity ( $k_{\text{cat}}/K_{\text{M}} = 34\,000 \text{ M}^{-1} \text{ s}^{-1}$  for (*R*)-methodol (*R*-**1**) with 480 : 1 *R* over *S* selectivity).<sup>64</sup> Such impressive improvement was attributed to the genesis of a catalytic Lys-Tyr-Asn-Tyr tetrad for proton shuffling. The tetrad forms a hydrogen bonding network which transfers proton to and from the reaction centre, stabilising formation of reaction transition states. RA95.5-8F was the first RA to be able to mediate aldol reactions between acetone and various aldehydes (*i.e.* an aldolase). It should be noted that previous RA's were inhibited by the formation of Schiff base with these aldehydes, whereas RA95.5-8F selectively forms enamines with acetone.

## Expanding the reaction profile of the RA95 family

A series of studies were conducted to expand the versatility of the RA95 family to catalyse different reactions (Fig. 5). Iminium catalysis mediated by RA95.5-8 was used as a means to mediate carbon-carbon bond formation, including conjugate additions (Fig. 5a and b),<sup>40,42,44</sup> Knoevenagel (Fig. 5c)<sup>43</sup> and Henry

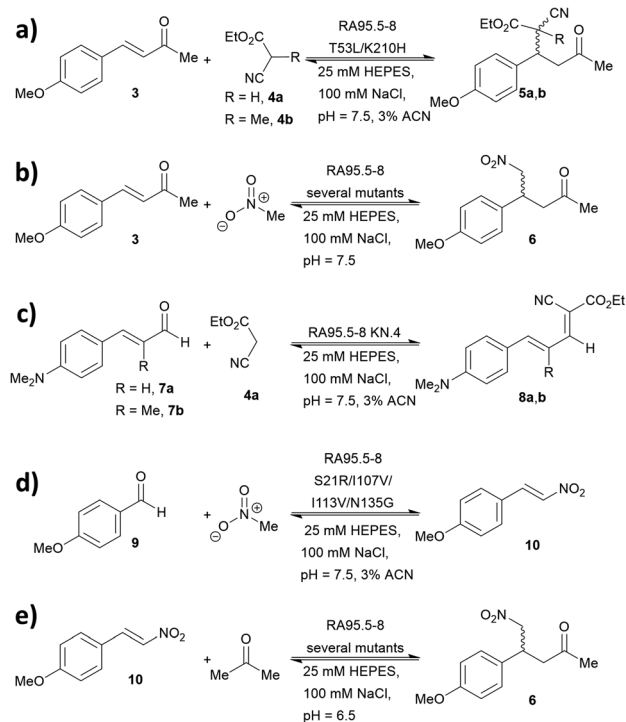


Fig. 5 Promiscuity of RA95.5-8 and variants for carbon-carbon bond forming reactions. Iminium catalysis includes: (a) conjugate addition of carbon nucleophiles; (b) conjugate addition of nitromethane; (c) Knoevenagel condensations of carbon nucleophiles with  $\alpha,\beta$ -unsaturated aromatic aldehydes and (d) Henry addition of nitromethane to aromatic aldehydes. Enamine catalysis includes: (e) conjugate addition of acetone to nitrostyrene.



condensations (Fig. 5d).<sup>41</sup> Enamine catalysis was also explored in the nitro-Michael addition of acetone to nitrostyrenes (Fig. 5e).<sup>42</sup> In some cases, formation of reactive iminium species was verified by reduction of the intermediates followed by mass spectrometric analysis.<sup>43,44</sup>

During the course of optimising RA95.5 to mediate different transformation (Fig. 5), several notes have been learned. Firstly, there is a positive correlation between stereoselectivity and catalytic efficiency.<sup>63–68</sup> Nevertheless, it should be noted that, during the optimisation process, stereoselectivity may be weak because the active site undergoes reconstruction (*e.g.* re-locating the catalytic residue);<sup>40,41,44</sup> eventually, stereoselectivity resumes and variants with kinetic parameters and selectivity similar to those of natural enzymes can be achieved. Furthermore, refined artificial enzymes often possess properties similar to those of natural enzymes. For instance, loop flexibility and residues that are distant from the active site (secondary shell and protein surface) could greatly affect the performance of the catalysis.<sup>41,42,44,105,106</sup> In another instance, it was indicated that catalysis is partially driven by a negative activation heat capacity, which is considered as a result of tight binding to the transition state forming an ordered complex.<sup>62</sup> Finally, the computationally designed 248-residued RA can be modified at approximately 30 positions. This signifies the genetic “plasticity”<sup>107,108</sup> of RA and echoes the fact that TIM-barrel fold is found in at least 15 families of enzymes.<sup>109–111</sup> The coupling of computational design (rational) and laboratory evolution with high-throughput screening (randomness) has proven to be an effective approach to create *de novo* enzyme. In recent years, this technology has been combined with others, including genetic code expansion (see below). We anticipate that the family of *de novo* enzymes will soon be vastly expanded.

## N-Terminal proline

### 4-Oxalocrotonate tautomerase

When located at the N-terminus of a protein, proline offers a secondary amine that can be used for iminium- and enamine-based organocatalysis. One such example is 4-oxalocrotonate tautomerase (4-OT) from *M. putida*, which is composed of six

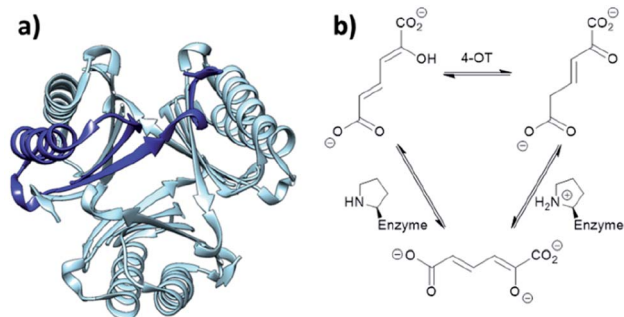


Fig. 6 (a) Hexameric crystal structure of 4-OT (PDB: 4X19), monomer subunit highlighted in dark blue. (b) Native reaction of 4-OT, showing the net reaction in the upper part and the function of the N-terminal proline as general base below.

homologous monomers carrying a catalytic N-terminal proline (Fig. 6a).<sup>112</sup> Naturally, this residue acts as a general base, catalysing the tautomerisation of a dienol into an unsaturated ketone (Fig. 6b).<sup>38,113,114</sup> Interestingly, this proline residue forms iminium intermediates with various carbonyl substrates.

Because of its significant substrate promiscuity, 4-OT has been used as an organocatalyst for chemical transformations. It has been demonstrated that 4-OT is able to catalyse enamine-based aldol reactions (Fig. 7a and b)<sup>37,70</sup> and conjugate additions (Fig. 7c).<sup>71</sup> Additionally, 4-OT has been exploited for iminium catalysis, including the conjugate addition of nitromethane (Fig. 7d).<sup>115</sup> Reduction of the intermediate iminium ion by sodium cyanoborohydride and subsequent mass spectrometry analysis provide evidence that supports the formation of the iminium intermediate.<sup>73</sup>

Mutagenesis *via* a combined computational and experimental approach has led to the identification of enhanced variants. Three residues in proximity were found to be crucial for catalysis, including Phe50, Met45 and Ala33. Mutability landscapes were used to determine ‘residue hotspots.’ The experiment consisted of singly mutating all amino acids with the exception of the catalytic Pro1.

Protein solubility of single point mutations was first assessed, followed by an activity screen of the tautomerization reaction and subsequently the Michael addition. An F50A mutation resulted in an increase of catalytic efficiency by a factor of 600 for cross-coupling aldol reactions.<sup>72</sup> In contrast, when both Phe50 and Met45 were replaced with valine and tyrosine respectively, the resulting variant was more effective at self-condensation reactions. The F50V/M45Y double mutant resulted predominantly in the *R* product, whereas a third mutant A33D selectively yielded the *S* enantiomer in the conjugate additions of acetaldehyde to  $\beta$ -nitrostyrenes.<sup>69</sup> Crystal

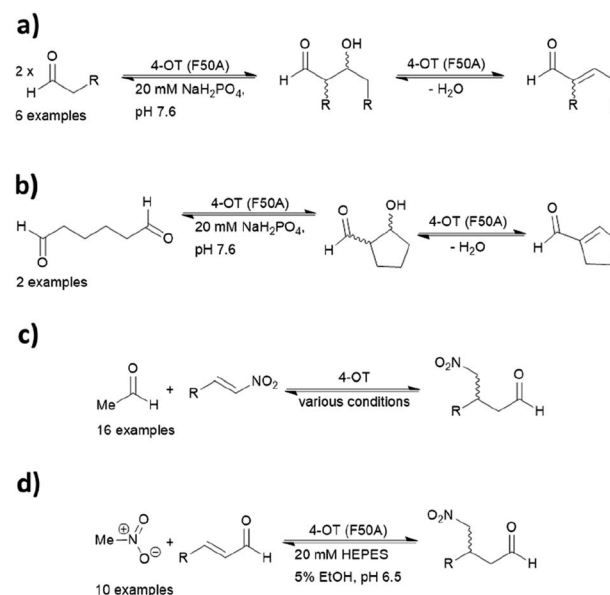


Fig. 7 Reactions catalysed by 4-OT include (a) intermolecular aldol; (b) intramolecular aldol; (c) nitro-Michael addition; and (d) enamine catalysed conjugate addition. 4-OT = 4-oxalocrotonate tautomerase.



structures of the two mutants have been obtained, but the N-terminal region was not resolved likely due to its inherent flexibility. Hence, the actual assembly in the active site remains unclear.

4-OT and its variants have been used for a range of applications including enzymatic<sup>115</sup> and chemoenzymatic cascades,<sup>116</sup> alongside whole cell catalytic systems.<sup>117–119</sup> The anti-anxiety drug pregabalin and three of its analogues were synthesised by coupling the 4-OT reaction with catalysis by aldehyde dehydrogenase (ALDH, Fig. 8).

Acetaldehyde was added stereoselectively to  $\alpha,\beta$ -unsaturated nitro substrates under the action of a 4-OT variant, followed by oxidation by ALDH to yield the corresponding carboxylic acid (Fig. 8).<sup>116</sup> To recycle NADH, a cofactor recycling system operated by NAD oxidase (NOX) was included. Lastly, the nitro group was reduced to the amine using sodium borohydride in the presence of nickel chloride. These applications present evidence that protein-based organocatalysis can be used in combined synthesis which may not be readily achievable using traditional organocatalytic systems.

Utilising only natural residues with no chemical modification needed, the N-terminal proline approach is arguably the simplest in establishing a biocompatible organocatalytic system. As a range of reactions have already been established, 4-OT is an attractive system for performing organic reactions in biological contexts. However, a major limitation is that it is only able to catalyse secondary amine organocatalysis. Other useful organocatalytic transformations (based on *e.g.* thiourea or counterion based catalysis) are unavailable and thus other approaches must be employed.

## Genetic code expansion

### Fundamentals of genetic code expansion

Genetic code expansion enables site-specific incorporation of unnatural amino acids, which can be used to mediate bio-orthogonal chemical reactions. To achieve this goal, a pair of orthogonal aminoacyl-tRNA synthetase/tRNA pair is needed. Specifically, the orthogonal tRNA decodes a blank codon,

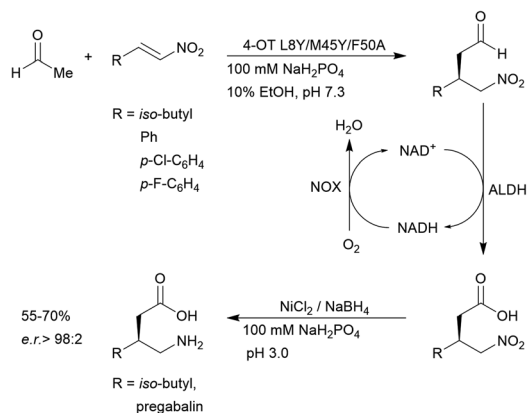


Fig. 8 Chemoenzymatic synthesis of pregabalin and three of its analogues using 4-OT. NAD = nicotinamide adenine dinucleotide, ALDH = aldehyde dehydrogenase, NOX = NADH oxidase.

commonly the amber stop codon (TAG) as it is often the least used codons in most organisms. To produce recombinant proteins that contain unnatural amino acids in *E. coli*, pyrrolysyl-tRNA synthetase/tRNA and tyrosyl-tRNA synthetase/tRNA pairs from archaea are the most versatile and popular choices.<sup>120</sup> The pyrrolysyl-tRNA synthetase/tRNA pair is particularly useful as it naturally decodes the amber codon.<sup>121</sup> To incorporate the unnatural amino acid, a TAG codon is then introduced into the gene of interest at the position of choice. Double transformation of *E. coli* with plasmids containing the gene of interest and the synthetase are conducted. By including the unnatural amino acid in the medium, the orthogonal synthetase specifically charges the orthogonal tRNA with the unnatural amino acid, which will allow for production of full-length protein with the unnatural amino acid at the desired position. To date, over 200 unnatural amino acids can be genetically incorporated into a protein of interest using this technique, so there exists a vast opportunity to exploit these unnatural amino acids for organocatalytic transformations (Fig. 9).<sup>91</sup>

### The multidrug regulator protein LmrR

LmrR is a dimeric protein isolated from *Lactococcus lactis* that has a hydrophobic pore in the centre, allowing for the

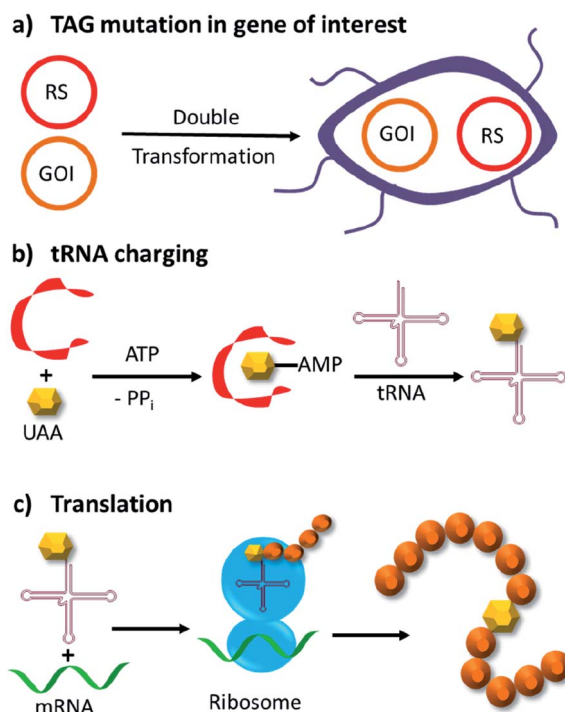


Fig. 9 Incorporation of unnatural amino acids by genetic code expansion in *E. coli*. (a) Double transformation of two plasmids, in which one bears an exogenous amino acid tRNA synthetase (RS) and cognate tRNA, whereas the other contains the gene of interest (GOI) with a site-specific TAG mutation. (b) Expression of the tRNA synthetase and addition of the unnatural amino acid (UAA) allows the tRNA to be charged with the UAA. (c) Ribosomal translation of the GOI with the unnatural amino acid incorporated site specifically into the protein. ATP = adenosine triphosphate, PP<sub>i</sub> = inorganic pyrophosphate.



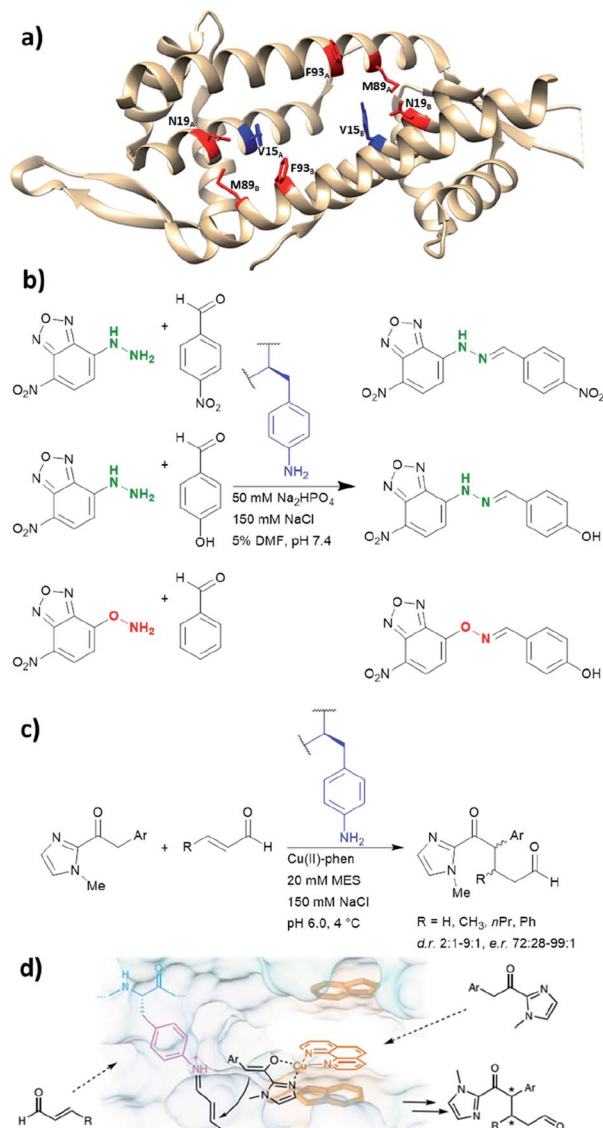


Fig. 10 (a) Crystal structure of the homodimeric protein LmrR (PDB: 3F8F). Residues in red are those targeted for unnatural amino acid incorporation (Asn19, Met89, Phe93). Residues in blue (Val15) show the most promising result, when they are replaced with the unnatural amino acid *p*-amino-phenylalanine. (b) Hydrazone and oxime ligation performed by the unnatural amino acid. (c) Conjugate addition catalysed by dual substrate activation using LmrR V15pAF and a copper complex. (d) Postulated mechanism for the conjugate addition *via* dual activation from (c). (d) Adapted from ref. 122, <https://www.nature.com/articles/s41929-019-0420-6>, with permission of Springer Nature, copyright 2020. Further permissions related to the material excerpted should be directed to Springer Nature. DMF = dimethylformamide, phen = phenanthroline, pAF = *p*-aminophenylalanine.

recruitment of organic molecules (Fig. 10a). Four positions located within the hydrophobic pore (Val15, Asn19, Met89 and Phe93) were individually mutated to a TAG codon and tested for the incorporation of the unnatural amino acid *p*-azidophenylalanine under the action of an evolved tyrosyl-tRNA synthetase from *Methanococcus jannaschii*. The azido group was chosen and subsequently reduced to the catalytically active aniline, because

direct incorporation of *p*-aminophenylalanine proved to be challenging.<sup>75</sup> The designer enzyme was then tested for hydrazone and oxime formation. It was found that unnatural amino acid replacement at the Val15 position yielded the most promising result (Fig. 10b).<sup>75</sup> Laboratory evolution was used to screen the library variants in 96 well plates by measuring the loss of the UV absorbance from the substrate.<sup>50</sup> The resulting variant which carries additional mutations, including A11L, N19M, A92R and F93H, showed a 74-fold increase in catalytic efficiency. Based on the knowledge of these positions from previous structures, Leu11 and Met19 are thought to help position the aniline in a more “reaction-ready” position. Furthermore, Arg92 was reasoned to stabilise the build-up of negative charge that appears during the condensation of the aniline with the carbonyl group. Lastly, His93 was proposed to serve as proton shuttle assisting in the formation of iminium ion intermediates and promoting the transamination processes.

Recently, the *p*-aminophenylalanine/LmrR system has been further modified for a novel dual substrate activation strategy.<sup>122</sup> Through combination with a supramolecularly bound Lewis acidic Cu(II) complex, the resulting artificial enzyme was able to mediate a Michael reaction that involves both formation of a Cu-enolate and an organocatalytic iminium intermediate. Yields of this novel reaction mode were up to 90%, with d.r. and ee up to 9 : 1 and >99% respectively. This work highlights that importance of developing different approaches to artificial enzyme design (*e.g.* genetic code expansion and supramolecular approach), as proteins can be used to host multiple catalytic centres for coupled reaction cascades.

### De novo designed BH32

BH32 is an enzyme originally created by Rosetta to perform the Morita-Baylis-Hillman reaction,<sup>101</sup> and this protein has been further re-engineered into a potent hydrolase through the combined use of genetic code expansion and laboratory evolution.<sup>74</sup> Substitution of the catalytic His23 with methyl-histidine was achieved by using an evolved variant of the pyrrolysyl-tRNA synthetase and its cognate tRNA (Fig. 11a). The resulting enzyme was able to perform ester hydrolysis for a range of compounds that fluoresce upon reaction (Fig. 11b). Screening for variants with improved activity was performed using 96 well plates on a plate reader where formation of the fluorescein product could be monitored. Six mutations resulted in a 15-fold increase in enzyme activity. Mutations resulting from the evolution were L10P, A19H, S22M, E46N, P63G and D125G. Based on the data derived from crystallography and kinetic investigations, the authors concluded that the aromatic ester formed between the substrate and Me-His was significantly more prone to hydrolysis (Fig. 11c). In contrast, the neutral acyl enzyme intermediate formed from the natural amino acid histidine hydrolyses slowly under the same condition.

The technique of genetic code expansion allows exploration beyond the limit of what natural amino acids offer, thus holding great promise in contemporary enzymology. Incorporation of



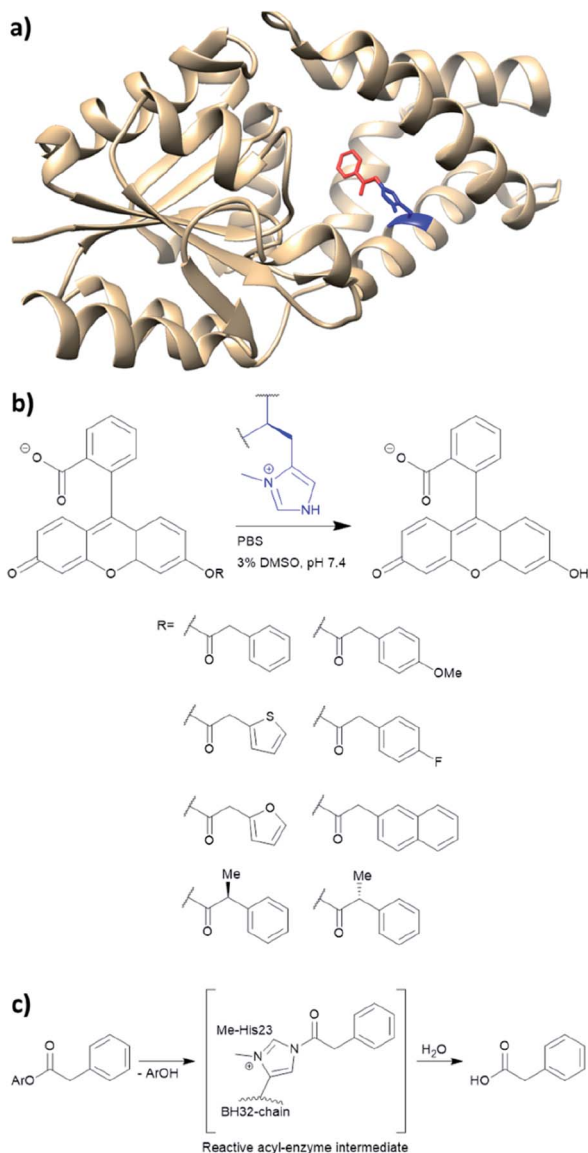


Fig. 11 (a) Crystal structure of the protein BH32 (PDB: 6Q7N). Residue in blue is the unnatural amino acid methyl-histidine bound to acetophenone (red). (b) Substrate scope of the ester hydrolysis performed by BH32 with the unnatural amino acid Me-His. (c) Shortened mechanism of the acyl enzyme intermediate formation of BH32 Me-His23 with aromatic esters. PBS = phosphate-buffered saline, DMSO = dimethyl sulfoxide.

unnatural amino acids *in vivo* enables laboratory evolution in a fashion similar to those of natural enzymes. Consequently, artificial enzymes made by this fashion can also be applied to whole cell catalysis or synthetic biological pathways. However, the efficiency of incorporation greatly depends on the unnatural amino acid used. The choice of protein to harbour the amino acid also needs to be considered carefully. Both LmrR and BH32 have been previously used in artificial enzyme design (LmrR for artificial metallo-enzymes and BH32 was computationally designed for carbon-carbon bond forming reactions).<sup>47,92</sup> Both examples have shown promise in performing biocompatible organocatalysis. As genetic code expansion has become more

readily available, this technique will likely gain increasing popularity in the future of enzyme design.

## Non-covalent supramolecular systems

### Harnessing non-covalent interactions

Non-covalent but strong protein-ligand interactions have been exploited to generate organocatalytic artificial enzymes. In these systems, a catalytic moiety is covalently attached to a section of a ligand that is only weakly involved in protein binding and introduced to the protein partner. Consequently, the resulting protein-ligand complex is converted into a potential catalytic entity (Fig. 12).

When compared to other approaches, a supramolecular complex has little restrictions on the choice of the catalytic motifs. Preparation of the modified ligands tends to be straightforward, involving simple synthetic techniques such as amide bond coupling and click chemistry.<sup>35,39,123-126</sup> Hence, the supramolecular approach enables researchers to screen activity for a broad range of candidates within a short period of time. In addition, the protein hosts can still be engineered *via* rational design or laboratory evolution.<sup>46,48,127-129</sup> To this end, the supramolecular approach is an important technique for creating artificial enzymes. As a rule of thumb, the supramolecular catalytic complexes are built based on protein-ligand interactions that have dissociation constants ( $K_D$ ) ranging from low  $\mu\text{M}$  to  $\text{pM}$ .<sup>123-125,130</sup>

The ligand needs to possess a site for easy functionalisation while causing minimal effect on protein-ligand interaction. One such pair is the (strept)avidin and biotin, whose  $K_D$  value is approximately  $10^{-14} \text{ M}^{-1}$ .<sup>130</sup> The (strept)avidin-biotin system has already been exploited in the late 1970s to tether a rhodium catalyst to the valeric motif of biotin for asymmetric hydrogenations.<sup>131</sup> Subsequently, a variety of streptavidin based artificial metallo-enzymes operated by iridium, rhodium, ruthenium and palladium have been reported.<sup>35,48,123,126,127,132,133</sup> Below we describe two different types of organocatalytic artificial enzymes based on biotin-streptavidin.

Anion- $\pi$ -catalysis has become a contemporary topic in organocatalysis.<sup>9,134-139</sup> In this catalytic mode, anion intermediates formed during the reaction can be stabilised by  $\pi$ -acidic molecules such as naphthalenediimides (NDIs, bold blue core in 11, Fig. 13a), which possess a positive quadrupole moment. This consequently facilitates organic transformations such as conjugate additions (Fig. 13b). Whereas all natural aromatic amino acids are  $\pi$ -basic and interact with cations, the

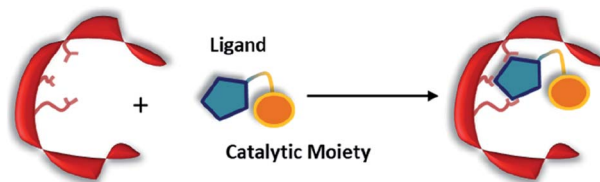


Fig. 12 Combination of a catalytically inactive protein scaffold with a ligand-catalyst conjugate leads to a catalytically active supramolecularly assembled protein complex.



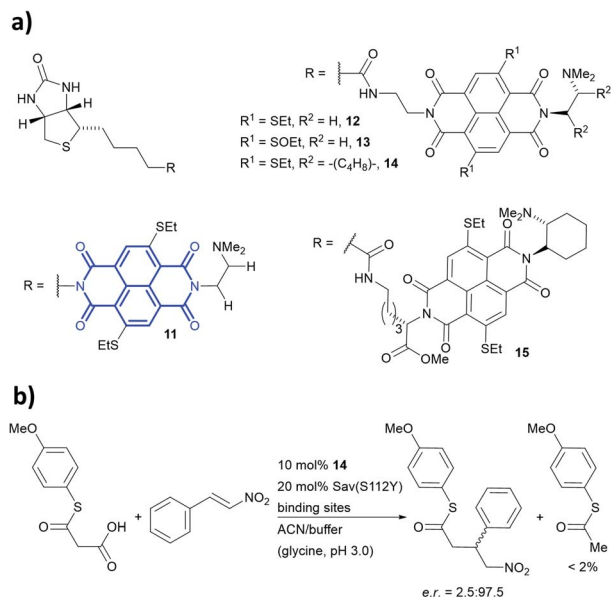


Fig. 13 (a) Reported biotin–NDI–amine organocatalyst conjugates, NDI fragment in bold and blue.<sup>36</sup> (b) Decarboxylative Michael addition reaction catalysed by **14** within S112Y mutant streptavidin. Sav = streptavidin.

streptavidin–biotin technology was recently used to create an organocatalytic artificial enzyme that drives catalysis by anion– $\pi$  interactions.<sup>36,76</sup>

To add anion– $\pi$  interactions into the repertoire of enzyme catalysis, a combined chemical and genetic screening approach was used. A library of five bifunctional catalytic moieties were attached to biotin (compounds **11**–**15**, Fig. 13a) that contain both an NDI motif and a tertiary amine connected through a linker of different length. The  $\pi$ -acidic surface of the NDI motif was proposed to be able stabilise the enolate intermediate formed in the reaction, whereas the tertiary amine acts as a base and localises the enolate intermediate over the NDI moiety.<sup>140</sup> Hence, their ability to mediate a decarboxylative alkylation between thioester malonates and nitrostyrenes was evaluated (Fig. 13b).<sup>36</sup>

Ligand **14** was identified to be most reactive, and the activity was screened using a streptavidin library of 20 variants. The combination of ligand **14** and S112Y variant yields an organocatalytic artificial enzyme that selects for product formation over the decarboxylated starting material at a ratio >30 : 1. The conversion in ACN : glycine buffer at pH 3.0 was found to be 90% with e.r. up to 97.5 : 2.5.

Based on the site-directed mutagenesis studies and docking simulations, a plausible mechanism operated by ligand **14**/Sav-S112Y was proposed. A medium sized linker between biotin and NDI (*i.e.* ligand **14**) is essential to accommodate the catalytic unit close to the biotin-binding vestibule, whilst not causing any steric clash. Large electron-withdrawing substituents at the NDI motif were found to weaken the binding (**13** vs. **14**, Fig. 13a), while a flexible dimethylene bridge instead of a rigid one (**12** vs. **14**, Fig. 13a) hampers both the conversion and selectivity. The tertiary amine/NDI motif locates in close proximity to the

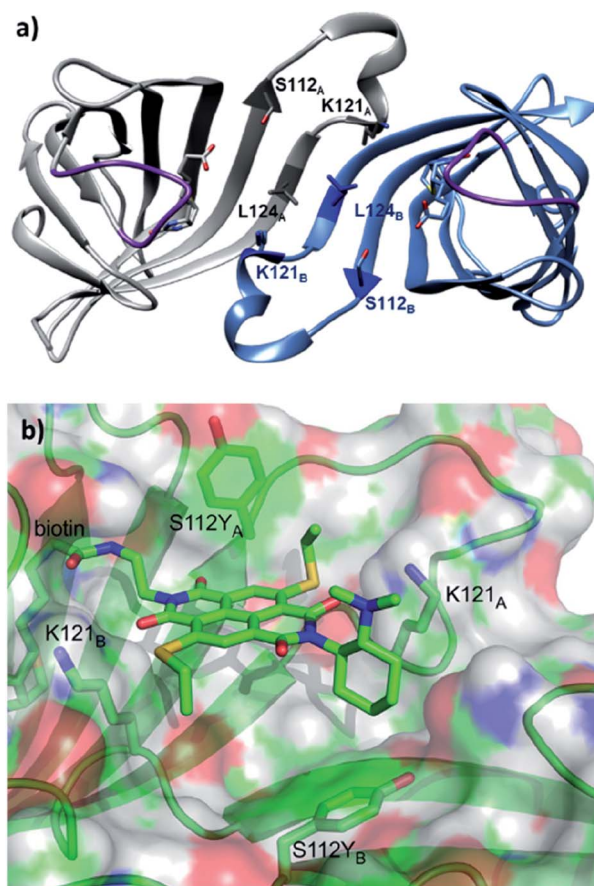


Fig. 14 (a) Cartoon overview of the assembly of streptavidin with full binding-site occupation with D-biotin in both binding sites, monomeric unit in light blue. The  $C_2$  symmetric interface of two streptavidin subunits is illustrated (PDB: 1MK5). Amino acids Ser112, Lys121, and Leu124 are highlighted. Purple loop regions represent amino acids 46–52. The other two subunits of the homotetrameric streptavidin are omitted for illustration purpose. (b) Cartoon overview of a single binding-site of anion– $\pi$  catalyst **14** in Sav S112Y. (b) Adapted from ref. 36, <https://pubs.acs.org/doi/abs/10.1021/acscentsci.6b00097>, with permission of ACS, copyright 2016. Further permissions related to the material excerpted should be directed to the ACS.

intersubunit interface of the homotetrameric streptavidin, which has a  $C_2$  symmetry (Fig. 14a). Hence, residues from both monomers can interact with the catalyst and substrates,<sup>141</sup> and the docking studies revealed that the S112Y mutation from each monomer, namely S112Y<sub>A</sub> and S112Y<sub>B</sub>, is essential to the catalysis by ligand **14**.

When the ligand is bound to monomer A, the NDI motif forms  $\pi$ – $\pi$ -interactions with S112Y<sub>A</sub>; this is supported by the observation that the mutant S112E and S112W resulted in decreased activity, while the S112F mutant showed similar reactivity to that of S112Y (Fig. 14b). In contrast, S112Y<sub>B</sub> shielded its own biotin binding site. Accordingly, optimal activity was obtained when the catalyst to free binding-sites ratio was kept at 1 : 2. The wild type lysine residues Lys121<sub>A</sub> and Lys121<sub>B</sub> anchor the NDI at the designated location. Furthermore, Lys121<sub>A</sub> helped maintaining a low pK<sub>a</sub> value for the tertiary amine of **14**, keeping it in its deprotonated form for reaction



## Review

(even at pH 3.0). Mutation of Lys121 led to a detrimental effect on the activity and selectivity. This study revealed the intricate interactions between the residues and catalytic motif, thereby highlighting that screening of both ligands and variants is critical to obtain an efficient and selective supramolecular system.

The hybrid catalyst system of streptavidin and conjugate **14** was further employed to perform a bioorthogonal domino-Michael-aldol reactions between diketones and nitrostyrenes (Fig. 15).<sup>76</sup> With 1–5 mol% catalyst loading, the bicyclic products were obtained in moderate yields ( $\approx 50\%$ ), decent enantioselectivities (0–80% ee) and significant diastereoselectivity ( $>20 : 1$ ) after screening with four streptavidin mutants. Interestingly, the protein–ligand assembly lead to an inversion of stereoselectivity when compared to the nascent biotin-catalyst conjugate.

The biotin-binding-sites in wild-type Sav are rather shallow, exposing a good portion of the catalytic moiety to the solvent. The lack of amino acid side chains in proximity makes mutational optimisation difficult to achieve (Fig. 14b). This led to the development of chimeric Sav variants, which contain insertions of amino acid loops around the biotin-binding sites of Sav like naturally occurring random loops or  $\alpha$ -helices.<sup>55</sup> Eight chimeric Sav variants containing random coils and alpha helix motifs inserted between residues 46–52 (purple region, Fig. 14a) and one with an addition at the C-terminus have been tested as host for the decarboxylative alkylation catalysed by ligand **14** (Fig. 13b). Though initially thought to increase stereoselectivity and reactivity, three of these chimeric protein hosts were completely inactive and the rest showed lower yields and enantioselectivities than the previously optimised mutant S112Y. Nonetheless, there are similar levels of selectivity for product formation over the decarboxylated starting material ( $>30 : 1$ ).

### Secondary amine organocatalysis

We have recently employed the streptavidin–biotin technology to create protein-based secondary amine organocatalytic systems. Seven biotinylated secondary amines (ligands **16–22**, Fig. 16a) were prepared *via* either copper-catalysed azide–alkyne cycloaddition or amide bond coupling reactions.<sup>39</sup> These catalysts can be broadly segregated into three types: MacMillan-like imidazolidinones (**16–19**), prolines (**20, 21**) and pyrrolidines (**22, 23**), and their ability to catalyse the Michael addition of nitromethane to aromatic  $\alpha,\beta$ -unsaturated aldehydes was tested (Fig. 16b).

Both (*R*)- and (*S*)-**22** alone are not enantioselective. However, when introduced to the tetrameric streptavidin, they were found

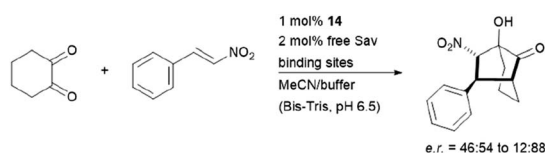


Fig. 15 Domino-Michael–Aldol-reaction catalysed by **14**. Bis-Tris = bis(2-hydroxyethyl)amino-tris(hydroxymethyl)methane.

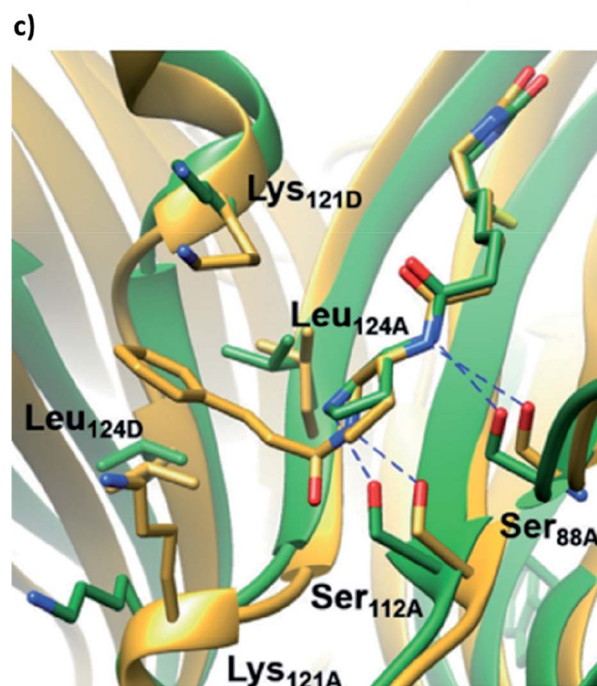
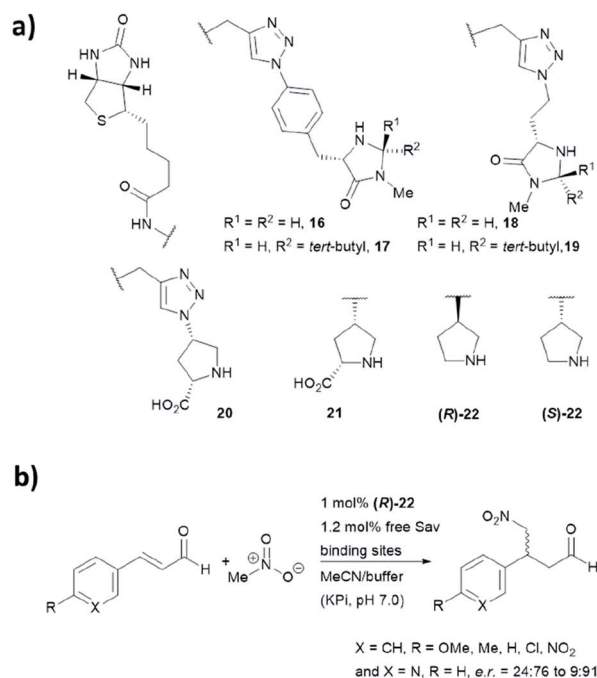


Fig. 16 (a) Reported biotin–secondary amine organocatalyst conjugates.<sup>39</sup> (b) Set of Michael addition reactions catalysed by **22** within a recombinant core streptavidin. (c) Cartoon overview of Sav:(*R*)-**22** crystal structure (green, PDB: 6GH7) and aminol adduct obtained from QM/MM simulations (golden), and it was adapted from ref. 39, which is an open access article under the terms of the Creative Commons Attribution License, published by Wiley-VCH, copyright 2018, the authors.

to be able to mediate the model reaction with high reactivity and stereoselectivity.<sup>39</sup> Moderate to good yields (37–80%) were obtained using only 1 mol% of protein catalyst and 1 : 1 MeOH/potassium phosphate buffer as reaction medium. Notably, these two protein complexes, namely Sav:(*R*)-**22** and Sav:(*S*)-**22**,



differed by only one chiral centre, but their stereoselectivity was opposite, with the former favouring for the *S* enantiomer and latter for the *R* enantiomer. Through crystallographic and computational structural studies, the position of the secondary amine motif was found to be in proximity to Ser112<sub>A</sub>. The lysine and leucine residues located at the dimer interface (Lys121<sub>A/B</sub> and Leu124<sub>A/B</sub>) dictate the face for which the intermediate was exposed for nucleophilic addition, thereby dictating both regio- (1,2 vs. 1,4-addition) and enantioselectivity (*R* and *S*) of the reaction (Fig. 16c).<sup>39</sup>

Based on the precedence of metallo-enzyme development and supramolecular capsules,<sup>142,143</sup> two organocatalytic artificial enzymes that operate distinctively different mechanisms have been designed. Nevertheless, the conditions developed so far are not completely biocompatible, as acidic conditions (pH 3.0) and/or a large volume of organic co-solvents are needed (though the latter was mostly due to the use of substrate with poor solubility in aqueous environments).<sup>23</sup> Furthermore, activity of these non-covalent complexes could be potentially optimised *via* laboratory evolution, as demonstrated by the existing Sav-based catalytic systems.<sup>46,48,127,128</sup> Though being a robust and reliable system, issues related to the *C*<sub>2</sub> symmetry of the inter-subunit interface of Sav was only recently addressed by the creation of “dimeric” Sav.<sup>141</sup> This “dimeric” Sav variant will facilitate mechanistic studies and the design of tailored and asymmetric scaffolds for chemical catalysis. In addition to the streptavidin:biotin system, other protein–ligand systems should serve as inspiration for novel protein-based organocatalytic systems, including the siderophore binding proteins<sup>124</sup> or coumarin binding albumins.<sup>144</sup>

## Conclusions and outlook

In this review, we summarised five approaches which are currently employed to perform organocatalysis within proteins (Table 1). The supramolecular tethering and N-terminal proline approaches have proven to be successful, and chemical catalysis with improved biocompatibility has been exploited in different applications including chemo-enzymatic synthesis<sup>116</sup> and gene switches.<sup>145</sup> In turn, covalent modification, computational *de novo* design and genetic code expansion are anticipated to excel, as related technologies have vastly improved and gained popularity in recent years.<sup>146–148</sup> Importantly, a much-improved system can be achieved by combining different approaches. This can be exemplified by the recent development of LmrR modified with dual catalytic groups.<sup>122</sup> Genetic code expansion can also be used to introduce novel catalytic functionalities into a *de novo* designed enzyme active site. This has been demonstrated in a recently reported artificial metalloenzyme, in which the designed active site includes the unnatural amino acid bipyridylalanine for metal binding.<sup>149</sup>

Despite all these exciting opportunities, there are aspects that need to be immediately addressed in the area of organocatalytic artificial enzyme design. Notably, many of the current systems suffer from poor reactivity, with enzyme loadings up to 20 mol% needed for reaction. However, the development of RA95, aniline/LmrR and methylated histidine/BH32 have

demonstrated that laboratory evolution is a feasible approach for activity improvement. The choice of protein scaffold and screening system likely play critical roles during the design. Furthermore, most protein-based organocatalytic systems are based on enamine and iminium catalysis that have similar counterparts in Nature. Useful bioorthogonal reactions that are frequently used in small molecule synthesis have not been tested, including  $\alpha$ -fluorinations, aziridinations and Diels–Alder reactions.<sup>4</sup> Also, sophisticated catalytic modes such as singly occupied molecular orbital (SOMO)<sup>150</sup> activation or photo-radical chemistry<sup>151</sup> can also be explored. In turn, other useful catalysts, including hydrogen bonding activators (thio-ureas and squaramides),<sup>152,153</sup> N-heterocyclic carbene<sup>32,154</sup> and ion pairing catalysis<sup>155</sup> have yet been explored. Additionally, repurposing flavin-dependent enzymes for novel photo-redox reactions represent a valuable avenue for artificial enzyme design.<sup>156–158</sup> In summary, this review illustrated that the design of artificial organocatalytic enzymes has become an exciting area of research and it will play critical roles in both chemical and synthetic biology research in future.

## Conflicts of interest

There are no conflicts to declare.

## Acknowledgements

We would like to thank for the financial support provided by Leverhulme Trust (RPG-2017-195), Royal Society (RG170187) and Wellcome Seed Trust (202056/Z/16/Z).

## Notes and references

- M. Tavakolian, S. Vahdati-Khajeh and S. Asgari, *ChemCatChem*, 2019, **11**, 2943.
- Y. Qin, L. Zhu and S. Luo, *Chem. Rev.*, 2017, **117**, 9433.
- Y. B. Wang and B. Tan, *Acc. Chem. Res.*, 2018, **51**, 534.
- D. W. MacMillan, *Nature*, 2008, **455**, 304.
- T. D. Beeson and D. W. C. MacMillan, *J. Am. Chem. Soc.*, 2005, **127**, 8826.
- S. G. Ouellet, J. B. Tuttle and D. W. MacMillan, *J. Am. Chem. Soc.*, 2005, **127**, 32.
- W. Notz, F. Tanaka and C. F. Barbas III, *Acc. Chem. Res.*, 2004, **37**, 580.
- O. V. Serdyuk, C. M. Heckel and S. B. Tsogoeva, *Org. Biomol. Chem.*, 2013, **11**, 7051.
- Y. Zhao, Y. Cotellet, L. Liu, J. Lopez-Andarias, A. B. Bornhof, M. Akamatsu, N. Sakai and S. Matile, *Acc. Chem. Res.*, 2018, **51**, 2255.
- J. Lou, F. Liu, C. D. Lindsay, O. Chaudhuri, S. C. Heilshorn and Y. Xia, *Adv. Mater.*, 2018, **30**, 1705215.
- R. J. Spears, R. L. Brabham, D. Budhadev, T. Keenan, S. McKenna, J. Walton, J. A. Brannigan, A. M. Brzozowski, A. J. Wilkinson, M. Plevin and M. A. Fascione, *Chem. Sci.*, 2018, **9**, 5585.
- R. J. Spears and M. A. Fascione, *Org. Biomol. Chem.*, 2016, **14**, 7622.





- 13 F. R. Bisogno, M. G. López-Vidal and G. de Gonzalo, *Adv. Synth. Catal.*, 2017, **359**, 2026.
- 14 M. Heidlindemann, G. Rulli, A. Berkessel, W. Hummel and H. Gröger, *ACS Catal.*, 2014, **4**, 1099.
- 15 G. Rulli, N. Duangdee, K. Baer, W. Hummel, A. Berkessel and H. Gröger, *Angew. Chem., Int. Ed.*, 2011, **50**, 7944.
- 16 K. Baer, M. Krausser, E. Burda, W. Hummel, A. Berkessel and H. Gröger, *Angew. Chem., Int. Ed.*, 2009, **48**, 9355.
- 17 M. P. van der Helm, B. Klemm and R. Eelkema, *Nat. Rev. Chem.*, 2019, **3**, 491.
- 18 N. K. Devaraj, *ACS Cent. Sci.*, 2018, **4**, 952.
- 19 L.-H. Qin, W. Hu and Y.-Q. Long, *Tetrahedron Lett.*, 2018, **59**, 2214.
- 20 E. M. Sletten and C. R. Bertozzi, *Angew. Chem., Int. Ed.*, 2009, **48**, 6974.
- 21 A. Mondal, S. Bhowmick, A. Ghosh, T. Chanda and K. C. Bhowmick, *Tetrahedron: Asymmetry*, 2017, **28**, 849.
- 22 S. Bhowmick, A. Mondal, A. Ghosh and K. C. Bhowmick, *Tetrahedron: Asymmetry*, 2015, **26**, 1215.
- 23 C. Jimeno, *Org. Biomol. Chem.*, 2016, **14**, 6147.
- 24 Y.-Q. Yu and Z.-L. Wang, *J. Chin. Chem. Soc.*, 2013, **60**, 288.
- 25 L. Burroughs, M. E. Vale, J. A. R. Gilks, H. Forintos, C. J. Hayes and P. A. Clarke, *Chem. Commun.*, 2010, **46**, 4776.
- 26 A. Seingeot, Y. Charmasson, M. Attolini and M. Maffei, *Heteroat. Chem.*, 2017, **28**, e21352.
- 27 W. W. Y. Leong, X. Chen and Y. R. Chi, *Green Chem.*, 2013, **15**, 1505.
- 28 J. Yan, R. Sun, K. Shi, K. Li, L. Yang and G. Zhong, *J. Org. Chem.*, 2018, **83**, 7547.
- 29 N. Mase, Y. Nakai, N. Ohara, H. Yoda, K. Takabe, F. Tanaka and C. F. Barbas III, *J. Am. Chem. Soc.*, 2006, **128**, 734.
- 30 G. Zhong, R. A. Lerner and C. F. Barbas III, *Angew. Chem., Int. Ed.*, 1999, **38**, 3738.
- 31 B. S. Vachan, M. Karuppasamy, P. Vinoth, S. V. Kumar, S. Perumal, V. Sridharan and J. C. Menendez, *Adv. Synth. Catal.*, 2020, **362**, 87.
- 32 C. K. Prier and F. H. Arnold, *J. Am. Chem. Soc.*, 2015, **137**, 13992.
- 33 F. Rudroff, M. D. Mihovilovic, H. Gröger, R. Snajdrova, H. Iding and U. T. Bornscheuer, *Nat. Catal.*, 2018, **1**, 12.
- 34 F. Schwizer, Y. Okamoto, T. Heinisch, Y. Gu, M. M. Pellizzoni, V. Lebrun, R. Reuter, V. Kohler, J. C. Lewis and T. R. Ward, *Chem. Rev.*, 2018, **118**, 142.
- 35 T. Heinisch and T. R. Ward, *Acc. Chem. Res.*, 2016, **49**, 1711.
- 36 Y. Cotelle, V. Lebrun, N. Sakai, T. R. Ward and S. Matile, *ACS Cent. Sci.*, 2016, **2**, 388.
- 37 M. Rahimi, E. M. Geertsema, Y. Miao, J. Y. van der Meer, T. van den Bosch, P. de Haan, E. Zandvoort and G. J. Poelarends, *Org. Biomol. Chem.*, 2017, **15**, 2809.
- 38 E. Zandvoort, E. M. Geertsema, B. J. Baas, W. J. Quax and G. J. Poelarends, *Angew. Chem., Int. Ed.*, 2012, **51**, 1240.
- 39 A. R. Nödling, K. Świderek, R. Castillo, J. W. Hall, A. Angelastro, L. C. Morrill, Y. Jin, Y.-H. Tsai, V. Moliner and L. Y. P. Luk, *Angew. Chem., Int. Ed.*, 2018, **57**, 12478.
- 40 X. Garrabou, D. S. Macdonald, B. I. M. Wicky and D. Hilvert, *Angew. Chem., Int. Ed.*, 2018, **57**, 5288.
- 41 X. Garrabou, D. S. Macdonald and D. Hilvert, *Chem.–Eur. J.*, 2017, **23**, 6001.
- 42 X. Garrabou, R. Verez and D. Hilvert, *J. Am. Chem. Soc.*, 2017, **139**, 103.
- 43 X. Garrabou, B. I. Wicky and D. Hilvert, *J. Am. Chem. Soc.*, 2016, **138**, 6972.
- 44 X. Garrabou, T. Beck and D. Hilvert, *Angew. Chem., Int. Ed.*, 2015, **54**, 5609.
- 45 L. Li, C. Li, Z. Zhang and E. Alexov, *J. Chem. Theory Comput.*, 2013, **9**, 2126.
- 46 M. Hesticová, T. Heinisch, L. Alonso-Cotchico, J. D. Maréchal, P. Vidossich and T. R. Ward, *Angew. Chem., Int. Ed.*, 2018, **57**, 1863.
- 47 G. Roelfes, *Acc. Chem. Res.*, 2019, **52**, 545.
- 48 A. D. Liang, J. Serrano-Plana, R. L. Peterson and T. R. Ward, *Acc. Chem. Res.*, 2019, **52**, 585.
- 49 C. Zeymer and D. Hilvert, *Annu. Rev. Biochem.*, 2018, **87**, 131.
- 50 C. Mayer, C. Dulson, E. Reddem, A. W. H. Thunnissen and G. Roelfes, *Angew. Chem., Int. Ed.*, 2019, **58**, 2083.
- 51 Y. Wang, J. Chen and Z. Kang, *Biochemistry*, 2019, **58**, 1451.
- 52 V. Vaissier Welborn and T. Head-Gordon, *Chem. Rev.*, 2019, **119**, 6613.
- 53 H. Kries, R. Blomberg and D. Hilvert, *Curr. Opin. Chem. Biol.*, 2013, **17**, 221.
- 54 C. Trindler and T. R. Ward, in *Effects of Nanoconfinement on Catalysis*, ed. R. Poli, Springer International Publishing, Cham, 2017, ch. 49, pp. 49–82, DOI: 10.1007/978-3-319-50207-6\_3.
- 55 M. M. Pellizzoni, F. Schwizer, C. W. Wood, V. Sabatino, Y. Cotelle, S. Matile, D. N. Woolfson and T. R. Ward, *ACS Catal.*, 2018, **8**, 1476.
- 56 H. J. Davis and T. R. Ward, *ACS Cent. Sci.*, 2019, **5**, 1120.
- 57 Z. P. Wu and D. Hilvert, *J. Am. Chem. Soc.*, 1990, **112**, 5647.
- 58 D. Häring, E. Schüler, W. Adam, C. R. Saha-Möller and P. Schreier, *J. Org. Chem.*, 1999, **64**, 832.
- 59 C. J. Suckling and L.-M. Zhu, *Bioorg. Med. Chem. Lett.*, 1993, **3**, 531.
- 60 H. Kuang, M. L. Brown, R. R. Davies, E. C. Young and M. D. Distefano, *J. Am. Chem. Soc.*, 1996, **118**, 10702.
- 61 T. L. Williams, A. R. Nödling, Y. H. Tsai and L. Y. P. Luk, *Wellcome Open Res.*, 2018, **3**, 107.
- 62 H. A. Bunzel, H. Kries, L. Marchetti, C. Zeymer, P. R. E. Mittl, A. J. Mulholland and D. Hilvert, *J. Am. Chem. Soc.*, 2019, **141**, 11745.
- 63 C. Zeymer, R. Zschoche and D. Hilvert, *J. Am. Chem. Soc.*, 2017, **139**, 12541.
- 64 R. Obexer, A. Godina, X. Garrabou, P. R. E. Mittl, D. Baker, A. D. Griffiths and D. Hilvert, *Nat. Chem.*, 2017, **9**, 50.
- 65 R. Obexer, S. Studer, L. Giger, D. M. Pinkas, M. G. Grütter, D. Baker and D. Hilvert, *ChemCatChem*, 2014, **6**, 1043.
- 66 L. Giger, S. Caner, R. Obexer, P. Kast, D. Baker, N. Ban and D. Hilvert, *Nat. Chem. Biol.*, 2013, **9**, 494.
- 67 E. A. Althoff, L. Wang, L. Jiang, L. Giger, J. K. Lassila, Z. Wang, M. Smith, S. Hari, P. Kast, D. Herschlag, D. Hilvert and D. Baker, *Protein Sci.*, 2012, **21**, 717.
- 68 L. Jiang, E. A. Althoff, F. R. Clemente, L. Doyle, D. Röthlisberger, A. Zanghellini, J. L. Gallaher,



- J. L. Betker, F. Tanaka, C. F. Barbas III, D. Hilvert, K. N. Houk, B. L. Stoddard and D. Baker, *Science*, 2008, **319**, 1387.
- 69 J.-Y. van der Meer, H. Poddar, B.-J. Baas, Y. Miao, M. Rahimi, A. Kunzendorf, R. van Merkerk, P. G. Tepper, E. M. Geertsema, A.-M. W. H. Thunnissen, W. J. Quax and G. J. Poelarends, *Nat. Commun.*, 2016, **7**, 10911.
- 70 E. M. Geertsema, Y. Miao, P. G. Tepper, P. de Haan, E. Zandvoort and G. J. Poelarends, *Chem.-Eur. J.*, 2013, **19**, 14407.
- 71 Y. Miao, E. M. Geertsema, P. G. Tepper, E. Zandvoort and G. J. Poelarends, *ChemBioChem*, 2013, **14**, 191.
- 72 E. Zandvoort, E. M. Geertsema, W. J. Quax and G. J. Poelarends, *ChemBioChem*, 2012, **13**, 1274.
- 73 E. Zandvoort, B.-J. Baas, W. J. Quax and G. J. Poelarends, *ChemBioChem*, 2011, **12**, 602.
- 74 A. J. Burke, S. L. Lovelock, A. Frese, R. Crawshaw, M. Ortmayer, M. Dunstan, C. Levy and A. P. Green, *Nature*, 2019, **570**, 219.
- 75 I. Drienovská, C. Mayer, C. Dulson and G. Roelfes, *Nat. Chem.*, 2018, **10**, 946.
- 76 L. Liu, Y. Cotelte, J. Klehr, N. Sakai, T. R. Ward and S. Matile, *Chem. Sci.*, 2017, **8**, 3770.
- 77 M. D. Toscano, K. J. Woycechowsky and D. Hilvert, *Angew. Chem., Int. Ed.*, 2007, **46**, 3212.
- 78 E. T. Kaiser and D. S. Lawrence, *Science*, 1984, **226**, 505.
- 79 D. Qi, C. M. Tann, D. Haring and M. D. Distefano, *Chem. Rev.*, 2001, **101**, 3081.
- 80 L. Polgar and M. L. Bender, *J. Am. Chem. Soc.*, 1966, **88**, 3153.
- 81 L. Polgar and M. L. Bender, *Biochemistry*, 1967, **6**, 610–620.
- 82 K. E. Neet, A. Nanci and D. E. Koshland Jr, *J. Biol. Chem.*, 1968, **243**, 6392.
- 83 Z. P. Wu and D. Hilvert, *J. Am. Chem. Soc.*, 1989, **111**, 4513.
- 84 H. L. Levine, Y. Nakagawa and E. T. Kaiser, *Biochem. Biophys. Res. Commun.*, 1977, **76**, 64.
- 85 S. Mao, Z. Dong, J. Liu, X. Li, X. Liu, G. Luo and J. Shen, *J. Am. Chem. Soc.*, 2005, **127**, 11588.
- 86 J. C. Maza, D. L. V. Bader, L. Xiao, A. M. Marmelstein, D. D. Brauer, A. M. ElSohly, M. J. Smith, S. W. Krska, C. A. Parish and M. B. Francis, *J. Am. Chem. Soc.*, 2019, **141**, 3885.
- 87 C. B. Rosen and M. B. Francis, *Nat. Chem. Biol.*, 2017, **13**, 697.
- 88 P. G. Isenegger and B. G. Davis, *J. Am. Chem. Soc.*, 2019, **141**, 8005.
- 89 B. Bhushan, Y. A. Lin, M. Bak, A. Phanumartiwath, N. Yang, M. K. Bilyard, T. Tanaka, K. L. Hudson, L. Lercher, M. Stegmann, S. Mohammed and B. G. Davis, *J. Am. Chem. Soc.*, 2018, **140**, 14599.
- 90 S. R. G. Galan, J. R. Wickens, J. Dadova, W.-L. Ng, X. Zhang, R. A. Simion, R. Quinlan, E. Pires, R. S. Paton, S. Caddick, V. Chudasama and B. G. Davis, *Nat. Chem. Biol.*, 2018, **14**, 955.
- 91 A. Dumas, L. Lercher, C. D. Spicer and B. G. Davis, *Chem. Sci.*, 2015, **6**, 50.
- 92 M. Morais, N. Forte, V. Chudasama and J. R. Baker, in *Bioconjugation: Methods and Protocols*, ed. S. Massa and N. Devoogdt, Springer, New York, NY, 2019, ch. 15, pp. 15–24, DOI: 10.1007/978-1-4939-9654-4\_2.
- 93 J. N. deGruyter, L. R. Malins and P. S. Baran, *Biochemistry*, 2017, **56**, 3863.
- 94 O. Boutureira and G. J. Bernardes, *Chem. Rev.*, 2015, **115**, 2174.
- 95 D. Hilvert, *Annu. Rev. Biochem.*, 2013, **82**, 447.
- 96 A. Zanghellini, L. Jiang, A. M. Wollacott, G. Cheng, J. Meiler, E. A. Althoff, D. Röthlisberger and D. Baker, *Protein Sci.*, 2006, **15**, 2785.
- 97 A. Leaver-Fay, M. Tyka, S. M. Lewis, O. F. Lange, J. Thompson, R. Jacak, K. W. Kaufman, P. D. Renfrew, C. A. Smith, W. Sheffler, I. W. Davis, S. Cooper, A. Treuille, D. J. Mandell, F. Richter, Y.-E. A. Ban, S. J. Fleishman, J. E. Corn, D. E. Kim, S. Lyskov, M. Berrondo, S. Mentzer, Z. Popović, J. J. Havranek, J. Karanicolas, R. Das, J. Meiler, T. Kortemme, J. J. Gray, B. Kuhlman, D. Baker and P. Bradley, in *Methods in Enzymology*, ed. M. L. Johnson and L. Brand, Academic Press, 2011, vol. 487, ch. 545, pp. 545–574.
- 98 D. J. Tantillo, C. Jiayang and K. N. Houk, *Curr. Opin. Chem. Biol.*, 1998, **2**, 743.
- 99 M. Merski and B. K. Shoichet, *Proc. Natl. Acad. Sci. U. S. A.*, 2012, **109**, 16179.
- 100 D. Röthlisberger, O. Khersonsky, A. M. Wollacott, L. Jiang, J. DeChancie, J. Betker, J. L. Gallaher, E. A. Althoff, A. Zanghellini, O. Dym, S. Albeck, K. N. Houk, D. S. Tawfik and D. Baker, *Nature*, 2008, **453**, 190.
- 101 S. Bjelic, L. G. Nivón, N. Çelebi-Ölçüm, G. Kiss, C. F. Rosewall, H. M. Lovick, E. L. Ingalls, J. L. Gallaher, J. Seetharaman, S. Lew, G. T. Montelione, J. F. Hunt, F. E. Michael, K. N. Houk and D. Baker, *ACS Chem. Biol.*, 2013, **8**, 749.
- 102 M. Hennig, B. D. Darimont, J. N. Jansonius and K. Kirschner, *J. Mol. Biol.*, 2002, **319**, 757.
- 103 B. Kuhlman, G. Dantas, G. C. Ireton, G. Varani, B. L. Stoddard and D. Baker, *Science*, 2003, **302**, 1364.
- 104 T. A. Kunkel, *Proc. Natl. Acad. Sci. U. S. A.*, 1985, **82**, 488.
- 105 A. R. Buller, P. van Roye, J. K. B. Cahn, R. A. Scheele, M. Herger and F. H. Arnold, *J. Am. Chem. Soc.*, 2018, **140**, 7256.
- 106 Y. Zhang, P. Doruker, B. Kaynak, S. Zhang, J. Krieger, H. Li and I. Bahar, *Curr. Opin. Chem. Biol.*, 2019, **62**, 14.
- 107 D. L. Trudeau and D. S. Tawfik, *Curr. Opin. Chem. Biol.*, 2019, **60**, 46.
- 108 M. A. Maria-Solano, E. Serrano-Hervas, A. Romero-Rivera, J. Iglesias-Fernandez and S. Osuna, *Chem. Commun.*, 2018, **54**, 6622.
- 109 R. K. Wierenga, *FEBS Lett.*, 2001, **492**, 193.
- 110 R. K. Wierenga, E. G. Kapetaniou and R. Venkatesan, *Cell. Mol. Life Sci.*, 2010, **67**, 3961–3982.
- 111 A. D. Goldman, J. T. Beatty and L. F. Landweber, *J. Mol. Evol.*, 2016, **82**, 17.



## Review

- 112 J. Lazic, J. Spasic, D. Francuski, Z. Tokic-Vujosevic, J. Nikodinovic-Runic, V. Maslak and L. Djokic, *J. Serb. Chem. Soc.*, 2016, **81**, 871–881.
- 113 T. K. Harris, R. M. Czerwinski, W. H. Johnson Jr, P. M. Legler, C. Abeygunawardana, M. A. Massiah, J. T. Stivers, C. P. Whitman and A. S. Mildvan, *Biochemistry*, 1999, **38**, 12343.
- 114 E. A. Burks, C. D. Fleming, A. D. Mesecar, C. P. Whitman and S. D. Pegan, *Biochemistry*, 2010, **49**, 5016.
- 115 C. Guo, M. Saifuddin, T. Saravanan, M. Sharifi and G. J. Poelarends, *ACS Catal.*, 2019, **9**, 4369.
- 116 L. Biewenga, T. Saravanan, A. Kunzendorf, J. Y. van der Meer, T. Pijning, P. G. Tepper, R. van Merkerk, S. J. Charnock, A. W. H. Thunnissen and G. J. Poelarends, *ACS Catal.*, 2019, **9**, 1503.
- 117 T. Narancic, J. Radivojevic, P. Jovanovic, D. Francuski, M. Bigovic, V. Maslak, V. Savic, B. Vasiljevic, K. E. O'Connor and J. Nikodinovic-Runic, *Bioresour. Technol.*, 2013, **142**, 462.
- 118 L. Djokic, J. Spasic, S. Jeremic, B. Vasiljevic, O. Prodanovic, R. Prodanovic and J. Nikodinovic-Runic, *Bioprocess Biosyst. Eng.*, 2015, **38**, 2389.
- 119 J. Radivojevic, G. Minovska, L. Senerovic, K. O'Connor, P. Jovanovic, V. Savic, Z. Tokic-Vujosevic, J. Nikodinovic-Runic and V. Maslak, *RSC Adv.*, 2014, **4**, 60502.
- 120 A. R. Nödling, L. A. Spear, T. L. Williams, L. Y. P. Luk and Y.-H. Tsai, *Essays Biochem.*, 2019, **63**, 237.
- 121 J. W. Chin, S. W. Santoro, A. B. Martin, D. S. King, L. Wang and P. G. Schultz, *J. Am. Chem. Soc.*, 2002, **124**, 9026.
- 122 Z. Zhou and G. Roelfes, *Nat. Catal.*, 2020, **3**, 289.
- 123 I. S. Hassan, A. N. Ta, M. W. Danneman, N. Semakul, M. Burns, C. H. Basch, V. N. Dippon, B. R. McNaughton and T. Rovis, *J. Am. Chem. Soc.*, 2019, **141**, 4815.
- 124 D. J. Raines, J. E. Clarke, E. V. Blagova, E. J. Dodson, K. S. Wilson and A.-K. Duhme-Klair, *Nat. Catal.*, 2018, **1**, 680.
- 125 F. W. Monnard, E. S. Nogueira, T. Heinisch, T. Schirmer and T. R. Ward, *Chem. Sci.*, 2013, **4**, 3269.
- 126 T. R. Ward, *Acc. Chem. Res.*, 2011, **44**, 47.
- 127 M. T. Reetz, J. J. Peyralans, A. Maichele, Y. Fu and M. Maywald, *Chem. Commun.*, 2006, 4318.
- 128 T. Heinisch, F. Schwizer, B. Garabedian, E. Csibra, M. Jeschek, J. Vallapurackal, V. B. Pinheiro, P. Marliere, S. Panke and T. R. Ward, *Chem. Sci.*, 2018, **9**, 5383.
- 129 M. Jeschek, R. Reuter, T. Heinisch, C. Trindler, J. Klehr, S. Panke and T. R. Ward, *Nature*, 2016, **537**, 661.
- 130 A. Zocchi, N. Humbert, T. Berta and T. R. Ward, *Chimia*, 2003, **57**, 589.
- 131 M. E. Wilson and G. M. Whitesides, *J. Am. Chem. Soc.*, 1978, **100**, 306.
- 132 L. Olshansky, R. Huerta-Lavorie, A. I. Nguyen, J. Vallapurackal, A. Furst, T. D. Tilley and A. S. Borovik, *J. Am. Chem. Soc.*, 2018, **140**, 2739.
- 133 C.-C. Lin, C.-W. Lin and A. S. C. Chan, *Tetrahedron: Asymmetry*, 1999, **10**, 1887.
- 134 R. E. Dawson, A. Hennig, D. P. Weimann, D. Emery, V. Ravikumar, J. Montenegro, T. Takeuchi, S. Gabutti, M. Mayor, J. Mareda, C. A. Schalley and S. Matile, *Nat. Chem.*, 2010, **2**, 533.
- 135 Y. Zhao, Y. Domoto, E. Orentas, C. Beuchat, D. Emery, J. Mareda, N. Sakai and S. Matile, *Angew. Chem., Int. Ed.*, 2013, **52**, 9940.
- 136 Y. Zhao, Y. Cotelle, A.-J. Avestro, N. Sakai and S. Matile, *J. Am. Chem. Soc.*, 2015, **137**, 11582.
- 137 Y. Zhao, C. Beuchat, Y. Domoto, J. Gajewy, A. Wilson, J. Mareda, N. Sakai and S. Matile, *J. Am. Chem. Soc.*, 2014, **136**, 2101.
- 138 A. J. Neel, M. J. Hilton, M. S. Sigman and F. D. Toste, *Nature*, 2017, **543**, 637.
- 139 M. Giese, M. Albrecht and K. Rissanen, *Chem. Commun.*, 2016, **52**, 1778.
- 140 Y. Cotelle, S. Benz, A.-J. Avestro, T. R. Ward, N. Sakai and S. Matile, *Angew. Chem., Int. Ed.*, 2016, **55**, 4275.
- 141 S. Wu, Y. Zhou, J. G. Rebelein, M. Kuhn, H. Mallin, J. Zhao, N. V. Igareta and T. R. Ward, *J. Am. Chem. Soc.*, 2019, **141**, 15869.
- 142 T. M. Brauer, Q. Zhang and K. Tiefenbacher, *J. Am. Chem. Soc.*, 2017, **139**, 17500.
- 143 T. M. Brauer, Q. Zhang and K. Tiefenbacher, *Angew. Chem., Int. Ed.*, 2016, **55**, 7698.
- 144 S. Eda, I. Nasibullin, K. Vong, N. Kudo, M. Yoshida, A. Kurbangalieva and K. Tanaka, *Nat. Catal.*, 2019, **2**, 780.
- 145 Y. Okamoto, R. Kojima, F. Schwizer, E. Bartolami, T. Heinisch, S. Matile, M. Fussenegger and T. R. Ward, *Nat. Commun.*, 2018, **9**, 1943.
- 146 B. D. Weitzner, Y. Kipnis, A. G. Daniel, D. Hilvert and D. Baker, *Protein Sci.*, 2019, **28**, 2036.
- 147 I. Drienovská and G. Roelfes, *Nat. Catal.*, 2020, **3**, 193.
- 148 K. Chen and F. H. Arnold, *Nat. Catal.*, 2020, **3**, 203.
- 149 J. H. Mills, S. D. Khare, J. M. Bolduc, F. Forouhar, V. K. Mulligan, S. Lew, J. Seetharaman, L. Tong, B. L. Stoddard and D. Baker, *J. Am. Chem. Soc.*, 2013, **135**, 13393.
- 150 T. D. Beeson, A. Mastracchio, J. B. Hong, K. Ashton and D. W. Macmillan, *Science*, 2007, **316**, 582.
- 151 M. Silvi and P. Melchiorre, *Nature*, 2018, **554**, 41.
- 152 R. R. Knowles and E. N. Jacobsen, *Proc. Natl. Acad. Sci. U. S. A.*, 2010, **107**, 20678.
- 153 B. L. Zhao, J. H. Li and D. M. Du, *Chem. Rec.*, 2017, **17**, 994.
- 154 D. M. Flanigan, F. Romanov-Michailidis, N. A. White and T. Rovis, *Chem. Rev.*, 2015, **115**, 9307.
- 155 M. Mahlau and B. List, *Angew. Chem., Int. Ed.*, 2013, **52**, 518.
- 156 K. F. Biegasiewicz, S. J. Cooper, X. Gao, D. G. Oblinsky, J. H. Kim, S. E. Garfinkle, L. A. Joyce, B. A. Sandoval, G. D. Scholes and T. K. Hyster, *Science*, 2019, **364**, 1166.
- 157 M. J. Black, K. F. Biegasiewicz, A. J. Meichan, D. G. Oblinsky, B. Kudisch, G. D. Scholes and T. K. Hyster, *Nat. Chem.*, 2020, **12**, 71.
- 158 B. A. Sandoval, A. J. Meichan and T. K. Hyster, *J. Am. Chem. Soc.*, 2017, **139**, 11313.



# ChemComm

Chemical Communications

Accepted Manuscript

This article can be cited before page numbers have been issued, to do this please use: N. Santi, L. C. Morrill, K. Swiderek, V. Moliner and L. Y. Lu, *Chem. Commun.*, 2021, DOI: 10.1039/D0CC08142F.



This is an Accepted Manuscript, which has been through the Royal Society of Chemistry peer review process and has been accepted for publication.

Accepted Manuscripts are published online shortly after acceptance, before technical editing, formatting and proof reading. Using this free service, authors can make their results available to the community, in citable form, before we publish the edited article. We will replace this Accepted Manuscript with the edited and formatted Advance Article as soon as it is available.

You can find more information about Accepted Manuscripts in the [Information for Authors](#).

Please note that technical editing may introduce minor changes to the text and/or graphics, which may alter content. The journal's standard [Terms & Conditions](#) and the [Ethical guidelines](#) still apply. In no event shall the Royal Society of Chemistry be held responsible for any errors or omissions in this Accepted Manuscript or any consequences arising from the use of any information it contains.

## Transfer Hydrogenations catalyzed by Streptavidin-hosted Secondary Amine Organocatalyst

Nicolò Santi,<sup>a</sup> Louis C. Morrill,<sup>a,b</sup> Katarzyna Świderek,<sup>c</sup> Vicent Moliner,<sup>c</sup> Louis Y. P. Luk<sup>\*,a,b</sup>

<sup>a</sup> School of Chemistry, Main Building, Cardiff University, Cardiff CF10 3AT, UK

<sup>b</sup> Cardiff Catalysis Institute, School of Chemistry, Main Building, Cardiff University, Cardiff CF10 3AT, UK

<sup>c</sup> Departament de Química Física i Analítica, Universitat Jaume I, 12071 Castelló, Spain.

\*E-mail: [lukly@cardiff.ac.uk](mailto:lukly@cardiff.ac.uk); Tel.: +44 (0)29 2251 0161



## COMMUNICATION

**Transfer Hydrogenations catalyzed by Streptavidin-hosted Secondary Amine Organocatalyst**Nicolò Santi,<sup>a</sup> Louis C. Morrill,<sup>a,b</sup> Katarzyna Świderek,<sup>c</sup> Vicent Moliner,<sup>c</sup> Louis Y. P. Luk<sup>\*,a,b</sup>Received 00th January 20xx,  
Accepted 00th January 20xx

DOI: 10.1039/x0xx00000x

Here, the streptavidin-biotin technology was applied to enable organocatalytic transfer hydrogenation. By introducing a biotin-tethered pyrrolidine (**1**) to the tetrameric streptavidin (T-Sav), the resulting hybrid catalyst was able to mediate hydride transfer from dihydro-benzyl nicotinamide (BNAH) to  $\alpha$ ,  $\beta$ -unsaturated aldehydes. Hydrogenation of cinnamaldehyde and some of its aryl-substituted analogues was found to be nearly quantitative. Kinetic measurements revealed that the T-Sav:1 assembly possesses enzyme-like behavior, whereas isotope effect analysis, performed by QM/MM simulations, illustrated the step of hydride transfer is at least partially rate-limiting. These results have proven the concept that T-Sav can be used to host secondary amine-catalyzed transfer hydrogenations.

In biological systems, nicotinamide is frequently used in the transfer of electrons and hydrogen atoms<sup>1, 2</sup> and is typically found in the form of NAD(P)H attached to an adenosine dinucleotide appendix.<sup>3</sup> While the adenosine dinucleotide motif is crucial for molecular recognition and metabolic regulation in cell,<sup>4</sup> this appendix is a large and complex molecular burden that needs to be addressed when it comes to synthetic applications.<sup>5</sup> Consequently, various cofactor recycling systems have been designed.<sup>6, 7</sup> In an alternative and potentially simpler approach, small organic molecules can be used as hydride donors,<sup>8, 9</sup> such as the Hantzsch ester,<sup>10</sup> dihydro-benzyl nicotinamide (BNAH) and their derivatives.<sup>11, 12</sup> Nevertheless, there are only a handful of protein-based catalysts reported to use simple hydride donors for reactions, including ene-reductases (ERs),<sup>6, 13</sup> salicylate (SalH), *para*-hydroxybenzoate (PHBH) and hydroxybenzoate (3HB6H)

hydroxylases,<sup>14</sup> cytochrome P450,<sup>15</sup> 2-hydroxybiphenyl 3-monoxygenase (HbpA)<sup>16</sup>, Old Yellow Enzyme (TsOYE),<sup>17</sup> and glucose dehydrogenases (GDH).<sup>18</sup> Here, we aim to expand this collection by proving the concept that organocatalytic artificial enzymes can catalyze transfer hydrogenation using BNAH as a hydride source.<sup>19</sup>

Artificial enzymes can be created by docking chemical catalysts into a designated protein scaffold, and the resulting complex can potentially use hydride donors for reactions.<sup>7</sup> Different approaches such as computational design, genetic code expansion, supramolecular approach and amino acid modifications have been used to accommodate chemical catalytic systems for bioorthogonal reactions.<sup>19-25</sup> Previously, the streptavidin-biotin technology has been applied to host Ru and Ir-mediated transfer hydrogenation with the use of NAD(P)H and formic acid as hydride donors.<sup>7, 26-28</sup> Recently, streptavidin has also been used to host organocatalysis, including secondary amine, anion- $\pi$  and DMAP catalysis;<sup>19, 20, 23, 29, 30</sup> however, the reaction profile of these organocatalytic systems remains largely unexplored, and their possibility of mediating organocatalytic transfer hydrogenation reaction has not been tested.

Here, we demonstrate that secondary amine hosted by streptavidin can be used to catalyze transfer hydrogenation reactions (**Fig. 1**). Hybrid catalysts have been created by introducing biotinylated secondary amines (**1** and **2**) to the tetrameric streptavidin (**T-Sav**) or the monomeric counterpart (**M-Sav**). Upon optimization, conversion of cinnamaldehyde (**3**) to its reduced counterpart (**5**) was found to be >90% (**Table 1**). This work lays the basis for enabling organocatalytic transfer hydrogenation in biological contexts.

In previous work, we have demonstrated that biotinylated catalysts (**1** and **2**) were able to mediate Michael addition and aldol condensation when introduced to the tetrameric streptavidin (**T-Sav**).<sup>31</sup> In this work, the reduction of cinnamaldehyde **3** by dihydrobenzyl nicotinamide (BNAH, **4**) in KP<sub>i</sub> buffer (10 mM, 10% methanol, pH 7.0) at room temperature serves as the model transfer hydrogenation reaction and was assessed by <sup>1</sup>H NMR spectroscopy (**Table 1**).

<sup>a</sup> School of Chemistry, Main Building, Cardiff University, Cardiff CF10 3AT, UK<sup>b</sup> Cardiff Catalysis Institute, School of Chemistry, Main Building, Cardiff University, Cardiff CF10 3AT, UK<sup>c</sup> Departament de Química Física i Analítica, Universitat Jaume I, 12071 Castelló, Spain.

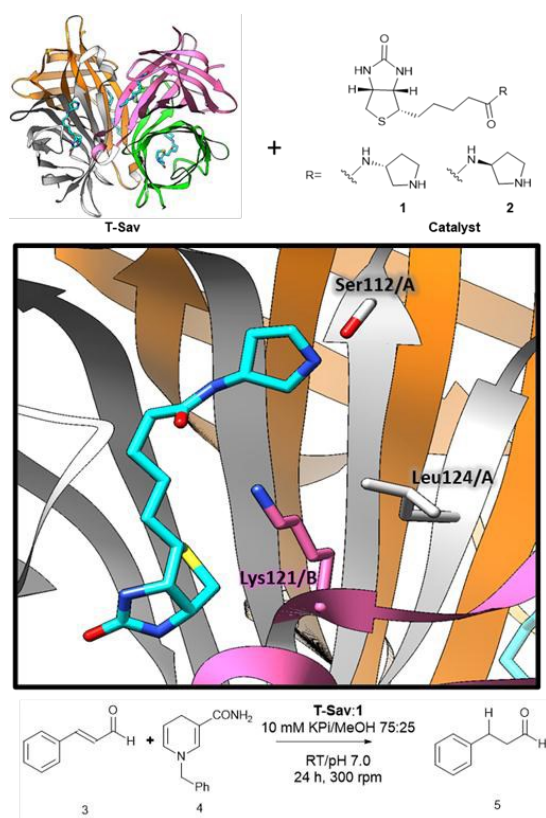
\*E-mail: lukly@cardiff.ac.uk; Tel.: +44 (0)29 2251 0161

† Footnotes relating to the title and/or authors should appear here.

Electronic Supplementary Information (ESI) available: [details of any supplementary information available should be included here]. See DOI: 10.1039/x0xx00000x



In the absence of protein or catalysts, only 3 % of dihydrogenated product was observed after 24-hour incubation when two equivalents of BNAH was used (**Entry 1**). Similarly, **T-Sav** (and its monomeric counterpart **M-Sav**<sup>32, 33</sup>) have negligible effects in catalyzing hydride transfer (**Entry 2-3**). When 1 mol% of catalyst **1** or **2** is used, the estimated reaction conversion increased to about 25% (**Entry 4-5**). When both **T-Sav** and catalyst **1** are included (1:1.2 ratio of catalyst to protein), the estimated conversion increased to 77 and 95% at 1 and 2 mol% respectively (**Entry 6-7**). These results are in line with the findings that organocatalysis is favored when executed in an environment that has low dielectric constant, such as organic solvents and protein surface or interior.<sup>19</sup> Increasing the amount of BNAH to 5 equivalents in a 75:25 KPi:MeOH mixture enhances the conversion up to 94% with only 1 mol% of **T-Sav:1** (**Entry 8**). Interestingly, when no shaking was applied to the reaction mixture, the product conversion decreases to 53% (**Entry 9**). Lastly, in agreement with the previous work which illustrated catalyst **2** is more flexible and solvent-exposed when bound to **T-Sav**,<sup>20</sup> the conversion was lower when catalyst **2** was used (**Entry 10**).



**Fig. 1.** Combining the tetrameric streptavidin (**T-Sav**) with biotinylated organocatalysts **1** or **2** to generate organocatalytic artificial enzymes (**T-Sav:1**, PDB: 6GH7, 1.08 Å) for transfer hydrogenation reactions.

**Table 1.** Screening reaction for transfer hydrogenation from BNAH to cinnamaldehyde<sup>a,b,c</sup>  
DOI: 10.1039/D0CC08142F

Entry	Host	Guest	Hydrogen Donor	Loading (mol%)	% Estimated conversion <sup>a</sup>
1	N.A.	N.A.	BNAH ( <b>4</b> )	N.A.	3
2	<b>T-Sav</b>	N.A.	BNAH ( <b>4</b> )	1	5
3	<b>M-Sav</b>	N.A.	BNAH ( <b>4</b> )	1	4
4	N.A.	<b>1</b>	BNAH ( <b>4</b> )	1	26
5	N.A.	<b>2</b>	BNAH ( <b>4</b> )	1	25
6	<b>T-Sav</b>	<b>1</b>	BNAH ( <b>4</b> )	1	77
7	<b>T-Sav</b>	<b>1</b>	BNAH ( <b>4</b> )	2	95
8	<b>T-Sav</b>	<b>1</b>	BNAH ( <b>4</b> )	1	94 <sup>d</sup>
9	<b>T-Sav</b>	<b>1</b>	BNAH ( <b>4</b> )	1	53 <sup>e, f</sup>
10	<b>T-Sav</b>	<b>2</b>	BNAH ( <b>4</b> )	1	51
11	<b>M-Sav</b>	<b>1</b>	BNAH ( <b>4</b> )	1	21
12	<b>M-Sav</b>	<b>2</b>	BNAH ( <b>4</b> )	1	10
13	<b>T-Sav</b>	<b>1</b>	NADH ( <b>5</b> )	1	5
14	<b>T-Sav</b>	<b>1</b>	Hantzsch ( <b>6</b> )	1	0

<sup>a</sup> Estimated conversion was determined by ratio of corresponding <sup>1</sup>H NMR peak integration (see SI); <sup>b</sup> Reactions performed in a mixture 90:10 KPi 10 mM:MeOH at pH 7.0 using 1 equivalent of aldehyde (6.6 mM) and 2 equivalents of **4** (13.2 mM); <sup>c</sup> In the absence of catalyst, partial oxidation of BNAH was observed, but the oxidation rate is negligible when compared to the protein-hosted organocatalytic reaction. <sup>d</sup> Reactions performed in a mixture 75:25 KPi 10 mM:MeOH at pH 7.0 using 1 equivalent of aldehyde (6.6 mM) and 5 equivalents of **4** (33 mM); <sup>e</sup> 0 rpm, side-product observed; <sup>f</sup> ppt observed. 1 mol% of **T-Sav/M-Sav** correspond to 66 nmol catalytic sites. N.A. indicates not added

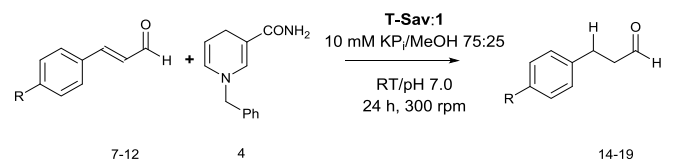
In most streptavidin-based artificial enzymes, the catalytic centers are surrounded by residues at the intersubunit interface.<sup>24, 34</sup> It however has recently been demonstrated that such a shielded environment might not be ideal for some of the chemical catalytic reactions; indeed, the monomeric variant **M-Sav** can be a superior host to **T-Sav** for Rh-catalyzed reactions.<sup>33</sup> **M-Sav** was thus tested as an alternative host for the organocatalytic transfer hydrogenation reaction. Nevertheless, in this case the conversion dropped to 21% and 10% by catalyst **1** and **2** in **M-Sav**, respectively (**Entry 11-12**). This observation suggests that secondary amine-catalyzed transfer hydrogenation prefers a more shielded protein scaffold. To see how a change in hydride donor affects the conversion rate, alternative hydride donors including Hantzsch ester (**5**) and NADH (**6**) were tested, but their use resulted in significant lower conversion (**Entry 13-14**). The negligible conversion observed with NADH (**5**) could be caused by its structural complexity, whereas the low solvent solubility of Hantzsch ester (**6**) in aqueous buffer can influence its ability to transfer hydride within the **T-Sav** scaffold.

Having optimal conditions determined (**Table 1, Entry 8**), various aromatic  $\alpha$ ,  $\beta$ -unsaturated aldehydes were tested as alternative substrates. The **T-Sav:1** assembly showed significant substrate promiscuity; cinnamaldehyde analogues with chloro, fluoro or nitro substituent added at the *para* position can be converted into the corresponding dihydro-products (**Table 2**), while the background reactions remain negligible. Supported by NMR analysis, modest conversion was



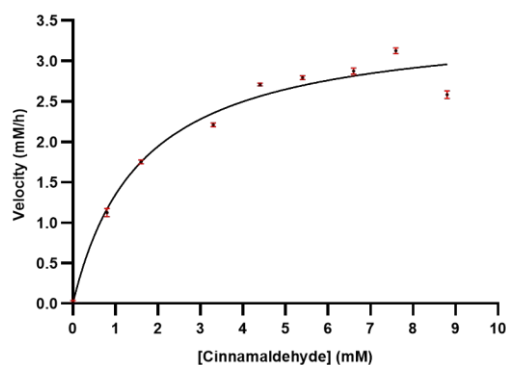
also observed for the methyl, bromo and methoxy analogues (60–76%). Together, these observations suggest that the efficiency of hydride transfer is largely affected by electrostatic properties of the substituents.

**Table 2.** Substrate scope for transfer hydrogenation from BNAH to aromatic  $\alpha$ ,  $\beta$ -unsaturated aldehydes mediated by **T-Sav:1** assembly.<sup>a</sup>



Aldehyde	% Estimated conversion <sup>b</sup>
Cinnamaldehyde ( <b>3</b> )	94
<i>p</i> -Cl ( <b>8</b> )	94
<i>p</i> -F ( <b>9</b> )	>99
<i>p</i> -Br ( <b>10</b> )	60
<i>p</i> -OCH <sub>3</sub> ( <b>11</b> )	69
<i>p</i> -NO <sub>2</sub> ( <b>12</b> )	>99 <sup>c</sup>
<i>p</i> -CH <sub>3</sub> ( <b>13</b> )	76

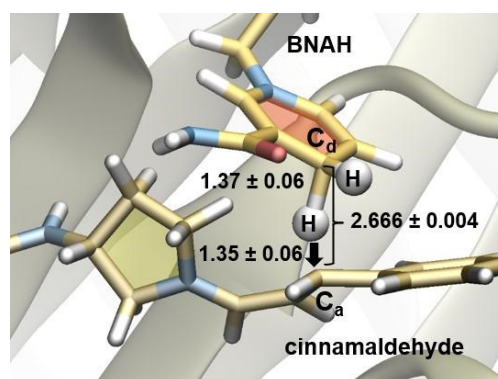
<sup>a</sup> Estimated conversion was determined by ratio of corresponding <sup>1</sup>H NMR peak integration (see SI); <sup>b</sup> Reactions performed in a mixture 75:25 KPi 10 mM:MeOH at pH 7.0 using 1 equivalent of aldehyde (6.6 mM) and 5 equivalents of **4** (33 mM) with 1 mol% of **T-Sav:1**; <sup>c</sup> Reaction performed in a mixture of 9:1 KPi 10 mM:MeOH at pH 7.0 using 1 equivalent of aldehyde (6.6 mM) and 2 equivalents of **4** (13.2 mM). 1 mol% of **T-Sav/M-Sav** correspond to 66 nmol catalytic sites.



**Fig. 2.** Kinetic evaluation of **T-Sav:1** complex for transfer hydrogenation from BNAH to cinnamaldehyde.

Kinetic properties of the streptavidin-based transfer hydrogenation system were evaluated. The protein-based catalyst demonstrates enzyme-like kinetic behaviours with catalytic efficiency ( $k_{\text{cat}}/K_{\text{M}}^{\text{cinnamaldehyde}}$ ) estimated to be  $8.50 \pm 0.5 \text{ M}^{-1}\cdot\text{s}^{-1}$  at 25 °C (**Fig. 2**). The corresponding  $k_{\text{cat}}/K_{\text{M}}$  for flavoprotein was reported to be  $5900 \text{ M}^{-1}\cdot\text{s}^{-1}$ . Furthermore, BNAH has been used for aromatic hydroxylation and the reduction of  $\alpha,\beta$ -unsaturated carbonyl substrate; their biomolecular reaction rate constants were measured to be  $1.2 \cdot 10^4$  and  $1.9 \cdot 10^6 \text{ M}^{-1}\cdot\text{s}^{-1}$ , respectively.<sup>13, 14</sup> Although these values are significantly higher than that of the streptavidin

system, the presented bottom-up approach has not yet been engineered and offers significant flexibility in design. QM/MM molecular dynamics (MD) simulations were conducted to obtain detailed understanding of the hydride transfer step in the **T-Sav:1** system. Exploration of the free energy surface at M06-2X:RM1/MM level enabled identification of the isolated structures of reactants (in solution as solvated species and in the active site of the protein scaffold as the “Michaelis complex”) and the hydride transfer transition state (see SI for details). Hence, the magnitude of the [1,2-<sup>2</sup>H/<sup>1</sup>H] KIE were computationally assessed, including quantum tunneling corrections required for chemical reactions involving the transfer of a light particle such as the hydride transfer. The resulting KIE was found to be  $3.89 \pm 0.15$  when the ground state of BNAH in aqueous solution was used, and this parameter further increased to  $4.28 \pm 0.18$  when the equilibrium between the Michaelis complex and the hydride transfer transition state were used for calculation (see SI for details). These values are similar to those previously obtained for hydride transfer processes catalyzed by NADH-dependent enzymes,<sup>35, 36</sup> including  $\text{L}$ -lactate dehydrogenase (in the range between 3.36–2.80)<sup>37</sup> and morphinone reductase ( $8.4 \pm 1.6$ ),<sup>38</sup> but significantly higher than that of the experimental counterpart measured in the present study. Interestingly, regarding the hydride donor-acceptor distance and the relative orientation of the different involved moieties, the nature of the optimized transition state can be considered as equivalent to those located in previous studies (**Fig. 3**).<sup>35–38</sup> It therefore suggests that the hydride transfer step in the **T-Sav** artificial enzyme is at least partially rate-limiting.



**Fig. 3.** Detail of the transition state for the hydride transfer from BNAH to cinnamaldehyde in the active site of **T-Sav:1** optimized at M06-2X/MM level. Average distances in Å.

In summary, we have described the use of streptavidin as host for organocatalytic transfer hydrogenations. At 1 mol%, the **T-Sav:1** assembly was able to mediate the hydrogenation of various aromatic  $\alpha$ ,  $\beta$ -unsaturated aldehydes in excellent conversions, and the resulting products have been used in the synthesis of pharmaceutical compounds.<sup>39</sup> Moreover, **T-Sav:1** possesses Michaelis Menten kinetic properties for the organocatalytic transfer hydrogenation, presenting as a great





starting point for artificial enzyme engineering. Studies focusing on the reaction mechanisms, the use of prochiral aldehydes and potential applications in cascade reactions are currently ongoing.

### Conflicts of interest

There are no conflicts to declare.

### Acknowledgements

This work was supported by Cardiff University through the start-up fund provided by the Cardiff School of Chemistry, the Leverhulme Trust through grant to L.Y.P.L. (RPG-2017-195), the Royal Society through grant to L.C.M. (RG150466), the UK's Wellcome Trust through grants to L.Y.P.L. (202056/Z/16/Z).

### Notes and references

1. S.-i. Oka, C.-P. Hsu and J. Sadoshima, *Circ. Res.*, 2012, **111**, 611-627.
2. L. Josa-Culleré, A. S. K. Lahdenperä, A. Ribaucourt, G. T. Höfler, S. Gargiulo, Y.-Y. Liu, J.-H. Xu, J. Cassidy, F. Paradisi, D. J. Opperman, F. Hollmann and C. E. Paul, *Catalysts*, 2019, **9**, 207-218.
3. S. Yasui and A. Ohno, *Bioorg. Chem.*, 1986, **14**, 70-96.
4. Y. Yang and A. A. Sauve, *Biochim. Biophys. Acta*, 2016, **1864**, 1787-1800.
5. A. Geddes, C. E. Paul, S. Hay, F. Hollmann and N. S. Scrutton, *J. Am. Chem. Soc.*, 2016, **138**, 11089-11092.
6. C. E. Paul, S. Gargiulo, D. J. Opperman, I. Lavandera, V. Gotor-Fernández, V. Gotor, A. Taglieber, I. W. C. E. Arends and F. Hollmann, *Org. Lett.*, 2013, **15**, 180-183.
7. Y. Okamoto, V. Köhler and T. R. Ward, *J. Am. Chem. Soc.*, 2016, **138**, 5781-5784.
8. Q.-A. Chen, K. Gao, Y. Duan, Z.-S. Ye, L. Shi, Y. Yang and Y.-G. Zhou, *J. Am. Chem. Soc.*, 2012, **134**, 2442-2448.
9. C.-H. Lim, A. M. Holder, J. T. Hynes and C. B. Musgrave, *J. Am. Chem. Soc.*, 2014, **136**, 16081-16095.
10. T. M. Bräuer, Q. Zhang and K. Tiefenbacher, *J. Am. Chem. Soc.*, 2017, **139**, 17500-17507.
11. C. E. Paul, E. Churakova, E. Maurits, M. Girhard, V. B. Urlacher and F. Hollmann, *Bioorg. Med. Chem.*, 2014, **22**, 5692-5696.
12. N. Falcone, Z. She, J. Syed, A. Lough and H.-B. Kraatz, *ChemBioChem*, 2019, **20**, 838-845.
13. T. Knaus, C. E. Paul, C. W. Levy, S. de Vries, F. G. Mutti, F. Hollmann and N. S. Scrutton, *J. Am. Chem. Soc.*, 2016, **138**, 1033-1039.
14. A. Guarneri, A. H. Westphal, J. Leertouwer, J. Lunsonga, M. C. R. Franssen, D. J. Opperman, F. Hollmann, W. J. H. van Berkel and C. E. Paul, *ChemCatChem*, 2020, **12**, 1368-1375.
15. J. D. Ryan, R. H. Fish and D. S. Clark, *ChemBioChem*, 2008, **9**, 2579-2582.
16. J. Lutz, F. Hollmann, T. V. Ho, A. Schnyder, R. H. Fish and A. Schmid, *J. Organomet. Chem.*, 2004, **689**, 4783-4790.
17. Y. Okamoto, V. Köhler, C. E. Paul, F. Hollmann and T. R. Ward, *ACS Catalysis*, 2016, **6**, 3553-3557.
18. C. Nowak, A. Pick, P. Lommes and V. Sieber, *ACS Catal.*, 2017, **7**, 5202-5208.
19. A. R. Nödling, N. Santi, T. L. Williams, Y.-H. Tsai and L. Y. P. Luk, *RSC Adv.*, 2020, **10**, 16147-16161.
20. A. R. Nödling, K. Swiderek, R. Castillo, J. W. Hall, A. Angelastro, L. C. Morrill, Y. Jin, Y. H. Tsai, V. Moliner and L. Y. P. Luk, *Angew. Chem., Int. Ed.*, 2018, **57**, 12478-12482.
21. C. Zeymer and D. Hilvert, *Annual Review of Biochemistry*, 2018, **87**, 131-157.
22. C. Mayer, C. Dulson, E. Reddem, A.-M. W. H. Thunnissen and G. Roelfes, *Angew. Chem., Int. Ed.*, 2019, **58**, 2083-2087.
23. Y. Zhao, Y. Cotelte, L. Liu, J. Lopez-Andarias, A. B. Bornhof, M. Akamatsu, N. Sakai and S. Matile, *Acc. Chem. Res.*, 2018, **51**, 2255-2263.
24. H. J. Davis and T. R. Ward, *ACS Cent. Sci.*, 2019, **5**, 1120-1136.
25. R. B. Leveson-Gower, C. Mayer and G. Roelfes, *Nat. Rev. Chem.*, 2019, **3**, 687-705.
26. J. Zhao, J. G. Rebelein, H. Mallin, C. Trindler, M. M. Pellizzoni and T. R. Ward, *J. Am. Chem. Soc.*, 2018, **140**, 13171-13175.
27. T. Heinisch and T. R. Ward, *Acc. Chem. Res.*, 2016, **49**, 1711-1721.
28. Y. Okamoto and T. R. Ward, *Biochemistry*, 2017, **56**, 5223-5224.
29. Y. Cotelte, V. Lebrun, N. Sakai, T. R. Ward and S. Matile, *ACS Cent. Sci.*, 2016, **2**, 388-393.
30. H. Lechner, V. R. Emann, M. Breuning and B. Höcker, *bioRxiv*, 2020, 2020.2003.2005.978098.
31. N. Santi, L. C. Morrill and L. Y. P. Luk, *Molecules*, 2020, **25**.
32. D. Demonte, C. M. Dundas and S. Park, *Appl. Microbiol. Biotechnol.*, 2014, **98**, 6285-6295.
33. I. S. Hassan, A. N. Ta, M. W. Danneman, N. Semakul, M. Burns, C. H. Basch, V. N. Dippon, B. R. McNaughton and T. Rovis, *J. Am. Chem. Soc.*, 2019, **141**, 4815-4819.
34. F. Schwizer, Y. Okamoto, T. Heinisch, Y. Gu, M. M. Pellizzoni, V. Lebrun, R. Reuter, V. Kohler, J. C. Lewis and T. R. Ward, *Chem. Rev.*, 2018, **118**, 142-231.
35. M. Roca, J. J. Ruiz-Pernía, R. Castillo, M. Oliva and V. Moliner, *Phys. Chem. Chem. Phys.*, 2018, **20**, 25722-25737.
36. K. Świderek, A. Kohen and V. Moliner, *Phys. Chem. Chem. Phys.*, 2015, **17**, 30793-30804.
37. K. Świderek, I. Tuñón, S. Martí and V. Moliner, *ACS Catal.*, 2015, **5**, 1172-1185.
38. M. Delgado, S. Görlich, J. E. Longbotham, N. S. Scrutton, S. Hay, V. Moliner and I. Tuñón, *ACS Catal.*, 2017, **7**, 3190-3198.
39. D. Wang and D. Astruc, *Chem. Rev.*, 2015, **115**, 6621-6686.



Article

# Streptavidin-Hosted Organocatalytic Aldol Addition

Nicolò Santi <sup>1</sup>, Louis C. Morrill <sup>1,2</sup> and Louis Y. P. Luk <sup>1,2,\*</sup>

<sup>1</sup> School of Chemistry, Main Building, Cardiff University, Cardiff CF10 3AT, UK; SantiN@cardiff.ac.uk (N.S.); MorrillLC@cardiff.ac.uk (L.C.M.)

<sup>2</sup> Cardiff Catalysis Institute, School of Chemistry, Main Building, Cardiff University, Cardiff CF10 3AT, UK

\* Correspondence: lukly@cardiff.ac.uk; Tel.: +44 (0)29 2251 0161

Academic Editor: Isabella Rimoldi

Received: 5 May 2020; Accepted: 20 May 2020; Published: 25 May 2020

**Abstract:** In this report, the streptavidin-biotin technology was applied to enable organocatalytic aldol addition. By attaching pyrrolidine to the valeric motif of biotin and introducing it to streptavidin (Sav), a protein-based organocatalytic system was created, and the aldol addition of acetone with *p*-nitrobenzaldehyde was tested. The conversion of substrate to product can be as high as 93%. Although the observed enantioselectivity was only moderate (33:67 er), further protein engineering efforts can be included to improve the selectivity. These results have proven the concept that Sav can be used to host stereoselective aldol addition.

**Keywords:** organocatalysis; streptavidin; artificial enzyme; protein; aldol; enamine; catalysis; biocompatible

## 1. Introduction

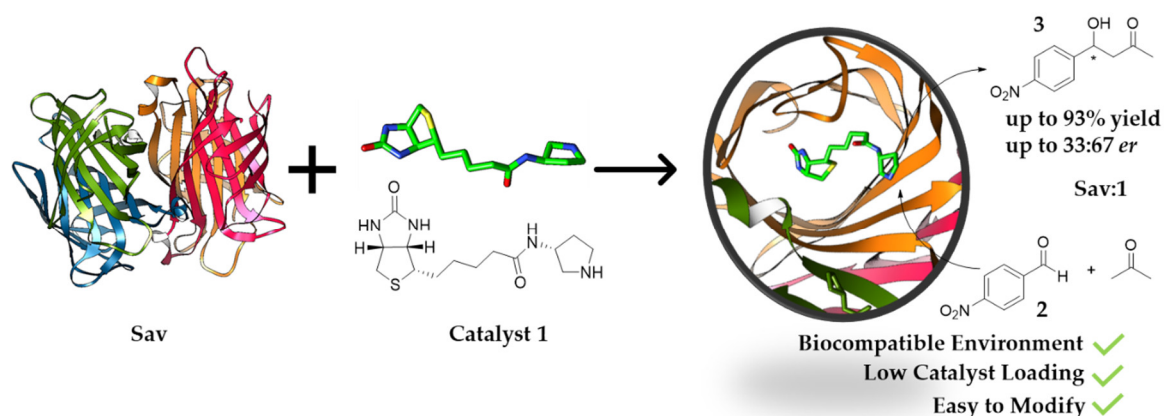
Representing a major mode of carbon–carbon bond formation, aldol addition is an appealing tool that has been broadly used in chemical and synthetic biology research [1–3]. Important applications include chemo-enzymatic synthesis of chiral synthons and bioactive chemicals [4–10], as well as labelling of biomolecules (protein, DNA and RNA) [3,11]. Given its usefulness, different approaches have been developed to mediate aldol addition [4,12–16]. Naturally occurring and de novo aldolases are excellent options. Most of these enzymes contain a catalytic active lysine residue that forms an enamine intermediate as nucleophile for conjugation [17,18]. Though often recognized for their catalytic efficiency, significant engineering efforts are typically needed in order to accept relevant substrates. Hence, the use of alternative catalysts has been examined.

Many secondary amine organocatalysts are known for their abilities to perform aldol addition [19–21]. Since they tend to accept a broader range of substrates and have stronger nucleophilicity than primary amines [22], it is of great interest to enable secondary amine organocatalytic aldol addition in biological contexts [23]. One simple solution is to incorporate catalytic amines within a recombinant protein as a means to enhance the biocompatibility of organocatalysis [17,24–27]. Indeed, the *N*-terminal proline of 4-oxalocrotonate tautomerase (4-OT) and its variants have been used as protein-based organocatalytic systems for stereoselective aldol addition [12,15]. Though efficient, the 4-OT system is largely limited to the use of *N*-terminal proline. However, as illustrated by traditional organocatalysis studies, modifications of the catalyst motif can lead to significant improvement in performance (selectivity and reactivity) [28–36]. To this end, it is of fundamental interest to explore other protein-based systems, where secondary amine catalysts other than *N*-terminal proline can be used.

Streptavidin (Sav) is an ideal host for chemical catalysis [23,24,37–41]. As the valeric acid motif of biotin is largely not involved in binding, it can be covalently added with an organocatalyst and introduced to Sav. Consequently, streptavidin can be used to host chemical catalysis [23,24,37,42],

and applications ranging from dynamic kinetic resolution and biomolecular labeling to molecular switch design can be established [43–48]. Importantly, it has been demonstrated that nucleophiles can be generated via organocatalysis within Sav [24]. Indeed, biotin can be modified with pyrrolidine and introduced into Sav, creating a protein-based secondary amine organocatalytic system [24]. While this catalytic motif (catalyst **1**) contains essentially no bulky or H-bonding substituents adjacent to the reacting nitrogen atom, this Sav-based system was able to mediate carbon–carbon bond formation (i.e., 1,4-Michael addition) in good yield and stereoselectivity [24]. Bringing these findings together, Sav is seemingly an ideal host for organocatalytic aldol addition reactions.

Here, we developed an alternative Sav-based system for aldol addition. By using biotinylated pyrrolidine, Sav is converted into a system suitable for the organocatalytic aldol addition reaction between acetone and *p*-nitrobenzaldehyde derivatives (Figure 1). Using only 1 mol% of catalyst, the estimated conversion can reach up to 93%. This work demonstrates that aldol addition can be achieved using the streptavidin-biotin technology.

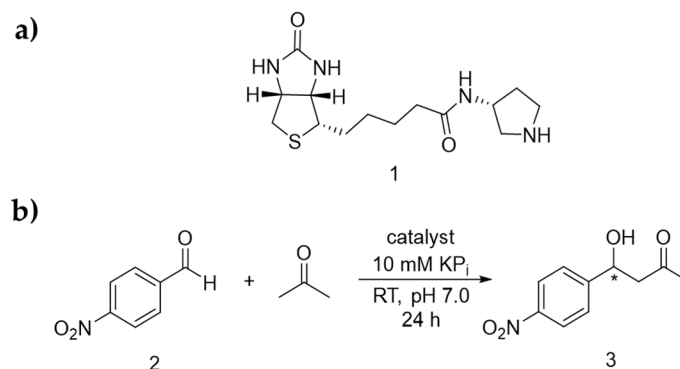


**Figure 1.** Streptavidin (Sav):1 assembly (1 mol%, (PDB: 6GH7, 1.08 Å)) used for aldol addition reaction under biocompatible conditions.

## 2. Results and Discussion

### 2.1. Screening for Optimised Conditions

Previously, a family of biotinylated secondary amine catalysts were prepared, including ones that contain imidazolidinone, proline and pyrrolidines [24]. We learned that all the biotinylated imidazolidinones were relatively difficult to prepare, involving multiple chemical steps and chromatographic steps. Furthermore, they are not active in different reactions, including hydride transfer, aromatic substitution, and Michael addition (data not shown here). Similarly, all the proline derivatives, though simpler to prepare, are not active under neutral pH. Hence, in this work, ligand **1**, which bears a minimally substituted pyrrolidine moiety, was tested for aldol addition (Scheme 1a). *p*-Nitrobenzaldehyde (**2**) was initially used as it contains a reactive carbonyl group and do not possess any enolisable  $\alpha$ -hydrogen, whereas acetone was chosen as the nucleophile for C-C bond formation (Scheme 1b).



**Scheme 1.** (a) Structure of the biotinylated catalyst **1**. (b) Enamine catalysed aldol addition reaction presented in this report.

In the absence of catalyst or protein, 17% racemic product (**3**) was observed when one equivalent of **2** was added to buffer (KP<sub>i</sub> 10 mM at pH 7.0) containing 20 vol% of acetone (>400 equivalent), as accessed by <sup>1</sup>H-NMR spectroscopy (Table 1, Entry 1). When the biotinylated organocatalyst **1** was included at 1 mol%, the reaction yield increased to 36% (Entry 2). Interestingly, when Sav but not the catalyst was included, the reaction yield was also mildly enhanced from 16% to 33% with increasing protein loading (0.1 mol%–1 mol%, Entry 3–5). In any case, no enantioselectivity was observed.

**Table 1.** Screening for assessing the best conditions to perform enamine-catalysed aldol addition.

Entry	Catalyst	Eqv. Acetone	Co-solvent	Loading (mol%)	Estimated Conversion <sup>a</sup> %	er (R:S)
1	None			None	17	50:50
2	<b>1</b>			1	36	50:50
3	Sav			0.1	16	50:50
4	Sav			0.5	23	50:50
5	Sav			1	33	50:50
6	Sav: <b>1</b>	20 vol%	NA	0.1	47	38:62
7	Sav: <b>1</b>			0.5	79	33:67
8	Sav: <b>1</b>			1	93	33:67
9 <sup>b</sup>	Sav: <b>1</b>			1	92	33:67
10 <sup>c</sup>	Sav: <b>1</b>			1	37	34:66
11	Sav: <b>1</b>	5	25% MeOH	1	20	33:67
12	Sav: <b>1</b>	5	25% ACN	1	12	33:67
13	Sav: <b>1</b>	5		1	1	NA
14	Sav: <b>1</b>	10	25% <i>i</i> -PrOH	1	5	NA
15	Sav: <b>1</b>	20		1	9	36:64
16	Sav: <b>1</b>	50		1	18	33:67

<sup>a</sup> The estimated conversion was calculated by measuring the integral ratio between the substrate and product peaks from the reaction crude <sup>1</sup>H-NMR. <sup>b</sup> 1 mol% trifluoroacetic acid (TFA) used as additive.

<sup>c</sup> Reaction run at 10 °C.

To see if the aldol addition reaction could proceed organocatalytically, both streptavidin and ligand **1** (1:1 ratio) were included and the reaction yield increased up to 93%. Furthermore, the enantiomeric ratio (er) of *R* to *S* isomer was measured to be 33:67, thus suggesting that stereoselectivity of the aldol addition was originated from the binding of ligand **1** to Sav (Entry 6–8). There was also a small amount of elimination product observed (5%, see section 6.1.8 in the SI). Similar to previous observation [24], enantioselectivity was only observed when Sav was included, thereby providing evidence that the organocatalytic reaction takes place within the protein scaffold. With the goal to further enhance stereoselectivity, we modified the reaction conditions, including the

addition of co-catalyst trifluoroacetic acid (1%, [49–51] Entry 9) and decrease of the reaction temperature (10 °C, Entry 10). Changing the amount of acetone used or including the amount of cosolvents (i.e., methanol, acetonitrile, and isopropanol) did not lead to improved stereoselectivity (Entry 11–16). Nevertheless, in all cases, neither the yield nor selectivity was improved.

## 2.2. Site-Directed Mutagenesis of the Protein Host

Based on previous analysis via X-ray crystallography and molecular dynamics (MD) studies [24], Ser112 and Lys121 were found to be in proximity to the pyrrolidine catalyst, and these residues were modified to see if performance of the aldol addition reaction can be affected (Table 2).

**Table 2.** Screening for assessing the best conditions to perform enamine-catalysed aldol reactions.

Catalyst	Estimated Conversion <sup>a</sup> /%	er (R:S)
Sav:1	93	33:67
T-rSav:1	92	35:65
S112E:1	14	39:61
K121A:1	89	44:56

<sup>a</sup> The estimated conversion was calculated by measuring the integral ratio between the substrate and product peaks from the reaction crude <sup>1</sup>H-NMR.

A reduced tetrameric streptavidin variant (T-rSav) was used to create the variants [47]. Ser112 was found to be in hydrogen-bonding distance with the pyrrolidine motif [24]. When this residue was modified to glutamate, a vastly different electrostatically charged residue, the resulting S112E variant, was found to be a poor host, producing a poor reaction yield (14%). On the other hand, Lys121 was found to be in close proximity to the tetrahedral intermediate [24]. When this residue was replaced with a non-charged and small residue such as alanine, the resulting protein-based complex could yield 89% of the aldol product. However, poor stereoselectivity was observed.

## 3. Materials and Methods

Reactions were performed in oven dried glassware without precautions to exclude air. Reaction temperatures are stated as heating device temperature (e.g., oil bath, shaker, etc.), if not stated otherwise. Concentrations under reduced pressure were performed by rotary evaporation at 40 °C at the appropriated pressure, unless otherwise noted. Deionized water was obtained by a PURELAB® Option system (15 MΩ·cm, ELGA LabWater, High Wycombe, UK). Analytical and preparative thin layer chromatography (TLC) was carried out with silica gel 60 F254 aluminum sheets (Merck KGaA, Darmstadt, Germany). Detection was carried out using UV light ( $\lambda = 254$  nm and 366 nm), followed by immersion in permanganate staining solution with subsequent development via careful heating with a heat gun. Flash column chromatography was performed using silica gel (pore size 60 Å, 0.040–0.063 mm, Global Life Sciences Solutions USA LLC, Marlborough, USA).

*para*-Nitrobenzaldehyde (**2**) for aldol addition reactions with Sav was obtained commercially (Merck KGaA, Darmstadt, Germany) and if necessary purified by washes with sodium bicarbonate pH 8.3, subsequent drying with magnesium sulphate and stored under inert atmosphere at 4 °C. All other solvents and reagents were obtained from commercial sources and used as received.

Sav (Streptavidin *Streptomyces avidinii* recombinant, tetramer,  $M_w \approx 52$  kDa), a recombinant variant of streptavidin processed at the C and N termini and carrying amino acids 13–139, was obtained commercially (PRO-791, ProSpec-Tany TechnoGene Ltd., Ness-Ziona, Israel) as lyophilized powder in 10 mM KPi pH 6.5 and stored at −23 °C upon receipt until further use. According to the supplier Sav has the following amino acid sequence:

MAEAGITGTWYNQLGSTFIVTAGADGALTGTYESAVGNAESRYVLTGRYDSAPATDGSALTG  
WTVAWKNNYRNAHSATTWSGQYVGGAEARINTQWLLTSGTTEANAWKSTLVGHDTFTKVKPS  
AAS

The plasmid for tetrameric reduced streptavidin (T-rSav) (encoding for a Streptavidin *Streptomyces avidinii* recombinant, tetramer,  $M_w \approx 50$  kDa, “reduced” Streptavidin with amino acids 16–133) was obtained as gift from Takeshi Sano (pTSA-13, Addgene plasmid #17327, <http://n2t.net/addgene:17327>, RRID:Addgene\_17327) [47]. The gene encoding for *T-rSav* translates to the following amino acid sequence:

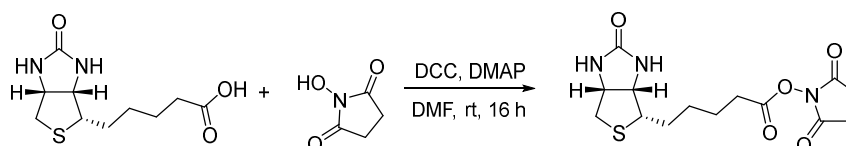
MGITGTWYNQLGSTFIVTAGADGALTGTYESAVGNAESRYVLTGRYDSAPATDGSALTALGWTV  
AWKNNYRNAHSATTWSGQYVGGAEARINTQWLLTSGTTEANAWKSTLVGHDTFTKV

A 3510 benchtop pH Meter (VWR International, Radnor, USA) connected to a Universal pH electrode (VWR International, Radnor, USA) was used for the pH adjustment of buffers and reaction mixtures employing either 1.0 M or 0.1 M sodium hydroxide solution or hydrochloric acid. Shaking of the reactions (300 rpm) at 25 °C was achieved using a thermoshaker Mini shake lite (VWR International, Radnor, USA) or a Incubating Orbital Shaker (VWR International, Radnor, USA).  $^1\text{H}$ - and  $^{13}\text{C}$ -NMR spectra were recorded in  $\text{CDCl}_3$  or  $\text{DMSO-}d_6$  on Bruker Fourier 300, Ultrashield 400, or Ascend 500 instruments (Bruker Corporation, Billerica, USA). Chemical shifts are reported in parts per million (ppm) and are referenced to the residual solvent resonance as the internal standard ( $\text{CHCl}_3$ :  $\delta = 7.26$  ppm for  $^1\text{H}$ ;  $\text{DMSO}$ :  $\delta = 2.54$  ppm for  $^1\text{H}$ ). Data are reported as follows: chemical shift ( $\delta$ ), multiplicity (br s = broad singlet, s = singlet, d = doublet, dd = double doublet, td = triple doublet, t = triplet, dt = double triplet, q = quartet, p = pentet, sept = septet, br m = broad multiplet, m = multiplet, mc = centrosymmetric multiplet), coupling constants (Hz) and integration. Size exclusion chromatography was performed using a AKTA Purifier workstation (Global Life Sciences Solutions USA LLC, Marlborough, USA) system with the respective column mentioned in the detailed procedure.

### 3.1. Experimental Details for the Synthesis of Catalyst 1.

Catalyst 1 was synthesized following a two-step procedure previously reported from our group (Scheme 2 and 3). [24]

Synthesis and  $^1\text{H}$ -NMR Assignment for the Synthesis of (+)-Biotin NHS ester

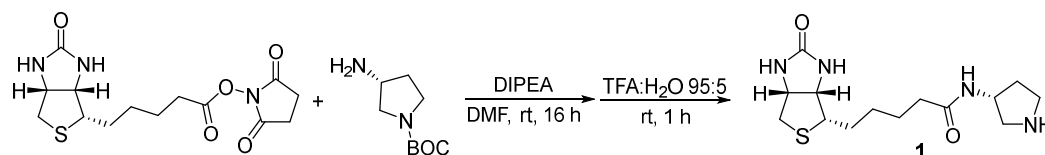


**Scheme 2.** Synthesis of (+)-biotin NHS ester by coupling reaction.

(+)-Biotin (960 mg, 4.0 mmol, 1.0 eq), *N*-hydroxysuccinimide (NHS, 920 mg, 8.0 mmol, 2.0 eq), and 2-(dimethylamino)pyridine (DMAP, 24 mg, 0.2 mmol, 0.05 eq) were dissolved in dry DMF (ca. 40 mL) under inert atmosphere. The solution was cooled to 0 °C with an ice bath. Dicyclohexylcarbodiimide (DCC, 908 mg, 4.4 mmol, 1.1 eq) dissolved in dry DMF was then added dropwise. The reaction mixture was left stirring at room temperature overnight and formed a precipitate was removed via vacuum filtration. Crude NHS ester was precipitated by the addition of  $\text{Et}_2\text{O}$ , collected by filtration, and washed with deionized water and  $\text{Et}_2\text{O}$ . The crude product was recrystallized from iso-propanol, collected via filtration, and washed with  $\text{Et}_2\text{O}$  to afford the active ester as white solid after drying under fine vacuum (272 mg, 0.8 mmol, 20% yield).

$^1\text{H}$ -NMR (400 MHz,  $\text{DMSO-}d_6$ ):  $\delta = 6.43$  (s, 1H), 6.37 (s, 1H), 4.32 (mc, 1H), 4.13 (mc, 1H), 3.10 (mc, 1H), 2.87–2.78 (m, 5H), 2.67 (t,  $J = 7.3$  Hz, 1H), 2.58 (d,  $J = 12.6$  Hz, 1H), 1.71–1.28 (m, 6H) ppm. The analytical data are in accordance with the literature [24].

Synthesis and  $^1\text{H}$ -NMR Assignment for the Synthesis of (*R*)-3-(5-((3*aS*,4*S*,6*aR*)-2-oxohexahydro-1*H*-thieno[3,4-*d*]imidazol-4-yl)pentanamido)pyrrolidin-1-ium formate (Catalyst 1)



**Scheme 3.** Synthesis of catalyst **1**.

(+)-Biotin NHS ester (100 mg, 0.29 mmol, 1.0 eq) and (3*R*)-3-amino-1-Boc-pyrrolidine (64 mg, 0.29 mmol, 1.0 eq) were dissolved in dry DMF. Di-iso-propylethylamine (DIPEA, 106  $\mu$ L, 0.58 mmol, 2.0 eq) was added and the reaction was allowed to proceed under stirring overnight at room temperature. The solvent was removed under reduced pressure at 80  $^{\circ}$ C. The residue was dissolved in a mixture of trifluoroacetic acid (TFA):H<sub>2</sub>O (95:5, 5.0 mL) and stirred at room temperature for 1 h. Excess TFA was removed under reduced pressure, the residue was dissolved in a minimal amount of H<sub>2</sub>O and lyophilized. The crude product was purified by preparative HPLC (High Performance Liquid Chromatography) using a Supelcosil C18 column (25 cm  $\times$  21.2 mm, 12  $\mu$ m; gradient H<sub>2</sub>O:MeCN 99:1 to 50:50 over 30 min, 0.1% HCO<sub>2</sub>H, 10 mL $\cdot$ min<sup>-1</sup>, 20  $^{\circ}$ C,  $\lambda$  = 210 nm, Merck KGaA, Darmstadt, Germany) and catalyst **1** was obtained as white solid (43 mg, 0.12 mmol, 42% yield).

<sup>1</sup>H-NMR (400 MHz, D<sub>2</sub>O):  $\delta$  = 4.57 (dd,  $J$  = 7.8, 4.9 Hz, 1H), 4.45–4.35 (m, 2H), 3.54 (dd,  $J$  = 12.5, 7.0 Hz, 1H), 3.46–3.35 (m, 2H), 3.30 (dt,  $J$  = 9.6, 4.1 Hz, 1H), 3.19 (dd,  $J$  = 12.5, 4.9 Hz, 1H), 2.95 (dd,  $J$  = 13.1, 4.9 Hz, 1H), 2.74 (d,  $J$  = 13.1 Hz, 1H), 2.38–2.27 (m, 1H), 2.23 (t,  $J$  = 7.2 Hz, 2H), 1.99 (td,  $J$  = 13.5, 6.8 Hz, 1H), 1.76–1.47 (m, 4H), 1.45–1.31 (m, 2H) ppm. The analytical data are in accordance with the literature [24].

### 3.2. Experimental Details for the Preparation and Purification of T-rSav and Mutants.

Tetrameric reduced streptavidin (T-rSav) and relative mutants were expressed using an *E. coli* expression system with the following protocol. Plasmid pTSA-13 containing the desired *T-rSav* gene in a pET-3a vector was transformed into calcium competent BL21(DE3) pLysS cells and grown for 16 h on LB agar plates containing 100  $\mu$ g/mL ampicillin and 34  $\mu$ g/mL chloramphenicol. A single colony from the plate was picked to inoculate a 15 mL MTP (per 1 L: 10 g tryptone, 10 g NaCl, 5 g yeast extract, 2.2 g Na<sub>2</sub>HPO<sub>4</sub>, 1 g KH<sub>2</sub>PO<sub>4</sub>, pH = 6.9) starter culture containing 100  $\mu$ g/mL ampicillin and 34  $\mu$ g/mL chloramphenicol, which was incubated at 37  $^{\circ}$ C and 180 rpm overnight. The culture was diluted to 40 mL with 20% glucose and then added to 1 L MTP medium containing 100  $\mu$ g/mL ampicillin and 34  $\mu$ g/mL chloramphenicol, yielding a final glucose concentration of 0.05%. The cultures were grown at 37  $^{\circ}$ C and 225 rpm to an OD<sub>600</sub> of 1.0–1.2 and induced with IPTG (Isopropyl  $\beta$ -D-1-thiogalactopyranoside) at a final concentration of 1 mM. The culture was grown at 25  $^{\circ}$ C for 16 h and the cell pellet was harvested after centrifugation at 4000 rpm at 4  $^{\circ}$ C for 25 min and stored at –20  $^{\circ}$ C.

The pellet was subjected to a freeze–thaw cycle, resuspended in 25 mL of lysis buffer (50 mM Tris, 100 mM NaCl, 1 mM PMSF, pH 8.0) and lysed by sonication (7 min, 5 s on, 10 s off). The insoluble fraction was isolated by centrifugation at 15000 rpm for 25 min at 4  $^{\circ}$ C. The supernatant was discarded and the insoluble fraction was washed with wash buffer 1 (4 $\times$  resuspension in 50 mM Tris, 110 mM EDTA, 1.5 M NaCl, 1 mM PMSF, 0.1% Triton X-100, pH 8.0 and pellet re-isolation by centrifugation at 11000 rpm and 4  $^{\circ}$ C) and wash buffer 2 (4 $\times$  resuspension in 50 mM Tris, 110 mM EDTA, 1.5 M NaCl, 1 mM PMSF, pH 8.0 and pellet re-isolation by centrifugation at 11000 rpm and 4  $^{\circ}$ C). The insoluble fraction was resuspended in denaturing buffer 1 (5 mL/g pellet, 6 M GdnHCl, 50 mM Tris-HCl, pH 1.5) and incubated at 37  $^{\circ}$ C and 180 rpm for 16 h. The insoluble fraction was removed by centrifugation at 15000 rpm and 4  $^{\circ}$ C. The supernatant was diluted to 200 mL with denaturing buffer 2 (6 M GdnHCl, 50 mM Tris-HCl, pH 6.5) and dialysed against 3 L of 6 M GdnHCl, 50 mM Tris-HCl, pH 6.5 for 3 h at room temperature. The dialysis bag was then placed into fresh 3 M GdnHCl, 50 mM Tris-HCl, pH 6.5 (denaturing buffer 2 was reused up to 5 times). T-rSav was refolded by gradient dialysis, pumping in refolding buffer (0.5 mg/L catalyst **1**, 10 mM KPi, pH 7.0) at 4 mL/min, constant stirring of the mixture at 4 mL/min for 48 h at room temperature. Towards the

end of this process a varying amount of precipitation was observed. The precipitate was removed via centrifugation at 15000 rpm at 4 °C and the supernatant was concentrated to 20 mL by Amicon ultra centrifugation using a 3.5 kDa cut-off. The concentrated solution was transferred into a centrifugal concentrator with a 10 kDa cut-off and the buffer was exchanged five times by concentration to 2.5 mL and refilling to 20 mL (10 mM KPi, pH 7.0). The protein solution was finally concentrated to obtain a protein concentration of 2 mg/mL as determined by nanodrop (Thermo Fischer Scientific, Waltham, USA) measurement at 210 nm. This was used for catalysis of the aldol addition reaction without further purification. A sample of the solution was loaded on SDS-PAGE to check the purity (>95%, see pg S2, Figure S1) of the protein (15% *w/v*).

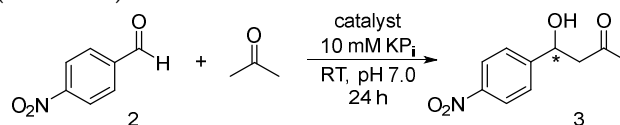
The mutations K121 or S112 were introduced by site-directed mutagenesis PCR using PrimeStar HS DNA polymerase (Takara Bio Inc., Kusatsu, Japan) and the accompanying buffers, dNTPs and primers mentioned in Table 3 below. Due to the high GC content of the region of interest a variety of methods and temperatures had to be screened, as primer insertions were observed, especially for mutations at K121. Hence, a 50 µL PCR was prepared according to the instructions and the reaction mixture distributed equally (12.5 µL) over 4 PCR tubes. These were then subjected to the following conditions, using a gradient to achieve a different annealing temperature for each tube. Method 1: Initial denaturing (4 min, 95 °C), 33 cycles of (10 s at 98 °C, 5 s at 58/60/62/64 °C, 5 min at 72 °C), final extension (10 min, 72 °C) and hold (4 °C). Method 2: Initial denaturing (4 min, 95 °C), 15 cycles of (10 s at 98 °C, 5 s at 58/60/62/64 °C, 5 min at 72 °C), 15 cycles of (10 s at 98 °C, 5 s at 61/63/65/67 °C, 5 min at 72 °C) and final extension (5 min, 72 °C) and hold (4 °C). Method 3: Initial denaturing (4 min, 95 °C), 3 cycles of (10 s at 98 °C, 5 s at 55/57/59/61 °C, 5 min at 72 °C), 3 cycles of (10 s at 98 °C, 5 s at 58/60/62/64 °C, 5 min at 72 °C), 30 cycles of (10 s at 98 °C, 5 s at 61/63/65/67 °C, 5 min at 72 °C) and final extension (10 min, 72 °C) and hold (4 °C). In the case of the K121 mutation, Method 1 and 3 were also applied using 3% DMSO (Dimethyl sulfoxide), if no positive results were obtained without DMSO. The mutant constructs were confirmed by DNA sequencing (Eurofins Genomics Germany GmbH, Ebersberg, Germany) using the T7 promoter primer (TAATACGACTCACTATAGG).

**Table 3.** List of primers used for the introduction of mutations in tetrameric reduced streptavidin (T-rSav) at positions S112 and K121.

Mutation	Primer (5' to 3')
S112E	Forward
	GGCTGCTGACCGAAGGCACCACCGAGG
	Reverse
CCTCGGTGGTGCCTTCGGTCAGCAGCC	
K121A	Forward
	ACCGAGGCCAACGCCTGGGCGTCCACGCTGGTCGGC
	Reverse
GGCGTTGGCCTCGGTGGTGCCGGA	

### 3.3. Experimental Details for the Activity Screening of Catalysts 1 for the Aldol Addition Reaction of Acetone and *p*-Nitrobenzaldehyde

<sup>1</sup>H-NMR Based Screening for Yield Determination of Aldol Addition Reaction of Acetone and *p*-Nitro benzaldehyde (Scheme 4).



**Scheme 4.** Aldol addition reaction of acetone to *p*-nitrobenzaldehyde.

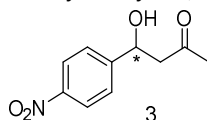
A stock solution of catalyst **1** (0.50 mg, 1.59 µmol) was prepared dissolving the catalyst in 1 mL of KPi (pH 7.0, 10 mM) into a 1.5 mL Eppendorf tube. *p*-Nitrobenzaldehyde (**2**, 20 mg, 132.34 µmol) was dissolved in 1 mL of acetone to create a stock solution. Commercial Sav (0.58 mg, 1 mol%, 33



nmol) was weighted into a 1.5 mL Eppendorf tube and dissolved in 379.25  $\mu\text{L}$  of  $\text{KPi}$  (pH 7.0, 10 mM). An aliquot of 20.75  $\mu\text{L}$  (1 mol%) of the catalyst stock solution was added to the Sav Eppendorf tube. Subsequently, an aliquot of 24.93  $\mu\text{L}$  (1 eq.) of the *p*-nitrobenzaldehyde stock solution was added to the Eppendorf tube. An amount of 75.07  $\mu\text{L}$  of acetone was added to reach a final acetone volume of 100  $\mu\text{L}$ . The mixture was shaken at 300 rpm at 25  $^{\circ}\text{C}$  for 24 h. The mixture was extracted with  $\text{CH}_2\text{Cl}_2$  ( $500 \times 3 \mu\text{L}$ ) and the organic phase evaporated under reduced pressure. The crude of reaction was dissolved in  $\text{CDCl}_3$  (620  $\mu\text{L}$ ) and subjected to  $^1\text{H-NMR}$  analysis.

### 3.4. Synthesis and $^1\text{H-NMR}$ Assignment of Aldol Addition Reaction Product

Synthesis and  $^1\text{H-NMR}$  assignment of 4-hydroxy-4-(4-nitrophenyl) butan-2-one (**3**) (Scheme 5).



**Scheme 5.** 4-hydroxy-4-(4-nitrophenyl) butan-2-one.

4-hydroxy-4-(4-nitrophenyl) butan-2-one (**3**) was synthesised as previously reported (see pg S3, Figure S2) [48].  $^1\text{H-NMR}$  (400 MHz,  $\text{CDCl}_3$ ):  $\delta$  = 8.20 (d,  $J$  = 8.8 Hz, ArH, 2H), 7.53 (d,  $J$  = 8.8 Hz, ArH, 2H), 5.26 (m, ArCH(OH)CH<sub>2</sub>, 1H), 3.61 (br s, ArCH(OH)CH<sub>2</sub>, 1H), 2.85 (m, CH<sub>2</sub>COCH<sub>3</sub>, 2H), 2.22 (s, CH<sub>2</sub>COCH<sub>3</sub>, 3H) ppm. The analytical data were found to be in good agreement with the reported data [48].

### 3.5. Chiral HPLC Data of Activity and Selectivity Screening

#### 3.5.1. Screening Reactions

Analytical chiral HPLC analysis of product **3** was performed on a 1260 Infinity Quaternary LC system (Agilent Technologies, Santa Clara, USA) using a Lux Amylose-1 column (Phenomenex, Torrance, USA), 4.6 mm  $\times$  250 mm (0.5 mL/min, 25  $^{\circ}\text{C}$ , *n*-hexane/iso-propanol 75:25, 50 min). Slight variations on the retention time are due to the change of the column guard throughout the measurements. The peaks were assigned using signal at 280 nm.

## 4. Conclusions

In summary, we reported the use of streptavidin as a host for organocatalytic aldol addition. The reaction yield is nearly quantitative using only 1 mol% of catalyst. When compared to other protein-based aldol addition systems, such as ones catalyzed by 4-OT [12,15], catalytic antibodies [52] and RA95.5-8F [17], both the enantioselectivity and reactivity can further be improved in the Sav-based system, and thus additional protein engineering efforts are needed. However, in contrast with the other existing system, the performance of the Sav-based catalytic system can be improved by modifying both the catalytic motif and the protein scaffold. Indeed, by site-directed mutagenesis studies, this work illustrated that Ser112 and Lys121 are crucial in dictating the reaction conversion and stereoselectivity, respectively. The roles of these residues will be further investigated with the aim to improve the performance of this Sav-hosted aldol addition reaction. Hence, we anticipate this proof-of-concept study will be converted into applications for organocatalytic aldol addition in chemical and synthetic biology research in future.

**Supplementary Materials:** The following are available online. Figure S1: SDS-PAGE of T-rSav and mutants, Figure S2:  $^1\text{H-NMR}$  spectrum for the aldol product **3**, Figure S3–S18: Chiral-LC spectra for the aldol product **3** using different catalysts and conditions, Figure S19–S37:  $^1\text{H-NMR}$  spectrum for aldol reactions using different catalysts and conditions.

**Author Contributions:** Conceptualisation, L.Y.P.L. and L.C.M.; methodology, L.Y.P.L. and N.S.; investigation, N.S.; data curation, N.S.; writing—original draft preparation, N.S.; writing—review and editing, L.Y.P.L.; supervision, L.Y.P.L.; funding acquisition, L.Y.P.L. and L.C.M. All authors have read and agreed to the published version of the manuscript.

**Funding:** This work was supported by Cardiff University through the startup fund provided by the Cardiff School of Chemistry, the Leverhulme Trust through grant to L.Y.P.L. (RPG-2017-195), the Royal Society through grant to L.C.M. (RG150466), the UK's Wellcome Trust through grants to L.Y.P.L. (202056/Z/16/Z).

**Acknowledgments:** We thank Ms Alina Stein and Professor Thomas R Ward at the University of Basel for their discussion on improving the recombinant preparation of T-Sav. We also would like to thank Dr Yu-Hsuan Tsai and Dr Alexander Nödling at Cardiff University for their useful suggestions during the development of this project.

**Conflicts of Interest:** The authors declare no conflict of interest. The funders had no role in the design of the study; in the collection, analyses, or interpretation of data; in the writing of the manuscript, or in the decision to publish the results.

## References

1. van der Helm, M.P.; Klemm, B.; Eelkema, R. Organocatalysis in aqueous media. *Nat. Rev. Chem.* **2019**, *3*, 491-508, doi:10.1038/s41570-019-0116-0.
2. Bhowmick, S.; Mondal, A.; Ghosh, A.; Bhowmick, K.C. Water: the most versatile and nature's friendly media in asymmetric organocatalyzed direct aldol reactions. *Tetrahedron: Asymmetry* **2015**, *26*, 1215-1244, doi:10.1016/j.tetasy.2015.09.009.
3. Howard, T.S.; Cohen, R.D.; Nwajiobi, O.; Muneeswaran, Z.P.; Sim, Y.E.; Lahankar, N.N.; Yeh, J.T.H.; Raj, M. Amino-Acid-Catalyzed Direct Aldol Bioconjugation. *Org. Lett.* **2018**, *20*, 5344-5347, doi:10.1021/acs.orglett.8b02265.
4. Schober, L.; Ratnam, S.; Yamashita, Y.; Adebar, N.; Pieper, M.; Berkessel, A.; Hessel, V.; Gröger, H. An Asymmetric Organocatalytic Aldol Reaction of a Hydrophobic Aldehyde in Aqueous Medium Running in Flow Mode. *Synthesis* **2019**, *51*, 1178-1184, doi:10.1055/s-0037-1610404.
5. Heidlindemann, M.; Rulli, G.; Berkessel, A.; Hummel, W.; Gröger, H. Combination of Asymmetric Organo- and Biocatalytic Reactions in Organic Media Using Immobilized Catalysts in Different Compartments. *ACS Catal.* **2014**, *4*, 1099-1103, doi:10.1021/cs4010387.
6. Rulli, G.; Duangdee, N.; Baer, K.; Hummel, W.; Berkessel, A.; Gröger, H. Direction of Kinetically versus Thermodynamically Controlled Organocatalysis and Its Application in Chemoenzymatic Synthesis. *Angew. Chem. Int. Ed.* **2011**, *50*, 7944-7947, doi:10.1002/anie.201008042.
7. Baer, K.; Krauß, M.; Burda, E.; Hummel, W.; Berkessel, A.; Gröger, H. Sequential and Modular Synthesis of Chiral 1,3-Diols with Two Stereogenic Centers: Access to All Four Stereoisomers by Combination of Organo- and Biocatalysis. *Angew. Chem., Int. Ed.* **2009**, *48*, 9355-9358, doi:10.1002/anie.200900582.
8. Avila-Ortiz, C.G.; Pérez-Venegas, M.; Vargas-Caporali, J.; Juaristi, E. Recent applications of mechanochemistry in enantioselective synthesis. *Tetrahedron Lett.* **2019**, *60*, 1749-1757, doi:10.1016/j.tetlet.2019.05.065.
9. Kamo, S.; Maruo, S.; Kuramochi, K.; Tsubaki, K. Synthesis of enantiomerically pure juglomycin C and NHAB. *Tetrahedron* **2015**, *71*, 3478-3484, doi:10.1016/j.tet.2015.03.073.
10. Varun; Sonam; Kakkar, R. Isatin and its derivatives: a survey of recent syntheses, reactions, and applications. *Med. Chem. Commun.* **2019**, *10*, 351-368, doi:10.1039/C8MD00585K.
11. Samanta, B.; Seikowski, J.; Höbartner, C. Fluorogenic Labeling of 5-Formylpyrimidine Nucleotides in DNA and RNA. *Angew. Chem. Int. Ed.* **2016**, *55*, 1912-1916, doi:10.1002/anie.201508893.
12. Saifuddin, M.; Guo, C.; Biewenga, L.; Saravanan, T.; Charnock, S.J.; Poelarends, G.J. Enantioselective Aldol Addition of Acetaldehyde to Aromatic Aldehydes Catalyzed by Proline-Based Carbogases. *ACS Catal.* **2020**, *10*, 2522-2527, doi:10.1021/acscatal.0c00039.
13. Spears, R.J.; Brabham, R.L.; Budhadev, D.; Keenan, T.; McKenna, S.; Walton, J.; Brannigan, J.A.; Brzozowski, A.M.; Wilkinson, A.J.; Plevin, M., et al. Site-selective C-C modification of proteins at neutral pH using organocatalyst-mediated cross aldol ligations. *Chem. Sci.* **2018**, *9*, 5585-5593, doi:10.1039/C8SC01617H.
14. Roldán, R.; Hernandez, K.; Joglar, J.; Bujons, J.; Parella, T.; Sánchez-Moreno, I.; Hélaïne, V.; Lemaire, M.; Guérard-Hélaïne, C.; Fessner, W.-D., et al. Biocatalytic Aldol Addition of Simple Aliphatic Nucleophiles to Hydroxyaldehydes. *ACS Catal.* **2018**, *8*, 8804-8809, doi:10.1021/acscatal.8b02486.

15. Rahimi, M.; Geertsema, E.M.; Miao, Y.; van der Meer, J.Y.; van den Bosch, T.; de Haan, P.; Zandvoort, E.; Poelarends, G.J. Inter- and intramolecular aldol reactions promiscuously catalyzed by a proline-based tautomerase. *Org. Biomol. Chem.* **2017**, *15*, 2809–2816, doi:10.1039/c7ob00302a.
16. Yamashita, Y.; Yasukawa, T.; Yoo, W.-J.; Kitanosono, T.; Kobayashi, S. Catalytic enantioselective aldol reactions. *Chem. Soc. Rev.* **2018**, *47*, 4388–4480, doi:10.1039/C7CS00824D.
17. Zeymer, C.; Hilvert, D. Directed Evolution of Protein Catalysts. *Annu. Rev. Biochem.* **2018**, *87*, 131–157, doi:10.1146/annurev-biochem-062917-012034.
18. Obexer, R.; Godina, A.; Garrabou, X.; Mittl, P.R.E.; Baker, D.; Griffiths, A.D.; Hilvert, D. Emergence of a catalytic tetrad during evolution of a highly active artificial aldolase. *Nat. Chem.* **2016**, *9*, 50, doi:10.1038/nchem.2596
19. Mase, N.; Nakai, Y.; Ohara, N.; Yoda, H.; Takabe, K.; Tanaka, F.; Barbas, C.F. Organocatalytic Direct Asymmetric Aldol Reactions in Water. *J. Am. Chem. Soc.* **2006**, *128*, 734–735, doi:10.1021/ja0573312.
20. Raj, M.; Vishnumaya; Ginotra, S.K.; Singh, V.K. Highly Enantioselective Direct Aldol Reaction Catalyzed by Organic Molecules. *Org. Lett.* **2006**, *8*, 4097–4099, doi:10.1021/ol0616081.
21. List, B.; Lerner, R.A.; Barbas, C.F. Proline-Catalyzed Direct Asymmetric Aldol Reactions. *J. Am. Chem. Soc.* **2000**, *122*, 2395–2396, doi:10.1021/ja994280y.
22. Oliveira, V.G.; Cardoso, M.F.C.; Forezi, L.S.M. Organocatalysis: A Brief Overview on Its Evolution and Applications. *Catalysts* **2018**, *8*, doi:10.3390/catal8120605.
23. Nödling, A.R.; Santi, N.; Williams, T.L.; Tsai, Y.-H.; Luk, L.Y.P. Enabling protein-hosted organocatalytic transformations. *RSC Adv.* **2020**, *10*, 16147–16161, doi:10.1039/D0RA01526A.
24. Nödling, A.R.; Świderek, K.; Castillo, R.; Hall, J.W.; Angelastro, A.; Morrill, L.C.; Jin, Y.; Tsai, Y.-H.; Moliner, V.; Luk, L.Y.P. Reactivity and Selectivity of Iminium Organocatalysis Improved by a Protein Host. *Angew. Chem., Int. Ed.* **2018**, *57*, 12478–12482, doi:10.1002/anie.201806850.
25. Zhao, Y.; Cotelle, Y.; Liu, L.; Lopez-Andarias, J.; Bornhof, A.B.; Akamatsu, M.; Sakai, N.; Matile, S. The Emergence of Anion- $\pi$  Catalysis. *Acc. Chem. Res.* **2018**, *51*, 2255–2263, doi:10.1021/acs.accounts.8b00223.
26. Guo, C.; Saifuddin, M.; Saravanan, T.; Sharifi, M.; Poelarends, G.J. Biocatalytic Asymmetric Michael Additions of Nitromethane to  $\alpha,\beta$ -Unsaturated Aldehydes via Enzyme-bound Iminium Ion Intermediates. *ACS Catal.* **2019**, 4369–4373, doi:10.1021/acscatal.9b00780.
27. Leveson-Gower, R.B.; Mayer, C.; Roelfes, G. The importance of catalytic promiscuity for enzyme design and evolution. *Nat. Rev. Chem.* **2019**, *3*, 687–705, doi:10.1038/s41570-019-0143-x.
28. Jacobsen, E.N.; MacMillan, D.W.C. Organocatalysis. *Proc. Natl. Acad. Sci. U. S. A.* **2010**, *107*, 20618, doi:10.1073/pnas.1016087107.
29. MacMillan, D.W.C. The advent and development of organocatalysis. *Nature* **2008**, *455*, 304–308, doi:10.1038/nature07367.
30. Donslund, B.S.; Johansen, T.K.; Poulsen, P.H.; Halskov, K.S.; Jorgensen, K.A. The Diarylprolinol Silyl Ethers: Ten Years After. *Angew. Chem., Int. Ed.* **2015**, *54*, 13860–13874, doi:10.1002/anie.201503920.
31. Jensen, K.L.; Dickmeiss, G.; Jiang, H.; Albrecht, L.; Jorgensen, K.A. The diarylprolinol silyl ether system: a general organocatalyst. *Acc. Chem. Res.* **2012**, *45*, 248–264, doi:10.1021/ar200149w.
32. Mukherjee, S.; Yang, J.W.; Hoffmann, S.; List, B. Asymmetric Enamine Catalysis. *Chem. Rev.* **2007**, *107*, 5471–5569, doi:10.1021/cr0684016.
33. Anebousevly, K.; Shruthi, K.S.; Ramachary, D.B. Asymmetric Supramolecular Organocatalysis: A Complementary Upgrade to Organocatalysis. *Eur. J. Org. Chem.* **2017**, 2017, 5460–5483, doi:10.1002/ejoc.201700611.
34. Bertelsen, S.; Jorgensen, K.A. Organocatalysis—after the gold rush. *Chem. Soc. Rev.* **2009**, *38*, 2178–2189, doi:10.1039/b903816g.
35. Zou, Y.-Q.; Hörmann, F.M.; Bach, T. Iminium and enamine catalysis in enantioselective photochemical reactions. *Chem. Soc. Rev.* **2018**, *47*, 278–290, doi:10.1039/C7CS00509A .
36. Erkkila, A.; Majander, I.; Pihko, P.M. Iminium catalysis. *Chem. Rev.* **2007**, *107*, 5416–5470, doi:10.1021/cr068388p.
37. Davis, H.J.; Ward, T.R. Artificial Metalloenzymes: Challenges and Opportunities. *ACS Cent. Sci.* **2019**, *5*, 1120–1136, doi:10.1021/acscentsci.9b00397.
38. Pellizzoni, M.M.; Schwizer, F.; Wood, C.W.; Sabatino, V.; Cotelle, Y.; Matile, S.; Woolfson, D.N.; Ward, T.R. Chimeric Streptavidins as Host Proteins for Artificial Metalloenzymes. *ACS Catal.* **2018**, *8*, 1476–1484, doi:10.1021/acscatal.7b03773.
39. Schwizer, F.; Okamoto, Y.; Heinisch, T.; Gu, Y.; Pellizzoni, M.M.; Lebrun, V.; Reuter, R.; Kohler, V.; Lewis, J.C.; Ward, T.R. Artificial Metalloenzymes: Reaction Scope and Optimization Strategies. *Chem. Rev.* **2018**, *118*, 142–231, doi:10.1021/acs.chemrev.7b00014.

40. Hassan, I.S.; Ta, A.N.; Danneman, M.W.; Semakul, N.; Burns, M.; Basch, C.H.; Dippon, V.N.; McNaughton, B.R.; Rovis, T. Asymmetric  $\delta$ -Lactam Synthesis with a Monomeric Streptavidin Artificial Metalloenzyme. *J. Am. Chem. Soc.* **2019**, *141*, 4815–4819, doi:10.1021/jacs.9b01596.
41. Lechner, H.; Emann, V.R.; Breuning, M.; Höcker, B. An Artificial Cofactor catalyzing the Baylis-Hillman Reaction using Designed Streptavidin as Protein Host. *bioRxiv* **2020**, 2020.2003.2005.978098, doi:10.1101/2020.03.05.978098.
42. Cotellet, Y.; Lebrun, V.; Sakai, N.; Ward, T.R.; Matile, S. Anion- $\pi$  Enzymes. *ACS Cent. Sci.* **2016**, *2*, 388–393, doi:10.1021/acscentsci.6b00097.
43. Le, Q.; Nguyen, V.; Park, S. Recent advances in the engineering and application of streptavidin-like molecules. *Applied Microbio. & Biotech.* **2019**, *103*, 7355–7365, doi:10.1007/s00253-019-10036-5.
44. Okamoto, Y.; Kojima, R.; Schwizer, F.; Bartolami, E.; Heinisch, T.; Matile, S.; Fussenegger, M.; Ward, T.R. A cell-penetrating artificial metalloenzyme regulates a gene switch in a designer mammalian cell. *Nat. Commun.* **2018**, *9*, 1943, doi:10.1038/s41467-018-04440-0.
45. Raines, D.J.; Clarke, J.E.; Blagova, E.V.; Dodson, E.J.; Wilson, K.S.; Duhme-Klair, A.-K. Redox-switchable siderophore anchor enables reversible artificial metalloenzyme assembly. *Nat. Catal.* **2018**, *1*, 680–688, doi:10.1038/s41929-018-0124-3.
46. Heinisch, T.; Schwizer, F.; Garabedian, B.; Csibra, E.; Jeschek, M.; Vallapurackal, J.; Pinheiro, V.B.; Marliere, P.; Panke, S.; Ward, T.R. E. coli surface display of streptavidin for directed evolution of an allylic deallylase. *Chem. Sci.* **2018**, *9*, 5383–5388, doi:10.1039/c8sc00484f.
47. Sano, T.; Pandori, W.M.; Chen, X.; Smith, L.C.; Cantor, R.C. A minimum-sized core streptavidin has enhanced structural stability and higher accessibility to biotinylated macromolecules. *J. Biol. Chem.* **1995**, *270*, 28204–28209, doi:10.1074/jbc.270.47.28204.
48. Hosseini, M.; Stiasni, N.; Barbieri, V.; Kappe, C.O. Microwave-Assisted Asymmetric Organocatalysis. A Probe for Nonthermal Microwave Effects and the Concept of Simultaneous Cooling. *J. Org. Chem.* **2007**, *72*, 1417–1424, doi:10.1021/jo0624187.
49. Gao, J.; Bai, S.; Gao, Q.; Liu, Y.; Yang, Q. Acid controlled diastereoselectivity in asymmetric aldol reaction of cycloketones with aldehydes using enamine-based organocatalysts. *Chem. Commun.* **2011**, *47*, 6716–6718, doi:10.1039/C0CC05224H.
50. Gryko, D.; Zimnicka, M.; Lipiński, R. Brønsted Acids as Additives for the Direct Asymmetric Aldol Reaction Catalyzed by l-Proline-thioamides. Direct Evidence for Enamine–Iminium Catalysis. *J. Org. Chem.* **2007**, *72*, 964–970, doi:10.1021/jo062149k.
51. Sutar, R.L.; Joshi, N.N. Role of Additives in Chiral Amine-Catalyzed Direct Aldol Reaction. *Synth. Commun.* **2014**, *44*, 352–360, doi:10.1080/00397911.2013.805231.
52. Zhong, G.; Lerner, R.A.; Barbas, I.C. Broadening the Aldolase Catalytic Antibody Repertoire by Combining Reactive Immunization and Transition State Theory: New Enantio- and Diastereoselectivities. *Angew. Chem., Int. Ed.* **1999**, *38*, 3738–3741, doi:10.1002/(sici)1521-3773(19991216)38:24<3738::aid-anie3738>3.0.co;2-2.

**Sample Availability:** Samples of the compound **3** are available from the authors.



© 2020 by the authors. Licensee MDPI, Basel, Switzerland. This article is an open access article distributed under the terms and conditions of the Creative Commons Attribution (CC BY) license (<http://creativecommons.org/licenses/by/4.0/>).